The 9th TUAT PVST

PHOTOVOLTAIC STUDENT THINK-IN

TUAT

第9回

東京農工大学　大学院　電気電子工学講座

太陽光発電システム研究発表会

論文集

2007年3月24日（土）

主催：　東京農工大学　大学院　黒川浩助研究室

黒川　浩助
e-mail: kurochan@cc.tuat.ac.jp
http://www.tuat.ac.jp/~kurochan/
国立大学法人　東京農工大学　大学院
共生科学技術研究部　生存科学研究拠点
〒184-8588 東京都小金井市中町2-24-16
TEL: 042-388-7132　　FAX: 042-385-7445

東京農工大学 大学院 電気電子工学講座
太陽光発電システム研究発表会
予稿集

開催日時

平成１９年3月２４日（土）１３時～１７時４０分

開催場所

東京農工大学　小金井キャンパス

新１号館　１階　講堂

主催:東京農工大学 大学院 電気電子工学講座 黒川浩助研究室

太陽光発電システム研究発表会
プログラム

平成 19 年 3 月 24 日（土）　13 時～17 時 40 分
東京農工大学　小金井キャンパス　新 1 号館 1 階　講堂

Ⅰ. 始めに（挨拶）	（黒川浩助）	13:00～13:10	
Ⅱ. 研究発表			
1.　注目研究から（Ⅰ）			ページ
(1) PV System R&D in Tunisia	（工博 Ridha）	13:10～13:40	**3**
(2) 太陽光発電システム計測データを用いた運転特性高度解析手法に関する研究	（工博 植田）	13:40～14:10	**5**
(3) 波長離散光型 LED ソーラーシミュレータの開発	（M2 小柳）	14:10～14:40	**7**
休憩 （コーヒーブレイク・ポスタータイム）		14:40～15:20	
2.　注目研究から（Ⅱ）			
(1) PV インバータのディジタル制御機能の研究	（M2 瀬尾）	15:20～15:50	**9**
(2) デュアルセンサ型日射計の開発	（M2 平田）	15:50～16:20	**11**
(3) 空中写真を用いた都市地域の太陽光発電システムポテンシャルの推定	（B4 鈴木）	16:20～16:50	**13**
3.　今後の太陽光発電システム研究の方向性	（黒川浩助）	16:50～17:30	
Ⅲ. 終わりに	（黒川浩助）	17:30～17:40	
Ⅳ. 懇親会		18:00～	

研究発表会終了後，生協ホールにて懇親会を行います。（参加費無料）

◎ 休憩（コーヒーブレイク）中に，以下のポスタープレゼンテーションを行う予定です。

・ モンゴルにおける太陽光発電システムに関する研究	（PD アマル）	**15**
・ 太陽光発電の面的発電量推定技術に関する研究	（D3 大谷）	**16**
・ 太陽光発電システムの単独運転試験方法に関する研究	（D3 五十嵐）	**17**
・ 新型太陽電池の特性検証研究	（D3 筒井）	**19**
・ パワーエレクトロニクスによる配電系統の電力品質安定化に関する研究	（D2 李）	**21**
・ 太陽光発電変動特性評価法の研究	（D2 川崎）	**23**
・ 蓄電池あり系統連系システムに関する研究	（D1 嶋田）	**25**
・ 太陽電池の性能評価に関する研究	（D1 津野）	**26**
・ PV インバータ系統機能超縮小模擬試験装置の開発	（M2 中村）	**28**
・ マトリックスコンバータの電力系統への適用	（M2 鎌倉）	**30**
・ リモートセンシングによる太陽光発電システム資源量の推定	（M1 浜野）	**32**
・ 写真測量法による太陽光発電システムの日照障害特性の推定	（M1 渡辺）	**33**
・ パワーコンディショナの単独運転検出機能に関する研究	（M1 宮本）	**34**
・ TUAT-20kW 太陽光発電の測定データを生かした高度性能分析	（B4 石岡）	**36**
・ 集中連系型太陽光発電システムにおける計測データ処理法の研究	（B4 井出）	**37**
・ 各種太陽電池の屋外性能評価	（B4 角）	**38**
・ 縮小系統模擬分散電源の開発	（B4 東方田）	**39**
・ 配電系統の電圧制御に関する研究	（B4 山口）	**41**
・ 大規模太陽光発電システムに関する研究	（砂漠 WG 伊藤）	**43**

Photovoltaic System Research and Development in Tunisia

Dr. Ridha LANDOULSI

1. Introduction.

In an emerging country such as Tunisia, the international situation imposes an accurate technology transfer and an absolute leveling in sectors extremely interesting on very high added value, like that of renewable energies. This may be achieved by increasing the potential of research and development (R&D) laboratories and the transfer of valorized results towards industrial fields.

2. Energy Issues in Tunisia

The Tunisian energy context is currently characterized by an increase of the energy demand and a stagnation of the hydrocarbon resources, which leads to an energy deficit estimated at 8 Mtep by 2010.

The Tunisian government has a particular interest to promote durable energy and to adopt an energy strategy which takes account at the same time the requirements of the socio-economic development and safeguarding of the environment [1].

To face this situation, Tunisia committed itself in an energy policy compatible with the durable development which consist to :

- Intensification and reinforcement of the efforts leading to the development of the national hydrocarbon resources by the promotion of the use of the clean fuels such as the natural gas.
- The rational use of energy,
- Obligatory and periodic audits in the sectors: industry, transport and service,
- The promotion of the new techniques of energy economy such as the cogeneration, the thermal regulation of the habitats and the certification of the house electric apparatuses.
- The installation of an adequate lawful framework of energy mastering.
- The development of renewable energies which resulted in :
  - The development of wind power for the production of electricity by the installation of a wind park of 300 MW (2005-2011).
  - Diffusion on large scale of solar heaters of water,
  - Optimization of the rural electrification by PV systems. Beside this rather important market, Tunisia has approximately 300,000 surface wells. This should encourage to develop PV pumping systems. The photovoltaic energy will rise to 3.5 MW by 2010 (electrification rural, pumping, professional application).

System	units	2010	2020	2030
Wind	MW	310	1130	1840
Solar thermics	10^3 m^2	280	950	2500
photovoltaics	MWc	3.5	8.5	18
Biogas	MW	30	50	80
Economy energy (cumul)	Mtep	1.3	6.7	18.6
Avoided emission (cumul)	MTE CO2	3	15.7	43.6

Fig. 1. Development prospect of renewable energies in Tunisia

3. Historical background of PV research and development in Tunisia

	PV Research activities [2]
End of 1970's	A study was performed, in Tunisia, showing that many remote rural areas are in need of electric utility insuring a minimum of human comfort and preventing migration of the rural populations
1985	In the framework of a national project promoting renewable energies, a PV Pilot Plant (PVPP) was installed (1985) at INRST (National Institute for Research Science and Technology) by local competences.
1986	Since 1986, the role assigned to the PVPP is to apply renewable energies based national programmes, particularly related to the research and development (R&D) of PV materials and technologies.The first main objective was the development of a local PV technology that may produce monocrystalline Silicon solar cells and modules with efficiencies approaching international ones. The results of Research and Development (R&D) achieved on crystalline silicon solar cells and the demonstration projects realized within the PVPP, let the PV research team thought that Tunisia is not so far to industrialize PV technology. Several attempts have been made to promote and transfer the technological know acquired in the PVPP by inviting industrials both at national or international levels. All of them recognize the capability and the level attained by the PV group, which is the first Arabic and African research team who master and develop silicon solar cells processing and PV modules.

1997	In 1997 a research group on photovoltaic systems emerged within the photovoltaic laboratory. The research activities of this group were oriented on modeling, control and optimal management of PV systems used in pumping and desalination of water.
2001	In 2001 the PV group realized an important demonstration project financed by the ALECSO and consisting of producing 25 PV bags (distributed in the Arabic countries) for the education of technicians and engineers working in the field of renewable energy. Each bag contains a PV module having a power of 30 Watts, and encloses different applications (lighting, pumping …etc.)

Fig.2. Education PV system bags

Fig.3. PV water desalination by reverse osmosis unit.

4. National PV program

The ANER (National Agency for Renewable Energies) recently formerly (ANME) National Agency for Energy Conservation which is the governmental institution in charge of renewable energy promotion. ANME has assured until 2006[3]:

- the rural PV electrification of 12000 homes and 200 schools,
- 5 projects of PV public Lighting,
- 86 PV pumping systems.

(Totally: 2MWc of PV modules has been installed).

Theses PV applications have contributed to the development of the rural environment and enabled the manufacturing of special batteries and regulators, for the first time in Tunisia.

In the framework of a Japanese credit to Tunisia (financed by JBIC), ANME will assure the installation of 1200 PV home systems, 500 PV public Lighting, 48 PV pumping and 45 PV desalination systems.

Fig. 4. Solar Street-lighting in Ksar Ghilene, south of Tunisia.

5. Support of research programs and development

An important Presidential decision ordered the establishment of a technological pole (Techno-Park) on the site of Borj-Cedria, beside the INRST[4]. This Techno Park, included from 2006 : three Research and technologies Centers of Energy (CRTEn), Water, and Biotechnology, a Production Park, an Innovation Park, an University Park, and a Central Library.

This Techno Park is designed to promote innovative and competitive enterprises complying with the national, as well as international priorities, some formation and research activities of high level in relation with Industry, and new and high technologies. This may offer a setting to the enterprises in order to develop some new technologies (i.e., PV technology). This Techno Park may also receipt enterprises that may produce entire PV modules. It should be assisted by the LPVS researchers of CRTEn. (Research and Technologies of Energy Center).

6. Conclusion

The installation of renewable energies in Tunisia is justified by the increase of conventional energies price and the environmental protection. So, the promotion, the diffusion and the development of renewable energies have an unconditional support in Tunisia. However, so that these actions are durable, it would be necessary that they find technological supports by institutions of engineering and research laboratories of point**.**

References

[1] http://www.environnement.nat.tn

[2] Project for a technological leveling of the photovoltaic pilot plant of the National Institute of Scientific and Technical research, report prepared by Brahim Bessais ,Tunisia, May 2003.

[3] http://www.anme.nat.tn

[4] http://www.ecopark.rnrt.tn.

太陽光発電システム計測データを用いた運転特性高度解析手法に関する研究

植田　譲（博士(工学)）

1. はじめに

人類の持続可能な発展の実現に向け，再生可能エネルギーへの期待はますます高まっている。中でも太陽光発電(PV)はその発電過程で一切の排出ガスを発生しない事，入力エネルギーである太陽からの日射量が膨大である事などから，環境持続性を持った次世代エネルギーシステムの根幹を担うべき電源の一つとして期待されている。しかし，住宅用太陽光発電システムが既存配電系統の末端部分へ数百件規模で局所集中的に連系された場合，PV システムからの余剰電力の逆潮流による，配電系統の電圧上昇発生が懸念される。配電系統の電圧が管理範囲を超えて上昇する可能性がある場合，分散型電源である PV システムは出力を抑制し系統電圧の過度な上昇を回避しなければならない。そのため，日本国内において用いられる PV システム用パワーコンディショナ(PCS)は出力抑制機能を搭載しているが，この機能は，系統電圧上昇時には数秒～数分の時間で出力を抑制するため，PVシステムの運転特性評価に辺り，出力抑制機能による損失量を定量化するには数分以下の時間解像度を持つ評価手法が必要となる。

本研究では，1分周期で収録されたPVシステムの計測データを用い，系統電圧上昇時の出力抑制機能による損失を含む，系統連系型太陽光発電システムの発電特性と損失発生要因を高度に解析する手法を開発する事を目的する。また，開発した手法を用い，独立行政法人新エネルギー・産業技術総合開発機構により平成 14 年度から行われている「集中連系型太陽光発電システム実証研究」における 553 軒の住宅用太陽光発電システムの運転特性解析を行った。

2. システム出力係数と損失量の定量化

PVシステムでは，入力エネルギーである日射が太陽電池アレイ面に入射し太陽電池セルにおいて直流電力に変換された後，PCS から交流電力として出力が得られるまでの間に様々な損失が生じる。これらの様々な要因による損失量を定量化する手法の一つとして，東京農工大学にて現在も開発が続けられているSV法が挙げられる。SV法では，PVシステムの性能評価指標として，システム出力係数を用いる。システム出力係数とは，等価日システム運転時間を等価日太陽日照時間で除した値として定義され，[%]で表わしている。また，損失に関しても発電量と同様に，日射量から算出される理想的な出力電力量に対して発電できなかった電力量の割合を損失要因毎に定量化する。解析期間は30日を基本としており，これは，解析期間中にある程度の快晴日，種々の損失が極小である状態のデータが必要な為である。

本研究において損失量の定量化が可能な PV システムの損失要因は以下の通りである。

- PCS オフ状態による損失
- PCS 容量不足による損失
- 出力抑制機能による損失
- アレイ温度上昇による損失
- 変動による損失
- PCS での損失
- 定格ばらつき，汚れ，劣化等
- 入射角による損失
- 直流回路抵抗による損失
- 日陰による損失
- MPPミスマッチ高電圧側による損失

3. 結果および考察

「集中連系型太陽光発電システム実証研究」では 2003 年 12 月から実証試験地域での PV システム設置を開始し，2004 年 1 月から部分的に計測を開始した。これ以降，順次，設置数を増加させ，約 2 年半後の 2006 年 5 月に全 553 軒の設置・計測開始を完了した。PV アレイの総設置容量は約 2.13[MW]，PCS 定格出力ベースでの全設置容量は約 2.16[MW]である。PVモジュールは日本国内の大手4社，三菱電機，三洋電機，京セラ，シャープ社製のモジュールを主に使用し，PCS は各社の市販品の他，蓄電池付き PV システム用に開発した一体型 PCS も 250 軒に設置した。

これらの計測データの中から，安定してデータが取得できた 2004 年 10 月以降のデータを用いて全553軒のPVシステムの運転特性を解析した。結果の中から，本稿では特に系統電圧上昇回避の為の出力抑制による損失に着目し，結果を報告する。

始めに，2004年10月以降の毎日の出力抑制による損失量をまとめたのが Fig.1 である。グラフ中の縦棒が一日毎の出力抑制による損失を示しており，折れ線は実証研究地域に連系された全 PV アレイ容量を右側縦軸に示している。グラフより，季節的には春・秋の中間期に多くの出力抑制が発生していることが分る。この理由としては，中間期には日射量が多く晴天率が高いこと，気候的に空調などの負荷が少なく，系統全体での負荷が軽くなる傾向があること等が考えられる。一方，発電量に占める損失量の割合は，

出力抑制による損失が最大であった 2006 年 3 月 25 日においても，約 10.3[MWh]の日積算発電量に対して 0.3[MWh]と少ない量に収まっている。しかし,この結果には実証研究地域の配電系統がオール電化住宅等の普及により一般的な住宅地域の配電系統よりも低いインピーダンスとなっている可能性や，実証研究地域の配電系統の上位側の負荷状態・電圧制御などが影響している可能性など，実証研究地域特有の要因が影響していると考えられるため，一般化を行なうには更なるデータの蓄積と考察が必要である。

次に，2004 年 10 月～2007 年 1 月までの全ての出力抑制による損失を曜日別にまとめたのが Fig.2 である。結果より，週末にほとんどの出力抑制が発生している事が明らかである。また，時刻別に見た Fig.3 では，ほとんどの出力抑制が 10 時から 14 時の間に発生している様子が分る。実証研究地域の電圧は，週末に近隣の工業負荷が無くなり高めの電圧になる傾向があるため，週末の日射量が豊富な時間帯に PV システムからの逆潮流による電圧上昇幅が大きくなり，出力抑制が発生していると考えられる。

また，システム毎に出力抑制による損失量をまとめた Fig.4 では，設備導入時期の違いから全 553 軒において集計期間が同一では無いが，特定の数十軒に偏って出力抑制による損失が発生している様子が分る。損失が特定のシステムに偏る原因としては，線路インピーダンスの違いや柱状変圧器以下のシステムの連系状況，更には各 PCS の出力抑制制御方式の違いなど，多くの要因が影響していると考えられる。このような偏りは，今後の PV システムの大量普及段階においては大規模な系統連系に対する障害となる可能性もあるため，PV システム設置者への公平性の確保のためにも，更なる解析を続けていく予定である。

4. まとめ

本研究では，1 分周期の計測データを用いて PV システム運転特性の高度解析が可能な手法を開発し，系統電圧上昇時の出力抑制による損失を定量化可能とした。また，開発した手法を用いて「集中連系型太陽光発電システム実証研究」における計測データ解析を行ない，評価手法の有効性を示すと共に，出力抑制による損失の発生傾向を明らかにした。

「集中連系型太陽光発電システム実証研究」は平成 19 年度まで継続される。今後も，本研究の成果を応用し，更なる PV システムの普及拡大に資するべく，研究を継続していく予定である。

なお，本研究は，「集中連系型太陽光発電システム実証研究」の一環として行っている。このような機会を与えていただいた(独)新エネルギー・産業技術総合開発機構，及び様々なご協力をいただいた関係者各位に，この場を借りて感謝の意を表する。

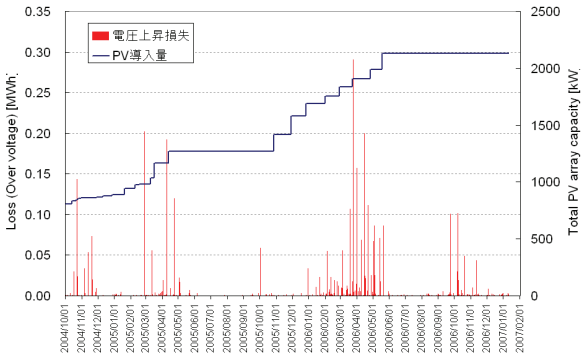

Fig. 1 Summary of the output energy loss due to the high grid voltage

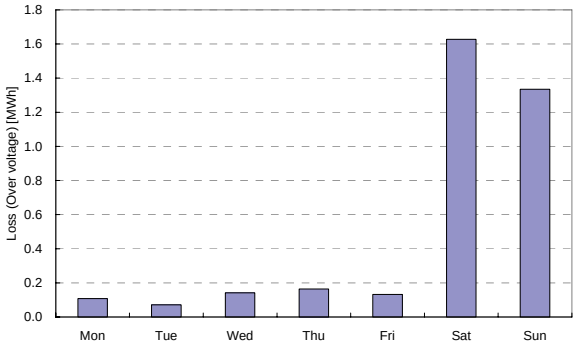

Fig. 2 Summary of the output energy loss for each day of the week

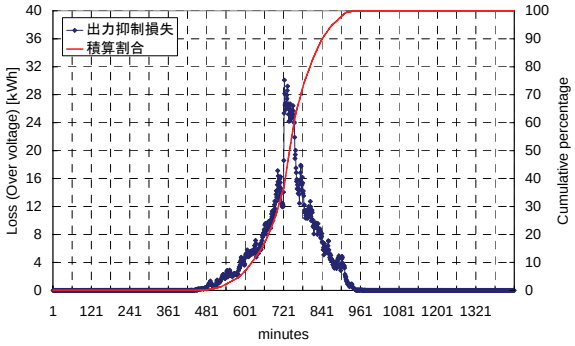

Fig. 3 Summary of the output energy loss due to the high grid voltage for each minute

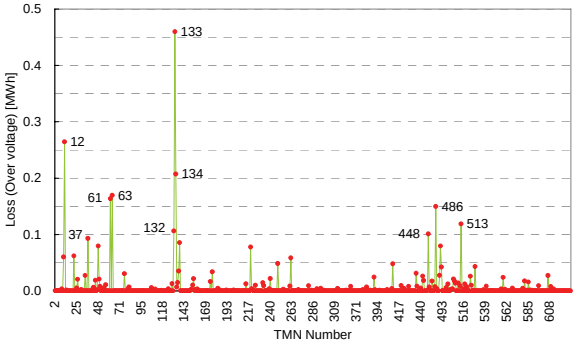

Fig. 4 Summary of the outputenergy loss due to the high grid voltage for each syste m

波長離散型 LED ソーラシミュレータの基礎実験

小柳　淳（M2）

1．はじめに

太陽電池の定格出力評価はシステム設計や価格決定において非常に重要である。一般的に，出力評価にはキセノンランプを光源としたソーラシミュレータを用いるが，キセノンランプは赤外域で特有の輝線スペクトルを持ち，連続した基準太陽光スペクトルの模擬が難しいという問題がある。現在，赤外域の補正を行ったソーラシミュレータが開発されているが，装置が高価であり，また光学フィルタなどを用いるため，効率が悪く消費電力が大きくなり，さらにランプの寿命が短いため，測定コストがかさむなどの様々な問題を抱えている。

本研究室では，LED を光源としたソーラシミュレータによる結晶 Si 太陽電池セルの評価手法を提案している[1]。LED は小型，長寿命で省電力という長所を持ち，LED メーカーの競争から照度が向上し，かつ安価に入手できるため，現在注目の光源である。LED を用いることにより装置が安価に作れ，測定コストも下げられることから，太陽電池の価格を下げ，更なる普及拡大が期待できる。この LED ソーラシミュレータを用いた手法は，青，赤，赤外 LED の持つスペクトルにより別個に測定した３つの分光感度から，全体の分光感度を算出し標準状態における短絡電流を算出する手法，および異なる照度で測定した２つの IV 特性から標準状態における IV 特性を算出するという手法である。しかしながら，精度良い出力評価法が確立しておらず，製品化に向けて精度の向上が求められている。そこで，本研究ではこれまでの評価手法を検証し，精度良く測定するために改良，改善を試みた。

2. 算出手法

〈2.1〉分光感度算出手法　　結晶 Si 太陽電池セルを図 1 に示す，n 層，空乏層，p 層をもったモデルで考える。LED ソーラシミュレータを用い，それぞれの層に対して別個に感度がある離散光（青，赤，赤外）をそれぞれ照射し，実測値より３つの離散分光感度を得る。半導体において，少数キャリア連続の方程式を解くことにより各層の少数キャリアの濃度分布が求まるが，多くのパラメータを含むため，材料定数（膜厚，吸収係数など）に代表値を用いることで，各式での変数を 1 つに絞る。この変数は実測した離散分光感度にフィッティングすることにより定まるため，半導体に光が入射したときのセルの電流を求めることができ，最終的に実測していない全体の分光感度を算出できる。具体的に用いる変数は n 層での表面再結合速度，表面反射率，p 層での少数キャリア拡散長である。フィッティングには最小二乗法を用いる。算出した分光感度に基準太陽光を積算することで，標準状態における太陽電池の短絡電流値が求まる。

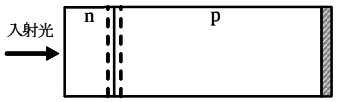

図 1　分光感度の算出に用いたセルのモデル

〈2.2〉IV 特性算出手法　　現在用いている LED ソーラシミュレータは太陽光に比べて放射照度が低く，標準状態（100mW/cm²）を再現できない。このため，異なる照度で実測した IV 特性を，照度と電流が比例するとして計算可能な補正式[2]を用いて，標準状態を外挿により算出する。算出には 2 つの IV 特性と 2.1 で求めた短絡電流を用いる。

3. 手法および測定の改善

これまでは図 1 のモデルで出力を算出していたが，検証には封止された太陽電池セルを用いたため，これに即したモデルでの評価が必要である。このため，セルを封止するための樹脂：EVA（Ethylene-Vinyl Acetate）や BSF（Back Surface Reflector）構造などを反映させた図 2 に示すモデルによる分光感度算出を行った。

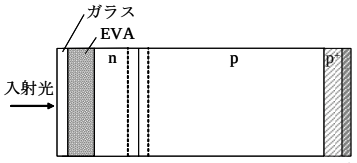

図 2　封止された太陽電池セルのモデル

〈3.1〉紫外吸収剤による影響　　新しいモデルにおける EVA には，EVA を劣化から防ぐために紫外吸収剤が含まれる[3]。そこで，紫外吸収剤の代表例として CYTEC 社の CYASORBE®の特性をデータシートより読み取り，この特性の近似式を作成した（式 1）。

$$f(\lambda)=1-\frac{1}{1+e^{\frac{\lambda-\lambda_0}{\alpha}}} \qquad \text{(式 1)}$$

なお，λ_0：変化の中心（＝395[nm]），α：変化率（＝5.5）である。結果を図 3 に示す。この近似式を分光感度に掛け合わせ改善した。

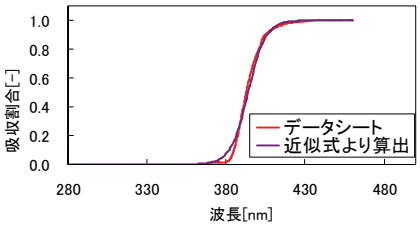

図 3　紫外吸収の近似式化

〈3.2〉　内部反射による影響　　これまでの算出結果は，1000～1200[nm]において規格値に比べ急に減少していた。しかし，算出法やパラメータを検討したが，改善がみられなかったため，新たにセルの内部で吸収されなかった光が裏面の金属電極などにより反射され再度吸収による増加していると考え，この影響を加えた。2.1 において用いた式からセルの裏面に達した光を求め，反射率 0.7[4]で内部反射するとして求めた分光感度を図 4 に示す。増分からセルで吸収されずに裏面に達する光が存在することがわかった。

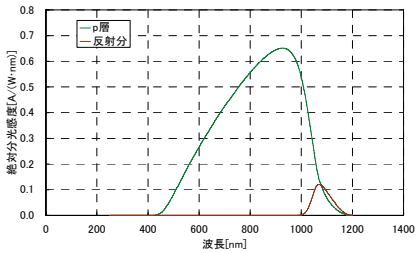

図 4　内部反射による分光感度の増加

〈3.3〉 測定の改善　　LED ソーラシミュレータの放射照度が低いため，測定において回路の抵抗による影響，外挿による測定誤差の拡大が認められた。このため，結晶 Si 太陽電池にとって感度が高い赤外域で高い放射照度を有する LED を用い，LED の実装密度を高めた新しい LED ソーラシミュレータを作製した。またバイポーラ電源を用いた回路の損失を抑え，一定範囲の温度で実測を行った。この結果，従来に比べ精度よく離散分光感度，IV 特性を測定できた。

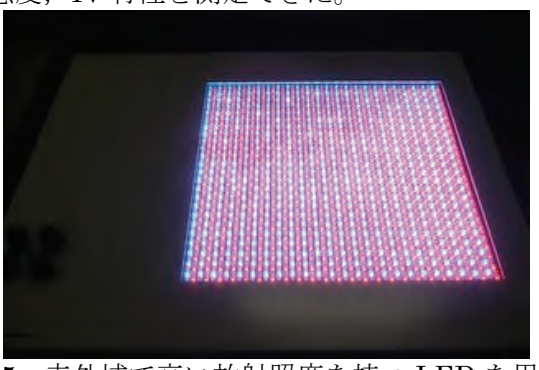

図 5　赤外域で高い放射照度を持つ LED を用い作製した LED ソーラシミュレータ

4. 改善後の算出結果

結果を図 6，図 7 および表 2 に示す。測定の改善により実測離散値が増加し，また手法の改善により，全体を精度よく算出できた。

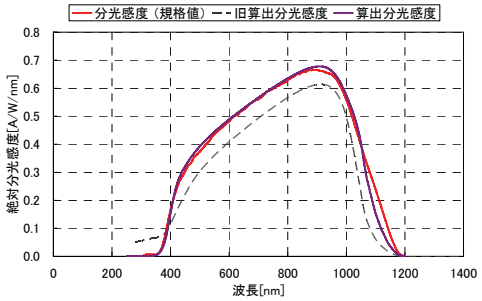

図 6　改善後の分光感度算出結果

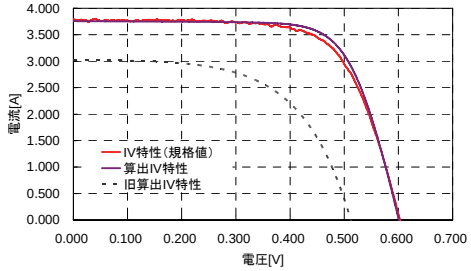

図 7　改善後の IV 特性算出結果

表 2　改善後の算出結果と規格値の比較

		規格値	算出結果	
短絡電流	Isc	3.760	3.757	[A]
開放電圧	Voc	0.603	0.601	[V]
最大出力	Pmax	1.553	1.648	[W]
最大出力点電流	Ipmax	3.370	3.468	[A]
最大出力点電圧	Vpmax	0.461	0.475	[V]
曲線因子	F.F.	68.50	72.99	[%]

5. まとめ

これまでの手法に改善を加えることにより，LED ソーラシミュレータを用いて結晶 Si 太陽電池の出力を高精度で算出可能にした。

6. 謝辞

本研究は文部科学省科学研究費萌芽研究の補助を受けた。関係者各位に感謝の意を表す。

文　　献

(1)　Shogo Kohraku, Kosuke Kurokawa : “A fundamental experiment for discrete-wavelength LED solar simulator”, 14th International Photovoltic Science and Engineering Conference (2004)
(2)　菱川善博，井村好宏，関本 巧，大城壽光：「各種太陽電池の IV 特性における放射照度依存性及び補正の検討」，電気学会論文誌，Vol.122-B，No.1，pp.26-32. (2002)
(3)　F.J.Pern : “Factors That Affect The EVA Encapsulant Discoloration Rate Upon Accelerated Exposure”, 1st WCPEC pp.897-900 (1994)
(4)　オーム社『薄膜太陽電池の基礎と応用』p.163 (2001)

PV インバータのディジタル制御機能の研究

瀬尾　祐介（M2）

1. まえがき

2001 年に示された「PV2030」では，2030 年までに総量 100GW の導入を目指しており，そのためには年産10～20GWの自動生産ラインによる大量生産が必要となる。これには，太陽電池モジュールはもちろんインバータについても革新的な技術が必要とされる [(1)]。

本研究では，高速処理，並列処理能力をもった Field Programmable Gate Array（以下，FPGA とする）単体のみで構成されるディジタルコントローラの開発をした。本稿では，その試験結果を報告する。

2. PV インバータの制御項目

図 1 に，PV インバータの制御項目を示す。PV インバータの制御項目は, 下から基本 PWM 制御, 連系制御，定電流制御，MPPT 制御，単独運転検出と階層状になっている。この制御項目は，下位制御の方がスイッチング周波数レベルでの高速制御を要し，上位制御では系統周波数レベルでの低速制御を要する。

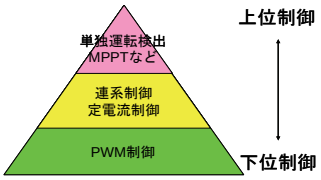

図 1　PV インバータの制御項目

3. システム構成概要

本研究で用いたデジタルインバータの構成図を**図 2** に示す。本システムは，FPGA ボードとインバータ本体が一つになった FPGA インバータと既存のディジタルコントローラの 2 つからなっている。インバータの回路パラメータを表 1 に示す。

図中，DCV，DCI は直流電圧，電流，ACV，ACI は交流電圧，電流を表している。

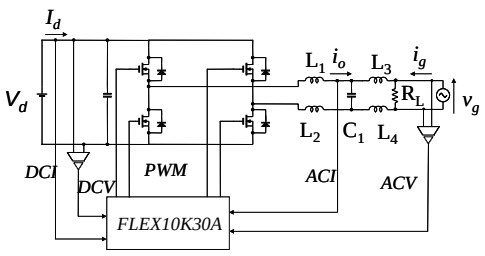

(a)　概要図

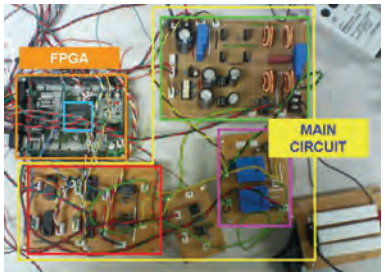

(b)　実回路

図 2　システム構成図

表 1　システムパラメータ

L_1, L_2, L_3, L_4	430 μ H	C_1	4.75 μ F
R_L	50 Ω	Carrier Frequency	50kHz
MOS-FET	IRF644	FPGA	FLEX10K30A

4. FPGA デザイン

図 3 に FPGA の内部構成を示す。下位制御部分と上位制御部分（ここでは，MPPT のみ）が並列に配置されている。系統電圧波形からサイクル信号 Cycle Pulse のみを取り出し, Digital PLL にて内部に格納された正弦波データと系統との同期制御を行う。系統と同期した正弦波データに, MPPT ブロックから出力された電流係数 k を乗算することで，基準電流波形を変化させ電力制御を行う。その後，定電流制御をかけ PWM 信号を出力する。

（1）MPPT ロジック

このコントローラで用いている MPPT 制御は，以下の**（1）式**にて行っている。

$$i_o = i_{o\_max} \times \ k \qquad (1)$$

ただし，i_{o_max}:インバータ定格出力電流

(1)式より, k の調整により交流出力電流が変化し，その結果直流入力電圧，電流の調整が可能である。

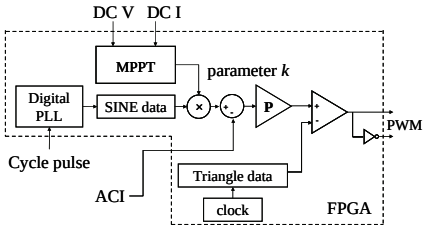

図 3　FPGA 内部構成図

5. 下位制御系の試験結果

図 4 に系統連系時における出力電流波形を示す。系統側には実際の系統波形をトランスによって降圧したものを使用した。ここでは，ディジタルコントローラボードは使用せず,電流定数 k は一定としている。

電流指令波形 v_{ref} からは系統波形のサイクル信号を取り出している。**図 5** に各次の電流歪率の計算結果を示す。また，その計算結果より総合電流歪率の計算を行ったところ，3.48%となった。これより，出力電流の歪率は電気技術指針で述べられている総合歪率 5%，各次歪率 3%以内の規定内であった。

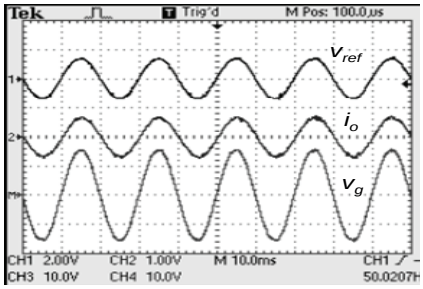

図 4　定電流制御時の波形

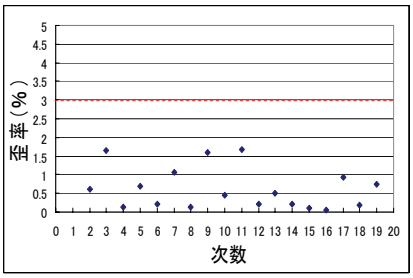

図 5　各次における歪率

6. 上位制御系の試験結果

前節にて開発した下位制御系に，MPPT を搭載することで上位・下位一体型のディジタルコントローラとしての試験を行った。

試験では，直流安定化電源に摺動抵抗を直列に接続することで太陽電池の特性を模擬した。摺動抵抗には，20 [Ω] を接続した。交流側には系統として交流バイポーラ電源を接続した。

試験結果を**図 6**，**図 7** に示す。結果より，時間の経過と伴い，インバータ出力電流波形の振幅が増加している。また，一定時間で電流出力は一定となり，FPGA が最大電力点を決定しているのがわかる。拡大波形を見ると，系統電流と出力電流が同相になっているのに対し，系統電流は逆相となっている。余剰電力を系統側に送り込む逆潮流状態であることを示している。**図 7** には，使用した電源の特性と，試験結果より得られた最大電力点をプロットしている。最大電力 16.2 [W] に対し，結果は 15.08 [W] となった。これより，MPPT 追従率は，93.09 [%] であることが確認された。

以上の結果より，FPGA を用いた MPPT 制御が正常に行われていることが確認できた。また，上位制御を行いながらも逆潮流を問題なく行うことができ，連系状態における下位制御系も正常に機能していることが確認できた。

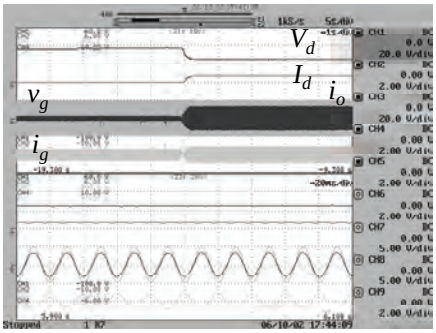

図 6　MPPT 動作時の波形
（Horizontal: upper: 1 s /div,　bottom: 20ms/div）

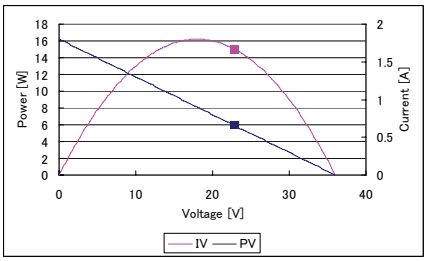

図 7　IV, PV カーブと動作点

7. まとめ

本稿では，市販の評価用 FPGA ボードをコントローラとして用いた FPGA インバータの開発，試験を行い，オールディジタルの PV インバータ用コントローラとしての動作を確認した。

また，試験により，下位制御系では，PWM 制御，同期制御，定電流制御，系統連系制御の開発を行い，正常動作が確認された。

上位制御では，MPPT 制御を開発し，正常動作が確認された。また，単独運転検出に必要となる各計算ロジック（実効値や 3 次高調波成分）の開発をし，シミュレーションにて制度良く計算されていることが確認された。

文　献

(1) K. Kurokawa, “Mass Production Scale of PV Modules and Components in 2030s and beyond” *in Proc. 15th International Photovoltaic Science & Engineering Conference (PVSEC-15)*, pp272-274, Shanghai, China, Oct 11-15, 2005.

デュアルセンサ型日射計の開発

平田　啓二（M2）

1. 研究背景と目的

太陽光発電システムの発電量推定や評価を行う上で，日射量は重要な要素である。本研究では，安価で長期安定性に優れた半導体素子を二種類用いることで，従来の Si 日射計の弱点であるスペクトル誤差を改善し，高精度な日射の計測を可能とするデュアルセンサ型日射計(Dual 日射計)の開発を目的としている。

現在，データの収集は太陽追尾装置を用いて，屋外で計測している。これは，日射計内の各センサから得られる実測出力電圧にはスペクトル誤差の他，日射計自体の諸特性である温度特性や角度特性による誤差が同時に存在するため，これの諸特性による影響を最小限に抑えるためである。

本稿では，各センサの理論出力電圧を用いた理論検証，及び実測出力電圧を用いた実証検証を行い，日射計測における Dual 日射計の精度，及び組み合わせを評価した。

2. デュアルセンサ型日射計

Dual 日射計は，Si センサ(分光感度域：320～1100nm)，及び GaAsP センサ(分光感度域：300～680nm)で補うことができない日射の長波長域に分光感度を持つ InGaAs センサ(分光感度域：900～1700nm)を追加することで，二種類のセンサから得られる出力電圧により，高精度な日射計測が期待できる。各センサの相対分光感度特性と基準太陽光スペクトルを図 1 に示す。また，図 1 に示すように，Dual 日射計の組み合わせは，Si+InGaAs と GaAsP+InGaAs の二通りが考えられる。

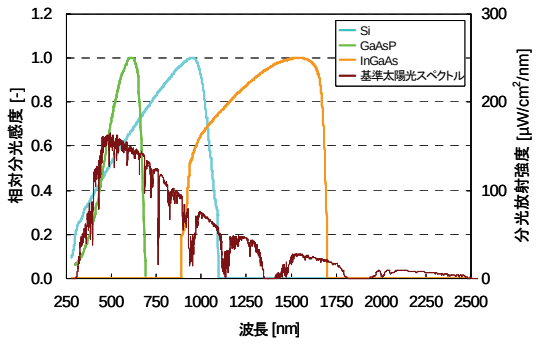

図 1：各センサの分光感度と基準太陽光スペクトル

また，Dual 日射計の日射強度は，次式から求められる[1]。

$$G_{dual} = \mathrm{K}_{short\_wave} \times E_{short\_wave} + \mathrm{K}_{long\_wave} \times E_{long\_wave} \quad (1)$$

ここで，G_{dual} は全天日射強度[kW/m²]，E_{short_wave}，E_{long_wave} は各センサの出力電圧[mV]，K_{short_wave}，K_{long_wave} は各センサの感度定数[kW/m²/mV]である。

3. 検証方法

3.1 理論出力電圧を用いた検証方法

Dual 日射計では，Si 日射計では感知することができない長波長域の日射変動を捉えることで，センサの分光感度特性による生じるスペクトル誤差を減少させる。そこで，式(2)に示すように，日射の分光放射強度と各センサの分光感度から各センサの理論出力電圧を推定することで，日射計自体の諸特性による影響を受けずに，Dual 日射計で生じるスペクトル誤差のみを Si 日射計と比較することで理論的に評価する[2]。

$$E_{theory} = \left(\sum_{\lambda 1}^{\lambda 2} I_{\lambda} \times K_{\lambda} \right) \times \mathrm{S} \times \mathrm{R} \quad (2)$$

ここで，E_{theory} は各センサの理論出力電圧[mV]，I_{λ} は分光放射強度[μW/cm²/nm]，K_{λ} は各センサの絶対分光感度[A/W]，S は各センサの受光面積[mm²]，R は検出抵抗値[Ω]，$\lambda 1$ は各センサの感度波長域における始点波長，$\lambda 2$ は各センサの感度波長域における終点波長とする。

3.2 実測出力電圧を用いた検証方法

複数のフォトダイオードを同一円筒内の日射計に搭載することは，拡散板の特性などを含めた総合的な光学特性が非常に複雑なため，現状では諸特性を満足させる Dual 日射計を作製することは困難である。そのため，市販の小型日射計(VM)に対して Si，GaAsP，及び InGaAs センサをそれぞれ個別に搭載し，太陽追尾装置を用いて追尾全天日射強度を計測したときの Dual 日射計の精度を実証検証する。

3.1 及び 3.2 では，任意の快晴日 1 日を検定日と定め，分光放射強度と各センサの出力電圧を用いて感度定数を決定する[1]。得られた感度定数を用いて，天候別の出力電圧を回帰式(1)に適用し，Dual 日射計の日射強度を求め，二次準器である精密日射計(MS-801：EKO)で計測された日射強度(精密日射強度)を基準値とし，その値と比較することより，Dual 日射計である Si+InGaAs と GaAsP+InGaAs の評価をそれぞれ行う。また，Dual 日射計の比較対象として，Si 日射計の日射強度に関しても，同様の算出方法を用いて求める。

4. 検証結果

4.1 理論出力電圧を用いた検証方法

快晴日 216 データ，曇天日 192 データの分光放射強度から各センサの理論出力電圧を式(2)より推定した。そして，2005/04/06 を検定日と定め，各センサの感度定数を決定し[1]，式(1)より各日射計の水平面全天日射強度を算出した。

基準値は精密日射強度を用い，式(3)より Si+InGaAs，GaAsP+InGaAs，及び Si 日射計における基準値からの誤差を算出した。評価指標である MBE，標準偏差，RMSE の結果を表 1 に示す。

$$Error = G_s - G \qquad (3)$$

ここで，G_s は各日射計の日射強度[kW/m²]，G は精密日射強度[kW/m²]とする。

表 1：各日射計における評価指標値

	天候	MBE [W/m²]	標準偏差 [W/m²]	RMSE [W/m²]
Si+InGaAs	快晴	2.0	4.0	4.0
	曇天	−1.0	7.0	7.0
GaAsP+InGaAs	快晴	−8.0	3.0	8.0
	曇天	−12.0	5.0	13.0
Si 日射計	快晴	−6.0	7.0	9.0
	曇天	16.0	9.0	18.0

Dual 日射計の Si+InGaAs と GaAsP+InGaAs で生じるスペクトル誤差は，Si 日射計と比較して，共に改善の傾向が見られる。特に，Si+InGaAs において，その傾向が顕著に表れており，RMSE では快晴時に 5 W/m²，曇天時に 11 W/m²，Si 日射計からの改善が見られる。

4.2 実測出力電圧を用いた検証方法

2007/01/08～2007/01/31 の期間で各センサから得られる実測出力電圧のデータ収集を行った。そして，2007/01/09 を検定日と定め，4.1 と同様の方法で各日射計の追尾全天日射強度を算出した。天候別の各日射計における RMSE を表 2，精密日射強度からの誤差の分布を図 2 にそれぞれ示す。

表2：各日射計におけるRMSE[W/m²]

	快晴	曇天	薄曇	変動	合計
Si+InGaAs	10.0	2.0	12.0	6.0	12.0
GaAsP+InGaAs	9.0	6.0	15.0	8.0	15.0
Si 日射計	11.0	2.0	17.0	6.0	15.0

データの収集が短期間にも関わらず，Dual 日射計の Si+InGaAs では，Si 日射計の RMSE と比較した場合，『快晴』で 1 W/m²，『薄曇』で 5 W/m² の改善が確認される。また，天候別に示した誤差分布からは，Dual 日射計の Si+InGaAs が GaAsP+InGaAs や Si 日射計と比較して，天候の影響による誤差分布のばらつきが最も小さく，且つ精密日射強度からの誤差が 0 付近で安定している。

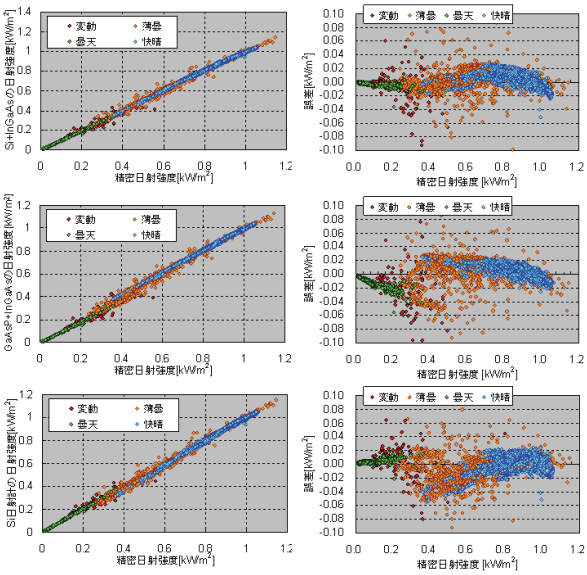

図 2：精密日射計との相関および各日射計の誤差分布

5. まとめ

安価で長期暴露にも安定した出力の得られる Si フォトダイオードなどの半導体素子を 2 種類用いることで，高精度な日射の計測を可能とする Dual 日射計を提案した。

理論検証では，各センサの理論出力電圧を推定することで，各日射計で生じるスペクトル誤差のみを評価した。その結果，Dual 日射計は，天候に関係なく Si 日射計よりもスペクトル誤差が減少することが確認された。また，実証検証では，追尾全天日射強度の精度を比較した。その結果，データの収集が短期間にも関わらず，天候別に示した誤差分布からは，Dual 日射計の Si+InGaAs が，天候の影響による誤差分布のばらつきが最も小さく，且つ誤差が 0 付近で安定することが明らかになった。さらに，両検証結果より，Dual 日射計の組み合わせに関しては Si+InGaAs が最適であることが示された。

参 考 文 献

[1] K.Hirata, Y.Miyake, T.Kato, K.Nakamura and K.Kurokawa: “Development of a Reliable, Long Life Pyranometer Compsed of Multiple photo sensors”, Proceeding of the 15th International Photovoltaic Science and Engineering Conference, pp.832-833, October 2005.

[2] 平田，黒川，三宅，加藤，中村：「二種類のフォトセンサを持つ新型日射計におけるスペクトル誤差の解析手法の開発」，電気学会 電力・エネルギー部門大会，琉球大学，沖縄，2006 年 9 月

空中写真を用いた都市地域における太陽光発電システムポテンシャルの推定

鈴木　真美（B4）

1 研究背景・目的

太陽光発電システムを設置する際，日射条件が良く，電力需要地に近接している戸建住宅は適した設置場所である。2005 年末における太陽光発電の国内全導入量 1422MW[1]の 8 割以上が，戸建住宅に設置されている。また，太陽光発電に関するロードマップ「PV2030」[2]では，2030 年までの国内導入目標量 102GW のうち，約半数にあたる 45GW を戸建住宅への導入と想定している。これに加えて地球温暖化問題への関心が高まっていることもあり，今後ますます太陽光発電は広まっていくと考えられる。

太陽光発電を含む分散型電源の普及に伴い，系統連系などの問題が起こるため，地域ごとに電力需給バランスを最適化していくことが望まれる。そこで，太陽光発電システムの普及を促進し，地域的なエネルギー計画の指針となるべき太陽光発電システムの導入ポテンシャルを推定することが重要となっている。

2 研究内容

研究機関や地方自治体などによるこれまでの調査事例では，太陽光発電システムポテンシャルの推定に既存の統計データが用いられている。しかし，この方法は統計データの存在する市区町村や都道府県ごとの評価であるため，評価できる地域が限定されており，また設置場所の具体的な分布を把握することが出来ない。

そこで本研究では，地域における太陽光発電システムの導入ポテンシャルを効率的に推定するために，航空機から撮影された空中写真を用いている。具体的には，太陽光発電システムの設置対象として有望な住宅の屋根を空中写真より認識し，その面積に太陽電池モジュールの設置割合などを反映させ，導入ポテンシャルを推定する手法を開発する。

3 解析手法の検討

3.1 トレーニングデータの再考

従来の方法では，灰色や黒の屋根が未抽出となるケースが多くあった。そこで，地表面被覆分類のトレーニングデータに改良を加えた。従来，灰色・黒屋根は，道路として分類していたため，そのトレーニングデータは道路から切り出したものであった。今回は考えを逆転し，道路を灰色・黒屋根として分類，つまりトレーニングデータを灰色・黒屋根から切り出すことにより，未抽出の減少を試みた。

また，黒屋根と分類されるべき領域が，水域とされてしまうことが多くあったため，水域と分類された領域においても屋根の可能性のある領域として扱った。

3.2 地表面被覆分類の優先度設定

最尤法による地表面被覆分類の際，屋根である可能性の高い順に 3 段階に分類した。分類項目を以下に示す。

・カラー屋根領域：屋根である可能性が高い
・グレー領域：灰色・黒屋根の可能性がある
・グリーン領域　　：樹木や草地のような自然物

この手順の追加により，カラー屋根の未抽出や，自然物の誤抽出を減少させることが出来る。

3.3 地図情報の導入

道路の誤抽出を減少させるため，地図を用いて道路・水域を認識する手順を加えた。国土地理院発行の数値地図 2500 を使用し，道路中心線と水域の情報を持つ地図画像と解析空中写真画像を画素ごとに比較し，地図のポリゴンと領域分割された写真画像の領域が 400pixel 以上重複した部分を道路もしくは水域と判断し，屋根である可能性のある領域から除外した。この方法により，影によって分断された道路領域なども抽出することができる。

4. 解析手順

今回行なった解析の手順を図 1 に示す。流れとしては，トレーニングデータの取得，領域分割，最尤法による地表面被覆分類，地図情報の利用，の 4 段階で成り立っている。

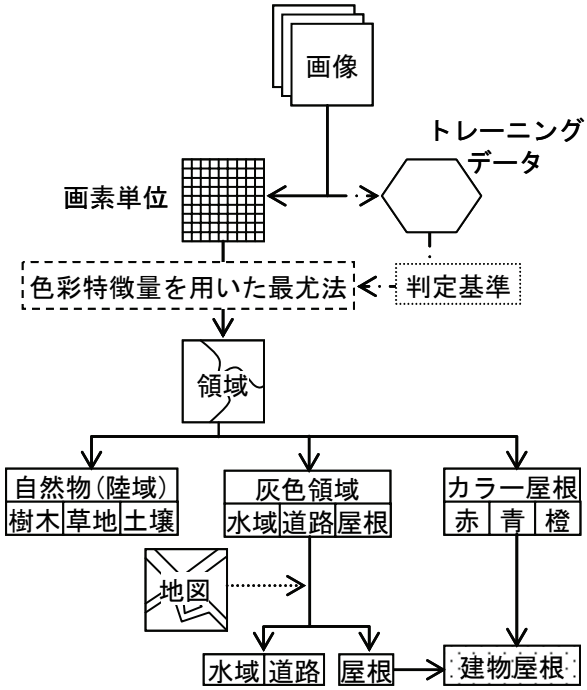

図 1. 解析手順

5. 解析結果

5.1 テストエリアにおける解析

小金井市から任意に住宅地を選び，5 箇所のテストエリアを設定した。テストエリアにおける解析の結果，領域が正しく分類されているかを示す的中率の平均が 82.9%，理想屋根面積と解析結果画像の面積を比較する面積率の平均が 101.5%となった。灰色・黒屋根領域の未抽出は減少したが，逆に道路領域の誤抽出が増加した。地図を用いた効果が存分に発揮できていないと考える。一方，分類項目ごとに優先度を与えたため，カラー屋根の未抽出は減少した。

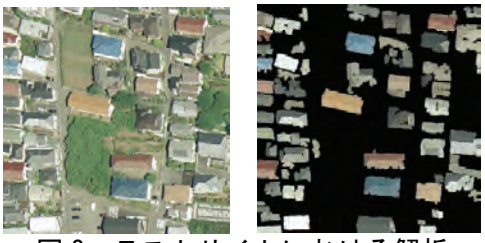

図 2. テストサイトにおける解析
（左：元画像，右：結果画像）

5.2 小金井市における解析

ケーススタディとして小金井市全域の解析を行った。抽出された全屋根面積 4057 万 pixel で，実際の面積に換算すると 2.54km² であった。小金井市全域が 11.33km² であるから市の 2 割強が住宅の屋根ということになる。

統計により得られる屋根の形状，方位，傾斜，日射量のパラメータを用いて，ポテンシャル評価を行った。このとき，設置可能面積は 1.72km² であり，導入可能量は 258MW であった。

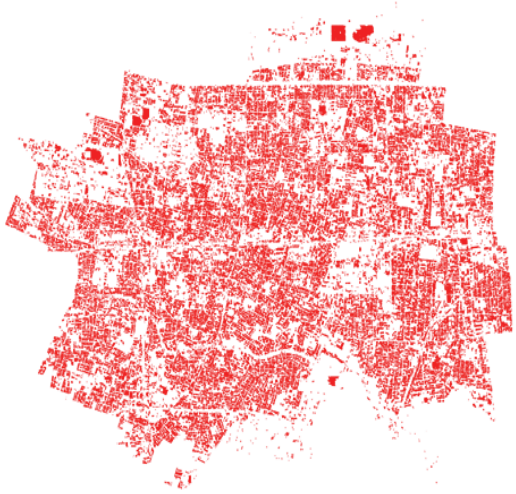

図 3. 小金井市解析結果

6. まとめ・今後の課題

今回，従来の解析法において主に灰色・黒色領域(屋根・道路・水域)に焦点を当て，新たな解析手順を検討した。それらにより灰色・黒の屋根を正しく分類できる画素は増加した。一方，道路の除外が未だに不完全であるので，地図情報の使用手法の改良が求められる。

また，太陽光発電システムの設置において，屋根の形状や方位，傾斜，高さも重要である。現在は，建築データにより条件を設定しているので，今後，空中写真画像から直接これらのパラメータを求める方法を検討する。

参考文献

[1]「Trends in photovoltaic applications. Survey report of selected IEA countries between 1992 and 2005」, IEA PVPS Task1, Report IEA – PVPS T1-15,2006
[2] NEDO 技術開発機構,「2030 年に向けた太陽光発電ロードマップ（PV2030）検討委員会 報告書」, 2004

モンゴルにおける太陽光発電システムに関する研究

アマルバヤル・アジヤバト（PD）

１． はじめに

乾燥・半乾燥地域の産業は第一次産業が主でその中でも草地を利用した牧畜が多い。逆に，世界の牧畜業は，全陸地面積の 25%にも及ぶ広大な土地を利用しており，そのほとんどは乾燥地である。発展途上国の乾燥地では，分散して移動を繰り返す，遊牧民文化が一般的であり，上記と同様に人口の増加進み，貧困層の拡大が深刻な問題となっている。地域格差と情報不足と過放牧，過剰な薪の採集に伴う砂漠化とその悪循環が広がっている。

遊牧民の生活水準と生産性の向上，更には，教育・社会福祉サービスの向上と情報共有のインフラ整備として電化が不可欠である。独立小型の太陽光発電システム（SHS）は，遊牧民のライフスタイルに適し，かつ地域資源の有効利用に繋がるため電化対策の有望な選択肢として期待されている。

２． 研究目的と方法

本研究では，乾燥地・半乾燥地における遊牧民世帯および村落などへ太陽光発電システムを導入していく場合の地域適合性を検証するためのモデルを構築し，ケーススタディとしてモンゴル地域における地域適合性を検証した。アプローチとして，まず技術面から，太陽エネルギー資源の詳細評価と太陽電池モジュールの暴露試験・性能評価，実フィールドにおける小型太陽光発電システムの損失の分離・評価を行っている。また，社会的側面から，太陽光発電システムの利用者に対する意識調査によって満足度，利用形態，ニーズ，問題点について分析を行い，普及・定着の方向性を明らかにした。分析結果から，太陽光発電システムの設計，施工，運行管理に必要な地域の特性を含むパラメータから設計の最適化を行っている。

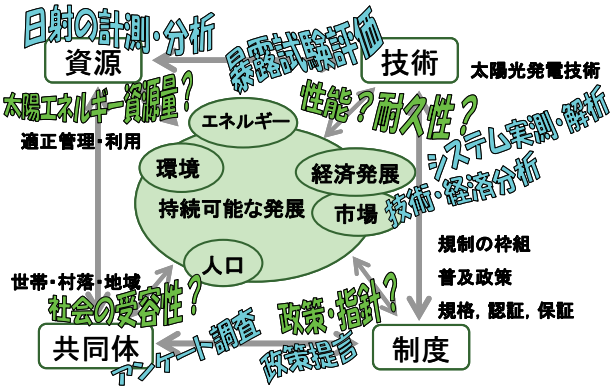

図 1. モンゴルにおける太陽光発電技術の適用

３．研究の成果

- **村落のエネルギーシステムと太陽光発電**

地域エネルギー資源の有効利用と環境負荷低減および安全保障の向上を評価するために村落のエネルギーフローのモデル化を構築した。エネルギーフローを熱エネルギーと電気エネルギーおよび輸送エネルギー需給に分けて積み上げ法によってモデル化した。

環境への影響を示す評価基準として，各種エネルギー機器の一次エネルギー消費と CO2 排出量で示す。エネルギー源の多様化によるエネルギー安全性の向上も検討した。また，現地調査によって，現状の村落エネルギーフローを定量的に把握した。また，対象地域の自然エネルギー資源の程度による最適システムの領域を算出した（図 2）。

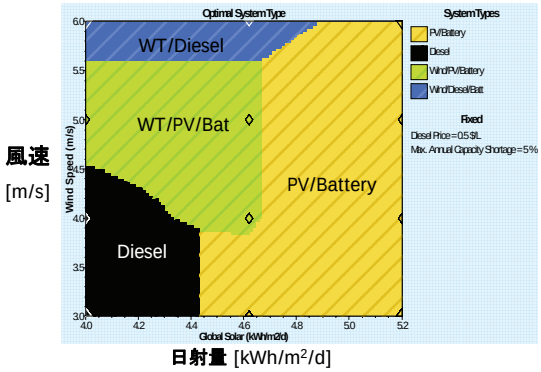

図 2. 地域の資源特性による最適システム領域

３． まとめ

本研究の成果として，乾燥地・半乾燥地における太陽光発電システムの地域適合性を検証するためのモデルを構築し，ケーススタディとしてモンゴル地域における地域適合性を検証した。
豊富な日射量と冷涼な大陸性気候を持つ乾燥・半乾燥地域では，温度係数の大きな結晶シリコン太陽電池が有効であることが示された。また，乾燥・半乾燥地域に多く見られる，牧畜業のため移動を繰り返すライフスタイルに独立小型の太陽光発電システムが適合していることが示された。

４． 参考文献

[1] Amarbayar Adiyabat, Kenji Otani, Kosuke Kurokawa, et al.（2006）Evaluation of Solar Energy Potential and PV module Performance in the Gobi Desert of Mongolia, Progress in Photovoltaics

[2] アジヤバト・アマルバヤル，黒川浩助（2005）モンゴルにおける独立小型太陽光発電システム実証研究のデータ解析･システム評価，太陽エネルギー，168 Vol.31 No.4, 2005, p83-88

太陽光発電の面的発電量推定技術に関する研究

大谷 謙仁（D3）

太陽光発電システムの国内導入量が 2001 年に累積で 45 万 kW を越え、日本は世界一の太陽光発電システム設置国となっている。この設備容量は、東京電力（株）福島第 1 号原子力発電所の出力（46 万 kW）に匹敵する。2010 年における政府の導入目標は 482 万 kW であり、これは現時点の 10 倍の規模である。2000 年における 8 月最大需要電力と比較すると、北海道電力の 457 万 kW や、北陸電力の 521 万 kW、四国電力の 535 万 kW と同程度である。また、導入件数で見ても、住宅への導入件数は 10 万件を越えており、2010 年には 100 万件を超えると考えられる。

このように大規模かつ多数の太陽光発電システムが 2010 年に実現することを想定すると、国家のエネルギー戦略の一環として、その総合的な発電出力（kW）及び発電量（kWh）の定量化を行うことが必要になってくると思われる。つまり、太陽光発電システムが大規模に導入されることによって生じる、既存発電設備の代替量（kW 価値）や燃料消費の節約量・CO2 排出削減量（kWh 価値）を日本全国または地域ブロックで包括的に把握する必要が発生すると思われる。もし、kW 価値の包括的な定量化が行えないままであれば、太陽光発電システムの大規模導入は電源計画の不確実性が増加するだけで、電気事業者にとって経済的利益を生まない可能性がある。この状態では、大規模な太陽光発電システムはエネルギー戦略上で単なるお荷物となり、「お日様任せの」あてにならない発電設備群としてしか取り扱うことが出来ない。このため、太陽光発電システムの大規模導入に対して政府及び電力事業者の理解を得られず、大規模導入が円滑に進まなくなることが予想されるため、全国包括的な kW 価値及び kWh 価値の評価手法を早期に開発する必要がある。

そこで本研究では、太陽光発電システムの全国大の発電出力（kW・kWh）を包括的にリアルタイムで把握するための計測技術を開発することを目的とする。このために、以下のような要素技術の開発を順次行っていく。

- 太陽光発電システムのモニタリングデータの活用
  - ✓ 住宅用太陽光発電システムの実測運転データ（約 150 件）から太陽光発電システムの運転特性を明らかにし、近傍の太陽光発電システムの発電出力を推定可能とする気象情報の抽出技術の開発
  - ✓ 太陽光発電システムの性能分布、信頼性に関する統計的情報の評価
- 面的発電量推定技術
  - ✓ 面的な発電量を 100 万件の計測計画ではなく少数のサンプリングで補完・計測する技術の開発
    - ✧ 気象庁配信データ（アメダス気象、メソ数値予報 GPV、気象衛星画像など）を用いた日射量のリアルタイム推定技術の開発
    - ✧ 太陽光発電出力のリアルタイム計測値から、日射量推定値を高精度化する補完推定技術の開発
    - ✧ 持続可能なモニタリングシステムの概念設計

参考文献

K.Otani et al., Field Experience with Large-scale Implementation of Domestic PV Systems and with Large PV Systems on Buildings in Japan, Prog. Photovolt: Res. Appl. 2004; 12:449-459

太陽光発電システムの単独運転試験方法に関する研究

五十嵐 広宣（D3）

１．はじめに

近年，急速に普及に設置が進む住宅用の太陽光発電システムは，発電電力と家庭内で使用する電力の差を余剰電力として，一般電気事業者の配電線へ連系し売電できる系統連系型システムが主流である。

本研究は，系統連系を行なう際に最も重要とされる単独運転現象の防止試験に用いられている回転機負荷について着目し，回転機負荷の特性について検討を行い，単独運転検出装置に与える影響について検証を行っている。

２．回転機負荷の特性

〈2･1〉回転機負荷の概要　単独運転検出装置の評価に用いている回転機負荷は，一般に市販されているグラインダーと言われる機器である。グラインダーの仕様を表 1 に示す。

表 1　回転機負荷の仕様
Table 1.　Spec of the motor load.

Electric ratings	Size of motor W[m] × H［m]	The size of the Flywheel D[m]W[kg]	Moment of inertia [kg･m2]
1Φ100V , 6.5A , 50/60Hz , Output power 645W	W:0452 H:0267	D:0.205×2 W:1.300×2	0.015

通常グラインダーは，誘導電動機のシャフトに研磨用の砥石を取り付け，回転している砥石部分に鉄等の切れ端部分を当て，研磨を行う機器である。グラインダーを単独運転検出装置の評価用負荷として使用する場合は，グライダーを空回転（無負荷）状態にて運転をする。回転している砥石は，砥石自身の重さと大きさによって運動エネルギーである慣性モーメントを持ち，誘導電動機への電力供給が無くなった後も慣性によって回転を継続する。砥石の慣性によって回転を継続する回転機負荷は，誘導電動機の状態から発電機へと変化し，単独運転検出装置へ影響を与えると考えられている。

〈2･2〉回転機負荷の発電について　回転機負荷は，主巻線と副巻線にコンデンサを直列接続した一般的なコンデンサ誘導電動機である。

発電状態の確認は，図 1 に示す回路図にて以下の手順に従い主巻線電流［Am］, 副巻線電流［As］, コモン電流［Ac］, 電圧［V_1］及び回転数［rpm］の計測を行った。

① 回転機負荷を定常運転状態（無負荷）で運転する。

② 並列抵抗負荷［R］を 10［Ω］に設定し，SW_r を投入する。

③ t=0 のタイミングで開閉器 SW_{mg} を開放する。

開閉器 SW_{mg} 開放前後の波形を測定する。

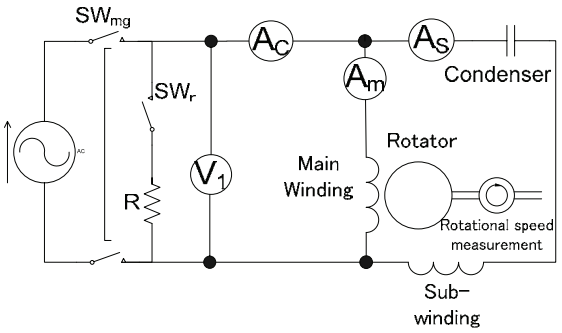

図 1　回転機負荷の回路図
fig. 1.　Circuit chart of motor load.

計測結果は，図 2 に示すとおりに SW_{mg} 解放後にコモン電流及び主巻線電流の流れる方向が反転し，回転機負荷から放出していることが確認できた。

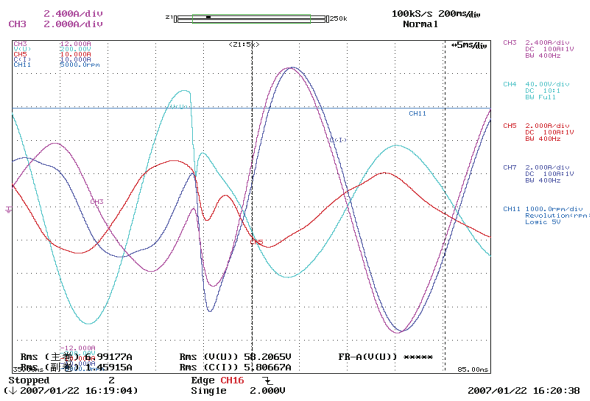

図 2　回転機負荷の発電状態計測結果
fig. 2.　Circuit chart of motor load.

主巻線電流[Am]及びコモン電流［Ac］の流れる向きが反転する現象は，回転機負荷が負荷として電力の供給を受けていたが，SW_{mg} 解放後に発電状態に変化することにより回転機負荷から外部へ電力を放出したことによると考えられる。しかし，計測結果の波形からでは，実際に誘導電動機が発電機状態に変化したか不明確である。そのため，回転機負荷が発電状態であることが明確に示されるすべり[S]を求めることにより，回転機負荷が発電状態であるかの確認を行うこととした。

〈2･3〉発電状態の解析　回転機負荷が発電状態となるには，回転数が同期速度を越えているかを確認することにより明確になると考えた。回転機負荷は，誘導電動機であることから通常すべりが 0～1 の範囲で運転されている。そのため，すべりが，0 よりも小さくなるのであれば回転機負荷が発電状態であると考えてよいことになる。

すべり[S]は，(1)式の同期速度と回転数から求められる。

$$S = \frac{(Ns - N)}{Ns} \quad \cdots\cdots(1)$$

S　：すべり　[S]
Ns　：同期速度　[rpm]
N　：回転数　[rpm]

しかし，SW_{mg} 開放後の同期速度は，電力の供給が無くなることから常に周波等が変化する。そのため，変化する周波数に合わせて同期速度も時々刻々と変化することになる。

通常同期速度は，(2) 式によって求めることが出来る。

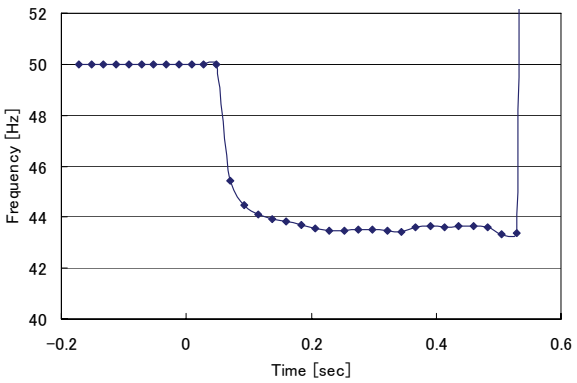

図 3　周波数の算出結果
fig. 3.　Calculation result of frequency.

$$Ns = \frac{120\ f}{p} \quad \cdots\cdots(2)$$

Ns　：同期速度　[rpm]
f　：周波数　[Hz]
P　：磁極の数

SW_{mg} 開放後の同期速度を求める方法は，通常運転時の同期速度から回転機負荷の磁極数を求められるので，変化する周波数が分かれば，同期速度が求められることになる。

周波数の算出方法は，電圧波形から電圧がゼロを通過するゼロクロス点を求め，一周期毎の時間から周波数を求めた。算出した周波数を図 3 に示す。

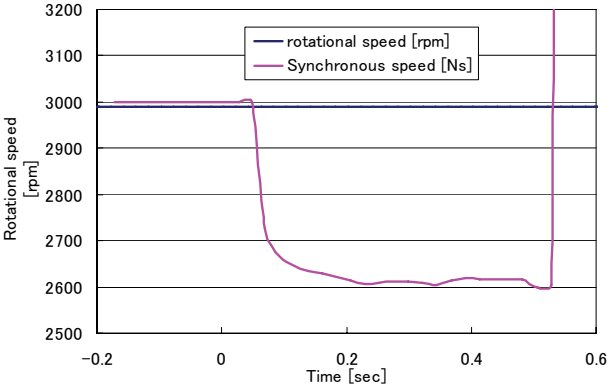

図 4　同期速度の計算結果
fig. 4.　Calculation result at synchronous speed.

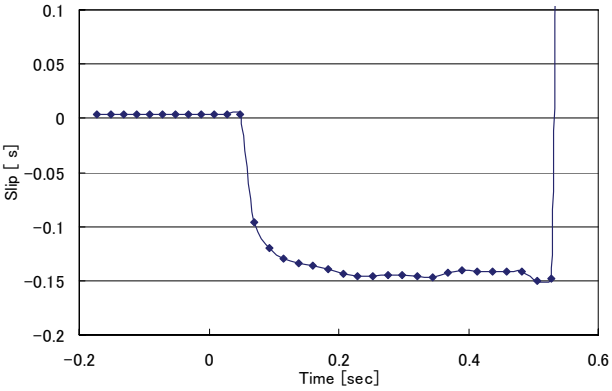

図 5　すべりの算出結果
fig. 5.　Calculation result at Slip.

同期速度は，電圧波形から算出した周波数を(2)式に代入し求めた。算出した同期速度は，図 4 に示すとおりの結果となった。また，求められた同期速度と計測した回転数を(1)式に代入しすべりを算出した。算出したすべりを図 5 に示す。

算出されたすべりは，SW_{mg} 開放後にマイナス($S<0$) になっていることが確認できた。すなわち，すべりが 0 より小さい結果となっていることから，回転機負荷は発電状態であることが確認できた。回転機負荷が発電状態になった要因として考えられるのは，慣性エネルギーを持つ砥石の影響を受け回転子の回転速度が低下しなかったことが考えられる。

3．まとめ

電力の供給を停止された後の回転機負荷は，慣性エネルギーを持つ砥石が回転子の回転数を維持させることにより，発電機へと状態を変化することが確認できた。

発電状態となる回転機負荷は，実際の単独運転防止装置へどのような影響を与えるのを検証するために今後は，実際のパワーコンディショナと組み合わせて単独運転実験を行う予定である。

新型太陽光発電モジュールのシステム特性検証研究

筒井　淳（D3）

１．はじめに

昨今の地球温暖化が原因と思われる異常気象は、世界の各地で徐々に現われ始めている。温暖化の原因とされる二酸化炭素の増加は年々増え続ける一方、世界の一次エネルギーに占める石油の割合は、約35%程度である。石油の消費は、大量の二酸化炭素を発生するため、抑制していかなければならない。このように、エネルギー、経済、環境を両立させるためにはクリーンでかつ無尽蔵な太陽光を使った太陽電池の普及が必要不可欠である。

２．目的

本研究の目的は、既に市販されている数種類の太陽電池モジュールを屋外に設置し、基本的な運転性能を定量的に明らかにすることである。ここでの基本的な性能とは、温度特性や照度特性、スペクトル依存性を指す。本年度は昨年度に引き続き、日射強度と太陽電池温度を入力パラメータとし、その入力パラメータから屋外稼動条件下での発電電力を推定する手法（以下 Energy Rating）に着目し、研究を進めた。現在 Energy Rating は、各国機関が新たな手法の開発や推定精度向上に取り組んでいるが、今回は AIST や津野らが提案[1]する直線補間法を用いて屋外性能を予測し、本実験サイトの実測結果との比較を行った。

３．計測設備の紹介

本実験サイトは、市販されている数種類の結晶系太陽電池と化合物系太陽電池、それと多接合型太陽電池の合計 7 種類を傾斜角 30 度、方位角 0 度で並べて計測を行っている。発電性能の計測はこれら太陽電池の I-V curve を専用の切替機によって 1 分間隔でほぼ同時に行っている。計測機は英弘精機製 I-V カーブトレーサー（MP160）を使用し、それ以外の計測機器として標準的な日射計・気温計の他、分光放射照度（350～1050nm）を 1 分間隔で測定可能な回折格子型分光放射計（MS-700）を設置した。なお日射計および分光放射計は太陽電池と同傾斜で設置した。またモジュール温度は、各々の太陽電池のバックシート裏面に取り付けた熱電対を専用の切替機により I-V 測定と同時に測定している。計測場所は、東京農工大学小金井校舎屋上（北緯 35.69 度、東経 139.52 度、海抜 58m）である。

設置したシステム構成機器の概観図を Fig.1 に示す。

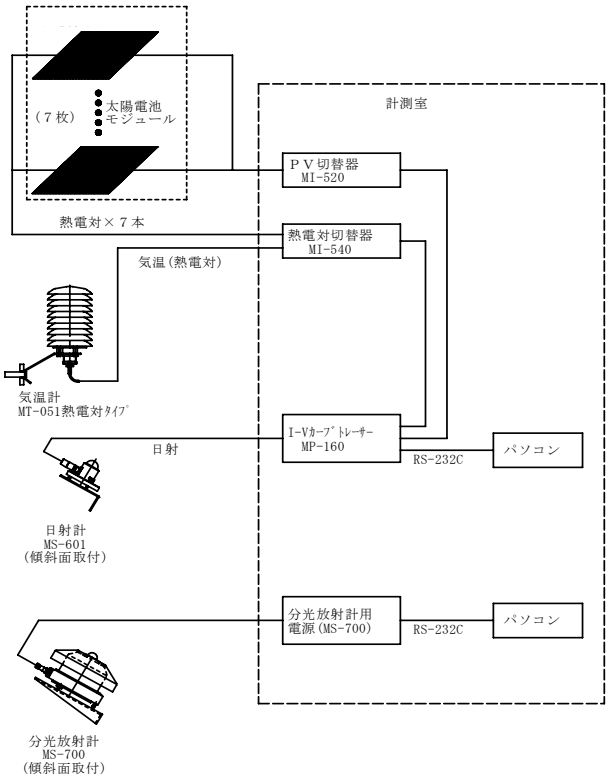

Fig.1 システム構成機器

４．直線補間法の紹介

本手法は、日射および温度条件の異なる 4 つの I-V curve を用いて任意の日射強度・動作温度における I-V curve を描き、そこから任意の発電出力を推定する手法である。本手法の特徴は、従来の任意出力を推定する際に必要であった直列抵抗や曲線因子を算出するような煩雑さがない点で、非常に簡素な手法である。以下に直線補間法の式を示すが、(1)式は温度補間を示すのに対し、 (2)式は照度補間を表す。また図 2,3 に各々の補間の様子を示す。

$$V_{T3}(I) = V_{T1}(I) + \frac{T_3 - T_1}{T_2 - T_1} \cdot \left(V_{T2}(I) - V_{T1}(I)\right) \qquad (1)$$

$$I_{E3}(V) = I_{E1}(V) + \frac{E_3 - E_1}{E_2 - E_1} \cdot \left(I_{E2}(V) - I_{E1}(V)\right) \qquad (2)$$

$V_T(I)$　：ある温度における V-I カーブ点
$I_E(V)$　：ある照度における I-V カーブ点
T_1　：低温度　　E_1：低日射
T_2　：高温度　　E_2：高日射
T_3,　：任意温度　E_3：任意日射

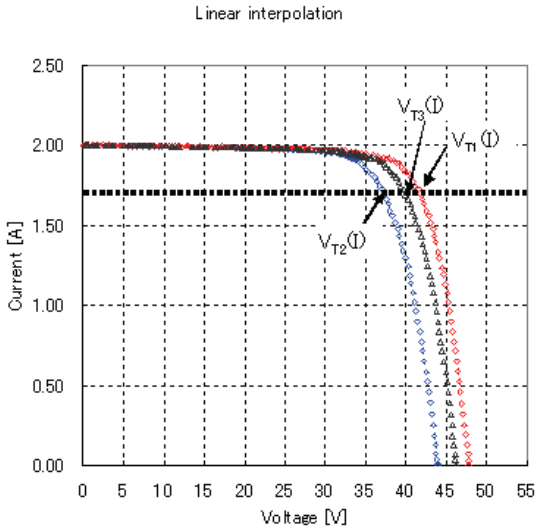

Fig.2 温度補間

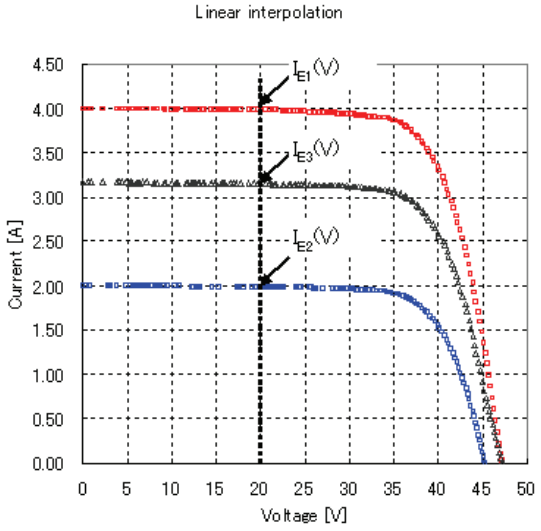

Fig.3 照度補間

本手法の入力パラメータは、任意の日射強度と動作温度であるが、今回の推定では日射強度の代わりに実測の短絡電流と、(3)式で推定した短絡電流の 2 種類を用いて任意出力を計算した。短絡電流を用いた場合の推定式は、(2)式から(4)式へと置き換えられる。

$$I_{sc-cal} = \frac{E}{E_0} \cdot I_{sc-STC} \cdot \{1 + \alpha(T - T_0)\} \qquad (3)$$

I_{sc-cal} ：推測短絡電流
I_{sc-STC} ：STC 時の短絡電流
E ：日射強度　E_0：1.0 [kW/m2]
T ：動作温度　T_0：25
α ：温度係数[%/　]

$$I_{E3}(V) = I_{E1}(V) + \frac{I_{sc3} - I_{sc1}}{I_{sc2} - I_{sc1}} \cdot (I_{E2}(V) - I_{E1}(V)) \qquad (4)$$

5．計測結果

はじめに、(3)式での推定値と実測値との誤差について述べる。図 4 の横軸は、絶対誤差（予測－実測）に STC 時の短絡電流で除算した結果、縦軸は頻度を表したヒストグラムである。推定に用いた太陽電池は単結晶 Si である。計算の結果、ヒストグラムの平均値が-0.02%、標準偏差 1.01%となった。これは、99%の確率で誤差が 3%以内に収まることを意味する。次にこの推定値と実測値を用いて(1)、(4)式の直線補間を行った結果が、図 5 である。図 5 の結果から、発電出力の推定誤差は図 4 で示した短絡電流の σ=1.01%が直接反映する形で推定精度を 0.5%から 1.1%へと落とす原因となる。

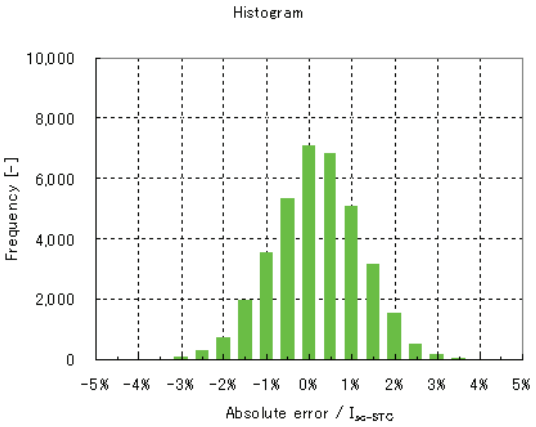

Fig.4 絶対誤差（I_{sc}）のヒストグラム

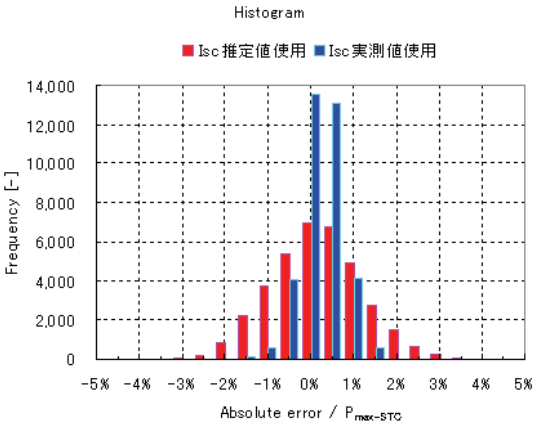

Absolute error (%)	Ave.	σ
推定値の場合	-0.06%	1.11%
実測値の場合	-0.01%	0.47%

Fig.5 絶対誤差（P_{max}）のヒストグラム

6．まとめ

直線補間法を用いた発電出力の予測は、短絡電流の推定値を用いても σ=1.1%の推定精度で推定可能であることが判った。

7．参考文献

[1]Y. Tsuno, “Temperature and Irradiance Dependence of the I-V Curves of various Kinds of Solar Cells”, PVSEC-15, 2005

パワーエレクトロニクスによる配電系統の電力品質安定化に関する研究

李 庚垂（D2）

１．はじめに

太陽光発電システム、特に住宅用太陽光発電システムが系統へ集中連系する場合、太陽光発電システムの逆潮流によって電圧上昇の問題が発生する。そこで、パワエレを用いた Distribution - Unified Power Flow Controller (D-UPFC)を提案する。D-UPFC は交流―交流コンバータと変圧器で構成される。本研究では、配電系統の電圧を安定的に運用するため、三つの D-UPFC topology を検討し、電圧上昇の制御のシミュレーションを行う。

２．研究内容

電圧上昇が発生する現在の配電系統と D-UPFC を設置する概念を図 1 に示す。集中連系 PV システムは一つの柱上変圧器に連系される。また、D-UPFC は柱上変圧器と集中連系型 PV システム内に設置されて動作する。

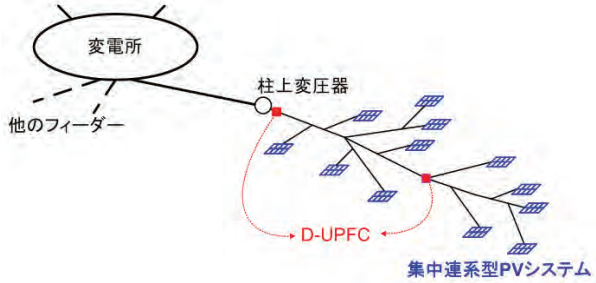

図 1. 配電系統の PV システムと D-UPFC

2. 1 D-UPFC の topology 分析

D-UPFC は配電系統の電圧安定化、特に PV システムが系統に連系されている場合での負荷側の電圧を安定化するために運用する。ここで、第一 topology は変圧器の二次側を二つに分けて一部分は系統の電圧を持ち、他方は交流―交流コンバータの電圧が入力される。

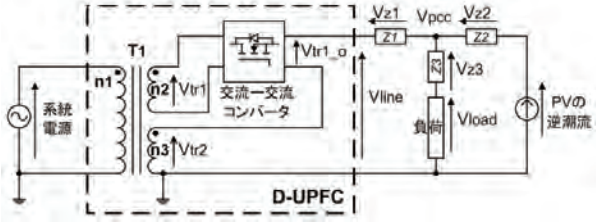

図 2. D-UPFC の第一 topology

PV の逆潮流により配電系統に変動が発生する場合、D-UPFC の出力電圧は交流―交流コンバータの出力を適正に制御することにより、系統電圧の制御を行う。

図 2 に第一の topology を示す。D-UPFC の出力電圧 V_{line} は、

$$V_{line} = \frac{(D \times n_2) + n_3}{n_1} \times V_s = V_{tr1\_o} + V_{tr2} = (V_{tr1} \times D) + V_{tr2}$$

ここで、D は duty ratio である。

第二 topology は D-UPFC の内にある変圧器の一次側の電圧の一部分を二次側に接続されている交流―交流コンバータの出力電圧に加える。図 3 に第二 topology の回路を示す。

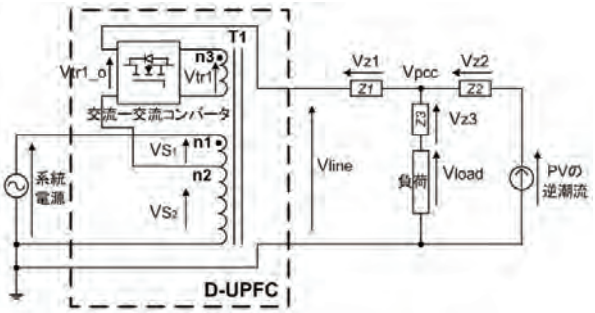

図 3. D-UPFC の第二 topology

D-UPFC の出力電圧は

$$V_{line} = V_{s2} + V_{tr1\_o} = (\frac{n_2}{n_1} \times V_s) + (V_{tr1} \times D)$$

第三 topology は UPFC の topology のように直列、並列変圧器を用いて D-UPFC を運用する。

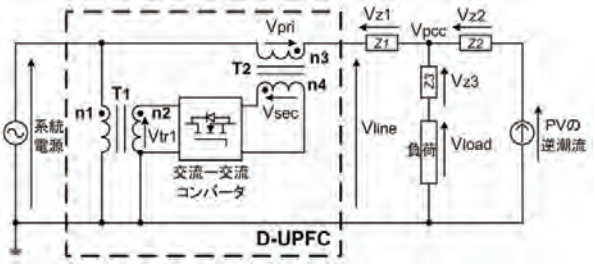

図 4. D-UPFC の第三 topology

D-UPFC の出力電圧は

$$V_{line} = V_s + V_{pri} = V_s + (V_{tr1} \times D) = V_s + (\frac{N_2}{N_1} \times V_s \times D)$$

また、図 2 の二次側の利用する電圧 Vtr_2 によって Vtr_1 の交流―交流コンバータが担当する容量が変わる。同じように図 3 では一次側の VS_2 によって Vtr_1 交流―交流コンバータの容量が変わる。図 4 の第三 topology の場合、並列変

圧器 T_1のタップ n_1によって交流ー交流コンバータの容量が決定される。

2. 2 変圧器のタップを用いた電圧制御

系統電圧に対して D-UPFC の出力電圧が一定及び制御範囲以内(正常状態)では D-UPFC が動作しない。しかし、電圧問題が起きると D-UPFC は図 5 と 6 に示す電圧制御を行う。

D-UPFC の第一、第二 topology が図 5 のように系統電圧の一部電圧を持ち、目標電圧まで交流―交流コンバータの電圧を一緒に含み制御を行う。

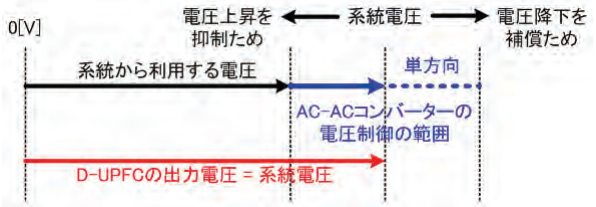

図 5. 系統電圧の一部と交流ー交流コンバータの電圧を含む電圧制御

これに対し、図 6 は系統電圧を全部使用して電圧制御では交流ー交流コンバータが電圧を上、下しながら動作する。D-UPFC の第三 topology では制御を行う。

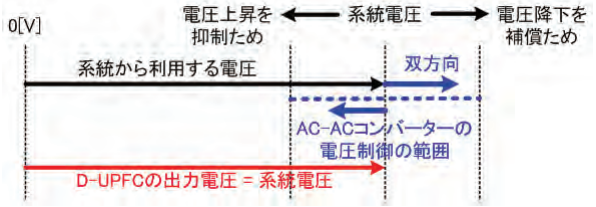

図 6. 系統電圧の全部と交流ー交流コンバータの電圧を含む電圧制御

図 6 で使用する D-UPFC の第三 topology は制御電圧を基準から双方向に制御するので交流ー交流コンバータで使用するスイッチ数が topology 1 と 2 に対し 2 倍になる。

2. 3 D-UPFC のシミュレーション

D-UPFC の電圧制御を検証するために配電系統モデルを想定した。

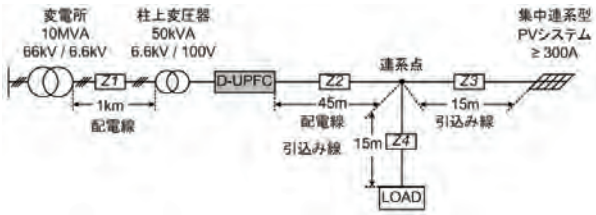

図 7. 集中連系型 PV システムのシミュレーションモデル

一つの柱上変圧器に 3[kW]の住宅用 PV システムが 10 件連系する。また、各住宅の負荷は 33.3[Ω]である。シミュレーションモデルを図 7 に、そのパラメータを表 1 に示す。

表 1. シミュレーションモデルのパラメータ

変電所の二次側電圧	6.6[kV,rms]
柱上変圧器の二次側電圧	100[V,rms]
配電線インピーダンス Z_1	0.025+j0.034[Ω/km]
配電線インピーダンス Z_2	0.011+j0.013[Ω/km]
引込み線インピーダンス Z_3 Z_4	0.00345+j0.00015[Ω/km]
負荷(10 件の住宅を想定)	3.33[Ω]
PV の逆潮流(最大)	300[A,rms]

電圧上昇(PV から逆潮流)のシミュレーションの結果を図 8 に示す。ここで、D-UPFC の電圧マージン(目標電圧より 2[V,rms]以内)を入れて電圧制御を行った。D-UPFC 制御の目標電圧は 101[V,rms]にして PV から逆潮流を 0[A,rms]から 100[A,rms]まで変化した。D-UPFC 後の線路電圧が 103[V,rms]の以上になる PV の出力電流が 70[A,rms]から D-UPFC の電圧制御が行った。70[A,rms] では制御前の配電線路の電圧が 104.3[V,rms]、制御後の電圧は 102.7[V,rms]となった。PV の出力電流が 100[A,rms] では 107.2[V,rms]、制御電圧は 103.7[V,rms]となった。

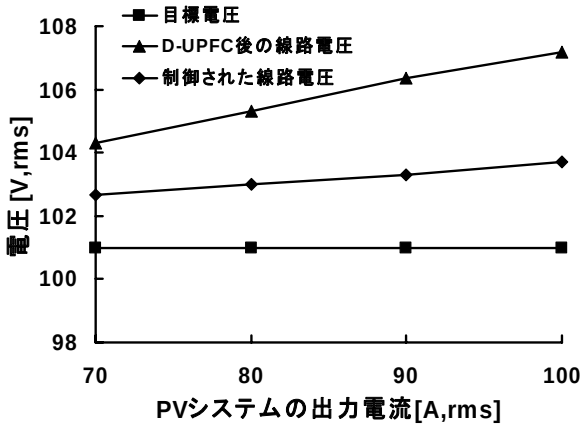

図 8. 電圧上昇のシミュレーション

3. まとめ

低圧配電系統で電圧上昇を制御する D-UPFC topology と手法を提案した。変圧器タップによって制御方法、D-UPFC の容量が変更することが分かった。配電系統の集中連系型 PV システムのモデルを用いて電圧上昇のシミュレーションを行った。今後は D-UPFC 内のタップによる D-UPFC の容量変化の分析、正確なシミュレーションモデルの確立、D-UPFC の実験を通して配電系統の最適な電圧制御について研究を行う予定である。

太陽光発電変動特性評価法の研究

川﨑　憲広（D2）

1. はじめに

わが国では，太陽光発電（PV）システムの導入目標量を 2010 年までに 4.82[GW]としている。また，PV2030（2030 年に向けた太陽光発電ロードマップ）[1]によれば，2030 年までの技術発展を想定したときの国内推定導入量は 102[GW]とされている。このように PV システムが急速に普及すれば，配電系統では局所集中的に連系（集中連系）するシステムが増加すると予想される。

一方，PV システムの発電電力は気象の変化に伴い不安定であり，集中的に系統連系する場合，電圧変動や周波数変動などの障害の要因になると懸念されているので，変動の対策が重要な課題になる。変動の対策は，系統側では負荷周波数制御（LFC），需要家側では電力貯蔵装置によって行うことができる。しかし，これらは既存の設備に付加するものなので，最適な容量を選定することが望ましい。そこで「ならし効果」[2]という現象を考慮する必要があると考えられる。これは，面的な広がりをもった PV システムで起こる出力変動の平滑化効果であるので，前述の設備の過剰な設置を避けることができる。

本研究では，ならし効果を考慮した PV システムの変動特性を定量的に評価する手法を開発し，ならし効果を評価することを目的としている。今回は，集中連系型太陽光発電システム実証試験地区で PV システム 553 軒の連系が完了したので，500 軒規模の変動特性の解析結果を報告する。

2. ならし効果

PV システムにおいて短時間で変動する要因は，ほとんどが移動する雲による日射の低下である。そのため，ならし効果のイメージは**図 1** のようになり，雲の移動による日射の低下は各地点で時間的なずれが生じるので，全体的な特性としては平均化される。これがならし効果の原理である。

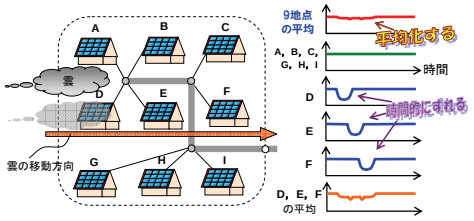

図 1. ならし効果のイメージ

3. 評価手法

これまでに開発した評価手法は，2 つの周波数解析法を用いて「1 日全体の周波数特性を周波数帯毎に把握する」方法と「1 日における周波数帯毎の最大の変動の大きさを抽出する」方法である。周波数解析法は前者がフーリエ変換，後者がウェーブレット変換によるものである。今回は，後者の評価手法を用いて評価した結果について述べている。

変動周期（周波数帯）毎の最大の変動幅（「最大変動幅」と定義）をウェーブレット変換で抽出する手法は**図 2** に示すように，変動周期の帯域毎に算出されるウェーブレット・パワースペクトルの最大値を用いる。その最大値が現れる時間を中心に各変動周期に対応した窓を対象とするデータ（ここでは日射強度）に適用し，その窓内の日射強度の最大値と最小値の差が最大変動幅となる。

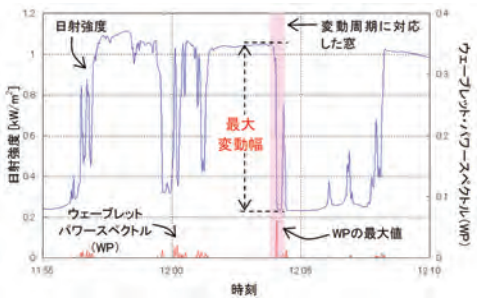

図 2. 最大変動幅の抽出方法（日射強度での例）

4. 評価対象データと解析パターン

前述のように現在，集中連系型 PV システム実証試験地区では PV システム 553 軒の連系が完了しており，順調に計測を継続している。そのため，500 軒規模の集中連系型 PV システムの変動特性の解析が可能となった。

今回，評価の対象としたデータは PV システムの発電電力で 1 秒値を用いた。また，本稿では**図 3** に示す日射強度の日に関する解析結果について議論する。解析には，変動解析に適切な計測データのみを用いているため，この日は 553 軒中 495 軒のデータを採用した。この 495 軒の PV システムの配置は**図 4** に示すとおりである。また，ならし効果を解析するためには，PV システムを増加させるパターンが重要になるが，今回は実証試験地区の中心の PV システムから同心円状に増加させるパターンで行った。

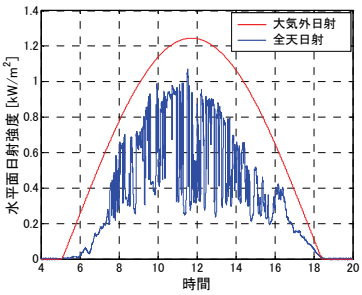

図 3. 解析に用いた日（2006/8/18）の日射強度

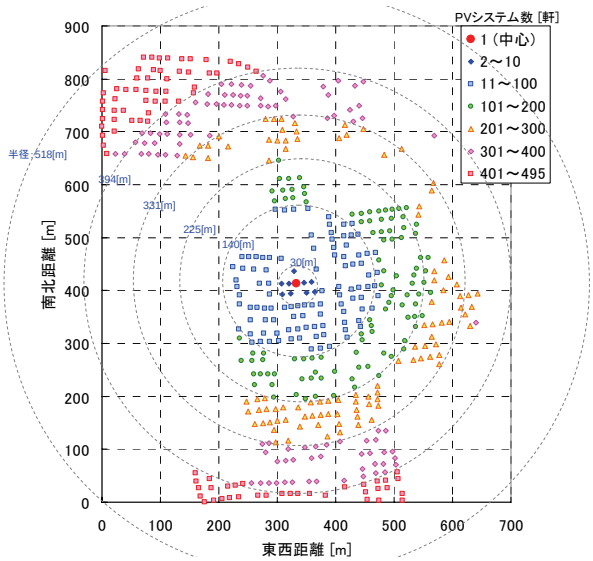

図 4. 実証試験地区における PV システムの配置図
（2006/8/18 における解析に有効なシステムのみ）

5. 集中連系型 PV システムの変動特性

ならし効果によりどの程度の変動を低減できたかを評価するには，ならし効果を考慮した結果とそうでない結果が必要である。そこで，ならし効果の考慮の有無を以下のように定義した。

・ならし効果無
　1 軒毎に最大変動幅を算出しておき，解析パターンに基づき，最大変動幅を加算していく。これにより各システムの変動の最悪ケースが考慮される。

・ならし効果有
　解析パターンに基づき，解析対象データを加算していき，加算したデータに対して最大変動幅を算出する。これにより時間的なずれ等が考慮される。

今回設定した条件で解析した結果を**図 5** 以降に示した。**図 5** は 1 軒毎の最大変動幅を加算していったので，ならし効果がない状況を意味している。それに対し，**図 6** はシステム間の解析対象データ（PV 発電電力）の時間的なずれが考慮されており，短周期変動成分で最大変動幅が大きく低減されていることがわかる。**図 7** は，ならし効果無とならし効果有の差分の最大変動幅であり，ならし効果によって最大変動幅がどの程度低減できたかを示している。これによれば，変動周期がおよそ 100 秒までの短周期成分において 400[kW]以上の最大変動幅の低減が確認できる。

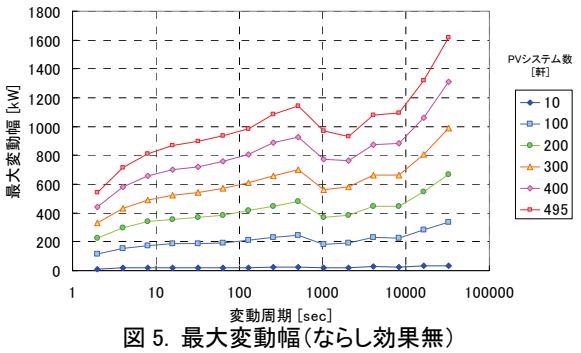

図 5. 最大変動幅（ならし効果無）

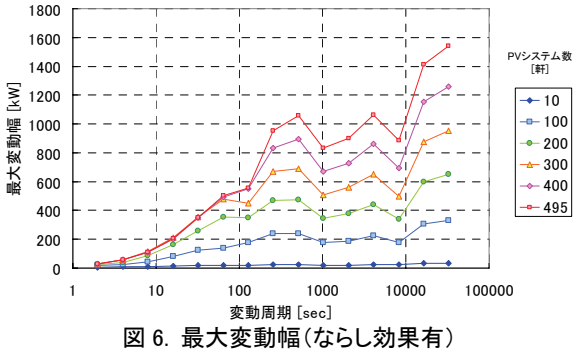

図 6. 最大変動幅（ならし効果有）

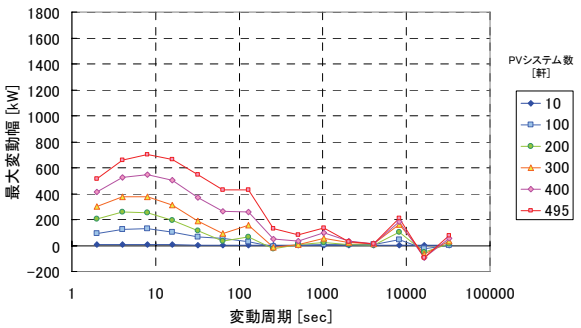

図 7. 最大変動幅の低減

また，**図 8～10** は**図 5～7** を設備容量で割った結果となっている。**図 8** はならし効果無のときの最大変動幅であり，この結果から各システムの平均的な変動特性が読みとれ，変動周期 2 秒のときの最大変動幅は設備容量の 30%である。それに対し，ならし効果有のときの**図 9** は PV システムの導入規模が大きくなると最大変動幅が低減する傾向が確認できる。変動周期約 10 以下は 100 軒程度でもならし効果があるが，100 秒程度になると規模の大きさの影響が強くなることがわかる。また，**図 10** からも同様のことがいえる。

6. まとめ

500 軒規模の集中連系型 PV システムの変動特性の評価を行った。ならし効果の有無からその効果を定量的に示すことができた。

謝辞

本研究は，NEDO 技術開発機構の委託研究「集中連系型太陽光発電システムの実証研究」の一環として実施している。関係者各位に感謝する。

参考文献

[1] NEDO 技術開発機構；「2030 年に向けた太陽光発電ロードマップ（PV2030）検討委員会　報告書」，2004
[2] 箕輪・大谷・津田・作田・黒川：「地域面平均日射の推定による太陽光発電システムの kW 価値分析」，太陽／風力エネルギー講演論文集 1998，p.17-20 (1998)

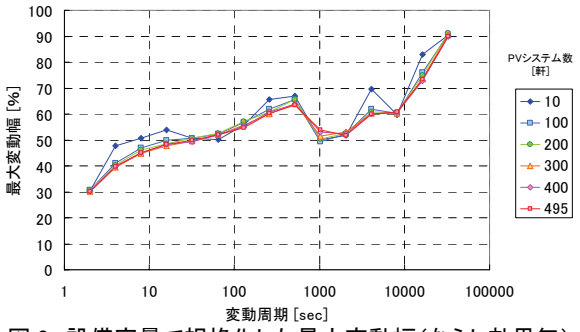

図 8. 設備容量で規格化した最大変動幅（ならし効果無）

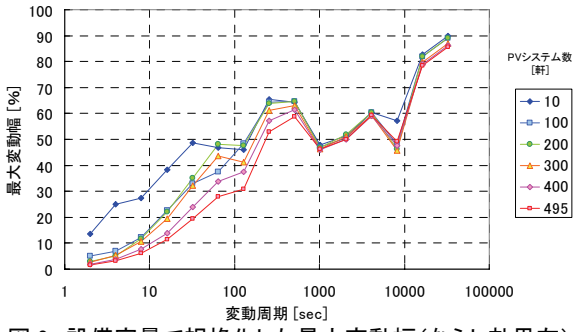

図 9. 設備容量で規格化した最大変動幅（ならし効果有）

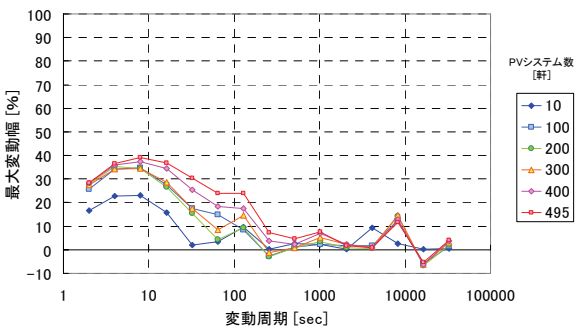

図 10. 設備容量で規格化した最大変動幅の低減

蓄電池あり系統連系太陽光発電システム
～天気予報を用いた日射予測の当日補正について～

嶋田　尊衛（D1）

１．はじめに

近年，急速に普及が進む住宅用の太陽光発電システムは大部分が系統連系型であり，発電電力と使用電力の差を電力系統と融通し処理している。今後，太陽光発電システムが持続的に発展していくために，電力系統への依存度を低下させた「自律度向上型」システムの登場が期待されている。

この研究では，従来のシステムに蓄電池を導入した，例えば図１に示すシステム構成において，予測を用いた適切な電池運用方法を開発することで，設置者のメリットを確保しつつシステムの自律度を向上し，将来の太陽光発電システムの理想的な姿を追求することを目的としている。

これまでに，３時間ごとの天気予報を用いて，翌日の日射量を１時間値で予測する手法を開発した[1]。今回，前述の手法によって前日に予測された日射を，当日の日射状況により逐次補正する当日補正手法を開発したので報告する。

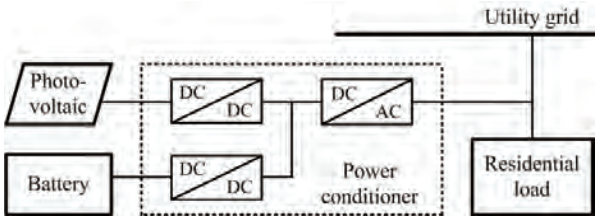

図１　PV システム構成例

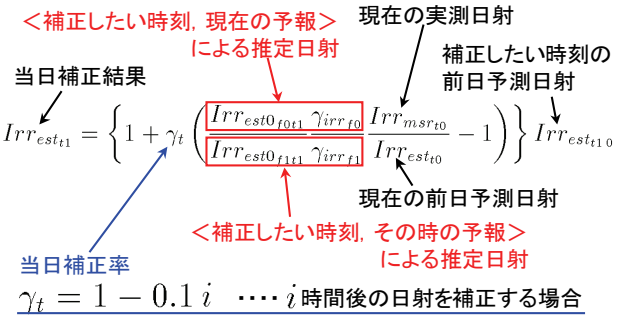

図２　当日補正手法

２．当日補正手法

前日に予測した日射は，１日を通して同じ方向（正負）に誤差が出ることが多い。この現象に着目して開発した当日補正の手法を図２に示す。ここで，予報とは日射予測に用いた天気予報を意味する。基本的には，前日に予測された日射を実測日射と比較して補正するが，このとき補正したい時刻の予報と現在の予報との違いを考慮している。当日補正率 γ_t は，近い将来ほど補正効果が大きくなるように補正力を調整する 0～1 の係数である。

なお，実際のシステムで実測日射が得られない場合には，PV 出力で代用できる可能性がある。

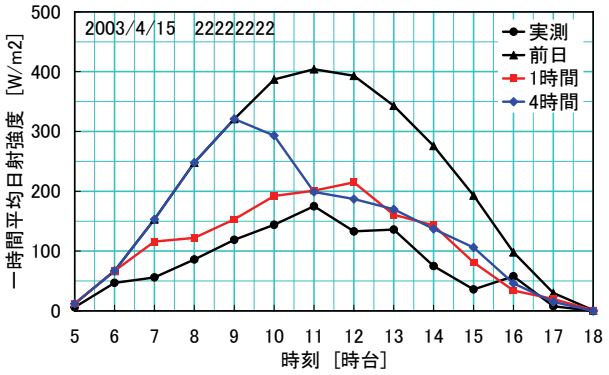

図３　当日補正結果の一例

３．補正結果

図３は，2003 年 4 月 15 日に，１時間ごとに当日補正した結果である。この日の天気予報は，１日を通して曇が出されており，予報からの日射予測が難しい典型例である。図中，１時間，４時間とは，それぞれ１時間後，４時間後を毎時，当日補正した結果である。当日補正により前日に予測された日射が修正されており，効果が確認できる。

４．まとめ

前日に予測された日射を当日に補正する手法を開発し，その効果を確認した。

今後は，この手法を有効に活用した自律度向上型 PV システムを検討する。

参考文献

[1] T. Shimada, K. Kurokawa, “Grid-connected Photo-voltaic Systems with Battery Storages Control based on Insolation Forecasting Using Weather Forecast”, *Renewable Energy 2006*, Chiba JAPAN, 2006, O-Pv-6-1

太陽電池の性能評価に関する研究

津野　裕紀（D1）

1. はじめに

自動車の燃費はどのような条件で測定されているかご存知だろうか？一般的な燃費の測定は,10・15 モードと呼ばれる,減速や加速など,ある程度現実的な走行を模擬した条件を用いている。これがもし,60km/h の定地燃費を使用していたら,低速走行時に威力を発揮するハイブリッド車の性能は数値に表れないであろう。

太陽電池にとっての燃費は出力(効率)である。出力測定は,国際的に定められた,一定の条件下(標準試験条件)で測定される。太陽電池の種類が結晶 Si 系のみであったときは,この出力の大小は屋外条件での出力の大小とほぼ同じであり,発電電力量を比較する上で問題は生じなかった。しかし,近年様々な種類や構造を有する太陽電池が開発され,市場に出回りつつある。これら新型太陽電池は,結晶 Si 系太陽電池とは特性が異なるため,標準試験条件下での出力の大小と,屋外条件での出力の大小が異なるという実験結果が数多く報告されている。このことから,現状の標準試験条件下での出力の他に,自動車の 10・15 モードのような,実条件を考慮した新たな性能指標を望む声が高まっている。

しかしながら,太陽電池の屋外条件における出力を再現することは非常に難しい。自動車の場合,走行条件はドライバーが決定できるが,太陽電池の場合,条件は,自然が決めるものであり再現することは不可能である。そこで数点の測定値を用いて,任意の条件に補正を行うのだが,この方法は各研究機関で種々提案されており手法は様々である。また,公平な値付けのためには,屋外条件を定めなくてはならない。自動車の場合もそうだが,測定条件によっては市場の妨げになり,余計な混乱を与える可能性があるため,慎重に決定しなければならない。これらの問題は,現在,国際電機標準化会議(IEC)TC82WG2 において議論されている。

本研究では,太陽電池の屋外条件における出力を評価するための様々な問題に対し,解決手法の提案を行い,国際的に認められる評価手法を確立させることを目指している。

2. Energy Rating モデルの提案

標準試験条件での出力評価の単位は,発電電力[W]で,その値付けを Power Rating と呼ぶのに対し,屋外特性を考慮した出力評価の単位は,発電電力量[Wh]で,値付けを Energy Rating と呼ぶ。この研究は,1980 年代後半から欧米で始まり,現在では,太陽光発電システムではなく,太陽電池モジュールに対し評価が行われている。日本で太陽電池モジュールの Energy Rating に関する研究は,約 20 年遅れ,近年に NEDO プロジェクトとして開始されている。

本提案手法は, I-V 特性の補正に必要な測定点が 3 点から 4 点のみで,他の機関が提案する手法に比べ非常に少なく容易なことが特徴である。また,I-V 特性を算出することができるため,電力だけでなく電圧,電流も把握することができる。

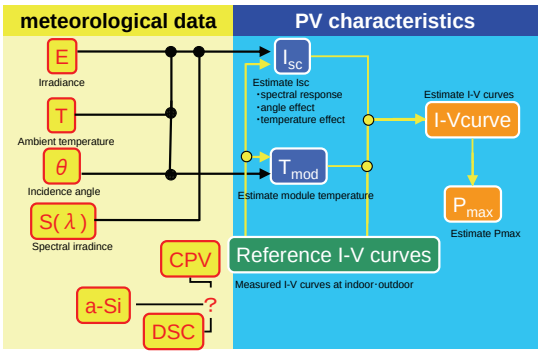

図 1　Energy Rating モデル

3. I-V 特性の直線補間/補外法

I-V 特性の直線補間/補外法：**Linear Interpolation / Extrapolation of I-V curves** (LINEX-IV)法は,Reference として測定した数点の I-V 特性から,様々な条件での I-V 特性に補正することが可能である。この手法は,多接合太陽電池に関する JIS 規格の素案に採用され,IEC などにも提案されている。我々は結晶 Si 系をはじめ,CIS や HIT など,様々な太陽電池に適用可能であることを証明した。

現在 2 種類の手法を提案している。ひとつは 4 つの I-V 特性を使用し,電流値に制限がある手法(Ver.1)。他方は 3 つもしくは 4 つの I-V 特性を使用し,制限はほとんどない手法(Ver.2)である。補正に用いるパラメータは,モジュール温度と I_{sc}(もしくは日射)である。ただし,日射をパラメータとした場合,スペクトルミスマッチなどにより多少精度が悪くなる。従って,日射やその他の条件から I_{sc} を推測する手法の開発が非常に重要である。

この手法は補外に対しても十分な精度を発揮する。しかしながら,温度の測定精度に気をつけねばならない。補外誤差の解析の結果,温度測定の精度が±1℃程度であれば,2 倍の補外まで 2%以内の精度で求めることができる。温度幅の異なる 2 種類の Reference I-V 特性(図 2)を用いて算出し,実

測値と比較したところ,表1のように標準偏差で約±0.8%であった。従って,ある程度の温度幅を確保することができれば,補間も補外も精度良く算出することが可能である。

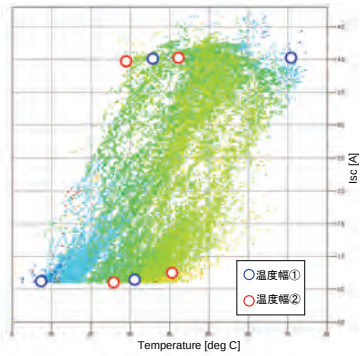

図2　2種類の Reference I-V の条件
(①は温度の外挿点が少なく,②は多い)

表1　Reference I-V の温度幅の違いと算出精度

	温度幅①	温度幅②
誤差の標準偏差[%]	0.57	0.82
誤差の平均値[%]	-0.18	-0.30

4. Energy Rating に必要な要因

Energy Rating の精度を向上させるには数多くの要因を考慮しなければならない。発電電力の精度はもちろん重要であるが,最終的には発電電力量が必要であるため,ある程度精度を犠牲にしても,容易に発電電力量を求める必要性も出てきている。そこで,LINEX-IV 法を用いて,屋外特性の各種要因が年間発電電力量に与える影響を解析した。単結晶太陽電池とヘテロ接合太陽電池の解析の結果を図3に示す。解析には2004年9月から,2005年8月までの一年間のデータ(一分値)を使用し,各要因が発電量に与える影響示した。負の場合は損失,正の場合は利得を示す。(注;データはある程度のフィルタリングを行っているため，正確な値ではない。)

推測電力量と測定値は 0.1%の誤差で,非常に精度が良い。両者を比較すると,PR はヘテロ接合の方が良い。周知の様に,温度特性が最も影響を与えているのだが,最大電力(あるいは効率)の照度依存性も無視できない。今回のサンプルでは,温度一定状態において,ヘテロ接合太陽電池は,1SUN よりも約0.7SUNで効率が最大となり,約0.5SUNまで効率が低下しないのに対し,単結晶太陽電池では,1SUN で最大となり,照度の減少とともに効率も低下することがわかっている。LINEX-IV 法は,このような解析も可能で,他のモデルではこの現象の把握が難しく,測定点が多数必要となるが,LINEX-IV 法は,3から4点の測定で充分である。I_{sc}と照度のミスマッチは分光放射照度や角度特性などが含まれるが,図 3 から,その影響はほとんど無視できることがわかる。しかしながら感度波長の異なる他の太陽電池にとっては無視できない要因であろう。

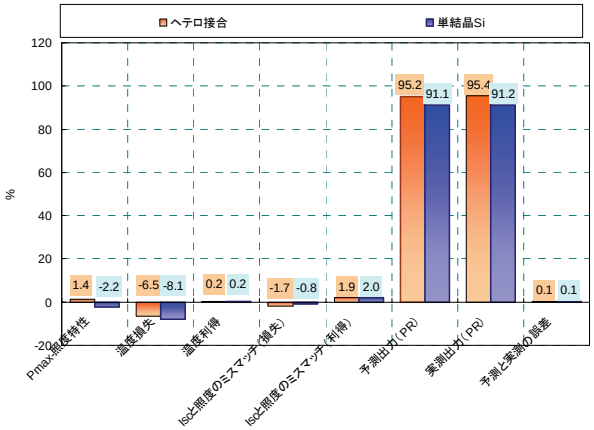

図3　各種要因が年間発電電力量に与える影響

5. その他の研究事項

本手法の適用範囲は,a-Si を除く単接合太陽電池に限られる。なぜならば,a-Si は温度の影響により特性が変化するためである。分光放射照度により特性(特に FF)が変化する多接合太陽電池も同様である。現在,多接合太陽電池の特性を調査しており,LINEX-IV 法の適用を模索している最中である。

また,要求精度によってはスペクトルミスマッチを考慮する必要がある。欧米では,基準セルとカラーフィルタなどを用いて分光感度を近似させ,これを日射計の代わりに用いる例が報告されている。これは,高価なスペクトルラジオメータを購入する必要が無く Energy Rating に有効である。日本ではほとんど使われた例が無い。

さらに,Energy Rating に用いる Reference I-V 特性を容易に,かつ2-3時間で測定する手法も開発中である。もちろん精度が要求される場合や効率的な評価を行うには屋内測定が最適でありこちらの開発も進行中である。

また,スペクトルミスマッチを解析する上で重要なモジュールの分光感度測定手法に関しても研究を進めている。

6. おわりに

Energy Rating の重要性と進捗状況を述べた。今後は,各種太陽電池における Energy Rating の精度を実証する予定である。ただ,太陽光発電システムはモジュールだけで構成されるものではない事を忘れてはならない。モジュールの Energy Rating は,例えると自動車としてではなく,エンジン単体の Rating といったところか?

PV インバータ系統機能超縮小模擬配電系統試験装置の開発

中村 祐介（M2）

1. まえがき

近年、一般家庭を中心に系統連系される太陽光発電(以下，PV)システムが急速に普及しており，将来的には一本の配電線に PV システムが多数台連系される可能性がある。PV システムを電力系統に接続する場合，設置前に単独運転防止機能や電力系統保護機能などの安全機能を試験する必要がある。直接的な試験としては実規模の独立した模擬配電系統を用いればよいが、これは大規模な設備になるため大学や研究機関の実験室に設置することは不可能である。このため当研究室では配電系統をインピーダンス変換によって縮小した等価回路を，受動素子で置き換えたシミュレータを開発した。このシミュレータは実験室に設置できるサイズではあるが，設置面積が大きく、コストも高額である。また多数台連系試験に適応するために試験装置を拡張させると設置面積が数十 m^2 程度にもなり、拡張することは容易でない。そこで当研究室では，シミュレータを電子回路で構成することにより，大きさやコスト，拡張性にメリットがある新しい配電系統シミュレータの開発を行ってきた。

本稿では超縮小模擬配電系統シミュレータのモデルを提案し、試作を行ったので報告する。

2. 超縮小模擬配電系統シミュレータ

<2･1> 構成 シミュレータの構成を図 1 に示す。提案したシミュレータは電子回路で作成された電子化縮小模擬配電系統シミュレータと能動式電力変換装置（Active Power Inter face :API）から構成され，API の片端に実規模の PV インバータが接続される構成とする。電子化縮小模擬配電系統は配電系統をインピーダンス変換によって縮小して等価回路に置き換え，RLC 素子によって配電系統を模擬する。

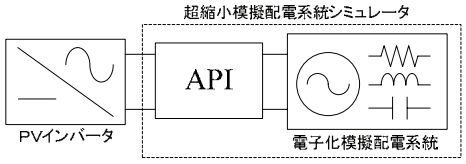

図 1 超縮小模擬配電系統シミュレータの基本構成

<2･2> モデル 図 2 に想定した配電系統のモデルを示す。日本の平均的な配電線の線路定数等のデータを使用し、主に低圧系統を中心にモデル化している。

モデルは，個々の低圧需要家に焦点を当て，低圧系統の一部を詳細に模擬したモデル（モデル A）と，マクロな視点で複数の柱上変圧器，低圧負荷，PV システムを集合体とみなし，配電線全体の挙動を検証するモデル（モデル B）の 2 モデルを作成した。

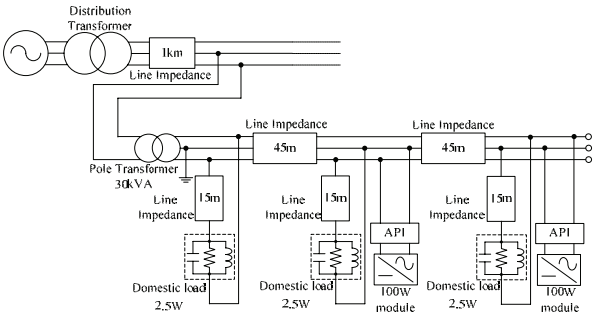

図 2 超縮小模擬配電系統シミュレータのモデル図

<2･3> 能動式電力変換装置 API API のブロック図を図 3 に示す。API は，電力レベルの異なる機器の等価的な接続を可能にするインターフェースである。API はインバータ側(端子 1)の電圧，電流を忠実に 1/*M*，1/*N* 倍させた電流，電圧を系統側(端子 2)の電圧，電流とし，これと同時にインバータ側の電圧，電流を忠実に *M*，*N* 倍した電流，電圧を系統側の電圧，電流とする。

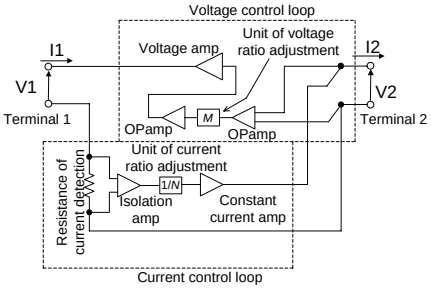

図3 APIのブロック図

API の拡大/縮小の精度検証の結果，電圧，電流比ともに設定した比率通りに拡大/縮小できていることが確認された。また周波数特性評価の結果，電圧は 20kHz までの変化を伝達できていることが確認され，電流は 410Hz までの変化を伝達できていることが確認された。

3. シミュレータの作成

<3･1>　シミュレータの作成　超縮小模擬配電系統シミュレータの作成を行った。シミュレータの主な仕様を表 1 に示し、設置状況を図 4 に示す。シミュレータ内の各模擬装置はそれぞれユニットとして構成されているため、自由に結線することができ、任意の試験回路を構成できる。特に低圧配電線，低圧負荷はインピーダンスを可変できるため，様々な形態の配電系統を模擬できる。

API は 2 ユニット試作し、最大 2 台の PV インバータの並列試験が可能である。ただし API の容量は 120W 程度であるため、実験で使用するインバータは海外製 AC モジュールインバータとする。

表 1.シミュレータの主な仕様

	実スケール	シミュレータ（モデル A）	シミュレータ（モデル B）
変圧器容量	30kVA	10VA	0.5VA
定格電圧	200V	10V	10V
配電用変圧器および高圧配電線	0.25+j0.34 Ω	考慮しない	0.03+j0.04 Ω
低圧配電線（45m）	0.25+j0.29 Ω	0.08+j0.10 Ω	0.34+j0.39 Ω
引込み線	2.3+j0.10 Ω	0.26+j0.01 Ω	考慮しない
最大低圧負荷	－	10 軒分	214 軒分

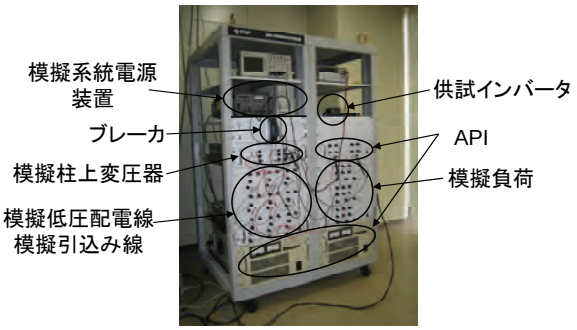

図 4. 超縮小模擬配電系統シミュレータの設置状況

<3･2>　シミュレータの性能評価　試作したシミュレータを周波数応答特性（ボード線図）の測定を行った。また測定回路の等価回路から，計算により理論値を求め，測定値と理論値を比較することによって 2.4kHz までの性能を評価した。測定値と実測値の誤差は，実際の系統に換算した値によって表示した。

低圧配電線に対する性能評価では，試験装置の低圧配電線 45mは，実際の系統では 50.3m程度に見えていることが確認された。住宅地区の架線状況や電線のたるみを考慮すると，許容できる誤差であるといえる。

低圧負荷に対する性能評価では，負荷の設定を 2 章で示したモデル 2 に対応させて任意に 30kW，18.4kVar に設定した。これは低圧需要家約 43 軒分に相当する負荷である。性能評価の結果，実際の系統ではそれぞれ 30.12kW，18.96kVar の負荷として見えていることが確認された。この誤差は負荷の変動としても十分に考えられる範囲であるといえる。また負荷の設定を変えた場合においても，同等程度の誤差であった。

次に模擬装置を結線して，実験回路を構成した場合の評価を行った。測定した回路は，実際の配電系統で想定される範囲内におけるインピーダンス値，組み合わせを任意に決定した。図 6 に実験回路を構成した場合の一例，図 7 にその測定結果を示す。この測定回路は配電用変圧器から 1km 離れた位置に柱上変圧器が連系し，低圧需要家が配電系統の末端（柱上変圧器から 90m離れた位置）に集中して連系している状態を模擬した回路である。この実験回路において実測値と理論値の誤差はほぼ，個々の模擬装置が持つ誤差を合計した値であり，個々の模擬装置を結線して実験回路となった場合においても実際の配電系統を模擬できていることが確認された。

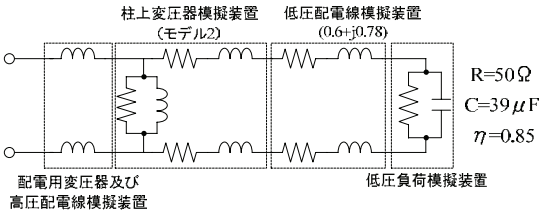

図 6 実験回路を構成した場合の一例

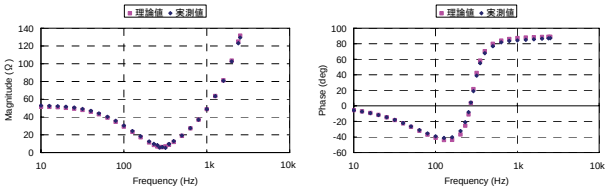

(a) 絶対値　　(b) 位相

図 7 実験回路（図 6）を構成した場合の周波数特性

4. まとめ

本研究により得られた成果についてまとめる。

① サイズ，コスト，拡張性にメリットのある新しい配電系統シミュレータを提案した。
② 低圧系統を中心とした配電系統のモデル化を行い，シミュレータの作成を行った。
③ 能動式電力変換装置 API の評価を行い，その特性を評価して有効性を示した。
④ シミュレータの評価を行い，2.4kHz までの周波数領域において，実際の配電系統を模擬できていることを確認した。

電力系統へのマトリックスコンバータの適用

鎌倉 輝男（M2）

1. はじめに

電力系統の調整余力を前提としている現在の太陽光発電（PV）システムは，連系される PV の総量が増加すれば系統への負担が増加し，導入量には限界があると考えられる。この問題に対し，地域での PV 導入 100%を目的とする自律度向上型太陽光発電システム（以下 AE-PVC：Autonomy-Enhanced PV Clusters）が提案されている。AE-PVC では需要家 PV による逆潮流はコミュニティとよばれる地域系統内で完結し，余剰電力はコミュニティ内での AC 蓄電ステーションに貯蔵される。これにより，コミュニティにおいて基本的に潮流を内部で完結し，外部系統にじょう乱を波及させない。AE-PVC 構成イメージを図 1 に示す。基本的にコミュニティでの需用電力は PV 及び AC 蓄電ステーションで賄われ，外部系統との電力の融通は極力少なくなるが，季節変動など緩やかな変動に対しては系統用ルータ機器と呼ばれるパワーエレクトロニクスを用いたアクティブ潮流制御機器を用いて外部系統との電力の融通を行う。このとき，基本的に自立する AE-PVC においては外部系統と同期をとる必要のない非同期連系が望ましい。また，図 2 に示すこのようなコミュニティが複数存在し，隣接した場合は外部系統接続の場合とは異なり，互いの電力状況に応じてその過不足分を補い合う。そのため，この場合のルータ機器は，AE-PVC 間の電力潮流をその方向を含めて急峻に制御することが求められる。また，ルータ機器両端での自端情報（有効，無効電力，周波数）での自律制御を行うことが考えられている。そのため，非同期に加え周波数の異なるコミュニティ間での潮流制御機能（異周波連系機能）も必要となる。

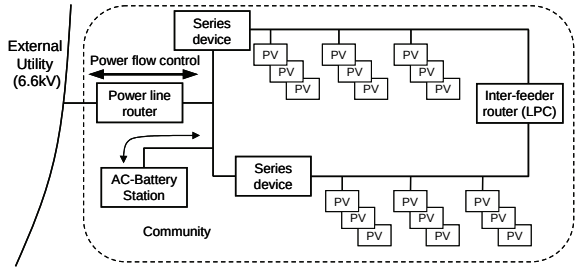

図 1. 自律度向上形太陽光発電システム（AE-PVC）

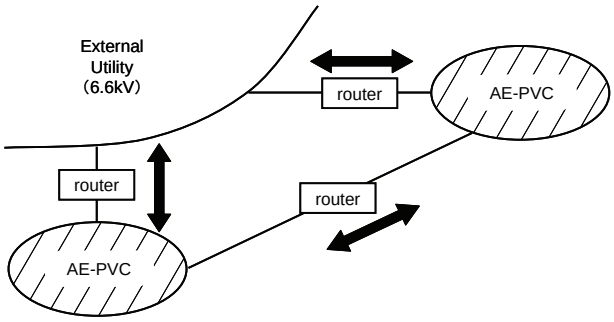

図 2　AE-PVC 広域展開

2. 系統間ルータ用変換回路方式

パワーエレクトロニクスを用いた系統間ルータ機器の構成としては，従来法である交流－直流－交流の変換プロセスをたどる Back-to-Back（以下 BTB）方式と，マトリックスコンバータ（以下 MC）方式が考えられる。図 3 に示す MC 方式は，BTB 方式において中間部に存在する大型直流リンクコンデンサを省略することが可能である。また直接変換方式であることから機器の小型化，長寿命化，導通損失低減が見込めるなど有利な点が多く，主に電動機分野において近年活発な研究活動がなされ，急速に実用化されつつある。本研究では，これらの優れた特徴を持つマトリックスコンバータの AE-PVC における系統用ルータ機器への適用を検討するものである。

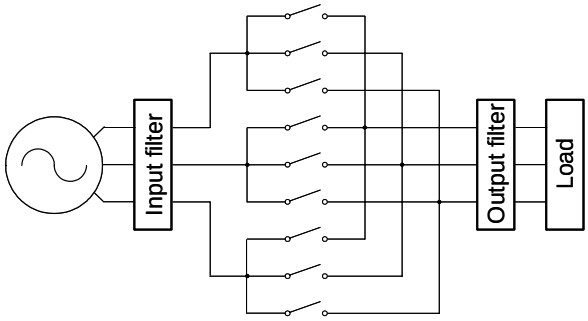

図 3. マトリックスコンバータ回路

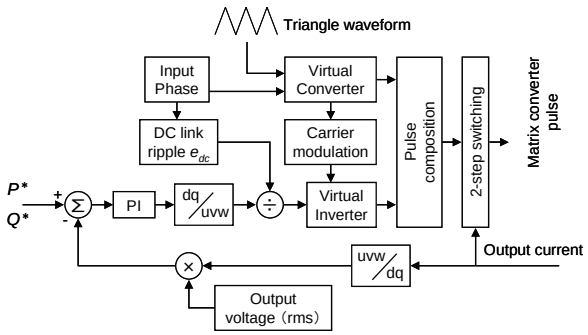

図 4　ルータ制御ブロック図

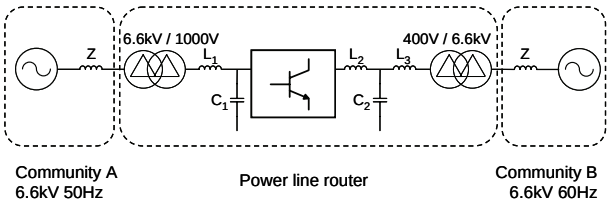

図 5　シミュレーションシステムの構成

3.　系統間ルータ制御法・シミュレーション

図 4 に本研究で作成したルータ制御用ブロック図を示す。本研究では MC の制御に仮想 AC/DC/AC 方式と呼ばれる方式を用いている。仮想 AC/DC/AC 方式では MC を中間に存在するバッファを含まない BTB 方式と見立てて制御を行う。これにより，複雑な MC の制御を従来法であり，比較的制御の行いやすい BTB 方式に立脚し，実績のある三角波比較法を用いることが可能となる。図 5 にシミュレーションシステムの構成を示す。本シミュレーションではその周波数が極端に異なるケースを仮定し，現在系統周波数として一般的な 50Hz，60Hz 間の連系を使用する。PV，AC 蓄電ステーションにより電圧が固定されるコミュニティ内部は三相電圧源による模擬を行った。

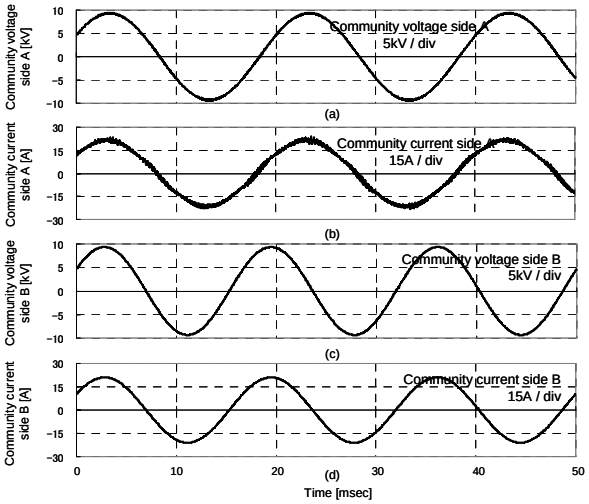

図 6　電圧 / 電流波形（順方向動作）

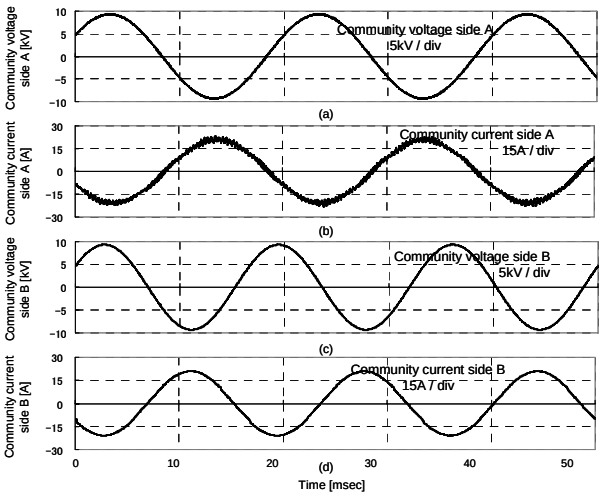

図 7　電圧 / 電流波形（逆方向動作）

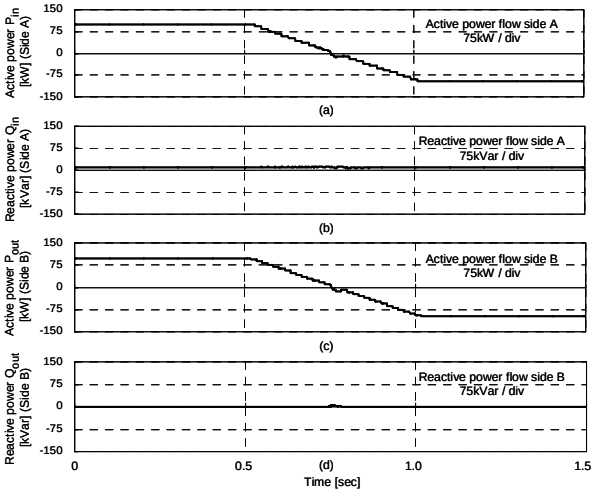

図 8　有効/無効電力の独立制御，潮流反転

4.　シミュレーション結果

有効電力指令 P=100kW，無効電力指令 Q=0kVar としたときの順方向動作，逆方向動作時の波形情報を図 6，7 に示す。この結果より，本方式でのルータ機器は各波形を良好に制御していることが判る。また，時間 t=0.5 から 1.0sec において有効電力指令 P=100kW より -100kW へ変更し，無効電力指令 Q=0kVar 固定としたときのシミュレーション結果を図 8 に示す。この結果から，AE-PVC において求められる P，Q 独立制御，高速な潮流反転制御を行うことができ，求められる要件を満足することができることを示した。

5.　謝辞

本研究は New Energy and Technology Organization（NEDO）による受託研究，自律度向上型太陽光発電システム（AE-PVC）の一部として実施されてものであり，関係者各位に感謝する。

リモートセンシングによる太陽光発電システム資源量の推定

浜野　祐貴（M1）

１．はじめに

近年，世界の経済成長に伴い化石燃料枯渇の問題は益々深刻になっており，新たなエネルギー源の開発を早急に行う必要がある。さらに，地球環境の面からも環境負荷の少ない再生可能エネルギーへの期待が高まっている。その中でも特に注目されているのが，発電時に CO_2 を排出しない太陽光発電システムである。

また，IEA により，全陸地面積の約 1%を占めるゴビ砂漠の半分に太陽電池を設置すると，2002 年の世界一次エネルギー供給量に匹敵するエネルギーを発電することができるという試算も出されている。

２．研究目的

砂漠などの未利用地に太陽光発電システムを設置すれば，大きなエネルギーを得ることが出来るが，砂漠だからといってどこにでも設置できるわけではない。しかし面積が広大なため，現地へ行って調査するのは現実的ではない。そこで，衛星画像を利用したリモートセンシングにより，砂漠などの未利用地から太陽光発電システムの設置に適した場所を選定し，資源量を推定することが本研究の目的である。

３．研究内容

３．１．適地の定義

太陽光発電システムの設置場所の適地として，本研究では「平坦で安定した未利用地」を太陽光発電システムの設置場所の適地と定義する。つまり，砂漠では礫砂漠が該当し，山岳地帯や砂丘地帯，河川付近と，植生が豊富な場所は除外する。

３．２．解析対象地域と使用データ

本研究では世界中の砂漠を解析する予定だが，まずはゴビ砂漠の約 243 万 km^2 を解析対象地域とした。解析に使用している衛星データは，メリーランド大学の HP で無償公開されているランドサット 7 ETM+の衛星画像を使用した。

４．解析手法

４．１．植生変動解析

植生指標値 NDVI を元に，植生の少ない場所を選定した。これまではランドサットの画像から算出した NDVI を使用して植生量を解析していたが，本研究では撮影時期の異なる画像を使用しているため，植生変動解析には限界があった。そこで，千葉大学の HP で公開されている NDVI のデータセット（約 10 日毎に平均化した年間 36 枚の NDVI データ）から年間最大 NDVI を算出して植生変動を解析することで対応した。

４．２．起伏地の抽出

山岳地帯や砂丘地帯は，太陽光発電システムの建設が困難であるだけではなく，砂丘地帯では砂嵐の影響もあるので，太陽光発電システムの設置場所として不適である。これらの場所は影があるため，輝度差が大きいという特徴がある。そこで，ラプラシアンフィルタを利用してエッジ検出を行い,起伏地を抽出した。

４．３．最尤法による土地被服分類

最尤法（maximum likelihood classifier）を用いて土地被服分類を行った。分類クラスとして，dune，gobi，desert_steppe，meadow，lake の 5 クラスを設定した。

５．解析結果

ゴビ砂漠の適地解析結果を図に示す。一部で衛星画像のつなぎ目で解析結果が異なってはいるものの，ゴビ砂漠では西へ行くに従って乾燥が厳しくなっていくが，解析結果も同じような傾向となっているので，満足のいく結果となった。なお，ゴビ砂漠の解析対象地域での太陽光発電システムの設置可能面積率は約 47%だった。また，グラウンドトゥルースの結果，解析精度は約 76%だった。

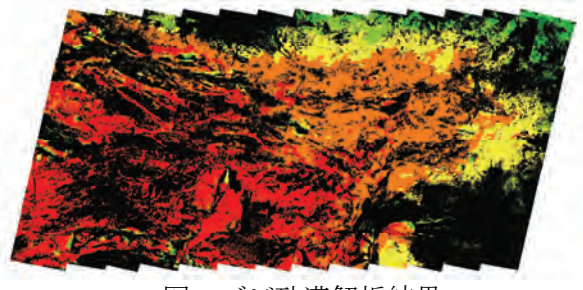

図　ゴビ砂漠解析結果

６．今後の課題

現在の解析手法では，画像によって起伏地抽出結果が異なる問題がある。この問題を解決した後，資源量の推定と，解析対象地域の拡大へ研究を進めていきたい。

写真測量法による影の定量評価システム

渡辺　優一（M1）

１．はじめに

太陽光発電（以下 PV）は太陽光を取り入れることで発電するために，PV アレイの設置場所は，日射が障害物などの影響を受けない場所が望ましい。しかし，実際はそのような理想的な場所に設置できるのはわずかであり，建物や木などの影がかかる場所に設置することがほとんどである。設置予定の PV アレイの出力を予測するためにも，影の定量評価を含めたシステム評価の必要性が重要となってくる。

これまでに本研究室では，写真測量・影推定において，研究が行なわれてきた。そこで，本研究ではこれまでの研究を含めた，現場向きの手軽な影定量評価システムを提唱する。さらに，写真測量の改善点について述べる。

２．影定量評価システム

影定量評価システムには，5 つの段階がある。この構造を図 1 に示す。

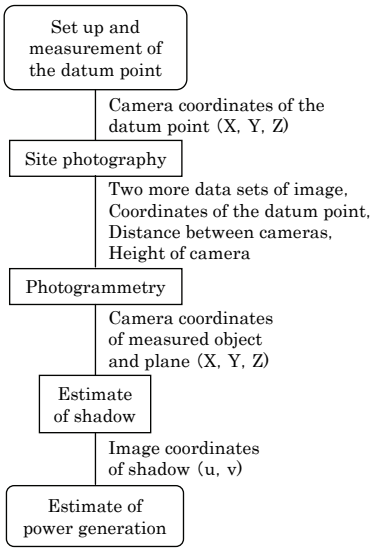

図 1 影定量評価システムの構造

このようにして，障害物が作る影を推定し，発電量の推定を行う。

３．写真測量

カメラで撮影する画像には，少なからずブレや回転が生じることがある。そこで，回転変換をかけて平行座標に変換し，測量物体の 3 次元座標を算出する。カメラの回転としては，傾き・仰角・水平方向の回転の 3 つの回転が存在する。

傾きは，シャッターを押すときに生じる回転で，鉛直方向の 2 点から傾きから算出する。

仰角・水平方向の回転については，基準点と基準画像を用いて，三角測量の原理から 2 枚目の平行座標上における理論値を算出する。その算出した座標と，実際に取り込んだ画像のズレから，回転角度を推定する。

図 2 から回転角度は

$$\gamma = \tan^{-1}\frac{f(v-v')}{f^2+vv'} \qquad (1)$$

と算出される。

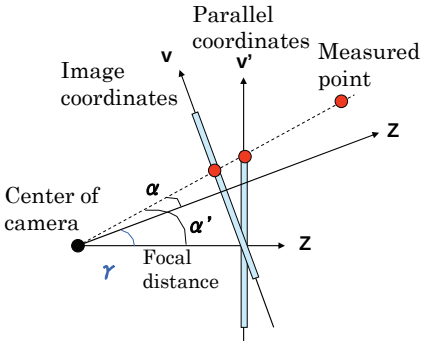

図 2 仰角・水平回転

４．結果・まとめ

理論通りに座標が算出できているかを確認するために，実際に撮影した画像を用いて，検証を行った。画像はそれぞれ三脚を使い固定し，基準画像に対して上下左右に回転させたものを使用した。

表 1　測量結果

	Actual measurement (X,Y,Z)[mm]	Estimated measurement (X,Y,Z)[mm]	Error (X,Y,Z)[mm]
①-②	(450, 1600, 3850)	(388, 1796, 4114)	(62, 196, 264)
①-③	(450, 1600, 3850)	(379, 1810, 4186)	(71, 210, 336)
①-④	(450, 1600, 3850)	(449, 1819, 4224)	(1, 219, 374)
⑤-⑥	(420, 1600, 3850)	(286, 1704, 3863)	(134, 104, 13)

表 1 から，Z 軸方向では多少誤差があるが，精度よく測量できている。

基準点付近に測量物体がある場合は，表 1 のようになったが，測量物体が離れている場合は，うまく測量できていないことがわかった。今後は，撮影するカメラのアングルと精度の関係を把握し，どういった条件で撮影すればある程度の精度を見込めるのかを検討する。また，影を表示することを進めていく。

パワーコンディショナの単独運転検出機能に与える電動機の影響に関する研究

宮本　和典（M1）

1. はじめに

近年，環境問題に対する意識は高まっており，太陽光発電は発電時に地球温暖化の原因となる二酸化炭素を排出しないクリーンなエネルギー源として広く普及が進みつつある。

そのような太陽光発電システムに欠かせない電力変換装置であるパワーコンディショナには，電力系統と連系するための保護機能を具備している。しかし負荷に電動機が接続された場合は，単独運転を検出することが困難となりうることが指摘されている。

本研究では，パワーコンディショナに負荷として接続された電動機の挙動を解析し，特に電源から切り離した後の電動機について，再現性の高い一般化モデルを開発することを目的としている。

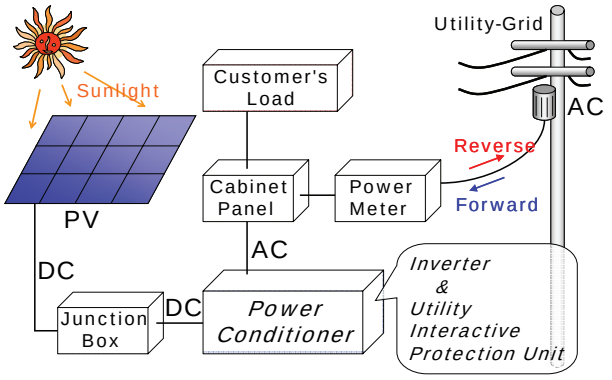

図 1　住宅用太陽光発電システムの構成例

2. 単独運転とは

単独運転とは，商用電源から切り離された電力系統内において，太陽光発電システムのような発電設備の運転によって生じる電力供給のみで，当該系統に電気が通じている状態のことを指す。このような状態では，公衆や作業員の感電，系統に接続されている機器の損傷，消防活動の妨害，事故の拡大や復旧の遅れが発生する恐れがある。このため保護継電器等を用いて単独運転を検出し，発電設備を系統から解列できるような単独運転防止策をとることを原則としている。[(1)]

3. 研究概要

同一配電線内に負荷として電動機が存在する場合に，パワーコンディショナが単独運転現象を検出し難いという知見[(2)]がある。そこで本研究では，研削加工用機器として広く用いられているグラインダ（砥石研削機，単相誘導電動機）を用いて，系統から解列後の電動機の電気的な挙動を回路理論によって一般化し，再現性の得られるモデルを構築することを目標としている。

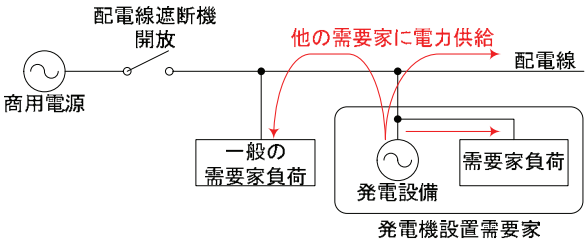

図 2　単独運転の概念図

4. 発電現象の確認

まず系統停電と同時にそれまで負荷として動作していたグラインダが発電機のように振舞うことが原因となり，パワーコンディショナの有する単独運転検出のアルゴリズムが系統停電を検出できないのではないかと考えた。そこで図 3 に示すような実験回路を構成し，トライアックによるスイッチでグラインダを電源から切り離した後の挙動を調査した。グラインダは定格消費電力が 645W のコンデンサモータを用いた。グラインダに並列に接続した負荷抵抗 R_L を 10W, 100W, 200W と変化させた時の消費電力を測定した結果を図 4 に示した。

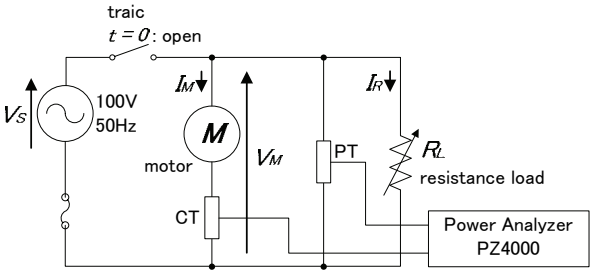

図 3　発電モード確認実験回路

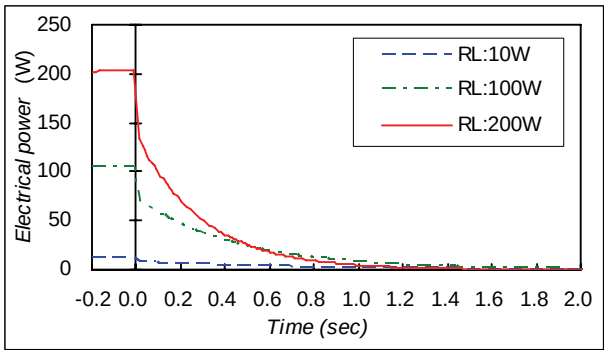

図 4　並列可変抵抗での消費電力

図 4 より，電源から切り離した直後の 1 秒間程度はグラインダから抵抗負荷に電力が供給されていることがわかる。

またグラインダ極間電圧の周波数 f_{VM} と回転子回

転数 f_{Rotor}から，式（1)によって算出したすべりを図 5 に示す。電源オフと同時にすべりが負に変化していることから，グラインダが発電モードへ移行していることが確認できる。

$$S = \frac{f_{VM} - f_{Rotor}}{f_{VM}} \quad [\text{-}] \cdots\cdots (1)$$

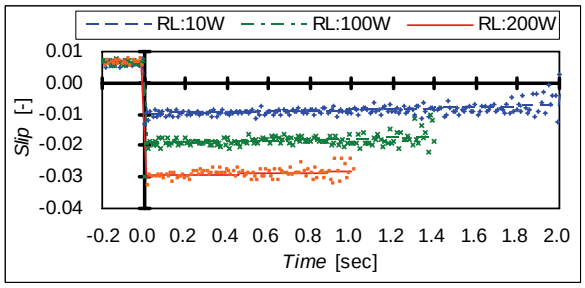

図 5　すべりの変化

図 4 に示した「抵抗負荷での消費電力」と，図 5 に示した「モータ端子間電圧周波数 f_{VM}と回転数 f_{Rotor}から求めたすべり」の双方において，グラインダが電力供給を断った直後の 1 秒間程度は発電することが確認された。

5.　回転体の運動エネルギーの変化

前述のような発電現象のエネルギー源は回転体の慣性運動にあるのではないかと考え，回転子の慣性運動による運動エネルギーに着目した。そこで回転子の回転速度変化から回転子の仕事率の算出を行った。

まず回転子の慣性モーメント J を式(2)より算出した。結果を表 1 に示す。

$$J = \frac{1}{8} MD^2 \quad [\text{kg}\cdot\text{m}^2] \qquad (2)$$

表 1　供試グラインダの慣性モーメント

PARTS	Mass (kg)	Diameter (m)	Inertia moment (kg·m²)
Left grind stone	1.370	0.205	7.197E-03
Right grind stone	1.360	0.205	7.144E-03
Others	3.520	0.027	3.208E-04
TOTAL			**1.466E-02**

次に求まった慣性モーメントから式(3)～(5)を用いて，回転体の運動エネルギーを算出した。ここで ω は角速度，$\dot{\omega}$ は角加速度，T はトルク，P は仕事率を表す。結果を図 6 に示す。

$$\omega = 2\pi \cdot f_{Rotor} \qquad (3)$$

$$T = J \cdot \dot{\omega} \qquad (4)$$

$$P = \omega \cdot T \qquad (5)$$

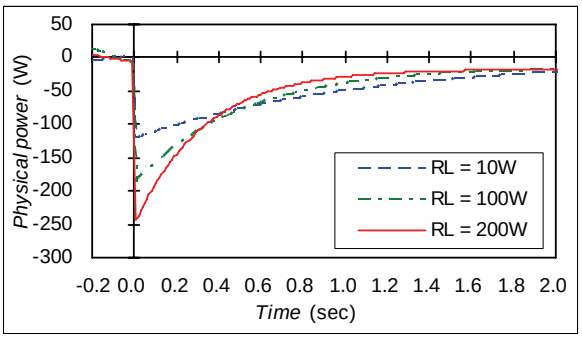

図 6　回転体の仕事率変化

図 6 よりグラインダの発電電力の変化は，回転体の仕事率の変化と類似していることが分かる。しかしそれらの絶対値は一致していない。それは機械損，慣性モーメント算出時の近似誤差などが原因と考えられる。

6.　まとめ

今回用いたグラインダは単相誘導電動機であるが，電動機が回転中に持つエネルギーによって、外部の励磁電源やトルクの受け渡しが無くとも、発電モードへと移行する現象が観測された。また回転体の運動エネルギーは、グラインダの発電現象に寄与する可能性が示された。

7.　今後の展望

グラインダの発電電力と回転体の仕事率の変化の相関性について，各特徴的なエネルギー量の計算などを行い，より詳細な分析・比較を行う。それらを元に停止過渡時での発電現象を模擬できる回転機モデルの作成を行い，回転機が単独運転検出機能に与える影響の解明へと発展させたい。

また単独運転検出機能には周波数変化や電圧位相跳躍を検出する方式があり，電動機の周波数特性も単独運転検出機能に影響を与える要因であると考えられ，今後検討を行う。

回転機がパワーコンディショナに与える影響を明確にするためには，系統の変動や急変に対する電動機の応答が，正確に再現されるような回転機モデル作成を目標に研究を進めていく。

参考文献

系統連系規定　JEAC9701-2006，社団法人　日本電気協会系統連系専門部会，オーム社，2006。
五十嵐広宣：“単独運転防止試験時の電動機負荷影響について”，平成 17 年度電気学会全国大会，2005。
見城 尚志，三宅 博：“小型 AC モータの設計と制御”，オーム社，1984。

TUAT-20kW 太陽光発電測定データを生かした高度性能分析

石岡　伸晃（B4）

１．背景・目的

近年，CO_2 増加による地球温暖化問題を背景に環境負荷の少ない太陽光発電に注目が集まっている．そこで本研究は TUAT-20kW の運転特性を評価し，効率向上のための事象の把握を目的とする。

２．測定

(TUAT-20kW 太陽光発電システム)

東京農工大学講義棟屋上に設置された定格システム出力 20[kW]の太陽光発電システム(12 直 14 並列)について表１に示す測定データを収集し運転特性の分析に用いた．

表 1．計測データ一覧

傾斜面日射量	[kWh/m２]
ｲﾝﾊﾞｰﾀ出力電力量	[kWh]
ｲﾝﾊﾞｰﾀ交流電圧	[V]
ｲﾝﾊﾞｰﾀ交流電流	[A]
ﾓｼﾞｭｰﾙ温度[15 点]	[℃]
外気温度	[℃]
太陽電池電力量	[kWh]
太陽電池直流電流	[A]
太陽電池直流電圧	[V]
ﾈｯﾄﾜｰｸｶﾒﾗによるｱﾚｲ画像	
直列接続部(ｽﾄﾘﾝｸﾞ)の直流電流	[A]

３．解析手法

解析についてはシステムの発電特性と損失の分離をおこない，続いて TUAT-20kW の測定データを活用した損失解析を行った．まず，システムの損失を分離する方法として，本研究室で開発・改良されてきた Sophisticated Verification(SV)法について説明する．太陽光発電において，入力エネルギーである太陽光が電気に変換される間に様々な損失が存在する．SV 法では傾斜面日射量・モジュール温度・アレイ出力電力・システム出力電力の一時間値を用いて，システムの損失を図１に示す 8 つに分離することができる．本解析手法を用いて，TUAT-20kW 太陽光発電システムの損失内容を調査した．

また，ストリング直流電流の計測データおよびネットワークカメラによるアレイ面画像を用いてストリングごとの I-V カーブをシミュレーションにより求め，「I-V カーブの重ね合わせ法」によって合成し，システム全体の電流電圧特性について解析を行った．

４．結果

4.1　SV 法を用いたシステム損失分離

SV 法によって 2006 年 1 月～12 月までの 1 年間における損失分離を行った．ｲﾝﾊﾞｰﾀ損失（λC）および温度損失（λPT）の影響が大きいことが確認できた．図１に一年間の損失割合を示す．

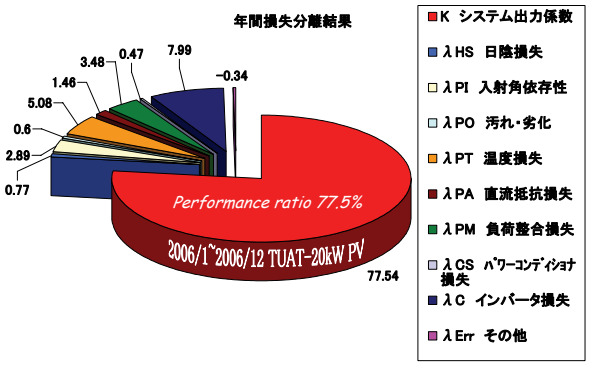

図 1　ＳＶ法損失分離結果(2006/1~2006/12)

次に，毎月の損失の変動について解析を行った．

図２に示すように，システム出力係数の月間変化は温度損失（λPT）の年変動に由来している．

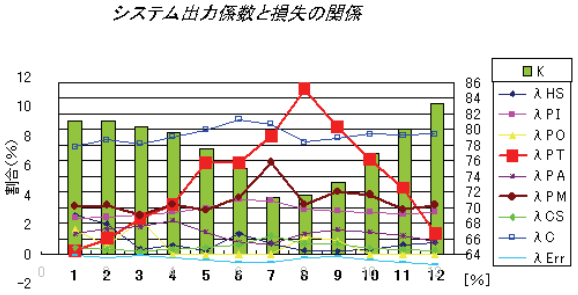

図 2　SV 法損失分離の季節変化(2006/1~2006/12)

4.2　I-V カーブシミュレーション

部分陰を有するアレイについて，本研究室で開発されている太陽電池の等価式を用いたシミュレーションツールを用いて解析し，部分陰がかかったストリングの影響でアレイ全体の I-V カーブの最大電力点が低下することがわかった．

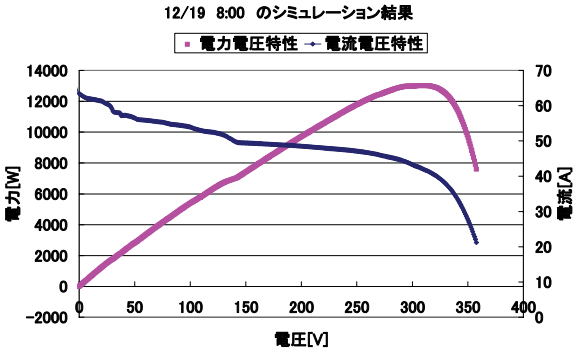

図 3 I-V カーブの部分陰の影響（2005/12/19　8:00)

５．まとめ

SV 法を用いて 2006 年の TUAT-20kW 太陽光発電システムの運転特性を解析した．発電の効率を示すシステム出力係数は，温度損失を主な原因に夏季に減少することがわかった．部分陰の影響を I-V カーブ推定から示した．今後の課題としては残る損失要因について分析を深めることである。

集中連系型太陽光発電システムにおける計測データ処理法の研究

井出　翔太（B4）

1. 研究背景・目的

(独)新エネルギー・産業技術総合開発機構では，太陽光発電（以下，PV）システムの円滑かつ健全な普及拡大のための技術を開発するため，「集中連系型太陽光発電システム実証研究」を実施している。実際に群馬県太田市の新興住宅地において系統連系型 PV システムを 553 軒の住宅に設置し，様々なデータを計測している。計測端末は全ての住宅に設置され，1 軒あたりの計測項目が 50 項目以上，計測周期が 1 秒（統計値として 1 分値，1 時間値，1 日値を収録）という計測環境は他に類を見ない規模である。このことから計測データは PV システムの運転特性や各種現象の把握をするために多くの研究者に注目されている。この実証実験における PV システム 1 軒の計測箇所を**図 1** に示す。

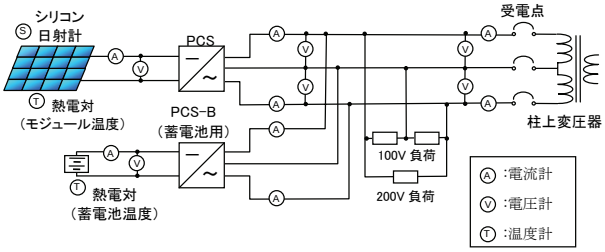

図 1　PV システムの計測箇所の例

その計測規模からデータ量は膨大であり，複数の大容量ハードディスクに実証研究専用のバイナリ形式のデータで蓄えられている。このデータを各種プログラム言語等で汎用的に使用するには，CSV 形式等に変換されていると扱いやすい。そのため，解析に必要な項目，特定の期間，特定の範囲の住宅等を選択でき，一括で CSV 形式等に変換できるツールが求められる。そして，多くの PV システム研究者が実証研究の計測データを利用し易くなることは，研究開発全体の発展のために大変有益なことである。

そこで，効率的なデータ処理を行って研究者を支援できるツールを開発することを本研究の目的とする。

2. データ処理ツール

それぞれの研究者の要求するデータは研究内容に応じて異なってくることが予想される。そこで，開発されるデータ処理ツールは多様な研究に対応できるよう自由度が高い必要がある。盛り込まれる機能としては計測項目，データサンプリング周期，出力期間，出力端末の必要に応じた自由選択，そして出力ファイルサイズを小さくする機能である。膨大なデータは解析の作業を繁雑にさせ研究の効率を悪くしてしまう。全体のデータサイズを落とすことにより，データ解析の効率向上が期待できる。データサイズを落とすには必要の無いデータの合理化，例えば未計測データや重複データを整理することや，多数ある項目を減らすことが考えられる。作成したデータ処理ツールの操作画面を**図 2** に示す。

計測項目，データサンプリング周期，出力期間，出力端末は簡便な操作で自由に選択できる。その他，出力ファイルサイズ推定機能をつけた。

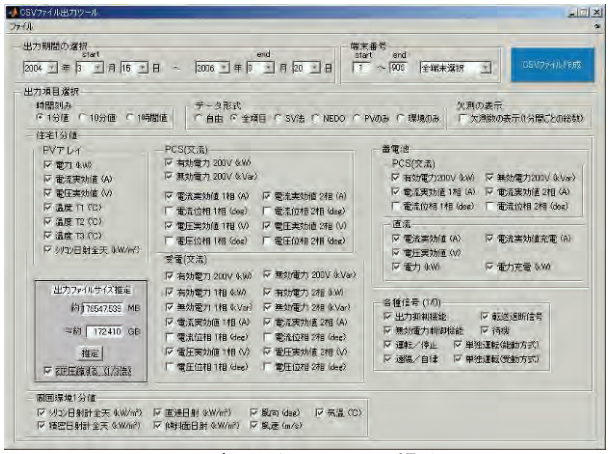

図 2　データ処理ツール操作画面

3. 出力テスト

開発したデータ処理ツールを用いて統計 1 分値から約 40 項目を選択し CSV 形式の 1 分値の出力を行った。期間は 2004 年 3 月から 2006 年 9 月までとし，出力結果を**図 3** に示す。その結果，532[GB]の統計 1 分値データから項目を選択し，CSV 形式に変換することで 87.2[GB]とすることができた。これは，16.4[%]の圧縮効果になる。

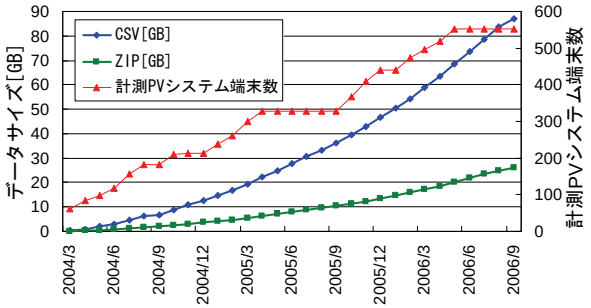

図 3　CSV ファイル出力結果

4. まとめ

効率的な PV システム解析の支援ができるデータ処理ツールを開発した。多種多様な研究に対応するために，操作性の高い選択機能などを付加した。

各種太陽電池の屋外性能評価

角　京子（B4）

1. 背景と目的

近年，化石燃料の使用過多で二酸化炭素などの排出で，地球温暖化などの環境問題が深刻化している。その中，二酸化炭素の廃棄物の排出を軽減できるクリーンなエネルギーとして太陽光発電の普及が期待されている。

現在最も普及しているのはシリコン系太陽電池であるが，新型太陽電池などの研究・開発が進められている。シリコン系太陽電池と比較し，低コスト（発電コストも含む）・材料費・製造エネルギーの削減などの優れた特徴がある。一方で規格・評価技術が整っておらず，今後の太陽光発電システム発展のためにも特性を把握する必要がある。

太陽電池の測定は通常屋内で行うが，実際使用するのは気象条件で特性の異なる屋外である。本研究では，シリコン系太陽電池と新型太陽電池を屋外の同一サイトに設置し，太陽電池の屋外での性能を評価する事を目的としている。

2. 研究内容

3 号館屋上に設置している太陽電池について紹介する。現在，3 号館屋上には結晶 Si 太陽電池 3 種類，CIS 系太陽電池 2 種類，ヘテロ接合太陽電池，多接合型太陽電池の計 7 種類を傾斜角度 30 度，方位角度 0 度で並べ同じ条件の下，性能評価を行っている。表 1 に太陽電池の種類と公称最大出力を,表 2 に変換効率を示す。

表 1.　太陽電池の種類と公称最大出力

種類	c-Si	Poly-Si(1)	Poly-Si(2)	CIGS	CIS	ヘテロ接合型	多接合型
公称最大出力[W]	167	132	167	112	40	190	36.5

表 2.　各太陽電池の変換効率

	c-Si	Poly-Si1	Poly-Si2	CIS-1	CIS-2	ヘテロ接合	多接合
変換効率[%]	15.8	12.8	12.8	9.1	7.9	16.1	8.3

本研究では，各種太陽電池の季節ごとのシステム出力係数の変動を評価する。

システム出力係数の算出式を式（1）に示す。

$$\text{システム出力係数} = \frac{\text{等価システム運転時間[kWh/kW]}}{\text{等価太陽日射時間[(kWh/m2)/ (kW/m2)]}} \quad (1)$$

3. これまでの成果

年間のシステム出力係数を図 1 に示す。

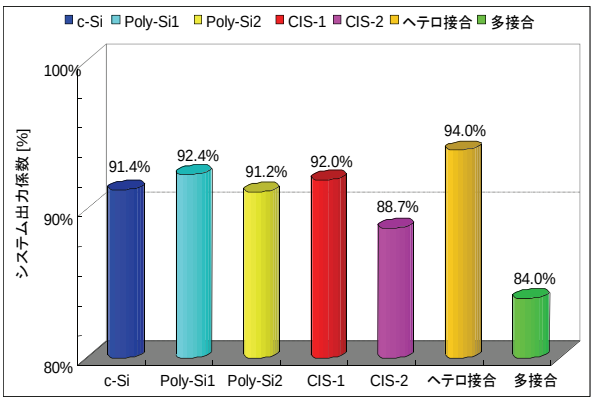

図 1.　各太陽電池のシステム出力係数

図 1 よりシステム出力係数が最も大きいのはヘテロ接合である。入力エネルギーが出力エネルギーに変換される割合が最も大きい。ここで，各種太陽電池のシステム出力係数が季節でどのように変動するか検証する。グラフを図 2 に示す。季節は

12 月…冬　　3 月　…春

6 月　…夏　　9 月　…秋

とした。（冬至，春分，夏至，秋分があり，最も季節性があるのではと考えた）

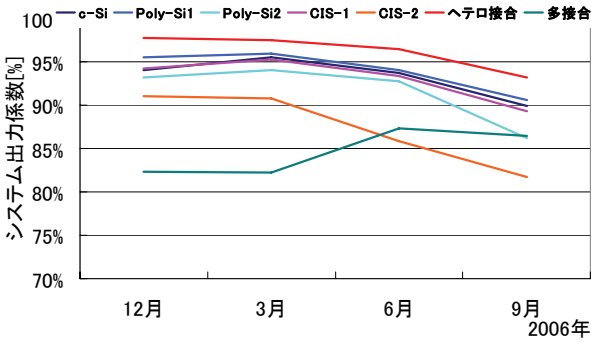

図 2.　各種太陽電池のシステム出力係数の変動

図 2 より，多接合太陽電池を除いて冬にシステム出力係数が高く，夏に低くなるという傾向になることがわかる。また，表 1，表 2 より公称最大出力，変換効率の大きいものがシステム出力係数は高い傾向にある。

4. まとめ

- システム出力係数は公称最大出力，変換効率の大きいものが高い傾向にある。
- 多接合太陽電池を除いては冬にシステム出力係数が大きくなり，夏には小さくなるという事が分かった。
- データの計測を重ねることで，今までにない傾向がみられるのではないかと考える。

縮小系統模擬分散電源の開発

東方田 敏彰（B4）

1.研究背景

近年，環境問題やエネルギー問題に注目が集まり，太陽光発電（以下，PV）システムなどのクリーンエネルギーを用いた分散型電源（以下，DG）が住宅を中心に普及している。DG が配電系統に多数台連系されると，電圧上昇や高調波などによる電力品質，単独運転などによる安全性の低下が懸念されている。そのため，事前に DG の多数台連系試験を行なうことが必要である。

従来の試験装置には，実際の太陽電池や家電製品などの実際の負荷などを利用した実規模の試験装置があるが，この試験装置は非常に大型で設備コストが高いために，限られた研究機関でしか使用することができなかった。そのため当研究室において，実際の配電系統を電気回路によって縮小模擬した縮小模擬配電系統シミュレータが開発された[1]。この試験装置において実規模の PV インバータを数台接続して試験することは可能であるが，より多くの PV インバータを接続するために試験装置を拡張すると大きな設置スペースが必要となるうえ，多大なコストも必要である。このような理由から，当研究室において更にサイズ，コスト，拡張性に優れた，超縮小模擬配電系統シミュレータが開発された[2]。この試験装置は配電系統を電子回路によって模擬しているため，電力レベルの違いから実規模の DG を直接接続できない。そのため，超縮小模擬配電系統シミュレータでは電力変換装置である API（Active Power Interface）[3]を搭載することにより，実規模の DG を接続可能にしている。しかし，超縮小模擬配電系統シミュレータにおいて DG の多数台連系試験を行なう場合には，実規模の DG の台数分 API が必要となることから，複数台の API，DG の設置スペース，購入コストが必要となる。

本研究では，超縮小模擬配電系統シミュレータにおいて様々な条件の多数台連系試験を省スペース，低コストで行なうために，実際の DG を電子回路により縮小模擬した，縮小系統模擬 DG を提案する。本稿では，DG の中でも PV システムに注目し，PV 用パワーコンディショナ（以下，PCS）を模擬した模擬 PCS を開発する。

2.模擬 PCS

2.1 仕様

模擬 PCS に求められる要件として，実規模の PV 用 PCS と同等な制御・機能を搭載すること，模擬 PCS の機能が選択可能であること，小型であること，超縮小模擬配電系統シミュレータに適応することが挙げられる。本研究では，これらの要件を満たすために，Field Programmable Gate Array（以下，FPGA）を用いる。FPGA は並列処理能力を持つことから，ひとつの FPGA に制御周波数の異なる複数の機能を搭載することができ，同時に模擬 PCS を小型にできる。また，FPGA はプログラムの書き換えにより内部回路が変更できるため，模擬 PCS の機能が選択できるようになる。要件を満たすための模擬 PCS の仕様を表 1 にまとめる。定格出力，出力電圧，出力電流，周波数は超縮小模擬配電系統シミュレータに適応するために設定している。また，実規模 PCS が持つ機能・制御として系統保護機能，その他の機能・制御を挙げる。

表 1　模擬 PCS の仕様

定格出力	0.1[W]
出力電圧	5/10[V]
出力電流	20[mA]
周波数	50[Hz]
系統保護機能	● OVR/UVR*1 ● OFR/UFR*2 ● 単独運転検出機能 （受動的方式＋能動的方式）
その他の機能・制御	● 起動停止制御 ● 同期制御 ● 力率制御 ● 定電流制御 ● 電圧上昇抑制機能 ● 出力変動機能 ● 高調波発生機能

*1: OVR/UVR：過電圧・不足電圧継電器
*2: OFR/UFR：周波数上昇・低下継電器

2.2 回路構成

図 1 に作成した模擬 PCS の回路構成を示す。

Grid phase signal circuit（系統位相信号回路）において，系統電圧波形の位相情報を持つ Grid phase signal（系統位相信号）を作成し，FPGA（FLEX10K30ATC144-3, Altera）に入力する。これにより，系統電圧波形に対し FPGA に格納されている 8bit 正弦波データを同期するように出力する。また，FPGA から出力される 8bit 正弦波データは D/A コンバータ（DAC0800, National Semiconductor）により D/A 変換されるが，今回用いた D/A コンバータは 180° 位相の違う波形が

2 つのピンから出力されるため，Differential circuit（差分回路）を接続することにより所望の波形を得ている。

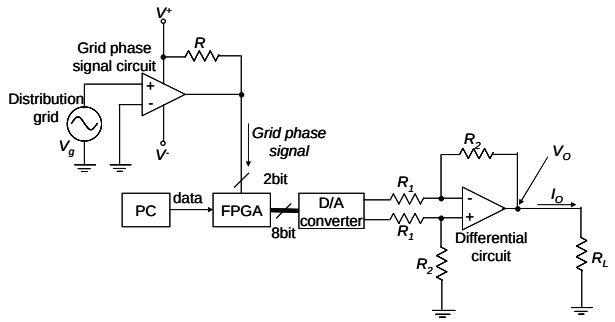

図 1　模擬 PCS 回路

3.同期制御

図 1 の回路において，模擬 PCS の出力を系統電圧波形に同期させる同期制御の実験を行なった。実験で用いた回路パラメータを表 2，実験結果を図 2 に示す。図 2 より模擬 PCS の出力電圧 Voは系統電圧波形 V_gと同期したことが確認できる。

表 2　回路パラメータ

Parameter	Value
V_g	3 [V]
f_g	50 [Hz]
R_1= R_2	10 [kΩ]
R_L	1 [kΩ]
R	10 [kΩ]

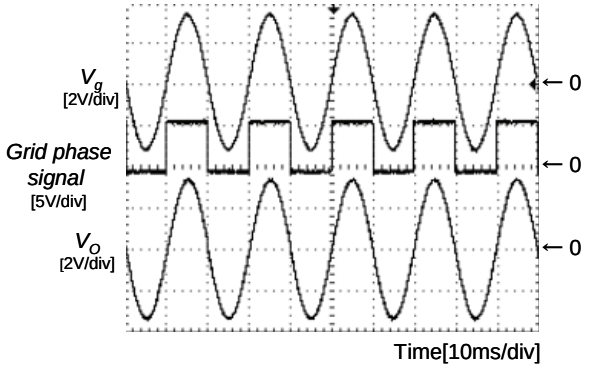

図 2　同期制御実験結果

4.周波数上昇・低下検出

系統保護機能である OFR/UFR を機能させるために，系統周波数に安全運転範囲を設け，周波数の上昇･低下を検出して模擬 PCS を停止する実験を行なった。この実験では安全運転範囲を 49～51Hz と設定した。また，45～55Hz まで 0.1Hz 刻みで変化する系統位相信号を FPGA 内部で作成したため，図 1 の回路から系統位相信号回路を除いた回路において実験を行なった。実験結果を図 3 に示す。図 3（b），（c）より，模擬 PCS が運転した周波数は 49.09～51.04Hz であることがわかる。これにより，模擬 PCS が系統周波数上昇・低下を検出することで模擬 PCS が停止し，設定した安全運転範囲で動作することが確認できる。

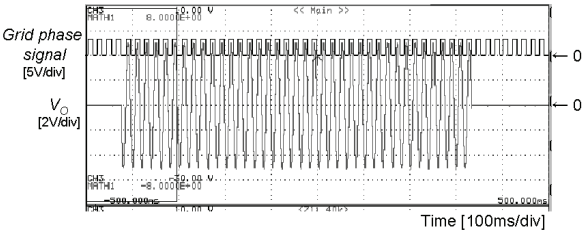

（a）全体図

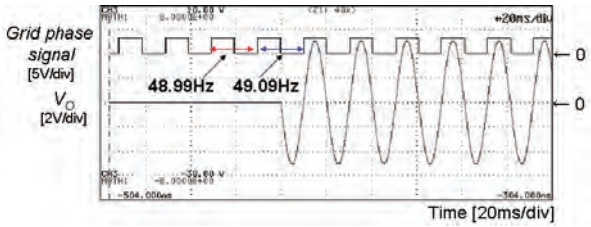

（b）運転開始時拡大図

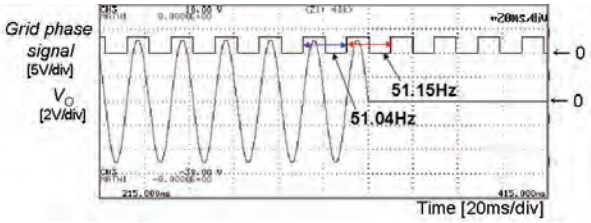

（c）運転停止時拡大図

図 3　周波数上昇・低下検出実験結果

5.まとめと今後の課題

制御系に FPGA を用いた模擬 PCS を作成し,出力電圧の同期制御，系統周波数上昇・低下検出を行なった。その実験結果より，これらの制御，機能が有用であることを確認した。

今後の課題として，表 1 に示した模擬 PCS の仕様に基づき，出力電流の増幅，実規模 PCS が持つすべての機能を搭載することが挙げられる。また，これらが作成され次第，超縮小模擬配電系統シミュレータを用いた系統連系試験を行なう。

文　献

[1] Y. Noda, T. Mizuno, H. Koizumi, K. Nagasaka, K. Kurokawa, “The deployment of a scaled-down simulator for distribution grid and its application for verifying interference behavior among a number of module integrated converters (MIC),” in *Proc. 29th IEEE Photovoltaic Special Conf.*, pp.1545-1548, May 2002.

[2] K.Takeuchi, H.Koizumi, H. Nagayoshi, and K.Kurokawa, “A new type of scaled-down network simulator composed of power electronics”, in Proc. 3th World Conference and Exhibition on Photovoltaic Solar Energy Conversion, May 2003, pp.2039-2042 vol.2

[3] Yusuke Nakamura, Hirotaka Koizumi, and Kosuke Kurokawa, “A new type of scaled-down network simulator for testing PV inverters,” in *Proc. RENEWABLE ENERGRY 2006,* pp 278-281, October 2006.

配電系統の電圧制御に関する研究

山口 健一郎（B4）

1. 研究背景

近年，CO2 をはじめとした環境負荷の低減，省エネルギー，電力供給信頼度の維持，コスト削減などの様々な観点から，分散型電源と呼ばれる小容量の電源が注目を集めている。

国内においては，一次エネルギーに占める石油の依存度を下げ，太陽光，風力，バイオマスといった自然(再生可能)エネルギーを利用した分散型電源の導入量拡大が目指されている。

このように分散型電源の配電系統への連系は今後ますます増加するものと予測されるが，太陽光発電システムのように自然エネルギーを利用した分散型電源は，気象条件によって出力が大きく変動するため，高密度に分散型電源を連系した配電系統においては想定外の電圧分布が発生する可能性が考えられる。

従来の電圧調整機器は大型でコストが高く，また分散型電源からの逆潮流による電圧変動を想定して設計されていないため，分散型電源の瞬時の出力変動に対応できない可能性がある。

そこで本研究では，パワーエレクトロニクスを導入した AC/AC コンバータに注目し，小型で高速制御が可能な電圧調整機器の開発を行った。

2. 研究内容

2.1 電圧調整回路の構成

今回開発した回路は柱上変圧器の低圧側に設置し，多数台連系された PV システムとの間で電圧制御を行なうことを想定している。この回路は図 1 に示すように，変圧器と AC/AC コンバータ，フィードバック制御回路から構成されており，太陽光発電システム(以下 PV システム)からの逆潮流で v_{line} が変動したときに AC/AC コンバータによって電圧の調整を行う。

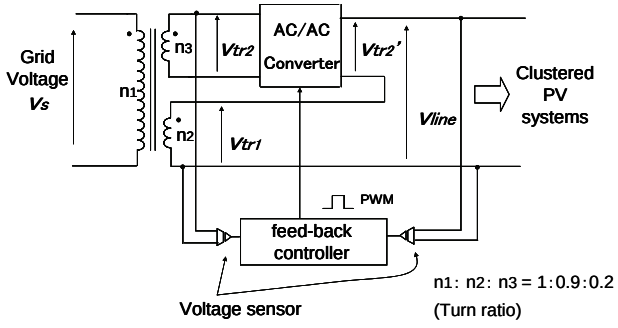

図 1　電圧調整回路の構成図

2.2 AC/AC コンバータ

電圧調整回路に用いる AC/AC コンバータは，図 2 に示すように 4 つの半導体スイッチと入出力フィルタから構成されており，各スイッチは表 1 に示すスイッチングパターンで動作する。この時，入力 v_{tr2} と出力 v_{tr2}'の関係は

$$v_{tr2}' = D \times v_{tr2} \qquad (1)$$

となる。D は各スイッチに入力される PWM 信号のデューティ比で理論的には 0 から 1.0 の値まで変化させることができる。

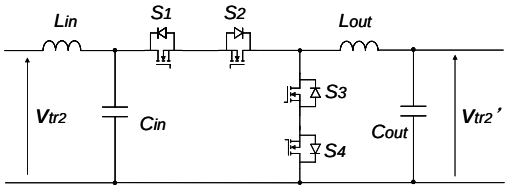

図 2　AC/AC コンバータ回路

表 1　スイッチングパターン

$V_{tr2} > 0$	$S1$:PWM $S3$: $\overline{S1}$ $S2$:ON $S4$:ON
$V_{tr2} < 0$	$S1$:ON $S3$:ON $S2$:PWM $S4$: $\overline{S2}$

2.3 フィードバック制御回路

図 3 はフィードバック制御回路のブロック図を示している。検出した電圧調整回路の出力電圧 v_{line} と目標電圧 v_{ref} との誤差 v_{error} は PI 制御がかけられた後，比較器によって三角波電圧 v_{tri} と比較され PWM 信号を生成する。生成された PWM 信号は Dead-time 発生回路とスイッチング制御回路を通って各スイッチに入力される。

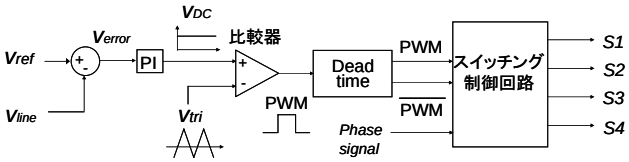

図 3　フィードバック制御回路

3. 電圧調整回路のシミュレーション

3.1 シミュレーション条件

図 4 は今回用いた配電系統のシミュレーションモデルである。このモデルは 30kVA の柱上変圧器から 4.5[m]離れたところに開発した電圧調整回路を設置し，そこからさらに 45[m]離れたところに，15 軒の需要家が 10[m]間隔で連系している状態を設定した。

各需要家には最大出力電流 Ipv = 20[A,rms]の PV システムと 14.29[Ω]の負荷インピーダンス $Zload$ が 15[m]の引き込み線で接続されている状態を設定した。なお，配電線と引込み線の線路インピーダンス Z_1，Z_2，Z_3，Z_4 については表 2 にそれぞれ値を示す。

柱上変圧器から需要家への送り出し電圧 vs は 104[V,rms]と仮定し，電圧調整回路の目標電圧 v_{ref} は 101[V,rms]と設定している。

また，AC/AC コンバータの入出力フィルタに用いる Lin, $Lout$, Cin, $Cout$ の値はそれぞれ 0.15[mH], 0.16[mF]としている。

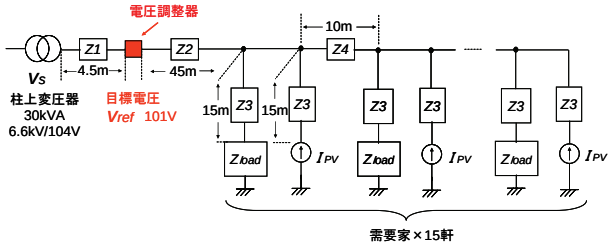

図 4　配電系統のシミュレーションモデル

表 2　線路インピーダンスのパラメータ

Z_1	0.0011+j0.0013[Ω]
Z_2	0.011+j0.0013[Ω]
Z_3	0.0345+j0.0015[Ω]
Z_4	0.0025+j0.0029[Ω]

3.2 シミュレーション結果

図 4 のモデルにて，各需要家の PV が一斉に 20[A,rms]で発電したときの配電線の電圧分布を図 5 に示す。電圧調整回路を設置していない場合送り出し電圧は 104[V,rms]から始まり，系統末端においては電圧値が適正範囲の 107[V,rms]を逸脱していることがわかる。通常，需要家の電圧が適正範囲を超えるときは PV インバータの出力抑制機能が働くが, 今回これは考慮していない。一方，電圧調整回路を設置した場合の送り出し電圧は目標電圧の 101[V,rms]に固定され，系統末端の電圧は 107[V,rms]を逸脱しないことがわかる。

以上より，開発した電圧調整回路は出力端の電圧を目標電圧値に制御し，配電線の電圧を適正範囲内に維持することが可能であるといえる。

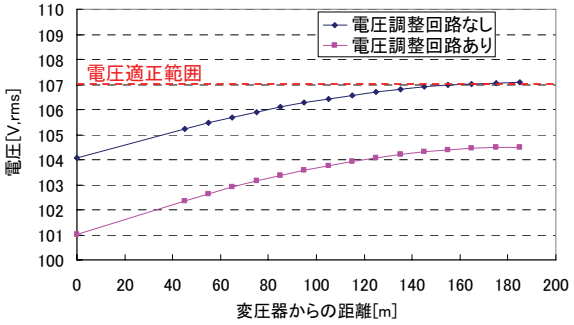

図 5　配電線の電圧分布

4. AC/AC コンバータの実験

4.1 実験回路

図 2 で示した AC/AC コンバータを 2[V]85[mW]レベルにて製作し，実験を行った。回路図を図 6 に示す。入力に AC 電源 vin = 2[V,rms]，出力に抵抗 R = 47[Ω]を接続し，各スイッチの制御には FPGA (Field Programmable Gate Array)を用いて実験を行った。入出力フィルタに用いる Lin，$Lout$，Cin，$Cout$ の値はそれぞれ 2.5 [mH]，1[uF]としている。

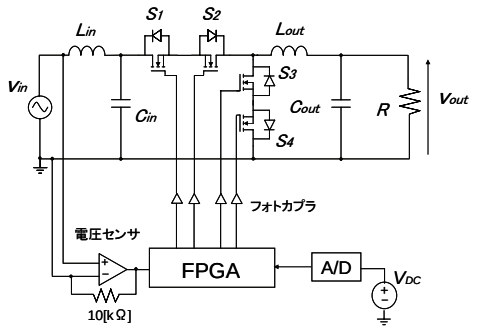

図 6　AC/AC コンバータの実験回路

4.2 実験結果

図 7 に作成した AC/AC コンバータの入出力波形を示す。出力電圧 $vout$ は入力電圧 vin とほぼ同位相であり，デューティ比 D によって振幅値が変化していることがわかる。また，表 3 に D と $vout$ の関係を示す。$vout$ の値は(1)式で示したように D に比例して変化していることがわかる。

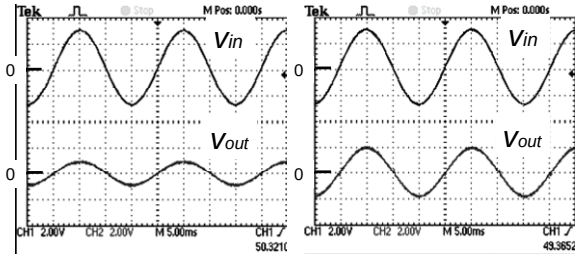

D = 0.3　　D = 0.7

図 7　AC/AC コンバータの入出力波形
(2.0[V/div], 5.0[ms/div])

表 3 デューティ比 D と出力電圧 $vout$ の関係

D	0	0.3	0.5	0.7	1.0
$Vout$ [V,rms]	0	0.66	1.09	1.33	1.88

5.まとめと今後の課題

シミュレーションより，今回開発した電圧調整回路の基本動作を確認することできた。また，2[V]85[mW]クラスの AC/AC コンバータを試作し，その電圧制御性を確認することができた。

今後はフィードバック制御回路の制作を行い電圧調整回路の完成を目指す。また，今回のシミュレーションで目標電圧の値は任意に設定したが，今後はその設定方法についても検討して行く。

大規模太陽光発電システムに関する研究

伊藤 雅一（砂漠 WG）

1. はじめに

「持続可能な発展」が様々な場所から提案されているが，その提案の中で太陽光発電システムへの期待は高い。なかでも，ドイツの WBGU が作成した持続的発展のシナリオでは，2100 年には太陽エネルギーが世界のエネルギー需要の 3 分の 2 を占めると予測している。

本研究は砂漠の広大な土地と強い日射，そして太陽光発電システムを組合せ，エネルギー問題や地球温暖化などの問題に取り組むことを大目的としている。図 1 に示すように，国際エネルギー機関（IEA）のもと，PVPS 部門の大規模太陽光発電システムの可能性評価を行う Task8 国際ワーキンググループ（WG）を中心とし，実行部隊である Task8 の国内 WG, そして農工大生存科学 COE の砂漠 WG の 3 つの WG が重なり合って大目的の達成を目指す。

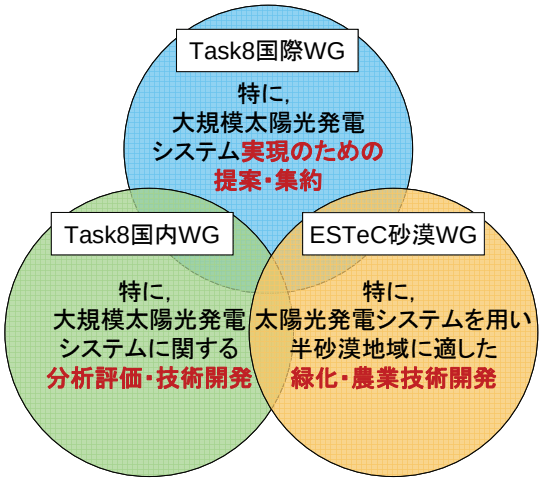

図 1 砂漠地域における太陽光発電システム開発に関わるワーキンググループ

図 2 農と工の融合による研究開発

2. 農工大 COE 砂漠 WG

本 WG は、日射量が豊富かつ広大な、砂漠等の未利用地への設置を想定し、人口増加による食糧危機への対応、多種多様性の維持のための緑化・農業開発、そしてエネルギー問題解決のための太陽光発電システム開発と、それぞれに必要な雨量、日射、環境図等の整備、さらに砂漠等未利用地域における太陽光発電システム技術、緑化・農業開発技術の集合を行う。各技術の各地域のおける適用を行い、経済性・エネルギー性・廃棄物性・実現性・地域性に有利なコミュニティの提案、そして改善点を示す。

図 2 は砂漠 WG での議論から，乾燥地域に向けた持続可能なコミュニティの提案である。

3. IEA/PVPS Task8

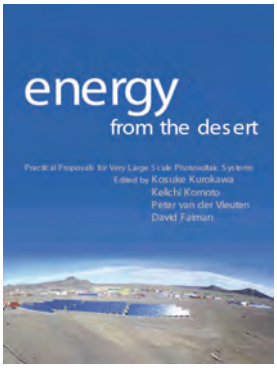

Task8 は砂漠地域における大規模太陽光発電システムの可能性を明らかにするため，1998 年に Task6 Subtask5 として発足し，1999 年に Task8 となった。第一期では主に可能性の検討を実施し，環境性に優れ，モジュールコストが下がれば経済的に成り立つと結果を得て報告書 Energy from the Desert（James and James 社）を発行した。第二期ではいくつかの地域を想定し，より実際的なケーススタディを行い，報告書 Energy from the Desert II（James and James 社）を発行した。現在，第三期が進行中であり，より詳細なケーススタディや，手引き書の作成，将来オプションの検討について議論している。

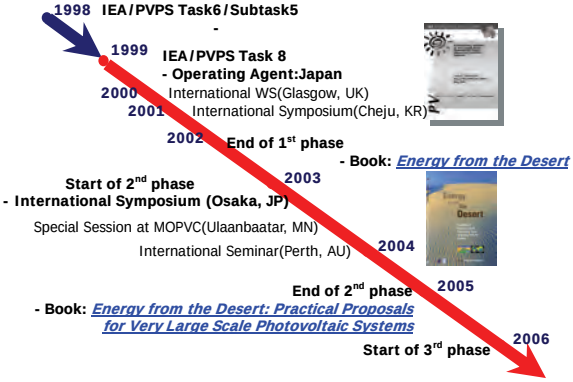

図 3 IEA/PVPS Task8 のこれまでの流れ

東京農工大学　大学院

電気電子工学講座

黒川浩助　研究室

論文リスト[2000 年～2007 年]

東京農工大学 大学院 電気電子工学講座
黒川浩助 研究室 論文リスト[2000 年～2007 年]

〈2000 年〉

(1) 黒川：太陽光発電の現状と展望，計測と制御，Vol.39, No.1, pp.8-13, 2000.
(2) 黒川：太陽光発電の課題と将来展望，エネルギー変換懇話会，日本科学技術振興財団，2000.1.31.
(3) 黒川：太陽光発電システムの動向，日本電気工業会第 27 回新エネルギー講演会，2000.2.10.
(4) 大谷，作田，加藤，杉浦，内田，山口，黒川：住宅用太陽光発電システムの運転特性評価，電気学会新エネルギー環境研究会「再生可能エネルギー」2000.3.15.
(5) 野崎, 秋山, 川口, 黒川 : EDLC 併用型独立型太陽光発電システムに用いるコンバータの設計方法と効率特性，電気学会全国大会，東工大，2000.3.
(6) 川口，黒川，野崎：独立型太陽光発電システムの出力係数に関する検討，電気学会全国大会，東工大，2000.3.
(7) 登守，大谷，作田，黒川：写真測量による日陰推定誤差の検討，電気学会全国大会，東工大，2000.3.
(8) 石川，黒川，岡田，滝川：太陽光発電システム複数連系時における運転特性－電圧上昇抑制特性のモデル化，電気学会全国大会，東工大，2000.3.
(9) 山口，内田，黒川：ＳＶ法による太陽光発電システムの損失因子の詳細化，電気学会全国大会，東工大，2000.3.
(10) 黒川：エネルギー創出時代，住まいの文化誌別巻「地球環境」，ミサワホーム総合研究所刊（著書），2000
(11) 黒川：太陽光発電システム技術動向，シーエムシー，（著書）
(12) 黒川：太陽光発電地域発電特性に関する基礎的問題の解明，第１２回太陽光発電連絡会，虎ノ門，2000,4.17（口頭発表）
(13) K. Kurokawa: PV systems in urban environment, Solar Energy Materials and Solar Cells, ????, 2000. ?.
(14) K. Kurokawa, O. Ikki: The Japanese experiences with national PV system Programme, Solar Energy, Topical Issue on Grid Connected Photovoltaics, 2000.?.
(15) K. Kurokawa, D. Uchida, A. Yamaguchi: Intensive introduction of residential PV systems and their monitoring by citizen-oriented efforts in Japan, 16th EU-PVSEC, Glasgow, May 1-5 2000.
(16) K. Kurokawa, P. Menna, F. Paletta, K. Kato, K. Komoto, T. Kichimi, S. Yamamoto, J. Song, W. Rijssenbeek, P. Van der Vleuten, J. Garcia Martin, A de Julian Palero, G. Andersson, R. Minder, M. Sami Zannoun, M. Aly Helal: A preliminary analysis of very large scale photovoltaic power generation (VLS-PV) systems, 16th EU-PVSEC, Glasgow, May 1-5 2000.
(17) H. Nagayoshi, K. Kurokawa, T. Ohashi, H. Nishita, T. Deguchi: Feasibility study of peak-power reduction system using 100kW PV and battery combined system at Shonan Institute of Technology, 16th EU-PSEC, Glasgow, May 1-5 2000.
(18) K. Kurokawa : Realistic PV Performance Values Obtained by a Number Grid-Connected Systems in Japan, World Renewable Energy Congress, Brighton, July 1-7, 2000 （国際会議）
(19) 黒川：太陽光発電システムの開発動向，第１７回太陽光発電システムシンポジウム，発明会館，2000,6.14-16（口頭発表）
(20) 黒川：太陽光発電の課題と将来展望，第８回高効率太陽電池および太陽光発電システムワークショップ，福井フェニックスプラザ，2000. 7.20-21（招待講演）
(21) 桜井，黒川：太陽電池アレイ分布定数回路シミュレーション～アレイ等価回路の提案～，電気学会電力・エネルギー部門大会，北海道大学，2000.8.2-4
(22) 川口，黒川，野崎：電気二重層キャパシタを組み込んだ独立型太陽光発電システム，電気学会電力・エネルギー部門大会，北海道大学，2000.8.2-4
(23) 輿石，黒川：太陽光発電における最大電力点追従制御システムの評価，電気学会電力・エネルギー部門大会，北海道大学，2000.8.2-4
(24) 石川，黒川，岡田，滝川：太陽光発電システムの複数台連系時における運転特性評価，電気学会電力・エネルギー部門大会，北海道大学，2000.8.2-4
(25) 山口，黒川，都筑，大谷：太陽光発電システムの評価に関する検討～アメダスデータ等を用いた日射量の推定方法～，電気学会電力・エネルギー部門大会，北海道大学，2000.8.2-4
(26) 谷口，大谷，黒川：衛星雲画像を利用した雲アルベドの動的分析，電気学会電力・エネルギー部門大会，北海道大学，2000.8.2-4
(27) H.Taniguchi,K.Otani,K.Kurokawa: The motional analysis of cloud albedo patterns by using GMS images,28th IEEE PVSC, Alaska September 15-22 2000
(28) T.Tomori, K.Otani, K.Sakuta, K.Kurokawai: On-site BIPV array shading evaluation tool using stereo-fisheye photographs,28th IEEE PVSC, Alaska September 15-22 2000
(29) H.Matsukawa,M.Shioya,K.Kurokawa: Study on simple assessment of BIPV power generation for architects,28th IEEE PVSC, Alaska September 15-22 2000
(30) 黒川：エネルギー・環境問題と太陽光発電システムへの期待，NEDO フォーラム２０００，東京ビッグサイト，2000,9.26-28（講演）
(31) 松川，塩谷，黒川，杉浦：太陽光発電システムの建築的利用に関する研究（その１）部分日陰が発電特性に及

ぼす影響評価，日本建築学会，日本大学，2000.9
(32) 塩谷，松川，黒川：太陽光発電システムの建築的利用に関する研究（その２）異傾斜角・異方位角の混在が発電特性に及ぼす影響評価，日本建築学会，日本大学，2000.9
(33) 塩谷，伊藤，松川，黒川，杉浦：建物条件の不均一が太陽光発電システムの発電特性に及ぼす影響評価，日本建築学会，日本大学，2000.9
(34) K. Kurokawa: Solar RD&D in Japan, IEA0CERT Expert Workshop, Paris, France, Oct. 27, 2000（口頭発表）
(35) 石川，黒川，岡田，滝川：太陽光発電システム複数台連系時における運転特性評価―電圧上昇抑制機能の検討―，日本太陽エネルギー学会，No.12，金沢工業大学，2000.11.8-9
(36) 大関，井澤，山口，大谷，黒川：太陽光発電システムの経年特性，日本太陽エネルギー学会，No.14，金沢工業大学，2000.11.8-9
(37) 加藤，大谷，作田，杉浦，黒川：導入地域の広がりを考慮した太陽光発電システムの kW 価値の検討，日本太陽エネルギー学会，No.15，金沢工業大学，2000.11.8-9
(38) 山下，黒川：ＰＶインバータのディジタル制御～ワンチップマイコンによる制御技術～，日本太陽エネルギー学会，No.22，金沢工業大学，2000.11.8-9
(39) 輿石，黒川：太陽光発電システムにおける最大電力点追従制御の評価，日本太陽エネルギー学会，No.25，金沢工業大学，2000.11.8-9
(40) 高宮，黒川：台形公式によるＰＶインバータの動作解析-ＰＶインバータの適正な入力容量のための解析-，日本太陽エネルギー学会，No.26，金沢工業大学，2000.11.8-9
(41) 大谷，加藤，作田，杉浦，黒川：パラメータ分析法を基にした太陽光発電システム・シミュレーションの住宅用システムによる検証，日本太陽エネルギー学会，No.31，金沢工業大学，2000.11.8-9
(42) 桜井，黒川：太陽光発電アレイ分布定数回路シミュレーション～シミュレーション手法の検討～，日本太陽エネルギー学会，No.81，金沢工業大学，2000.11.8-9
(43) 山田，梅谷，中村，杉浦，大谷，作田，黒川：モジュール直並列合成ＩＶカーブを利用した日陰損失シミュレーション技術の開発，日本太陽エネルギー学会，No.92，金沢工業大学，2000.11.8-9
(44) 田村，黒川，大谷：観測日射量の瞬時直散分離に関する研究，日本太陽エネルギー学会，No.126，金沢工業大学，2000.11.8-9
(45) 川口，黒川，野崎，谷内：EDLC を組み込んだ独立型太陽光発電システムのシミュレーション，電子通信エネルギー研究会，機械振興会館，2000.11.17
(46) 黒川：太陽光発電の課題と将来展望，政策総合研究所，エネルギーの有効利用と環境保全，2000.12.10.（執筆原稿）

〈2001 年〉

(1) 黒川：21 世紀に羽ばたく太陽光発電，太陽光発電協会「太陽光発電」誌寄稿，2001.1
(2) 谷口，大谷，黒川：衛星雲画像を用いた雲アルベドの動的分析，電気学会論文誌 B，Vol.121-B, No.2，2001.2
(3) 石川，黒川，岡田，滝川：太陽光発電システム複数台連系時における運転特性評価，電気学会新エネルギー・環境研究会，FTE-01-4，2001.2.21
(4) 井澤，大関，大谷，都筑，黒川：，電気学会全国大会，名古屋大学，2001.3.21-23
(5) 高宮，黒川：ＰＶインバータの適正な入力容量の決定方法に関する研究，電気学会全国大会，名古屋大学，2001.3.21-23
(6) 輿石，黒川，濱田，劉：太陽電池模擬電源による最大電力転追従制御の評価，電気学会全国大会，名古屋大学，2001.3.21-23
(7) Kosuke Kurokawa: PV systems in urban environment, Solar Energy Materials & Solar Cells Vol.67 (2001), Nos.1-4, March 2001,
(8) T.Doi, I.Tsuda, H.Unagida, A.Murata, K.Sakuta, K.Kurokawa: Experimental study on PV module recycling with organic solvent method, Solar Energy Materials & Solar Cells, Vol.67 (2001) , Nos.1-4, March 2001
(9) H.Unozawa, K.Otani, K.Kurokawa: A simplified estimating method for in-plane irradiation using minute horizontal irradiation, Solar Energy Materials & Solar Cells, Vol.67 (2001) , Nos.1-4, March 2001
(10) H.Taniguchi, K.Otani, K.Kurokawa: Hourly forecast of global irradiation using GMS staellite images, Solar Energy Materials & Solar Cells, Vol.67 (2001) , Nos.1-4, March 2001
(11) D.Uchida, K.Otani, K.Kurokawa: Evaluation of effective shading factor by fitting a clear-day pattern obtained from hourly maximum irradiance data, Solar Energy Materials & Solar Cells, Vol.67 (2001), Nos.1-4, March 2001
(12) M.Kusakawa, H.Nagayoshi, K.kamisako,K.Kurokawa: Further improvement of a transformerless, voltage-boosting inverter for AC modules, Solar Energy Materials & Solar Cells, Vol.67 (2001) , Nos.1-4, March 2001
(13) 黒川：明日の世界を支える太陽光発電エネルギー，春期応用物理学関係連合講演会シンポジウム「太陽光発電-現在から未来へ-」，明治大学，2001.3.28-31

(14) 黒川：都市地域における太陽光発電地域特性に関する基礎的問題の解明，H12 年度 NEDO 委託業務成果報告書，2001.3.
(15) 黒川：太陽光発電用分散型パワーコンディショナの研究開発，NEDO 地域コンソーシアム研究開発委託業務成果報告書，2001.3.
(16) 黒川：太陽光発電と分散電源，名古屋大学大学院集中講義，2001.05.17.
(17) K.Kurokawa, O.Ikki: The Japanese experiences with national PV system Programmes, Solar Energy, Vol.70, No.6 (Topical Issue on Grid Connected Photovoltaics), June 2001
(18) 黒川：太陽光発電システムの開発動向，18 回太陽光発電システムシンポジウム，イイノホール，2001.6.5-7.
(19) Kosuke Kurokawa: TOWARD LARGE-SCALE PV POWE GENERATION, 12th PVSEC, JEJU,June 11-15 2001
(20) M.Ito, K.Kato, H.Sugihara, T.Kichimi, J.Song, K.Kurokawa: A Preliminary Study on Potential for Very Large-Scale Photovoltaic Power Generation (VLS-PV) System on the Gobi Desert from Economic and Environmental Viewpoints, 12th PVSEC, JEJU,June 11-15 2001
(21) P.Menna, U.Ciorba, F.Pauli, K.Komoto, K.Kato, J.Song, K.Kurokawa: Analysis of the Impacts of Transferring a Photovoltaic Module Manufacturing Facility, 12th PVSEC, JEJU,June 11-15 2001
(22) T.Ishikawa, K.Kurokawa, N.Okada, K.Takigawa: EVALUATION OF OPERATION CHARACTERISTICS IN MULTIPLE INTERCONNECTION OF PV SYSTEMS, 12th PVSEC, JEJU,June 11-15 2001
(23) H.Matsukawa, K.Koshiishi, H.Koizumi, K.Kurokawa, M.Hamada, L.Bo: Dynamic Evaluation of Maximum Power Point Tracking Operation with PV array Simulator, 12th PVSEC, JEJU,June 11-15 2001
(24) J.Tamura, K.Kurokawa, K.Otani: A study of measuring estimating for in-plane irradiation using minute horizontal Global Irradiation, 12th PVSEC, JEJU,June 11-15 2001
(25) A.Yamaguchi, K.Kurokawa, T.Uno, M.Takahashi: Reflection and Absorption Characteristics of Electromagnetic Waves for PV Modules, 12th PVSEC, JEJU,June 11-15 2001
(26) K.Otani, K.Sakuta, T.Tomori, K.Kurokawa: Shading loss analysis of PV systems in urban area, 12th PVSEC, JEJU,June 11-15 2001
(27) T.Oozeki, T.Izawa, K.Otani, K.Kurokawa: The Evaluation Method of PV Systems, 12th PVSEC, JEJU,June 11-15 2001
(28) T.Sugiura, T.Yamada, H.Nakamura, M.Umeya, K.Sakuta, K.Kurokawa: Measurements, Analysis and Evaluation of Residential PV Systems by Japanese Monitoring Program, 12th PVSEC, JEJU,June 11-15 2001
(29) J.Song, K.Kurokawa, P.Menna, K.Kato, N.Enebish, D.Collier, S.C.Shin: International Symposium on “Potential of Very Large Scale Power Generation System on Desert, 12th PVSEC, JEJU,June 11-15 2001
(30) Y.Nozaki, K.Akiyama, T.Yachi, H.Kawaguchi, K.Kurokawa: Operating characteristics of an EDLC-battery hybrid stand-alone photovoltaic system, IECE Tans Communications, E84B (7), July 2001
(31) K.Kurokawa: The state-of-the-art in Photovoltaic, 1st MOPVC, Ulaanbaatar, September 5-7 2001
(32) K.Otani: Solar Energy Mapping for Eastern Asia by Satellite Images, 1st MOPVC, Ulaanbaatar, September 5-7 2001
(33) M.Ito, Kazuhiko Kato, Hiroyuki Sugihara, Tetsuo Kichimi, Jinsoo Song, Kosuke Kurokawa: A life-cycle analysis of Very Large Scale Photovoltaic (VLS-PV) System in the Gobi desert, 1st MOPVC, Ulaanbaatar, September 5-7 2001
(34) A.Amarbayar, K.Kurokawa: Performance analysis of Portable photovoltaic power generation systems based on measured data in Mongolia, 1st MOPVC, Ulaanbaatar, September 5-7 2001
(35) 黒川：日本における太陽光発電の現状と今後の動向，関電工太陽光発電国際シンポジウム「太陽光発電は地球を救えるか」，品川コクヨホール，2001.9.18
(36) 黒川：太陽光発電にかける夢，NEDO フォーラム-パネル太陽技術分科会，ホテルニューオータニ，2001.9.20
(37) K.Otani, K.Sakuta, T.Sugiura, K.Kurokawa: Performance analysis and simulation on 100 Japanese residential grid-connected PV systems based on four years’ experience, 17th EU-PVSEC, Munich, October 22-26 2001
(38) M.Ito, K.Kato, H.Sugihara, T.Kichimi, J.Song, K.Kurokawa: A Preliminary Study on Potential for Very Large-Scale Photovoltaic Power Generation System (VLS-PV) on the World Desert, 17th EU-PVSEC, Munich, October 22-26 2001
(39) J.Tamura, K.Kurokawa, K.Otani: Measuring and estimating for In-plane Irradiation, 17th EU-PVSEC, Munich, October 22-26 2001
(40) A.Yamaguchi, K.Kurokawa, T.Uno, M.Takahashi: A New Added Value of Photovoltaic Module ~Absorption Characteristics of Electromagnetic wave~, 17th EU-PVSEC, Munich, October 22-26 2001
(41) H.Koizumi, T.Kaito, Y.Noda, K.Kurokawa, M.Hamada, L.Bo: Dynamic Response of Maximum Power Point Tracking Function forIrradiance and Temperature Fluctuation in Commercial PV Inverters, 17th EU-PVSEC, Munich, October 22-26 2001
(42) 黒川：最近の太陽光発電研究・成果と今後の動向，田友会，学士会館，2001.11.09
(43) 野田，水野，小泉，黒川：太陽光発電が連系した配電系統のシミュレータの開発，日本太陽エネルギー学会，徳島文理大学，2001.11.8-9
(44) 山下，小泉，黒川，名島，川崎：PV インバータのディジタル制御，日本太陽エネルギー学会，徳島文理大学，2001.11.8-9

(45) 登守，大谷，作田，大野，飯田，黒川：都市環境における太陽光発電システムの日陰評価法，日本太陽エネルギー学会，徳島文理大学，2001.11.8-9
(46) 中村，杉浦，高橋，黒川：複数面設置された住宅用太陽光発電システムの発電量推定について，日本太陽エネルギー学会，徳島文理大学，2001.11.8-9
(47) アマルバヤル，黒川：モンゴルにおける携帯型発電システム実証研究のデータ解析・システム評価，日本太陽エネルギー学会，徳島文理大学，2001.11.8-9
(48) 井澤，大関，大谷，都築，黒川：太陽光発電システム計測データの品質診断法，日本太陽エネルギー学会，徳島文理大学，2001.11.8-9
(49) 大関，井澤，大谷，黒川：太陽光発電システムの計測データを用いた評価方法，日本太陽エネルギー学会，徳島文理大学，2001.11.8-9
(50) 竹内，金井，黒川：太陽電池単セルによる充電回路，電子情報通信学会電子通信エネルギー技術研究会，信学技報 EE 2001-33(2001-11)
(51) 黒川：太陽光発電の課題と将来展望，新政策（政策総合研究所），2001.11
(52) 黒川：太陽光発電技術の現状と将来動向，横浜市工業技術支援センター，2001.12.11

〈2002 年〉

(1) 黒川：太陽光発電システムの新展開，光協会成果報告書，2002.3
(2) 黒川：21 世紀世界の主役「太陽光発電」，JPEA 誌「光発電」，2002.2
(3) 黒川：私の学生時代，グリーンキャンパス，2002.3
(4) 黒川：世界へ向けた長期的な産業戦略が望まれる，PVTEC ニュース，2002.3
(5) 竹内，金井，黒川：太陽電池単セル昇圧回路への MPPT 制御の適用，日本機械学会情報・知能・精密機械部門，東京工業大学，2002.3.26
(6) 高橋，谷口，大谷，黒川：衛星雲画像の空間周波数を用いた日射量予測法の研究，電気学会全国大会，工学院大学，2002.3.26-29
(7) 大関，井澤，大谷，中村，高橋，杉浦，黒川：電圧上昇抑制運転状態の実例と SV 法解析結果との比較検討，電気学会全国大会，工学院大学，2002.3.26-29
(8) Paulo Sergio Pimentel, H. Matsukawa, T. Oozeki, T. Tomori, K. Kurokawa: PV System Integrated Evaluation Software, 29th IEEE PVSC, New Orleans, May 19-26 2002
(9) A. Amarbayar, K. Kurokawa: PERFORMANCE ANALYSIS OF PORTABLE PHOTOVOLTAIC POWER GENERATION SYSTEMS BASED ON MEASURED DATA IN MONGOLIA, 29th IEEE PVSC, New Orleans, May 19-26 2002
(10) Y. Noda, T. Mizuno, H. Koizumi, K. Nagasaka, K. Kurokawa: THE DEVELOPMENT OF A SCALED-DOWN SIMULATOR FOR DISTRIBUTION GRIDS AND ITS APPLICATION FOR VERIFYING INTERFERENCE BEHAVIOR AMONG A NUMBER OF MODULE INTEGRATED CONVERTERS (MIC), 29th IEEE PVSC, New Orleans, May 19-26 2002
(11) K. Kurokawa, K. Kato, M. Ito, K. Komoto, T. Kichimi, H. Sugihara: A COST ANALYSIS OF VERY LARGE SCALE PV (VLS-PV) SYSTEM ON THE WORLD DESERTS, 29th IEEE PVSC, New Orleans, May 19-26 2002
(12) A. Amarbayar, K. Kurokawa: PERFORMANCE ANALYSIS OF PORTABLE PHOTOVOLTAIC POWER GENERATION SYSTEMS BASED ON MEASURED DATA IN MONGOLIA, WREC-7, Warszawa, June 29 – July 5 2002
(13) 水野，野田，小泉，黒川：商用 PV インバータの単独運転検出要因の推定，電気学会部門大会，福井大学，2002.8.7-9
(14) 皆藤，五島，川崎，小泉，黒川：ディジタルインバータにおける MPPT 制御の検討，電気学会部門大会，福井大学，2002.8.7-9
(15) 谷口，高橋，大谷，黒川：AC モデルを用いた衛星雲画像による日射量予測の検討，電気学会部門大会，福井大学，2002.8.7-9
(16) H. Koizumi, K. Nagasaka, K. Kurokawa, N. Goshima, M. Kawasaki, Y. Yamashita, A. Hashimoto: DEVELOPMENT OF INTERCONNECTING MICRO CONTROLLER FOR PV SYSTEMS IN JAPAN, PV in Europe Conference and Exhibition From PV Technology to Energy Solutions, Rome, October 6-11 2002
(17) T. Mizuno, T. Ishikawa, Y. Noda, H. Koizumi, K. Kurokawa, Y. Arai, N. Goshima, M. Kawasaki, H. Kobayashi: THE ISLANDING DETECTION ALGORITHM OF A NEW AC MODULE FOR THE GRID CONNECTION IN JAPAN, PV in Europe Conference and Exhibition From PV Technology to Energy Solutions, Rome, October 6-11 2002
(18) 井澤，大関，黒川，大谷，都筑：太陽光発電システムの簡易評価，日本太陽エネルギー学会，仙台国際センター，2002.11.7-8
(19) 田村，大谷，黒川：多傾斜面日射量の測定と評価に関する研究，日本太陽エネルギー学会，仙台国際センター，2002.11.7-8
(20) 伊藤，加藤，河本，杉原，吉見，黒川：ゴビ砂漠における大規模太陽光発電システムのライフサイクル評価，日本太陽エネルギー学会，仙台国際センター，2002.11.7-8

〈2003 年〉

(1) 伊藤，加藤，河本，杉原，吉見，黒川：世界の砂漠における 100MW 大規模太陽光発電システム(VLS-PV)のライフサイクル評価, 第19回エネルギーシステム・経済・環境コンファレンス, 虎ノ門パストラル, 2003.1.30-31

(2) パウロ，松川，大関，黒川：太陽光発電システム発電特性の統合評価ソフトウェア(PVI)の住宅用システムによる検証，電気学会全国大会，東北学院大学，2003.3.17-19

(3) 高橋，谷口，黒川，大谷：衛星雲画像の空間周波数分析を用いた日射予測，電気学会全国大会，東北学院大学，2003.3.17-19

(4) 皆藤，小泉，黒川，五島，川崎：太陽光発電用インバータ向けディジタル MPPT 法の開発，電気学会全国大会，東北学院大学，2003.3.17-19

(5) 公楽，黒川：LED ソーラーシミュレータによる太陽電池新測定法，電気学会全国大会，東北学院大学，2003.3.17-19

(6) 岡田，小林，石川，滝川，黒川：ループコントローラによる系統故障時の区間自立運転のための潮流制御の検討，電気学会全国大会，東北学院大学，2003.3.17-19

(7) 黒川：アジアにおける PV 技術開発／導入普及の現状と今後の課題，第２回 アジアに於ける PV 技術開発／導入普及の現状と将来展望，東京国際交流館, PVTEC/JEMA，2003.2.14

(8) 黒川：太陽光発電のトピックス～WCPEC-3 へ向けて，2003 年春季 50 回応物学会，神奈川大 2003.3.27-30

(9) 黒川：わが家の エネルギー・太陽光発電，国立科学博物館，2003.3.29

(10) 黒川：太陽光発電システムの新展開，光協会成果報告書, 2003.3.

(11) K. Kurokawa, editor.: Energy from the Desert, James & James Ltd., May, 2003(単行本)

(12) M. Ito, K. Kato, K. Komoto, T. Kichimi, K. Kurokawa: An analysis of variation of very large-scale PV (VLS-PV) systems in the world deserts, WCPEC-3, Osaka, May 11-18

(13) T. OOZEKI, T. IZAWA, H. KOIZUMI,K. OTANI, K. KUROKAWA: An evaluation result of PV system field test program for indusry use by means of the SV method, WCPEC-3, Osaka, May 11-18, 2003

(14) H. Matsukawa, Paulo Sergio Pimentel, T. Izawa, S. Ike, H. Koizumi, K. Kurokawa: An Integrated design software for photovoltaic systems, WCPEC-3, Osaka, May 11-18

(15) S. Kohraku, K. Kurokawa: New methods for solar cell measurement by LED solar simulator, WCPEC-3, Osaka, May 11-18

(16) H. Koizumi, K. Nagasaka, K. Kurokawa, N. Goshima, M. Kawasaki, Y. Yamashita, A. Hashimoto: Interconnecting micro controller for PV systems in Japan, WCPEC-3, Osaka, May 11-18

(17) K. Takeuchi, H. Koizumi, K. Kurokawa: A new type of scaled-down network simulator composed of power electronics, WCPEC-3, Osaka, May 11-18

(18) T. Mizuno, Y. Noda, H. Koizumi, K. Nagasaka, K. Kurokawa, H.Kobayashi: The experimental results of islanding detection method for Japanes AC modules, WCPEC-3, Osaka, May 11-18

(19) Batsukh, D. Ochirvaani, Ch. Lkhagvajav, N. Enebish, Ts. Baatarchuluun, K. Otani, Koichi Sakuta, A. Amarbayar, K. kurokawa: Evaluation of solar energy potentials in Gobi desert area of Mongolia, WCPEC-3, Osaka, May 11-18

(20) Junsetsu Tamura, Hiroyuki Nakamura, Yoshinori Inoue, Kenji Otani, Kosuke Kurokawa: A new method of calculating in-plane irradiation by one-minute local solar irradiance, WCPEC-3, Osaka, May 11-18

(21) A.Adiyabat, K. Kurokawa: An Optimal design and use of solar home system in Mongolia, WCPEC-3, Osaka, May 11-18

(22) N. Okada, H. Kobayashi, K. Takigawa, M. Ichikawa, K. Kurokawa: Loop power flow controll and volatge characteristics of distribution system for distributed generation including PV system, WCPEC-3, Osaka, May 11-18

(23) N. Okada, T. Nanahara, K. Kurokawa: Estimation of distribution system load characteristics with time series data of PV system output, WCPEC-3, Osaka, May 11-18

(24) Namjil Enebish, M. Battushig, M. Altanbagana, K. Otani, K. Sakuta, A. Adiyabat, K. Kurokawa: Performance monitoring of PV modules for VLS-PV systems in Gobi desert of Mongolia, WCPEC-3, Osaka, May 11-18

(25) K. Sakakibara M. Ito, K. Kurokawa: A resource analysis on solar photovoltaic generation by a remote sensing approach,, WCPEC-3, Osaka, May 11-18

(26) 黒川：太陽光発電システムの普及とその可能性，太陽光発電所ネットワーク設立記念シンポジウム，国連大学会議場, 2003.5.24

(27) 黒川：シンポジウム２０年の歩み，第 20 回太陽光発電システムシンポジウム, 2003.7.1-3

(28) 黒川：太陽光発電システムの研究開発の方向性，第 20 回太陽光発電システムシンポジウム, 2003.7.1-3

(29) 松川，山田，塩谷，黒川：多面アレイ構造太陽光発電システムに対応したシミュレーション・ツールの開発，電気学会電力・エネルギー部門大会，東京電機大学, 2003.8.6-8

(30) 嶋田，黒川，吉岡：蓄電池あり系統連系太陽光発電システム，電気学会電力・エネルギー部門大会，東京電機大学, 2003.8.6-8

(31) 市川，岡田，黒川：系統故障時における BTB 式ループコントローラの特性解析，電気学会電力・エネルギー部門大会，東京電機大学, 2003.8.6-8

(32) 井上，黒川，三宅，中村，加藤：デュアルセンサ型日射計の開発，電気学会電力・エネルギー部門大会，東京電機大学, 2003.8.6-8
(33) M. Ito, K. Kato, K. Komoto, T. Kichimi, H. Sugihara, K. Kurokawa: An analysis of very Large-scale tracking PV (VLS-PV) sysytems in the world deserts, 2nd Mogolian PV Conf., Ulaanbaatar, 2003.9.4-6
(34) A. Adiyabat, K. Kurokawa: An optimal design and use of solar home system in Mongolia, 2nd Mogolian PV Conf., Ulaanbaatar, 2003.9.4-6
(35) K. Kurokawa: The State-of-art in Photovoltaic Research and Development, 2nd Mogolian PV Conf., Ulaanbaatar, 2003.9.4-6
(36) K. Komoto, K. Kato, K. Kurokawa: Scenario Study on Very Large Scale Photovoltaic (VLS-PV) Power Generation System for the Sustainable Growth, 2nd Mogolian PV Conf., Ulaanbaatar, 2003.9.4-6
(37) K. Kato, K. Otani, K. Komoto, M. Ito, K. Kurokawa, J. Song, D. Faiman, Peter van der Fleuten, L. Verhoef, D. Collier and N. Enebish: Study on Very Large-Scale Photovoltaic Power Generation System on Deserts Extended Activity of IEA/PVPS Task 8 from 2003 to 2005 –,2nd Mogolian PV Conf., Ulaanbaatar, 2003.9.4-6
(38) K. Kato, K. Otani, K. Komoto, M. Ito and K. Kurokawa: Cost estimation of Very Large-Scale Photovoltaic Power Generation System on World Deserts, 2nd Mogolian PV Conf., Ulaanbaatar, 2003.9.4-6
(39) M.Battushig, N.Enebish, M.Altanbagana, Ch.Lkhagvajav, K. Otani, K. Sakuta, K. Kurokawa, A.Amarbayar: Performance monitoring of PV modules for VLS-PV systems in Gobi desert of Mongolia, 2nd Mogolian PV Conf., Ulaanbaatar, 2003.9.4-6
(40) A. Adiyabat, K. Kurokawa: Techno-economics analysis of PV /Wind/ Diesel Hybrid systems in Villages of Mongolia, 2nd Mogolian PV Conf., Ulaanbaatar, 2003.9.4-6
(41) K. Kurokawa: Very Large-Scale PV (VLS-PV) System: Its background and concept, 2nd Mogolian PV Conf., Ulaanbaatar, 2003.9.4-6
(42) T. Shimada, K. Kurokawa, T. Yoshioka : Grid-connected Photovoltaic System with Battery, STORE, Aix en Provence, 2003.10.20-21
(43) M. Ito, T. Nishimura, K. Kurokawa: A Preliminary Study on Utilization of Desert with Agricultural Development and Photovoltaic Technology - Potential of Very Large-scale Photovoltaic Power Generation (VLS-PV) systems -,Desert Technology 7, 2003.11.9-14
(44) K. Kato, K. Otani, K. Komoto, M. Ito, K. Kurokawa, J. Song, D. Faiman, Peter van der Fleuten, L. Verhoef, P.Menna, D. Collier, N. Enebish: 'Energy from the Desert' - Feasibility Study on Very Large-Scale Photovoltaic Power Generation System on Desert Areas -, Desert Technology 7, 2003.11.9-14
(45) K. Sakakibara, M. Ito, K. Kurokawa: A Resource Analysis on Solar Photovoltaic Generation System on the Gobi Desert by a Remote Sensing Approach, Desert Technology 7, 2003.11.9-14
(46) K. Kurokawa: Considerations on technological standardization in sloar photovoltaics, 1st Renewable Energy Forum in North-East Asia, Nov. 10-11, 2003
(47) 大関，小泉，黒川，大谷：蓄電池付き太陽光発電システムの評価方法の開発，日本太陽エネルギー学会，足利工業大学, 2003.11.6-7.
(48) 公楽，黒川：離散光波長型ＬＥＤソーラーシミュレータの原理実験，日本太陽エネルギー学会，足利工業大学, 2003.11.6-7.
(49) 竹内，小泉，黒川：超縮小規模配電系統を用いたＰＶインバータ試験装置の基本原理，日本太陽エネルギー学会，足利工業大学, 2003.11.6-7.
(50) 黒川：市民のエネルギー・太陽光発電システム，小金井市民講座，2003.11.15.
(51) 黒川：100 年先から見てみよう-新エネルギー・物質代謝と生存科学の構築，産総研 LCA 研究センター：地域施策への LCA の新たな展開，2003.11.21.
(52) 黒川：21 世紀を担うエネルギー・太陽光発電，月刊オプトロニクス 2004 年 1 月号, 2004.1

〈2004 年〉

(1) 黒川：21 世紀を担うエネルギー・太陽光発電，月刊オプトロニクス 2004 年 1 月号，2004.1
(2) M. Ito, K. Kato, K. Komoto, T. Kichimi, H. Sugihara, K. Kurokawa: An Analysis of Very Large-Scale PV (VLS-PV) Systems Using Amorphous Silicon Solar Cells in the Gobi Desert, PVSEC-14, Bangkok, 2004.1.26-30
(3) K. Sakakibara, M. Ito, K. Kurokawa: A Resource Analysis on Solar Photovoltaic Generation System in the Gobi Desert by a Remote Sensing Approach, PVSEC-14, Bangkok, 2004.1.26-30
(4) T. Oozeki, T. Izawa, H. Koizumi, K. Otani, K. Tsuzuku, T. Koike, K. Kurokawa: A Performance Evaluation by Only One Monitoring Data Item for Citizens' PV House Project, PVSEC-14, Bangkok, 2004.1.26-30
(5) K. Takeuchi, T. Kaito,T. Mizuno, T. Oozeki, H. Koizumi and K. Kurokawa: Development of Ultra-Small-Scaled-Down Network Simlator for Testing PV Inverter Functions, PVSEC-14, Bangkok, 2004.1.26-30
(6) H. Tada, K. Kurokawa, T. Uno, M.Takahashi, S. Yatabe: Reflection and Absorption Characteristics of Electromagnetic Waves by PV Modules, PVSEC-14, Bangkok, 2004.1.26-30
(7) S. Kohraku, K. Kurokawa: A fundamental experiment for discrete-wavelength LED solar simulator, PVSEC-14, Bangkok, 2004.1.26-30
(8) N. Okada, M. Ichikawa, K. Kurokawa: Experiment and Evaluation of Loop Power Flow Control for

Distribution System Adaptable to a Large Number of Distributed PV Systems, PVSEC-14, Bangkok, 2004.1.26-30
(9) N. Kawasaki, T. Oozeki, K. Otani, K. Kurokawa: An Evaluation Method of the Fluctuation Characteristics of Photovoltaic Systems by Using Frequency Analysis, PVSEC-14, Bangkok, 2004.1.26-30
(10) A. Adiyabat, K. Kurokawa: Photovoltaic Systems for Village Electrification in Mongolia: Techno-Economic Analysis of Hybrid System in Rural Commnunity Centers, PVSEC-14, Bangkok, 2004.1.26-30
(11) T. Kaito, H. Koizumi, N. Goshima, M.Kawasaki, K. Kurokawa: Development of MPPT Algorithm for a Digital Controlled PV Inverter, PVSEC-14, Bangkok, 2004.1.26-30
(12) H. Matsukawa, H. Koiumi, K. Kurokawa: A Thermal Analysis for Photovoltaic Systems at Short Time Interval, PVSEC-14, Bangkok, 2004.1.26-30
(13) K. Kurokawa: Recent Advances in Solar PV System Engineering, PVSEC-14, Bangkok, 2004.1.26-30
(14) G. Yu, K. S. Lee, Y.S. Jung, J. So, J.H. Choi, K. Kim, K. Kurokawa: PVSEC-14, Bangkok, 2004.1.26-30
(15) K. Kurokawa: The state-of-art of photovoltaics in Asia, 3rd PVTEC Asia Seminar, Kasumigaseki Bldg. Feb. 9, 2004.
(16) 黒川：ＰＶ開発の方向性，JPEA 誌「光発電」，No.27，2004.3.
(17) 池，黒川：写真測量法による太陽光発電システムの日射障害物の推定，電気学会全国大会，青山学院大学，2004.3.17-3.19
(18) 井上, 黒川, 三宅, 中村, 加藤:デュアルセンサ型日射計の開発, 電気学会全国大会, 青山学院大学, 2004.3.17-3.19
(19) 黒川：太陽光発電システムの新展開，光協会成果報告書, 2004.2.修正
(20) 松川，山田，塩谷，黒川：多面アレイ構造太陽光発電システムに対応したシミュレーション・ツールの開発，電気学会 B 部門誌, Vol.124, No.3, pp.447-454, 2004.3
(21) K. Kurokawa: The state-of-art of photovoltaics in Asia, 3rd PVTEC Asia Seminar, Kasumigaseki Bldg. Feb. 9, 2004
(22) 黒川：ＰＶ開発の方向性，JPEA 誌「光発電」，No.27，2004.3, p.26-35
(23) 黒川：市民のエネルギー・太陽光発電システム，シロウマサイエンス・セミナー，黒部，2004.4.23.
(24) K. Kurokawa: State-of-art in PV research and development, INRST Seminar, Borji Cedria, Tunis, 4 May 2004.
(25) K. Kurokawa: Future target and recent advances in solar PV system engineering, 1st AIST RC-PV Workshop, 12 May 2004.
(26) K. Kurokawa: Future target and recent advances in solar PV system engineering, 三菱重工諫早工場セミナー, 14 May 2004.
(27) H. Koizumi, K. Kurokawa, S. Mori: Analysis of Class D inverter with irregular driving patterns, IEEE International Symposium on Circuits and Systems 2004 (ISCAS 2004), Vancouver, Canada, 2004.5
(28) K. Kurokawa: PV in Tunisian Sahara, IEA PVPS Task 8 expert meeting, Paris, 6 June 2004
(29) K. Kurokawa, F. Aratani: Perceived technical issues accompanying large PV development and Japanese "PV2030" 19th EU-PVSEC, Paris, 2004.6.7-11
(30) T. Oozeki, H. Koizumi, K. Otani, and K. Kurokawa: IDENTIFING OPERATION STATUSES OF GRID CONNECTED PV SYSTEMS WITH BATTERIES UNDER LIMITED DATA ITEMS - APPLYING THE SV METHOD TO EVALUATE GRID CONNECTED PV SYSTEMS WITH BATTERIES", 19th EU-PVSEC, Paris, 2004.6.7-11
(31) M. Ito, K. Kato, K. Komoto, T. Kichimi, H. Sugihara, K. Kurokawa : COMPARATIVE STUDY OF FIXED AND TRACKING SYSTEM OF VERY LARGE-SCALE PV (VLS-PV) SYSTEMS IN THE WORLD DESERTS, 19th EU-PVSEC, Paris, France, 2004.6.7-11
(32) 黒川：サンシャイン計画から 30 年　技術開発と今後の見通し，第 21 回太陽光発電システムシンポジウム，朝日ホール, 2004.6.16～18
(33) K. Kurokawa: PV in Tunisian Sahara, JBIC-Tunisia Seminar, Tokyo, 14 July 2004.
(34) 黒川：太陽光発電システム　－　今後の方向性，新日本石油本社セミナー, 2004.7.29.
(35) H. Koizumi, K. Kurokawa: Analysis of Class DE inverter with thinned-out driving patterns, 35th IEEE Power Electronics Specialists Conference 2004 (PESC 2004), Aachen, Germany, 2004.6
(36) 岡田，市川，黒川：BTB 式ループコントローラと需給バランスの検討，電気学会電力・エネルギー部門大会，名古屋大学，2004.8.5-7
(37) 五十嵐，末永：太陽電池からの電磁雑音，電気学会電力・エネルギー部門大会，名古屋大学，2004.8.5-7
(38) 五十嵐，末永：太陽光発電システム用パワーコンディショナの電磁環境性，電気学会電力・エネルギー部門大会，名古屋大学，2004.8.5-7
(39) 大関，井澤，都筑，大谷，黒川：太陽光発電システムの評価に関する日射量の推定方法，電気学会電力・エネルギー部門大会，名古屋大学，2004.8.5-7
(40) 植田，大関，黒川，伊藤，北村，宮本，横田，杉原：集中連系型太陽光発電システム実証研究におけるシステム運転性能の測定評価手法，電気学会電力・エネルギー部門大会，名古屋大学，2004.8.5-7
(41) 市川，岡田，黒川：BTB 式ループコントローラと過渡的な需給バランスのシミュレーション，電気学会電力・エネルギー部門大会，名古屋大学，2004.8.5-7
(42) 多田，黒川，宇野，高橋，谷田部：太陽電池の電磁波反射・吸収特性に関する研究，電気学会電力・エネルギ

一部門大会，名古屋大学，2004.8.5-7
(43) 中田，大関，黒川，小池：住宅用太陽光発電システムの長期運転特性の評価に関する研究，電気学会電力・エネルギー部門大会，名古屋大学，2004.8.5-7
(44) 川崎，大関，大谷，黒川：太陽光発電システム変動特性の評価，電気学会電力・エネルギー部門大会，名古屋大学，2004.8.5-7
(45) K. Kurokawa: 100 year sustainability scenario in solar photovoltaic, Workshop on Sustainability and Survival Paths over 100 years, Denver, Aug. 29, 2004
(46) K. Kurokawa: Energy from the Desert, WREC-8. Denver, PV064, Aug. 30-Sept. 3, 2004
(47) A. Adiyabat, K. Kurokawa, K. Otani, N. Enebish,G. Batsukh, M. Battushig, D. Ochirvaani, B. Ganbat: EVALUATION OF SOLAR ENERGY POTENTIAL AND PV MODULE PERFORMANCE IN THE GOBI DESERT OF MONGOLIA, 8th WREC, Denver, 2004.8.26-9.3
(48) M. Ito, K. Kato, T. Kichimi, H. Sugihara, K. Kurokawa : Comparative Study on Potential of Very Large-Scale PV Systems (VLS-PV) in the Gobi and Sahara Desert, 8th WREC, Denver, 2004.8.26-9.3
(49) 津野，菱川，黒川：多接合太陽電池における各要素セルの I-V 特性の分離法の検討，応用物理学会，2004.09.01-04
(50) 黒川：Future target and recent advances in solar PV system engineering，富士電機アドバンストテクノロジー・セミナー，2004.9.10
(51) 畠山，高橋，宇野，有馬，黒川：太陽電池モジュールによる地上デジタル放送波の反射損失，電子情報通信学会論文誌, Vol.J87-B, No.9, 2004.9
(52) 黒川：２１世紀人類のための太陽光発電，第３回英弘シンポジウム「太陽光発電への期待」，学士会館，2004.10.12
(53) M. Ito, T. Nishimura, K. Kurokawa: A preliminary study on utilization of desert with agricultural development and photovoltaic technology potential of vry large -scale photovoltaic power generation (VLS-PV) systems, Journal of Arid Land Studies (日本沙漠学会誌「沙漠研究」), Vol.14S, October 2004
(54) 松川，黒川：太陽電池モジュールの短時間間隔における温度特性解析，日本太陽エネルギー学会，北九州研究学園都市，2004.11
(55) 筒井，佐々木，黒川：新型太陽光発電モジュールのシステム特性検証研究，日本太陽エネルギー学会，北九州研究学園都市，2004.11
(56) 植田，大関，黒川，伊藤，北村，宮本，横田，杉原：太陽光発電システムにおけるアレイ面方位角の推定手法，日本太陽エネルギー学会，北九州研究学園都市，2004.11
(57) 池，黒川：写真測量法による太陽光発電システムの日影予測，日本太陽エネルギー学会，北九州研究学園都市，2004. 11
(58) 津野，菱川，黒川：多接合太陽電池における各要素セルの I-V 特性分離法の検討，日本太陽エネルギー学会，北九州研究学園都市，2004.11
(59) 川崎，大関，大谷，北村，杉原，西川，黒川：太陽光発電システム変動特性評価法の研究，日本太陽エネルギー学会，北九州研究学園都市，2004.11
(60) H. Koizumi, K. Kurokawa: Analysis of Class E inverter with switch-voltage elimination, The 30th Annual Conference of the IEEE Industrial Electronics Society (IECON 2004), Busan, Korea, 2004.11
(61) 大関，井澤，都筑，大谷，黒川：太陽光発電における計測データの品質診断方法，太陽エネルギー，Vol.30,No.6, pp47-55，2004.11

〈2005 年〉

(1) 大関，井澤，都筑，大谷，黒川，「太陽光発電システムの評価に関する日射量の推定方法」，電気学会部門誌 B, pp118-126，125 巻 1 号，2005.1
(2) K. Kurokawa: PHOTOVOLTAIC TECHNOLOGY DIRECTION - JAPANESE "PV2030", 31st IEEE PVSC, Orland, Florida, 2005.1.3-7
(3) H. Matsukawa, K. Kurokawa: Temperature Fluctuation Analysis of Photovoltaic Modules at Short Time Interval, 31st IEEE PVSC, Orland, Florida, 2005.1.3-7
(4) T. Oozeki, K. Otani, and K. Kurokawa, "Accuracy of estimated shading loss ratio by means of the SV method ~ An extraction algorithm of maximum pattern ~, 31st IEEE PVSC, Orland, Florida, 2005.1.3-7
(5) M. Ito, K. Kato, K. Komoto, T. Kichimi, K. Kurokawa: Analysis of transmission losses of Very Large-Scale Photovoltaic power generation systems (VLS-PV) in world desert, 31st IEEE PVSC, Orland, Florida, 2005.1.3-7
(6) H. Igarashi, S. Suenaga:Electromagnetic Noise from Solar Cells, 31st IEEE PVSC, Orland, Florida, 2005.1.3-7
(7) Y. Ueda, T. Oozeki, K. Kurokawa, T. Itou, K. Kitamura, Y. Miyamoto, M. Yokota, H. Sugihara, S. Nishikawa: ANALYTICAL RESULTS OF OUTPUT RESTRICTION DUE TO THE VOLTAGE INCREASING OF POWER DISTRIBUTION LINE IN GRID-CONNECTED CLUSTERED PV SYSTEMS, 31st IEEE PVSC, Orland, Florida, 2005.1.3-7
(8) S.Ike, K.Kurokawa: Photogrammetric Estimation of Shading Impacts on Photovoltaic Systems, 31st IEEE PVSC, Orland, Florida, 2005.1.3-7
(9) K. Sakakibara, M. Ito, K. Kurokawa: RESULTS OF PV RESOURCE SURVEY FOR WORLD 6 DESERTS

BY A MODIFIED REMOTE SENSING APPROACH, 31st IEEE PVSC, Orland, Florida, 2005.1.3-7
(10) H. TADA, K. KUROKAWA, T. UNO, M. TAKAHASHI, Satoru YATABE, T. ARIMA: DEVELOPMENT OF TV WAVE ABSORBING PV MODULE BY REARRANGING SOLAR CELLS, 31st IEEE PVSC, Orland, Florida, 2005.1.3-7
(11) Y. Tsuno, Y. Hishikawa, K. Kurokawa: SEPARATION OF THE I-V CURVE OF EACH COMPONENT CELL OF MULTI-JUNCTION SOLAR CELLS, 31st IEEE PVSC, Orland, Florida, 2005.1.3-7
(12) K. Kurokawa: PHOTOVOLTAIC TECHNOLOGY DIRECTION TOWARD JAPANESE "PV2030", 1st JSPS Workshop on the Future Direction of Photovoltaics, Aogaku-Kaikan, Tokyo, 3-4 March 2005
(13) 五十嵐：単独運転防止試験時の回転機負荷影響について，電気学会全国大会，徳島大学，2005.3.17-19
(14) 市川，岡田，黒川：BTB 式 LPC が連系する区間の特性と簡易推定法の検討，電気学会全国大会，徳島大学，2005. 3.17-19
(15) 嶋田，黒川，吉岡：蓄電池特性の高精度シミュレーションモデル，電気学会全国大会，徳島大学，2005.3.17-19
(16) 中田，大関，黒川，小池：簡易評価手法を用いた温度損失評価，電気学会全国大会，徳島大学，2005.3.17-19
(17) N. Okada, H. Kobayashi, T. Ishikawa, K. Takigawa, K. Kurokawa : Simulation of isolated operation in fault condition by loop power flow controller, Control Engineering Practice, pp1537-1543, Vol.13, 2005.3
(18) 岡田，黒川：自端情報によるループコントローラの制御と係数の決定法，電気学会論文誌 B，pp381-389，Vol.125，No4，2005.4
(19) 岡田, 黒川 : 6.6kV-100kVA BTB 式ループコントローラの制御試験, 電気学会論文誌 B, pp390-398, Vol.125, No4，2005.4
(20) 黒川：太陽光発電の普及状況と将来像，「太陽エネルギーを市民の手に」シンポジウム，愛知万博地球市民村，2005.5.4
(21) H. Koizumi, K. Kurokawa, S. Mori: Thinned-out controlled Class D inverter with delta-sigma modulated 1-bit driving pulses, IEEE International Symposium on Circuits and Systems 2005 (ISCAS 2005), pp. 1322-1325, Kobe, Japan, 2005.5.23-26
(22) 黒川 : 自律度向上型太陽光発電システム先導研究開発，自律度向上型太陽光発電システム先導研究開発公開ワークショップ，高輪プリンスホテル，2005.5.25
(23) K. Kurokawa, S. Wakao, Y. Hayashi, I. Ishii, K. Otani, M. Yamaguchi, T. Ishii, Y. Ono : CONCEPTUAL STUDY ON AUTONOMY-ENHANCED PV CLUSTERS FOR URBAN COMMUNITY TO MEET THE JAPANESE PV2030 REQUIREMENTS, 20th EU-PVSEC, Barcelona, 2005.6.6-10
(24) T. Oozeki, K. Otani, K. Kurokawa: AN ACCURACY OF THE SV METHOD FOR EVALUATED SHADING LOSSES ~ COMPARED WITH RESULTS USING THE FISH-EYE-PHOTOGRAM METHOD ~, 20th EU-PVSEC, Barcelona, 2005.6.6-10
(25) M. Ito, K. Kato, K. Komoto, T. Kichimi, K. Kurokawa: COMPARATIVE STUDY OF M-SI, A-SI AND CDTE SYSTEM OF VERY LARGE-SCALE PV (VLS-PV) SYSTEMS IN DESERT, 20th EU-PVSEC, Barcelona, 2005.6.6-10
(26) H. Igarashi1, S. Suenaga, K. Kurokawa : CHARACTERISTICS OF THE ELECTROMAGNETIC ENVIRONMENTS OF POWER CONDITIONERS FOR PV GENERATING SYSTEMS, 20th EU-PVSEC, Barcelona, 2005.6.6-10
(27) J. Tsutsui, K. Kurokawa : The Comparison of System Performance Measuring Multiple Modules, 20th EU-PVSEC, Barcelona, 2005.6.6-10
(28) Y.Ueda, T.Oozeki, K.Kurokawa, T.Itou, K.Kitamura, Y.Miyamoto, M.Yokota, H.Sugihara, S.Nishikawa: DETAILED PERFORMANCE ANALYSES RESULTS OF GRID-CONNECTED CLUSTERED PV SYSTEMS IN JAPAN -FIRST 200 SYSTEMS RESULTS OF DEMONSTRATIVE RESEARCH ON CLUSTERED PV SYSTEMS, 20th EU-PVSEC, Barcelona, 2005.6.6-10
(29) N. Kawasaki, T. Oozeki, K. Otani, K. Kitamura, H. Sugihara, S. Nishikawa, K.Kurokawa: IMPACT STATEMENT OF DISTRIBUTION NETWORK BY FLUCTUATION OF PV SYSTEM OUTPUT BY USING FREQUENCY ANALYSIS, 20th EU-PVSEC, Barcelona, 2005.6.6-10
(30) S. Taguchi, K. Kurokawa: PV Resource Survey for Urban Areas by means of Aerial Photographs, 20th EU-PVSEC, Barcelona, 2005.6.6-10
(31) K. Hayashi, T. Shimada, H. Koizumi, Y. Ohashi, K. Kurokawa : A Novel Cascaded PV Inverter by Utilizing Ready-Made ICs for Digital Audio Amplifier, 20th EU-PVSEC, Barcelona, 2005.6.6-10
(32) Y. Nakamura, H. Koizumi, K. Kurokawa: Performance Assessment with Different Inductance Model in the Ultra Scaled-Down Distribution Grid Simulator, 20th EU-PVSEC, Barcelona, 2005.6.6-10
(33) A.Amarbayar，黒川浩助：ゴビ砂漠地域開発の分析モデルの構築～エネルギー資源フローの調査分析～，第 24 回エネルギー・資源学会研究発表会，虎ノ門パストラル，2005.6.9～10
(34) A.Amarbayar，黒川浩助：ゴビ砂漠地域開発の分析モデル構築：現地調査による地域システムの分析，第 6 回 国際開発学会春季大会，文教大学湘南キャンパス，2005.6.11
(35) H. Koizumi, K. Kurokawa: A novel maximum power point tracking method for PV module integrated converter, 36th IEEE Power Electronics Specialists Conference 2005 (PESC 2005), pp. 2081-2086, Recife, Brasil, 2005.6.12-16
(36) 黒川：太陽光発電システム研究開発の方向性，第 22 回太陽光発電システムシンポジウム，朝日ホール，p.2-21~37，2005.6.15-17

(37) アマルバヤル，黒川：モンゴルにおける独立小型太陽光発電システム実証研究のデータ解析・システム評価，太陽エネルギー学会，pp83-88，vol.31，No4，2005.7
(38) 大関，井澤，大谷，都筑，小池，黒川：システム出力電力量のみの計測における太陽光発電システムの評価方法に関する研究，電気学会電力・エネルギー部門大会，大阪大学，2005.8.10-12
(39) 五十嵐，末長，佐藤，黒川：回転機負荷の違いによる単独運転防止装置への影響について，電気学会電力・エネルギー部門大会，大阪大学，2005.8.10-12
(40) 植田，大関，黒川，伊藤，北村，宮本，横田，杉原：系統連系型太陽光発電システムにおける出力抑制による発電量損失の定量化手法，電気学会電力・エネルギー部門大会，大阪大学，2005.8.10-12
(41) 川崎，大関，大谷，北村，杉原，西川，黒川：面的広がりを考慮した太陽光発電変動特性の分析，電気学会電力・エネルギー部門大会，大阪大学，2005.8.10-12
(42) K. Kurokawa：Mass Production Scale of PV Modules and Components in 2030s and beyond, 15th PVSEC, Shanghai, China, 2005.10.10-15
(43) A. Adiyabat, K. Kurokawa, K. Otani, N.Enebish, G.Batsukh, M. Battushig, D.Ochirvaani, B.Ganbat, D.Otgonbayar：PV Module Performance in the Ulaanbaatar of Mongolia, 15th PVSEC, Shanghai, China, 2005.10.10-15
(44) H. Igarashi, S. Suenaga, T. Sato, K. Kurokawa：About the Influence on the Islanding Detection Device by the Difference in the Motor Load, 15th PVSEC, Shanghai, China, 2005.10.10-15
(45) Y. Ueda, T. Oozeki, K. Kurokawa, T. Itou, K. Kitamura, Y. Miyamoto, M. Yokota, H. Sugihara, S. Nishikawa：Advanced analysis of shading effect using minutely based measured data for PV systems, 15th PVSEC, Shanghai, China, 2005.10.10-15
(46) K. Lee, K. Kurokawa：Study on D-UPFC in the clustered PV System with Grid, 15th PVSEC, Shanghai, China, 2005.10.10-15
(47) N. Kawasaki, T. Oozeki, K. Otani, K. Kitamura, H. Sugihara, S. Nishikawa, K. Kurokawa：An Evaluation Method of Area-dependency Equalization of Output Fluctuation from Distributed PV System by Using Frequency Analysis, 15th PVSEC, Shanghai, China, 2005.10.10-15
(48) Y. Tsuno, Y. Hishikawa, K. Kurokawa: Temperature and Irradiance Dependence of the I-V Curves of Various kinds of Solar Cells, 15th PVSEC, Shanghai, China, 2005.10.10-15
(49) K. Hayashi, T. Shimada, H. Koizumi, Y. Ohashi, K. Kurokawa：A New Grid-Connected Inverter by Utilizing Ready-Made PWM ICs for Audio Power Amplifier, 15th PVSEC, Shanghai, China, 2005.10.10-15
(50) J. Yokkaichi, T. Oozeki, K. Kurokawa：Irradiation Monitoring from Sunshine Hours given by JapaneseMeteorological Observation Network, 15th PVSEC, Shanghai, China, 2005.10.10-15
(51) K. Hirata, K. Kurokawa, Y. Miyake, T. Kato, K. Nakamura：Development of a Reliable, Long Life Pyranometer Compsed of Multiple photo sensors, 15th PVSEC, Shanghai, China, 2005.10.10-15
(52) 植田，大関，黒川：太陽電池モジュール入射角特性の屋外測定と解析，日本太陽エネルギー学会・日本風力エネルギー協会合同研究発表会，諏訪東京理科大学，2005.10.20-21
(53) 川崎，大関，大谷，北村，杉原，西川，黒川：太陽光発電システム変動特性の評価 ～導入面積・導入数の検討～，日本太陽エネルギー学会・日本風力エネルギー協会合同研究発表会，諏訪東京理科大学，2005.10.20-21
(54) 李，黒川：A Proposal of D-UPFC as a Voltage Controller in the Distribution System，日本太陽エネルギー学会・日本風力エネルギー協会合同研究発表会，諏訪東京理科大学，2005.10.20-21
(55) 田口，黒川：空中写真を用いた太陽光発電システム導入可能量の推定（住宅屋根の認識と日野市における実例），日本太陽エネルギー学会・日本風力エネルギー協会合同研究発表会，諏訪東京理科大学，2005.10.20-21
(56) 津野，菱川，黒川：内挿補間を用いた各種太陽電池 I-V 特性の温度・照度補正法，日本太陽エネルギー学会・日本風力エネルギー協会合同研究発表会，諏訪東京理科大学，2005.10.20-21
(57) 四日市，大関，黒川：地域性を考慮した日射量推定法の補正方法，日本太陽エネルギー学会・日本風力エネルギー協会合同研究発表会，諏訪東京理科大学，2005.10.20-21
(58) H. Koizumi, K. Kurokawa：A novel maximum power point tracking method for PV module integrated converter using square root functions, 31th IEEE Industrial Electronics Society (IECON 2005), NC, USA, pp2511-2516, 2005.11.6-11
(59) 黒川：太陽光発電のこれから，電気学会東北支部電力技術懇談会講演会，山形大学，2005.11.10
(60) 黒川：21 世紀の太陽光発電の可能性，太陽光発電コラボレーション事業総括報告会，2005.11.22
(61) 大関，井澤，大谷，黒川：システム出力電力量のみの計測における太陽光発電システムの評価方法に関する研究，電気学会論文誌 B，pp1299-1307，Vol.125，No12，2005.12
(62) 植田，大関，伊藤，北村，宮本，横田，杉原，黒川：系統連系型太陽光発電システムにおける出力抑制による発電量損失の定量化手法，電気学会論文誌 B，pp1317-1326, Vol.125，No12，2005.12

〈2006 年〉

原著論文

(1) ○植田，黒川，北村，赤沼，横田，杉原：太陽光発電システム評価における傾斜面日射量算出精度の検証と誤差の評価，太陽エネルギー，p.45 – 53，Vol.32，No.5，Jan. 2006

(2) ○アマル，中島，大谷，黒川：独立小型太陽光発電システムの利用実態と課題－モンゴルの遊牧民を事例として－，農業情報研究，p.139-154，第 15 巻 2 号，Feb. 2006

(3) ○H. Koizumi, K. Kurokawa, S. Mori : Analysis of class D inverter with irregular driving patterns，IEEE Trans. Circuits & Systems，p.677-687，Vol.53，No.3，Mar. 2006

(4) ○A Adiyabat., K. Otani, K. Kurokawa, N. Enebish, G. Batsukh, M. Battushig, D. Ochrvaani, B. Ganbat : Evaluation of solar energy potential and PV module performance in the Gobi Desert of Mongolia，Progress in Photovoltaics, in press，p.553-566，Vol.14，issue6，Sep. 2006

(5) ○ N. Kawasaki, T. Oozeki, K. Otani, K. Kurokawa : An Evaluation Method of the Fluctuation Characteristics of Photovoltaic Systems by Using Frequency Analysis，Solar Energy Materials & Solar Cells，p.3356-3363，Volume 90，Issues 18-19，23. Nov. 2006

(6) ○S. Kohraku, K. Kurokawa : A fundamental experiment for discrete-wavelength LED solar simulator, Solar Energy Materials & Solar Cells，p.3364-3370，Volume 90，Issues 18-19，23. Nov. 2006

(7) ○H. Koizumi, T. Mizuno, T. Kaito, Y. Noda, N. Goshima, M. Kawasaki, K.Nagasaka, and K. Kurokawa : A novel micro controller for grid-connected photovoltaic systems，IEEE Trans. Industrial Electronics，pp. 1889-1897，vol. 53，no. 6，Dec. 2006

(8) ○植田，黒川，伊藤，北村，赤沼，横田，杉原，森本：系統連系型太陽光発電システム運転特性の高度解析と蓄電池導入効果の検証，電気学会論文誌 B，p.247-258，Vol.127，No.1，Jan. 2007

(9) ○五十嵐，佐藤，小林，津田，黒川：共振負荷と回転機負荷の相違と単独運転試験への影響について，電気学会論文誌 B，p.192~199，Vol.127，No.1，Jan. 2007

(10) ○Y Ueda, T Oozeki, K Kurokawa, T Itou, K Kitamura, Y Miyamoto, M Yokota, H Sugihara : Quantitative Analysis Method of Output Loss due to Restriction for Grid-connected PV Systems，Electrical Engineering in Japan，pp9-19，Vol. 158，No. 2，30. Jan. 2007

国際学会・招待講演

(11) K. Kurokawa : Photovoltaic technology direction - Japanese "PV2030"，KIER-TUAT Joint Seminar，Taejon，KOREA，8. Mar. 2006

(12) ○K. Kurokawa, S Wakao, Y Hayashi, H Yamaguchi, K Otani, M Yamaguchi, T Ishii and Y Ono : Autonomy-Enhanced PV Cluster Concept for Solar Cities to Meet the Japanese PV2030 Roadmap，2nd International Solar Cities Congress，Oxford UK，7E.2，3-6. Apr. 2006

(13) ○K. Kurokawa : A conceptual study on solar pv cities for 21st century，WCPEC-4，Hawaii，p.2283-2288，7-12. May. 2006

(14) ○M Ito, K. Kato, K. Komoto, T. Kichimi, K. Kurokawa : A SENSITIVITY ANALYSIS OF VERY LARGE-SCALE PHOTOVOLTAIC POWER GENERATION(VLS-PV) SYSTEMS IN DESERTS，WCPEC-4，Hawaii，p.2387-2390，7-12. May. 2006

(15) ○K Lee, H Koizumi, K Kurokawa : Voltage sag/swell controller by means of D-UPFC in the distribution system，WCPEC-4，Hawaii，p.2427-2430，7-12. May. 2006

(16) ○J Tsutsui, Y Sato, K Kurokawa : Modeling the performance of several photovoltaic modules，WCPEC-4，Hawaii，p.2258-2261，7-12. May. 2006

(17) ○Y Ueda1, K Kurokawa, T Itou, K Kitamura, Y Miyamoto, M Yokota, H Sugihara : Performance ratio and yield analysis of grid connected clustered pv systems in Japan，WCPEC-4，Hawaii，p.2296-2299，7-12. May. 2006

(18) ○Y Tsuno, Y Hishikawa, K Kurokawa : Translation equations for temperature and irradiance of the I-V curves of various PV cells and modules，WCPEC-4，Hawaii，p.2246-2249，7-12. May. 2006

(19) ○H. Igarashi, T. Sato, H. Kobayashi, I. Tuda, K. Kurokawa : RESULT OF REVIEW BY ELECTRIC ENERGY AMOUNT COMPARISON WITH RESONANCE LOAD TURNED TO MOTOR LOAD STANDARDIZATION，WCPEC-4，Hawaii，p.2415-2418，7-12. May. 2006

(20) ○K Otani, T Takashima, K Kurokawa : Performance and reliability of 1MW photovoltaic power facilities in AIST - The first year's results，WCPEC-4，Hawaii，p.2046-2049，7-12. May. 2006

(21) ○H. Koizumi, K. Kurokawa, S. Mori : A comparison of output envelope waveforms of the delta-sigma modulated Class D series resonant inverter，Proc. IEEE International Symposium on Circuits and Systems 2006 (ISCAS 2006)，pp. 253-256，21-24. May. 2006

(22) ○K Lee, H Koizumi, K Kurokawa : Voltage Control of D-UPFC between a Clustered PV System and Distribution System，PESC06，Jeju，p.1367-1371，18-22. Jun. 2006

(23) ○K Hayashi, H Koizumi, Y Ohashi, and K Kurokawa : A single-phase grid-connected inverter by utilizing ready-made PWM power IC，Proc. IEEE International Symposium on Industrial Electronics 2006 (ISIE 2006)，pp. 1138-1142，9-13. Jul. 2006

(24) ○H Koizumi, K. Kurokawa : Plane division maximum power point tracking method for PV module integrated converter, Proc. IEEE International Symposium on Industrial Electronics 2006 (ISIE 2006), pp. 1265-1270, 9-13. Jul. 2006

(25) ○K Kurokawa, K Komoto, P Vleuten, D Faiman : A NEW KNOWLEDGE HOW TO MAKE THE VERY LARGE SCALE PVS HAPPEN ON THE DESERT!, 21th EU-PVSEC, Dresden, p.2590-2596, 3-10. Sep. 2006

(26) ○Y Ueda, K Kurokawa, T Itou, K Kitamura, Y Miyamoto, M Yokota, H Sugihara : Performance Analyses of Battery Integrated Grid-connected Residential PV Systems, 21th EU-PVSEC, Dresden, p.2580-2584, 3-10. Sep. 2006

(27) ○H Igarashi, A. Tasai, K. Kurokawa : The Status Report of the PV System Ream Inter-Connected Guideline in 5 Countries of Asia, RENEWABLE ENERGY 2006, P-Ot-5, 10-13. Oct. 2006

(28) ○H Igarashi, T. Sato, K. Kurokawa : About the Examination of an Alternative Technique of the Motor Load According to the Resonance Load, RENEWABLE ENERGY 2006, P-Pv-17, 10-13. Oct. 2006

(29) K.Otani, T. Takashima, K. Kurokawa : Comparison of Performance and Energy Yield of PV Modules by Using Two-Axis Tracking Array, RENEWABLE ENERGY 2006, O-Pv-6-6, 10-13. Oct. 2006

(30) ○Y.Ueda, K. Kurokawa, T. Itou, K. Kitamura, K. Akanuma, M. Yokota, H. Sugihara : Analysis Results of Maximum Power Point Mismatch on Grid-Connected PV Systems, RENEWABLE ENERGY 2006, O-Pv-3-7, 10-13. Oct. 2006

(31) ○M.Ito, K. Kato, K. Komoto, T. Kichimi, K. Kurokawa : Suitable Very Large-Scale Photovoltaic Power Generation Systems (VLS-PV) for Desert Regions from Four Types of Case Studies by Using Life-Cycle Analysis Method, RENEWABLE ENERGY 2006, O-Pv-6-4, 10-13. Oct. 2006

(32) ○A. Adiyabat, M. Nakajima, K. Otani, E. Namjil, K. Kurokawa : A Study on the Evaluation of Solar Home System Viewed by Users: -A case of Nomadic Families in Mongolia-, RENEWABLE ENERGY 2006, P-Pv-25, 10-13. Oct. 2006

(33) ○N.Kawasaki, K. Kurokawa, K. Kitamura, H. Sugihara, S. Nishikawa : An Evaluation of Area-Dependency Equalization of Fluctuation Characteristics from Distributed PV Systems, RENEWABLE ENERGY 2006, P-Pv-90, 10-13. Oct. 2006

(34) ○K Lee, K.yamaguchi, H.Koizumi, K.Kurokawa : D-UPFC as a Voltage Regulator in the Distribution System , RENEWABLE ENERGY 2006, P-N-5, 10-13. Oct. 2006

(35) ○ Y.Tsuno, Y.Hishikawa, K.Kurokawa : TRANSLATION EQUATIONS FOR TEMPERATURE AND IRRADIANCE OF THE I-V CURVES OF Various PV Cells and Modules by Linear Interpolation, RENEWABLE ENERGY 2006, O-Pv-5-4, 10-13. Oct. 2006

(36) ○ T.Shimada, K.Kurokawa : HIGH PRECISION SIMULATION MODEL OF BATTERY CHARACTERISTICS, RENEWABLE ENERGY 2006, P-Pv-1, 10-13. Oct. 2006

(37) ○ T.Shimada, K.Kurokawa : GRID-CONNECTED PHOTOVOLTAIC SYSTEMS WITH BATTERY STORAGES CONTROL BASED ON INSOLATION FORECASTING USING WEATHER FORECAST, RENEWABLE ENERGY 2006, O-Pv-6-1, 10-13. Oct. 2006

(38) ○T.Kamakura, K.Hayashi, Y.Ohashi, K.Kurokawa : CONSIDERATIONS ON POWER LINE ROUTER BY USING MATRIX CONVERTER, RENEWABLE ENERGY 2006, P-Pv-7, 10-13. Oct. 2006

(39) ○Y.Nakamura, H.Koizumi, K.Kurokawa : A new type of scaled-down network simulator for testing PV inverters, RENEWABLE ENERGY 2006, P-Pv-11, 10-13. Oct. 2006

(40) ○J.Koyanagi, K.Kurokawa : A Fundamental Experiment of Solar Cell's I-V Characteristics Measurement Using LED Solar Simulator, RENEWABLE ENERGY 2006, P-Pv-9, 10-13. Oct. 2006

(41) ○Y.Seo, K. Hayashi, K. Kurokawa : Development of FPGA-based Digital Controller for PV Inverter, RENEWABLE ENERGY 2006, P-Pv-6, 10-13. Oct. 2006

(42) ○K.Hirata, K.Nakamura, T.Kato, K.Kurokwa : Spectral Error Analyses of Pyranometers Composed of Multiple Photodiodes, RENEWABLE ENERGY 2006, O-Pv-3-4, 10-13. Oct. 2006

国内学会

(43) 五十嵐，佐藤，小林，津田，黒川：単独運転試験方法の共振負荷及び回転機負荷の違いによる単独運転検出装置へ与える影響について，電気学会電力・エネルギー部門大会，琉球大学，p.25-11~20，13-15. Sep. 2006

(44) ○五十嵐，佐藤，黒川：共振負荷による回転機負荷の代替検討について，電気学会電力・エネルギー部門大会，琉球大学，No.159，p.7-25~26，13-15. Sep. 2006

(45) 植田，黒川，伊藤，北村，赤沼，横田，杉原，森本：系統連系型太陽光発電システム運転特性の高度解析と蓄電池導入効果の検証，電気学会電力・エネルギー部門大会，No.9，p.11-1~11，13-15. Sep. 2006

(46) ○川崎，植田，北村，杉原，西川，黒川：太陽光発電システム出力変動の検出時間別発生確率分布を用いた変動特性定量化手法，電気学会 B 部門大会，No.188，p.11-13~14，13-15. Sep. 2006

(47) ○平田, 黒川, 三宅, 中村：二種類のフォトセンサを持つ新型日射計におけるスペクトル誤差の解析手法の開発，電気学会 B 部門大会，No.183，p.10-5~6，13-15. Sep. 2006

(48) ○中村, 小泉, 黒川：超縮小模擬配電系統を用いたＰＶインバータ試験装置の開発, 電気学会 B 部門大会, No.182,

p.10-3~4，13-15. Sep. 2006

(49) ○鎌倉, 林, 黒川:マトリックスコンバータを用いた系統連系用ルータ機器の開発, 電気学会 B 部門大会, No.185, p.10-9~10，13-15. Sep. 2006

(50) ○瀬尾, 黒川:ＦＰＧＡを用いたＰＶインバータ用デジタルコントローラの開発, 電気学会 B 部門大会，No.197, p.11-31~32，13-15. Sep. 2006

(51) ○小柳, 黒川:LED ソーラーシミュレータを用いたＩＶ特性測定の改良基礎実験, 電気学会Ｂ部門大会, No.184, p.10-7~8，13-15. Sep. 2006

シンポジウム・解説

(52) ○黒川：太陽光発電システム研究開発の方向性と再生可能エネルギー2006 国際会議，第 23 回太陽光発電システムシンポジウム，朝日ホール，14-16，Jun，2006

(53) ○黒川：New Trends Shaping IEC Standards

(54) ○大谷：世界のトップを走る太陽光発電，精密工学会誌 Vol.73，No.1，p48-51，Jan，2007

○：主要論文別刷りに掲載

○印のついていない論文も黒川研究室ホームページの「黒川研データベース」からダウンロードできます。
URL：http://pv.ei.tuat.ac.jp/database/database_main.htm

東京農工大学　大学院

電気電子工学講座

黒川浩助　研究室

主要論文別刷り[2006 年～2007 年]

原著論文

[2006 年～2007 年]

研究論文

太陽光発電システム評価における傾斜面日射量算出精度の検証と誤差の評価

Verification of Calculating Accuracy of Tilted Surface Irradiation and Error Analysis for PV Systems Performance Evaluation

植田 譲 *1 Yuzuru UEDA
黒川浩助 *1 Kosuke KUROKAWA
北村清之 *2 Kiyoyuki KITAMURA
赤沼克己 *3 Katsumi AKANUMA
横田昌治 *3 Masaharu YOKOTA
杉原裕征 *3 Hiroyuki SUGIHARA

Abstract

This paper describes the calculating accuracy of tilted surface irradiation using one minute average of secondly measured irradiance data. Calculation model for hourly irradiation is applied for minutely data. Accuracy of annual calculated irradiation and the range of variation are quantitatively summarized for three azimuths. As a result, accuracy of minutely calculated data and the range of the variations are slightly better than that of the hourly data's. Calculating error due to the error of tilt angle, azimuth, albedo, and effect of distance are also analyzed. The effect of each factors for the annual irradiation and the range of error are quantitatively summarized.

キーワード：日射量，傾斜面，太陽光発電システム
Key Words : Irradiation, Tilted surface, PV systems

1．はじめに

近年の世界的な太陽光発電(PV)システムの普及拡大と共に，PV システム運転特性評価の重要性もますます高まってきている．特に，住宅用 PV システムが局所集中的に電力系統に連系された場合に懸念される電圧上昇問題等に対する解析では，従来の 1 時間積算値を用いたエネルギー面での評価から，より短い計測周期で記録されたデータを用いた，瞬時的な発電特性の評価が重要となる．[1)]

一方，PV システムを評価する際に入力エネルギーとして用いる日射量の計測においては，様々な傾斜角度・方位に設置された PV アレイ面の日射量を，それぞれの面に実際に日射計を設置して計測する方法が理想的であると言える．しかし，多くのシステムを評価する際には日射計の設置コストやメンテナンスコストの削減の為，代表点にて計測した水平面全天日射量，及び追尾架台を用いて計測した法線面直達日射量をもとに任意の傾斜面日射量を算出する方法が有効である．この算出方法としては，全天日射は直達成分・天空散乱成分・地面反射成分の 3 成分から構成されていると考え傾斜面における個々の成分を個別に算出した後，それぞれを足し合わせることにより算出する方法が一般的であり，直達成分の算出には直接法を，天空散乱成分の算出には Perez モデル [2)]を，地面反射成分の算出には均一反射モデルを用いる方法が最も高精度であるとされている．[3)] しかし，天空散乱成分を算出する代表的なモデルである Perez モデルは 1 時間積算値を用いて構築されており，より短時間での計測周期における算出精度の検証は十分には行われていない．また，日本国内において一般的に利用可能な気象庁等により計測されている日射データや，独立行政法人 新エネルギー・産業技術総合開発機構(NEDO)による「太陽光発電新技術等フィールドテスト事業」にて収録されたデータにおいても，1 時間積算値により収録している場合が多く，より短い計測周期での大規模な計測データは，利用可能なものが限定的であった．

本論文では，NEDO により平成 14 年度から行われている「集中連系型太陽光発電システム実証研究」において計測されている 1 秒サンプリングによる 1 分値を用いる事により，短い計測周期でのデータを用いた年間を通した傾斜面日射量の算出精度，および瞬時的な日射強度の算出精度を検証し，PV システム評価における誤差要因を併せて評

*1 東京農工大学（〒184-8588 東京都小金井市中町 2-24-16）
e-mail: yzrueda@cc.tuat.ac.jp
*2 株式会社 明電舎
*3 株式会社 関電工
（原稿受付：2006 年 6 月 9 日）

価した．

2．データ取得地域と計測機器

本論文において用いた日射データの計測地点である「集中連系型太陽光発電システム実証研究」の実証研究地域は群馬県太田市にあり，中心部は北緯 36.311°，東経 139.337°に位置する．本実証研究では南北約 1[km]，東西約 0.5[km]の地域に集中的に太陽光発電システムを導入し同一配電系統に連系する事により，太陽光発電システムの運転特性の評価や電力系統に及ぼす影響などについて研究を行っている．日射等を計測する周辺環境計測システムは実証研究地域内 6 カ所，それぞれのシステムが水平面全天日射計，直達日射計，水平面に設置したシリコンセンサを用いた小型日射計，及び傾斜角 30 度で異なる方位に設置された傾斜面日射計を備え，Station1 ではさらに風速，風向，気温が計測されている．実証研究地域の概略図とそれぞれの周辺環境計測システムの位置(Fig.1)，周辺環境計測システムの写真(Fig.2)，および傾斜面日射計の設置方位角(Table 1)を以下に示す．また，Table 2 には各計測機器の型番をまとめた．なお，精密日射計には結露等を防止するためファン付きの日射計を用いている．

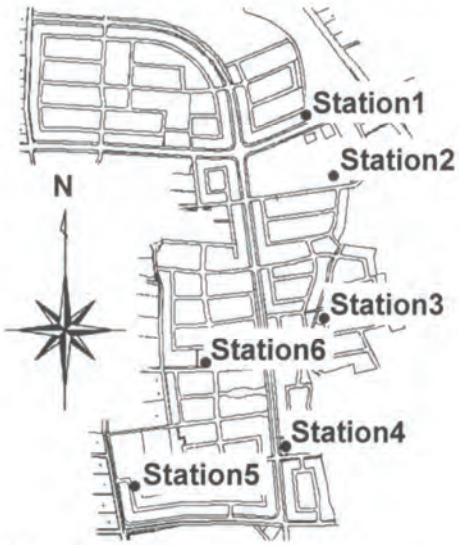

Fig.1 Map of demonstrative research area and locations of meteorological stations.

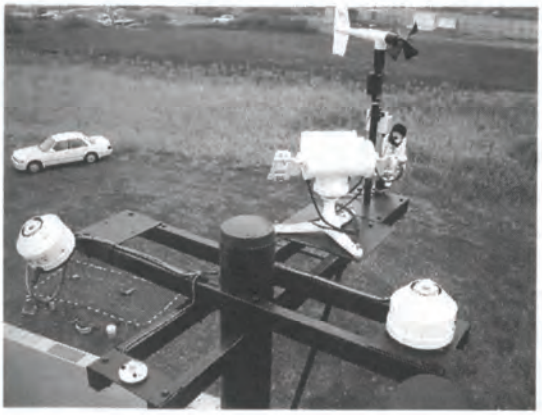

Fig.2 Picture of meteorological station.

Table 1 Azimuth of pyranometers for tilted surface.

Station #	1	2	3	4	5	6
Azimuth [deg]	-13	-52	-97	3	37	86

Table 2 Model numbers of measurement equipments.

	型番	メーカ
精密全天日射計(水平面)	MS-802F	英弘精機(株)
直達日射計	MS-54	同上
太陽追尾装置	STR-22	同上
小型日射計	ML-020VM	同上
精密全天日射計(傾斜面)	MS-802F	同上

以上に示した周辺環境計測システムにて計測された日射データの内，2004 年 10 月～2005 年 9 月までの 1 年間に安定してデータを取得できた Station1～Station3 のデータを用いて以下に示す検証と評価を行った．各日射計は約 1 年に 1 回の頻度で較正を行っており，清掃は数ヶ月に一度行っている．上記期間における Station1 の欠測は 2005 年 2 月 25 日(日射計較正の為)の他，複数の日に数十分ずつ，計 300 分間の欠測があったが，これらのデータは単純に欠測(日射無し)として扱っている．また，Station2 の欠測日は 2005 年 7 月 15 日，Station3 の欠測日は 2004 年 10 月 29 日と 2005 年 8 月 19 日であり，これらの欠測日を除外した Station1～Station3 における年積算水平面全天日射量の誤差は 0.5[%]以下であった．

なお，本論文における方位角は真南を 0[deg]とし，真東を-90[deg]，真西を 90[deg]として表すこととする．

3．傾斜面日射強度算出手法

任意の傾斜面日射強度を，水平面全天日射強度と直達日射強度を用いて算出する方法として，本論文では 1 節で述べたように，時積算傾斜面日射量を算出する手法を採用した．本手法では，傾斜面日射量を直達成分・天空散乱成分・地面反射成分に分けて個別に算出した後，それぞれをたしあわせることにより任意の傾斜面日射量を算出する．以下にその概略を述べる．

3．1 傾斜面直達成分の算出手法

傾斜面直達成分は直達日射計にて計測された日射量をもとに，直接法を用いて(1)式にて算出する．

$$H_{Ab} = H_n \cdot \cos\theta \qquad (1)$$

ここで，

H_{Ab} ：傾斜面直達日射量 [kWh/m²]
H_n ：法線面直達日射量 [kWh/m²]
θ ：入射角 [deg]

3．2 天空散乱成分の算出手法

天空散乱成分はPerezモデルを用いて，(2)式により算出する．

$$H_{Ad} = H_d\{0.5(1+\cos\beta)(1-F_1') + F_1'(a/c) + F_2'\cdot\sin\beta\} \quad (2)$$

ここで，

H_{Ad} ：傾斜面天空散乱日射量 [kWh/m²]
H_d ：水平面散乱日射量 [kWh/m²]
β ：傾斜角 [deg]
F'_1 ：太陽の位置，天空の明るさ，晴天度によって決定される係数
F'_2 ：太陽の位置，天空の明るさ，晴天度によって決定される係数
a ：太陽周辺光が占める立体角を傾斜面への平均入射により重み付けした値
c ：太陽周辺光が占める立体角を水平面への平均入射により重み付けした値

係数 F'_1，F'_2，の決定方法，及び a，c の決定方法に関しては文献2)，3)に詳しいため，ここでは省略する．なお，係数 a，c の決定に用いる太陽周辺光の視半径には25[deg]を用いた．

3．3 地面反射成分の算出手法

均一反射モデルでは水平面全天日射量を用いて(3)式により傾斜面の反射成分を算出する．なお，アルベド値には一般的な住宅地域の値として0.2を用いることとした．

$$H_{Ar} = \rho\cdot H_g\cdot\frac{1-\cos\beta}{2} \quad (3)$$

ここで，

H_{Ar} ：傾斜面反射日射量 [kWh/m²]
H_g ：水平面全天日射量 [kWh/m²]
ρ ：地表面アルベド= 0.2

3．4 日射量と日射強度の取扱い

日射の計測に用いている水平面全天日射計と直達日射計はセンサ部分にサーモパイルを用いたものであり，その応答速度は95%の変動に対して約5～7秒程度[4]となっている．そこで，本論文では日射計の応答速度より早い日射急変による誤差を低減するため，1秒周期で計測された瞬時的な日射強度の1分平均値を，その1分間における日射量として扱うと共に，より瞬時的な解析においてはその1分間における日射強度としても用いる事とした．PVシステム運転特性評価においては，評価の対象となる太陽電池は半導体素子であり，その出力はサーモパイル型日射計と比べて日射強度の変化に対しほぼ瞬時的に応答する．そのため，このような早い時間での変動に対して評価を行う場合には，シリコンセンサを用いた小型日射計等の使用が考えられるが，日射強度の絶対値の計測精度においてはサーモパイル型日射計に及ばず，また本実証研究では主に1分値を用いて太陽光発電システム運転特性の解析を行っている事から，このような取り扱いとした．

4．日射概況

傾斜面日射強度の算出精度を検証する前に，実証研究地域の日射概況を本節にてまとめる．Table 3には水平面とそれぞれの傾斜面における実測の年間日射量を，Fig.3には月別の推移をまとめた．なお，本論文では実測された日射データに関しては，水平面，傾斜面とも，0付近の誤差を取り除くため，日射計の計測値が0.001[kW/m²]以上のデータのみを用いる事とした．

Table 3 Annual irradiations on the global and tilted surfaces.

Station #	1	1	2	3
Tilt angle [deg]	0	30	30	30
Azimuth [deg]	N/A	-13	-52	-97
Irradiation [kWh·m^{-2}·Year^{-1}]	1388	1639	1519	1261

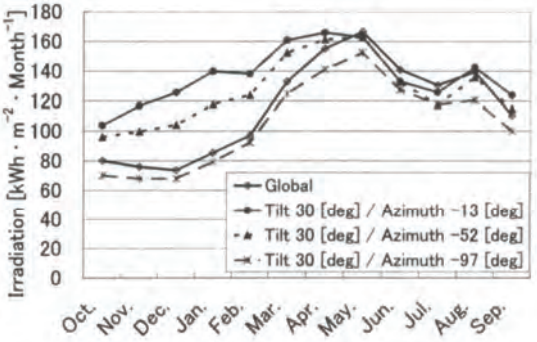

Fig.3 Monthly irradiation on each surface.

次に，Station1の傾斜面(傾斜角30[deg]，方位角-13[deg])における，日射強度別データ数(=日射強度 0.001[kW/m²]以上の時間[min])が，各月の月積算データ数，及び年積算データ数に占める割合をFig.4に，同じく日射強度別の日射量が月積算日射量，及び年積算日射量に占める割合をFig.5に，日射強度0.1[kW/m²]毎にまとめた．グラフ中の各レベルは低い方から白(黒点)，灰，黒(左下斜線)，白(横破線)，灰(格子)，黒(縦線)，白(横実線)，灰(斜格子)，黒(右下斜線)，白(斜破線)，灰(菱形)，黒，白である．これらの結果より，日射強度0.1[kW/m²]以下のデータ数（=時間）

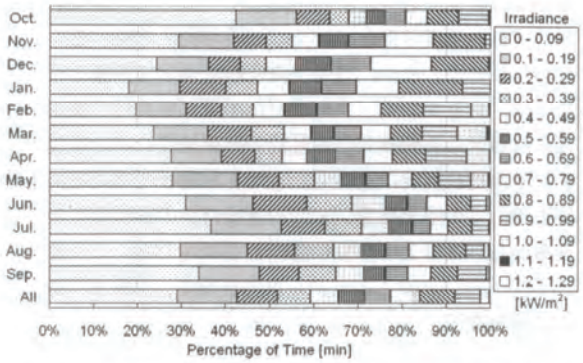

Fig.4 Percentage of time for each irradiance level.

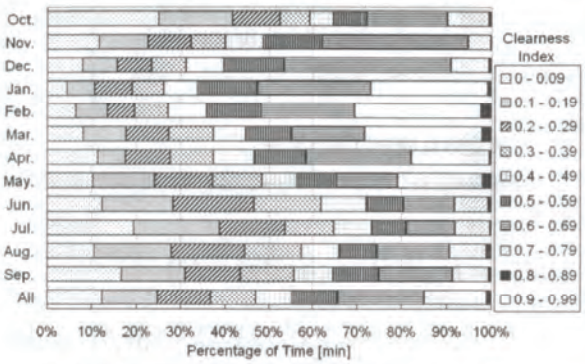

Fig.6 Percentage of time for each clearness index.

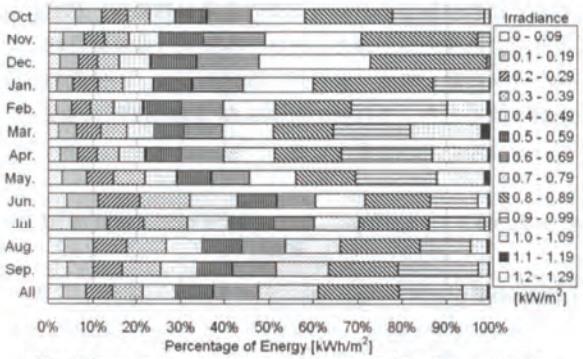

Fig.5 Percentage of energy for each irradiance level.

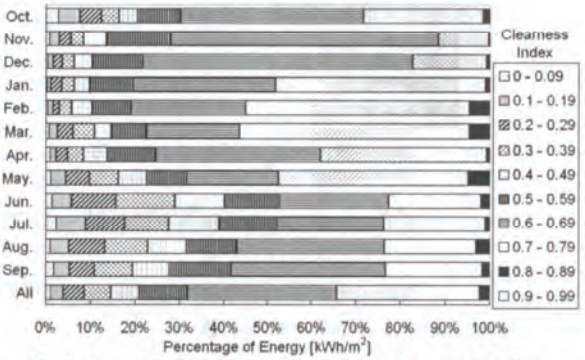

Fig.7 Percentage of energy for each clearness index.

が年間に占める割合は 29.4[%]であるが，その時間に供給している日射量の年積算日射量に占める割合は 3.2[%]にしかすぎない事等が分る．

また，日射強度別と同様に晴天指数別の時間と日射量を Fig.6，Fig.7 に，散乱比別の時間と日射量を Fig.8，Fig.9 にまとめた．グラフ中の各レベルは低い方から白(黒点)，灰，黒(斜線)，白(横破線)，灰(格子)，黒(縦線)，白(横実線)，灰(斜格子)，黒，白である．これらのグラフより，太田市では冬季の晴天率が高く，年間の全日射量のうち 34.3[%]が晴天指数 0.7 以上の時間に供給された(Fig.7)ことが読み取れる．また，散乱比の傾向は Fig.8，9 の通りであり，年間全日射量のうち 55.5[%]が直達光により供給された日射量であった．このような気象概況を知ることは，PV システム評価における入力エネルギーとして日射データを扱う際には，より発電特性に影響を与える日射レベルや気象条件等を判断する際に有用である．

なお，晴天指数，散乱比の定義は(4)，(5)式の通りであり，日射状況を説明する指数として用いている．一般に，晴天指数が大きい(1 に近づく)ほど天気が良く，散乱比が大きい(1 に近づく)ほど天気が悪いと言える．

$$CI = \frac{H_g}{H_o} \qquad (4)$$

ここで，

CI　：晴天指数

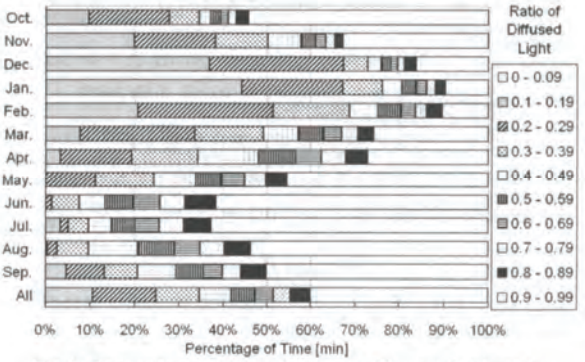

Fig.8 Percentage of time for each diffused light ratio.

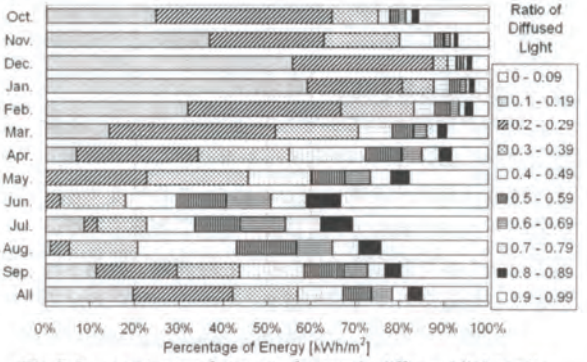

Fig.9 Percentage of energy for each diffused light ratio.

Ho　：大気外水平面日射量 [kWh/m²]

$$K_d = \frac{H_d}{H_g} \tag{5}$$

ここで,

K_d　：散乱比

5．傾斜面日射強度算出精度の検証

2004 年 10 月から 2005 年 9 月までの 1 年間に計測されたデータを用いて，3 節で示した方法により傾斜面日射強度の 1 分値を算出し，同一地点において実測された傾斜面日射強度と比較する事により，その算出精度を検証した．算出結果の一例として，Station1 にて計測された，水平面全天日射強度と直達日射強度を用いて算出した傾斜面日射強度の 1 分値を横軸に，同じく Station1 で実際に傾斜面にて計測された日射強度の 1 分値を縦軸に，月毎に分けて散布図としてプロットした結果を Fig.10 に示す．

これらのデータの算出精度を検証するため，平均的な誤差を見るための指標として平均誤差(MBE)を，各算出値における誤差の平均誤差に対するばらつきを見る指標として標準偏差(1Sigma)を，同じく，誤差の広がりを見る指標として二乗平均平方根誤差(RMSE)を，また全体の推定精度を見るための指標として，最小二乗法を用いて原点を通る直線で近似したときの直線の傾き(α)を用いて評価した．以下に MBE，1Sigma，RMSE の定義を示す．

$$\mathrm{MBE} = \frac{1}{N}\sum_{i=1}^{N}(X_i - X_{0i}) \tag{6}$$

$$1\mathrm{Sigma} = \left\{\frac{1}{N}\sum_{i=1}^{N}((X_i - X_{0i}) - \mathrm{MBE})^2\right\}^{\frac{1}{2}} \tag{7}$$

$$\mathrm{RMSE} = \left\{\frac{1}{N}\sum_{i=1}^{N}(X_i - X_{0i})^2\right\}^{\frac{1}{2}} \tag{8}$$

ここで,

X_i : 算出値

X_{oi} : 実測値

N: データ数

また，α の算出には次式を用い，最小二乗法により傾きを決定した．

$$X_{0i} = \alpha X_i \tag{9}$$

Table 4 には，Station1～3 における，それぞれの地点での傾斜面日射強度の算出精度検証結果を示す．また，天候別の算出精度を検証するため，文献 3)に合わせ，晴天の定義として晴天指数 0.7 以上を，曇天の定義として散乱比 0.95 以上(小数点以下 2 桁四捨五入で 1.0 になる範囲)を用

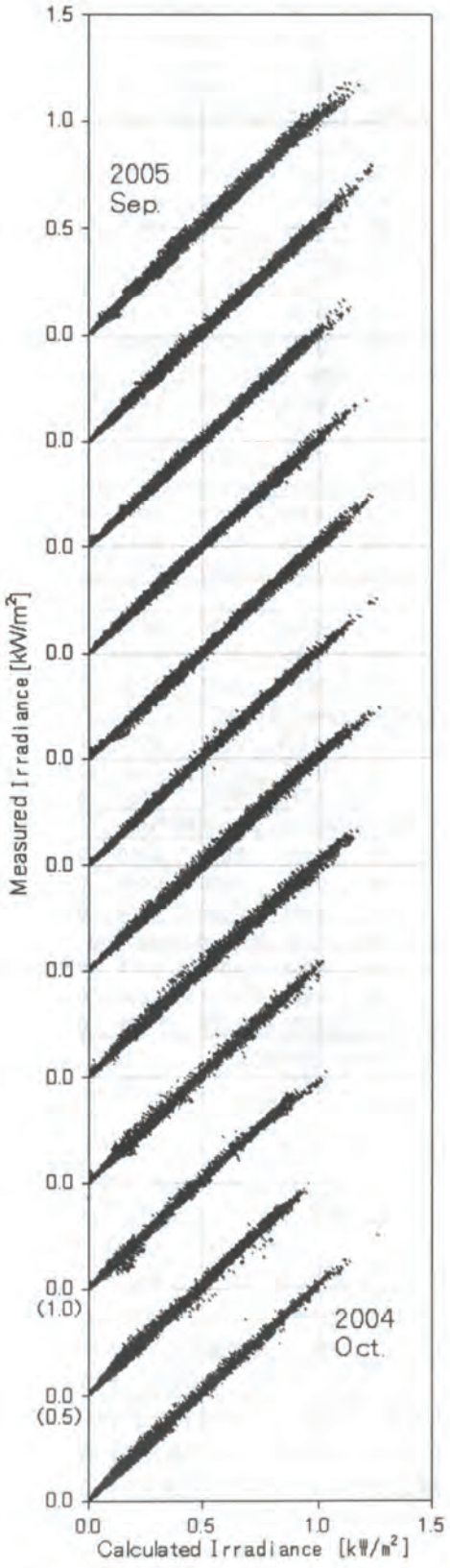

Fig.10 Scatter plot of calculated irradiance and measured irradiance using 1 minute data. Data collected from 2004/10 to 2005/9 at Station1.

Table 4 Verification results of calculation accuracy of tilted surface irradiance.

Station#	Azimuth [deg]	MBE [kW/m^2]	1Sigma [kW/m^2]	RMSE [kW/m^2]	α	Number of data
All (1m)						
1	−13	−0.005	0.012	0.013	1.013	258913
2	−52	−0.001	0.012	0.012	1.002	261848
3	−97	0.001	0.012	0.012	0.996	258729
Clear (Clearness Index > 0.7) (1m)						
1	−13	−0.008	0.014	0.016	1.009	39061
2	−52	0.004	0.013	0.014	0.996	40436
3	−97	0.004	0.012	0.013	0.991	41857
Cloudy (Ratio of Diffused Light > 0.95) (1m)						
1	−13	0.000	0.009	0.009	1.004	108115
2	−52	−0.001	0.009	0.009	1.004	115258
3	−97	0.001	0.009	0.009	0.991	112069
Other (Conditions except clear and cloudy) (1m)						
1	−13	−0.008	0.013	0.015	1.017	112772
2	−52	−0.004	0.014	0.015	1.007	107474
3	−97	0.000	0.015	0.015	1.001	105697
All (1h)						
1	−13	−0.002	0.015	0.016	1.002	4237
2	−52	0.015	0.023	0.028	0.956	4320
3	−97	0.021	0.027	0.034	0.929	4221
Clear (Clearness Index > 0.7) (1h)						
1	−13	−0.014	0.020	0.025	1.008	983
2	−52	0.023	0.033	0.040	0.959	961
3	−97	0.041	0.032	0.052	0.928	959
Cloudy (Ratio of Diffused Light > 0.95) (1h)						
1	−13	0.000	0.010	0.010	0.992	1452
2	−52	0.001	0.008	0.009	0.983	1615
3	−97	0.003	0.009	0.009	0.969	1538
Other (Conditions except clear and cloudy) (1h)						
1	−13	0.002	0.014	0.014	0.998	1872
2	−52	0.021	0.021	0.030	0.951	1814
3	−97	0.024	0.026	0.035	0.927	1790
Reference (Hourly irradiation)						
Ref.	0	0.021		0.042		4461

いて，晴天，曇天，それ以外の天候における算出精度も合わせて示した．さらに，これらの結果を従来の時積算傾斜面日射量の算出精度と比較するため，Table 4 の下段には 1 分値から作成した 1 時間値を用いて傾斜面日射量を算出した場合の精度を示し，最下段には参照値として文献 3)より引用した時積算傾斜面日射量の全天候での算出精度評価結果を加えた．1 分値，1 時間値ともデータ計測開始時刻をそのデータの時刻としており，例えば 9 時 0 分 0 秒～9 時 0 分 59 秒までの計測値から得られた 1 分値を 9 時 0 分として扱っており，9 時 0 分～9 時 59 分の計測値から得られた 1 時間値を 9 時のデータとして扱っている．

結果より，1 時間値を用いることにより算出精度が低下する傾向が見られた．この理由の一つとして，傾斜面日射量の算出に用いる太陽の位置を算出する際に，特に 1 時間値において時刻の誤差が大きくなってしまう事が考えられる．そこで，1 時間値の計測時刻を毎時 30 分として(9 時 0 分～9 時 59 分の計測値から得られた 1 時間値を 9 時 30 分のデータとする)太陽の位置を算出した場合の傾斜面日射量算出精度を Table 5 にまとめた．結果より，毎時 30 分における太陽の位置を用いて傾斜面日射量を算出した方が算出精度は良くなり，1 分値における算出精度とほぼ同等の精度が得られる事が分った．今回用いたデータは 1 分値，1 時間値とも，1 秒サンプリングによる値であり，全天候，全方位角において文献 3)と同等以上の精度が得られた．

Table 5 Verification results of calculation accuracy of hourly tilted surface irradiance using half-hour time stamp.

Station#	Azimuth [deg]	MBE [kW/m^2]	1Sigma [kW/m^2]	RMSE [kW/m^2]	α	Number of data
All (1h)						
1	−13	−0.004	0.010	0.011	1.012	4282
2	−52	−0.001	0.010	0.010	1.001	4335
3	−97	0.001	0.010	0.010	0.996	4288
Clear (Clearness Index > 0.7) (1h)						
1	−13	−0.006	0.011	0.012	1.007	500
2	−52	0.005	0.010	0.011	0.995	525
3	−97	0.003	0.010	0.010	0.992	550
Cloudy (Ratio of Diffused Light > 0.95) (1h)						
1	−13	0.001	0.005	0.005	0.989	1534
2	−52	0.000	0.004	0.004	0.995	1623
3	−97	0.001	0.005	0.005	0.992	1593
Other (Conditions except clear and cloudy) (1h)						
1	−13	−0.007	0.011	0.013	1.015	2282
2	−52	−0.003	0.012	0.012	1.005	2225
3	−97	0.001	0.012	0.012	0.998	2178

以上の結果より，3 節に示した時積算傾斜面日射量の算出手法は，1 分値のような，より短周期の瞬時的な日射強度を算出する際にも有効であることが示されたと言える．

6．傾斜面日射強度算出における誤差の評価

本節では，水平面での日射計測データから算出した傾斜面日射強度を用いて PV システム運転特性評価を行う際に，誤差要因になると考えられる項目について，その影響を調べた結果をまとめる．

6．1 方位角誤差の影響

PV システムの運転特性の評価には，入力エネルギーであるアレイ面日射量が不可欠である．しかし，住宅用太陽光発電システムなどの場合，必ずしも正確な方位角が計測されているとは限らず，南，東，西等のおおまかな方位のみ把握されている場合も多い．このようなシステムを評価する際には，アレイ面方位角情報と実際の方位角のずれが存在し，このずれは 1 分値のような短い計測周期で計測されたデータを用いて解析を行う際には誤差の原因になってしまうと考えられる．そこで，傾斜面日射強度を算出する際に，意図的に方位角をずらし，実際の方位角において計測された日射強度とのずれを評価した．評価には Station1

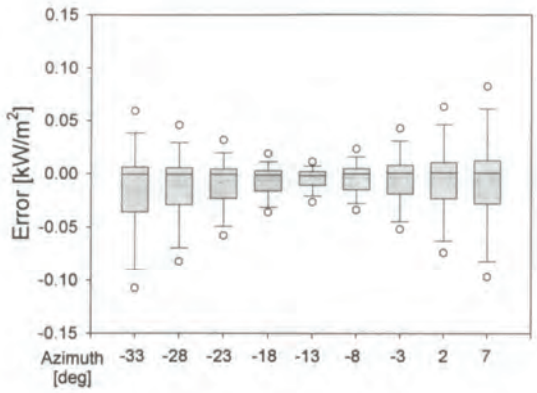

Fig.11 Box chart of azimuth error effect.

Table 6 Verification results of azimuth error.

Delta [deg]	Azimuth [deg]	MBE [kW/m²]	1Sigma [kW/m²]	RMSE [kW/m²]	α
−20	−33	−0.013	0.047	0.049	1.028
−15	−28	−0.010	0.037	0.038	1.023
−10	−23	−0.008	0.026	0.027	1.019
−5	−18	−0.006	0.017	0.018	1.015
0	***−13***	***−0.005***	***0.012***	***0.013***	***1.013***
5	−9	−0.004	0.017	0.018	1.011
10	−3	−0.004	0.027	0.027	1.010
15	2	−0.004	0.038	0.038	1.009
20	7	−0.005	0.049	0.050	1.010

の計測データを用い，実測の方位角である-13[deg]に対して東西両方向に5[deg]刻みで方位角をずらして傾斜面日射強度を算出し，実測の傾斜面日射強度との誤差を箱ひげ図(Fig.11)にまとめた．箱ひげ図では一つの方位角での算出結果を一つのグループとし，箱の中の実線は中央値(50%)を，破線は平均値を表している．箱の上辺，下辺は全データ中の 75%，25%をそれぞれ表しており，上側のひげは 90%を，下側のひげは 10%を表している．今回の解析では用いたデータ数が多く，ひげの外側にも多くのデータが存在するため，単純な計測誤差や発生頻度の低いばらつきを取り除き全体の分布を見るために，ひげの外側の上下に 95%, 5%のデータ点をそれぞれプロットした．また，Table 6 には方位角をずらした場合の各評価指標値をまとめた．

結果より，方位角がずれるに従って，算出値のばらつきの範囲は広がっていき，標準偏差や RMSE の値も大きくなる事が分る．1 分程度の時間間隔で PV システムの瞬時的な運転特性を評価する場合には，±10[deg]の方位角ずれに対して標準偏差や RMSE の値は倍以上に増加していることから，求める評価精度に合わせて方位角の許容できる誤差範囲を適切に設定する必要性があると言える．

一方で平均誤差に目を向けると，東側へずらした場合は平均誤差がマイナス側(実際より少なく算出している)へ動くのに対し，西側へずらした場合，算出する傾斜面の方位角が真南に近づく事から，平均誤差はわずかではあるがプラス側にずれている事が分る．いずれの場合も平均誤差の変化は方位角を±10[deg]動かしても大きな変化ではなく，これは，午前と午後の天候に大きな違いが無い場合には，午前中に多く(少なく)見積もった日射量を午後に少なく(多く)見積もる事で相殺される事が原因だと考えられる．このように，午前と午後で比較的天候が安定している地域では，1 日以上の期間におけるエネルギー量の評価に対して，方位角誤差が及ぼす影響は軽微であると考えられる．

6．2 傾斜角誤差の影響

PV システムのアレイ面傾斜角の測定は方位角と比べると容易であり，設計図などがあれば比較的正確な値を得ることが可能である．ここでは，実際の傾斜角 30[deg]に対して，±10[deg]の範囲でずらした場合の傾斜面日射強度の誤差を評価した．評価結果を，6.1 同様，箱ひげ図(Fig.12)と Table 7 に示す．なお，Fig.12，Table 7 には傾斜角と方位角を同時にずらした場合の誤差評価結果も併せて示した．

結果より，方位角同様，傾斜角をずらす事によってもばらつきの範囲は広がっていく事が分る．また，平均誤差に関しては，傾斜角を 30[deg]より大きい方向にずらした場合にはあまり変化しないが，より水平に近い方向へずらした場合には，平均誤差がマイナス方向へとずれていき，ばらつきの範囲もマイナス方向へと広がっている．方位角，傾斜角をそれぞれ同時に 5[deg]ずらした場合にも，ばらつきの範囲は傾斜角を 25[deg]にした場合の方が多い．

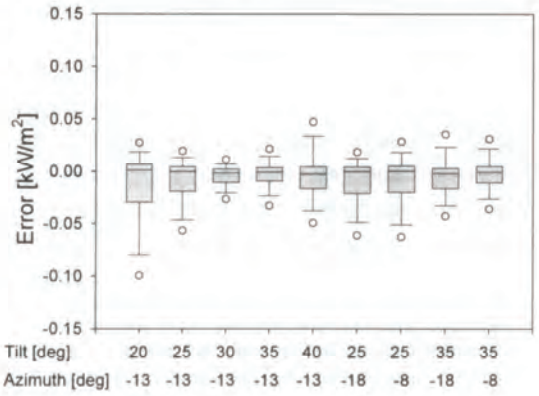

Fig.12 Box chart of tilt angle error effect.

Table 7 Verification results of tilt error and azimuth error.

Tilt [deg]	Azimuth [deg]	MBE [kW/m²]	1Sigma [kW/m²]	RMSE [kW/m²]	α
20	−13	−0.014	0.038	0.040	1.044
25	−13	−0.008	0.023	0.024	1.026
30	***−13***	***−0.005***	***0.012***	***0.013***	***1.013***
35	−13	−0.003	0.016	0.016	1.005
40	−13	−0.003	0.027	0.027	1.001
25	−18	−0.010	0.024	0.026	1.028
25	−8	−0.008	0.026	0.027	1.024
35	−18	−0.004	0.022	0.022	1.007
35	−8	−0.002	0.019	0.019	1.003

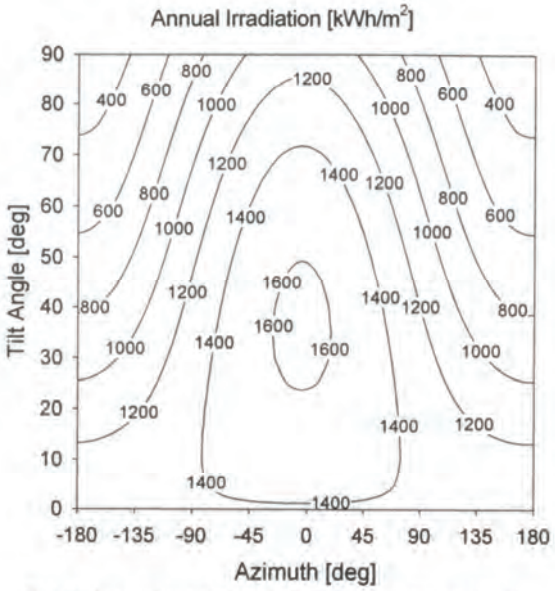

Fig.13 Annual irradiations of all tilt angle and azimuth.

このような違いは，各方位角，傾斜角における年間日射量の違いによって説明ができる．Fig.13 には 3 節で示した方法により，Station1 の水平面全天日射量と直達日射量を用いて算出した，全方位，全傾斜角の年間日射量を示した．このグラフからも分るとおり，30[deg]付近の最適傾斜角から傾斜角が大きくなる方向では 40[deg]辺りでも年間日射量に大きな違いは無いが，より水平に近づく方向では年間日射量が低下しており，方位角 0[deg]，傾斜角 20[deg]での年間日射量 1579[kwh/m²]に対し，傾斜角 30[deg]では 1622[kwh/m²]，傾斜角 40[deg]では 1628[kwh/m²]となっている．このように，方位角，傾斜角の誤差によって生じる平均値のずれやばらつきの広がり方は，対象とする傾斜面がどの方位・角度に向いているかによってその付近での日射量の変化に差があることから，同じ角度誤差に対しても異なる値となるため，注意が必要である．

6．3 アルベドの影響

住宅用 PV システムは様々な面に設置されるため，屋根の色や材質，陸屋根に架台を設けて設置されたシステムなど，周辺環境の違いによって，反射光の影響も様々であると考えられる．しかし，全ての環境においてアルベドを実測する事は現実的ではないため，本手法では一般的な住宅地域の値として，アルベド値を 0.2 に固定して傾斜面日射強度を算出している．アルベド値の誤差が年間日射量に及ぼす影響を評価するため，Station1 の年間計測データを用いてアルベドを 0.5,0.8 と変化させた結果を Fig.14 の左側と Table 8 にまとめた．なお，アルベド値 0.8 とは新雪の雪面の反射率に相当する値である．

結果より，アルベド値を大きくするに従い，平均誤差はプラス側(日射強度を多く算出する側)にずれていくが，そのずれ量は限定的で，ばらつきの範囲もほとんど変化しない．この結果より，アルベド値の誤差に関しては傾斜面日射強度算出に及ぼす影響は軽微であると言える．

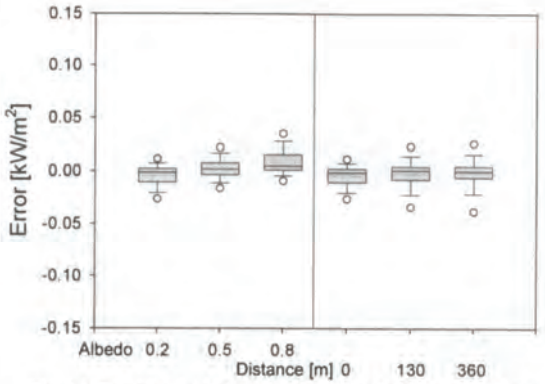

Fig.14 Box chart of albedo effect and distance effect.

Table 8 Verification results of albedo effect.

Albedo	MBE [kW/m²]	1Sigma [kW/m²]	RMSE [kW/m²]	α
0.2	***−0.005***	***0.012***	***0.013***	***1.013***
0.5	0.002	0.012	0.012	0.996
0.8	0.008	0.014	0.016	0.980

Table 9 Verification results of distance effect.

Distance [m]	MBE [kW/m²]	1Sigma [kW/m²]	RMSE [kW/m²]	α
0	***−0.005***	***0.012***	***0.013***	***1.013***
130	−0.002	0.030	0.030	1.006
360	−0.002	0.050	0.050	1.000

6．4 距離の影響

評価対象とする全ての PV システムのアレイ面に日射計を設置することは，費用の面でも維持管理の面でも現実的ではない．本実証研究では地域内 6 カ所の代表地点にて日射強度を計測しているため，PV システムと日射計の間にある程度の距離が存在する．このような場合，移動する雲の影響などで，日射計，または PV システムのみが日陰になっているといった状況が発生し，傾斜面日射強度算出と PV システム運転特性評価における誤差要因となっている．ここでは，この距離の影響を調べるため，Station1 の実測傾斜面日射強度に対して，Station2，Station3 の水平面全天日射強度と直達日射強度を用いて算出した場合の誤差を評価した．結果を Fig.14 の右側と Table 9 に示す．なお，それぞれの日射計の位置関係は Fig.1 に示した通りであり，ほぼ南北に並ぶ形となっている．

結果より，日射計設置位置から距離がある場合の傾斜面日射強度算出においても，平均値の誤差は無視できる範囲に収まっていることが分る．しかしばらつきの範囲は大きく広がっていることから，瞬時値を用いた評価を行う場合

には，できるだけ近くの日射計を用いる等，ばらつきを抑える工夫が必要である．

7．まとめ

本論文では，従来から広く用いられてきた時積算傾斜面日射量の算出方法を分単位でのより瞬時的な傾斜面日射強度算出に適用し，その算出精度を明らかにした．また，算出した傾斜面日射強度を PV システム運転特性評価に用いる際に誤差要因となる項目について，その影響を明らかにした．用いたデータは「集中連系型太陽光発電システム実証研究」の実証研究地域において計測されたデータに限られるため，結果には地域的な特徴を含むが，晴天や曇天などの天候別に結果をまとめた事により，日本国内において他の地域を評価する際にもある程度参考として用いることが可能であると考える．今後も PV システムの大量普及と大規模な系統連系の増加により，電力品質の維持の為に，より瞬時的な現象に対して評価，解析が行われていく事が予想される．本論文におけるデータが，PV システム評価時の誤差範囲の算出の一助になることを期待する．

なお，本研究は，「集中連系型太陽光発電システム実証研究」の一環として行ったものである．このような機会を与えていただいた(独)新エネルギー・産業技術総合開発機構，及び様々なご協力をいただいた関係者各位に，この場を借りて感謝の意を表する．

参考文献

1)Y.Ueda, T.Oozeki, K.Kurokawa, T.Itou, K.Kitamura, Y.Miyamoto, M.Yokota, H.Sugihara, S.Nishikawa, "ANALYTICAL RESULTS OF OUTPUT RESTRICTION DUE TO THE VOLTAGE INCREASING OF POWER DISTRIBUTION LINE IN GRID-CONNECTED CLUSTERED PV SYSTEMS", 31st IEEE Photovoltaic Specialists Conference pp1631 (2005)

2)R.Perez, R.Seals, P.Ineichen, R.Stewart, D.Menicucci, "A NEW SIMPLIFIED VERSION OF THE PEREZ DIFFUSE IRRADIANCE MODEL FOR TILTED SURFACES", Solar Energy Vol.39(3) pp.221-231 (1987)

3)日本太陽エネルギー学会編，「新太陽エネルギー利用ハンドブック」 pp.26-30

4)英弘精機株式会社，「精密全天日射計 MS-802F カタログ」

農業情報研究 15(2), 2006. 139-154

原著論文

独立小型太陽光発電システムの利用実態と課題 ーモンゴルの遊牧民を事例としてー

アジヤバト アマルバヤル*1)・中島正裕2)・大谷謙仁3)・黒川浩助1)

1)東京農工大学工学部　〒184-8588　東京都小金井市中町2-24-16
2)東京農工大学農学部　〒183-8509　東京都府中市幸町3-5-8
3)産業技術総合研究所電力エネルギー研究部門　〒305-8568　つくば市梅園1-1-1

要旨

モンゴル国では，遊牧民の生活水準の向上を目的として住居（ゲル）を電化するために1999年から独立小型太陽光発電システム（SHS）が導入されている．本研究では，ヒアリング調査（67世帯）とアンケート調査（359票）によりSHS利用者の利用実態と未利用者の認識を明らかにし，今後のSHSの普及定着に向けての課題について検討した．主な知見として，以下の5つが得られた．

（1）SHSの導入によって照明とテレビの使用が可能になったことに対して，SHS利用者は高い満足感を得ていた．また，SHSは小型かつ軽量であり，燃料を必要としないため，他の電源と比較して，移動を繰り返す遊牧民のライフスタイルに適合する技術であることが示された．（2）SHSを導入した世帯の78%が「10万ソーラーゲル計画」による補助金と無利子ローンを活用しており，市場を通しての普及が進んでいない．（3）SHSの課題は，SHSの保証期間が1年以内と短いこと，修理店または技術者が近くの村落センターまたは県都にいないことなどである．（4）未利用者のSHSに対する認識度が高く，SHSを購入予定があるという回答者が多いことが分かった．（5）SHSの普及定着及びそれによる遊牧民の農牧業の生産性向上のための課題は，市場原理に向けた優遇措置の見直し，サポート体制の整備，農牧業情報の活用環境の整備である．

キーワード

電化，独立小型の太陽光発電システム，アンケート調査，利用実態，遊牧民世帯

はじめに

モンゴル国では農牧業がGDPの約20%を占める基幹産業であり，その内8割は遊牧民世帯が営む家畜業（以降，遊牧業とする）である（NSO 2004）．しかし，1991年の市場経済化以降，遊牧民世帯と家畜頭数の増加，都市と幹線道路の周辺地域における家畜の集中，さらには気候変動の影響による砂漠化など遊牧業を営む上で様々な問題が起きている．これらの社会的及び自然的要因によって，牧草地の荒廃が生じており（鈴木 2003），遊牧業の生産性が低下している．遊牧業の生産性とリスク管理の能力を向上させるために，遊牧業の伝統的な知恵の伝承と実践的スキルなどに関する農牧業情報の共有は重要な課題である．

こうした状況下，1996年には遊牧民のラジオ放送スタジオが3ヶ所に整備されており，遊牧民の能力開発と情報共有のために放送活動が行われている（Robinson 1997）．また，最新の科学的手法や技術導入が検討され，リモートセンシング技術を牧草管理に活用する実用的な研究開発が進め

* Corresponding Author
E-mail: amar@cc.tuat.ac.jp

られ（Erdenesaikhan 2002），情報配信システムと体制が提案されている（Tserendash 2000）．本多（1999）はモンゴル国において，人工衛星データを利用するリモートセンシング技術を活用して，地上の植物の分布状況と生産量や質（生育状況）を把握する手法を開発した．このように，遊牧業の生産性の向上と自然災害の回避に最新技術を駆使した高度情報の活用が期待されている．

遊牧民世帯は，こうした農牧業に関する高度な情報や日常的に得る天気予報，市場情報，教育情報などの入手と交換のためにはラジオやテレビ放送や短波通信機器が必要であり，電化が不可欠である．しかし，モンゴル全国における遊牧民世帯の電化率は，年々上昇傾向にあるものの2003年においてわずか16.8%である（表1）．遊牧民は，広く薄く分布する牧草資源を求めて移動を繰り返しているため，携帯性の良い独立電源システムが必要である．実際に利用されている独立電源システムの種類とそれぞれの特徴比較を表2に示す．安定的に高出力が得られる小型ガソリン発電機は古くから使用されているが，遠隔地では燃料の安定的な調達と貯蔵，運搬費が問題になるため，広く普及してないのが現状である．また，安価で携帯性が良い小型風力発電システムは，風力資源が局所的で風速や風向の変動が大きく（Nikolakaki 2001），冬営地などは風を直接受けない場所が選ばれるなどの理由があり，全国に約3千台しか使用されてない（ADB 2002）．

このような中，日射量が豊富なモンゴルでは，遊牧民の住居（ゲル）を電化するために独立小型太陽光発電システム[注1]（SHS：ソーラーホームシステム，図1）が注目されており，国家プロジェクト（「10万戸ソーラーゲル計画」）として，2005年4月時点で約3万2千戸にSHSが導入されている．

筆者らは，乾燥・半乾燥地域における遊牧民世帯及び集落へ太陽光発電システムを導入する場合の地域適合性を検証するために，ケーススタディとしてモンゴル国における太陽エネルギー資源のポテンシャル評価と太陽電池モジュールの暴露試験と性能評価（Amarbayar *et al.* 2004），SHSの運転データの分析と損失分離を行っている（アジヤバト アマルバヤル・黒川浩助 2005）．今後，モンゴル国におけるSHSのさらなる普及定着のた

表1　モンゴル全国における遊牧民世帯の生活水準指標の推移(NSO 2004b)

統計指標	2000	2001	2002	2003
遊牧民世帯数	191,526	185,546	175,911	172,412
電化率 [%]	10.7	13.4	13.7	16.8
TV所有率 [%]	12.8	15.7	16.7	19.3
自動車所有率 [%]	8.7	9.5	10.5	11.5
バイク所有率 [%]	16.6	18.3	18.5	19.4

表2　遊牧民世帯の利用に対する独立小型電源システムの特徴比較

電源の種類	利点	弱点
独立小型太陽光発電システム（SHS）	高い携帯性，設置と保守管理が簡易，維持管理費・低コスト，無騒音，燃料不要，太陽電池の寿命20年	初期コストが高価，時間帯と天候による出力制限，蓄電池交換
小型ガソリン発電機	高出力，安定的電力供給	燃料とその運搬費が高コスト，燃料の安定的調達と貯蔵が困難，騒音，排気ガス
独立小型風力発電システム	安価，高い携帯性，設置容易，燃料不要	風力資源は局所的，強風下での危険性，騒音，短寿命，蓄電池交換，保守管理が必要

農業情報研究 15(2), 2006. 139-154

めには，こうした技術的側面からのアプローチのみならず，SHSの利用者及び未利用者への意識調査を行い，それらの結果を今後のSHSに関する技術開発や施策に反映するための知見を得ることが必要である．また，世界的にみても，SHSは開発及び発展途上国を中心に2000年まで約130万台が導入されているが，SHSのフィールドモニタリングやSHSユーザの声を聞くことがほとんど行われておらず，SHSの利用実態が未解明である（Nieuwenhout ら（2001）．

そこで本研究では，SHSを利用している遊牧民の利用実態（導入動機，満足度，利用形態，ニーズや問題点等）と未利用者のSHSに対する導入の可能性を明らかにし，今後のSHSの普及定着に向けての課題について検討する．

調査・分析方法

本研究のアンケート調査対象者は，モンゴル国の西部，中部，南部の地域から6つの県（ホブド県，ザブハン県，ブルガン県，ドンドゴビ県，ドルノゴビ県，ヘンティー県）の遊牧民世帯とした（図2）．

SHSの利用実態のアンケート項目の作成にあたっては，文献調査（新エネルギー財団 2005）及びドルノゴビ県サインシャンド村落（11 世帯）とヘンティー県ダダル村落（12 世帯）の遊牧民に現地で予備調査（ヒアリング調査）を行い，SHS利用者に対して表3に示すようにSHSの導入の動機，SHSの故障や修理など6つのカテゴリーからなる20項目の質問を設定した．実施方

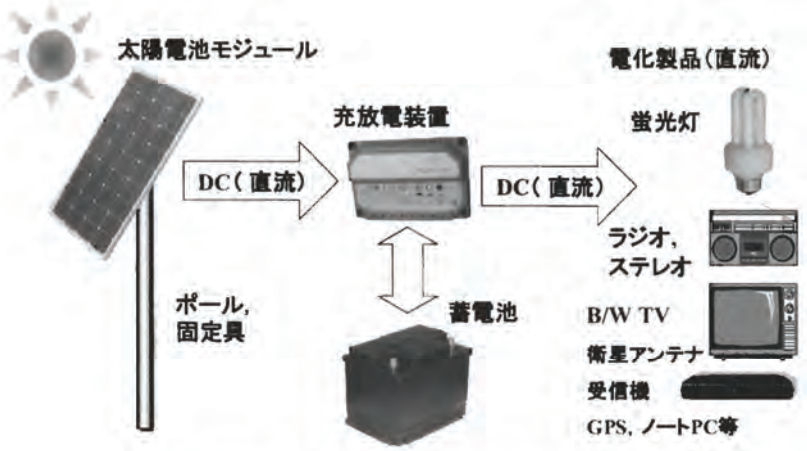

図1　独立小型の太陽光発電システム（SHS）の構成

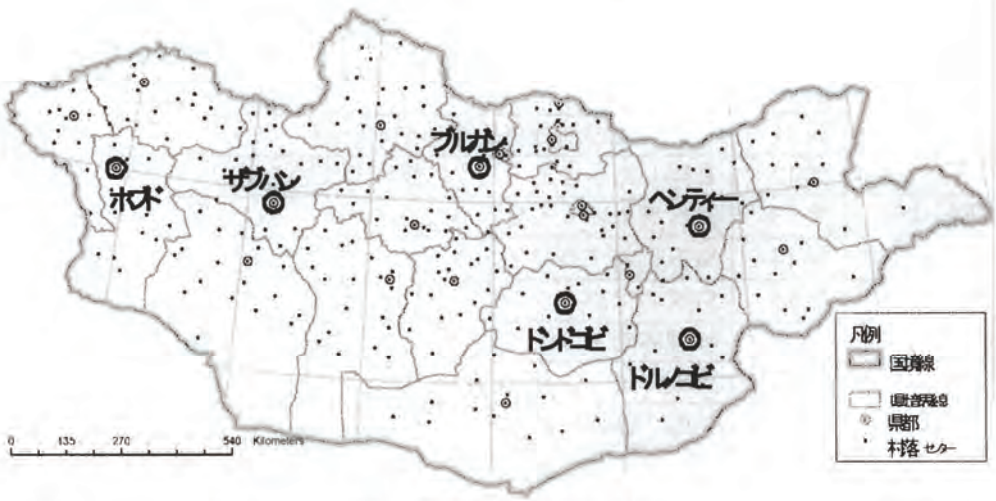

図2　調査対象地域の位置

法は，モンゴル国「燃料エネルギー省」の協力を得て，調査協力の得られた5県（ホブド県，ザブハン県，ブルガン県，ドンドゴビ県，ドルノゴビ県）の村落センターに合計3000部の調査票を郵送し（2005年6月21日），各村落センターを訪れた遊牧民の中で，SHSを所有する遊牧民に調査票が配布された．

アンケート実施の結果，359部（表5）が回収され，回収率は約12%であった．アンケート調査の回収率として12%は低いが，牧草地を求めて移動し住所が不確定などの特殊条件を有する遊牧民が対象者であること，調査に要する費用と時間が掛かること，さらには，既述したようにSHSの利用形態が未解明であることを考慮すると，359部でもSHSに対する利用者意識の傾向をみることは意義があると考えられる．しかしながら，アンケート調査からはSHSの利用実態の傾向を概括的には把握できるものの，使用しているSHSの性能（定格出力）別にみた利用実態の相違や発電量と消費電力量のバランスなどについては具体的に把握できない．そこで，この点を明らかにするために，代表的な定格出力のSHS（62W，50W，20W）をそれぞれ所有する3世帯の遊牧民のヒアリング調査結果を詳細に示す．

また，今後のSHSの導入の可能性を検討するため，SHS未利用者に対してSHSの認識程度や今後の購入予定など7つの項目を設定した（表4）．実施方法は，ブルガン県ヒシグウンドル村落（37世

表4　SHS未利用者に対するアンケート調査の質問項目

設問分類	設問	質問内容
アンケート回答者の属性	問1	回答者の家族数
	問2	年間の平均収入
	問3	家畜所有頭数
SHSの認識程度	問4	SHSに対する認識程度
	問5	SHSに関するコメント
SHSの導入可能性	問6	電源システムの購入の意思
	問7	導入したい電源の種類

表3　SHS利用者に対するアンケート調査の質問項目

設問分類	設問	質問内容
アンケート回答者の属性	問1	回答者の家族数
	問2	年間の平均収入
	問3	家畜所有頭数
SHSの導入，その動機	問4	SHSの購入先
	問5	使用開始時期
	問6	SHS導入の動機
	問7	SHSを購入する前にほかの電源を使用していたかどうか
	問8	ほかの電源ではなくSHSを選んだ理由
SHSの維持管理	問9	太陽電池の設置場所
	問10	故障の回数
	問11	SHSのどの部分が故障しやすいか
	問12	故障した場合どのように修理しているか
SHS導入による効果・影響	問13	SHS導入による良かった点
	問14	SHSに対するコメント
SHSの欠点，今後の要望	問15	SHSの欠点
	問16	修理体制・方法について
	問17	長期保証・品質について
	問18	SHSの価格・販売体制・その他について
SHSに対する総合的評価	問19	SHSに対する満足度
	問20	他人への勧め

農業情報研究 15(2), 2006. 139-154

帯), ドルノゴビ県サインシャンド村落 (6世帯) 及びヘンティー県 (7世帯) の遊牧民からSHSを利用していない遊牧民の協力を得て, 合計50世帯 (表5) に対面式アンケート調査を行った.

遊牧民へのSHSの導入経緯

モンゴル国では, 1989年に11W(定格最大出力)のアモルファスシリコン太陽電池で充電するランターン (中国製) が約2500セット販売されたことで[注2], 太陽電池が遊牧民に知られるようになった. その後, NEDO (1997) はモンゴル国において1992年から1996年にかけて携帯型の太陽光発電システムの実証研究を行い, モンゴルの非定住の社会システムをフィールドにして, 蓄電池やインバータ等の周辺機器を含むSHSの小型軽量化, 可搬性と信頼性の向上を図った.

これらの実証実験より, SHSが遊牧民の生活に適していることが明らかとなり, モンゴル国政府は1999年10月にモンゴル国会で, 遊牧民の住居 (ゲル) を電化する「10万戸ソーラーゲル計画」を議決した (Enebish 2000). この国家プロジェクトは, モンゴル国内約17万戸の無電化遊牧民世帯の内, 10万戸に対して2010年までに3つの段階を経てSHSを普及させるというものである. 初段階として初年度の2000年に約5千台, 第二段階として2001～2005年に約4万5千台, 第三段階の拡張と完成期として2006～2010年には約5万台のSHSをそれぞれ導入することを目標としている.

SHSの1セット当たりの市場価格は, 太陽電池モジュール1枚 (50W), 蓄電池 (12V, 75Ah), 充放電装置等を含めて約4万円である. 年間の平均所得が約124万Tg (NSO 2004) =約12万3千円注3)の遊牧民にとってSHSは非常に高額である. このため, 「10万戸ソーラーゲル計画」では1999年から無利子の1年間ローンを実施し, 2003-2004年には50%の補助金を交付するなどの措置を行った. モンゴル国「燃料エネルギー省」の推計では, 2000年までに約900台, 2005年4月までに約3万2千台のSHSが導入されている. 地域別の導入状況 (表6) をみると, 電化率の低い地域に対するSHSの導入件数が多い傾向にある.

表5 対象地域における面接調査と調査票の回収状況

県名	SHS利用世帯	未利用世帯
	郵送	面接
ドルノゴビ	63	6
ドンドゴビ	27	-
ブルガン	45	37
ヘンティー	-	7
ホブド	117	-
ザブハン	107	-
合計	359	50

SHS利用者へのアンケート調査結果

アンケート回答者の属性

SHS利用世帯の家族数は4人 (28.7%) または5人 (25.7%) の割合が多い (表7問1). SHS利用世帯の収入は100万Tg (9万4千円) 以下 (63.6%) の割合が多い (表7問2). 農村地域の世帯におけ

表6 県別遊牧民の世帯数, 電化率(2003年)とSHSの導入件数[注2](2005年3月)

県名	遊牧民世帯数	電化率[%]	SHSの導入数
アルハンガイ	17,077	6.7	2,190
バヤンウルギー	11,200	7.3	3,008
バヤンホンゴル	11,329	22.5	2,930
ブルガン	7,268	8.8	1,055
ゴビアルタイ	8,109	16.4	3,050
ドルノゴビ	4,092	24.7	425
ドルノド	4,803	16.0	750
ドンドゴビ	7,955	22.6	1,215
ザブハン	10,230	8.1	2,742
ウブルハンガイ	17,416	20.5	2,096
ウムヌゴビ	6,328	34.5	820
スフバートル	7,688	21.1	2,300
セレング	2,921	30.7	409
トゥブ	8,719	16.6	383
オブス	9,920	12.9	1,550
ホブド	9,117	14.6	3,570
ホブスグル	16,484	11.9	2,055
ヘンティー	7,352	15.4	705
ダルハンウール	919	36.8	100
ウラーンバートル	2,196	82.8	-
オルホン	794	43.7	150
ゴビスンベル	475	12.4	110
合計	172,392	16.7	31,613

る全国平均年収が124万Tg（約12万3千円[注3]）であるのに対して（NSO 2004），本研究のアンケート対象の遊牧民世帯の収入は低い傾向にある．この要因は，農村地域の世帯に現金収入が多い公務員，会社員の世帯も含まれるためであると考えられる．

また，家畜頭数は遊牧民の資産の主な指標となっており，一般的には50頭以下の家畜を所有している世帯を貧困層，150-250頭を所有している世帯が中間層とされている（Jargal *et al.* 2004）．モンゴル国統計局（NSO 2004）による全国の遊牧民の家畜所有頭数の分布と比較すると，SHSを所有する世帯は中間層以上に該当する世帯の割合が多いことが分かる（図3）．

表7　回答者の属性

選択項目	度数	[%]
問1 家族数		
3人まで	36	12
4人	86	28.7
5人	77	25.7
6人	61	20.3
7人以上	40	13.3
合計	300	100
問2 年間の平均収入		
40-60万Tg	93	31.3
60-80万Tg	47	15.8
80-100万Tg	49	16.5
100-140万Tg	44	14.8
140-200万Tg	37	12.5
200万Tg以上	27	9.1
合計	297	100

SHSの導入とその動機

SHSの購入先（表8問4）としては，「10万戸ソーラーゲル計画」による国からの購入が最も多い（78%）．「都市の販売店」や「訪問販売[注4]」から購入したケースは合計でも約16%であった．また，SHSの使用期間は，それぞれ1年以内が30%，2年間が41%，3年間が24%，3年以上が5%を示し，2年以内の世帯が71%であり，SHSの利用経験が少ないユーザが多いことが分かる．

SHSを導入した動機（表8問6）は，生活の利便性向上への欲求という意味での「電化製品を利用したい」（53.3%）が最も多く，次いで「近隣の家庭で体験して便利に感じた」（21%）であった．

SHSを導入する前に使用していた電源については，「電源を使用してなかった」（44%）が最も多い（表8問7）．SHSを導入するまでに発電機，風力発電システム，蓄電池など何らかの電源システムを使用したことがあり，電気の便利さを知っていた世帯は合計56%である．

また，他の電源システムではなくSHSを選んだ理由としては，「燃料が要らない」（51%）と「持ち運びが便利である」（19%）が多かった（表8問8）．小型ガソリン発電機を使用する遊牧民世帯では，燃料の宅配サービス等がないため，平均的に

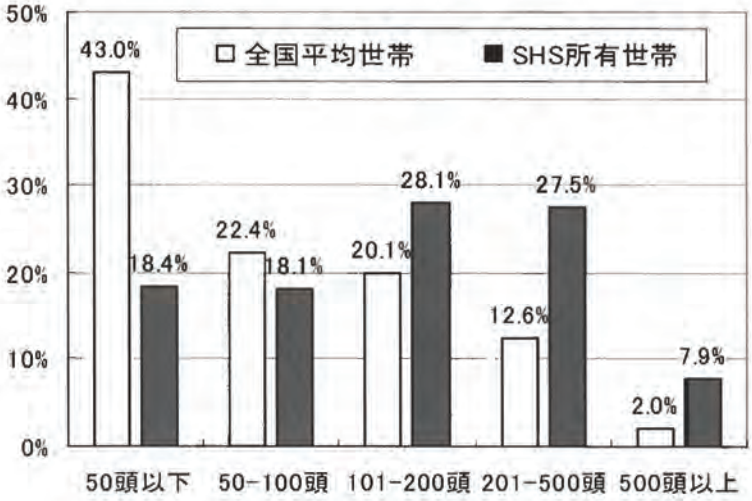

図3　SHS所有世帯と一般世帯の家畜所有頭数の比較

農業情報研究 15(2), 2006. 139-154

60km離れた村落センターからガソリン燃料を定期的に調達する必要がある．しかし，これには多額の経費が掛かるため，小型ガソリン発電機の継続的利用は困難である．

SHSの維持管理

SHSの太陽電池モジュールの設置場所（表9問9)は，「専用ポールに設置している」が最も多かった（71.6%）．しかし，住居（ゲル）の上に置いている世帯もあった（22.5%）．このような場合，モジュールの裏面が密閉された状態となり，開放状態の設置（専用ポールに設置）よりモジュール温度が上昇し出力が低下する．また，モジュールの高温状態はホットスポットや劣化の原因となり，火災の恐れもある．

SHSの故障しやすい部分は充放電装置やブレーカやヒューズなどを含む「コントロールボックス」（32.2%）と「蓄電池」（29.7%）である（表9問11）．しかし，故障回数[注5]（問10）は，1回が44件，2回以上が23件であり，故障頻度は比較的少ないといえる．これはSHSを購入して1，2年しか経ってない世帯が多いからであると考えられる．また，これ以外には，ヒアリング調査の結果から「遊牧で移動して再度SHSを組み立てる際に接続ミスによる短絡」が多いことが分かった．

故障したときの対処方法は（表9問12），現在はSHSの修理とサポートを行う業者と修理店が少ないため，故障した際には「電気に詳しい知人に頼む」（54.5%）が最も多く，次いで「自分たちで対応する」が多かった（19.4%）．

SHSの保守管理の作業内容としては，機材の掃

表8　SHSの導入，その動機について

選択項目	度数	[%]
問4 SHSの購入先		
都市の販売店	27	8.2
10万戸ソーラーゲル計画	258	77.9
訪問販売	25	7.6
その他	21	6.3
合計	331	100
問6 SHS導入の動機		
電化製品を利用したい	184	53.3
近隣の家庭で体験して便利に感じた	72	20.9
10万戸ソーラーゲル計画による優遇措置を知った	63	18.3
友人に勧められた	25	7.2
その他	1	0.3
合計	345	100
問7 SHSを購入する前に電源を使用していたかどうか		
電源はなかった	128	43.8
小型ガソリン発電機	79	27.1
風力発電システム	20	6.8
蓄電池	31	10.6
その他	34	11.6
合計	292	100
問8 ほかの電源と比べてSHSを選んだ理由（複数回答）		
燃料が要らない	252	51.2
騒音がなく，安全	45	9.1
持ち運びが便利	93	18.8
他に選択肢がなかった	30	6
環境に優しい・趣味	63	12.8
他の理由	11	2.2
合計	493	100

表9　SHSの維持管理について

選択項目	度数	[%]
問9 太陽電池の設置場所		
専用ポール等に設置	232	71.6
ゲルの上に固定	73	22.5
その他	19	5.9
合計	324	100
問11 SHSのどの部分が故障しやすいか		
太陽電池	26	10.9
蓄電池	71	29.7
コントローラ	77	32.2
ケーブル	21	8.8
パネル固定具	19	7.9
その他	25	10.5
合計	239	100
問12 故障した場合どのように修理しているか		
自分達で対応する	79	29.4
電気に詳しい人に頼む	147	54.6
購入先・修理店に依頼	25	9.29
その他	18	6.69
合計	269	100

除，太陽電池モジュールの固定具等の設置の安全点検，コントローラや蓄電池の電圧やインジケータ等の正常動作の確認，さらには開放型の蓄電池を使用している場合には電解液の補充確認がある．これらの維持管理についてはSHSの種類や導入時期によっても異なり，適宜行われていた（ヒアリング記録より）．

SHS導入の日常生活と農牧業への効果

SHS導入による日常生活の変化の中で良かった点（表10）については，「テレビ放送のニュースや市場情報などを即時に入手している」が最も多かった（53.8%）．これは，新聞，雑誌などの情報媒体が遊牧民の元に届くのは一週間以上遅れるという現状があり，SHSの導入により電源が確保できたことで，テレビを通じて都市地域の住民と格差なく，様々な情報を即時に得られるようになったことを意味する．

次いで多かったのが，「天気予報を詳細に把握できる」（22.9%）である．天気予報は遊牧民が放牧計画を立てる上で重要な情報である．具体的な例を2つ示すと，大雪や大雨が予想されるの場合は，放牧せず畜舎や柵に待避させておく．強風が予想される場合は，予め風が吹く方向に放牧し，風が強まったときに追い風によって容易に帰宅するなどの工夫がなされている．

さらには，SHSにより畜舎に照明の設置が可能となり，オオカミによる家畜被害の防止対策にもなる．SHS導入の効果について調査結果では，情報入手の環境が改善されたことが挙げられた（表10）．遊牧業を営む上で，気象環境と牧草地と家畜という3つの基本要素に加えて市場と生活状況の情報を巧みに活用しなければ，自然災害などに遭遇する恐れがある．2000年に大寒波（ゾド）により約240万頭の家畜が凍死したという惨事が起こった（森永由紀・篠田雅人2003）が．今後，気象情報を的確に入手し，被害回避の対策を取れば，大きな被害を未然に防ぐことができると考えられる．

なお，SHSの導入によって悪影響が見られた点としては，ドルノゴビ県サインシャンド村落（11世帯）とヘンティー県ダダル村落（12世帯）の遊牧民への予備調査（ヒアリング調査）において，「子供達がテレビを見すぎる」という意見が数軒でみられた程度で，それ以外には「特に無い」という意見が多かった．

表10　SHS導入による良かった点（問13，複数回答）

選択項目	度数	[%]
テレビ放送のニュース・市場情報などを即時に入手している	279	53.8
天気予報を詳細に把握できる	119	22.9
映画やドラマを楽しめるようになった	75	14.5
教育番組が見られるようになった	32	6.2
テレビ鑑賞を通じて近所との交流が深まった	7	1.3
その他	6	1.2
合計	519	100

SHSの欠点と今後の要望

SHSの欠点（表11問15）としては，「価格が高い」（48.9%）が最も多く，次いで「利用時間の制限」（22.7%）が多かった．「価格が高い」に関しては，「10万ソーラーゲル計画」によりSHSの購入への優遇措置（補助金，無利子融資）はあるものの，年間収入からすると割高感がみられる．

今後の要望を3つのカテゴリー別にみると，修理方法に関しては「村落センターに修理店の設立」（39.1%）と「ユーザマニュアルの充実化」（36.8%）への要望（表11問16）がほぼ同様の割合で高い．簡単な故障についてはユーザが対応できるようになりたいため，「ユーザマニュアルの充実化」が高い割合を示したと考えられる．保証・品質（表11問17）に関しては，「保証期間の長期化」（61.0%）の割合が高い．その背景には，「10万ソーラーゲル計画」から購入したSHSの保証期間は1年であり，また販売店や商人による訪問販売では商品が保証されないことがある．また，SHSの価格・販売体制・その他（表11問18）に関しては，「SHSの販売価格の値下げ」（46.6%）が最も多い．次いで，「SHSと蛍光灯，蓄電池などが村落内で購入可能に」（28.5%）と「SHSのサイズ拡大，出力増加」（24.9%）とほぼ同様の割合を示した．「SHSのサイズ拡大，出力増加」は，冷蔵庫などの消費電力の大きい電化製品も使用したいという要望によるものと考えられる．

農業情報研究 15(2), 2006. 139-154

表11　SHSの欠点，今後の要望(複数回答)

選択項目	度数	[%]
問15 SHSの欠点		
価格が高い	153	48.9
利用時間の制限	71	22.7
頻繁に故障する	20	6.4
操作が難しい	21	6.7
その他（欠点なし，分からない）	48	15.4
合計	313	100
問16 修理体制・方法について		
村落センターに修理店の設立	136	39.1
ユーザマニュアルの充実化	128	36.8
修理派遣員の巡回	84	24.1
合計	348	100
問17 長期保証・品質について		
保証期間の長期化	159	61
周辺機器の品質向上	87	33.2
その他(特にない，有料保証の延長)	15	5.8
合計	261	100
問18 SHSの価格・販売体制・他について		
SHSの販売価格の値下げ	79	46.6
SHSと蛍光灯，蓄電池などが村落内で購入可能に	48	28.5
SHSのサイズ拡大，出力増加	42	24.9
合計	169	100

表12　SHSに対する総合的評価

選択項目	度数	[%]
問19 SHSに対する満足度		
満足している	308	89.3
どちらでもない	29	8.4
満足していない	8	2.3
合計	345	100
問20 他人へSHSを勧めるかどうか		
勧める	252	75.9
どちらでもない	60	18.1
勧めない	15	4.5
分からない	5	1.5
合計	332	100

総合評価

SHSを導入したことによる満足度としては，89%の世帯が導入して満足している(表12問19)．また，76%の世帯がSHSを他人に勧める(表12問20)と答えている．これらの結果より，SHSを導入したことによる遊牧民の総合評価は高い傾向にあるといえる．ただし，SHSを導入して2年未満の世帯が7割以上を占めており，この評価はあくまでSHS導入の初期段階のものである．利用年数が経つにつれて，表11で明らかとなった様々な欠点や要望を如何に解決するかが，今後のSHSに対する評価に影響を及ぼすと考えられる．

SHSの性能ごとに見た遊牧民の生活の実態

ここでは，使用しているSHSの性能(太陽電池の定格出力：62W，50W，20W)別にみた利用実態を述べるとともに発電量と消費電力量のバランスを試算する．

定格出力62Wのケース(世帯A)

トゥブ県ナライフ村落の6人家族の世帯Aでは，2003年10月から表13に示す仕様のSHSセットを利用している(図4)．SHSの導入の動機は，ラジオ番組で「10万ソーラーゲル計画」の内容とその優遇措置(補助金と1年間無利子ローン)を知ったことであった．この世帯の年収は約80万Tg(約7万5千円)であり，所有する家畜頭数は120頭である．購入したSHSセットの価格は37万Tg(約3万5千円)であり，価格の50%は補助金を受けて残額(18万5千Tg)は1年間の無利子ロー

図4　SHSの設置状況(世帯A)

ンで支払った. SHSの導入により,「照明とテレビが使えるようになったので大変満足している」とのことであった.

世帯Aは, 蛍光灯, ステレオ, テレビを使用し(表14, 図5), 平均的に夏季は184Wh/日, 冬季は169Wh/日の電力消費をしている. そこで, 日射量が少ない冬季の発電量を推定し, 電力の需給バランスについて検討した. 気象観測所(ナライフ)の12月の平均水平面日射量は1.1kWh/m²/日であり, 傾斜角60° に対する推定日射量は3.2kWh/m²/日である[注6]. 従って, 太陽電池モジュール62Wから198Wh/日の発電量を期待できるため, 消費電力量169Wh/日に対して需給バランスが取れているといえる.

定格出力50Wのケース(世帯B)

ドルノゴビ県サインシャンド村落の家族5人の世帯Bでは, 表13に示す仕様のSHSセットを2004年10月から使用している. SHSの導入の動機は,「10万ソーラーゲル計画」の優遇措置を知ったことであった. 年間収入は約100万Tg(約9万4千円)であり, 所有家畜頭数は約250頭であった. この世帯では, 中継アンテナから離れているため, テレビ放送は受信できないが, テレビゲーム機能が付いたビデオCD・DVDの再生機を使用していた. 世帯主は,「SHSは故障したがこと無い, 性能に対して大変満足している, 他人に勧めたい, 要望はテレビ放送の受信可能範囲の拡張である」とコメントした.

この世帯における平均的な消費電力を計算すると, 夏季246Wh/日, 冬季193Wh/日となった(表

表13 対象世帯のSHSの仕様

世帯	SHSの要素	製造国, メーカ	定格出力
A	太陽電池	日本, Sharp	62W
	充放電装置	タイ, Leonics	12V, 6/10A
	蓄電池	中国, Toyo	12V, 70Ah
B	太陽電池	中国, Sunpower	50W
	充放電装置	中国, Steca	12V, 6/10A
	蓄電池	中国, Toyo	12V, 65Ah
C	太陽電池	中国, Suntech	20W
	充放電装置	中国, Steca	12V, 6/10A
	蓄電池	中国, Toyo	12V, 38Ah

表14 対象世帯の電化製品の仕様と平均使用時間

世帯	電化製品	製造国	消費電力[W]	平均使用時間[h]	
				夏	冬
A	蛍光灯	タイ	11	4	6
	ステレオ	中国	15	2	1
	白黒テレビ	中国	22	5	4
B	蛍光灯	中国	11	4	6
	ラジオ	ロシア	1	2	2
	白黒テレビ	中国	30	5	2.5
	ビデオCDプレーヤー	中国	20	5	2.5
C	蛍光灯	中国	11	1	4
	白黒テレビ	中国	30	2	0.5

図5 ゲル内の電化製品(世帯A)

農業情報研究 15(2), 2006. 139-154

14). 日射量が少ない冬季や消費電力が多い時は太陽電池モジュールを太陽に向けて置き直す工夫をしているという.

著者ら (2004) は, サインシャンド市において太陽電池の暴露試験を行っている. モジュールの傾斜角を45° に設置した, この世帯と同タイプ (多結晶) の太陽電池は夏季には約6[h/日]等価稼働時間注7), 冬季には約4[h/日]等価稼働時間の発電することが示された. これにより, 50W太陽電池モジュールの発電量は夏季に約300Wh/日, 冬季に約200Wh/日と推定され, 発電量と消費電力量は平均的にバランスが取れているといえる.

定格出力20Wのケース (世帯C)

ヘンティー県ダダル村落, 家族4人の世帯Cは, 定格出力が20WのSHS (表13) を2003年11月から使用している. SHSの導入動機はこれまで使用していたローソクではなく, 電気でもっと明るい照明を点けたいということであった. 購入先は首都ウラーンバートル市内の販売店で, 購入価格が約15万Tg (約1万4千円) であった. 所有する家畜頭数は約100頭, 平均年収は約60万Tg (約5万6千円) である.

ダダル気象観測所の12月の平均水平面日射量は1.3kWh/m²/日であり, 傾斜角60° に対する推定日射量は3.6kWh/m²/日である(注6). 従って, 太陽電池モジュールのサイズが20Wでは, 12月には約72Wh/日の発電量しか期待できない. そのため, 照明だけでも使用時間が最大で6時間, テレビだけでは2時間程度と限定される. 実際の電化製品の利用時間から見ても世帯A, BのSHSと比べてかなり少ないことが分かる (表14).

しかしながら,「とにかく, 照明が日常的に使用できることが大事なので, その点においては現在のSHSに満足している」という意見が世帯主から聞かれた. 将来は大きいサイズのSHSを購入する考えがある.

SHS未利用者へのアンケート調査結果

アンケート回答者の属性

家族数は4人または5人家族の割合が多く (表15問1), SHS利用世帯の家族数の分布 (表7問1) とほぼ同じであった. 家畜頭数 (図6) と平均年収の分布 (表15問2) では, SHSの未利用世帯はSHSを利用する世帯より, いずれも少ないという傾向がみられた.

SHSに対する認識程度と今後の導入可能性

SHSについて, 約半数の世帯が名前のみではなく, 性能等もよく知っていることが明らかになった (表16問4). 今後, 電源システムを購入する予定がある世帯は55%, 購入したいが経済的に困難という世帯が31%, 電源は特に要らないという世帯は14%であった (表16問5). また, 導入したい電源の種類ではSHSが72%と大半を示して

表15 SHS未利用の回答者の属性

選択項目	度数	[%]
問1 家族数		
3人まで	10	20
4人	14	28
5人	16	32
6人以上	10	20
合計	50	100
問2 年間の平均収入		
40-60万Tg	15	34.1
60-80万Tg	14	31.8
80-100万Tg	9	20.5
100-140万Tg	4	9.1
140-200万Tg	2	4.5
合計	44	100

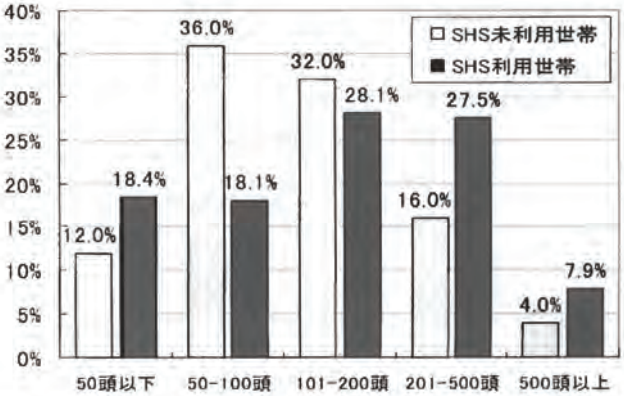

図6 SHS利用と未利用世帯の家畜所有頭数の比較

いる（表16問6）．従って，認識程度の結果（表16問4）も踏まえると，今後SHSが普及するポテンシャルは高いと考えられる．

考察

SHSの導入に伴い，2000年に10.7%であった遊牧民の電化率が2005年3月の推定では約29%となり5年間で約3倍に向上した．今後もSHSの導入件数が増加すると予想される．ここでは，本研究の調査結果を踏まえて，今後のSHSの普及定着の課題と農牧業の生産性向上におけるSHSの活用の可能性について検討する．

「10万戸ソーラーゲル計画」による優遇措置の見直し

「10万戸ソーラーゲル計画」は遊牧民のSHS購入に際して，当初，無利子の1年間ローンの実施，さらにその後50%の補助金と利子0%の1年間ローンを実施してきた．こうした優遇措置によって，2005年までに約3万2千世帯の遊牧民にSHSが導入された注2)．今回のアンケート調査において回答者の78%が10万戸ソーラーゲル計画の優遇措置を利用した（表8問4）ことからも，優遇措置はSHSの普及が促進される要因になったと考えられる．しかし，表8問6のSHS導入の動機について，「電化製品を利用したい」（53.3%）と「近隣の家庭で体験して便利に感じた」(20.9%)が合わせて74.2%を示す．このように生活の利便性の向上への要望や満足が，「10万ソーラゲル計画による優遇措置を知った」(18.3%)を上回ることから，今後も優遇措置に関係なくSHSを導入したいという世帯が増える可能性はある．また，モンゴル国の今後の財政状況を考慮すると，今後持続的なSHSの普及定着のためには，現在の「10万戸ソーラーゲル計画」による補助金に依存した形態ではなく，市場原理の中でSHSを販売していくことが望ましい．このため，例えば現行の補助金の割合を30%，15%などと段階的に引き下げる代わりに，ローンの期間を1.5年，2年と長期化するなどの対策が必要であると考えられる．

表16　未利用者のSHSに対する認識程度と導入可能性

選択項目	度数	[%]
問4 SHSに対する認識程度		
名前のみ知っている	25	52.1
性能等も良く知っている	22	45.8
まったく知らない	1	2.1
合計	48	100
問6 電源システムの購入の意思		
購入予定がある	27	55.1
購入したいが，経済的に困難	15	30.6
電源は不要	7	14.3
合計	49	100
問7 導入したい電源の種類		
小型発電機	3	6.5
風力発電システム	1	2.2
SHS	33	71.7
蓄電池	4	8.7
その他	5	10.9
合計	46	100

SHSのサポート体制の整備

SHSの欠点として「利用時間の制限」(22.7%)があげられている（表11問15）．SHSは，雨などの悪天候が続き，蓄電池への充電が不足した場合，充放電制御装置の過放電の防止機能によって，電力利用が制限されることがある．SHSのこのような特性を認識した上で，天気予報から日照時間を把握して電力消費を節約するなどの電力需要の管理（DSM=Demand Side Management）を行う必要がある．そのためには，SHS導入時のユーザトレーニング（利用者研修）が不可欠である．また，回答結果から，SHS利用者は保証期間の長期化と修理店の設立を要望していた．修理専門店のネットワーク構築，技術者などの人材育成，さらには簡単なトラブルなどに対してSHS利用者自らが対処できるためにSHSの利用・管理方法に関するユーザマニュアルと参考書の充実が必要である．こうしたことから，SHSの総合的なサポート体制の構築が課題と考えられる．

農牧業情報の活用環境の整備

「はじめに」で述べたように社会的・自然的要因による様々な問題を克服し，農牧業の生産性を向上させていくためには，牧畜の伝統的な技法に加えて科学的手法と最新技術を積極的に用いる必要がある．特に，農牧業情報の活用環境の整備が

農業情報研究15(2), 2006. 139-154

不可欠である．具体的には，遊牧民を対象としたTVやラジオ放送の番組内容を充実させるなどして，遊牧民が農牧業の環境負荷，牧草地荒廃のメカニズムや要因等について理解を深めること，また，牧草地の植物分布・育成状況などの解析情報を遊牧民に定期的に提供する情報支援システムが必要である．さらには，GPSや通信機器を用いて家畜の位置確認や放牧経路の記録・蓄積によって牧草地の高度管理が可能となるであろう．

SHSは性能上，動力や熱利用などの高出力(1kW以上)を供給することはできず農牧業の生産性向上に直接的に寄与できる可能性は低い．しかし，その中でSHSが上述した農牧業の情報支援システムや通信機器の電源として活用すれば，遊牧民の生活水準のみならず農牧業生産性の向上に寄与できる．

まとめ

本研究では対面式及びアンケート票調査により，SHSを利用している遊牧民の利用実態とSHS未利用者の認識を明らかにし，今後の課題を整理した．本研究より明らかとなった，主な知見を以下に示す．

1) SHSを導入することによって照明とテレビを使用できるようになったことに対して，SHS利用者は高い満足感（89%）を得ていた．また，SHSは小型かつ軽量であり，また燃料を必要としないため，移動を繰り返す遊牧民のライフスタイルに適合する技術であることが示された．
2) 遊牧民の平均年収に比べて，SHSの販売価格は高価である．このため，市場を介しての普及が進んでおらず，SHSを導入した世帯の78%が「10万ソーラーゲル計画」による補助金と無利子ローンを利用して購入していた．
3) SHSは2003年から本格的にモンゴル国内で導入されたため，使用期間は2年以内の世帯が多く，現時点では故障発生回数は少なかった．しかし，現在の課題は，SHSの保証期間は1年以内と短いこと，修理店または技術者が近くの村落センターや県都にいないことである．
4) SHS未利用者に対する調査から，SHSに対する認識度が高く(98%)，SHSを購入予定があるという回答者が多い（72%）ことが分かった．
5) SHSの普及定着及びそれによる遊牧民の農牧業の生産性向上のための課題として，市場原理に向けた優遇措置の見直し，サポート体制の整備，電化率の更なる改善と共に農牧業情報の活用環境の整備が必要であると考えられる．

注

注1)SHSの特徴は，太陽電池モジュール，蓄電池，充放電装置，ケーブル，固定具から構成されたシンプルなシステムであり(図1)，設置が容易であるとともに軽量(総重量：30～50kg)である．日中は太陽電池で発電した電力を蓄電池に貯めておき，必要に応じてその電力を供給する．駆動部分がないため騒音はなく，他の電源システムと比べて長寿命で保守管理が比較的容易である．その反面で，初期投資コストが高価であり，日射量の変動(天候と時間帯)によって発電量が制限されるという欠点がある．

注2)2005年3月までの10万戸ソーラーゲル計画による導入量，モンゴル国燃料・エネルギー省，再生可能エネルギー課，専門家への聞き取り調査．

注3)モンゴル国の通貨単位はトゥグルクTgであり，2005年7月に1円=10.68Tg，2003年には1円=10.11Tgであった．Bank of Mongolia, <http://www.mongolbank.mn/rates.asp>, 2005年10月12日参照．

注4)商人が生活必需品などを販売するために各遊牧民世帯を訪問しており，その際にSHSも販売している．

注5)質問10と14の回答を表に示さず，文章で表現している．

注6)モンゴル国気象水文研究所(Institute of Meteorology and Hydrology of Mongolia)の各気象観測所の平均水平面日射量データに基づいた傾斜面推定値，<http://www.env.pmis.gov.mn/Meteoins>, 2005年10月12日参照．

注7)発電の電力積算量を定格出力で稼働する時間で示すパラメータである．

引用文献

アジヤバト アマルバヤル・黒川 浩助(2005)モンゴルにおける独立小型太陽光発電システム実証研究のデータ解析¥システム評価，太陽エ

ネルギー，168 Vol.31 No.4, 83-88pp.
Amarbayar, A. and Kosuke Kurokawa, *et al.* (2004) Evaluation of Solar Energy Potential and PV Module Performance in the Gobi Desert of Mongolia, WREC-8, Denver, Colorado, Aug. 2004.
ADB (2002) Mongolia's Environment Implications for ADB's Operations, East and Central Asia Department of Asian Development Bank, PSNo.090602, ISBN 971-561-468-x.
Enebish, N. (2000) National Photovoltaic Program "100,000 Solar House (GER) in Mongolia", 28th IEEE Photovoltaic Specialists Conference, September 15-22, 2000.
Erdenesaikhan, N. (2002) Time-series satellite data analysis for assessment of vegetation cover of Mongolia, ESRI's 22nd Annual User Conference.
本多嘉明(1999)衛星観測による植物生産量推定手法の開発，戦略的基礎研究推進事業，地球変動のメカニズム，平成10年度研究年報，JST資料番号J1529AA, 884-888pp.
本多嘉明(1999)人工衛星のデータから植物生産量を調べる手法を開発，<http://www.jst.go.jp/kisoken/seika/zensen/04honda/>, 2005年10月18日参照.
Jargal, G. and Y.Otgonbold, *et al.* (2004) Study Report "Bringing herders' assets into full economic and productive use", UNDP/SIDA, Ulaanbaatar, 31-33pp.
森永由紀・篠田雅人(2003)モンゴルの自然災害ゾド，科学，Vol.73 No.5, 2003年5月，573-577pp.
NEDO (1997) 太陽光発電システム実用化技術開発，携帯太陽光発電システム実証研究成果報告書，新エネルギー産業技術総合開発機構，<http://www.tech.nedo.go.jp/Index.htm>, 2005年10月18日参照.
Nieuwenhout, F.D.J. and Dijk, A.L. van, *et al.* (2001), Experience with solar home systems in developing countries: a review, Progress in Photovoltaics, Vol.9 (DOI: 10.1002/pip.392) 455-474pp.
Nikolakaki, E.Krontiris (2001) "Problems and Prospects of Autonomous Power Plants with Small Scale Wind Turbines in Isolated Areas, Demonstration Project of Rural Electrification in Mongolia", International Conference Renewable Energies for Islands: Towards 100% RES Supply, Chania - Crete, Greece, 14-16 June 2001.
NSO:National Statistical Office of Mongolia (2004) Statistical Year Book 2003, 141-147pp.
NSO:National Statistical Office of Mongolia (2004b) Statistical Year Book 1989-2002: "Mongolia in a Market System", 163-165pp.
Robinson, B. (1997) In the Green Desert: Nonformal Distance Education Project for Nomadic Women of the Gobi Desert, Mongolia. UNESCO's Education for All Innovations Series, No.12.
新エネルギー財団(2005)住宅用太陽光発電システム施工品質向上に関する調査報告書，平成17年3月.
鈴木由紀夫(2003)モンゴル国における農牧業の現状，科学，Vol.73 No.5, 2003年5月，549-553pp.
Tserendash, S. (2000) Some policy related issues for pasture management, Newsletter No. 6 (38), Mongolian Academy of Sciences, Ulaanbaatar.

受付日　2005年11月1日
受理日　2006年4月10日
担当部会　情報利用・普及部会

IEEE TRANSACTIONS ON CIRCUITS AND SYSTEMS—I: REGULAR PAPERS, VOL. 53, NO. 3, MARCH 2006

Analysis of Class D Inverter With Irregular Driving Patterns

Hirotaka Koizumi, *Member, IEEE*, Kosuke Kurokawa, *Member, IEEE*, and Shinsaku Mori, *Member, IEEE*

***Abstract*—This paper presents an analysis of Class D inverter when irregular driving patterns are given to the gate drive of the switch devices. The analysis has been carried out with focusing on the waveforms, harmonics, low-frequency components, output power, and equivalent dc resistance, which are numerically analyzed and discussed. Class D inverters with six different Q factors from 0.1 to 20 are analyzed about 2^{16} driving patterns for each Q. Superior four models of the six inverters are built and tested in circuit experiments. The calculated waveforms are compared to the experimental results. Both of them are agreed well in time domain and frequency domain. Analytical results show a possibility of a novel control method with irregular driving patterns. In spite of discontinuous control, the output power or voltage can be strictly changed as if continuous using the selected driving patterns in some ranges.**

***Index Terms*—Class D inverter, high-frequency inverter, resonant power source.**

I. Introduction

CLASS D inverter [1]–[4] is one of the high-frequency high-efficiency resonant power sources, which has been applied to dc/dc resonant converters, radio transmitters, and electronic ballasts for fluorescent lamps [4]. Its high dc/ac power conversion efficiency is achieved by the zero-current switching (ZCS), which enables its operation at several hundred kilohertz. To control its output power or voltage, the operating frequency is varied (FM control) or a phase shift is given using two switching legs. However, ZCS is not maintained when the operating frequency is shifted away from the resonant frequency, or when a phase shift is given between the two switching legs. Those may result in an increase of switching losses. Against the problem, this paper presents a novel method to control the output power or voltage of Class D inverter at a fixed operating frequency with maintaining ZCS. The proposed method gives irregular driving patterns instead of a uniform driving pattern for the gate drives of the switching devices (MOSFETs). The output resonant circuit is tuned to the operating frequency; therefore, the time for ZCS comes by half cycle. The irregular driving patterns cause the switching transition at the time for ZCS irregularly. The output power or voltage is changed by the various driving patterns with maintaining ZCS.

Manuscript received November 23, 2004; revised May 12, 2005. This paper was presented in part at the IEEE International Symposium on Circuits and Systems, Vancouver, BC, Canada, May 23–26, 2004. This paper was recommended by Associate Editor A. Ioinovici.

H. Koizumi and K. Kurokawa are with the Department of Electrical and Electronic Engineering, Tokyo University of Agriculture and Technology, Tokyo 184-8588, Japan (e-mail: koizumih@cc.tuat.ac.jp).

S. Mori is with the Department of Electrical and Electronics Engineering, Nippon Institute of Technology, Saitama 345-8501, Japan.

Digital Object Identifier 10.1109/TCSI.2005.858491

In the voltage source full bridge inverter with a series resonant circuit for induction heating, pulse density modulation (PDM) control is proposed [5]. In this method, operating frequency is fixed at the resonant frequency. All the switches always turn on and off at zero current. The superiority of the PDM control in reduction of switching losses and electromagnetic noises is described in [5]. In that research, probably because of the application, the discontinuity of output power or comparison between switching patterns in terms of low-frequency components is not discussed.

It has been pointed out that irregular driving patterns form various waveforms which include harmonics and low-frequency components. The purpose of this paper is to make it clear the characteristics from the viewpoints of the harmonics, low-frequency components, output power, and equivalent dc resistance by numerical analysis focusing on the waveforms caused by the irregular driving patterns.

Six Class D inverters with different Q factor from 0.1 to 20 are analyzed about 2^{16} driving patterns for each and compared. Superior four models of the six are built and tested in circuit experiments. The experimental waveforms correspond with the calculation results in time domain and frequency domain.

A similar control way was applied to Class DE inverter [6]. However, it could not prevent a small increase of power dissipation of switching loss, because its high efficient operation at a few megahertz is on the assumption of zero-voltage and zero-current switching [7]–[14]. On the contrary, Class D inverter does not require zero-voltage switching. Its operating frequency is less than that of Class DE inverter. Therefore, Class D inverter can operate with keeping high power conversion efficiency against various switching patterns.

Analytical results show a possibility of a novel control method with irregular driving patterns. In spite of discontinuous control, the output power or voltage can be strictly changed as if continuous using the selected driving patterns in some ranges.

II. Circuit Description

A Class D voltage-switching series resonant inverter [1]–[4], [15], which is fed by a dc voltage source, is shown in Fig. 1. It is composed of two switch devices S_1, S_2, a bandpass filter (BPF) L-C, and a load resistance R_L. The pair of switch devices performs as one switch which alternately connects with the dc voltage source V_I and an earth with keeping 0.5 duty ratio at the switching frequency f; i.e., while one device is ON the other is OFF in half period $T/2 = 1/2f$. The driving signals D_{r1} and D_{r2} keep the relation $D_{r1} = \overline{D_{r2}}$. The upper switch S_1 is driven through a transformer. To maintain the gate-turning-on voltage,

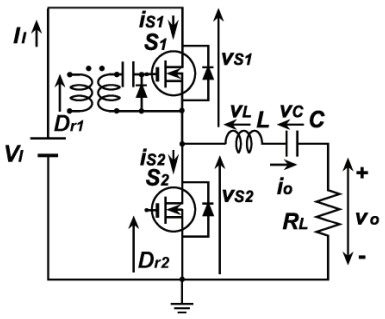

Fig. 1. Class D voltage-switching series resonant inverter.

a clamper is added between the transformer and S_1, which is effective when irregular driving pulses are given. In the regular operation, it keeps alternate operation by one period. This operation generates a uniform square waveform v_{S2} at the input terminal of the BPF at the switching frequency. An impedance of the BPF at the operating frequency is designed to be zero; therefore, only the fundamental component of the square waveform flows to the load resistance in ideal. The output current i_o becomes sinusoidal and it flows through each switch by half period. As shown in Fig. 2, while the switch current i_{S1} or i_{S2} is flowing through one switch, the voltage across the switch device v_{S1} or v_{S2} is zero, and the switching transition occurs at the zero current point; therefore, the 100% power conversion efficiency can be achieved.

In proposed method, the circuit topology itself is the same to the conventional Class D inverter, however the uniform driving pattern is rearranged, i.e., ON or OFF state sometimes appears in series. Regarding the square waveform patterns as binary codes, the regular pattern can be written as [1010...], which means $[V_I 0 V_I 0 \ldots]$ of the bottom switch voltage v_{S2}. In this paper, instead of the regular pattern, irregular patterns are given, for example [1100...] or [1000...]. Each pulse has half period of the operating cycle. The total patterns of 16 series pulses, which equal to 8 operating cycles, are applied to Class D inverter with six different Q factors.

III. Analysis

In regular operation, waveforms of Class D inverter are simply given based on the hypotheses of a loaded quality factor Q_L which is enough high to supply sinusoidal output current i_o, and by lossless ideal elements which ensure 100% efficiency. In the uniform driving operation, the input voltage of the BPF, i.e., v_{S2} becomes a square wave

$$v_{S2} = \begin{cases} V_I & \left(0 \le t < \frac{\pi}{\omega}\right) \\ 0 & \left(\frac{\pi}{\omega} \le t < \frac{2\pi}{\omega}\right) \end{cases} \tag{1}$$

where ω means operating angular frequency. According to the assumptions, the output voltage v_o becomes the fundamental component of the square wave, that is

$$v_o = V_o \sin \omega t \tag{2}$$

where its amplitude V_o is obtained by expanding the square wave into Fourier series

$$V_o = \frac{2V_I}{\pi} \simeq 0.637 V_I. \tag{3}$$

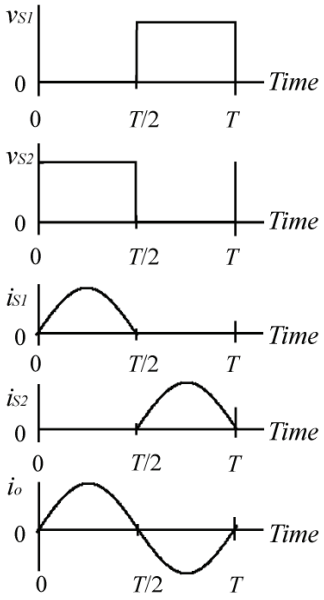

Fig. 2. Ideal waveforms in Class D inverter with infinite Q_L in regular operation.

However, if one of the two conditions, i.e., a high Q_L or the uniform driving pattern, is not satisfied, the inverter operation cannot be explained with the above theory. In case when the circuit is driven by irregular driving patterns, and/or it has low Q factor, waveforms need to be calculated from the differential equations. In the circuit of Fig. 1, the circuit equations are

$$C\frac{dv_C}{dt} = i_o \tag{4}$$

$$L\frac{di_o}{dt} = -v_C - R_L i_o + v_{S2} \tag{5}$$

where v_C and v_L are voltages across the capacitance C and the inductance L as depicted in Fig. 1. The loaded Q factor Q_L is given as

$$\frac{\omega L}{R_L} = \frac{1}{\omega C R_L} = Q_L. \tag{6}$$

In (5), v_{S2} takes V_I and zero according to the drive pattern. Thus, there exist two states, which are State 1 for $v_{S2} = V_I$, and State 0 for $v_{S2} = 0$. These states are symbolized by binary codes "1" and "0", respectively, for simplification. Each state is maintained within half period $(0 < t \le (\pi/\omega))$. According to the continuity of inductor current and capacitor voltage, the initial values of i_o and v_C in half period are given as the final values in the previous period. In a steady state, the last values should be equal to the initial values in a total period. Using this condition, the circuit equations (4) and (5) can be numerically solved with Runge-Kutta formula, then voltage and current waves are obtained. Before the calculation, the parameters have to be given. The input voltage and the load resistance are given as $V_I = 1$ V, and $R_L = 1\ \Omega$ for generalization of the analysis [14]. For circuits with $R_L \neq 1\ \Omega$ and/or $V_I \neq 1$ V, all voltages v must be replaced by v/V_I and all currents i must be replaced by $i \cdot R_L/V_I$. Six conditions of the loaded Q factor

TABLE I
THE VALUES OF THE RESONANT COMPONENTS IN THE COMPUTATION FOR $R_L = 1\ \Omega$ AT 200 kHz

Q_L	0.1	1	3	5	10	20
L	79.58 nH	795.8 nH	2.387 μH	3.979 μH	7.958 μH	39.79 μH
C	7.958 μF	795.8 nF	265.3 nF	159.2 nF	79.58 nF	7.958 nF

are given as $Q_L = 0.1$, 1, 3, 5, 10, and 20. The waveforms depend on the Q factor. Therefore, the operating frequency itself does not affect the waveform in principle if the resonant circuit is tuned to the operating frequency. In this study, $f = 200$ kHz is assumed and used. Under the condition, the resonant inductance and capacitance are given with (6). These are shown in Table I. In each case, the waveforms are computed with a regular driving pattern [1010...], which are shown in Fig. 3. The output voltage waveforms for $Q_L \geq 3$ correspond to the theoretical sinusoidal waveform. However, in case of $Q_L = 1$ and 0.1, those are different from sine wave, and zero-current switching is not maintained.

To clarify the characteristics of all the patterns, several parameters are calculated with considering the total period. Assuming that m-figure binary code is given as a driving pattern, the total period, i.e., the sum of m half periods becomes $mT/2$, where m is an even number. During the total period, the averaged input current I_I is

$$I_I = \frac{2}{mT} \int_0^{\frac{mT}{2}} i_{S1}(t)dt. \tag{7}$$

Similarly, the output power P_o is

$$P_o = \frac{2}{mT} \int_0^{\frac{mT}{2}} i_o^2(t) R_L dt. \tag{8}$$

Using (7), the input power P_I is obtained as $P_I = V_I I_I$ then the equivalent dc resistance R_{DC} is given as $R_{DC} = V_I/I_I$. The waveforms shaped with irregular driving patters are expected to be various in forms. To quantify them, the harmonics and low-frequency components are calculated. The fundamental component is on a basis of the operating frequency f; therefore the harmonics are obtained by the following equations with taking account of the total period $mT/2$:

$$a_n = \frac{2}{\frac{mT}{2}} \int_0^{\frac{mT}{2}} x(t)\cos(n\omega t)dt \tag{9}$$

$$b_n = \frac{2}{\frac{mT}{2}} \int_0^{\frac{mT}{2}} x(t)\sin(n\omega t)dt \tag{10}$$

where a_n and b_n are Fourier coefficients, and $x(t)$ can be v_o, v_C, v_{S2}, etc. Using (9) and (10), total harmonic distortion (THD) is

$$\mathrm{THD} = \sqrt{\frac{\sum_{n=2}^{\infty}(a_n^2 + b_n^2)}{a_1^2 + b_1^2}} \tag{11}$$

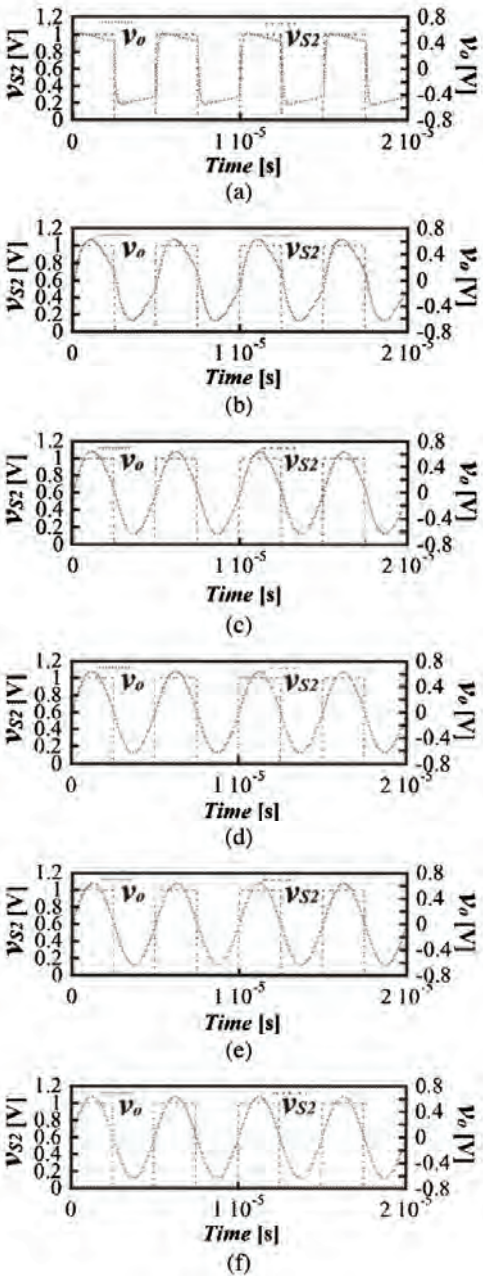

Fig. 3. Calculated waveforms of the switch voltage v_{S2} and the output voltage v_o in Class D inverter with the regular driving pattern [10 101 010...]. (a) $Q_L = 0.1$. (b) $Q_L = 1$. (c) $Q_L = 3$. (d) $Q_L = 5$. (e) $Q_L = 10$. (f) $Q_L = 20$.

where a_1 and b_1 are fundamental components. Then, regarding the total period as a basic period, low-frequency components are also calculated as

$$c_k = \frac{2}{\frac{mT}{2}} \int_0^{\frac{mT}{2}} x(t)\cos\left(\frac{k}{\frac{m}{2}}\omega t\right)dt \tag{12}$$

$$d_k = \frac{2}{\frac{mT}{2}} \int_0^{\frac{mT}{2}} x(t)\sin\left(\frac{k}{\frac{m}{2}}\omega t\right)dt \tag{13}$$

TABLE II
THE RANGE OF P_o, R_{DC}, AND TOTAL DISTORTIONS OF v_o

Q_L	THD	TLD	TD	FD	P_o [W]	R_{DC} [Ω]
0.1	$4.01e^{-1} - 6.22e^{3}$	$4.97e^{-1} - 2.53e^{11}$	$6.41e^{-1} - 2.53e^{11}$	$6.90e^{-1} - 2.61e^{11}$	$5.25e^{-2} - 2.39e^{-1}$	$4.23 - 1.91e^{1}$
1	$1.27e^{-1} - 3.70e^{5}$	$2.97e^{-1} - 6.83e^{15}$	$3.25e^{-1} - 6.83e^{15}$	$3.76e^{-1} - 8.14e^{15}$	$1.97e^{-2} - 1.78e^{-1}$	$5.68 - 5.08e^{1}$
3	$4.41e^{-2} - 1.31e^{3}$	$1.74e^{-1} - 5.50e^{9}$	$1.80e^{-1} - 5.50e^{9}$	$2.22e^{-1} - 6.82e^{9}$	$4.35e^{-3} - 1.63e^{-1}$	$6.16 - 2.30e^{2}$
5	$2.65e^{-2} - 1.46e^{3}$	$1.23e^{-1} - 3.35e^{10}$	$1.26e^{-1} - 3.35e^{10}$	$1.59e^{-1} - 4.25e^{10}$	$1.85e^{-3} - 1.59e^{-1}$	$6.29 - 5.39e^{2}$
10	$1.32e^{-2} - 8.15e^{2}$	$6.86e^{-2} - 2.71e^{8}$	$6.99e^{-2} - 2.71e^{8}$	$8.99e^{-2} - 3.48e^{8}$	$5.19e^{-4} - 1.56e^{-1}$	$6.40 - 1.92e^{3}$
20	$6.46e^{-3} - 1.36e^{3}$	$3.55e^{-2} - 1.98e^{7}$	$3.62e^{-2} - 1.98e^{7}$	$4.68e^{-2} - 2.56e^{7}$	$1.35e^{-4} - 1.55e^{-1}$	$6.44 - 7.42e^{3}$

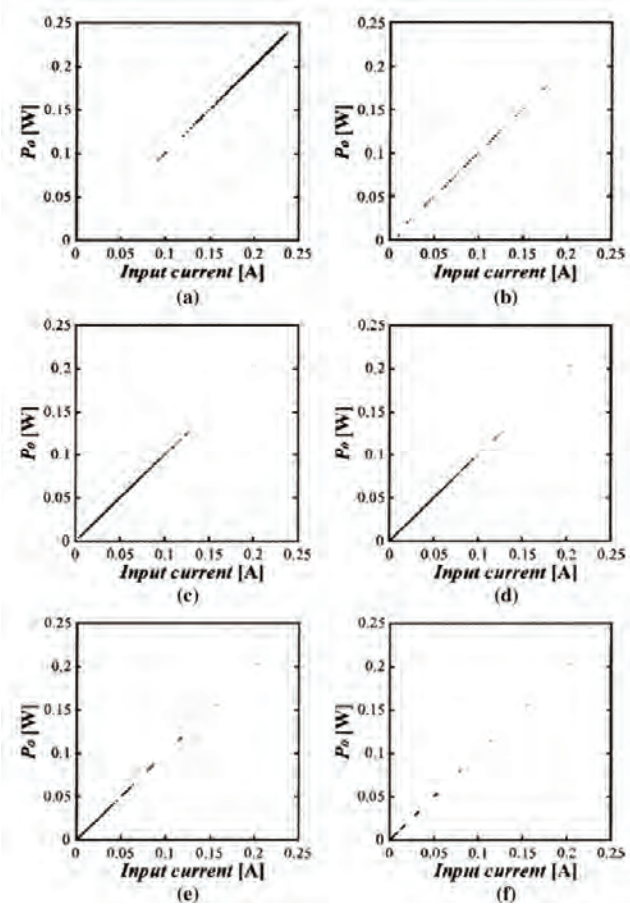

Fig. 4. Relationship between the output power P_o and the input current I_I. (a) $Q_L = 0.1$. (b) $Q_L = 1$. (c) $Q_L = 3$. (d) $Q_L = 5$. (e) $Q_L = 10$. (f) $Q_L = 20$.

where k is a natural number from 1 to $m/2 - 1$. Referring to (11), a parameter of total low-frequency-components distortion (TLD) which is normalized by the fundamental component is assumed as

$$\mathrm{TLD} = \sqrt{\frac{\sum_{k=1}^{\frac{m}{2}-1} (c_k^2 + d_k^2)}{a_1^2 + b_1^2}}. \tag{14}$$

In a similar way, total distortion (TD) is obtained with (11) and (14)

$$\mathrm{TD} = \sqrt{\frac{\sum_{n=2}^{\infty} (a_n^2 + b_n^2) + \sum_{k=1}^{\frac{m}{2}-1} (c_k^2 + d_k^2)}{a_1^2 + b_1^2}}. \tag{15}$$

In some patterns, the harmonics caused by the low-frequency components can be noticeable. To cover all of them, c_k and d_k are calculated about k over $m - 1$ in (12) and (13). In this case, the components given by (9) and (10) are also included. Referring to (15), a parameter including full-components distortion (FD) is given as

$$\mathrm{FD} = \sqrt{\frac{\sum_{k=1}^{\infty} (c_k^2 + d_k^2) - (a_1^2 + b_1^2)}{a_1^2 + b_1^2}}. \tag{16}$$

The waveforms have been analyzed using the above equations with $m = 16$ which is chosen because 2^n-digits-binary codes should be suitable not only for circuit experiments but also for practical applications. Those can be easily generated with a binary counter IC and some logic ICs. Eight bits provide 256 binary codes, which offer 33 of different cyclic patterns, i.e., 10000000, 01000000, 00100000, ..., are regarded as the same one, while 16 bits provide 65 536 binary codes which offer 4113 of different cyclic patterns. It is clear that only 33 plots form a discontinuous characteristic. In case of 32 bits, that is, 4 294 967 296 patterns, the calculation is too heavy to be solved with personal computers. Skipping the same patterns as a cyclic pattern, each parameter has been calculated in 2^{16} patterns. Substituting the output voltage v_o for $x(t)$, THD, TLD, TD, and FD are obtained. The harmonics higher than 14th are ignored. Based on the calculation results, the range of THD, TLD, TD, and FD about v_o, plus P_o and R_{dc} are shown in Table II except the patterns of all "1", all "0", and regular one. The relationship between the output power P_o and the input current I_I is shown in Fig. 4. Owing to the assumed 100% efficiency, all the plots are on the line of $P_o = R_L I_I$. The discontinuity, which has been pointed out in this type of regulation method, occurs. More bits of driving pattern generate more variations of output waveforms and powers, which make the density of plots higher. Besides, more bits result in longer cycle, which causes lower frequency components. Note that, 16-bit patterns include all the variations generated by 8, 4, and 2-bit patterns. The distribution of the plots has different characteristics by Q_L. In case of

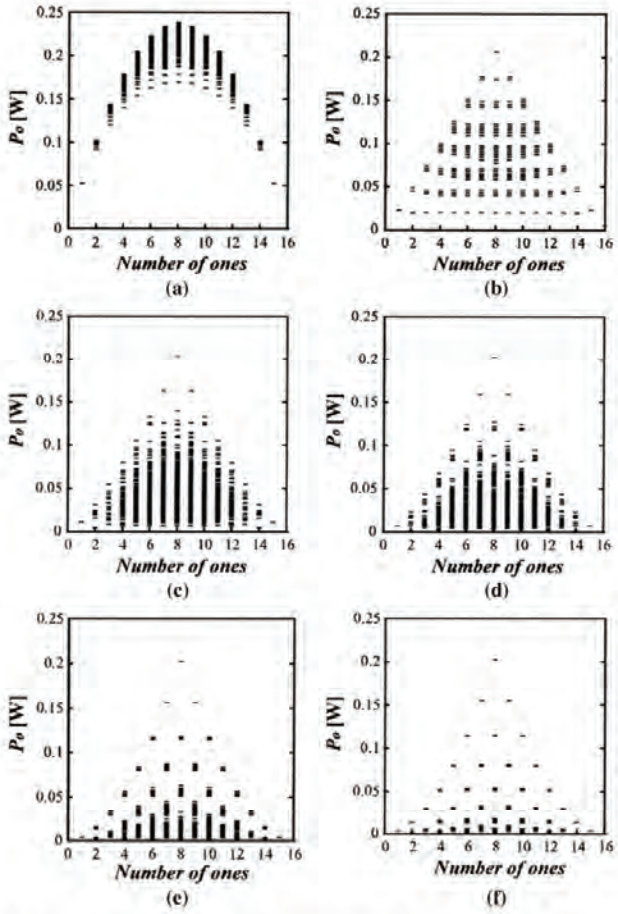

Fig. 5. Relationship between the output power P_o and the number of "1"s. (a) $Q_L = 0.1$. (b) $Q_L = 1$. (c) $Q_L = 3$. (d) $Q_L = 5$. (e) $Q_L = 10$. (f) $Q_L = 20$.

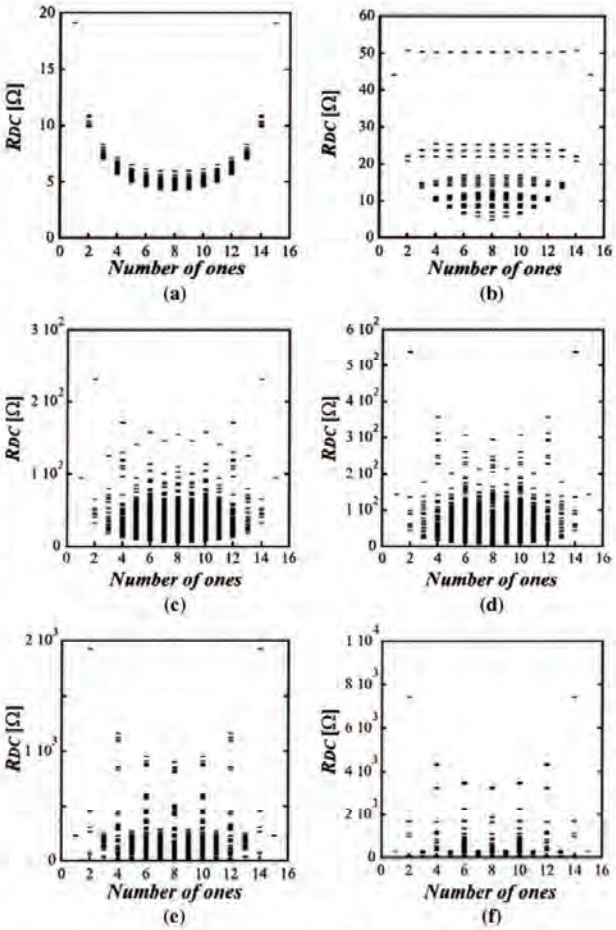

Fig. 6. Relationship between the equivalent dc resistance R_{dc} and the number of "1"s. (a) $Q_L = 0.1$. (b) $Q_L = 1$. (c) $Q_L = 3$. (d) $Q_L = 5$. (e) $Q_L = 10$. (f) $Q_L = 20$.

$Q_L = 0.1$, the plots get together in the upper right area which seems a continuous straight line. In case of $Q_L = 1$, the plots are spread like a broken line. In case of $Q_L = 3$ or 5, the plots get together in low power range, which also seems a continuous line. In case of $Q_L = 10$, the continuous segment is shorter than that of $Q_L = 5$. In $Q_L = 20$, the plots are dispersed in some groups of narrow range. The distribution of the plots is well understood in Fig. 5, where *Number of ones* means how many "1"s are included in the 16-figure driving pattern. The symmetrical characteristic reflects that the equivalent circuits in State 1 and State 0 are symmetric; therefore, [1000000000000000] and [0111111111111111] have the same characteristic. The relationship between the equivalent dc resistance and number of ones is shown in Fig. 6. In case of $Q_L = 0.1$, R_{DC} takes small values around 4 to 20 Ω. As Q_L becomes larger, R_{DC} increases. In case of $Q_L = 20$, R_{DC} stretches to several kilo-Ohms. According to the calculation results shown in Table II, all kinds of distortions are in wide range. However, we have no interest in the patterns which cause high distortion. Some of the patterns with high distortion have very small basic component and others include sharp turns in the waveform. The distribution of the distortions less than five are mapped out in Fig. 7 as functions of P_o. These have a tendency to be suppressed as Q_L rises. In case of $Q_L = 0.1$, most of the plots are in the right half, while, in cases of $Q_L = 3$, 5, 10, and 20, the plots are in the left half. The THD is visible in $Q_L = 0.1$ and 1. On the other hand, those are almost overlapped with the horizontal axis in $Q_L = 3$, 5, 10, and 20. In each case, TLD is larger than THD. The difference between FD and TD means the total distortion caused by the low-frequency components. In high Q_L, it can be negligible, however in low Q_L it becomes large. The TD and FD seem segments or broken lines, which tend to be vertical as Q_L grows. Judging from Fig. 7, there are few patterns with low distortions. Giving a standard FD = 1, which means the sum of the distortions of a pattern is equal to its fundamental component, all the patterns with FD over the standard are eliminated. The remaining patterns are plotted in Fig. 8 as P_o-I_I characteristics. In $Q_L = 0.1$ and 1, there are only 13 and 171 plots in each graph. In cases of $Q_L = 3$ and 5, of which characteristics seem to have large continuous ranges, include 735, and 1315 plots, respectively. In $Q_L = 10$ and 20, there are 2302 and 3238 plots. As Q_L takes larger value, more plots remain in narrow range.

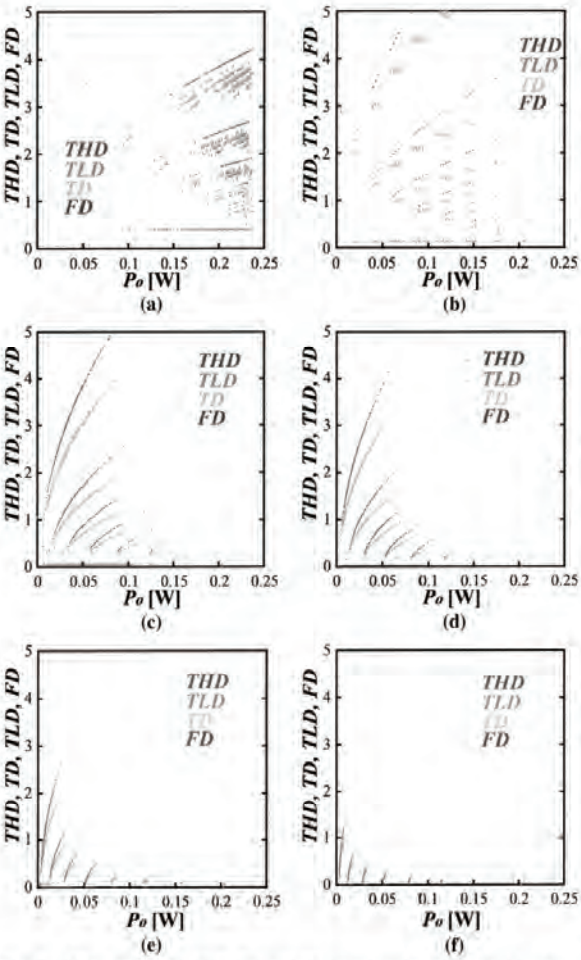

Fig. 7. Calculated THD, TLD, TD, and FD data plots for the output voltage v_o as functions of the output power P_o. (a) $Q_L = 0.1$. (b) $Q_L = 1$. (c) $Q_L = 3$. (d) $Q_L = 5$. (e) $Q_L = 10$. (f) $Q_L = 20$.

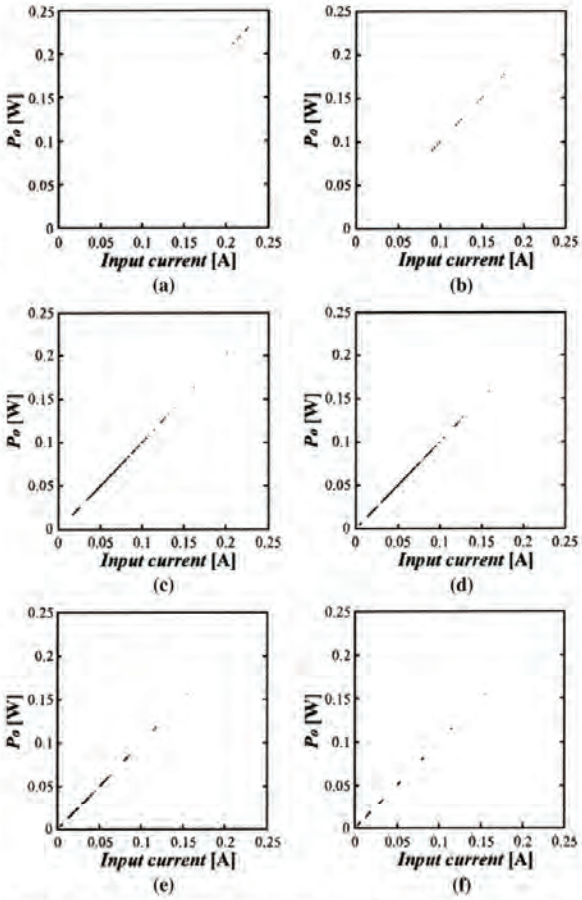

Fig. 8. Relationship between the output power P_o and the input current I_I. (a) $Q_L = 0.1$. (b) $Q_L = 1$. (c) $Q_L = 3$. (d) $Q_L = 5$. (e) $Q_L = 10$. (f) $Q_L = 20$.

Here, we discuss the characteristics of the six models. The model with $Q_L = 0.1$ has a continuous line in higher power range in the $P_o - I_I$ characteristic as shown in Fig. 4(a), however, most of the patterns include large FD. The output voltage waveform shown in Fig. 3(a) is rather close to square waveform, which results in 0.4 of the minimum value of THD. Further more, the large current jump at the switching transition is feared. The output voltage waveform is homothetic to the output current waveform. As seen in Fig. 3(a), at the switching instant, the output voltage is far from zero because of the low Q_L. Therefore, this model cannot maintain the high-efficiency operation achieved by zero-current switching which is the most important advantage of Class D inverter. Then, about the model of $Q_L = 1$, the dispersed $P_o - I_I$ characteristic is not suitable for continuous regulation as shown in Fig. 4(b). Therefore, these two models with low Q_L are left out of the research objects. The model with $Q_L = 20$ also has an intermittent $P_o - I_I$ characteristic. However, each segment includes many plots. In addition, this model is approximate to the ideal model with a high Q factor. Thus, the model with $Q_L = 20$ remains.

Even though the model with $Q_L = 3$ or 5, as is widely alleged, around the regular operation point, the distribution of the plots is obviously discontinuous in Fig. 4. It seems impossible to control an inverter's operation smoothly. On the other hand, in small P_o range, the plots exist in high density as if continuous. As shown in Fig. 8, most of them seem to remain after the selection with TD ≤ 1. According to the calculation results with considering the level of FD, P_o can be changed from 0.0306 to 0.0708 W at intervals within 0.001 W in case of $Q_L = 5$. With regard to $Q_L = 3$, P_o can be changed from 0.0192 to 0.0252 W, from 0.0356 to 0.0534 W, and from 0.0583 to 0.0664 W, under the same condition. Fig. 8(c) seems quite similar to Fig. 8(d), however, the intervals just over 0.001 W divide a segment into shorter ones. Short segments are caused by the low-density remaining plots. The number of remaining plots 735 in case of $Q_L = 3$ is equal to 56% of 1315 in case of $Q_L = 5$. As to $Q_L = 10$, major continuous segments are from 0.0131 to 0.0253 W, from 0.0291 to 0.0389 W, and from 0.0513 to 0.0594 W. In each range the intervals are kept within 0.001 W.

IV. Circuit Experiments

To confirm the waveforms, four models of experimental circuits with $Q_L = 3$, 5, 10, and 20 have been built and tested. A Class D inverter is designed following the conventional design

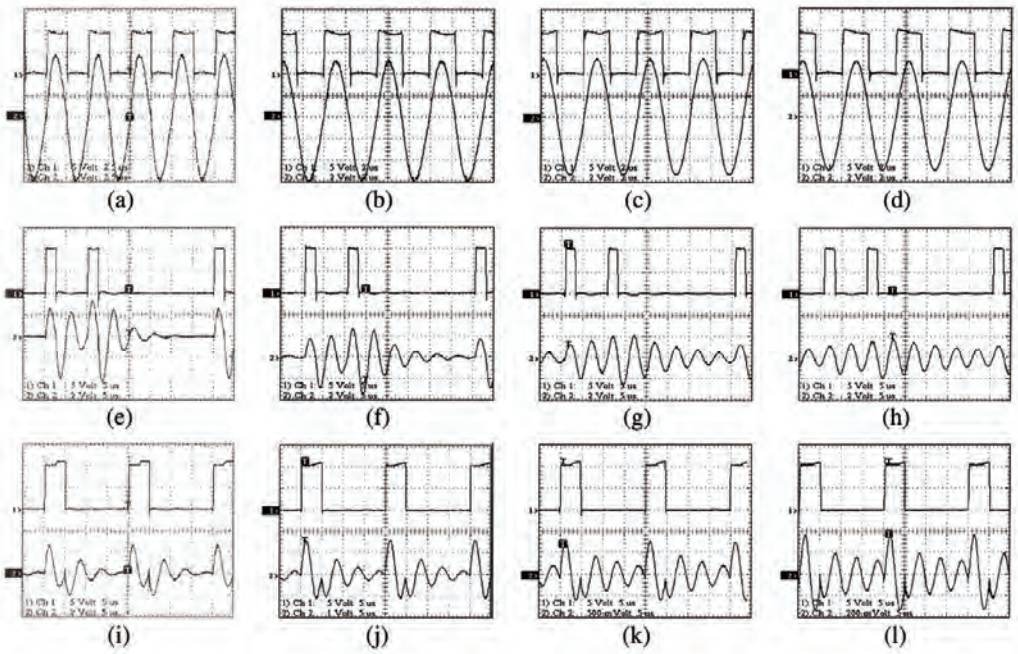

Fig. 9. Observed waveforms of the switch voltage v_{S2} (ch 1: top) and the output voltage v_o (ch 2: bottom), with the driving pattern [1010101010101010] from (a) to (d), [1000100000000000] from (e) to (h), and [1100000011000000] from (i) to (l). (a), (e), and (i) $Q_L = 3$; (b), (f), and (j) $Q_L = 5$; (c), (g), and (k) $Q_L = 10$; and (d), (h), and (l) $Q_L = 20$.

equations assuming 100% power conversion efficiency [15]. The following parameters are given; the switching frequency $f = 200$ kHz, input voltage $V_I = 10.0$ V, load resistance $R_L = 5.0\ \Omega$, and loaded quality factors of the series resonant circuit $Q_L = 3$, 5, 10, and 20. The resonant inductance and capacitance are calculated by the given parameters; for example, in case of $Q_L = 10$, $L = Q_L R_L/\omega = 39.79\ \mu$H and $C = 1/\omega^2 L = 1/\omega Q_L R_L = 15.9$ nF. The designed values and the measured ones with equivalent series resistance (ESR) are shown in Table III. The measured R_L was 4.95 Ω at 200 kHz. Two MOSFETs (IRF510) were used as switch devices. The input port was connected to a dc-power supply with an input capacitor. The voltage source was kept at 10.00 V in each test. The upper switch S_1 was driven through a transformer with a clamper. The four models were realized by replacing only the resonant circuit in the same board with the other components. The gate driver was manually regulated to give an intended pattern. Various driving patterns were given to the gate drive.

Fig. 9 shows the observed waveforms v_{S2} and v_o under the condition of $f = 200$ kHz, $V_I = 10.0$ V. Observed waveforms under the regular operation with the pattern of [1010101010101010] are shown in Fig. 9(a) to (d), which are in agreement with Fig. 2 and Fig. 3(c) to (f). The measured values of the output power were 2.91, 2.76, 2.79, and 2.40 W for $Q_L = 3$, 5, 10, and 20. The power conversion efficiencies were 80.3, 77.1, 72.7, and 72.4%, respectively. Arbitrary 10 patterns were applied to each model. The measured output power P_o and the power conversion efficiency are shown in Table IV. The blanks of the efficiency column mean that the input current was below the limitation of measurement. For the same reason, the efficiencies corresponding with the $P_o < 50$ mW have a

TABLE III
THE VALUES OF THE CIRCUIT COMPONENTS FOR $R_L = 5\ \Omega$ AT 200 kHz

Q_L	L	C	$L_{Measured}$ (ESR)	$C_{Measured}$ (ESR)
3	11.94 μH	53.05 nF	11.94 μH (146 mΩ)	53.04 nH (49 mΩ)
5	19.89 μH	31.83 nF	19.96 μH (148 mΩ)	31.97 nH (56 mΩ)
10	39.79 μH	15.92 nF	39.78 μH (270 mΩ)	16.02 nH (200 mΩ)
20	79.58 μH	7.958 nF	80.50 μH (160 mΩ)	7.91 nH (350 mΩ)

possibility of including errors. Generally, the power conversion efficiency kept more than 70%, however, as Q_L increases, it reduces slightly. In Class D inverter, the power losses are caused by the parasitic capacitor's discharge at the switching devices and the ESRs in all the circuit components. Using the measured values shown in Table III and an assumed output capacitance C_{out} of the switch device, the output power and the efficiency are calculated. The C_{out} and the drain–source resistance R_{DS} of IRF510 are assumed to be constant at 100 pF and 1 Ω because the driving pulses were about 5 V. Switching loss is given as $C_{\text{out}} \cdot V_I^2 \cdot (N_s \cdot f)/16$, where N_s is the number of switching transition during a driving pattern. Conduction losses are calculated with (8) replacing R_L with the sum of ESRs. In those calculations the used data of waveforms are recalculated based on the measured values. The obtained results are shown in Table V. Approximately, the Tables IV and V are agreed qualitatively. The differences can be caused by the reverse current flowing through the body diode of MOSFETs and undervoltage of driving pulses given for S_1.

For instance, observed waveforms with two driving patterns are shown in Fig. 9, where (e) to (h) are

TABLE IV
MEASURED OUTPUT POWER P_o [W] AND POWER CONVERSION EFFICIENCY [%]

	P_o [W]				Efficiency [%]			
Driving Pattern	Q_L=3	Q_L=5	Q_L=10	Q_L=20	Q_L=3	Q_L=5	Q_L=10	Q_L=20
1010101010101010	2.913	2.757	2.797	2.398	80.3	77.1	72.7	72.4
1000100010001000	0.887	0.812	0.738	0.658	82.1	78.9	72.5	74.7
1010000010100000	1.005	0.857	0.753	0.642	76.9	74.5	71.7	69.3
1010101000000000	1.192	1.027	0.839	0.691	76.3	74.7	70.0	68.0
1000000010000000	0.351	0.254	0.203	0.163	80.4	76.9	71.3	72.2
1000000000000000	0.162	0.110	0.068	0.047	81.2	79.5	69.2	77.6
1100000000000000	0.081	0.036	0.011	0.003	80.8	92.1	56.0	-
1010000000000000	0.489	0.360	0.240	0.180	76.7	75.6	71.1	66.2
1000100000000000	0.391	0.289	0.220	0.169	75.1	75.6	71.4	69.5
1100110000000000	0.146	0.062	0.019	0.005	78.7	79.3	21.2	-
1100000011000000	0.160	0.067	0.020	0.005	80.2	82.7	33.0	-

TABLE V
CALCULATED OUTPUT POWER P_o [W] AND POWER CONVERSION EFFICIENCY [%]

	P_o [W]				Efficiency [%]			
Driving Pattern	Q_L=3	Q_L=5	Q_L=10	Q_L=20	Q_L=3	Q_L=5	Q_L=10	Q_L=20
1010101010101010	3.307	2.675	2.453	2.410	81.3	81.2	77.8	77.4
1000100010001000	0.980	0.717	0.626	0.606	81.3	81.2	77.8	77.3
1010000010100000	1.152	0.793	0.649	0.612	81.3	81.2	77.8	77.3
1010101000000000	1.370	0.959	0.724	0.634	81.3	81.2	77.8	77.3
1000000010000000	0.408	0.242	0.174	0.156	81.3	81.1	77.7	77.2
1000000000000000	0.201	0.109	0.062	0.044	81.3	81.1	77.6	77.1
1100000000000000	0.097	0.035	0.010	0.003	81.2	80.8	76.4	72.1
1010000000000000	0.559	0.343	0.218	0.169	81.3	81.2	77.7	77.2
1000100000000000	0.444	0.277	0.192	0.162	81.3	81.1	77.7	77.2
1100110000000000	0.175	0.061	0.018	0.005	81.1	80.7	76.2	71.3
1100000011000000	0.192	0.067	0.018	0.005	81.2	80.8	76.3	71.4

with [1000100000000000]; and (i) to (l) are with [1100000011000000]. Using these patterns, the waveforms are calculated, which are shown in Fig. 10. Utilizing those waveforms, the states of switches can be briefly explained. The pair of switches performs as one switch; thus, S_1 is OFF while S_2 is ON, and *vice versa*. There are two cases of ON states; i.e., the switch current flows forward or reversely. There can be four independent modes; Mode 1: S_1 is ON with forward current, Mode 2: S_1 is ON with reverse current, Mode 3: S_2 is ON with forward current, and Mode 4: S_2 is ON with reverse current. The switching patterns [1000100000000000], and [1100000011000000] can be denoted with the number of modes, respectively, [1 343 134 343 434 343], and [1 234 343 412 343 434]. Fig. 10 is useful for understanding. While v_{S2} is "1", v_o is a similar figure of the current waveform i_{S1}. While v_{S2} is "0", v_o depicts a similar figure of $-i_{S2}$. After switching transition, always Mode 1 or Mode 3 appears. Mode 2 and Mode 4 never appears in series. The same Modes do not appear in series. The transitions between Modes 1 and 2, Modes 1 and 3, and Modes 3 and 4 give a smooth output waveform. The transitions from Mode 2 to 3, and Mode 4 to 1 are in one direction, which cause a sharp corner in the output waveform.

To compare the calculated waveforms with the observed ones, the voltages of the calculated ones have to be decupled. The v_{S2} has distortions in the square wave, which was caused by the distortions of gate drive waveform through a transformer. Therefore, the observed output voltage waveform does not fully accord with calculation results. In each case, including the regular pattern, the harmonics and the low-frequency components were measured with fast Fourier transform (FFT) function of an oscilloscope. Fig. 11 compares the measured data and the calculated ones. The calculated data are decupled. The spectra of v_{S2} are shown in the left side, which should have the same characteristic by the driving pattern. As shown in the twelve figures, the calculated spectra have the same characteristics by the patterns; in addition the observed ones are qualitatively agreed well with the calculation results in each pattern. The spectra of

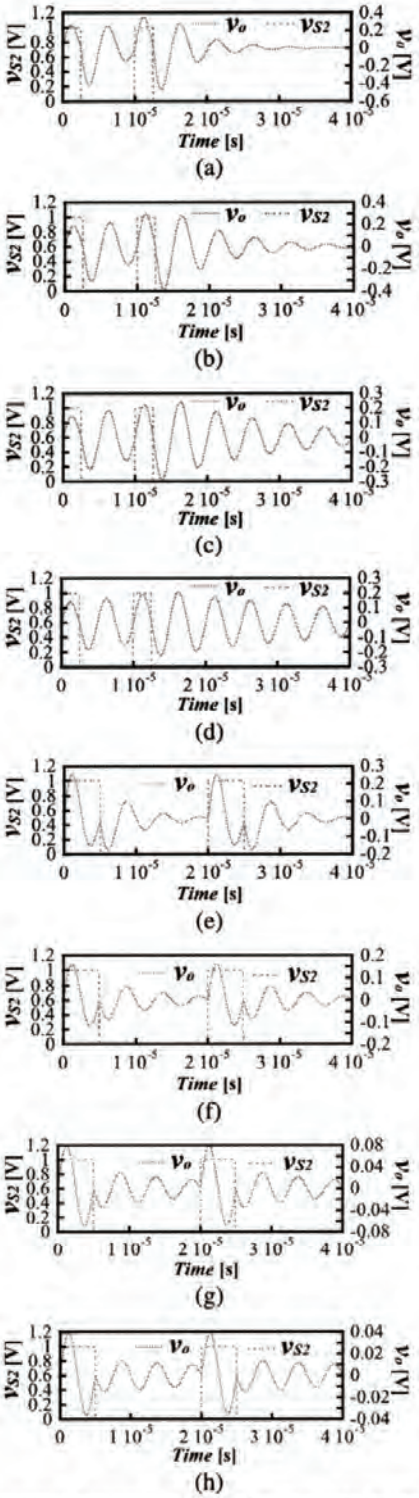

Fig. 10. Calculated waveforms in Class D inverter, with the driving pattern [1000100000000000] from (a) to (d) and [1100000011000000] from (e) to (h); switch voltage v_{S2} and output voltage v_o: (a) and (e) $Q_L = 3$, (b) and (f) $Q_L = 5$, (c) and (g) $Q_L = 10$, and (d) and (h) $Q_L = 20$.

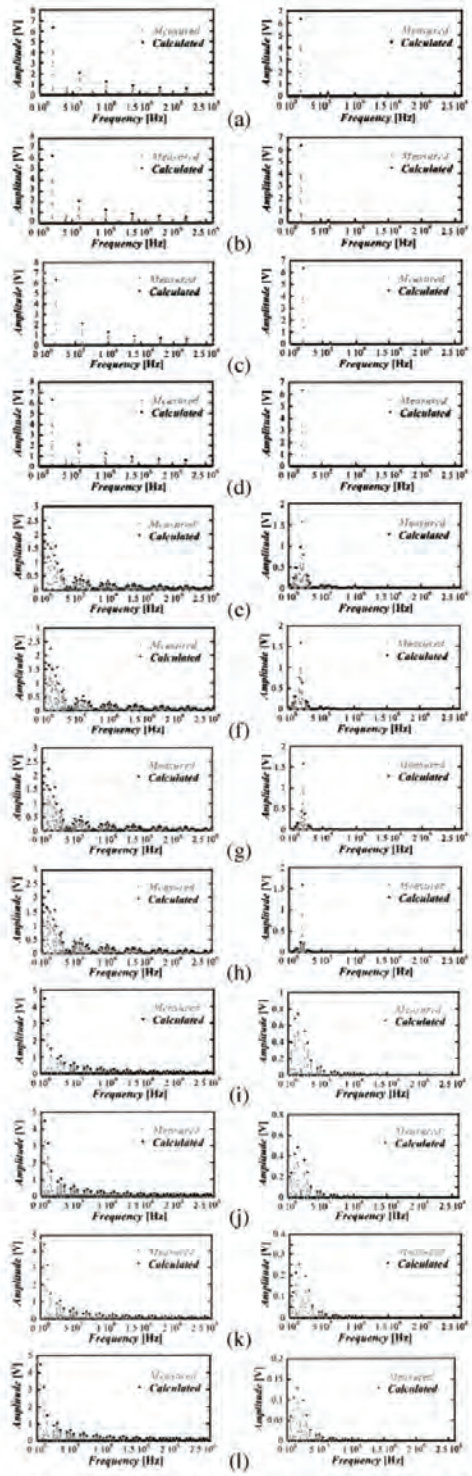

Fig. 11. Observed and calculated spectra of the switch voltage v_{S2} (left side) and the output voltage v_o (right side) with the driving pattern [1010101010101010] from (a) to (d), [1000100000000000] from (e) to (h), and [1100000 011000000] from (i) to (l). $Q_L = 3$ in (a), (e), and (i); $Q_L = 5$ in (b), (f), and (j); $Q_L = 10$ in (c), (g), and (k); and $Q_L = 20$ in (d), (h), and (l).

v_o are shown in the right side of Fig. 11, which also have similar characteristics by the driving patterns. However, except the regular pattern, the shape and amplitude are different by Q_L. The high Q_L forces narrow band output current and reduces the

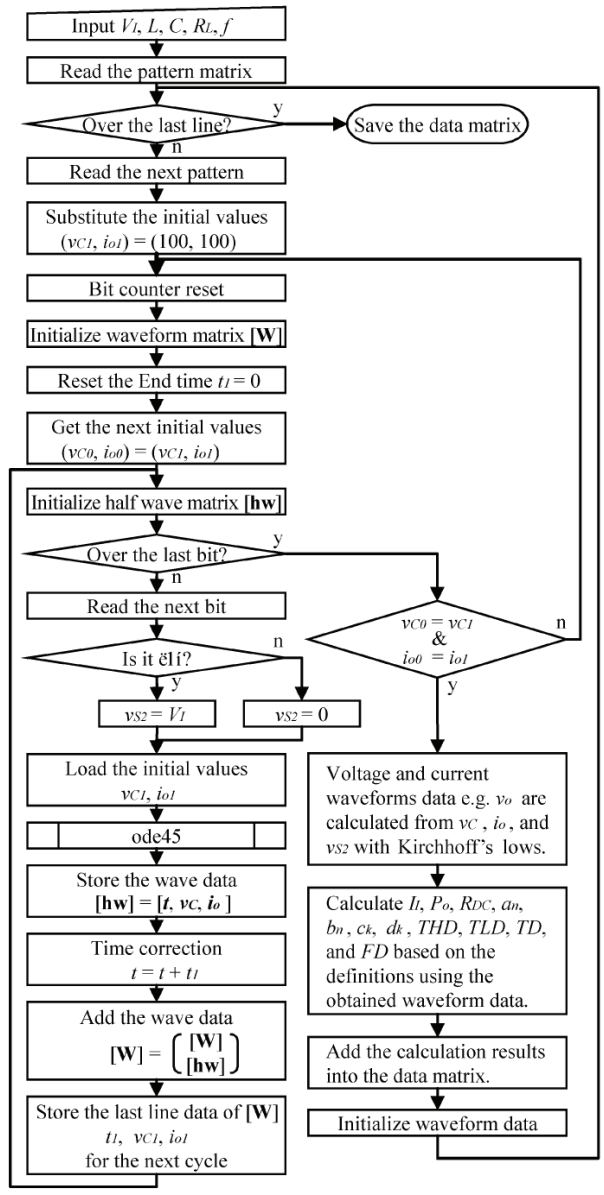

Fig. 12. Flowchart of numerical analysis.

output power. Also, as shown in the spectra of v_o, the calculated spectra and the observed ones are qualitatively agreed each other. The difference of the amplitude is mainly caused by the power losses, accuracy of measurements and using the flat top window in the circuit experiments. Above results confirm all the calculation results with the same program in this paper.

V. Conclusion

An analysis of Class D inverter with irregular driving patterns has been carried out. The various waveforms, output voltage, input current, THD, TLD, TD, FD, and equivalent dc resistance have been calculated and clarified about various loaded Q factors. Observed waveforms in the circuit experiments showed good agreement with the calculated ones in time domain and frequency domain. The analytical results show that, there exist some ranges where the output power can be controlled as if continuous using the selected low-distortion patterns. The distribution of the ranges is different by the Q factors. The models with low Q factors cannot maintain the zero current switching. High Q factor models cause dispersed several groups with similar output powers. In this paper, a model of $Q_L = 5$ has wider continuous output power range than the others. The power conversion efficiency can be kept about constant because the zero-current switching is maintained against various driving patterns. Those characteristics show that variation of driving pattern can be applied as a novel control method to Class D inverter. One can choose an appropriate model using the analytical results with taking into consideration the acceptable distortion level and the requested interval for the output power control.

Appendix

The numerical analysis has been carried out with MATLAB ver.6.1. In this paper, MATLAB ode45 solver in default configuration is utilized, which is based on Runge–Kutta (4,5) formula. The basic flow is shown in Fig. 12. At first, the values of circuit elements C, L, R_L, the input voltage V_I, and the switching frequency f are given. The driving patterns are generated as 16 digits binary codes in another program, where the same codes as a cyclic pattern are eliminated using bit shift and subtraction. The driving patterns are given as a matrix (4113 by 16 in this paper) with binary code 1/0. Each line gives a driving pattern. Waveforms are calculated by the pattern. Giving initial values, the differential equations (4) and (5) are solved with MATLAB ode45 solver by half cycle. The switch voltage v_{S2} takes V_I or zero by the digit of driving code "1" or "0". The half-waveform data of v_C and i_o are directly given as functions of time t, which are saved into a matrix [**hw**]. The combination of [**hw**]s forms a whole waveform matrix [**W**] step by step. Note that, the time t starts from zero in each half cycle; therefore it must be corrected for combination with a parameter t_1 which indicates the total time. Before the combination, the last line of [**W**] is deleted to avoid an overlap. At the end of half cycle, the data of v_C and i_o in the last line of [**hw**] are stored as v_{C1} and i_{o1}, which are given as the initial values for the next calculation. When 16 half cycles are combined, the initial values v_{C0} and i_{o0} are compared to the last values v_{C1} and i_{o1}. If the differences are within $\pm 1\mathrm{e}^{-6}$ and $\pm 1\mathrm{e}^{-8}$, respectively, the whole waveforms are obtained, or the same process is repeated with the same driving pattern. Then, based on the obtained waveform data of v_{C1} and i_{o1}, the other waveforms are calculated with Kirchhoff's lows. Then, following the definitions, I_I, P_o, R_{DC}, a_n, b_n, c_k, d_k, THD, TLD, TD, and FD are calculated. These are added into a data matrix. The above steps are repeated until the end of the pattern matrix.

Acknowledgment

A preliminary version of this paper which dealt with a specific circuit with a loaded Q factor $Q_L = 10$ was presented at ISCAS. In this paper, six circuits with different Q_L from 0.1 to 20 are analyzed, compared, and discussed. The analysis which was specialized to one circuit is generalized about the input voltage, the load resistance, and the loaded Q factor.

REFERENCES

[1] P. J. Baxandall, "Transistor sine-wave LC oscillators, some general considerations and new developments," *Proc. Inst. Elect. Eng.*, pt. B, vol. 106, pp. 748–758, May 1959.

[2] W. J. Chudobiak and D. F. Page, "Frequency and power limitations of Class-D transistor amplifier," *IEEE. J. Solid-State Circuits*, vol. SC-4, pp. 25–37, Feb. 1969.

[3] M. K. Kazimierczuk, "Class D voltage-switching MOSFET power inverter," *Proc. IEE., Pt. B, Electr. Power Appl.*, vol. 138, pp. 282–296, Nov. 1991.

[4] M. K. Kazimierczuk and W. Szaraniec, "Electronic ballast for fluorescent lamps," *IEEE Trans. Power Electron.*, vol. 8, no. 4, pp. 386–395, Oct. 1993.

[5] H. Fujita and H. Akagi, "Pulse-density-modulated power control of a 4 kW, 450 kHz voltage source inverter for induction melting applications," *IEEE Trans. Ind. Appl.*, vol. 32, no. 2, pp. 279–286, Mar./Apr. 1996.

[6] H. Sekiya, M. Matsuo, H. Koizumi, S. Mori, and I. Sasase, "New control scheme for class DE inverter by varying driving signals," *IEEE Trans. Ind. Electron.*, vol. 47, no. 6, pp. 1237–1248, Dec. 2000.

[7] M. K. Kazimierczuk and W. Szaraniec, "Class D voltage-switching inverter with only one shunt capacitor," in *Proc. Inst. Elect. Eng., Pt. B, Elect. Power Appl.*, vol. 139, Sept. 1992, pp. 449–456.

[8] H. Koizumi, M. Iwadare, S. Mori, and K. Ikeda, "A Class D type high frequency tuned power amplifier with Class E switching conditions," in *Proc. IEEE Int. Symp. Circuits Syst. (ISCAS'94)*, vol. 5, Jun. 1994, pp. 105–108.

[9] S. A. El-Hamamsy, "Design of high-efficiency RF Class-D power amplifier," *IEEE Trans. Power Electron.*, vol. 9, pp. 297–308, May 1994.

[10] H. Koizumi, M. Fujii, T. Suetsugu, and S. Mori, "New resonant dc/dc converter with Class DE inverter and Class E rectifier," *World Scientif. J. Circuits, Syst., and Comput.*, vol. 5, no. 4, pp. 559–574, Dec. 1995.

[11] H. Koizumi, T. Suetsugu, M. Fujii, K. Shinoda, S. Mori, and K. Ikeda, "Class DE high-efficiency tuned power amplifier," *IEEE Trans. Circuits Syst. I, Fundam. Theory Appl.*, vol. 43, no. 1, pp. 51–60, Jan. 1996.

[12] D. C. Hamill, "Class DE inverters and rectifiers for DC-DC converter," in *Proc. IEEE Power Electron. Specialist Conf. (PESC '96)*, Jun. 1996, pp. 854–860.

[13] K. Shinoda, T. Suetsugu, M. Matsuo, and S. Mori, "Idealized operation of Class DE amplifier and frequency multipliers," *IEEE Trans. Circuits Syst. I, Fundam. Theory Appl.*, vol. 45, no. 1, pp. 34–40, Jan. 1998.

[14] M. Albulet, "An exact analysis of Class-DE amplifier at any output Q," *IEEE Trans. Circuits Syst. I, Fundam. Theory Appl.*, vol. 46, no. 10, pp. 1228–1239, Oct. 1999.

[15] M. K. Kazimierczuk and D. Czarkowski, *Resonant Power Converters*. New York: Willey-Interscience, 1995.

Hirotaka Koizumi (S'98–M'01) was born in Tokyo, Japan, in 1970. He received the B.E., M.E., and Ph.D. degrees in electrical engineering from Keio University, Yokohama, Japan, in 1993, 1995, and 2001, respectively.

From 1995 to 2001, he was an electrical engineer with Tokyo Electric Power Company Inc.. From 1998 to 2001, he was also with the Graduate School of Keio University. He is currently with Tokyo University of Agriculture and Technology as a Research Assistant. His interests include photovoltaic systems, high-frequency high-efficiency tuned power amplifiers, resonant dc/dc power converters, dc/ac inverters, and high-frequency rectifiers, especially Class D, Class E, and Class DE circuits.

Dr. Koizumi is a member of the Institute of Electronics, Information and Communication Engineers (IEICE) of Japan.

Kosuke Kurokawa (M'04) graduated from Waseda University, Tokyo, Japan, in 1965 and received the Ph.D. degree in engineering from the same university in 1993.

He joined the Electrotechnical Laboratory (ETL), Ministry of International Trade and Industry (MITI), in 1965 where he has been engaged in research on energy systems technology. He studied at Polytechnic of Central London (presently University of Westminster), London, U.K., from 1971 to 1972. He was also with MITI and then joined New Energy Development Organization (NEDO) for solar energy R&D program, respectively. He has been a Professor with the Electrical and Electronic Engineering Department, Faculty of Technology, Tokyo University of Agriculture and Technology, since 1996. His current research interests include solar energy, photovoltaic systems engineering, and energy systems.

Dr. Kurokawa was the Project Leader for IEC61863 in IEC TC82/WG3 and has been the Operating Agent of Task VIII in photovoltaic system R&D program by International Energy Agency since 1998. He was the General Vice-Chairperson of the 2nd World Conference on Photovoltaic Solar Energy Conversion, 1998, and the General Chairperson of the 3rd World Conference, May 2003. He is a member of the International Solar Energy Society, Institute of Electrical Engineers of Japan, and the Japan Solar Energy Society.

Shinsaku Mori (M'80) was born in Kagoshima, Japan, in 1932. He received the B.E., M.E., and Ph.D. degrees in electrical engineering from Keio University, Yokohama, Japan, in 1957, 1959, and 1965, respectively.

From 1957 to 1997, he was with the Department of Electrical Engineering, Keio University. From 1978 to 1979, he was a Visiting Professor of Electrical Engineering at the University of Wisconsin, Madison. From April 1997 until his retirement in April 2004, he was with the Department of Electrical and Electronics Engineering, Nippon Institute of Technology, Miyashiro, Saitama, Japan. His research interests include circuit theory, communication engineering, synchronization, information theory, and medical engineering, especially nonlinear circuits, power electronics, chaos, phase-locked loops, modulation and coding, and hyperthermia.

Dr. Mori is a Fellow of the Institute of Electronics, Information, and Communication Engineers (IEICE) of Japan, the Japan Society for Simulation Technology, the Society of Instrument and Control Engineers, the Society of Information Theory and Its Applications (SITA), and the Japanese Society of Hyperthermic Oncology.

PROGRESS IN PHOTOVOLTAICS: RESEARCH AND APPLICATIONS
Prog. Photovolt: Res. Appl. 2006; **14**:553–566
Published online 16 May 2006 in Wiley InterScience (www.interscience.wiley.com). DOI: 10.1002/pip.692

Applications

Evaluation of Solar Energy Potential and PV Module Performance in the Gobi Desert of Mongolia‡

Amarbayar Adiyabat[1]*,†, Kosuke Kurokawa[1], Kenji Otani[2], Namjil Enebish[3], Garmaa Batsukh[3], Mishiglunden Battushig[3], Dorjsuren Ochirvaani[3] and Bathuu Ganbat[3]

[1]*Tokyo University of Agriculture and Technology (TUAT), Naka-cho 2-24-16, Koganei, Tokyo 184-8588, Japan*
[2]*National Institute of Advanced Industrial Science & Technology (AIST), Tsukuba Central 2, Tsukuba, Ibaraki 305-8568, Japan*
[3]*Inter-University Solar Energy Research Net-Center, National University of Mongolia, P.O. Box 46A/436, Ulaanbaatar 210546, Mongolia*

Here, we present the results of evaluation of solar energy potential and photovoltaic (PV) module performance from actual data measured over a period of more than 2 years in the Gobi Desert of Mongolia. To allow estimation of solar energy potentials and durability of PV systems in the Gobi Desert area, a data acquisition system, including crystalline silicon (c-Si), polycrystalline silicon (p-Si) modules, and two sets of precision pyranometers, thermometers, and anemometer, was installed at Sainshand City in October 2002. This system measures 23 parameters, including solar irradiation and meteorological parameters, every 10 min. High output gain was observed due to operation at extremely low ambient temperatures and the module performance ratios (PRs) were high (>1·0) in winter. In summary, the present study showed that a PV module with a high temperature coefficient, such as crystalline silicon, is advantageous for use in the Gobi Desert area. Copyright © 2006 John Wiley & Sons, Ltd.

KEY WORDS: PV module performance; solar energy potential; field tests; Gobi Desert

INTRODUCTION

The Gobi Desert, Mongolia, is one of the most promising candidate sites for introduction of the 100 MW class very large scale photovoltaic systems (VLS-PV) specified by Task 8 'Very Large Scale Photovoltaic Power Generation Systems' conducted as part of the IEA photovoltaic power systems program (IEA PVPS).[1] Within the framework of the IEA PVPS Task 8 activity, a conceptual design has been developed

* Correspondence to: Amarbayar Adiyabat, Tokyo University of Agriculture and Technology (TUAT), Naka-cho 2-24-16, Koganei, Tokyo 184-8588, Japan.
†E-mail: amar@cc.tuat.ac.jp
‡Amarbayar Adiyabat and Namjil Enebish are Ph.D. Students; Kosuke Kurokawa and Garmaa Batsukh are Professors; Kenji Otani, Mishiglunden Battushig, Dorjsuren Ochirvaani and Bathuu Ganbat are Reseachers.

Received 23 August 2005
Revised 12 November 2005

and a trial calculation of the costs associated with power generation and construction of a VLS-PV system in the Gobi Desert area has been performed.[2,3]

The meteorological environmental characteristics of the Gobi Desert may affect the PV system performance and design specifications. Therefore, it is necessary to clarify the factors that will affect the system design, operation, and maintenance. However, no useful reference data are available and there have been no case studies analyzing solar energy resources or performance for PV system installation in the Gobi Desert area.

In the Gobi Desert, Mongolia, we set up two types of photovoltaic (PV) modules and checking devices (e.g., *I–V* curve tracer, etc.) as well as meteorological devices to study the characteristics of PV system operation under such severe environmental conditions. The present study was performed to verify the output simulation technique for the VLS-PV to confirm the efficiency of using a large-scale concentrated PV system in this area, and to clarify the specific requirements for system design. To clarify the actual environmental capabilities (loss analysis) in the Gobi Desert, we measured meteorological data, such as the amount of solar irradiation and temperature, and the *I–V* characteristics of the PV modules.

EXPERIMENTAL SETUP

To determine the potential of VLS-PV in the Gobi Desert area, we installed two types of crystalline silicon PV module and checking devices (e.g., *I–V* curve tracer, etc.) as well as a new data acquisition system at the field site, Sainshand City (44°54' N and 110°07' E) (Figure 1), which is located in the southeastern part of Mongolia. The data acquisition system (Figure 2) is switched on automatically every 10 min and records the total solar irradiation received on the horizontal and 45° tilted surfaces, site meteorological data, and measures PV module current-voltage (*I–V*) curves.

The measurement items are listed below:

1. Global irradiance on the horizon
2. In-plane irradiance at 45°
3. Wind speed & direction
4. Air temperature
5. Humidity
6. Albedo
7. Short-circuit current (I_{sc})
8. Open-circuit voltage (V_{oc})

Figure 1. Overview of the experimental setup and horizontal pyranometer

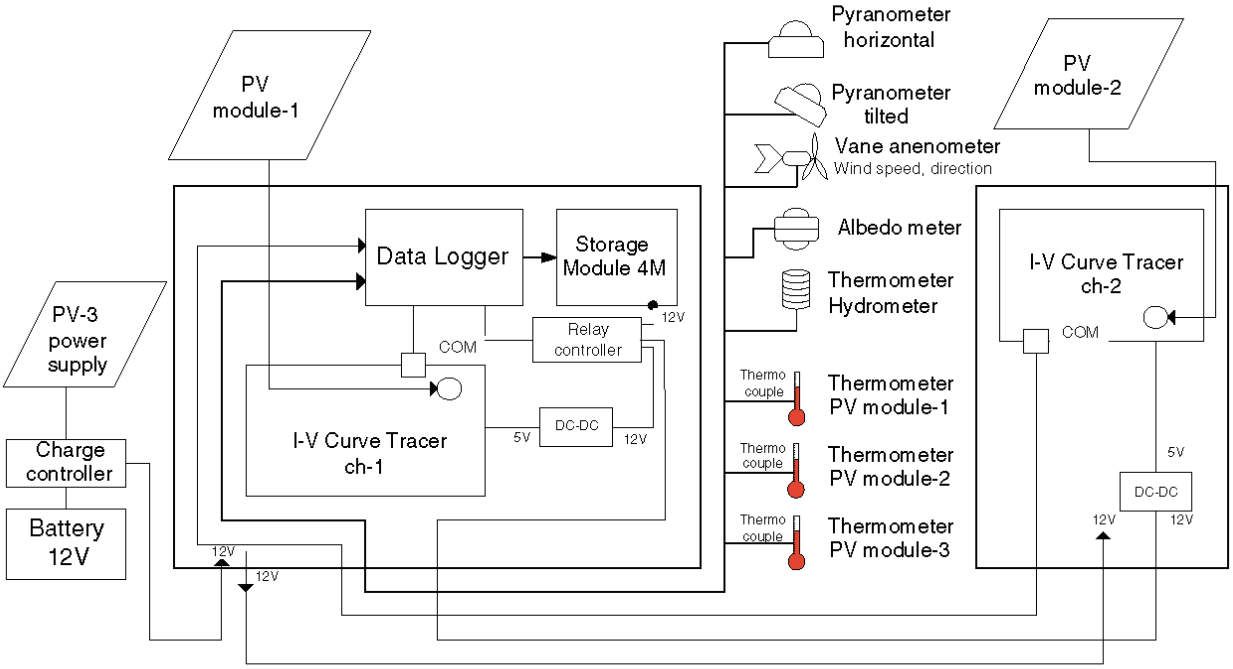

Figure 2. Schema of the data acquisition system

9. Current at maximum power (I_{pm})
10. Voltage at maximum power (V_{pm})
11. Temperature of modules (T_1, T_2)

The management system software package is installed in the data acquisition system, which is supplied by a 12 V battery at measurement time and data are loaded into the 4 MB storage module (SM4M).

The crystalline silicon (c-Si), polycrystalline silicon (p-Si) modules used in this exposure test, and the datasheet showing the electrical characteristics under standard test conditions (STC: 1000 W/m^2, AM 1·5 and module temperature of 25°C[4,5]) are shown in Table I. PV module 1 (80 W) uses multi-crystal silicon solar cells measuring 125 mm^2 with 12·6% module conversion efficiency. In addition, use of an anti-reflective coating and back surface field (BSF) structure improved cell conversion efficiency to 14%. White tempered glass, EVA resin, and a weatherproof film along with an aluminum frame were used. PV module 2 (75 W) was produced by a multistage proprietary texture optimized pyramidal surface (TOPS) process, which maximizes photon absorption from direct and diffused light. Ultra-clear tempered glass, torsion, and a corrosion-resistant anodized aluminum module frame were used.

Table I. Electrical characteristics of photovoltaic (PV) modules on STC (as manufacturer datasheets)

PV module name and Type		PV module-1 p-Si	PV module-2 c-Si
Parameters	Unit		
Short-circuit current (I_{sc})	A	5·3	4·8
Open-circuit voltage (V_{oc})	V	21·3	21·7
Current at maximum power (I_{pm})	A	4·7	4·4
Voltage at maximum power (V_{pm})	V	17·1	17·0
Maximum power rating (P_{max})	W	80	75
Temperature coefficient	W/°C	0·373	0·321

ANALYSIS METHOD

The field data analysis is divided into three parts regarding environmental conditions, solar energy resource evaluation, and PV performance. The environmental condition indices include ambient and module temperatures, average wind speed, humidity, and albedo. For evaluation of the solar energy resource, we use sunshine duration time, monthly average irradiation, and irradiation variable ratio. The PV Module performance indices include reference yield, array (module) yield, module performance ratio, temperature modification factor, and other loss factors of the PV module.

In this analysis, we used 2 years of data collected from March 2003 to February 2005. First, raw data obtained from the test site were checked and correctable noise was filtered.

Environmental condition indices

The average values of the ambient temperature, module backside temperature, wind speed/direction, humidity, and albedo were examined to determine the actual environmental conditions to which the PV modules are exposed. We compared measured meteorological data to the average annual data obtained from a local weather station, to evaluate the environmental conditions during the measurement period as compared to a normal year.

Solar energy resource indices

The horizontal and in-plane irradiation [kWh/m^2/day], duration of sunshine, $T_{\text{Meas.Duration}}$ [h/month], and fraction, F_{SD}, relative to possible duration of sunshine were used as indices of solar energy resources. Here, possible duration of sunshine was the mean duration for a fine day. We compared monthly irradiance and sunshine duration time to local weather station data, to evaluate the irradiance during the measurement period.

$$F_{\text{SD}} = T_{\text{Meas.Duration}}/T_{\text{Possible Duration}} \tag{1}$$

PV Module performance indices

All system performance data have been evaluated in terms of operational performance and reliability based on IEC Standard 61724.[8]

$$Y_{\text{r}} = H_{\text{A}}/G_{\text{S}} \tag{2}$$

$$Y_{\text{A}} = E_{\text{A,d}}/P_{\max} \tag{3}$$

$$\text{PR} = Y_{\text{A}}/Y_{\text{r}} \tag{4}$$

The *reference yield*, Y_{r}, is based on the in-plane irradiation, H_{A}, and represents the solar irradiance of reference, G_{S} ($= 1000\,\text{W/m}^2$), per day and kW$_{\text{p}}$. The *array yield*, Y_{A}, is the daily array energy output, $E_{\text{A,d}}$, per kW and represents the number of hours per day that the array would need to operate at its rated output power, $P_{\max}$, to contribute the same daily array energy to the system as it was monitored. The *array performance ratio*, PR, is the ratio of actual array output energy to the energy available theoretically (i.e., $Y_{\text{A}}/Y_{\text{r}}$). PR is independent of location and array size, and indicates the overall losses on the array's rated output due to module temperature and incomplete utilization of irradiation.[9] In this paper, the term 'array' means module.

To evaluate the effects of module temperature on output performance, the temperature, K_{temp}, and other loss modification factor, K_{oth}, were determined. These factors were calculated using Equations 5 and 6 from the module temperature, T_{cell}, temperature coefficient, $\alpha_{P_{\max}}$, and module performance ratio, PR, every 10 min.

The other loss modification factor, K_{oth}, covers incident angle, soil, shading, aging, and other unknown loss factors[10] except temperature loss of the PV module.

$$K_{temp} \quad 1 \quad \alpha_{P_{max}}(T_{cell} \quad 25) \tag{5}$$

$$K_{oth} \quad PR/K_{temp} \tag{6}$$

To compare the actual measured power values, $P_{max,real}$, with nominal power values, maximum power values were extracted from 1 year of data (March 2003–February 2004) under conditions of 1000 ± 10 W/m^2 irradiance, and extrapolated by the temperature correction procedure of JIS C8919[6] (IEC 60891[7]) for the STC.

RESULTS AND DISCUSSION

Environmental conditions

Table II shows a comparison of measured ambient temperature to the values for a normal year. Mean error of ambient temperature was 0·82°C and root mean square error (RMSE) was 0·35°C. Air temperature conditions were similar to those in a normal year.[11]

The daily transitions of ambient and module temperatures are shown in Figure 3 (Table III) by the monthly average hour values. The difference between daytime and nighttime air temperature was around 10°C, and the seasonal air temperature range ranged from 20°C to +30°C. The rise in module temperature was from

Table II. Comparison of measured ambient temperature to those in a normal year [°C]

Month	1	2	3	4	5	6	7	8	9	10	11	12	Year
Average year air temp	18	14	4·5	6·1	14·2	20·6	23·2	21·1	13·7	4·4	7·6	16	3·53
Measured average temp	19	13	3·4	8·1	15·4	21	24·3	20·9	15·8	6·06	7·8	15	4·35
Maximum ambient temp	4·0	1·8	18·3	31·4	32·6	33·4	35·3	34·3	29·5	19·9	13·0	3·0	4·0
Minimum ambient temp	31·1	30·0	17·2	4·5	0·9	0·0	12·9	10·7	0·0	6·6	19·4	25·6	31·1

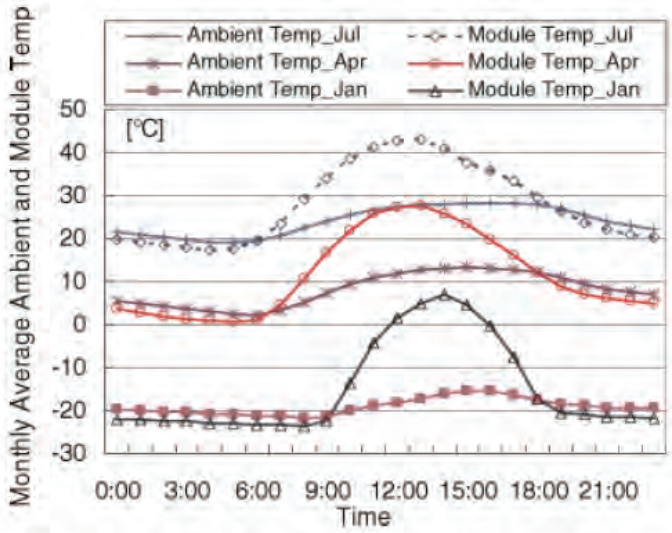

Figure 3. Daily transitions of ambient and module temperature represented by monthly average values

Table III. Daily transitions of ambient and module temperature represented by monthly average values [°C] (numerical values of Figure 3)

Month	Item		0:00	1:00	2:00	3:00	4:00	5:00	6:00	7:00	8:00	9:00	10:00	11:00	12:00	13:00	14:00	15:00	16:00	17:00	18:00	19:00	20:00	21:00	22:00	23:00
Jan	Module temp.	Avrg.	−22·1	−22·1	−22·3	−22·4	−23·0	−23·1	−23·2	−23·3	−23·6	−22·3	−13·5	−4·3	1·4	4·9	7·0	4·5	−0·4	−7·7	−17·3	−20·5	−21·0	−21·5	−21·6	−21·9
		Stdev	4·7	4·6	4·5	4·5	4·3	4·1	4·4	4·4	4·0	4·3	5·3	8·8	9·9	9·9	9·3	8·7	8·2	7·0	5·3	4·9	5·0	4·7	4·5	4·3
	Ambient temp.	Avrg.	−19·7	−20·0	−20·2	−20·4	−20·8	−21·0	−21·1	−21·3	−21·7	−21·5	−20·0	−18·8	−18·3	−17·2	−16·1	−15·6	−15·5	−16·3	−17·7	−18·6	−18·9	−19·5	−19·4	−19·5
		Stdev	4·1	4·2	4·2	4·0	3·8	3·8	4·0	3·9	3·6	3·7	3·6	3·9	3·6	3·5	4·1	4·2	4·4	4·3	4·3	4·4	4·5	4·3	4·0	3·8
Apr	Module temp.	Avrg.	3·5	2·8	1·9	1·3	0·8	0·7	0·9	4·5	10·5	16·6	21·8	25·7	27·2	27·4	25·9	23·3	19·8	16·1	12·1	8·8	6·9	6·0	5·4	4·8
		Stdev	4·3	4·3	4·3	4·0	3·7	3·7	3·5	4·0	5·2	6·2	7·7	8·2	8·3	9·0	9·1	8·7	7·9	6·9	6·1	5·2	4·9	4·9	5·0	5·2
	Ambient temp.	Avrg.	5·6	4·9	4·2	3·6	2·9	2·6	2·1	3·2	5·1	7·3	9·3	10·8	11·9	12·8	13·1	13·3	13·2	12·8	12·2	10·9	9·2	8·3	7·5	7·0
		Stdev	4·0	4·0	3·8	3·6	3·4	3·4	3·2	3·4	3·7	4·2	4·7	5·1	5·3	5·6	5·9	6·0	6·1	6·2	6·1	5·5	5·1	4·9	5·0	5·2
Jul	Module temp.	Avrg.	19·8	19·1	18·4	17·9	17·4	17·6	19·4	23·3	29·2	34·0	38·5	41·2	42·8	43·1	40·9	37·7	35·7	33·4	29·5	26·4	23·6	22·0	21·0	20·3
		Stdev	3·1	3·1	2·8	2·5	2·7	3·0	3·0	3·6	4·2	5·8	6·7	8·5	9·6	9·4	9·1	8·9	7·2	5·4	4·2	3·7	3·4	3·5	3·4	3·2
	Ambient temp.	Avrg.	21·6	20·9	20·3	19·7	19·2	18·9	19·3	20·7	22·4	24·0	25·5	26·5	27·2	27·7	28·0	28·1	28·1	28·3	28·0	27·0	25·4	24·1	23·0	22·2
		Stdev	3·2	3·0	2·8	2·7	2·7	2·9	2·8	2·9	3·1	3·3	3·4	3·7	4·0	4·3	4·4	4·5	4·5	4·2	4·1	3·8	3·6	3·6	3·5	3·3

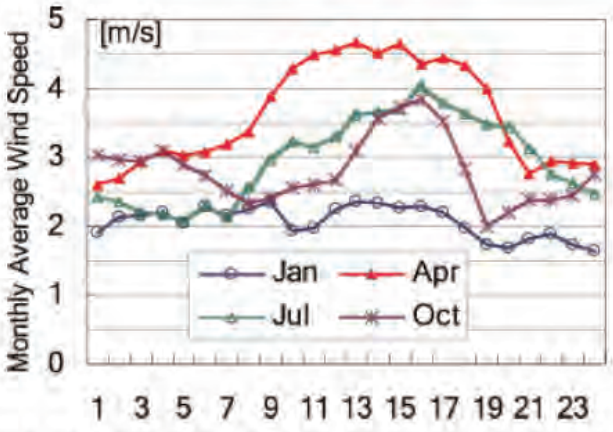

Figure 4. Daily transition of monthly average wind speed (3 m height)

15 to 20°C relative to ambient temperature, and module temperature was kept below the standard conditions of 25°C in April and January. Thus, the PV module, frame, and cable were working over a wide range of temperatures and were subjected to severe thermal stress.

Yearly average wind speed was 2·85 m/s, with standard deviation of 2·06 [m/s], and maximum wind speed recorded was 19·0 m/s at a height of 3 m. The daily transition of wind speed is shown in Figure 4 (Table IV). Daytime wind in spring was stronger (around 6 m/s) than nighttime wind. To determine the cooling effect of wind on module temperature, we extracted wind speed, module temperature, and ambient temperature data from measured data (See Figure 5). The rise in module temperature relative to ambient temperature (T_{module} $T_{ambient}$), is inversely related to wind speed at constant irradiance ($G_A \gg 0$). At midnight (G_A 0), the module temperature rise indicated a negative value until to 5°C due to the radiation cooling effect.

On the other hand, module temperature rise and in-plane irradiation are proportional at a constant wind speed (Figure 6). The absolute values of ambient temperature and wind direction did not appear to affect module temperature rise. In addition, the average temperature difference of modules 1 and 2 was 0·55°C (standard deviation 0·38°C), indicating that these modules have similar heat capacities.

In the warm season, the albedo was constant at 0·28 and increased to 0·4 in winter because of snow cover (See Figure 7, Table V). The winter albedo during the measurement period was less than 30% in an average year[11] as little snow fell in 2003–2005. The monthly average humidity was 40% during the warm season, and around 60% in the cold season.

Solar energy resource

Figure 8 shows the monthly variation in duration of sunshine and fraction relative to the ideal. The monthly durations of sunshine in winter and summer seasons were 200 and 300 h, respectively, in a normal year. The fraction of the duration of sunshine was 0·6 in summer, due to the rainy season, increasing to 0·8 or more in the cold season. There was only a small difference in the duration between a normal year (Table V)[12] and the measurement period, with a mean error of 4·5 h and RMSE of 7·5 h.

Figure 9 shows the monthly average values of horizontal and in-plane global irradiation. The annual mean of horizontal irradiation was 4·66 kW/m^2/day, which was 1·5-fold greater than that in Sapporo, Japan. The annual average of in-plane irradiation was 5·82 kW/m^2/day. The tilted irradiation data showed relatively small variation within a year, as precipitation is concentrated in the summer. The mean error between the measured horizontal irradiation and that in a normal year was 3·4% with RMSE of 7·5%.

PV module performance

Figure 10 shows the monthly average outputs of modules 1 and 2 in comparison to the rated output. The annual energy outputs of modules 1 (p-Si) and 2 (c-Si) were 404 and 351 Wh/day, respectively. Standard deviations were 43 and 40 Wh/day, respectively.

Table IV. Daily transition of monthly average wind speed [m/s] (numerical values of Figure 4)

Month	Time	0:00	1:00	2:00	3:00	4:00	5:00	6:00	7:00	8:00	9:00	10:00	11:00	12:00	13:00	14:00	15:00	16:00	17:00	18:00	19:00	20:00	21:00	22:00	23:00	Monthly average
Jan	Avrg.	1·9	2·1	2·1	2·2	2·0	2·3	2·2	2·2	2·4	1·9	2·0	2·3	2·4	2·3	2·3	2·3	2·2	2·0	1·7	1·7	1·8	1·9	1·7	1·6	3·6
	Stdev	2·2	2·2	2·1	2·3	2·2	2·4	2·4	2·5	2·6	2·2	2·5	2·3	2·1	2·0	1·7	1·6	1·4	1·4	1·6	1·9	2·1	2·3	2·1	2·0	2·3
Apr	Avrg.	2·6	2·7	2·9	3·1	3·0	3·1	3·2	3·4	3·9	4·3	4·5	4·6	4·7	4·5	4·6	4·3	4·4	4·3	4·0	3·2	2·7	2·9	2·9	2·9	3·6
	Stdev	2·1	2·1	2·5	2·6	2·6	2·3	2·3	2·2	2·3	2·2	2·3	2·5	2·6	2·6	2·6	2·4	2·3	2·1	2·3	2·4	2·3	2·1	2·1	2·3	2·3
Jul	Avrg.	2·4	2·4	2·2	2·2	2·1	2·3	2·1	2·6	3·0	3·2	3·1	3·3	3·6	3·7	3·7	4·0	3·8	3·6	3·5	3·4	3·1	2·8	2·6	2·5	3·0
	Stdev	1·7	1·8	1·6	1·7	1·3	1·7	1·6	1·4	1·2	1·2	1·2	1·5	1·9	1·9	1·7	1·6	1·7	1·6	1·7	1·7	1·8	1·8	1·6	1·4	1·6
Oct	Avrg.	3·0	3·0	2·9	3·1	2·9	2·7	2·5	2·3	2·4	2·5	2·6	2·7	3·1	3·6	3·7	3·8	3·5	2·8	2·0	2·2	2·4	2·4	2·4	2·7	2·8
	Stdev	2·3	2·4	2·5	2·7	2·6	2·5	2·2	2·1	2·1	1·8	1·4	1·1	1·1	1·3	1·3	1·5	1·6	1·6	1·3	1·6	2·0	1·9	2·1	2·3	1·9
Yearly	Avrg.	2·5	2·5	2·5	2·5	2·4	2·5	2·5	2·6	3·0	3·1	3·2	3·3	3·4	3·5	3·6	3·6	3·5	3·3	2·9	2·6	2·4	2·3	2·4	2·4	2·9
avrg.	Stdev	2·0	2·1	2·2	2·2	2·1	2·1	2·1	2·1	2·1	2·0	1·9	1·9	1·8	1·8	1·8	1·8	1·8	1·8	1·8	1·9	1·9	1·9	2·0	2·0	2·0

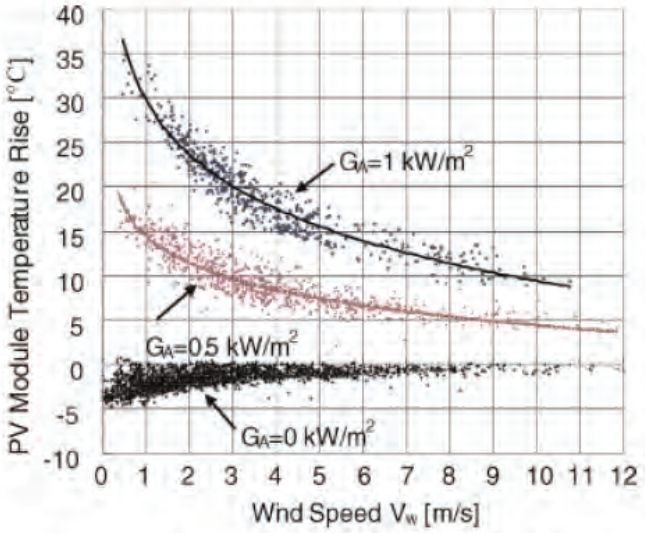

Figure 5. Module temperature rise ($T_{module} - T_{ambient}$) and wind speed relationship at constant irradiance

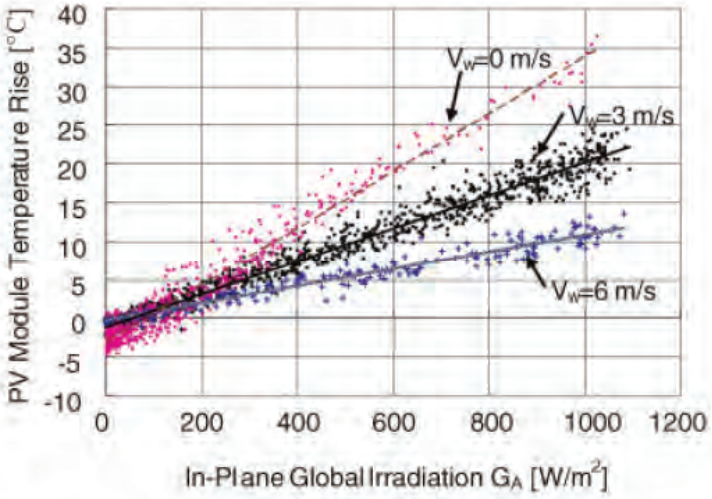

Figure 6. Module temperature rise ($T_{module} - T_{ambient}$) and in-plane irradiance relationship at constant wind speed

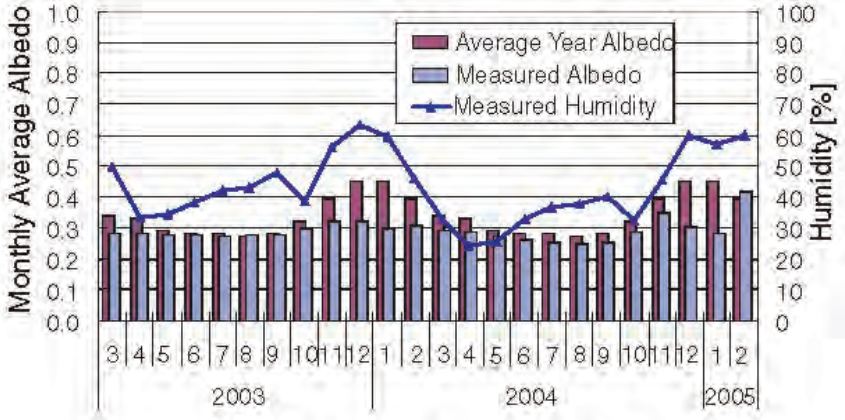

Figure 7. Albedo and Humidity variation

Table V. Numerical values of all parameters in the Figure 7–13

Year	2003												2004												2005	
Month	3	4	5	6	7	8	9	10	11	12	1	2	3	4	5	6	7	8	9	10	11	12	1	2
Average year albedo	0·34	0·33	0·29	0·28	0·28	0·27	0·28	0·32	0·39	0·45	0·45	0·39	0·34	0·33	0·29	0·28	0·28	0·27	0·28	0·32	0·39	0·45	0·45	0·39
Measured albedo	0·28	0·28	0·27	0·28	0·27	0·27	0·28	0·29	0·32	0·32	0·296	0·302	0·288	0·283	0·27	0·259	0·253	0·246	0·267	0·287	0·35	0·298	0·281	0·417
Measured humidity [%]	49·75	33·33	34·52	38·25	42·17	43·11	47·86	38·52	55·91	63·43	59·38	45·98	32·69	24·38	25·63	32·63	36·64	37·48	37·36	32·41	45·46	59·95	57·14	59·85
Average year sunshine duration [h]	262	258	298	308	302	297	278	258	213	198	210	217	262	258	298	308	302	297	278	258	213	198	210	217
Standard deviation [h]	28·4	25·5	23·2	27·3	29·8	25·7	22	20·8	21·2	15·5	27·2	27·2	28·4	25·5	23·2	27·3	29·8	25·7	22	20·8	21·2	15·5	27·2	27·2
Possible sunshine duration [h]	369	403	458	464	470	434	377	340	287	272	284	290	369	403	458	464	470	434	377	340	287	272	284	290
Average year fraction [h]	0·71	0·64	0·65	0·66	0·64	0·68	0·74	0·76	0·74	0·73	0·74	0·75	0·71	0·64	0·65	0·66	0·64	0·68	0·74	0·76	0·74	0·73	0·74	0·75
Measured sunshine duration [h]	279·5	269·8	284	283	288·2	277·8	263·7	275	213·2	229	235·8	234·7	256·3	298·5	307·2	281	300·3	282·5	268·7	275·7	235·5	202·5	244·3	236
Measured fraction	0·76	0·67	0·62	0·61	0·61	0·64	0·70	0·81	0·74	0·84	0·83	0·81	0·69	0·74	0·67	0·61	0·64	0·65	0·71	0·81	0·82	0·74	0·86	0·81
Horizontal irradiation [kW/m^2/d]	3·7	2·7	2·1	2·7	3·6	4·6	5·7	6·5	6·6	6·4	6·0	5·0	4·0	2·6	2·2	2·5	3·3	4·8	6·4	7·2	6·7	7·0	5·9	5·0
Average year horizontal irradiation [kW/m^2/d]	3·4	2·2	1·7	2·0	3·0	4·4	5·7	6·5	6·5	6·0	5·4	4·7	3·4	2·2	1·7	2·0	3·0	4·4	5·7	6·5	6·5	6·0	5·4	4·7
In-plane irradiation [kW/m^2/d]	5·6	5·2	4·2	4·9	5·8	6·2	6·2	6·2	6·0	5·8	6·2	6·3	6·5	4·9	4·9	5·1	5·6	6·0	7·2	6·9	6·2	6·6	6·2	6·2
Sapporo horizontal irradiation [kW/m^2/d]	2·6	1·6	1·3	1·5	2·3	3·3	4·3	4·8	5·0	4·6	4·2	3·5	2·6	1·6	1·3	1·5	2·3	3·3	4·3	4·8	5·0	4·6	4·2	3·5
Rated energy output 1 [Wh/d]	435	429	455	449	434	406	385	454	377	374	375	434	344	470	491	438	458	428	374	429	421	285	384	346
Rated energy output 2 [Wh/d]	408	402	426	421	407	381	361	426	354	351	352	407	322	440	460	411	430	402	351	402	394	267	360	324
Real energy output 1 [Wh/d]	409	388	397	377	370	346	338	421	375	381	379	426	328	418	428	366	369	352	324	388	422	293	385	349
Real energy output 2 [Wh/d]	366	345	352	335	328	308	302	377	324	328	326	362	277	352	355	305	315	303	281	344	360	245	333	297
In-plane reference yield [h/d]	6·31	6·21	6·18	6·02	5·85	6·18	6·30	6·45	4·88	4·89	5·11	5·65	6·18	7·21	6·91	6·16	6·60	6·25	6·23	6·32	5·44	4·11	5·34	6·00
Yield of module 1 [h/d]	5·93	5·63	5·39	5·05	4·98	5·27	5·52	5·98	4·86	4·98	5·17	5·54	5·90	6·41	6·02	5·14	5·30	5·13	5·39	5·63	5·46	4·22	5·35	6·07
Yield of module 2 [h/d]	5·66	5·34	5·10	4·79	4·72	5·01	5·26	5·71	4·47	4·58	4·73	5·03	5·32	5·76	5·32	4·58	4·83	4·71	4·98	5·32	4·96	3·77	4·94	5·51
Performance ratio of module 1	0·94	0·91	0·87	0·84	0·85	0·85	0·88	0·93	1·00	1·02	1·01	0·98	0·95	0·89	0·87	0·83	0·80	0·82	0·87	0·90	1·00	1·03	1·00	1·01
Temperature factor, K_{temp1}	1·05	1·01	0·97	0·95	0·93	0·94	0·96	1·01	1·08	1·10	1·10	1·07	1·06	0·99	0·97	0·93	0·92	0·93	0·97	1·00	1·05	1·09	1·09	1·09
Other loss factor, K_{oth1}	0·90	0·90	0·90	0·89	0·92	0·91	0·91	0·92	0·92	0·92	0·92	0·91	0·90	0·90	0·90	0·89	0·87	0·88	0·90	0·90	0·96	0·94	0·92	0·93
Performance ratio of module 2	0·90	0·86	0·82	0·80	0·81	0·81	0·83	0·88	0·92	0·94	0·93	0·89	0·86	0·80	0·77	0·74	0·73	0·75	0·80	0·85	0·91	0·92	0·93	0·92
Temperature factor, K_{temp2}	1·05	1·01	0·97	0·95	0·94	0·95	0·97	1·01	1·07	1·10	1·09	1·07	1·06	0·99	0·98	0·94	0·93	0·95	0·97	1·01	1·04	1·07	1·08	1·07
Other loss factor, K_{oth2}	0·86	0·85	0·85	0·84	0·86	0·85	0·86	0·88	0·86	0·85	0·85	0·83	0·81	0·81	0·79	0·79	0·78	0·80	0·82	0·85	0·88	0·86	0·86	0·86

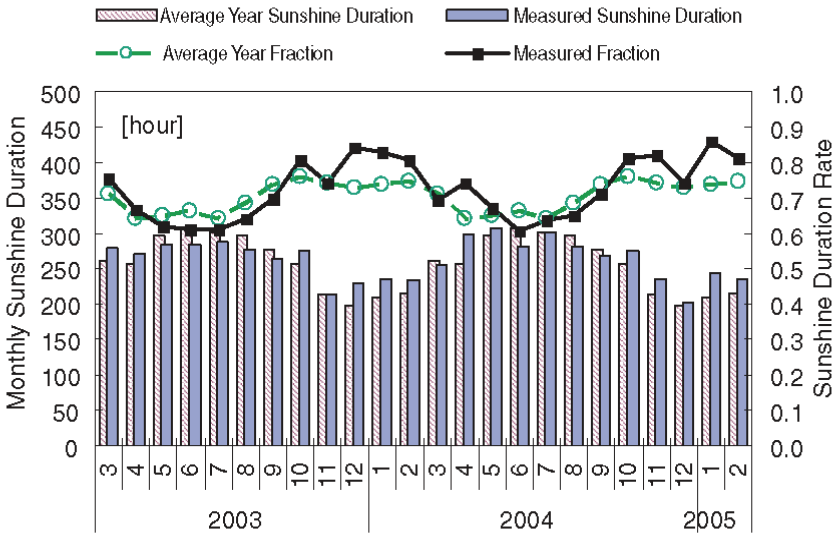

Figure 8. Comparison of the duration of sunshine and fraction relative to an average year

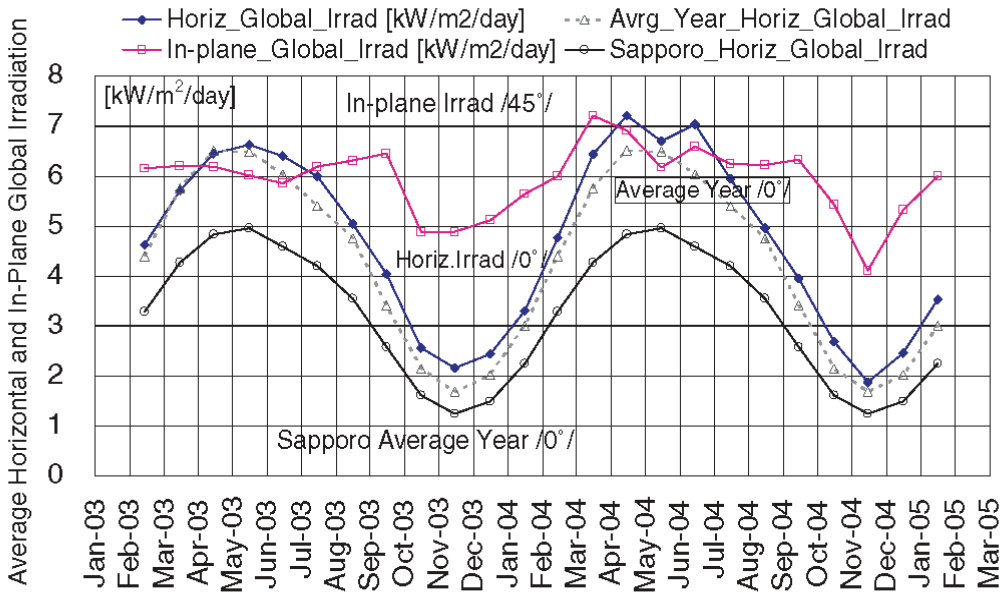

Figure 9. In-plane and horizontal global irradiation in comparison to data for an average year and for Sapporo

For comparison with other types of module, the reference yield, module yield, and performance ratio (PR) were calculated from measured data as shown in Figure 11 and Table V. The annual reference yields of horizontal and tilted irradiation were 1695 and 2137 h/y, indicating 1695 and 2137 h sunshine hours per year with a standard of 1 kW/m^2 solar energy. The annual module yields were $Y_{A,m1} = 1961$ h/y and $Y_{A,m2} = 1842$ h/y, indicating that each module worked for 1961 h and 1842 h by rated power, P_{max}, in the year.

Figures 12 and 13 show the variations in performance ratio, temperature, and other loss modification factors. Strong seasonal variations were apparent in the performance of both modules. The PR of module 1 showed very high values of >1·0 in winter and around 0·85 in the warm season due to the effect of module temperature. The other loss was stable at around 10%.

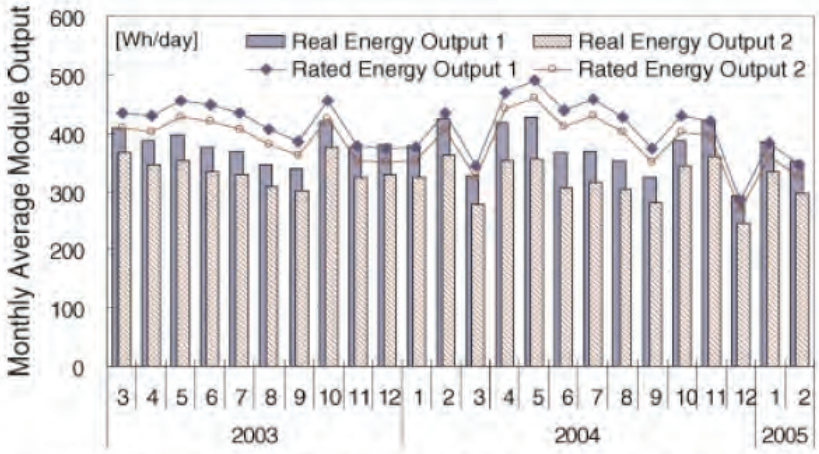

Figure 10. Average outputs of modules 1 and 2 in comparison to the rated output

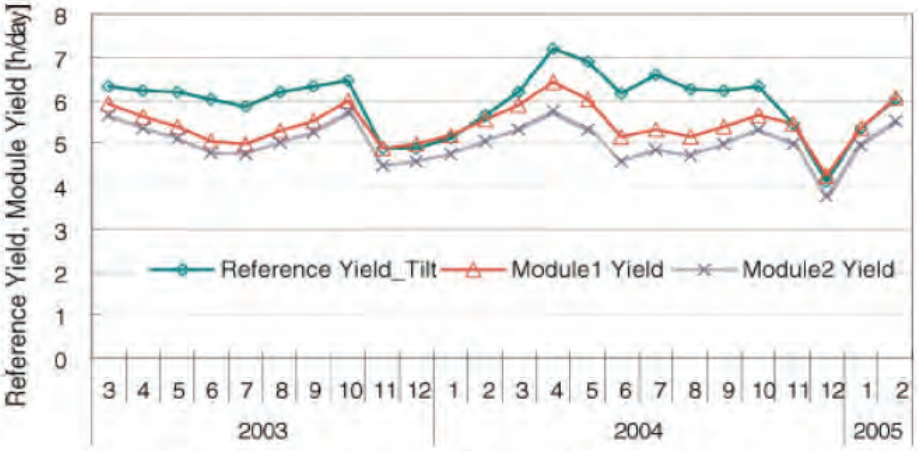

Figure 11. Reference yield, Y_A, and array yield, Y_r, of modules 1 and 2

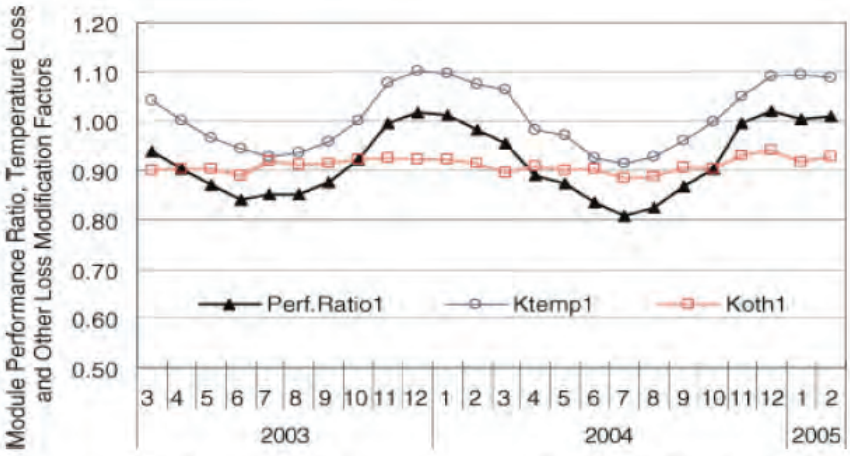

Figure 12. Monthly average performance ratio, temperature, and other loss modification factors of PV module 1

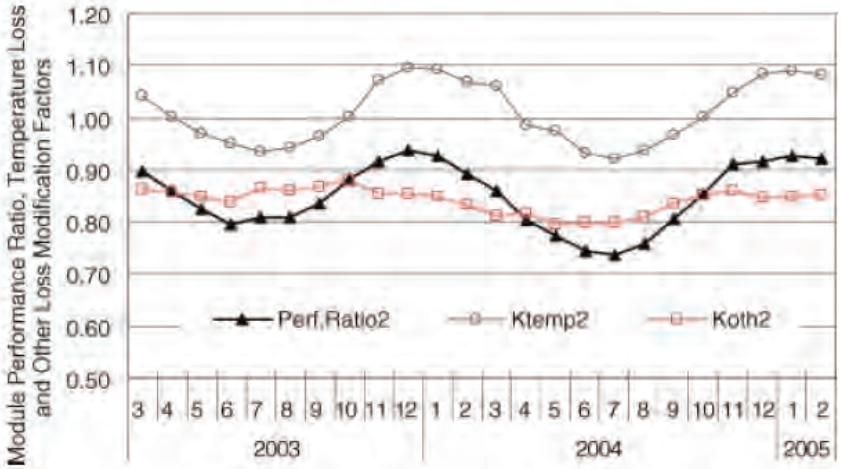

Figure 13. Monthly average performance ratio, temperature, and other loss modification factors of PV module 2

The performance of module 2 was 0·75–0·93, which was 0·1 lower than that of module 1. In addition, the value of K_{oth2} was lower than that of module 1. The nominal power values (according to the manufacturers) were used for yield and performance calculations. However, the average measured power values, $P_{max,real}$, of modules 1 and 2 were below the respective nominal power values of 76·3 W (95·4%) and 68·6 W (91·4%) within the allowed tolerance range ±10% (JIS C8990). This difference (4·6%, 8·6%) was included in the performance differences between module 1 and 2. In addition, module performance difference may have been due to differences in the materials used for module construction: for example, differences in glass reflection coefficient, etc.

Sandstorms, dust, and snow coverage did not appear to have significant effects on module performance.

CONCLUSIONS

Accurate determination of the performance of PV modules is crucial for the design of VLS-PV systems and their economic evaluation. To develop a conceptual design and calculation of the power generation and construction costs for a VLS-PV system for the Gobi Desert, an autonomous PV module performance monitoring and data acquisition system was developed. Outdoor performance tests of two types of PV module were conducted in Sainshand City, Mongolia.

The results described here indicated high output gain due to the extremely low ambient temperature and the module performance ratio showed very high values of >1·0 in winter. In summary, the results of the present study show that PV modules with high temperature coefficients, such as crystalline silicon, are advantageous for use in the Gobi Desert area. We are obtaining useful information for installation of the VLS-PV system in the Gobi Desert area, and will continue our field study to further evaluate the long-term performance of PV modules exposed to the severe environmental conditions in the Gobi Desert.

Acknowledgements

The study was carried out by the Japanese-Mongolian Research team within the cooperative framework between the National Institute of Advanced Industrial Science & Technology, Tokyo University of Agriculture & Technology, and Inter-University Solar Research Net-Center of the National University of Mongolia.

REFERENCES

1. IEA, Photovoltaic Power Systems Programme, Task 8: Very large scale photovoltaic power generation systems in remote areas, http://www.oja-services.nl/iea-pvps/tasks/index.htm.

2. Kurokawa K (ed.). *Energy from the Desert, Feasibility of Very Large Scale Photovoltaic Power Generation (VLS-PV) Systems*. James & James Ltd: UK, 2003; 195.
3. Ito M, Kato K, Sugihara H, Kichimi T, Song J, Kurokawa K. A preliminary study on potential for very large-scale photovoltaic power generation (VLS-PV) system in the Gobi desert from economic and environmental viewpoints. *Solar Energy Materials and Solar Cells* 2003; **75**(3–4): 507–517.
4. JIS C8990. Crystalline silicon terrestrial photovoltaic (PV) modules: Design qualification and type approval.
5. IEC 1215. Design and type approval of crystalline silicon terrestrial PV Modules.
6. JIS C8919. Outdoor measuring method of output power for crystalline solar cells and modules, 1995.
7. IEC 60891. Procedures for temperature and irradiance corrections to measured *I–V* Characteristics of crystalline silicon photovoltaic devices.
8. IEC 61724. The international electrotechnical commission. Photovoltaic system performance monitoring Guidelines for measurement, data exchange and analysis, 1998.
9. Jahn U, Mayer D, Heidenreich M, *et al*. International energy agency PVPS task 2: analysis of the operational performance of the IEA Database PV systems. 16th European Photovoltaic Solar Energy Conference and Exhibition, Glasgow, United Kingdom, May 2000.
10. Oozeki T, Izawa T, Otani K, Kurokawa K. An evaluation method of PV systems. *Solar Energy Materials and Solar Cells* 2003; **7**(3–4): 687–695.
11. Institute of Meteorology and Hydrology of Mongolia, www.env.pmis.gov.mn/Meteoins/
12. Davaadorj D, Gomboluudev P. Evaluation report of renewable energy resource in the Dornogobi province, June 1997.

原著論文 Papers

Available online at www.sciencedirect.com
ScienceDirect

Solar Energy Materials & Solar Cells

ELSEVIER

Solar Energy Materials & Solar Cells 90 (2006) 3356–3363

www.elsevier.com/locate/solmat

An evaluation method of the fluctuation characteristics of photovoltaic systems by using frequency analysis

Norihiro Kawasaki[a,*], Takashi Oozeki[a], Kenji Otani[a,b], Kosuke Kurokawa[a]

[a]*Kosuke Kurokawa Lab, Tokyo University of Agriculture and Technology, 2-24-16 Naka-cho, Koganei, Tokyo 184-8588, Japan*

[b]*National Institute of Advanced Industrial Science and Technology (AIST), Japan*

Received 24 May 2005; accepted 20 February 2006
Available online 4 August 2006

Abstract

Short-time fluctuations in solar irradiance will become an important issue with regard to future embedded photovoltaic (PV) systems. However, when PV systems are intensively installed, fluctuation of total output in clustered PV systems is not remarkable because there is the smoothing effect of irradiance in certain areas. In this paper, a new estimation method of irradiance fluctuation, which is based on the combination of the Fourier transform and the wavelet transform methods, is described.

Keywords: PV system; The smoothing effect; Fluctuation characteristic; Fourier transform; Wavelet transform

1. Introduction

The output of photovoltaic (PV) systems has a short-term fluctuation due to weather fluctuation. It may cause undesirable effects on an individual power system, and it lowers the capacity value (kW value) of the PV system. To clarify these phenomena, authors have studied "the smoothing effect" which is to smoother the total area irradiance. Fluctuation

*Corresponding author. Tel./fax: +81 42 388 7445.
E-mail address: norihiro@cc.tuat.ac.jp (N. Kawasaki).

0927-0248/$ - see front matter © 2006 Elsevier B.V. All rights reserved.
doi:10.1016/j.solmat.2006.02.034

of PV output is sensitive as for a few PV systems; however, fluctuation of total output in clustered PV systems is not remarkable because there is spatial-inhomogeneity of irradiance field in certain areas. According to the smoothing effect, the capacity value of PV systems is indicated to increase, and problems for utility that occurred by fluctuation of PV output power can be alleviated. Therefore, it is very important to quantitate this effect and to develop a new evaluation method.

Several important studies of the smoothing effect have already been approached based on irradiation data. One of the papers describes a definition of the irradiance fluctuation degree by using original parameter, moving average and standard deviation of irradiance data, and demonstrates improvement in kW value [1]. In another paper, the magnitude of the fluctuation and speed of fluctuation are defined, and the forecast of load frequency control (LFC) capacity is evaluated [2]. Both the studies have developed simulation methods of the smoothing effect based on irradiation as the relation between smoothing effect, area size and the value of the number of PV systems in a distribution network. Furthermore, the evaluation method is proposed to be more mathematical and to consider several time scales, and also it is necessary to demonstrate accuracy of simulations by using data obtained in real system. However, both the studies are not used in real measurement data of the distribution network.

The purpose of this paper is to develop a new evaluation method for smoothing effect. The evaluation method uses Fourier transform and wavelet transform [3] for frequency analysis. Measured data can be obtained from February 2004. This study is a part of "Demonstrative Research on Clustered PV Systems", funded by New Energy and Industrial Technology Development Organization (NEDO).

2. Measured data

Irradiance data have been recorded by 1 min sampling. Irradiance data used in analysis were obtained by the special monitoring system that consists of nine synchronized monitoring terminals from October 1995 to December 1997 (Fig. 1). Those terminals have been installed on a grid which covers an area measuring about 4 km × 4 km at 140°05′58″ east to 140°09′05″ east and 36°02′58″ north to 36°05′30″ north. The size of the grid is decided by considering the size of typical urban distribution network [1].

3. Approach

Applying the Fourier transform and the wavelet transform one can derive frequency domain properties of the recorded fluctuation patterns. Unlike Fourier transform, wavelet transform is localized in time by frequency analyzing. In other words, Fourier transform has only frequency information, and wavelet transform has time information and frequency information. However, if either of them is chosen, authors think that the fluctuation characteristic cannot be grasped correctly. Because Fourier transform gives fluctuation for the whole one day, and wavelet transform gives fluctuation for a local time, both of them are important in order to understand fluctuation characteristics. The flow of the calculation is shown in Fig. 2.

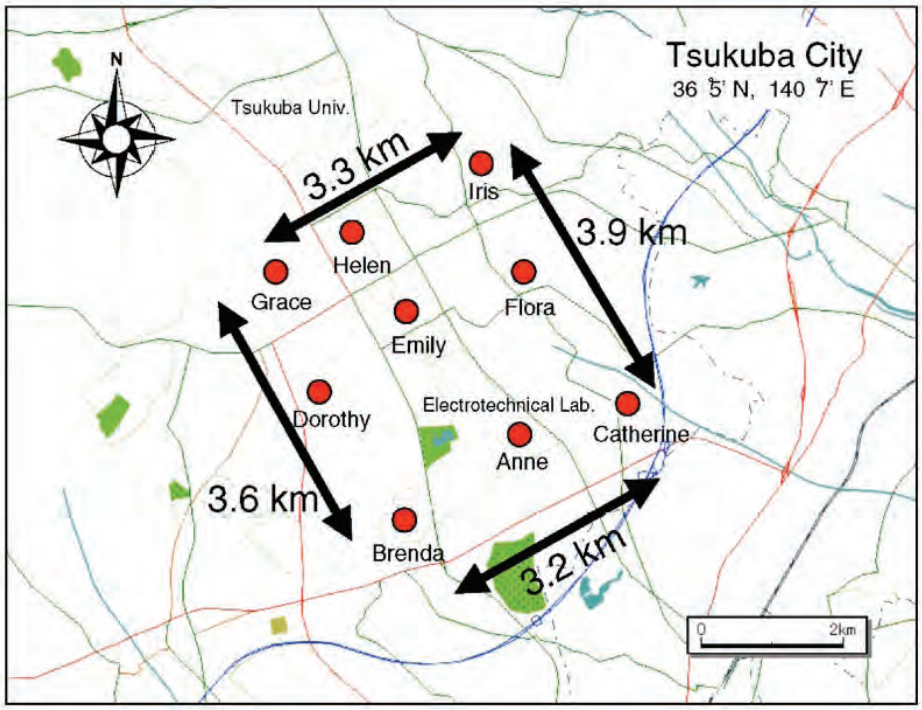

Fig. 1. Location of nine terminals of area irradiance monitoring system.

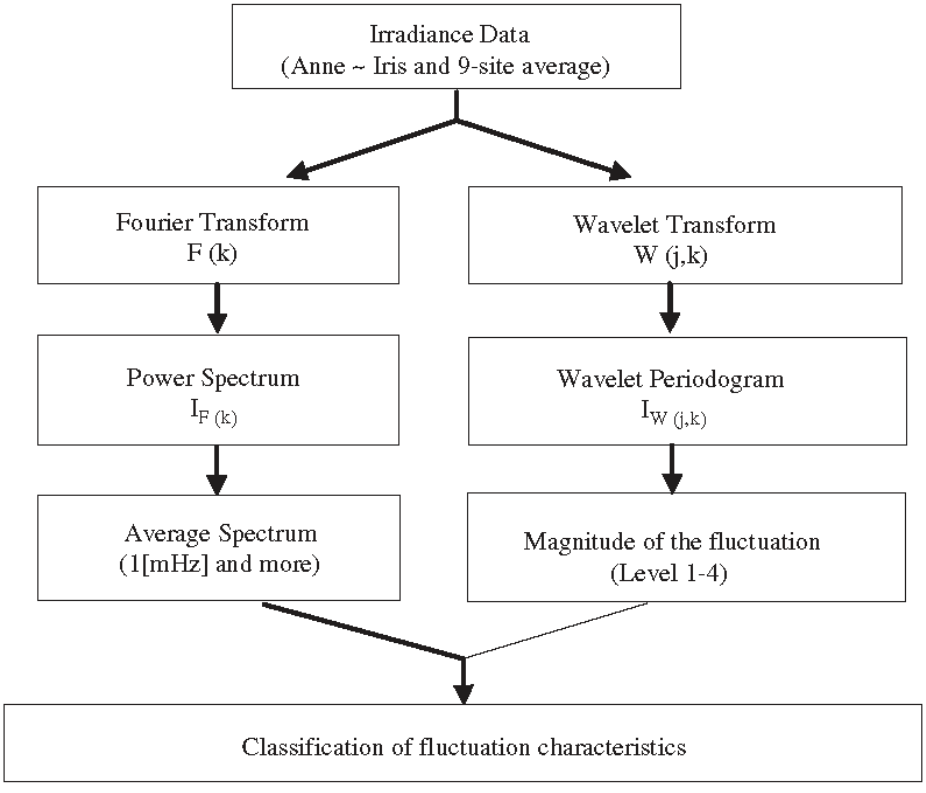

Fig. 2. Flow chart of the evaluation process.

3.1. Fourier analysis

The Fourier transform of discrete data is given by the following formula:

$$F(k) = \sum_{n=0}^{N-1} f(n) e^{-j2\pi kn/N}. \quad (1)$$

Power spectrums ($I_{F(k)}$) are calculated from the square of the coefficients of Fourier spectrum ($F(k)$):

$$I_{F(k)} = \frac{1}{N}|F(k)|^2. \quad (2)$$

The maximum frequency is $\frac{1}{120}$ Hz($= 8.33 \times 10^{-3}$ Hz) based on the sampling theorem, because irradiance data have been recorded by 1 min sampling. This time, power spectrum more than 1×10^{-3} Hz was averaged as an example. This is defined as "average spectrum". This corresponds to the frequency domain of LFC. The average spectrum means degree of the distribution of the fluctuation during the entire day. There is so much of fluctuation that this value is large.

3.2. Wavelet analysis

Wavelet transform W of a signal $f(n)$ is calculated as the inner product of $f(n)$ and the scaled and shifted wavelet base $\psi_{j,k}(n)$:

$$W(j,k) = \sum_{n=0}^{N-1} f(n)\psi_{j,k}(n), \quad (3)$$

$$\psi_{j,k}(n) = \frac{1}{2^{j/2}}\psi\left(\frac{n-k}{2^j}\right). \quad (4)$$

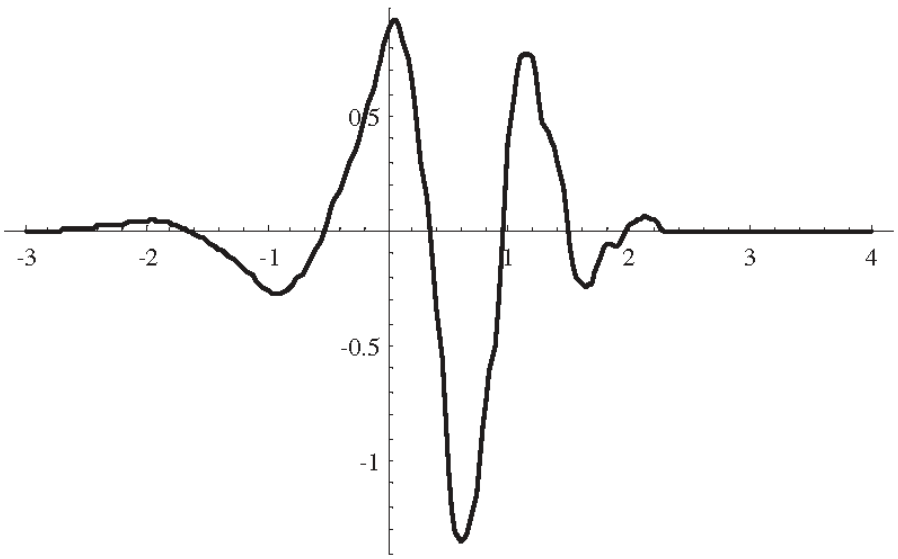

Fig. 3. Daubechies 4 (wavelet function).

Daubechies 4 (Fig. 3) has been chosen as a wavelet function ($\psi_{j,k}(n)$). Wavelet periodograms are calculated from the square of the coefficients of wavelet spectrum ($W(j,k)$):

$$I_{W(j,k)} = |W(j,k)|^2. \tag{5}$$

This time, the fluctuation cycle for 1 16 min was observed as an example. This corresponds to a level 4 from a level 1. Furthermore, this corresponds to the frequency domain of LFC. The maximum spectrum is looked up from these periodograms (Fig. 4). The maximum periodogram is detected and the width of irradiance fluctuation of this time is calculated. This is defined as "magnitude of fluctuation". The magnitude of fluctuation is not necessarily maximum of the day, because frequency band is limited. The greatest magnitude of fluctuation can be calculated for the target frequency.

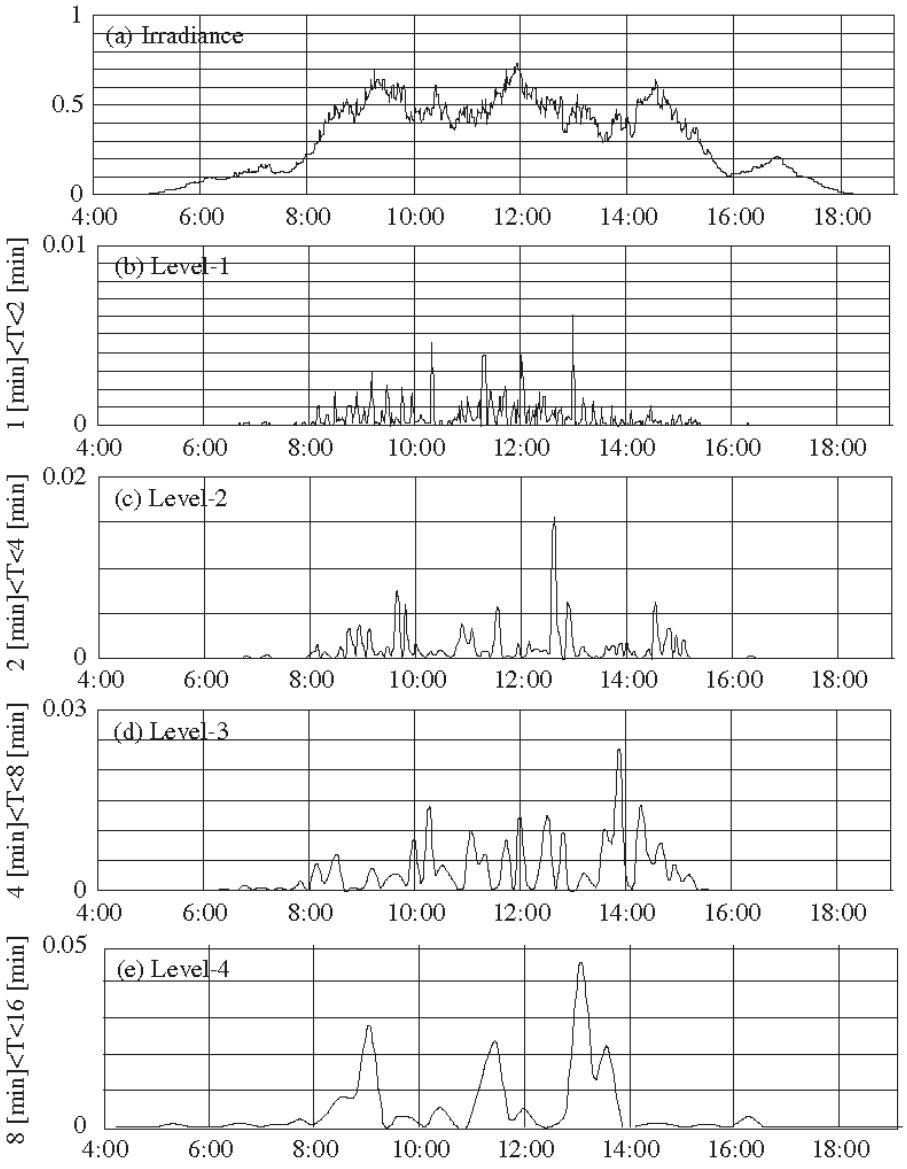

Fig. 4. Wavelet periodogram; average of nine-site measurements (19 August 1997).

4. Results and discussion

Result of the flow chart is shown in Fig. 5((a)3, (b)3, (c)3, (d)3) and Table 1. The horizontal axis serves as magnitude of the fluctuation, and the vertical axis serves as average spectrum in Fig. 5. Four patterns of a clear weather day (97/8/10), a cloudy after fine weather day (97/8/19), a slightly cloudy sky day (97/7/4), and a rainy weather day (97/7/10) are analyzed.

(1) Clear day: The real measured data of 10th July (see Fig. 5(a)) has been set for evaluation standards as a clear day. Average spectrum and magnitude of the fluctuation are, respectively, distributed over the range of about 0.005×10^{-3} and about $0.05\,\mathrm{kW/m^2}$ on this pattern. As a result, these fluctuations of irradiance are the smallest among the four patterns. But as for three points of Brenda, Helen, and Iris, magnitude of the fluctuation is larger than other points, according to the influence of the shade of the building. Influence of the shade of the building is contained on irradiation of nine-site average, according to the smoothing effect.

(2) Slightly cloudy day: There is fast and small fluctuation on each point in area. Average spectrum is distributed over the range about 1.0×10^{-3} 1.4×10^{-3}, magnitude of the fluctuation is distributed over the range about 0.2 $0.4\,\mathrm{kW/m^2}$. As compared with clear day, average spectrum is 200 times or more, and the magnitude of fluctuation is 10 times or more. Therefore, irradiance of each point had a sharper fluctuation. On the other hand, shape of irradiance of nine-site average is smoother than irradiance of each point. Comparing irradiance of nine-site average of this day with irradiance of clear day, average spectrum is about 30 times, and the magnitude of fluctuation is about the same. Average spectrum decreases to about $\frac{1}{10}$ and this means that short and fast fluctuations are contained, according to the smoothing effect.

(3) Cloudy, fine later day: Irradiance of this day has much quick and big fluctuation. Irradiance fluctuation of each point in the area is intense. Average spectrum is distributed over the range of about 5 9×10^{-3}, magnitude of fluctuation is distributed over the range of about 0.2 $0.6\,\mathrm{kW/m^2}$. As compared with clear day, average spectrum is 1400 times or more, and the magnitude of the fluctuation is 30 times or more. Therefore, irradiance of each point had a very sharp fluctuation. Comparing irradiance of nine-site average of this day with irradiance of clear day, average spectrum is about 130 times, and the magnitude of fluctuation is about 3 times. Average spectrum decreases to about $\frac{1}{12}$ and the magnitude of the fluctuation decreases to about $\frac{1}{4}$, according to the smoothing effect. This means that the smoothing effect is acquired well.

(4) Rainy day: On the whole, irradiance is small on this day. Therefore, since the absolute value of fluctuation becomes small, an average spectrum and the range of fluctuation become inevitably small: average spectrum is distributed over the range of about 0.02×10^{-3} 0.07×10^{-3}, magnitude of the fluctuation is distributed over the range of about 0.02 $0.07\,\mathrm{kW/m^2}$. Compared to clear day, average spectrum is 1400 times, and the magnitude of the fluctuation is 30 times. Therefore, irradiance of each point did not have very sharp fluctuation. Compared to irradiance of nine-site average of this day with irradiance of clear day, average spectrum is about 2 times, and the magnitude of fluctuation is about $\frac{1}{2}$. The smoothing effect is not obtained on this pattern.

(5) Summary of results: Fig. 5(b) and (c) are influenced by the short-time moving cloud, because irradiance drops and spikes are caused by passing fast clouds. Fig. 5(c) was deadened by the smoothing effect to level of Fig. 5(b). This is the result of "the smoothing

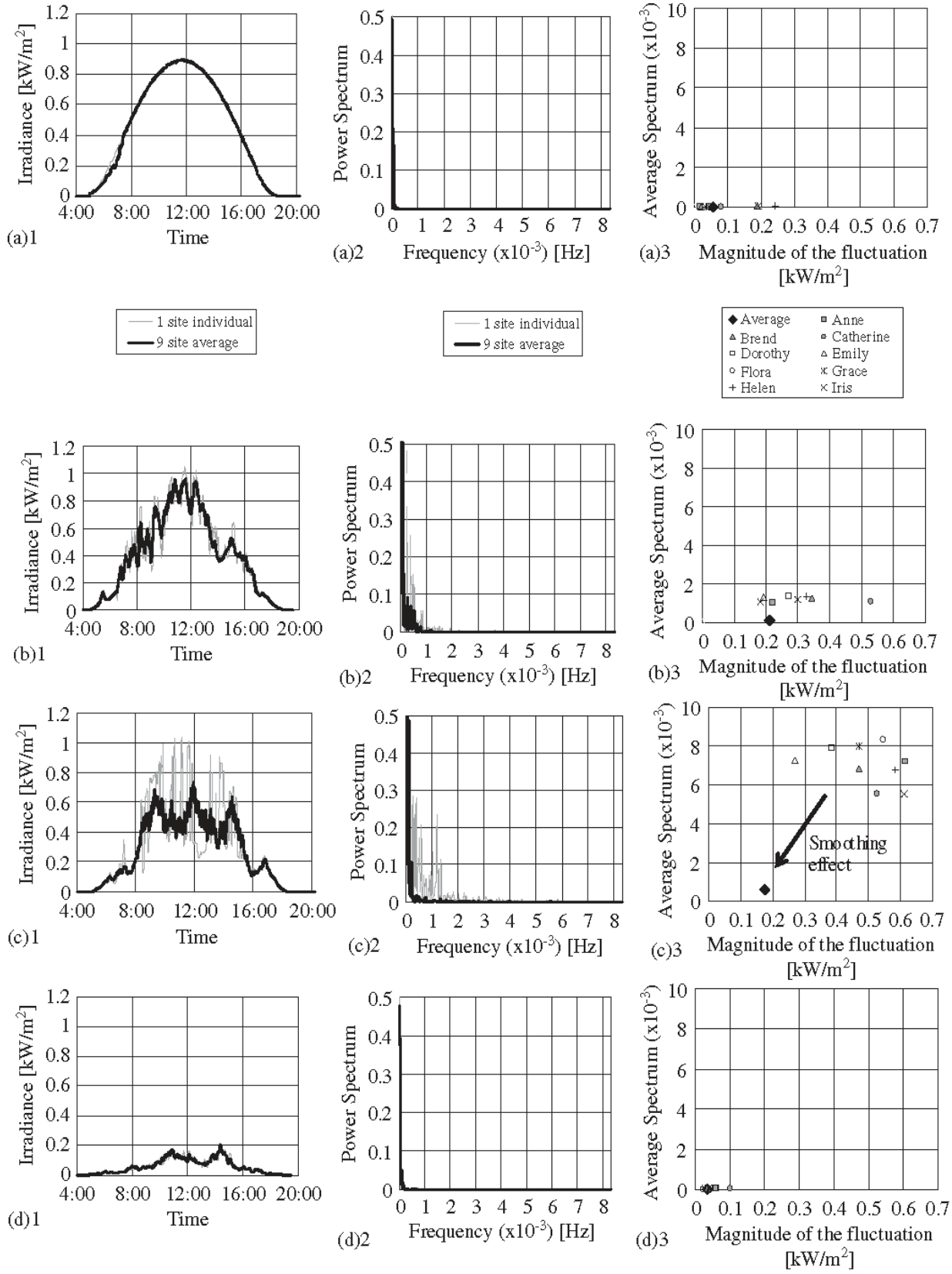

Fig. 5. Classification of fluctuation characteristic; relation of average spectrum and magnitude of the fluctuation. (a) 10 July 1997, (b) 4 July 1997, (c) 19 August 1997, (d) 10 August 1997. (1) Irradiance data, (2) result of Fourier transform, (3) fluctuation characteristic.

Table 1
Relation of average spectrum and magnitude of the fluctuation

	Clear		Slightly cloudy		Cloudy, fine later		Rainy	
	One-site individual	Nine-site average	One-site individual	Nine-site average	One-site individual	Nine-site average	One-site individual	Nine-site average
Average spectrum ($\times 10^{-3}$)	0.00465	0.00448	1.021	0.129	7.22	0.572	0.0508	0.00891
Magnitude of the fluctuation (kW/m^2)	0.0170	0.0565	0.221	0.212	0.615	0.175	0.0605	0.0352

One-site individual: Anne.

effect". Fig. 5(a) and (d) are scarcely influenced by the short-time moving cloud, thus this fluctuation characteristics (average spectrum, magnitude of the fluctuation) become very small value. The authors arrange the fluctuation patterns according to intensity; Fig. 5(c) > (b) > (d) > (a). This turn is the same as the turn that the smoothing effect has obtained. The smoothing effect can be quantified in every fluctuation frequency by using frequency analysis of Fourier transform and wavelet transform.

5. Conclusion

In this study, authors verified the smoothing effect using frequency analysis of Fourier transform and wavelet transform using irradiation data. From the results, the authors obtained the smoothing effect; Fig. 5(c) > (b) > (d) > (a) (in order of effect). This turn is equal to the irradiance fluctuation. Because of them, it is confirmed that the more the irradiance fluctuates, the more the smoothing effect is effective. Moreover, the smoothing effect can be quantified by this evaluation method. In a future work, the authors will model the simulation to consider the smoothing effect in actual grid including area size, the distance of station, and number of PV systems.

Acknowledgments

This work was supported by NEDO as a part of the "Demonstrative Research on Clustered PV Systems" under METI.

References

[1] K. Otani, J. Minowa, K. Kurokawa, Sol. Energy Mater. Sol. Cells 47 (1997) 281.
[2] S. Yanagawa, et al., Trans. IEE Jpn. 121 (9) (2001) 1094.
[3] A. Woyte, R. Belmans, J. Nijs, Analysing short-time irradiance fluctuations by their characteristic time scales, WCPEC-3, Osaka, Japan, 11–18 May 2003.

原著論文 Papers

Available online at www.sciencedirect.com
ScienceDirect
Solar Energy Materials & Solar Cells
ELSEVIER
Solar Energy Materials & Solar Cells 90 (2006) 3364–3370
www.elsevier.com/locate/solmat

A fundamental experiment for discrete-wavelength LED solar simulator

Shogo Kohraku*, Kosuke Kurokawa

Tokyo University of Agriculture and Technology (TUAT), Naka-cho 2-24-16, Koganei, Tokyo 184-8588, Japan

Received 24 May 2005; accepted 22 September 2005
Available online 30 August 2006

Abstract

This paper intends to report the possibility of using an light-emitting diode (LED) as a light source of a solar simulator for measuring solar cells. In our laboratory the LED solar simulator has been made up as the test production, and characteristics of monocrystalline Si solar cell have been measured by using it. As a result, spectral response (SR) and I–V characteristics of solar cells can be measured by the proposed method even though light intensity of the LED is in the range of approximately up to 10 mW/cm^2. Moreover, I–V characteristics under standard test conditions (STC) can be estimated by compensation.

Keywords: Light-emitting diode (LED); Spectral response; Measuring method

1. Introduction

For further market deployment of photovoltaic systems (PV systems), solar cells and modules must maintain sufficient reliability; therefore, technologies for measuring solar cell performances are very important. At present, the solar cell measurement performance has been improved, but it is still expensive since Xenon and Halogen lamp, which consist of the solar simulator have short life and require a lot of electric power. Meanwhile, it is widely recognized that light-emitting diode (LED) is energy saving, within budget, and needs a small light source, and recent technical innovation allows us to easily buy the high luminance LED. In a few studies, the solar simulator using LED as light source has been

*Corresponding author. Tel./fax: +81 42 388 7445.
E-mail address: kohraku@cc.tuat.ac.jp (S. Kohraku).

0927-0248/$ - see front matter © 2006 Published by Elsevier B.V.
doi:10.1016/j.solmat.2005.09.024

proposed. These simulators use white light LED instead of the previous lamps. However, their characteristics are not corresponding with characteristics of natural sunlight because the spectrum of LED is narrower and weaker than the spectrum of natural sunlight. Therefore, a suitable method is required in order to use the LED solar simulator.

This paper intends to propose that the LED solar simulator makes it possible to obtain the performance of solar cell, I V and spectal response (SR) characteristics, by the methodological measurement. Discrete SR can be measured in such a way that white and plural monochromatic light and the solar cell illuminate each other due to the fact that monochromatic light LED except white light has bright line spectrum. SR curve can be estimated by using discrete SR and least-squares method with physical model, and photocurrent under standard text conditions (STC) is obtained from SR curve. Moreover, the LED solar simulator is able to measure I V characteristics of STC by assuming that I V characteristics of Si solar cells are independent of light intensity.

2. Theory and experimental

2.1. Measuring method using LED

Fig. 1 shows the measurement procedure of SR using LED. A test cell is irradiated by monochromatic light together with white light as bias light, and its short circuit current (I_{sc}) is measured. Secondly, the cell is only exposed to white light and I_{sc} is measured in the same way. The difference of I_{sc} in the two conditions divided by incidence monochromatic irradiance is SR at the wavelength of the illuminating light. SR at discrete wavelength are derived by three monochromatic LED (this time, blue, red and infrared). Experimental discrete are supplemented by a theoretical curve of photocurrent, and then the whole SRs curve of the test cell is calculated [1]. The SR curve multiplied by the reference solar spectral distribution calculates photocurrent under STC. I V characteristics are measured under two different irradiations and calculated under STC by correction.

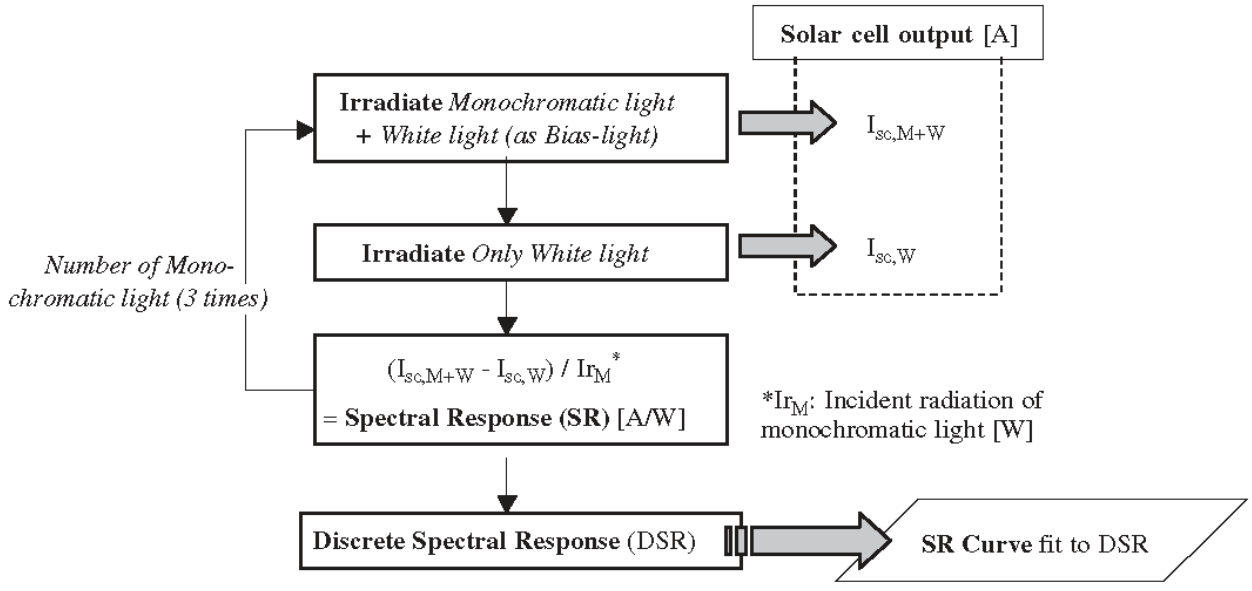

Fig. 1. Measurement procedure of spectral response using monochromatic light.

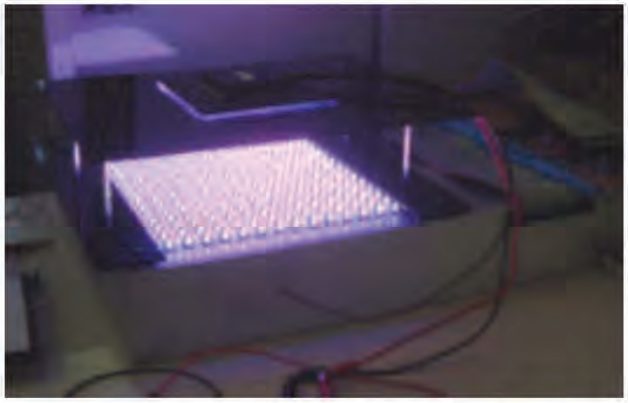

Fig. 2. Discrete-wavelength LED solar simulator.

Table 1
Specifications of LED

Color	Peak wave length (nm)	Spectral half bandwidth (nm)	Typical light intensity (cd)	Angle of beam spread (deg)	Typical forward current: I_F (mA)	Typical forward voltage: V_F (V)
Blue	470	25	1500	30	20	3.6
Red	644	18	800	30	20	1.9
Infrared	950	50	180 (mW/sr)	35	50	1.3
White	470 (570)	–	3100	35	20	3.6

2.2. Specification of LED solar simulator

LED solar simulator for a $100 \times 100\,mm^2$ solar cell is manufactured for trial (Fig. 2). This equipment has LED in four colors (blue, red, infrared and white), and the specification is shown in Table 1. Their angle of beam spread is around the middle (about 30°), and lamp-type LED is used. Each LED is arranged equally (7.62 mm between each LED, and 15.24 mm between same color). Fig. 3 shows schematic illustration of the LED arrangement. 14×14 LED per color are laid out on a grid, and the total number of LED is 784. The total area of light source is about $205 \times 205\,mm^2$. The distance of irradiation is adjusted with spacers. This time, light source irradiated a measuring object from a height of 84 mm, and had illumination unevenness per color of about 5%. The arrangement has lower illumination unevenness calculated by illuminant simulation [2] (Fig. 4).

The simulator is electrically designed as follows. A voluntary current can be passed through the LED controlled at each color and voluntary light intensity is available. Typical forward current (I_F) of LED is 20 mA (in the case of infrared, $I_F = 50\,mA$) in this SR measurement.

3. Results and discussion

3.1. Measurement of SR

The relation between the I_F and the irradiance of LED light was examined with a spectroradiometer for grasping the irradiance in measuring (Fig. 5). After this, the

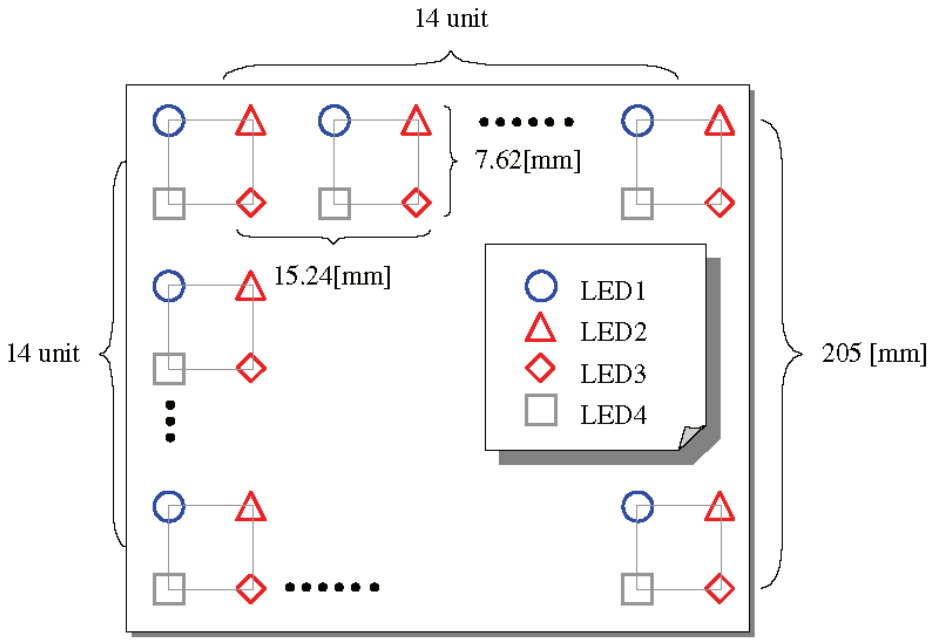

Fig. 3. Schematic illustration of LED arrangement.

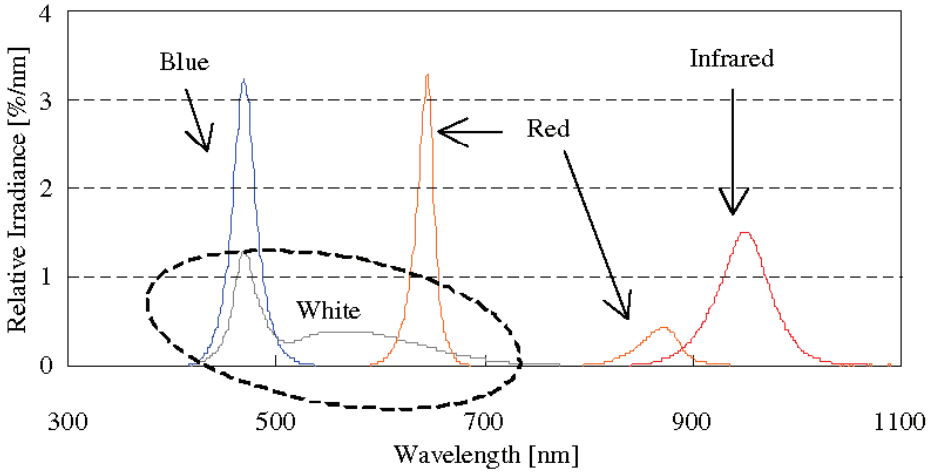

Fig. 4. Wavelength characteristics of LED built-in solar simulator.

irradiance of LED light is derived from each I_F (one needs to be careful about the irradiance time change of LED). Discrete SR measured by three LED was compensated with the photocurrent theoretical curve by least-squares method and the calculated and measured curve is compared (Fig. 6). Consequently, the measured and calculated photocurrents under STC were, respectively, 3.76 and 3.14 A, and the estimation is lower than the measurement one. The current is derived SR multiplied by AM1.5G standard spectrum.

3.2. *Measurement of I– V characteristics*

Shown in Fig. 7 are the experimental I V characteristics illuminated with white LED light, the calculated and the measured I V curves under AM1.5G spectrum. I V

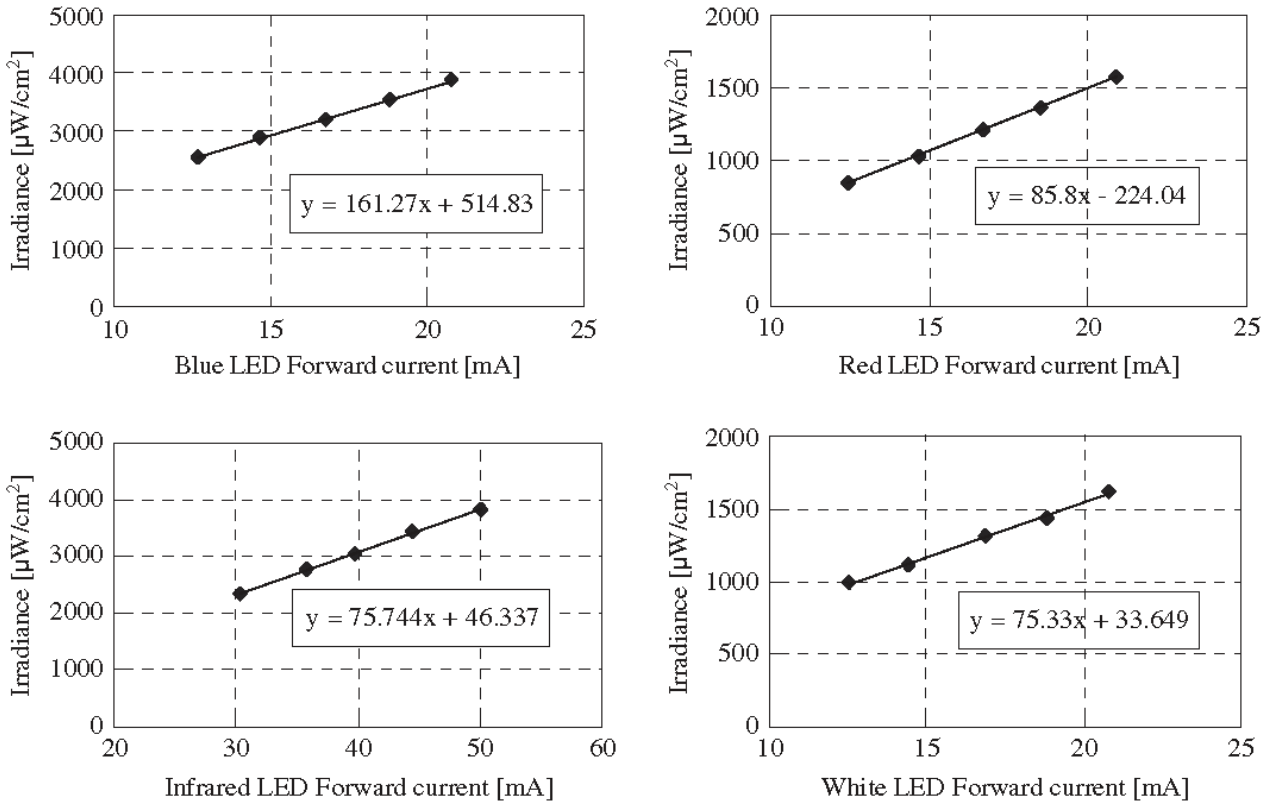

Fig. 5. Relations between each LED forward current (I_F) and irradiance.

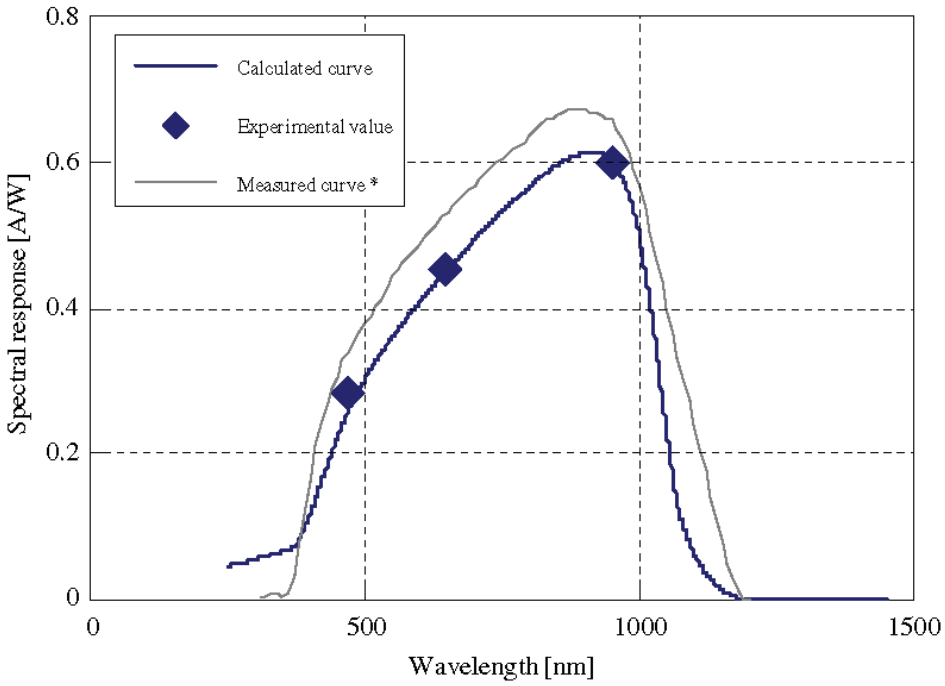

Fig. 6. Comparison of calculated and measured SR curve (* measured by AIST).

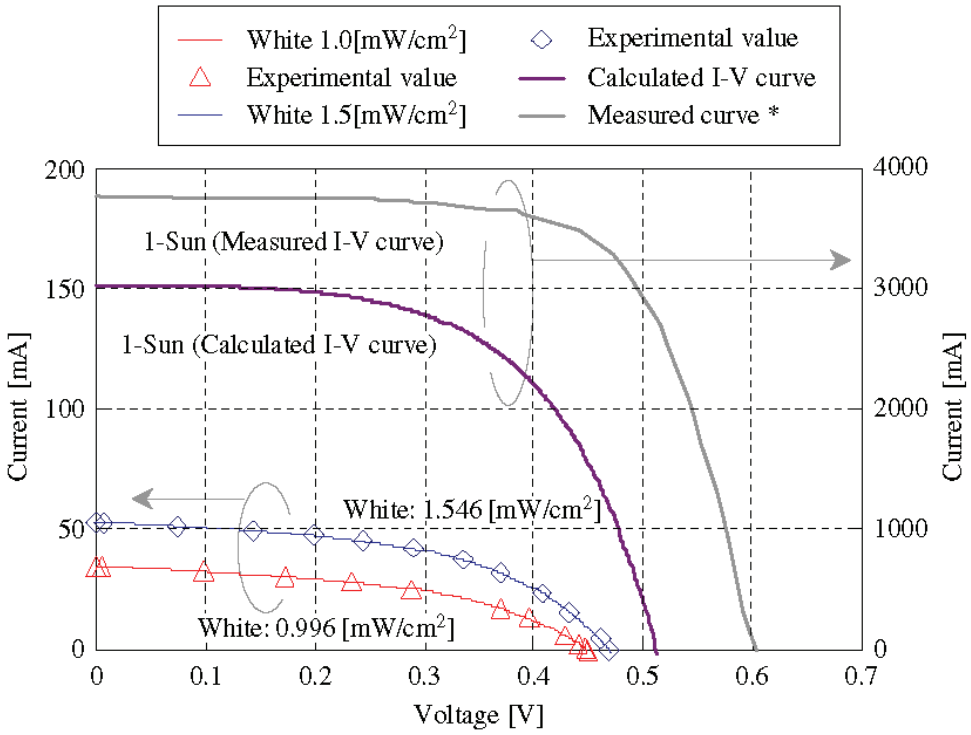

Fig. 7. Comparison of the results of calculated and measured I–V curve under 1-Sun (* measured by AIST).

Table 2
Measured and calculated value

	Calculated value	Measured value
V_{oc} (V)	0.51	0.60
I_{sc} (A)	3.02	3.76
V_{max} (V)	0.37	0.46
I_{max} (A)	2.47	3.37
F.F. (%)	58.59	68.50

characteristic under STC can be calculated from

$$V_2 = V_1 (= V_3),$$

$$I_2 = I_1 + (E_2 - E_1)\frac{I_3 - I_1}{E_3 - E_1},$$

where E_1, V_1, I_1 and E_3, V_3, I_3 are the irradiance, voltage, and current of the experimentally known I_{out} (V), respectively. E_2, V_2 and I_2 are those of the unknown I_{out} (V) [3]. The calculated and measured value is compared in Table 2, the former has smaller curve than the latter. The difference is caused by the errors including each irradiance under experiment, because the compensation widens these errors by over 10 times. Therefore, the accurate measurement of LED irradiance before the cell characterization is important. Any way, I V characteristics can be estimated roughly by correction.

4. Conclusion

In the present work, the four color LED (including three monochromatic) solar simulator is used for as light source and the measuring method of solar cells has been demonstrated by it. Assuming that SR and I–V characteristics of mono-crystalline Si solar cell do not depend on light intensity and wavelength, a test cell is measured. As a result, the estimated value is lower than the nominal one and examining the dependence will be required in the future. Nevertheless, it is notable that the low intensity light like LED can estimate the I–V characteristics under AM1.5G spectrum.

Acknowledgements

The authors would like to thank Y. Hishikawa of AIST for many helpful discussions.

References

[1] H.J. Hovel, Semiconductors and Semi-metals, vol.11, Academic Press, New York, 1975, pp. 8–37.
[2] S. Kohraku, K. Kurokawa, New methods for solar cells measurement by LED solar simulator, WCPEC-third, 2003.
[3] Y. Hishikawa, Y. Imura, T. Oshiro, Jpn. J. Appl. Phys. Part 2 39-7A (2000) L6.

IEEE TRANSACTIONS ON INDUSTRIAL ELECTRONICS, VOL. 53, NO. 6, DECEMBER 2006

A Novel Microcontroller for Grid-Connected Photovoltaic Systems

Hirotaka Koizumi, *Member, IEEE*, Tamaki Mizuno, Takashi Kaito, Yukihisa Noda, Norio Goshima, Manabu Kawasaki, Ken Nagasaka, and Kosuke Kurokawa, *Member, IEEE*

***Abstract*—The purpose of this paper is to develop a novel microcontroller for grid-connected photovoltaic (PV) systems. As a prototype model, a 100-W-class module-integrated converter composed of the proposed controller and a flyback inverter has been built and tested. The prototype model is designed to satisfy the Japanese grid-connection guideline. Basic functions as those of a grid-connected PV inverter, such as the maximum-power-point tracking and the anti-islanding protection, have been confirmed in the experiments using a distribution network simulator located in a laboratory. This paper presents the description of the controller and the experimental results. A microcontroller has been developed with a 50-MHz-class microcomputer and simple interfaces. By revising the program, the proposed controller can be applied to various types of PV systems or grid-connected equipment.**

***Index Terms*—AC module, anti-islanding, grid connection, grid-connected photovoltaic (PV) inverters, islanding detection, maximum power point tracking (MPPT).**

I. Introduction

ROOF-MOUNTED systems, which are the most popular photovoltaic (PV) systems for residential use, are exponentially increasing in recent years. When these roof-mounted systems are connected to the utility grid system, the grid-connected PV inverter needs to satisfy the standards for interconnection. Roof-mounted systems are classified into two types: one has a central PV inverter for interconnection, and the solar panels are connected with dc wirings. The other one, which is called the "ac module" has a small PV inverter behind each panel, which is individually interconnected with ac wiring. In the case of the central PV inverter, wires from PV modules are connected together in series and/or parallel. However, it is known that the partially shaded modules perform as resistance components. They reduce the total output power from the series/parallel-connected modules [1]–[3]. The same phenomenon is caused when several PV modules have different $I-V$ characteristics by means of the difference of irradiation or temperature. Residential areas usually bristle with buildings and plants, which often cast their shadow on the roof-mounted PV arrays. Furthermore, as roofs are in various shapes and sizes, therefore the generated power from each PV module is different by location. The ac module has an advantage in these issues. It can track and output the maximum power by each PV module [4]. It never performs as a resistance component against the other modules.

To develop a new ac module that is suitable for the Japanese grid-connection guideline [5], the "Regional Consortium Research and Development Program" was carried out. Our working group WG-2 took charge of the controller part. In the process of the development, system configurations composed of some ac modules, and the requirements for the controller in each configuration were discussed. A conventional ac module has all the functions of a power conditioner; however, in a roof-mounted system, several functions can be collectable in a master controller. As a variation, those functions can be set in a concentrated interconnection unit in or by the circuit breaker (CB). Consequently, the proposed controller is designed as an all-in-one system. The controller remains independent, and the interfaces are simplified to be adaptable to an ac module with various types of inverters designed for grid connection, a CB as an interconnection unit, and a master controller. The proposed controller is composed of a 50-MHz-class microcomputer and simple interfaces. A prototype of the module-integrated converter (MIC) for the ac module, which is composed of the proposed controller and a flyback inverter built by another working group WG-3, has been built and tested. Basic functions as those of a MIC including maximum power point tracking (MPPT) and islanding protection have been confirmed. Islanding tests with a distribution network simulator have been carried out. The MIC shows excellent performance in islanding protection. These functions are adaptable not only for an ac module controller but also for a master controller or for the equipment for interconnection. Furthermore, by changing the programs, it can be adjusted to any type of guideline for interconnection.

II. Basic Model

A model of an MIC with the proposed controller is shown in Fig. 1, except the master controller. The MIC locates between the PV module and the utility grid. The input is a direct

Manuscript received September 7, 2004; revised June 26, 2006. Abstract published on the Internet September 15, 2006. This work was supported in part by the New Energy and Industrial Technology Development Organization (NEDO) of Japan from FY2000 to FY2001 under the "Regional Consortium R&D Program" and in part by the Ministry of Economy, Trade, and Industry (METI) of Japan in FY2002.

H. Koizumi, K. Nagasaka, and K. Kurokawa are with the Tokyo University of Agriculture and Technology, Tokyo 184-8588, Japan (e-mail: koizumih@cc.tuat.ac.jp; bahman@cc.tuat.ac.jp; kurochan@cc.tuat.ac.jp).

T. Mizuno was with Tokyo University of Agriculture and Technology, Tokyo 184-8588, Japan. He is currently with Nippon Oil Corporation, Tokyo 105-8412, Japan.

T. Kaito and Y. Noda were with the Tokyo University of Agriculture and Technology, Tokyo 184-8588, Japan. They are currently with East Japan Railway Company, Tokyo 151-8578, Japan.

N. Goshima was with YEM Inc., Atsugi 243-0021, Japan.

M. Kawasaki is with YEM Inc., Atsugi 243-0021, Japan.

Digital Object Identifier 10.1109/TIE.2006.885526

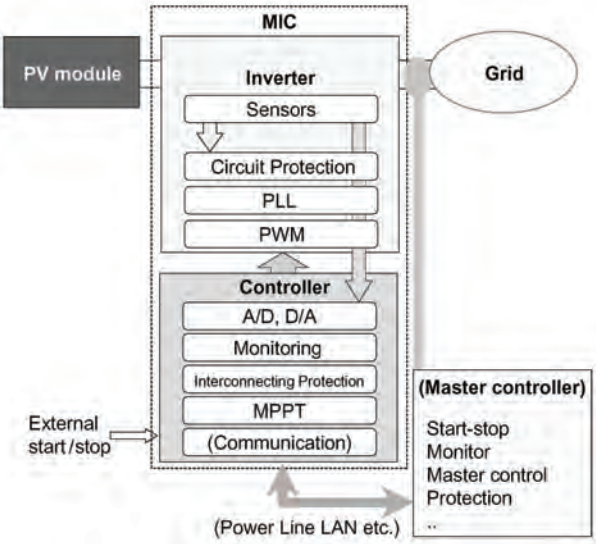

Fig. 1. System model with the proposed controller.

current from the PV module, and the output is an alternating current to the single-phase two-wire grid system. The MIC is composed of two boards. The inverter board has basic functions as those of a dc/ac converter, i.e., phase-locked loop, pulsewidth modulation (PWM), and circuit protection. The inverter has a flyback topology, which is built by another working group WG-3. The switching frequency of the main switch is 100 kHz. The input capacitor is 6600 μF. The output filter inductor and capacitor of the inverter are 470 μH, and 0.94 μF, respectively. The equivalent circuit is equal to [6, Fig. 4], which is introduced as a fundamental flyback inverter. The details including the circuit description and the principle of operation are described in [6]. Sensors are equipped on the same board. The measured voltages and currents are used in the inverter and sent to the controller through isolation amplifiers, which reduce the switching noise from the inverter board. The controller board has functions to control the MIC as a grid-connected PV system. Based on the measured data, the controller monitors the condition of the inverter and the grid, and orders the start/stop or the value of the output current. The functions of interconnecting protection and MPPT are also included in the program.

A. *Controller Board*

Fig. 2 shows the second-version controller board [7], which consists of a microcomputer, chip selecting (CS) PLD, I/O ports, A/D and D/A converters, memory PLDs, communication ports, and power supplies for ICs. Eight copies of the board were made and used in various tests. The latest board has been reduced to 150 mm × 210 mm with a four-layer board, which is still larger than common 100-W-class MICs in the market. For further reduction in size, the parallel I/O ports can be replaced by a serial one, and the space for the emulator probe adapter around the CPU and communication functions can be eliminated.

The relationship between the feature items shown in Fig. 2 is depicted in Fig. 3 as a block diagram. The controller board has

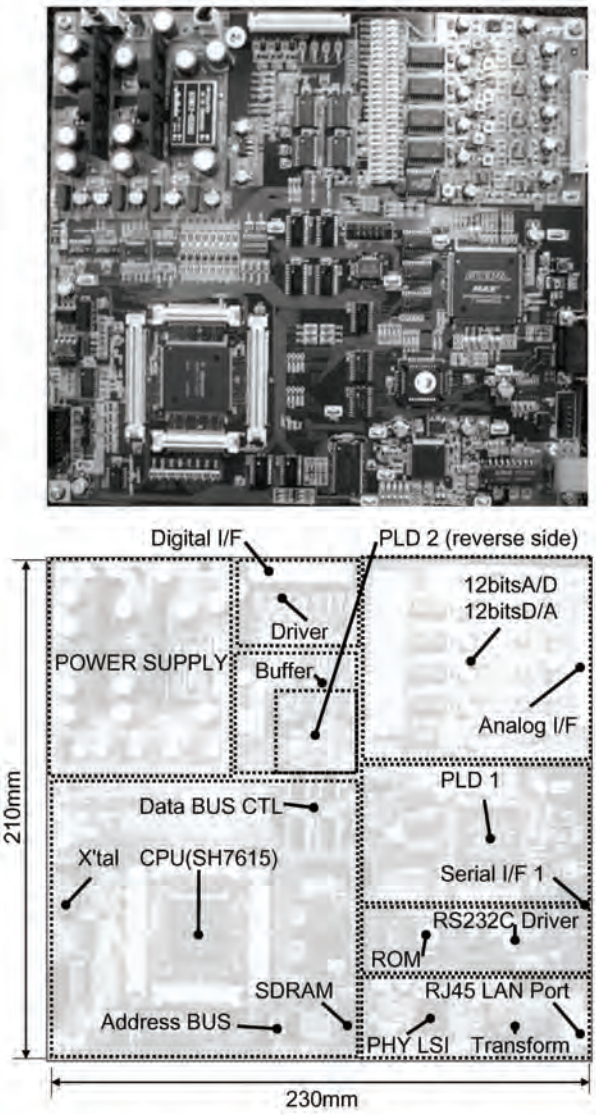

Fig. 2. Controller board and its layout.

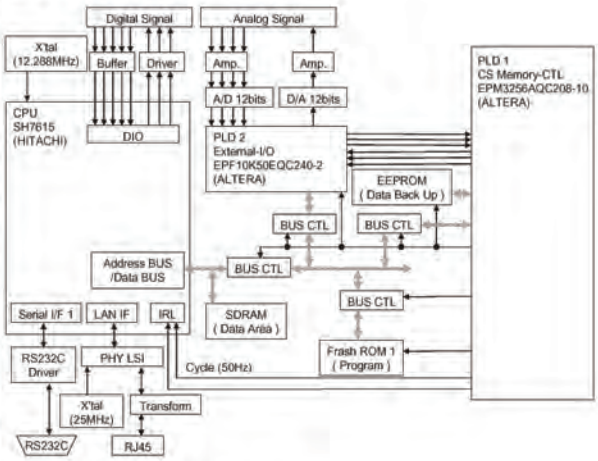

Fig. 3. Block diagram of the controller.

four input and one output analog ports and five input and three output digital ports. Analog signals of the measured voltages and currents are sent through the analog input ports. The output-current level is indicated through the analog output port. Two of the five digital input ports are used at the present stage. One conveys the controller whether the inverter is operating or not. The other one conveys the condition of the inverter board, i.e., if it can start or not. The remaining three can be used for indication of emergency stop or internal fault, etc. A digital output port is used to send a start/stop signal. Another port sends a standby command, which makes the inverter board ready to start. The rest is for turning on and off the interconnection CB, which is not used at the present stage. The measured voltage and current waveforms sent through the analog ports are changed into digital data and stored into the memory PLDs. The controller has two buffers. Assuming that the grid frequency range is between 47.5 and 52.5 Hz, the internal cycle clock of the controller is set at 34.4 Hz. Each buffer stores the data for one and a half cycle. The two buffers alternately starts by the internal clock; therefore, some part of the waveform data is stored into both buffers. Owing to this overlap, the monitoring is uninterrupted. It is stored in each buffer with at least one whole cycle of the grid-voltage waveform. In a series of data, there should be three zero-cross points. Each waveform is quantized in 256 levels and encoded into an 8-bit binary code with a sampling clock of 18.8 kHz. The zero-cross points are estimated with linear approximation. The grid frequency, its harmonics, the rms values of ac, and the average values of dc are calculated with the CPU (SH7615 HITACHI [8]).

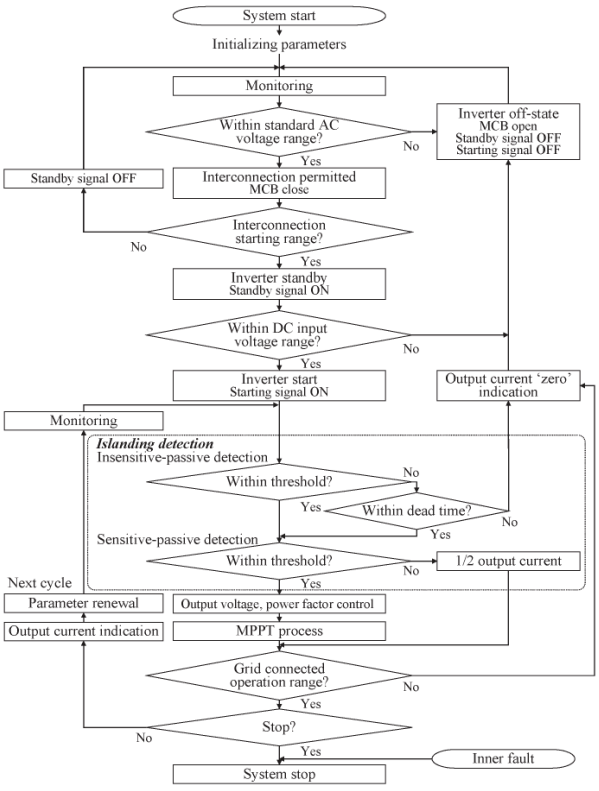

Fig. 4. Flowchart.

B. Fundamental Flow

A fundamental operating flow is shown in Fig. 4. The MIC starts with the starting command. During the operation, the controller continues monitoring the system condition from the data of input and output voltages and currents. When the grid voltage, which is equal to the output voltage, is within the standard ac voltage range (from 95 to 107 V, which was decided by the Japanese Electric Utility Law), the controller sends a memory control block (MCB)-close command. To avoid the repetition of the MCB being turned on and off, the starting condition range is narrower than the others. Second, the grid frequency, the grid voltage, and its third harmonic component are checked. The ranges of the frequency and the third harmonic component are based on the draft specification of the inverter for the ac module on [5, Appendix I, p. 178]. The range of the voltage is decided, taking into consideration the voltage range from 80 to 115 V shown in the same draft. Here, the grid frequency and the third harmonic component are checked before interconnection. The grid voltage is checked again, which is a backup function of the starting one. When these three conditions are satisfied, the inverter moves to the standby position. Then, the condition of the PV module is checked. If the open-circuit voltage of the module is in the dc input voltage range (from 7 to 50 V), the controller sends a starting command to the inverter board and starts it up. The dc voltage range is decided by the specification of the inverter board; therefore, an appropriate PV module has to be chosen. The input and output voltages and currents, the grid frequency, and the third harmonic component of the grid voltage waveform are calculated based on the stored data. During the grid-connected operation, the controller always monitors the grid condition.

The islanding detection and protection function is based on a combination method, which is proposed as the active–passive series method [9]. The islanding function used in the proposed controller has the following advantages [10], [11].

- As an active detection function, the output-current reduction method is used, which prevents the interference between grid-connected PV inverters.
- The output-current reduction is achieved in the same process as the MPPT function.
- The dead time after the insensitive–passive detection prevents the false detection and the stop by the instantaneous voltage drop.
- The function is written as a program; therefore, the parameter values are easily adjusted.

At the first step, a remarkable change is detected with the insensitive–passive detection algorithm. The insensitive–passive detection range is matched with the "interconnection starting range." The grid frequency, the grid voltage, and its third harmonic component are checked. If one of them is out of the proper range shown in Table I, the dead-time counter starts. Taking the instantaneous voltage drop into consideration, the dead time is set to 400 ms [11]. The lower limit of the grid voltage 90 V is also based on the data of the instantaneous

TABLE I
THRESHOLDS AND OPERATION RANGES

Items	Starting condition	Interconnection starting range	Standby condition	Insensitive-passive detection	Sensitive-passive detection	Grid connected operation range
Grid voltage [Vrms]	95-107	90-110	-	90-110	-	80-115
Grid frequency [Hz]	-	48.5-51.0	-	48.5-51.0	-	-
3rd harmonic component [%]	-	3	-	3	-	-
Ratio of grid-frequency change [%]	-	-	-	-	0.1	-
Ratio of 3rd harmonic component change [%]	-	-	-	-	0.5	-
DC input voltage [V]	-	-	7-50	-	-	7-50

voltage drop. Within the dead time, the grid condition is also checked by the sensitive–passive detection algorithm. This function observes the ratio of the grid-frequency change and that of the third harmonic component change. If one parameter exceeds the threshold, it reduces the value of the output-current indication to half of the present value. If the system is in islanding phenomenon, the current reduction amplifies the fluctuation by each cycle. In this case, the remarkable change should be repeatedly detected by the insensitive–passive detection function until the end of the dead time. When it goes over the dead time, the controller puts the inverter into OFF-state. This function operates as an active detection function required in the guideline [5]. Small deviation with possibility of islanding, which is not detected by the insensitive–passive detection function, is also detected with the sensitive–passive detection algorithm. Its thresholds are based on the simulation and the experiments [11], [12]. Table I shows all the thresholds and the operation ranges used in the controller.

The MPPT function is based on the algorithm that consists of the incremental conductance method (IncCond) and constant voltage (CV) method [13]. A flowchart is shown in Fig. 5. In the program, the present operating position on the $I-V$ curve is found with the dc input voltage and current values by each cycle using their average values. Comparing to the present value and the last one, a target value is calculated, following the IncCond method and with it given as a dc target voltage. The output current is controlled to make the input dc voltage close to the objective. When the monitored dc voltage comes close to the aim (within 0.05 V) or when it never comes within the range for a while, the program renews the data and calculates the next target voltage. When it is difficult to keep the maximum power point by means of rapid changing of irradiation or when the monitored input voltage is less than 15 V, the algorithm is changed to the CV method [14]. In this mode, after waiting 25 cycles, the target voltage is kept to 85% of the open-circuit voltage V_{OC} from 10 to 20 s [14].

Before going to the next cycle, the dc input voltage is checked because there is no other check process in the operation loop. The grid voltage is also checked with a wider range from 80 to 115 V, which is shown in the draft specification [5]. If one of them is out of the range, the inverter immediately puts into the OFF-state. Owing to the thresholds, in case of a serious fault, the MIC can stop without waiting for the end of the dead

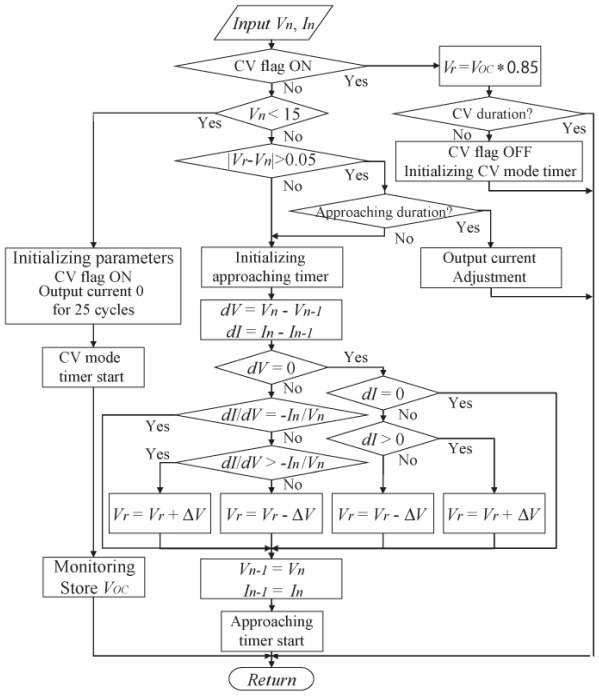

Fig. 5. Flowchart of the MPPT process.

time. The system stops if trouble is found in the controller or the inverter, or if stopping command is given.

Several functions can be integrated into one common unit in a group of ac modules via communication system. They are shown in a block of the master controller in Fig. 1. These functions are also installed into each controller board at the present stage.

III. DISCUSSION ON TOTAL SYSTEM

As a group system, several models composed of some ac modules are expected. As shown in Fig. 1, some functions installed into the controller board are able to be separated and set in a master controller, which is shared in one group. Fig. 6 shows three models of the total system. The Japanese grid-connection guideline requires an interconnection CB between

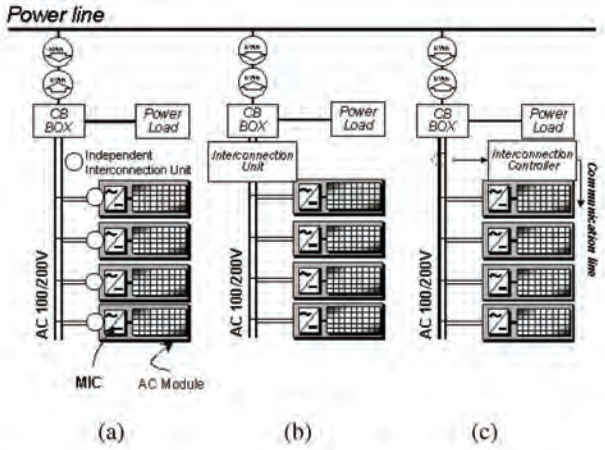

Fig. 6. Total system configurations. (a) Independent interconnection. (b) Concentrated interconnection. (c) Monitoring interconnection.

the generation systems and the grid system including the inner wires. Therefore, the CB box is drawn in all three models. As shown in Fig. 6(a), a conventional ac module has all the functions of a power conditioner. From a small system composed of a few modules to larger one, this type is equally adopted. However, in a roof-mounted system, several functions can be collectable in an extra controller, as shown in Fig. 1, e.g., start/stop, monitoring, islanding protection, and system protection. A system configuration shown in Fig. 6(b) has a concentrated interconnection unit in or by the CB. If the communication is available between the concentrated interconnection unit and ac modules, the functions can be divided among them, e.g., monitoring, detecting, and communicating are set in the unit, and operating, protecting, and communicating are in each module. This model is shown in Fig. 6(c). Considering the MPPT function, if a high-speed communication system with high reliability is available for a low price, it could be realized as a cost advantage; however, we agreed that the MPPT function should not be shared in the present. The proposed controller is built as an all-in-one system; therefore, it is adaptable to an ac module, a CB as an interconnection unit, and a master controller.

IV. Experimental Results

A. Basic Operation

The proposed controller has been tested. The experiments were carried out with a MIC composed of a second-version controller and a flyback inverter [6], as shown in Fig. 7. The output ports are connected to a reduced-scale distribution network simulator [15], and the input ports are connected to a Solar cell array simulator (Kernel) composed of a PWM-controlled current source with 160-kHz switching frequency and a 125-kHz PWM-controlled shunt regulator, which forms an $I-V$ characteristic under the given condition using DSP [16].

At first, the basic operation following the algorithm was tested. The gain of the isolation amplifiers was adjusted. Fig. 8 shows the observed waveforms in an interconnecting test. The

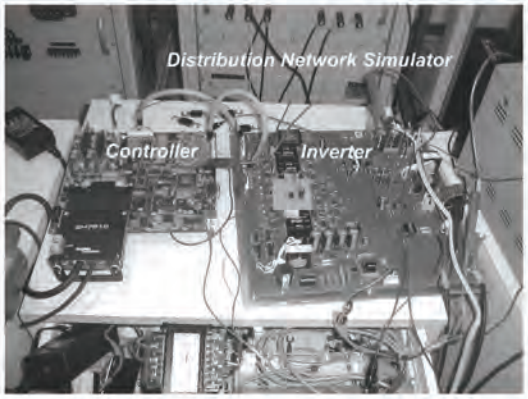

Fig. 7. Proposed system composed of the second-version controller and a flyback inverter.

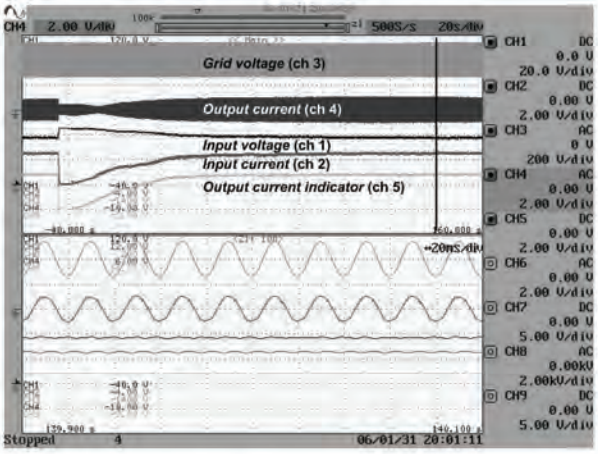

Fig. 8. Observed waveforms in an interconnecting test with the MIC. Horizontal: 20 s/div (upper) and 20 ms/div (bottom). Vertical: grid voltage (channel 3, 200 V/div), output current (channel 4, 2 A/div), input voltage (channel 1, 20 V/div), input current (channel 2, 2 A/div), and output current indicator (channel 5, 2 V/div).

waveforms were measured with the digital LPF function (the threshold is 1 kHz) of the digital scope DL716 (YOKOGAWA). During this time, the Solar cell array simulator was set and fixed at a condition of a fill factor of 0.7 with maximum output power of 95 W. The MPPT operation was observed in the waveforms. The control parameter arises to the maximum power and tracks the point. The MPPT function could keep the operation against rapid 10-W decrease and increase of the irradiation parameter. The MPPT operation tests were repeated and tuned under many $I-V$ curves with various fill factors ranging from 0.4 to 0.85 [14].

B. Islanding Tests

Before the islanding tests of the MIC with the proposed controller, two types of conventional 100-W-class inverters (inverter X and Y) were examined with the reduced-scale distribution network simulator. This method is not for strict tests following some standards. A configuration of the test system is

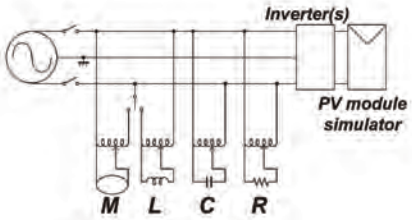

Fig. 9. Test system.

shown in Fig. 9. The islanding detection functions were tested under the following conditions.

1) The system is loaded with a parallel load composed of resistance R, capacitance C, and inductance L (RCL) or induction motor M (RCM).
2) Active power and reactive power are changed around the balancing point between the inverter output power and the load network.
3) The PV module simulator performs as a PV module under the fixed irradiance and temperature.
4) Grid fault is simulated by turning off the CB between the load network and the ac power source.
5) The test is started in steady state.
6) In each condition, the same tests are carried out five times.
7) Islanding phenomena, which are more than 5 s, are forced to stop.

Both inverters X and Y contain an anti-islanding system that observes the grid voltage and frequency. These functions are not enough to detect islanding in Japanese guideline. It requires that all types of inverters, including the ac module, equip a complete islanding protection. They should provide both passive and active methods. First, the islanding detection function was tested with a single inverter. Fig. 10 shows the observed maximum islanding time and the observed average islanding time about an inverter X under the conditions of RCM and RCL loads, respectively. The direction of the power flow from the ac power source to the load is defined as positive. The islanding point at which the islanding phenomenon is observed is expressed as a coordinate (unbalanced ratio of active and reactive power). Islanding phenomena (over 1 s) were caused at the balancing point (0, 0) every time. The test range was extended around the point; however, no islanding points were found. Then, the same tests were applied to an inverter Y. In case of the RCM load, the islanding phenomena were observed at (0, −10) and (10, −10). In case of the RCL load, they were observed when the unbalanced ratio of reactive power was −10% and that of active power was from −10% to +10%, as shown in Fig. 11. These results show that the inverters X and Y have islanding occurrence conditions near the balancing point. At least, these inverters have the possibility of islanding under these test conditions with repeatability.

Then, parallel operations were tested with five X inverters. Fig. 12 shows the results of the parallel operations with the RCM and RCL load. The test ranges were extended around the points where the islanding phenomenon was observed. The islanding range was clearly spread than that of a single operation. These results show that parallel operation of five

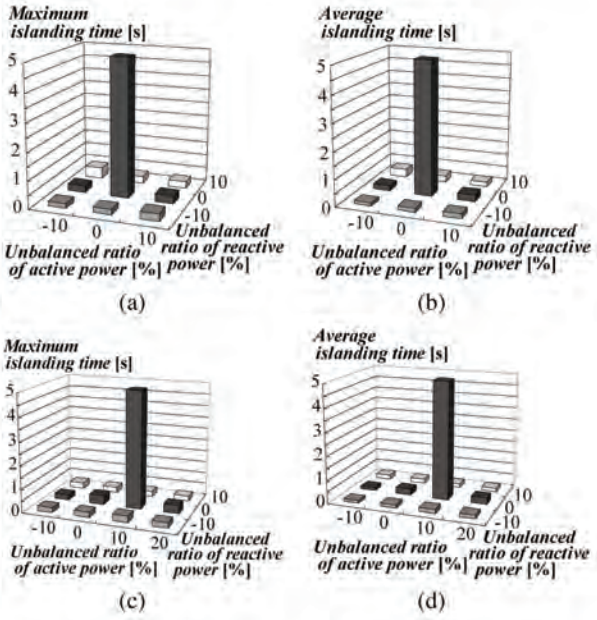

Fig. 10. Measured islanding time of an inverter X with RCM and RCL loads. (a) Maximum islanding time and (b) average islanding time with RCM load, and (c) maximum islanding time and (d) average islanding time with RCL load.

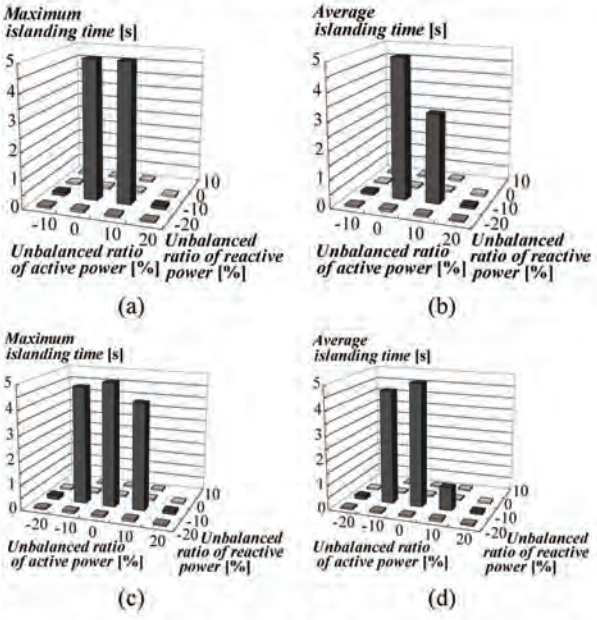

Fig. 11. Measured islanding time of an inverter Y with RCM and RCL loads. (a) Maximum islanding time and (b) average islanding time with RCM load, and (c) maximum islanding time and (d) average islanding time with RCL load.

X inverters made it easy to cause islanding comparison with the single operation. These conditions are more difficult for inverters to detect the islanding phenomenon. Therefore, they are rather suitable to test islanding detection and protection.

In order to verify the islanding detection function of the proposed controller, the single and parallel operations were tested. At first, the sensitive–passive detection function was

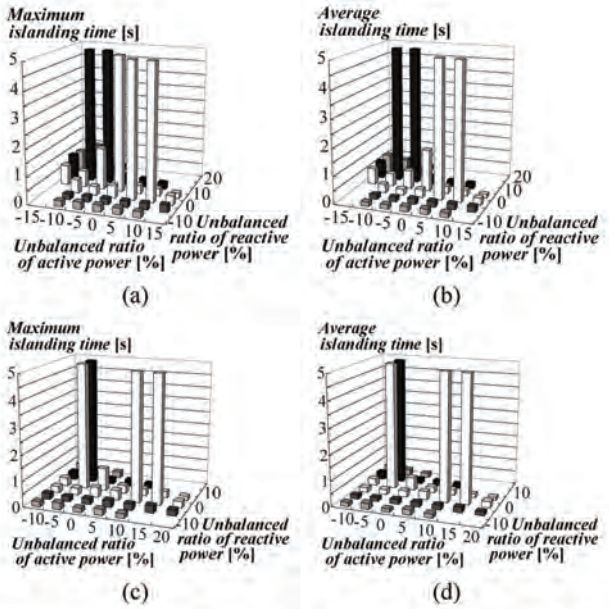

Fig. 12. Measured islanding time under the parallel operations of five X inverters with RCM and RCL loads. (a) Maximum islanding time and (b) average islanding time with RCM load, and (c) maximum islanding time and (d) average islanding time with RCL load.

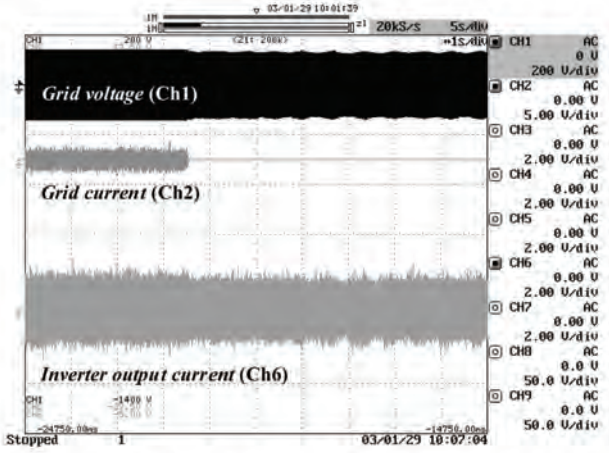

Fig. 13. Observed islanding phenomenon caused by a MIC with a proposed controller under the condition of the sensitive detection masked. Horizontal: 5 s/div. Vertical: grid voltage (channel 1, 200 V/div), grid current (channel 2, 5 A/div), and inverter output current (channel 6, 2 A/div).

masked in the program, i.e., islanding was detected only by the insensitive–passive detection function. In this test, an islanding phenomenon over 1 s was observed, as shown in Fig. 13, at the balanced load condition, which was similar to the phenomena observed at the previous tests with the conventional inverters. Then, the sensitive–passive detection function was enabled and tested. Fig. 14 shows the test results with the RCM and RCL loads. Based on the obtained results, it is confirmed that the proposed system is able to detect the islanding phenomena within 100 ms and that the threshold of each detection method is adequate to detect islanding.

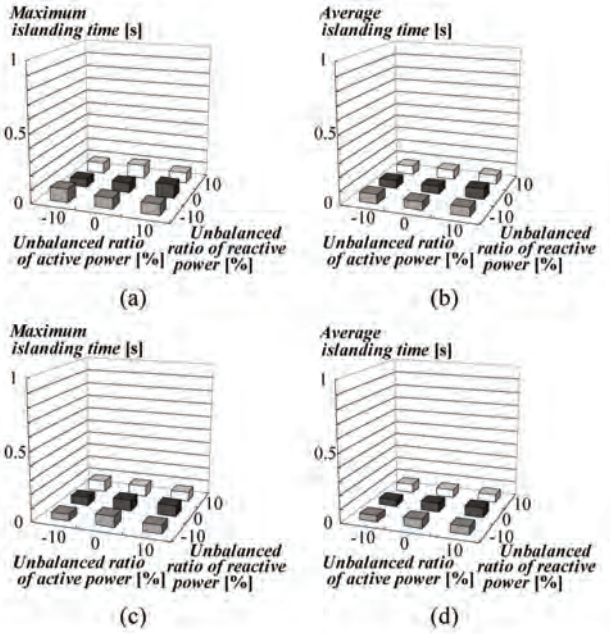

Fig. 14. Measured islanding time of a MIC with the proposed controller with RCM and RCL loads. (a) Maximum islanding time and (b) average islanding time with RCM load, and (c) maximum islanding time and (d) average islanding time with RCL load.

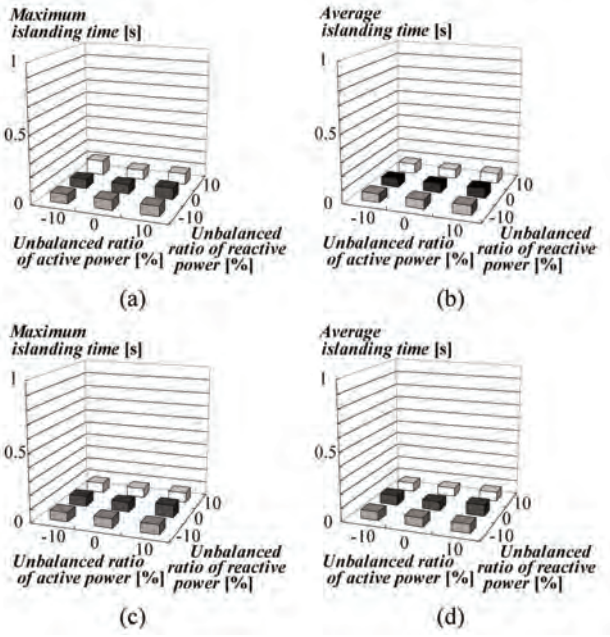

Fig. 15. Measured islanding time under the parallel operations of four MICs with the proposed controller with RCM and RCL loads. (a) Maximum islanding time and (b) average islanding time with RCM load, and (c) maximum islanding time and (d) average islanding time with RCL load.

To test them under more severe conditions, the same four inverters with the proposed controller were connected in parallel. Fig. 15 shows the islanding test results of the parallel operations. In these tests, no islanding phenomena over 1 s were

observed. All the islanding phenomena were detected within 100 ms. These results conclude that the proposed controller is able to detect islanding phenomena, which are difficult to be found by conventional 100-W-class inverters. There are still some rooms for future study, for instance, islanding tests under some strict conditions following some standards [17], and how to deal with the situation when several types of ac modules are connected to the same wire.

V. Conclusion

A novel microcontroller for Japanese PV systems has been developed with a 50-MHz-class microcomputer and simple interfaces. Prototype models for the ac module have been built and tested. Basic functions as those of a MIC including MPPT and islanding protection have been confirmed with the prototype models. Islanding tests with a distribution network simulator have been carried out. The proposed system shows excellent performance in islanding protection. Total system configuration and application of the controller have been discussed. The proposed controller is adaptable not only for a PV inverter but also for a master controller or independent equipment for grid connection. These applications and the development of control methods as a group system of ac modules are subjects in the future study.

Acknowledgment

The authors would like to thank Assoc. Prof. T. Shimizu of Tokyo Metropolitan University, Assist. Prof. K. Wada of Tokyo Institute of Technology, and K. Yasui of Niwa Electric Company, Ltd., for their helpful supports and advice on the inverter board. They would also like to thank T. Nakahira of Nippon Kernel System Company, Ltd., for his informative support on the Solar cell array simulator.

References

[1] C. Gonzalez and R. Weaver, "Circuit design considerations for photovoltaic modules and systems," in *Proc. 14th IEEE Photovoltaic Spec. Conf.*, Jan. 1980, pp. 528–535.

[2] N. F. Shepard, Jr. and R. S. Sugimura, "The integration of bypass diode with terrestrial photovoltaic modules and arrays," in *Proc. 17th IEEE Photovoltaic Spec. Conf.*, 1984, pp. 676–679.

[3] N. D. Kaushika and N. K. Gautam, "Energy yield simulations of interconnected solar PV arrays," *IEEE Trans. Energy Convers.*, vol. 18, no. 1, pp. 127–134, Mar. 2003.

[4] H. Oldenkamp and I. J. de Jong, "AC modules: Past, present and future," presented at the Installing the Solar Solution, Hatfield, UK, 1998. [Online]. Available: http://www.nkf.nl/electronics/photovoltaics/papers/files/ISS1998-AC%20modules.pdf

[5] Agency of natural resources and energy, *Guideline to Regulate Utility-Connection Technology*, 1998, Denryoku shinpo-sha. (in Japanese).

[6] T. Shimizu, K. Wada, and N. Nakamura, "A flyback-type single phase utility interactive inverter with low-frequency ripple current reduction on the dc input for an ac photovoltaic module system," in *Proc. IEEE 33rd Annu. Power Electron. Spec. Conf.*, Jun. 2002, vol. 3, pp. 1483–1488.

[7] H. Koizumi, K. Nagasaka, K. Kurokawa, N. Goshima, M. Kawasaki, Y. Yamashita, and A. Hashimoto, "Development of interconnecting micro controller for PV systems in Japan," in *Proc. PV Eur. PV Technol. Energy Solutions Conf. and Exhib.*, Rome, Italy, Oct. 2002, pp. 683–686.

[8] *Hitachi Releases SH-DSP Series RISC Microcomputer with On-Chip 10/100 Mbps Ethernet Controller*, Dec. 6, 1999. News release. [Online]. Available: http://global.hitachi.com/New/cnews/E/1999/991206B.html

[9] H. Kobayashi, K. Takigawa, and E. Hashimoto, "Method for preventing islanding phenomenon on utility grid with a number of small scale PV systems," in *Proc. 22nd IEEE Photovoltaic Spec. Conf.*, Oct. 1991, pp. 695–700.

[10] T. Mizuno, T. Ishikawa, Y. Noda, H. Koizumi, K. Kurokawa, Y. Arai, N. Goshima, M. Kawasaki, and H. Kobayashi, "The islanding detection algorithm of a new ac module for the grid connection in Japan," in *Proc. PV Eur. PV Technol. Energy Solutions Conf. and Exhib.*, Rome, Italy, Oct. 2002, pp. 703–706.

[11] T. Mizuno, "A study on islanding detection method for advanced ac module," M.S. thesis, Tokyo Univ. Agriculture Technol., Tokyo, Japan, Mar. 2004. (in Japanese).

[12] T. Mizuno, Y. Noda, H. Koizumi, and K. Kurokawa, "Interference of islanding detecting factor in commercial PV inverters," in *Proc. 13th Annu. Conf. Power and Energy Soc. IEE-J*, Aug. 2002, vol. A, pp. 597–598. No.191, (in Japanese).

[13] T. Kaito, H. Koizumi, N. Goshima, M. Kawasaki, and K. Kurokawa, "Development of MPPT algorithm for a digital controlled PV inverter," in *Proc. Tech. Dig. 14th Int. PVSEC-14*, Bangkok, Thailand, Jan. 2004, pp. 901–902.

[14] T. Kaito, "A study on digital MPPT function for PV inverters," M.S. thesis, Tokyo Univ. Agriculture Technol., Tokyo, Japan, Mar. 2004. (in Japanese).

[15] Y. Noda, T. Mizuno, H. Koizumi, K. Nagasaka, and K. Kurokawa, "The development of a scaled-down simulator for distribution grids and its application for verifying interference behavior among a number of module integrated converters (MIC)," in *Proc. 29th IEEE Photovoltaic Spec. Conf.*, May 2002, pp. 1545–1548.

[16] Nippon Kernel System Co., Ltd., *Product Catalog of Solar Cell Array Simulator*, Jan. 2006. (in Japanese and English). [Online]. Available: http://www.kernel-sys.co.jp/cell-h.pdf

[17] A. Woyte, R. Belmans, S. Member, and J. Nijs, "Testing the islanding protection function of photovoltaic inverters," *IEEE Trans. Energy Convers.*, vol. 18, no. 1, pp. 157–162, Mar. 2003.

Hirotaka Koizumi (S'99–M'01) was born in Tokyo, Japan, in 1970. He received the B.E, M.E., and Ph.D. degrees in electrical engineering from Keio University, Yokohama, Japan, in 1993, 1995, and 2001, respectively.

From 1995 to 2001, he was an Electrical Engineer with Tokyo Electric Power Company Inc., Tokyo, Japan. From 1998 to 2001, he was with the Graduate School of Keio University. Since 2001, he has been a Research Associate with the Department of Electrical and Electronic Engineering, Faculty of Technology, Tokyo University of Agriculture and Technology. His research interests include high-frequency high-efficiency tuned power amplifiers, resonant dc/dc power converters, dc/ac inverters, and high-frequency rectifiers, especially Class D, Class E, and Class DE circuits.

Dr. Koizumi is a member of the Institute of Electronics, Information and Communication Engineers of Japan.

Tamaki Mizuno was born in Shizuoka, Japan, in 1978. He received B.E. and M.E. degrees from Tokyo University of Agriculture and Technology, Tokyo, Japan, in 2002 and 2004, respectively.

He is currently with Nippon Oil Corporation, Tokyo. His research interests include islanding detection methods for ac module inverters.

Takashi Kaito was born in Ibaraki, Japan, in 1979. He received the B.E. and M.E. degrees in electrical engineering from Tokyo University of Agriculture and Technology, Tokyo, Japan, in 2002 and 2004, respectively.

He is currently with East Japan Railway Company, Tokyo. His research interests include the development of maximum-power-point-tracking function for photovoltaic inverters.

Yukihisa Noda was born in Kyoto, Japan, in 1979. He received the B.E. and M.E. degrees from Tokyo University of Agriculture and Technology, Tokyo, Japan, in 2001 and 2003, respectively.

He is currently with East Japan Railway Company, Tokyo. His research interests include studied islanding phenomena caused by dispersed generators, mainly photovoltaic systems, on distribution systems and development of grid simulators.

Norio Goshima was born in Japan in 1967. He graduated from Sogodenshi Computer College, Kanagawa, Japan.

From 1988 to 2005, he was a Development Engineer with YEM Inc., Atsugi, Japan. His research interests include research and development of HDTV peripheral equipment.

Manabu Kawasaki was born in Japan in 1957. He received the B.E. degree from Tamagawa University, Tokyo, Japan.

From 1980 to 1997, he was a Development Engineer with Kuwano Electrical Instruments Company, Ltd. Since 1998, he has been a Development Engineer with YEM Inc., Tokyo. His research interests include research and development of HDTV peripheral equipment.

Ken Nagasaka was born in Kermanshah, Iran, in 1956. He received the B.S. degree from Nihon University, Tokyo, Japan, in 1985, and the M.S. and Ph.D. degrees from Tokyo Metropolitan University, Tokyo, in 1987 and 1990, respectively, all in electrical engineering.

From 1990 to 1991, he was a Chief Researcher with Computer Software Development Company, Tokyo. From 1991 to 1994, he was a Visiting Professor at the University of Manitoba, Winnipeg, MB, Canada. From 1994 to 1998, he was a Scientist with the Central Research Institute of Electric Power Industry (CRIEPI), Tokyo. From 1995 to 1998, he was an Associate Professor with the Department of Electrical Engineering, Tokyo Metropolitan University. He is currently an Associate Professor with the Graduate School of Engineering, Tokyo University of Agriculture and Technology, Tokyo. He has published more than 150 scientific papers. His current research interests concern environmental energy engineering, particularly power system analysis, wind power, load forecasting, and application of intelligent systems to power systems.

Prof. Nagasaka is a member of the Institution of Electrical Engineers, U.K., the Institute of Electrical Installation Engineers of Japan, and the International Neural Network Society of the USA. He received a Paper Prize from the IEIE of Japan in 1991 for one of his papers and an award from the Ministry of Energy in 2002 for his contribution to the International Power System Conference (PSC-2002).

Kosuke Kurokawa (M'04) received the B.E. degree and the Doctorate Degree of Engineering from Waseda University, Tokyo, Japan, in 1965 and 1993, respectively.

He joined the Electrotechnical Laboratory (ETL), Ministry of International Trade and Industry (MITI) in 1965, where he was engaged in research on energy systems technology for 30 years. From 1971 to 1972, he studied at the Polytechnic of Central London (now the University of Westminster), London, U.K. He also has working experiences at MITI and the New Energy Development Organization under the solar energy R&D program. Since 1996, he has been a Professor with the Department of Electrical and Electronic Engineering, Faculty of Technology, Tokyo University of Agriculture and Technology, Tokyo. He was the Project Leader for IEC61863 in IEC TC82/WG3 and has been the Operating Agent of Task VIII in the photovoltaic system R&D program of the International Energy Agency since 1998. His current research interests include solar energy, photovoltaic systems engineering, and energy systems.

Prof. Kurokawa is a member of the International Solar Energy Society, the Institute of Electrical Engineers of Japan, and the Japan Solar Energy Society. He was the General Vice-Chairperson of the 2nd World Conference on Photovoltaic Solar Energy Conversion in 1998 and the General Chairperson of the 3rd World Conference in May 2003.

論　文

系統連系型太陽光発電システム運転特性の高度解析と蓄電池導入効果の検証

学生員 植田　譲*　正　員 黒川　浩助*
正　員 伊藤　孝充**　正　員 北村　清之**
非会員 赤沼　克己***　非会員 横田　昌治***
正　員 杉原　裕征***　正　員 森本　篤史****

Advanced Analysis of Grid-connected PV System's Performance and Effect of Battery

Yuzuru Ueda*, Student Member, Kosuke Kurokawa*, Member, Takamitsu Itou**, Member,
Kiyoyuki Kitamura**, Member, Katsumi Akanuma***, Non-member, Masaharu Yokota***, Non-member,
Hiroyuki Sugihara***, Member, Atsushi Morimoto****, Member

An advanced analysis method for grid connected PV systems is developed in this research. To investigate the issues which may happen in the clustered PV systems, "Demonstrative research on clustered PV systems" is being conducted from December, 2002, in Oota, Japan. More than 500 residential PV systems will be installed in the demonstrative research area, battery integrated PV systems are developed to avoid the restriction of output power due to the raising of grid voltage. Annual performance of commercial PV systems without battery is analyzed and resulted in around 80% of performance ratio on the average. Over voltage of power distribution line and snow are two major factors of very low performance ratio on daily basis. Effects of batteries are also analyzed, the results indicate that there will be some improvement for the energy loss due to the grid voltage but PCS's efficiency will be around 8% worse than that of the commercial PV systems. It is also found that the non-optimized operation of battery sometimes results in the fully-charged situation during the noontime and maximum reverse power flow may not be minimized in this situation.

キーワード：太陽光発電システム，評価，蓄電池，出力抑制，電圧上昇
Keywords: photovoltaic system, evaluation, battery, output restriction, over voltage

1. はじめに

地球温暖化と世界的な気候変動が懸念される中，温室効果ガス排出量の削減に向け再生可能エネルギーへの期待と需要はますます高まってきている。中でも，太陽光発電（PV）はその発電過程で一切の排出ガスを発生しない事，入力エネルギーである太陽からの日射量が膨大である事などから，環境持続性を持った次世代エネルギーシステムの根幹を担うべき電源の一つとして期待されている。しかし，日本国内において順調な普及が進む住宅用 PV システムにおいては，今後，既存配電系統の末端部分への数百件規模での局所的な集中連系が行われる事が予想され，このような場合 PV システムからの余剰電力の逆潮流による配電系統の電圧上昇が個別連系されたシステムよりも多く発生してしまうことが懸念される。配電系統の過度な電圧上昇を防止するため，現在日本において市販されている PV システム用パワーコンディショナ（PCS）には配電系統の電圧上昇を防ぐための出力抑制機能が搭載されているが，この機能は系統の電圧上昇時には十分な日射がある場合においても発電量を抑制してしまうため，PV システムのシステム効率

* 東京農工大学
〒184-8588　小金井市中町 2-24-16
Tokyo University of Agriculture and Technology
2-24-16, Naka-cho, Koganei 184-8588
** (株) 明電舎
〒103-8515　東京都中央区日本橋箱崎町 36-2 リバーサイドビル
Meidensha Corporation
Riverside Building, 36-2, Nihonbashi Hakozakicho, Chuo-Ku, Tokyo 103-8515
*** (株) 関電工
〒108-8533　東京都港区芝浦 4-8-33
Kandenko Co., Ltd.
4-8-33, Shibaura Minato-ku, Tokyo 108-8533
**** 松下エコシステムズ (株)
〒486-8522　春日井市鷹来町字下仲田 4017 番
Matsushita Ecology Systems Co., Ltd.
4017, Shimonakata, Takaki-cho, Kasugai 486-8522

を低下させる可能性のある事が確認されている[1]。

この出力抑制を回避する技術の一つとして蓄電池付きPVシステムがあげられる。平成14年度から行われている独立行政法人新エネルギー・産業技術総合開発機構による「集中連系型太陽光発電システム実証研究」は，この蓄電池付きPVシステムを出力抑制回避技術の一例として用いる事により，実証実験サイトに数百台規模で集中的に連系されたPVシステムの運転特性の評価及び出力抑制回避技術の効果等を検証するなど，汎用的な対策技術を開発し，その有効性を一般的な実配電系統において実証すると共に，PVシステムの集中連系に関する応用シミュレーション手法を開発することを目的としている[2]。本論文では，この実証研究から得られたデータを用いて，PVシステムの運転特性と蓄電池導入効果を発電電力量の面から解析する事を目的としている。

2. 蓄電池付き太陽光発電システム

〈2・1〉 蓄電池付き太陽光発電システム概要 「集中連系型太陽光発電システム実証研究」では，出力抑制回避技術として蓄電池付きPVシステムを開発し，その有効性や課題に対する実証研究を行っている。実際の配電系統に連系されたPVシステムに取付ける蓄電池には鉛蓄電池を用い，1システムあたりの設置容量は49[Ah]の蓄電池96セル（6セル×16個）直列接続を基本としている[2]。チャージコントローラはPVシステム用PCSとの組み合わせにより一体型と別置型を開発した。一体型はPVシステム用PCSの機能とチャージコントローラの機能の両方を備えたPCSであり，別置型は市販PVシステムのPCS出力側に接続されるチャージコントローラとなる。

〈2・2〉 一体型PCS概要 今回の解析では，蓄電池付きシステムとして，2005年1月から本格的な設置が始まった一体型PCSの結果を用いた。一体型PCSはFig. 1に示すようにアレイからのDC出力昇圧用D/Dコンバータ，チャージコントローラ用D/Dコンバータ，及びインバータで構成される。電力系統からの蓄電池充電は行わず，蓄電池から系統への逆潮流を防止するため，放電は受電点に150[W]以上の順潮流がある時のみ家庭内負荷に供給する形で行っている。蓄電池の充放電制御は逆潮流抑制運転[3]に設定した。この制御方式では，PVシステムからの発電電力を優先的に家庭内負荷に供給し，余剰電力は蓄電池へと充電される。系統への逆潮流は日中に蓄電池が満充電になった場合や，蓄電池充電電流制御範囲を超えて発電量がある場合にのみ行われる。蓄電池の放電は，PVシステムの発電電力が無い夜間に，家庭内負荷に対して行われる。

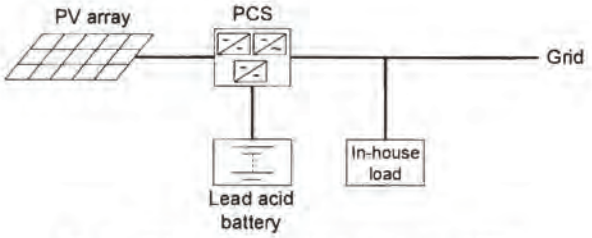

Fig. 1. Schematic view of battery-integrated PCS.

3. 損失要因と分離手法

〈3・1〉 システム運転特性評価指標と損失の定義 PVシステムの性能評価指標として，本研究ではシステム出力係数を用いている。システム出力係数とは，等価日システム運転時間を等価日太陽日照時間で除した値として定義され，[%]で表わしている。これは，ある評価期間内に太陽電池アレイ面に入射した日射量を基準とし，全ての日射量が基準太陽光で供給されたとして，PVシステムが常に定格状態で運転した場合に得られると考えられる発電量に対して，実際に発電された電力量の割合を示す値である。損失に関しても発電量と同様に，日射量から算出される理想的な出力電力量に対して，発電できなかった電力量の割合を損失要因毎に定量化した。解析に使用したデータは1秒周期で計測されたデータの1分平均値であり，個々の1分値の計測された時刻におけるアレイ面日射強度から期待される発電電力を算出し，実際の発電電力と比較する事により，システム出力係数と損失割合を求めた。解析期間は30日を基本としており，これは，解析期間中にある程度の快晴日，種々の損失が極小である状態のデータが必要だからである。なお，個々の1分値に対してその時の日射強度から期待される出力電力は，厳密には日射強度だけでなく分光放射照度分布も考慮する必要があるが，本研究では分光放射照度分布を計測していないため，太陽電池モジュールの分光感度特性に対して入射光の分光放射照度分布のずれが及ぼす影響に関しては，その他の損失，またはゲインとして扱っている。

〈3・2〉 定量化した損失要因と定義 筆者らは先の論文[1]にて，日陰の影響を受けない太陽光発電システムに対して，以下に示す要因により発生する発電電力の損失を分離，定量化する手法を開発し，出力抑制機能動作時の現象把握と，損失量の定量化を行った結果を報告した。

- PCSオフ状態による損失
- PCS容量不足による損失
- 出力抑制機能による損失
- アレイ温度上昇による損失
- 変動による損失
- PCSでの損失
- 定格ばらつき，汚れ，劣化等

本稿では，これらの損失要因に加え，以下の項目を新たに分離可能とし，解析を行った。

- 入射角による損失
- 直流回路抵抗による損失
- 日陰による損失
- MPPミスマッチ高電圧側による損失
- 蓄電池システムによる損失

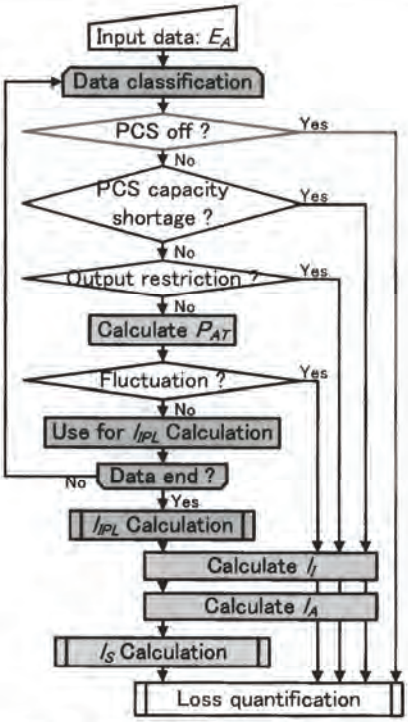

Fig. 2. Flow chart of data classification.

既に報告済みの損失要因の定義に関しては，本節に簡単な説明と式のみを示すが，本稿において新しく分離可能とした損失量算出時の表記に統一性を持たせるため，記号と呼称に若干の変更を加えている。

また，本節で説明する，計測データの損失要因毎の特徴を用いた分類の流れを Fig. 2 にフローチャートとして示した。本手法では，以下に示す(2)から(6)までの方法により各計測データを分類した後，どの条件にも当てはまらなかった，損失が極小と思われるデータのみを用いて(7)にて定格ばらつき，汚れ，劣化等の損失量を算出した後，〈3·3〉～〈3·5〉節において説明する手法で入射角による損失，直流回路抵抗による損失，日陰損失を算出している。

（1） アレイ標準出力電力量　太陽電池アレイ面に入射している日射（量）が基準太陽光であったとして，PV システムが常に定格状態で運転した場合に得られると考えられる発電電力（量）。

$$E_{AS} = P_{ACap} \cdot \frac{H_{Ag}}{G_S} \quad \cdots\cdots (1)$$

$$P_{AS} = P_{ACap} \cdot \frac{G_{Ag}}{G_S} \quad \cdots\cdots (2)$$

ここで，

E_{AS}：アレイ標準出力電力量 [kWh]
P_{AS}：アレイ標準出力電力 [kW]
P_{ACap}：定格アレイ容量 [kW]
H_{Ag}：アレイ面日射量 [kWh/m^2]
G_{Ag}：アレイ面日射強度 [kW/m^2]
G_S：標準試験条件での日射強度 = 1 [kW/m^2]，分光放射照度分布 = 基準太陽光

（2） PCS-OFF の判定　日射があるにもかかわらず PCS が停止状態にある場合を以下の式で判定する。メンテナンス目的での停止も含む。

$$ACIa_{PCS1} < 0.1\,[\mathrm{A}] \text{ or } ACIa_{PCS2} < 0.1\,[\mathrm{A}] \quad \cdots\cdots (3)$$

ここで，

$ACIa_{PCS1}$：交流電流実効値 PCS1 相 [A]
$ACIa_{PCS2}$：交流電流実効値 PCS2 相 [A]

（3） PCS 容量不足状態の判定

$$P_{AS} > P_{PCS} \times C_{PCS} \text{ and } P_A > P_{PCS} \quad \cdots\cdots (4)$$

ここで，

P_A：アレイ出力電力 [kW]
P_{PCS}：PCS 定格出力 [kW]
C_{PCS}：PCS 定格出力に対する入力許容電力の比

（4） 出力抑制機能動作有無の判定　アレイ出力電圧を縦軸（Y）に，アレイ温度を横軸（X）にとった散布図上の直線 (5) 式，及び，アレイ出力電流を縦軸（Y）に，アレイ面日射強度を横軸（X）にとった散布図上の直線 (6) 式を用い，出力電圧が最大出力動作電圧よりも開放電圧側にあり，かつ，出力電流が最大出力動作電流よりも少ない状態で，PCS 出力端電圧が 107 [V] を超えているデータを出力抑制状態にあるデータとして分類する。なお，以下に示す式に含まれる定数のうち，(5) 式中の電圧を判定する閾値に用いる C_V には 1 を（定数による補正無し），(6) 式中の傾きを決める定数 C_{loss} には 0.95 を，幅を決める定数 C_{range} にはそれぞれのアレイの定格出力電流の 5%を用いた。これらの値はアレイ出力電圧とアレイ温度の関係やアレイ出力電流とアレイ面日射強度の関係が，温度測定誤差やアレイストリング構成などの影響により理論的な値とは完全には一致しない場合に生じる誤差を補正するために導入した値である。厳密には個々のシステムに対して設定すべきであるが，今回の解析では，全てのシステムの解析結果から，最も精度良く抑制状態を判定可能であった値としてこれらの定数の値を決定した。

$$Y = V_{P\max} \times N_{series} \times C_V + \beta_{P\max} \times N_{series} \times (X - 25) \quad \cdots\cdots (5)$$

ここで，

Y：アレイ出力電圧 [V]
X：アレイ温度 [°C]
V_{Pmax}：モジュールの最大出力動作電圧 [V]
N_{serie}：直列接続されたモジュール数
β_{Pmax}：モジュール最大出力動作電圧の温度補正係数 [V/°C]
C_V：定数

$$Y = I_{P\max} \times N_{parallel} \times C_{loss} \times X \pm C_{range} \quad \cdots\cdots (6)$$

ここで，

Y：アレイ出力電流 [A]

X：アレイ面日射強度 [kW/m^2]

I_{Pmax}：モジュール最大出力動作電流 [A]

$N_{parallel}$：並列接続されたモジュール数

C_{loss}：定数

C_{range}：最大出力動作電流の幅を決める定数 [A]

なお，一体型 PCS に関しては研究目的にて出力抑制機能動作フラグが取得できるため，この情報を用いることにより更に確実な判定が可能である。

（5） アレイ出力温度補正

$$P_{AT} = \frac{P_A}{1 + (\alpha_{P_{max}} \cdot (T_C - 25))} \quad \cdots\cdots (7)$$

ここで，

P_{AT}：標準試験条件に温度補正後のアレイ出力電力 [kW]

α_{Pmax}：モジュール最大出力温度係数 [1/°C]

T_C：モジュール温度 [°C]

（6） 変動状態の判定　日射計測場所と PV システムアレイ面に若干の距離がある事から生じる計測誤差と，わずかではあるが，日射，または負荷急変動時の MPPT ずれが発生している可能性のあるデータを以下の基準にて分類する。

- 毎分のアレイ出力の変動量がアレイ容量の 3% [kW] 以上
- 毎分の全天日射強度の変動量が 0.03 [kW/m^2] 以上

さらに，変動状態であっても損失が無い事も考えられるため，(6) 式を用い，アレイ出力電流が最大出力動作電流の軌跡の範囲外にある時のみ，変動状態と分類し，出力が範囲内の場合には，変動損失は無いものとした。

（7） 定格ばらつき，汚れ，劣化等の損失量の算出　（2）から（6）の手順で，様々な損失が存在すると考えられる計測データを除外した後，以下の手順で Ideal performance line の作成を行い，得られた傾きから評価期間中常に一定の割合で存在した損失量として l_{IPL} を得る。

1. 各種損失が極小なデータの抽出
2. 抽出したデータを標準試験条件（25°C）に温度補正した後，入射角特性の影響を除外（〈3·3〉節参照）
3. アレイ面日射強度 0.4 [kW/m^2] 以上のデータのみ抽出
4. 抽出データを，縦軸アレイ出力電力，横軸アレイ面日射強度で散布図にプロット
5. 原点を通り，プロットした全データの上位 3% を通るように直線を引く

$$l_{IPL} = \sum (P_{AS} - P_{IPL}) = E_{AS} - E_{IPL} \quad \cdots\cdots (8)$$

ここで，

l_{IPL}：定格ばらつき，汚れ，劣化損失 [kWh]

E_{IPL}：Ideal performance line 上の出力電力量 [kWh]

P_{IPL}：Ideal performance line 上の出力電力 [kW]

〈3·3〉 入射角による損失の算出方法　入力エネルギーである日射強度は日射計で計測しており，使用している日射計の入射角特性は 3%以下である。一方，太陽電池モジュールはモジュール表面が平面であるため，入射角依存性により入射光の一部はモジュール表面のカバーガラス等で反射してしまいモジュール内太陽電池セルの発電層にまで到達しない[4]。本手法では，太陽電池モジュールのカバーガラスからセルに至るまでの各層の屈折率を実効屈折率という一つの屈折率の値で表わし，幾何光学的手法を用いて反射により失われる日射強度を算出し，発電電力の損失を定量化した[5]。そのモデル式を以下に示す。今，Fig. 3 のように異なる屈折率 n_1，n_2 を持った二つの媒質の境界を通過する光の屈折角 θ_2 は Snell の法則より，入射角 θ_1 を用いて以下のように表される。

$$n_1 \cdot \sin\theta_1 = n_2 \cdot \sin\theta_2 \quad \cdots\cdots (9)$$

また，この時の反射率 r は入射光強度 I_i と反射光強度 I_r の比となり，

$$r = \frac{I_r}{I_i} = \frac{1}{2}(r_\perp + r_\parallel) \quad \cdots\cdots (10)$$

ここで，

$$r_\perp = \frac{\sin^2(\theta_2 - \theta_1)}{\sin^2(\theta_2 + \theta_1)} \quad \cdots\cdots (11)$$

$$r_\parallel = \frac{\tan^2(\theta_2 - \theta_1)}{\tan^2(\theta_2 + \theta_1)} \quad \cdots\cdots (12)$$

太陽電池モジュールに入射する光の場合，n_1 は空気の屈折率であるため約 1 となり，n_2 は実験より求めた値[5] として 1.80 を用いた。アレイ面に入射する直達成分，散乱成分，反射成分のそれぞれに対して反射率を算出し，最終的に得られた全成分に対する反射率 r_{All} から，次式を用いて透過率 τ_{All} を得る。

$$\tau_{All} = 1 - r_{All} \quad \cdots\cdots (13)$$

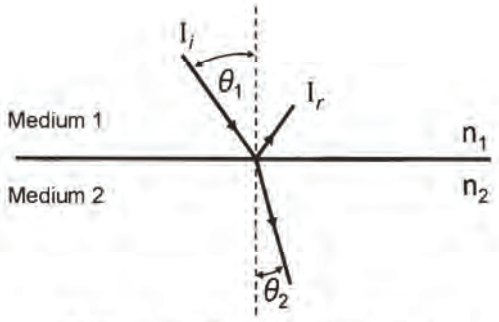

Fig. 3. Angle of incidence and refraction.

この値を定格出力測定時の透過率（入射角 = 0 度と仮定）で割ることにより，入射光の反射による損失係数 K_I を算出する。K_I を用いて入射角損失 l_I は以下のようになる。

$$l_I = (1 - K_I) \cdot E_{IPL} \quad \cdots\cdots (14)$$

ここで，
l_I：入射角による損失 [kWh]

〈3·4〉 直流回路抵抗による損失の算出方法 太陽電池アレイの各ストリング間に接続されるブロッキングダイオードの順方向電圧降下と，アレイから接続箱までの配線抵抗等により，直流電圧降下による損失が生じる。文献(7)を参考にこの損失 l_A を表わすモデル式として，以下の式を用いた。

$$l_A = \sum (0.6 \times DCI + 0.2 \times DCI^2) \times \frac{1}{1000} \quad \cdots\cdots (15)$$

ここで，
l_A：直流回路抵抗による損失 [kWh]
DCI：アレイ出力電流 [A]

この式は直流出力電流に対する 1 次項として（ブロッキングダイオードによる電圧降下分）0.6 [V]，2 次項としてケーブルの抵抗値 0.2 [Ω] を用いて直流回路抵抗による損失を算出している。なお，ケーブルの抵抗値は一般的な直流配線に用いられている CV ケーブル（2 mm^2）の抵抗値（9.24 [Ω/km]）を参考にし，ケーブル長は実証研究地域に設置された PV システムの最頻値として約 20 [m] を用いた。

〈3·5〉 日陰損失の算出方法 日陰の影響に関しては，移動する雲やその他非定常的な日陰は考慮せず，屋根の形状による自己陰，近隣の建築物や樹木による陰など，評価期間中に定常的に PV アレイ面にかかる日陰の影響のみを考慮する事とし，PV システムから見た天空を太陽の方位角，高度角に対して 5 度刻みでメッシュ状に区切り，分割した領域毎に日陰損失係数 K_S を算出した。K_S の値には，基本概念としては以下の式を用いた。

$$K_S = \frac{P_{AT}}{P_{IPL} - (1 - K_I) \cdot P_{IPL}} \quad \cdots\cdots (16)$$

これは，評価期間中の各領域での P_{AT}（標準試験条件に温度補正後のアレイ出力電力）の最大値をその時の日射強度から期待される出力電力から定格ばらつき，汚れ，劣化等の損失と入射角特性による損失を引いた値で除した値である。ただし，各領域での最大出力には，移動する雲の影響等によるエッジ効果による偶発的な強い日射を取り除くため，〈3·2〉節(6)の判定条件より変動状態にあると判断されたデータを除外した後，最大値から 2 番目と 3 番目の出力の平均値を最大出力として用いた。また，システムによっては直流回路抵抗による損失が大きい場合があるため，この場合には直流回路抵抗による損失の影響も (16) 式の分母より除外した。さらに，上記方法で各領域の日陰損失係数を算出した後，方位角 ±15 度の領域での日陰損失係数の平均値でさらに全領域の日陰損失係数を除する事とした。これは，モジュール温度計測誤差やその他誤差要因により日陰損失係数にかかる偏差が，割合としてはわずかであっても，日射量が豊富で発電量も豊富な南中時刻付近では無視できない量となってしまうからである。全 100 システム，1 年間を通じた方位角 ±15 度の領域での補正前の日陰損失係数の平均値は 0.96 程度であった。これは，補正すべき誤差が 4%程度であったことを意味する。なお，この補正方法では南中時刻付近に日陰のかかるシステムの場合には誤った補正をしてしまう事になるが，解析対象とした PV システムには，そのようなシステムは無い事を確認している。また，〈3·2〉節(7)において P_{IPL} を求める際にも日陰の影響を受けたデータを用いているが，複数の快晴日を含む，ある程度の期間（本稿では 30 日）のデータを用いて P_{IPL} を算出する場合には，その影響は軽微であると考えられる。これは，同じ太陽の位置においても大気状態等の違いにより日射強度は日々異なる値を示すからであり，ある太陽位置において日陰により受け取ることが出来なかった日射強度を，異なる太陽位置のデータが補う可能性が高い為である。本研究では，P_{IPL} の算出に用いる 0.4 [kW/m^2] 以上のアレイ面日射強度が期待できる範囲に，広範囲にわたり極端な日陰要因が存在するシステムが無いことを確認しているため，P_{IPL} の算出に日陰の影響は含まれないものとした。

補正後の最終的な日陰損失係数 K_S を用いて，日陰による損失は以下のようになる。

$$l_S = (E_{AS} - l_{IPL} - l_I - l_A) \cdot (1 - K_S) \quad \cdots\cdots (17)$$

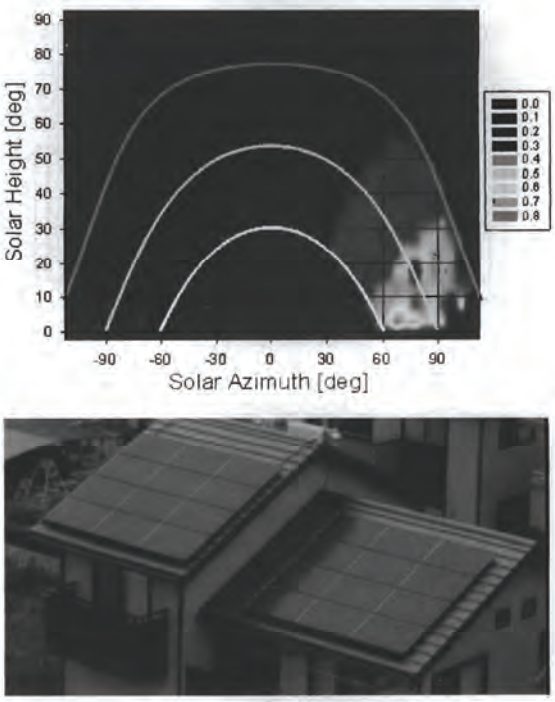

Fig. 4. Shading analysis result.

ここで，

l_S：日陰による損失 [kWh]

Fig. 4 には，本手法を用いて 2004 年 5 月から 1 年間の天空の各領域での日陰損失率（$=1-K_S$）を算出した結果の一例と，このシステムの写真を示す。グラフ中の方位は真南が 0 度，真西が +90 度であり，3 本の円弧は上からそれぞれ夏至，春分，冬至の日の太陽の軌道を表わしている。このシステムの方位角は南であり，結果から太陽が西にある時に段付き屋根による自己陰が生じ，特に太陽高度が低い冬季において大きな損失が発生している事が分る。

〈3･6〉 最大出力動作点ミスマッチ損失の取扱い 今回新たに定義した最大出力動作点（Maximum Power Point：MPP）ミスマッチ高電圧側による損失は，先の論文[1]では出力抑制機能による損失のうち系統電圧が 107 [V] 以下の時の損失として分類しており，これには PCS 内部の温度上昇による出力電流抑制などが含まれていたが，本稿では，日陰が生じているシステムや不均一なストリング構成を持つシステム等も解析対象に加えるにあたり，分類名と定義を変更した。これは，PV アレイ面の部分陰や不均一ストリング等による段付き I-V カーブの影響で動作点が開放電圧側にずれる事があるためであり（Fig. 5 参照），このような場合には出力抑制時と同様，動作点電圧は V_{Pmax} より高く，電流は I_{Pmax} より少ない状態として計測されるが，この情報だけでは PCS の出力抑制が原因なのか段付き I-V カーブが原因であるのかの判断ができないからである。アレイ出力電圧・電流から MPP ミスマッチとして判断される日陰損失に関しては，太陽の位置に依存して発生するという日陰損失の特徴を用いて〈3･5〉節で述べた手法により別途定量化が可能であるため，解析結果としては MPP ミスマッチ高電圧側による損失には含まれず日陰損失として定量化される事になるが，日陰以外の要因（不均一なストリング構成など）により生じる段付き I-V カーブ等による「出力抑制」ではない MPP ミスマッチ損失はこの損失に含まれる事になるため，名称を変更することとした。

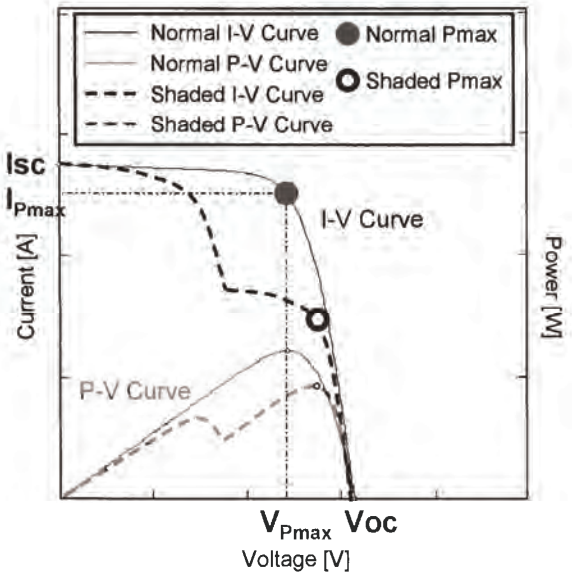

Fig. 5. Example of normal and stepped I-V curve.

一方で，動作点電圧が V_{Pmax} よりも低い側にずれる事により生じる MPP ミスマッチ損失も存在し，この時の動作点電流は I_{Pmax} よりも大きくなると考えられる。これには，日射強度が低い場合などに PCS が MPPT 制御を行わず，定電圧制御を行っている場合等が該当する。しかし，この場合の損失量が月積算発電電力量に対して占める割合を検討するため，定電圧制御を行う可能性のある日射強度を 0.1 [kW/m^2] 以下の日射強度とし，この時の発電量が全体に占める割合を算出した結果，4 [%] 程度であった。つまり，仮にそこに 1 割程度の損失が発生したとしても，その損失が全体に占める割合はわずかであると考えられ，また，このような低日射時には多くの誤差要因の影響が割合として大きくなる傾向がある事から，今回は MPP ミスマッチ低電圧側による損失はその他の損失として扱っている。

また，〈3･2〉節（6）で述べたように日射や負荷の急変動時に MPPT 制御が追いつかない事により生じる損失も考えられるが，これに関しては今まで通り，変動状態を閾値により判断した後，変動による損失として分類した。

〈3･7〉 各種損失量の定量化 以上の方法により，ある日射量における PV システムの理想的な発電電力量 E_{AS} と，すべての発電状態にあるデータに存在する「定格ばらつき，汚れ，劣化等の損失」，「入射角による損失」，「直流回路抵抗による損失」，「日陰損失」が算出された。これらの損失のうち，「入射角による損失」，「直流回路抵抗による損失」は，その損失要因に対するモデル式から個々のデータに対して直接算出したものであり，「定格ばらつき，汚れ，劣化等の損失」，「日陰損失」はそれ以外の損失が極小であると考えられるデータのみを用いて，それぞれの損失量を算出するモデルにあてはめる事により求めた値である。

これら以外の損失要因による損失量の定量化には，〈3･2〉節に示した手順にて損失要因毎に分類されたデータを用いる。本手法では以下に示す（1）から（6）の損失要因は排他的に発生すると仮定し，Fig. 6 に示した流れで定量化を行っている。各損失量の算出式を，その時の日射量から算出されるアレイ標準出力電力量 E_{AS} に対して発電量，損失量がどのように分離されたかを表わす形で要因毎に以下に示す。

（1） PCS-OFF による損失 PCS が停止状態にあると判定されたデータでは，その時の日射量から発電可能な全電力量が PCS 停止状態により失われたと考え，以下の式を用いて定量化する。

$$l_{PCO} = E_{IPL} = E_{AS} - l_{IPL} \quad \cdots\cdots\cdots\cdots\cdots\cdots (18)$$

ここで，

l_{PCO}：PCS-OFF 損失 [kWh]

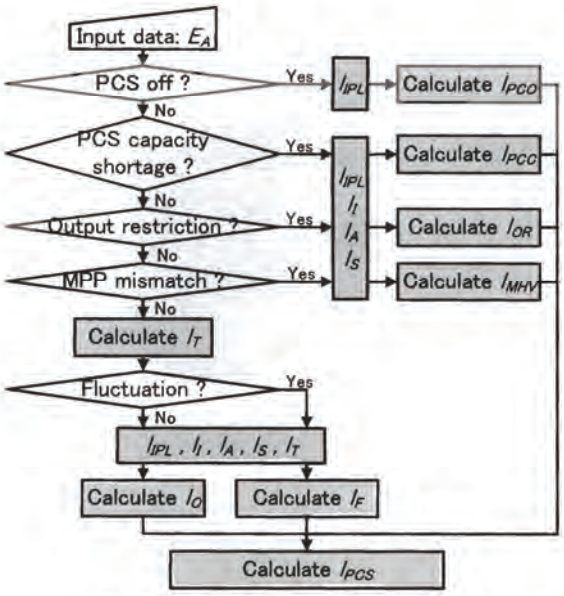

Fig. 6. Flow chart of loss quantification.

（2） PCS 容量不足による損失　P_{AS} が PCS の入力範囲を超える場合，アレイからの出力電力が制限され，損失が発生する。アレイからの出力電圧・電流のみを見た場合，現象としては MPP ミスマッチであるが，原因は PCS の容量不足にあることから分けて考えている。モジュール温度によらず出力電力により制限を受けるため，温度損失は考慮していない。なお，温度補正後の出力が PCS の入力範囲を超える場合の容量不足損失は，今回の解析目的では分離不要であったため，温度損失として取り扱っている。

$$l_{PCC} = E_{AS} - l_{IPL} - l_I - l_A - l_S - E_A \quad \cdots\cdots (19)$$

ここで，
l_{PCC}：PCS 容量不足損失 [kWh]
E_A：アレイ出力電力量 [kWh]

（3） 系統電圧上昇回避のための出力抑制による損失
PCS 出力端電圧が 107 [V] 以上であり，動作点から出力抑制状態にあると判断されたデータを用い，以下の式から損失量を算出する。L_{PCC} と同じ理由により，温度損失は考慮していない。

$$l_{OR} = E_{AS} - l_{IPL} - l_I - l_A - l_S - E_A \quad \cdots\cdots (20)$$

ここで，
l_{OR}：出力抑制損失 [kWh]

（4） MPP ミスマッチ高電圧側による損失　〈3·6〉節で述べたように厳密には出力抑制では無い場合の MPP ミスマッチ損失も含まれるが，ここでは基本的に電圧上昇回避以外の出力抑制制御として以下の式より損失量を算出する。

$$l_{MHV} = E_{AS} - l_{IPL} - l_I - l_A - l_S - E_A \quad \cdots\cdots (21)$$

ここで，l_{MHV}：MPP ミスマッチ高電圧側による損失 [kWh]

（5） 変動による損失　変動による損失は，実際には日射計測位置と PV システムの位置が離れていることによる計測誤差がほとんどである。温度損失を考慮し，以下の式によって損失量を算出する。

$$E_{AT} = \frac{E_A}{1 + (\alpha_{P_{max}} \cdot (T_C - 25))} \quad \cdots\cdots (22)$$

$$l_T = E_{AT} - E_A \quad \cdots\cdots (23)$$

$$l_F = E_{AS} - l_{IPL} - l_I - l_A - l_S - l_T - E_A \quad \cdots\cdots (24)$$

ここで，
l_T：温度損失 [kWh]
l_F：変動による損失 [kWh]
E_{AT}：標準試験条件に温度補正後のアレイ出力電力量 [kWh]

（6） その他損失　〈3·2〉節に示した方法でデータを損失要因毎に分類したとき，どの損失要因の特徴も持たなかったデータに含まれる損失をここで算出する。システムに明らかな損失要因が無い場合，ほとんどのデータはここに含まれる。

$$l_O = E_{AS} - l_{IPL} - l_I - l_A - l_S - l_T - E_A \quad \cdots\cdots (25)$$

ここで，
l_O：その他損失

（7） PCS での損失　アレイから出力された直流電力は PCS にて交流に変換される。この過程で生じる損失を以下の式で算出する。

$$l_{PCS} = E_A - E_{PCS} \quad \cdots\cdots (26)$$

ここで，
l_{PCS}：PCS での損失 [kWh]
E_{PCS}：システム出力電力量 [kWh]

〈3·8〉 システム出力係数と損失率の計算　以上の方法により求めた各値により，システム出力係数と各損失要因の損失率を求める。システム出力係数（Performance Ratio：P.R.）は

$$P.R. = E_{PCS}/E_{AS} \quad \cdots\cdots (27)$$

となり，各損失率は P.R. 同様，損失量を E_{AS} で除することにより求まる。

〈3·9〉 一体型 PCS における蓄電池充放電損失　今回から解析対象とした一体型 PCS における蓄電池充放電損失は，チャージコントローラ交流側・直流側での電力量の計測値が現時点で利用できなかったため，チャージコントローラによる損失・蓄電池の自己放電を含む充放電損失を，直交変換時の損失や PCS の消費電力と合わせて一体型 PCS による損失として扱った。PV アレイの出力は入力として

の日射があるときのみ計算しているが，一体型 PCS の交流側出力電力量は評価期間中 24 時間積算する事により求めている。これは，現在の蓄電池制御方式では系統からの充電を行っていない為，24 時間積算においても PCS からの出力は全て PV アレイ出力から得られた電力となるからである。

また，今回の解析では，評価開始・終了時刻は蓄電池の有無に関わらず 0 時としている。蓄電池の残存電力量を考慮すると，このような積算方法では，評価開始時の蓄電池の容量と充電状態が評価終了時のそれと同じでないときには，蓄電池残存電力量の差による誤差が生じる事になる。しかし，先に述べたように現時点では蓄電池の直流側入出力の計測値が利用できず，任意の時間における蓄電池の充電状態を高精度に把握することができなかったため，このような取扱いとした。ここで，評価開始・終了時刻を 0 時とした事による解析誤差について簡単にまとめる。30 日毎の平均的な等価システム運転時間を 100 時間とすると，平均的なシステム容量 4 [kW] のシステム発電電力量は 400 [kWh] となる。一方，蓄電池容量は約 9 [kWh] であり，放電深度 70%で制限をかけて利用した場合の蓄電池残存電力の最大誤差は 6.3 [kWh] となる。システム出力係数を 80%とすると，蓄電池残存容量の誤差が損失率に与える最大誤差は約 1.3%程度となる。

4. 結果および考察

〈4・1〉 PV システムの連系状況 今回の解析では，2004 年 10 月から 2005 年 9 月までの約 1 年間の計測結果を用いている。PV システムの導入数はこの期間中も順次増加しており，2005 年 9 月の時点での総連系システム数は約 300 軒，PV システム容量は 1 [MW] を超え，月間の総発電量は最大で 100 [MWh] 程度であった。柱上変圧器毎に見た場合の連系割合は最大で 100%であり，これは柱上変圧器以下の全住宅に PV システムが設置された状態を意味する。文献 (8) によれば，2030 年の日本国内の太陽光発電システム導入量 102 [GW] を実現するに辺り，PV システム設置可能な戸建住宅への普及率を約 50%と想定している。このような大量普及時代には，本実証研究地域にように，柱上変圧器以下に 100%PV システムが導入され，さらに地域一帯が同一配電線に連系される状態が多く発生すると考えられる。

〈4・2〉 市販 PV システムの出力特性 2004 年 10 月から 2005 年 9 月までの間に計測された約 1 年分のデータ用いて蓄電池を持たない市販 PV システムの運転特性を解析した。解析対象は期間中に順次系統連系された全 300 軒以上の中から，解析に必要なデータがそろっているシステムのみ 100 軒程度とし，解析の基本期間は 30 日とした。ただし，上記解析期間においては様々な要因により意図的に解列状態にあったシステムが多く，連続した約 30 日の解析期間のうちに解列状態にある日を含んでいる場合が多いため，後に示す日別の結果においては，一日の発電可能電力量のうち解列状態にあった割合が 5%以下の日のデータのみを用いている。Fig. 7 に，全システムの年間の運転特性の平均値を示した。P.R. は約 80%と良好であり，PCS による損失，温度損失，入射角損失などある程度避けられない損失以外に目立った損失は発生していない事が分る。

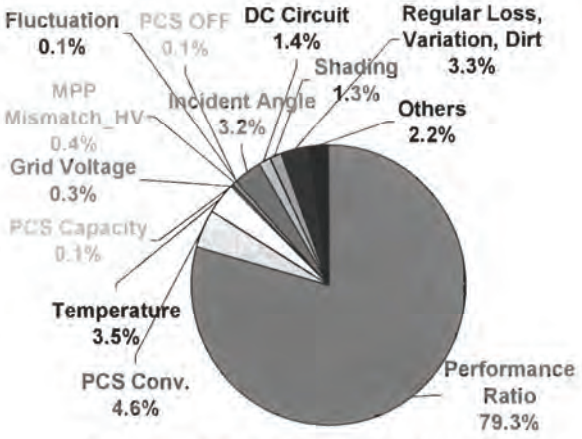

Fig. 7. Annual result of commercial PV systems.

今回の解析期間では，懸念されていた系統電圧上昇による出力抑制も，全体の結果では 0.3%と無視できる範囲に収まっている。出力抑制による損失は PCS 出力端電圧が抑制開始電圧（107 [V] 程度）以上になった場合に発生するが，PCS 出力端電圧は PV システムからの逆潮流電力や連系された線路のインピーダンス等により決まる電圧上昇幅（ΔV [V]）だけでなく，変電所からの送出電圧やタップ調整により決まる上位側の連系点電圧に強く依存する。文献 (9) では住宅地域配電線モデルケースとして，バンク容量 20 [MVA]・フィーダ数 8 回線・線路容量 2500 [kVA] を想定しており，このケースに当てはめて考えると解析期間の配電線容量に対する PV システムの連系容量は 40 [%] 程度となることから，相当量の出力抑制が予想される状態にある。実証研究から得られたデータより，逆潮流電力による電圧上昇幅はほぼ事前予想の範囲内にある[10]事から，今回の 0.3%という値は，住宅地域から見た上位側系統の電圧管理により電圧上昇が抑えられた結果であると推測される。

次に，30 日毎の評価期間中の 1 システム・1 日の結果を一つのデータ点として，月別に箱ひげ図にまとめた結果を Fig. 8 に示す。約 100 システム・30 日の結果であるため，月ごとに最大で約 3000 点のデータが存在していることになる。箱の中の実線が中央値，破線が平均値であり，箱の大きさは中央値に対して上下 25%のデータが含まれる範囲，ひげに相当する線は 90%，10%をそれぞれ示している。この範囲を超えたデータについては個別にプロットしているため，箱ひげ図により，平均値の推移だけでなく，大まかな発生頻度や最大値，最小値なども同時に示す事ができる。結果から P.R. の平均値は冬季に最大となり，夏季に向かって低下していく。これは，Fig. 8(b) に示したように，主に

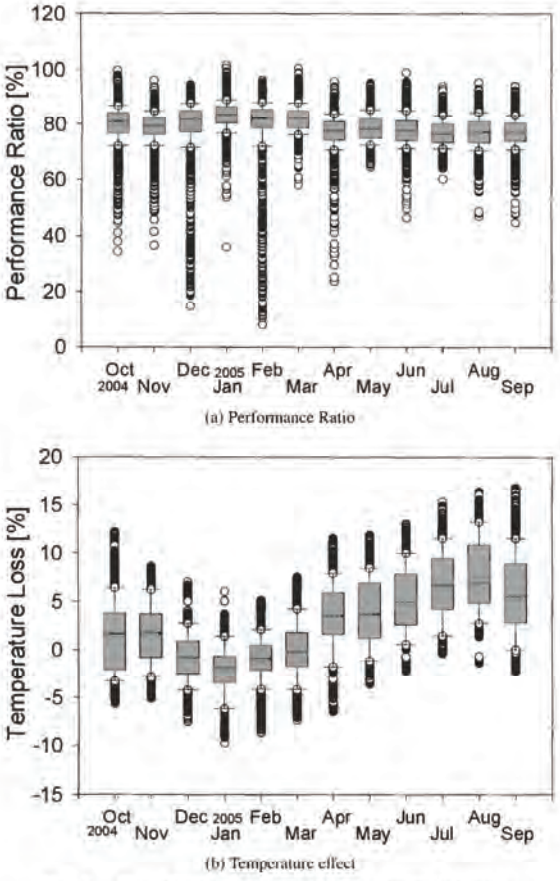

Fig. 8. Box chart of commercial PV system's results.

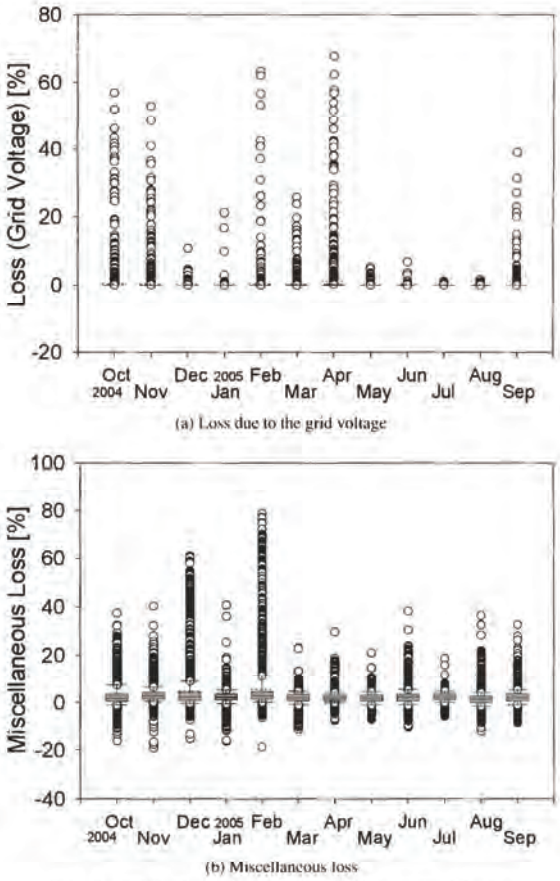

Fig. 9. Box chart of commercial PV system's Loss.

モジュール温度上昇による損失の影響であると考えられ，温度上昇による損失は冬季にはモジュール温度低下によりゲインとなっているが，夏季には 10%近い損失を記録しているシステムが多く見られる。本実証研究で使われているモジュールは Si 結晶系であり，−0.3～−0.5 [%/°C] と負の温度係数を持っている為このような結果となった。一方で P.R. が大きく低下しているデータに目を向けると，頻度は低いものの 2004 年 10 月，11 月 12 月，2005 年 2 月，4 月に 40%以下の P.R. が記録されている。解析の結果，これらの極端に低い P.R. の原因は系統電圧上昇回避のための出力抑制と積雪であった。Fig. 9(a) に電圧上昇による損失の結果を，Fig. 9(b) にその他の要因による損失の結果を示す。2004 年 10 月，11 月，2005 年 2 月，4 月に 50%を超える出力抑制による損失を記録しており，極端に低い P.R. のデータと一致している。また，2004 年 12 月，2005 年 2 月のその他の損失に極端に大きいデータがあるのは積雪の影響であり，これは，現地調査により確認済である。本研究では PV システムへの入力エネルギーである日射量を実証研究地域内 6 カ所に設置された環境計測システムにて，精密日射計を用いて計測しているが，雪の降った翌日に日射計に積もった雪が溶け日射が有りと計測されている時間帯に，多くの太陽電池モジュールは雪に覆われたままになっていることから生じた損失である。現象としては日陰損失とも考えられるが，本手法で対象とする日陰損失は評価期間中定常的にかかる日陰としているため，その他の損失として分類した。また，これら以外の要因により発生している損失に関しても，出力抑制，積雪（その他の損失）による損失同様，箱ひげ図により確認した結果，極端な P.R. の低下要因とはならず，ある程度予想可能な範囲内でのみ推移していた。以上より，系統連系型太陽光発電システムにおいては，系統電圧上昇回避のための出力抑制が，著しくシステムの発電性能を低下させる原因として最も注意すべきものであることが分る。出力抑制の発生確率は，先に述べたように PV システムが連系された配電線のインピーダンスや同一配電線に連系された負荷量等により決まる電圧上昇幅 ΔV の他，系統側の送出電圧等によって決定される連系点電圧に大きく依存するため，PV システムからの逆潮流電力量だけでは一概には判断できないが，電力品質の悪化を防ぎ，連系状態の違いによる抑制量の違いなど，設置者側の不公平感を無くすためにも，更なるデータ収集と解析を続けていく予定である。

〈4·3〉 蓄電池付き PV システムの出力特性　2005 年

2月から2005年10月までの間に計測された9ヶ月分のデータを用いて，蓄電池付きシステムの運転特性を解析した（Fig. 10参照）。対象としたシステム数は最終的に50システム程度であるが，評価期間中に順次導入されているため，2005年2月のシステム数は14，3月は36である。蓄電池充放電，インバータ部分を含めた一体型PCSの総合的な損失率は12.7%であり，蓄電池無し市販PCSの平均値である4.6%に比べて約8%余分な損失が発生した事になる（ただしこの値には〈3·9〉節で述べたように，蓄電池による損失の他，実証研究の為の制御系，計測系での消費電力も含まれている為，単純に一体型PCSの効率を表わすものではない）。温度損失が蓄電池無し市販PVシステムの年間結果に比べて高いのは，導入軒数の関係で多くのデータが夏季に取得された為であり，月別に見ると大きな差は見られなかった。また，系統電圧上昇回避のための出力抑制はほぼ0%であった。出力抑制回避効果の定量化には，蓄電池無し市販PVシステムとの連系状況の違い等を考慮し，より多くのデータを用いて解析を行う必要があるが，同時期に計測された蓄電池無し市販PVシステムでは出力抑制による損失が発生している事から，出力抑制回避に対しては

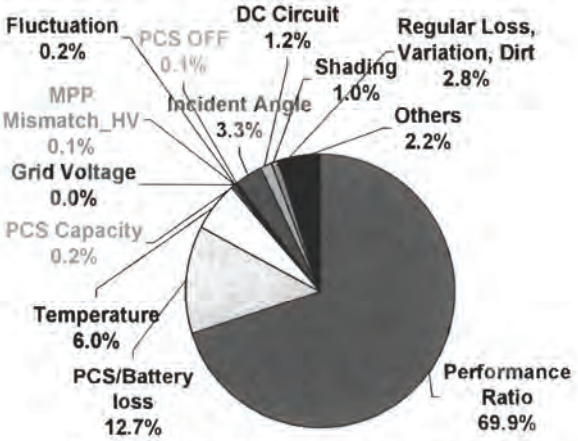

Fig. 10. Result of battery-integrated PV systems.

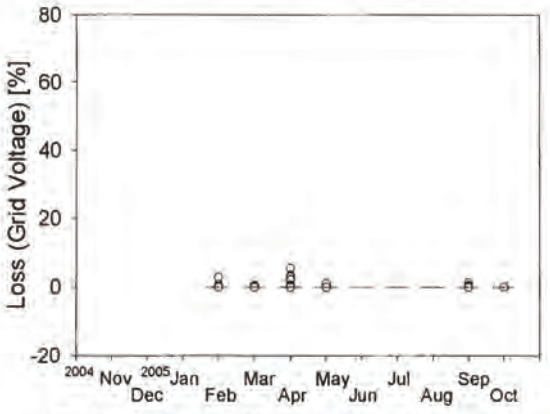

Fig. 11. Box chart of loss due to the grid voltage.

ある程度の効果が期待できると考えられる。個別に見た結果（Fig. 11）においても，出力抑制による極端な損失は発生していない事が分る。しかし，今回の結果のみを比較すると，出力抑制を回避することにより得られた電力量に対して，出力抑制回避装置（蓄電池）を導入することにより新たに発生した損失の方が多く，設置者側の蓄電池を導入するメリットが明確では無い結果となっている。これは，〈4·2〉節で述べたように，出力抑制による損失量がPVシステムの連系状態だけでなく，系統側の電圧調整の影響を強く受けるからであり，今後の大量普及時代を考慮すると，既存の配電系統において全てのPVシステム導入地域の電圧を本実証研究地域と同等に制御することは難しいと考えられる事から，導入規模の拡大に伴う出力抑制による損失量の増加とともに，蓄電池導入メリットも拡大していくと考えられる。

一方，PVシステムが系統に与える影響の一つとして，システム毎のPVアレイ容量1[kW]あたりの逆潮流電力量の割合を縦軸とし，月別の最大値1時間分をまとめたのがFig. 12である。この結果から，蓄電池付きシステムではひげの上側にあたる最大値が若干少なくなっているものの，平均値では市販PVシステムと大きな違いは無いことが分る。この原因を調べるため，最も大きな逆潮流電力量を記

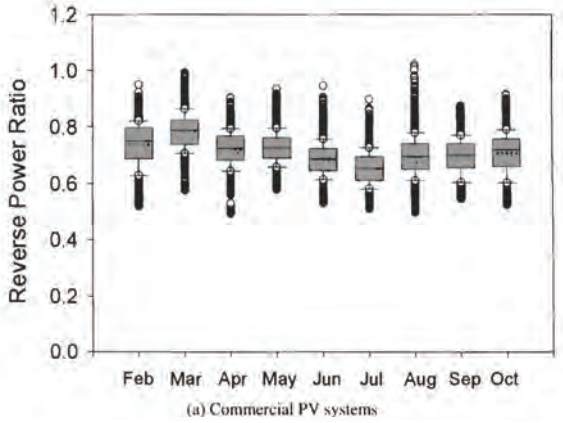

(a) Commercial PV systems

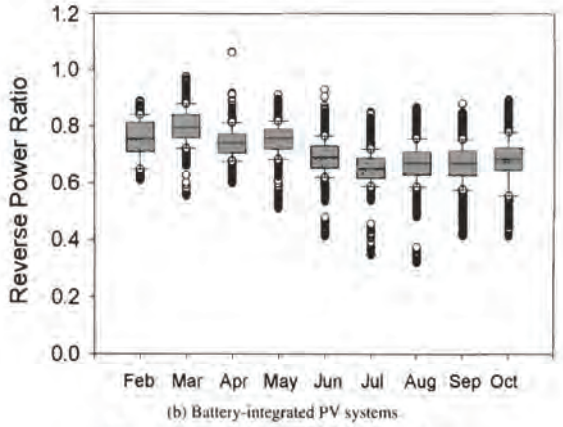

(b) Battery-integrated PV systems

Fig. 12. Maximum reverse power flow.

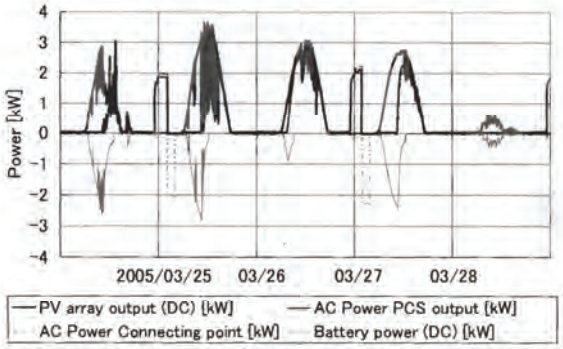

Fig. 13. Power flow of PV array, PCS, Connecting point and battery.

録した 2005 年 3 月 25 日前後のアレイ発電電力，PCS 出力電力，蓄電池充放電電力，受電点電力をグラフにまとめた (Fig. 13)。いずれの計測値も PV システムから出力される側をプラスとしており，蓄電池電力のマイナスは充電を，受電点電力のマイナスは系統からの買電を意味している。結果から，前日の放電が十分ではない場合や，午前中の発電量が多い時には正午前に蓄電池が満充電になっており，それ以降の PV アレイからの発電電力はそのまま系統に送られていることが分る。今回解析した期間は蓄電池設備の導入期間であり，蓄電池運用方式は先に述べたように逆潮流抑制運転に固定されていたため，このようなケースが見られたと思われる。

5. まとめ

本論文では，系統連系型太陽光発電システムの高度解析手法を提案し，その解析結果として「集中連系型太陽光発電システム実証研究」から得られたデータを用い，一般的な太陽光発電システムの運転特性の他，特に集中連系時に問題になるであろうと懸念される系統電圧上昇回避のための出力抑制による損失についても解析を行い，現状では発生頻度は低いものの，著しく PV システムの発電能力を低下させる原因になりうることを示した。また，新たに開発された蓄電池付き PV システムに関しては，一体型 PCS の導入段階での性能を分析し，一定の出力抑制回避効果がありそうな事，また，蓄電池の運用方式によっては必要なときに充電ができず，結果として逆潮流電力量の抑制効果が少なくなってしまう事を示した。今後も，様々な蓄電池運用方式に関してデータを収集し，解析を行っていく予定である。

なお，本研究は，集中連系型太陽光発電システム実証研究の一環として行っている。このような機会を与えていただいた（独）新エネルギー・産業技術総合開発機構，及び様々なご協力をいただいた関係者各位に，この場を借りて感謝の意を表する。

（平成 18 年 2 月 27 日受付，平成 18 年 5 月 30 日再受付）

文　献

(1) Y. Ueda, T. Oozeki, K. Kurokawa, T. Itou, K. Kitamura, Y. Miyamoto, M. Yokota, and H. Sugihara: "Quantitative Analysis Method of Output Loss due to Restriction for Grid-connected PV Systems", *IEEJ Trans. PE*, Vol.125, No.12, pp.1317–1326 (2005-12) (in Japanese)
植田　譲・大関　崇・黒川浩助・伊藤孝充・北村清之・宮本裕介・横田昌治・杉原裕正：「系統連系型太陽光発電システムにおける出力抑制による発電量損失の定量化手法」，電学論 B, **125**, 12, pp.1317–1326 (2005-12)

(2) （株）関電工：平成 14 年度 NEDO 委託業務成果報告書「集中連系型太陽光発電システム実証研究」(2003)

(3) Y. Miyamoto, M. Yokota, H. Sugihara, T. Tanabe, K. Kitamura, I. Shimoura, Y. Matumura, and S. Nishikawa: "MANAGEMENT OF SYSTEM TO AVOID RESTRICTION OF PHOTOVOLTAIC POWER GENERATION STSTEM OUTPUT", 20th European Photovoltaic Solar Energy Conference, pp.2717–2719 (2005)

(4) T. Yamada, H. Nakamura, T. Sugiura, K. Sakuta, and K. Kurokawa: "Refection loss analysis by optical modeling of PV module", Solar Energy Materials & Solar Cells, Vol.67, pp.405–413 (2001)

(5) Y. Ueda, T. Oozeki, and K. Kurokawa: "Outdoor measurement and analysis of incident angle effect of PV module", Proc. of JSES/JWEA Joint Conference, pp.51–54 (2005) (in Japanese)
植田　譲・大関　崇・黒川浩助：「太陽電池モジュール入射角特性の屋外測定と解析」，太陽/風力エネルギー講演論文集, pp.51–54 (2005) (in Japanese)

(6) Y. Ueda, T. Oozeki, K. Kurokawa, T. Itou, K. Kitamura, Y. Miyamoto, M. Yokota, and H.Sugihara: "Advanced analysis of shading effect using minutely based measured data for PV systems", 15th International Photovoltaic Science and Engineering Conference Technical Digest, pp.444–445 (2005)

(7) 財団法人日本品質保証機構：「太陽光発電システム評価技術の研究開発」，平成 6 年度新エネルギー・産業技術総合開発機構委託業務成果報告書 (1995)

(8) 独立行政法人新エネルギー産業技術総合開発機構：「2030 年に向けた太陽光発電ロードマップ」(2004)

(9) 財団法人エネルギー総合工学研究所・財団法人電力中央研究所・日本電池株式会社：「大量導入に向けた共通基盤技術の研究開発及び調査」，平成 13 年度新エネルギー・産業技術総合開発機構委託業務成果報告書 (2002)

(10) Y. Ueda, T. Oozeki, K. Kurokawa, T. Itou, K. Kitamura, Y. Miyamoto, M. Yokota, H. Sugihara, and S. Nishikawa: "DETAILED PERFORMANCE ANALYSES RESULTS OF GRID-CONNECTED CLUSTERED PV SYSTEMS IN JAPAN—FIRST 200 SYSTEMS RESULTS OF DEMONSTRATIVE RESEARCH ON CLUSTERED PV SYSTEMS", 20th European Photovoltaic Solar Energy Conference Proceedings, pp.2466–2469 (2005)

植田　譲　（学生員）　1972 年 8 月 24 日生。1995 年 3 月信州大学理学部物理学科卒業。同年，アプライドマテリアルズジャパン（株）入社。2003 年まで半導体製造プロセスの開発に従事。2004 年 4 月東京農工大学大学院工学府に入学。現在に至る。主に太陽光発電システムの評価に関する研究に従事。

黒川浩助　（正員）　1942 年 8 月 16 日生。1965 年 3 月早稲田大学第一理工学部電子工学科卒業。同年 4 月通産省工業技術院電気試験所（現産業技術総合研究所）入所。電子技術総合研究所エネルギー情報技術研究室長などを経て 1996 年 4 月東京農工大学工学部教授，現在に至る。主に太陽光発電システムの研究に従事。工学博士。日本太陽エネルギー学会理事，国際太陽エネルギー学会会員。

伊藤孝充  (正員) 1973年1月21日生。1997年3月新潟大学大学院自然科学研究科博士前期(修士)課程修了。同年4月(株)明電舎入社。電力系統の解析業務に従事。

横田昌治  (非会員) 1971年9月27日生。1996年3月東京農工大学大学院工学研究科博士前期課程修了。同年4月(株)関電工入社。現在,太陽光発電システムの研究に従事。

北村清之  (正員) 1957年11月4日生。1980年3月早稲田大学理工学部電気工学科卒業。同年4月(株)明電舎入社。現在,電力ソリューション営業技術部に勤務。主として,電力系統監視制御システムの開発業務に従事。技術士(情報工学),情報処理学会会員。

杉原裕征  (正員) 1950年8月15日生。1976年3月東京電機大学大学院工学研究科修士課程修了。同年4月(株)関電工入社。現在,技術開発本部に勤務。主に太陽光発電システムの研究に従事。工学博士。電気設備学会会員。

赤沼克己  (非会員) 1969年1月12日生。1992年3月明治大学工学部電気工学科卒業。同年4月(株)関電工入社。現在,太陽光発電システムの研究に従事。

森本篤史  (正員) 1968年10月24日生。1991年3月関西大学工学部電気工学科卒業。同年4月松下精工(株)(現松下エコシステムズ(株))入社。現在,技術センターに勤務。主に太陽光発電システム向けパワーコンディショナの研究開発に従事。

論　文

共振負荷と回転機負荷の相違と単独運転試験への影響について

正　員　五十嵐広宣*　　非会員　佐藤　孝則*
正　員　小林　広武**　　非会員　津田　泉***
正　員　黒川　浩助****

About the Influence on the Difference and the Islanding Test of the Resonance Load and the Motor Load

Hironobu Igarashi*, Member, Takashi Sato*, Non-member, Hiromu Kobayashi**, Member,
Izumi Tuda***, Non-member, Kousuke Kurokawa****, Member

The Islanding detection device of the most important protection instrument for the Utility—Interconnected Photovoltaic inverters the islanding phenomenon by the influence of the resurrection energy of the motor load and the resonance load. In the main discourse, it experimented on the individual operation by both measurements, and compared the amounts of electric energy of the motor load and the resonance load using PCS of a real machine and the effectiveness of the motor load was confirmed.

キーワード：太陽光発電システム，回転機負荷，共振負荷，単独運転検出装置，単独運転
Keywords: photovoltaic system, motor load, resonance load, Islanding detection device, Islanding

1. 緒　言

2004 年度の個人住宅用太陽光発電システムの設置軒数は，財団法人新エネルギー財団が実施している太陽光発電助成制度だけでも約 54,4 千軒を超えている[1]。2004 年度の設置軒数は，本助成制度が開始された 1994 年～1997 年の設置軒数（約 3.6 千軒）の約 17 倍以上と驚異的な数字である。

住宅用太陽光発電システムが，加速的に普及した要因には，1993 年の系統連系技術要件ガイドライン[2]（以下「ガイドライン」という）改定により，逆潮流型の連系運転が認められたことが考えられる。また，財団法人電気安全環境研究所（以下「JET」という）が行っている認証制度に適合した太陽光発電システム用パワーコンディショナ（以下「パワーコンディショナ」という）を設置する場合は，電力会社と設置者との間で行われる連系協議に係る時間短縮[3]をすることが可能となったことが関係していると考えられる。

認証制度は，新エネルギー産業技術総合開発機構の研究・開発成果[5]-[10]，ガイドライン及び電気用品取締法等の安全要求事項を包含した認証試験方法[4]によって，パワーコンディショナの安全性について試験を行うものである。

パワーコンディショナは，太陽電池から発電される直流電力を交流電力へ変換を行う逆電力変換部と単独運転検出装置や保護継電器等を兼ね備えたものであり，太陽光発電システムと一般配電線との連系を行う際に，重要な役割を果たしている。また，パワーコンディショナに具備されている単独運転検出装置は，太陽光発電システムが系統と連系運転している際に，連系している系統が停電状態等の異常状態になったことを検出し，系統から太陽光発電設備等を解列させる重要な検出装置である。

しかし，単独運転検出装置は，発電量と負荷量が平衡状態にある場合や，回生エネルギーを持つ回転機負荷や共振負荷等が系統内に負荷として存在する状態で系統と切り離された場合，分離した局所系統内の電圧や周波数にほとんど変化が発生せず，単独運転を検出することが困難であるとされている[5]-[10]。

* （財）電気安全環境研究所
〒151-8545　東京都渋谷区代々木 5-14-12
Japan Electrical Safety & Environment Technology Laboratories
5-14-12, Yoyogi, Shibuyaku, Tokyo 151-8545
** （財）電力中央研究所
〒201-8511　狛江市岩戸北 2-11-1
Central Research Institute of Electric Power Industry
2-11-1, Iwado Kita, Komae 201-8511
*** （独）産業技術総合研究所
〒305-8568　つくば市梅園 1-1-1
National Institute of Advanced Industrial Science and Technology
1-1-1, Umezono, Tukuba 305-8568
**** （国）東京農工大学工学教育部電子情報工学科
〒184-8588　小金井市中町 2-24-16
Tokyo University of Agriculture and Technology
2-24-16, Naka-cho, Koganei 184-8588

March 24, 2007
149

今回，著者らは，認証試験方法[4]で採用している回転機負荷（以下「回転機負荷」という）とIEC規格で採用している共振負荷（以下「共振負荷」という）の回生エネルギーを持つ負荷の相違について，各負荷に蓄積されるエネルギーの放出特性について測定を行った。また，同等のエネルギー放出特性を持つ共振負荷及び回転機負荷を用いて，実際のパワーコンディショナに具備されている単独運転検出装置に与える影響について検証を行った。

回転機負荷は，停電後の周波数維持特性が高いことから単独運転を広範囲で発生させる特性を持つことが示され，試験用負荷して具格条件が厳しいことが確認された。

2. 単独運転防止試験方法の概要

〈2・1〉 単独運転検出装置の目的 単独運転検出装置は，太陽光発電設備等の分散型発電設備が連系運転している系統や，その上位系統内で地絡や短絡事故等によって発生した系統擾乱等を検出し，パワーコンディショナの運転を停止させる目的で設置されている。単独運転検出装置が，系統停電を検出できなければ本来無電圧系統であるはずの系統に充電されることになり，人身および設備の安全に対して，公衆感電・機器損傷・消防活動への影響・事故点探査（除去）作業員の感電といった影響を与え，事故点の被害拡大や復旧遅れなどによる供給信頼度の低下を招く可能性があるとされ最も危険とされている[2]。

〈2・2〉 単独運転検出装置の概要 発電量と負荷量の関係が不平衡状態の場合は，停電後に電圧や周波数に顕著な変動が現れることから，過電圧継電器（OVR：Over Voltage Relay），不足電圧継電器（UVR：Under Voltage Relay），周波数上昇継電器（OFR：Over Frequency Relay），周波数低下継電器（UFR：Under Frequency Relay）等といった各種保護継電器が単独運転を検出することができる。

しかし，発電量と負荷量の関係が平衡状態の場合は，停電後に電圧や周波数にほとんど変化が発生しないため，電圧や周波数等の保護継電器では，単独運転を検出することが出来ない。そのため，ガイドラインでは，単独運転を確実に検出するために，単独運転検出装置の設置を要求している。

単独運転検出装置は，受動的単独運転検出装置と能動的単独運転検出方式の2種類の方式があり，それぞれの検出原理の長所を活かし単独運転の検出を行なっている。

受動的単独運転検出装置は，電圧位相跳躍検出方式，周波数変化率検出方式及び3次高調波電圧歪急増検出方式等といった検出方式があり，主に系統停電時に発生する電圧，電流，周波数等の系統擾乱を高感度で検出することから，高速性に優れている。しかし，発電量と負荷量が平衡状態では，停電時に発生する系統擾乱が発生し難ため単独運転を検出できない点や，高感度検出に検出を行うことから急激な負荷変動などによる誤検出等の欠点もある。

能動的単独運転検出装置は，周波数シフト方式，無効電力変動方式，有効電力変動方式及び負荷変動方式等といった検出方式があり，常時系統へ電圧や周波数等の変動を与えるため，単独運転移行時に顕著に発生する変動を検出することから，不感帯領域が無く確実性に優れている。しかし，同一能動信号の相互干渉による信号低下による不検出等の欠点もある。

〈2・3〉 回転機負荷による評価方法 認証試験方法の特徴は，負荷に回転機負荷を用いて評価を行っていることである。回転機負荷の意味合は，実際の配電線負荷として存在する回転機負荷を模擬するためである。また，もう一方では，多数の太陽光発電システム及び回転機発電機が並列運転する状況を模擬するものでもある。

空転する回転機負荷は，理想発電機として動作することから線路電圧及び周波数のパイロットとして作用し，単独運転状態を継続し易い状態とさせる。また，過去の研究成果[3]からは，周波数を変化させようとするパワーコンディショナに対しては，無効電力を供給・吸収する性能を有することから単独運転を発生しやすいとされている。

〈2・4〉 共振負荷の特徴 共振負荷による評価方法の特徴は，抵抗負荷，誘導性負荷及び容量性負荷を並列接続し，(1)式によって求める共振回路の鋭さを表す共振係数 Q_f が0.65と決められていることである。

$$Q_f = R\sqrt{\frac{C}{L}} \quad \cdots\cdots (1)$$

Q_f：共振係数
R：抵抗負荷 [Ω]
C：容量性負荷 [F]
L：誘導性負荷 [H]

試験回路の誘導性負荷量 P_{qL}[VAR_L] は，(1)式によって決定した共振係数 Q_f にパワーコンディショナの定格出力 P_{EUT} を乗算して求めている。(2)式は，(1)式から P_{qL}[VAR_L] を求める式としてIEC規格に記載されているものである。

$$P_{qL} = Q_f \times P_{EUT} \quad \cdots\cdots (2)$$

P_{qL}：誘導性負荷 [VAR_L]
P_{EUT}：パワーコンディショナ定格出力
Q_f ：0.65

また，共振負荷は，周波数の変化によって無効電力量を調整する特性を有しいているが，誘導性負荷や容量性負荷から発生する高調波電流によって，単独運転検出装置の検出方式に影響を与える特性を兼ね合わせて持っている。

3. 負荷のエネルギー放出特性の測定

〈3・1〉 負荷エネルギー放出特性の測定 単独運転検出装置は，停電直後に共振負荷及び回転機負荷に蓄積されたエネルギーが瞬時に放出されることによって，単独運転が検出できないものと考えられている。

共振負荷のエネルギー放出特性は，共振係数 Q_f が規定されているため，パワーコンディショナの定格出力に対し

表 1　回転機負荷の仕様

Table 1.　Spec of the motor load.

Spec of the motor load	The size of the Flywheel D[m]W[kg]	Moment of inertia
1Φ100V, 6.5A, 50/60Hz, Output645W	0.205*2 0.605*2	0.06 [N·m2]
1Φ100V, 6.3A, 50/60Hz, Output620W	0.205*2 0.605*2	0.06 [N·m2]
1Φ100V, 4.0/3.8A, 50/60Hz, Output 365W	0.150*2 0.605*2	0.03 [N·m2]
1 Φ 100V, 2.0/1.8A, 50/60Hz, Output 170W	0.150*2 0.539*2	0.03 [N·m2]

て常に一定である。それに対し，回転機負荷のエネルギー放出特性は，回転機の仕様等が明確に規定されたものがないため，使用する回転機負荷毎に異なる。

そのため，単独運転検出装置に与える影響についての検証を行う場合は，共振負荷と回転機負荷のエネルギー放出特性が同等でなければ評価を行うことができないことから，エネルギー放出特性の測定を行うこととした。

〈3・2〉 回転機負荷の選定　回転機負荷は，不特定多数あることから，JET 認証試験で使用している回転機負荷を基準とし，その約 1/2 定格出力 365 W と約 1/4 定格出力 170 W の代表機種 3 種類について計測を行った。また，定格出力 645 W の類似機種 620 W も同時に計測を行うこととした。

今回計測を行った回転機負荷を表 1 に示す。回転機負荷に取付けられているフライホイールは，回転運動の惰性による影響から，エネルギー放出特性に大きく関与することが考えられる。そのため，慣性モーメントの大きさについて (3) 式により求めた。

$$J = \frac{1}{8} \cdot W \cdot D^2 \quad [\mathrm{kg \cdot m^2}] \cdots\cdots (3)$$

W：フライホイールの重さ [kg]

D：フライホイールの直径 [m]

〈3・3〉 誘導性負荷量の選定　誘導性負荷量 P_{qL}[VAR_L] は，(2) 式によって決定されるためパワーコンディショナの定格出力を選定する必要がある。

定格出力の選定方法は，現在 JET 認証を取得しているパワーコンディショナの定格出力について調査を行い，最も多く認証を取得している定格出力 4 kW に決定した。これにより，共振負荷の誘導性負荷量は，(2) 式より求めた 2.6 kVar と決定した。

〈3・4〉 エネルギー放出時間の測定　エネルギー放出時間は，図 1 及び図 2 に示す回路図を用いて，以下に示す方法により測定した。

① 並列抵抗負荷 (R) を 0 W から 4000 W まで 100 W 刻み毎に増加させ，以下の②～④の手順とし繰り返し行う。

② t = 0 のタイミングで開閉器 SW_{CB} を開放する。

③ 線間電圧 V_1 が，20 V まで低下する時間 ΔX (Sec) を測定する。

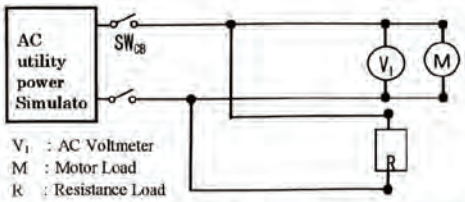

図 1　回転機負荷のエネルギー放出時間の測定回路

Fig. 1.　Measurement circuit at energy discharge time motor load.

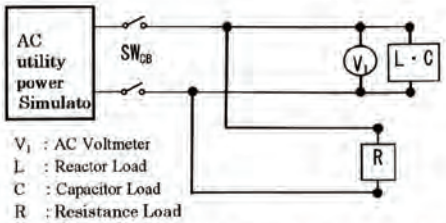

図 2　回転機負荷のエネルギー放出時間の測定回路

Fig. 2.　Measurement circuit at energy discharge time resonance load.

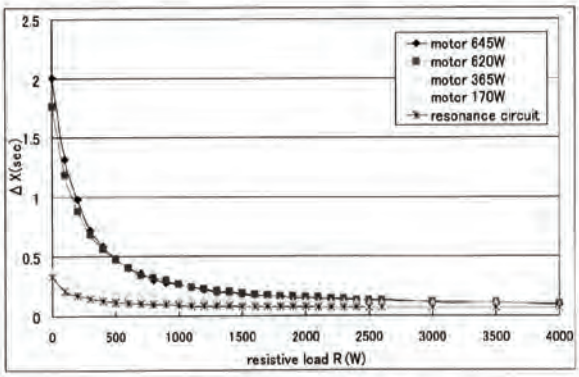

図 3　エネルギー放出時間の測定結果

Fig. 3.　Measurement result at energy consumption time.

④ 並列抵抗負荷で消費される電気的エネルギー量求める。

〈3・5〉 エネルギー放出時間の測定結果　エネルギー放出時間は，図 3 に示すとおり共振負荷と定格出力 170 W の回転機負荷が同等の測定結果となった。

また，計測時間は，並列抵抗負荷が増加すると伴に短くなり，抵抗負荷が 2500 W を超えたあたりからは，各負荷とも顕著な差がないことが確認できた。

しかし，共振負荷と回転機負荷は，エネルギーの蓄積や維持の特性が異なる点から，並列抵抗負荷によってエネルギーを消費する時間だけでは同等と判断することは難しい。そのため，共振負荷及び回転機負荷に蓄積されたエネルギーを，並列抵抗負荷で消費されるエネルギー量として比較を行うことにより，両負荷が持つエネルギー放出特性が明らかになると考え算出することとした。

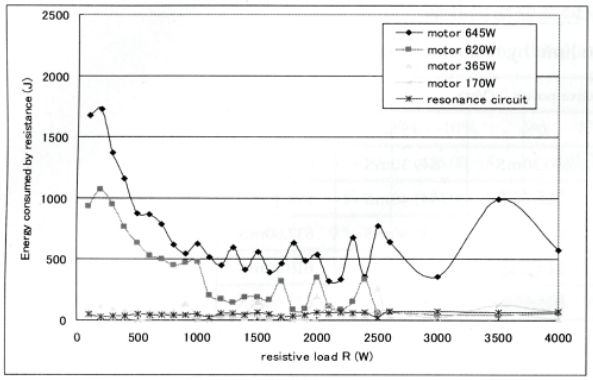

図 4　エネルギー放出特性の算出結果

Fig. 4.　Calculation result of amount of energy discharge.

〈3･6〉　エネルギー放出特性の算出　　共振負荷及び回転機負荷に蓄積されているエネルギー放出特性は，模擬電源と切り離した後に，並列抵抗負荷で消費する時間からエネルギー放出特性の算出を行った。エネルギー放出特性の算出は，並列抵抗負荷に流れる電流値（A）と負荷に電流が流れている時間（dt）の積分によって求められることから，(4) 式より行った。

$$J = R \times \int i^2 dt \quad \cdots\cdots (4)$$

J：電気的エネルギー量 [J]

R：抵抗値 [Ω]

i：抵抗に流れる電流 [A]

エネルギー放出特性は，図 4 に示すとおりの結果となり共振負荷と回転機負荷 170 W が同等であることが示され，エネルギー放出時間の測定結果と同じ結果になった。

また，並列抵抗負荷が 1000 W を超えた地点から，エネルギー放出時間では確認することができなかったエネルギー放出特性のばらつきが確認できた。この現象は，並列抵抗と各負荷の共振により，並列抵抗へ流れる電流が増加したものが要因として考えられる。

〈3･7〉　エネルギー放出特性の測定結果　　共振負荷と回転機負荷 170 W は，エネルギー放出時間及び放出特性から，同等のエネルギー放出特性を持つ負荷であることが示され，停電直後の単独運転検出装置に与える影響が同じであることが推測できる。そのため，単独運転検出装置に与える影響への検証は，今回計測した負荷を用いて，実際の単独運転実験を行うことにより検証を行うことした。

4.　単独運転実験による回転機負荷の有効性

〈4･1〉　単独運転実験条件　　単独運転検出装置の実験方法は，パワーコンディショナが系統と連系している状態から停電状態を発生させ，単独運転を検出し機器を停止させるまでの時間を計測するものである。

図 5 に示す単独運転実験回路は，実際の低圧配線に一般住宅用太陽光発電システムが，連系している配電モデルを縮小化したものある。また，当該回路図は，認証試験方法及び IEC 規格で採用されているものである。

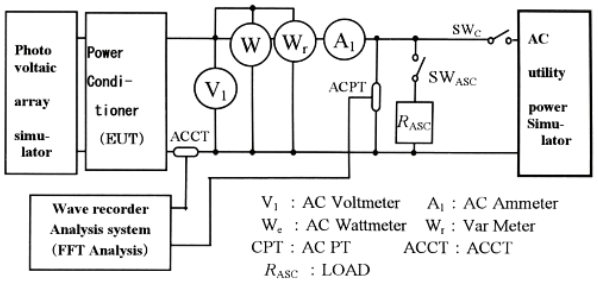

図 5　単独運転実験回路図

Fig. 5.　The circuit of islanding tests.

単独運転実験に使用したパワーコンディショナの仕様は，定格出力 4 kW のもので，受動的単独運転検出装置：電圧位相跳躍検出方式，能動的単独運転検出装置：周波数シフト検出方式を採用したものである。単独運転検出装置以外の保護継電器は，過電圧 OVR：115 V，不足電圧 UVR：85 V，過周波数 OFR：51 Hz，不足周波数 UFR：48.5 Hz とし，工場出荷時整定値に設定し実験を行った。

〈4･2〉　単独運転実験方法　　単独運転実験は，潮流点で消費される有効電力量及び無効電力量を調整し，図 5 に示す回路にて以下の実験方法で行った。

潮流点の有効電力量及び無効電力量は，パワーコンディショナの定格出力の −10%～+10%の範囲の 5%刻みで調整し単独運転実験を行う。そのため，単独運転実験の測定箇所は，有効電力及び無効電力の組み合わせによって合計 25 箇所を計測することになる。

（1）　有効電力量の調整は，パワーコンディショナの定格出力に対して −10%（3600 W），−5%（3800 W），0%（4000 W），+5%（4200 W），+10%（4400 W）の 5 箇所となるよう抵抗を調整する。

（2）　共振負荷での無効電力量の調整は，(2) 式によって求めた誘導性負荷量 P_{qL}[VAR_L] を固定値とし，パワーコンディショナが運転開始し定格出力になった後，パワーコンディショナの定格出力 −10%（2340 Var），−5%（2470 Var），0%（2600 Var），+5%（2730 Var），+10%（2860 Var）の 5 箇所となるよう容量性負荷量 P_{qC}[VAR_C] を調整する。

（3）　回転機負荷での無効電力の調整は，パワーコンディショナが運転を開始し定格出力になった後，容量性負荷を調整し，パワーコンディショナの定格出力に対して，−10%（−400 Var），−5%（−200 Var），−0%（0 Var）となるように調整する。また，無効電力を +5%（200 Var），+10（400 Var）に調整する場合は，誘導性負荷を調整し行う。

（4）　単独運転の計測は，系統交流模擬電源を t=0 のタイミングで開閉器（SW_{CD}）を開放し，パワーコンディショナが停止までの ΔX (Sec) を測定する。

〈4･3〉　共振負荷による単独運転実験結果　　共振負荷による単独運転実験結果は，図 6 及び表 2 に示すとおり，無

表2　共振負荷による単独運転検出時間

Table 2.　Islanding detection time limit by resonance load.

		Reactive power (Var)				
		-10%	-5%	0%	+5%	+10%
Active power (W)	-10%	635.90mS	Islanding	690.30mS	649.30mS	621.20mS
	-5%	653.10mS	802.30mS	Islanding	643.40mS	598.80mS
	0%	628.40mS	691.10mS	Islanding	632.40mS	637.60mS
	+5%	653.70mS	Islanding	Islanding	660.90mS	610.10mS
	+10%	674.20mS	758.90mS	Islanding	652.00mS	625.50mS

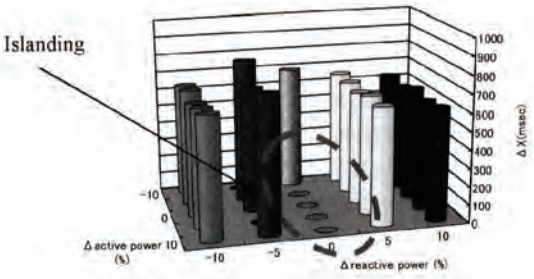

図6　共振負荷による単独運転検出時間

Fig. 6.　Islanding detection time limit by resonance load.

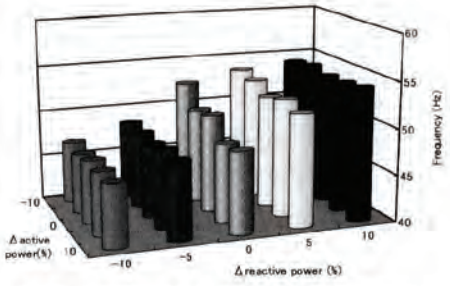

図7　停電後0.3後の周波数（共振負荷）

Fig. 7.　Frequency analysis result after 0.3 seconds after it blacks out (resonance load).

表3　停電後0.3秒後の周波数解析結果（共振負荷）

Table 3.　Frequency analysis result after 0.3 seconds after it blacks out (resonance load).

		Reactive power (Var)				
		-10%	-5%	0%	+5%	+10%
Active power (W)	-10%	46.75Hz	48.43 Hz	52.37 Hz	53.53 Hz	54.14 Hz
	-5%	46.47 Hz	48.25 Hz	50.21 Hz	53.12 Hz	54.46 Hz
	0%	46.88 Hz	48.05 Hz	50.59 Hz	52.09 Hz	54.03 Hz
	+5%	46.82 Hz	48.47 Hz	48.51 Hz	52.74 Hz	54.08 Hz
	+10%	46.78 Hz	48.35 Hz	48.81 Hz	52.12 Hz	54.39 Hz

効電力量が−5%～0%の範囲において有効電力量が−5%～+10%の範囲で，単独運転が発生していることが確認できた。

受動的単独運転検出装置は，電圧位相の変化を検出していることから，有効電力量がバランスしている影響を受ける。そのため，開閉器（SW_{CD}）開放後の電圧の位相が，検出レベルまで変化をしないことから受動的単独運転検出方式では検出できなかったと考えられる。

能動的単独運転検出方式は，周波数の変化を検出していることから，無効電力量のバランスの影響を大きく受ける。無効電力は，開閉器（SW_{CD}）開放前の状態では誘導性負荷及び容量性負荷によって平衡状態を保持している。また，開閉器（SW_{CD}）開放後では，パワーコンディショナが供給する無効電力量と負荷側が必要とする無効電力量が，周波数が変化することにより平衡状態を保持している。

そのため，無効電力量が平衡状態では，周波数に変化が発生しないことから，単独運転が発生したことが考えられる。しかし，無効電力量が不平衡の状態での単独運転は，周波数の変化により発生したと考えられる。

そこで，開閉器（SW_{CD}）開放前後の周波数を解析することにより，能動的単独運転検出装置の動作の有無について，検証を行うことができると考え，周波数の解析を行うこととした。なお，図6の単独運転現象は，パワーコンディショナの停止時間が測定できないため0秒として表す。

〈4・4〉　共振負荷の停電後における周波数解析　周波数の解析は，開閉器（SW_{CD}）開放前からパワーコンディショナ停止までの区間について解析を行った。図7及び表3は，開閉器（SW_{CD}）開放後0.3秒後の周波数について，記載したものである。

発電量と負荷量が不平衡の負荷条件では，開閉器（SW_{CD}）開放後に周波数が大きく変化しているため，能動的単独運転検出装置が単独運転を検出できたことが考えられる。

また，発電量と負荷量が平衡している負荷条件では，開

表 4　回転機負荷（170 W）による単独運転検出時限

Table 4.　Islanding detection time limit by motor load (170 W).

		Reactive power (Var)				
		-10%	-5%	0%	+5%	+10%
Active power (W)	-10%	655.00mS	Islanding	743.00mS	702.80mS	637.80mS
	-5%	644.60mS	684.80mS	Islanding	Islanding	Islanding
	0%	628.30mS	Islanding	Islanding	Islanding	650.82mS
	+5%	641.60mS	Islanding	Islanding	Islanding	621.60mS
	+10%	647.60mS	726.60mS	Islanding	Islanding	619.60mS

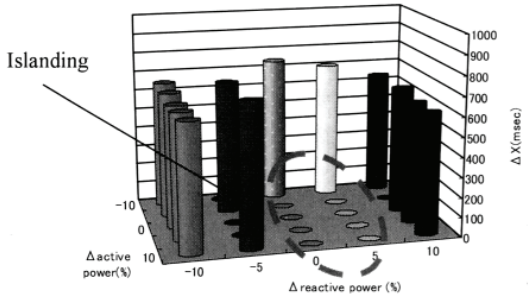

図 8　回転機負荷による単独運転検出時限

Fig. 8.　Islanding detection time limit by motor load.

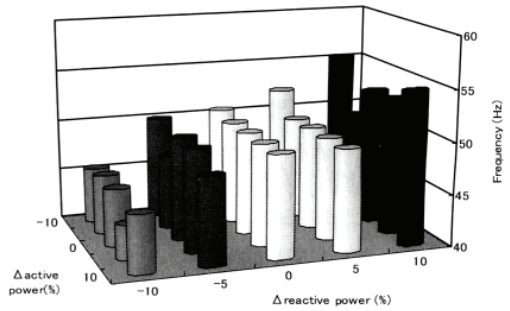

図 9　停電後 0.3 後の周波数（回転機負荷 170 W）

Fig. 9.　Frequency analysis result after 0.3 seconds after it blacks out (motor load 170 W).

表 5　停電後 0.3 秒後の周波数解析結果（回転機負荷 170 W）

Table 5.　Frequency analysis result after 0.3 seconds after it blacks out (motor load 170 W).

		Reactive power (Var)				
		-10%	-5%	0%	+5%	+10%
Active power (W)	-10%	45.45Hz	49.99Hz	50.51Hz	52.09Hz	55.24Hz
	-5%	45.84Hz	47.14Hz	50.05Hz	49.99Hz	50.00Hz
	0%	45.62Hz	50.05Hz	50.02Hz	50.04Hz	53.27Hz
	+5%	43.37Hz	49.96Hz	49.96Hz	49.99Hz	53.31Hz
	+10%	45.61Hz	48.51Hz	49.96Hz	49.97Hz	54.92Hz

閉器（SW_{CD}）開放後の周波数に変化が発生していない理由から，単独運転が発生したと考えられる。

能動的単独運転検出装置の閾値は，48.3 Hz を境に検出の有無が分かれていることから，能動的単独運転検出方式の下限検出周波数が，48.3 Hz 近辺であることが推測できる。

〈4･5〉　回転機負荷による単独運転実験結果　回転機負荷による単独運転実験結果は，図 8 及び表 4 に示すとおり無効電力量が −5%～+5%の範囲において有効電力量が −5%～+10%の広範囲で，単独運転が発生していることが確認できた。また，単独運転の発生箇所は，共振負荷の場合と類似している。回転機負荷による単独運転の発生は，検出原理が同じであることから，共振負荷と同様の理由が考えられる。しかし，単独運転の範囲が，広範囲になった要因については，回転機負荷特有の特性が関与していると考えられる。なお，図 8 の単独運転現象は，パワーコンディショナの停止時間が測定できないため 0 秒として表す。

〈4･6〉　回転機負荷による周波数解析結果　周波数の解析は，開閉器（SW_{CD}）開放前からパワーコンディショナ停止までの区間について解析を行った。図 9 及び表 5 は，開閉器（SW_{CD}）開放後 0.3 秒後の周波数について記載したものである。

単独運転が発生している負荷条件の周波数は，開閉器（SW_{CD}）開放前後では全く変化が無く周波数の維持特性が高いことが確認できる。しかし，それ以外の負荷条件では，開閉器（SW_{CB}）開放直後から極端に周波数が上昇又は低下をしていることが確認できた。

回転機負荷は，無効電力量が平衡状態の付近では開閉器（SW_{CB}）開放後に，自ら無効電力量を吸収又は供給することにより，周波数を維持しながら回転し，単独運転を発生させる特性を有していることが推測できる。

しかし，無効電力量の不平衡状態が大きい場合は，開閉器（SW_{CB}）開放後に，自ら調整できる無効電力量の許容

範囲を逸脱することにより，無効電力量がバランスした周波数に同期しながら回転することが考えられる。そのため，周波数が大きく変化した結果となったと推測できる。

5. 考　察

〈5・1〉 共振負荷における共振点の検討　共振負荷の実験は，IEC 規格に定められた共振係数（Q_f）0.65 を採用し，エネルギー放出特性や単独運転実験を行った。

単独運転実験は，回転機負荷が広範囲で単独運転ができる負荷であることが示されたが，共振係数を 0.65 から 1 へ変化させた場合，回転機負荷 170 W と同等の単独運転を発生させる可能性も考えられる。今後は，共振係数を変化させた場合の単独運転について検討を行うこととしたい。

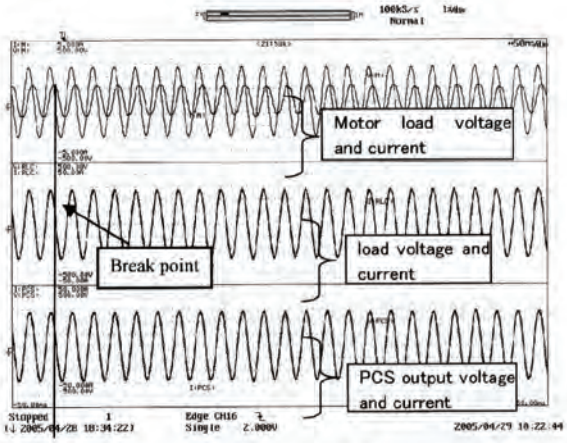

図 10　回転機負荷 170 W の各電圧電流波形

Fig. 10.　Each voltage current wave form of motor load 170 W.

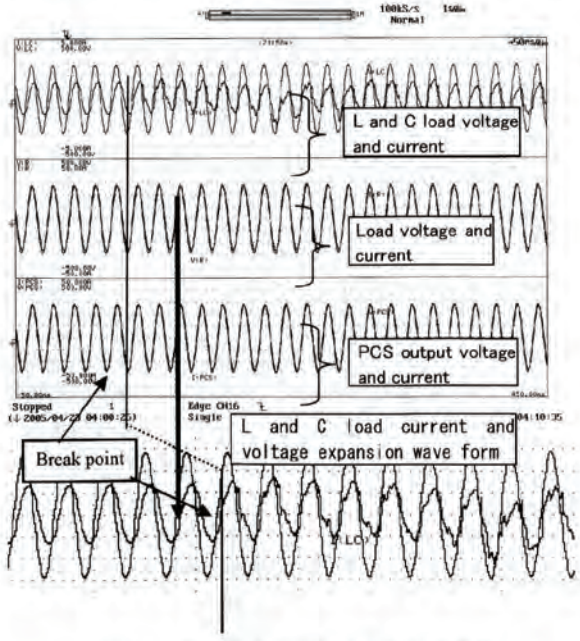

図 11　共振負荷による高調波電流波形

Fig. 11.　Harmonic current wave type by resonance load.

〈5・2〉 共振負荷の高調波問題　共振負荷は，系統停電後に共振負荷から発生する高調波電流の影響によって，単独運転検出装置の検出方式によっては，正しく単独運転現象を検出することが出来ない問題がある。

今回の単独運転実験結果は，系統停電直後から 25 箇所の全ての負荷条件において，図 11 に示す誘導性負荷及び容量性負荷から発生する高調波電流を観測した。また，図 10 に示すとおり回転機負荷は，高調波電流の発生は確認出来なかった。

高調波電流の発生要因は，誘導性負荷のヒステリシス特性等の磁気特性に起因するものと考えられる。しかし，高調波電流の直接の発生要因については，現在の特定出来ていない。そのため，今後は，高調波電流発生要因の特定の検討を行うこととしたい。

6. ま と め

本論文は，共振負荷と回転機負荷が蓄積するエネルギーを計測することにより，エネルギー放出特性について明らかにした。

また，計測結果から同等のエネルギー特性を持つ共振負荷と回転機負荷を用いて単独運転実験を行い，共振負荷よりも回転機負荷のほうが単独運転を広範囲で発生していることが確認できた。回転機負荷が，広範囲で単独運転を発生させる要因について単独運転実験の周波数の解析を行い，無効電力が平衡状態近辺では周波数を維持する特性があることが確認できた。

今回の結果から，回転機負荷は，周波数維持特性が高い特性を持つ負荷であり，広範囲の負荷条件において単独運転を発生させることが可能な負荷であることが示された。また，共振負荷は，回転機負荷よりも周波数維持特性が低いため，回転機負荷の特性を代替することが出来ないことが確認できた。

（平成 18 年 2 月 27 日受付，平成 18 年 8 月 23 日再受付）

文　献

（1） New Energy Foundation (NEF) Web site: http://www.solar.nef.or.jp/.htm (in Japanese)
http://www.solar.nef.or.jp/josei/h16_setti_kensu.htm
財団法人 新エネルギー財団 web site: http://www.solar.nef.or.jp/
（2） 解説電力系統連系技術要件ガイドライン 系統連系技術要件検討委員会報告'98 系統連系技術要件検討委員会技術評価作業部会
（3） 分散型電源系統連系技術指針 JEAG9701-2001 社団法人 日本電気協会分散型電源系統連系専門部会
（4） 太陽電池発電システム用系統連系保護装置等の試験方法作成：財団法人電気安全環境研究所 (2002-10)
（5） 『ニューサンシャイン計画新エネルギー・産業技術総合開発機構（NEDO）委託業務成果報告書』として，平成 5 年度 太陽光発電システム実用化技術開発「太陽光発電利用システム評価技術の研究開発」（周辺技術評価システムの研究開発）」
（6） 『ニューサンシャイン計画新エネルギー・産業技術総合開発機構（NEDO）委託業務成果報告書』として，平成 6 年度 太陽光発電システム実用化技術開発「太陽光発電利用システム評価技術の研究開発」（周辺技術評価システムの研究開発）」

(7) 『ニューサンシャイン計画新エネルギー・産業技術総合開発機構 (NEDO) 委託業務成果報告書』として，平成 7 年度太陽光発電システム実用化技術開発「太陽光発電利用システム評価技術の研究開発」(周辺技術評価システムの研究開発)』
(8) 『ニューサンシャイン計画新エネルギー・産業技術総合開発機構 (NEDO) 委託業務成果報告書』として，平成 8 年度 太陽光発電システム実用化技術開発「太陽光発電利用システム評価技術の研究開発」(周辺技術評価システムの研究開発)』
(9) 『新エネルギー・産業技術総合開発機構 (NEDO) 委託業務成果報告書』として，平成 4 年度 分散型新発電技術実用化実証研究に関する保護機能等試験方法の確立』
(10) 『新エネルギー・産業技術総合開発機構 (NEDO) 委託業務成果報告書』として，平成 5 年度 分散型新発電技術実用化実証研究に関する保護機能等試験方法の確立』
(11) H. Igarashi: "The tests of islanding have an influence on motor", 2005 National Convention Record IEE Japan, No.6-192, pp.341–342 (2005) (in Japanese)
五十嵐広宣：「単独運転防止試験時の回転機負荷影響について」，平成 17 度電気学会全国大会, No.6-192, pp.341–342 (2005)

五十嵐 広 宣 

(正員) 1972 年 11 月 19 日生。1993 年 3 月東京電機大学短期大学電気科卒業。1991 年 4 月 (財) 電気安全環境研究所入所。現在，(財) 電気安全環境研究所研究部先任主査。主として太陽光発電システムの系統連系保護装置の認証業務，太陽光発電システムの研究に従事。2004 年 10 月東京農工大学大学院工学教育部に入学。現在に至る。

佐 藤 孝 則 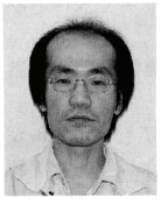

(非会員) 1973 年 2 月 24 日生。1996 年 3 月千葉大学工学部電気電子工学科卒業。同年 4 月常陽産業 (株) 入社。1999 年 5 月同社退社。同年 5 月 (財) 電気安全環境研究所入所。現在に至る。主に電力系統の解析業務に従事。

小 林 広 武 

(正員) 1956 年生。1982 年 3 月北海道大学工学部電子工学専攻修士課程修終。同年 4 月に (財) 電力中央研究所入所。現在，(財) 電力中央研究所入所システム技術研究所上席研究員。主として太陽光発電システム，蓄電池系統の研究に従事。1993 年オーム技術賞，1997 年電気学会学術振興賞論文賞受賞。博士 (工学)。太陽エネルギー学会員。

津 田 泉 

(非会員) 1955 年 1 月 23 日生。1979 年 3 月大阪大学大学院工学研究科前期 (修士) 課程修了。同年 8 月同大学院後期課程中退。同年 9 月日本オーチスエレベータ (株) 入社。1981 年 3 月同社退社。同年 4 月電子技術総合研究所入所。太陽エネルギー関連の研究開発に従事。

黒 川 浩 助 

(正員) 1942 年 8 月 16 日生。1965 年 3 月早稲田大学第一理工学部電子工学科卒業。同年 4 月通産省工業技術院電気試験所 (現産業技術総合研究所) 入所。電子技術総合研究所エネルギー情報技術研究室長などを経て 1996 年 4 月東京農工大学工学部教授，現在に至る。主に太陽光発電システムの研究に従事。工学博士。日本太陽エネルギー学会理事，国際太陽エネルギー学会会員。

Electrical Engineering in Japan, Vol. 158, No. 2, 2007
Translated from Denki Gakkai Ronbunshi, Vol. 125-B, No. 12, December 2005, pp. 1317–1326

Quantitative Analysis of Output Loss Due to Restriction for Grid-Connected PV Systems

YUZURU UEDA,[1] TAKASHI OOZEKI,[1] KOSUKE KUROKAWA,[1] TAKAMITSU ITOU,[2] KIYOYUKI KITAMURA,[2] YUSUKE MIYAMOTO,[3] MASAHARU YOKOTA,[3] and HIROYUKI SUGIHARA[3]

[1]Tokyo University of Agriculture and Technology, Japan
[2]Meidensha Corporation, Japan
[3]Kandenko Co., Ltd., Japan

SUMMARY

The voltage of power distribution lines will be increased due to reverse power flow from grid-connected PV systems. In the case of high-density grid connection, the voltage increase will be higher than in a stand-alone grid connection system. To prevent overvoltage on the power distribution lines, the PV system's output will be restricted if the voltage of the power distribution line is close to the upper limit of the control range. Because of this interaction, the output loss will be larger in the high-density case. This research has developed a quantitative analysis method for PV system output and losses in order to clarify the behavior of grid-connected PV systems. All the measured data are classified into loss factors using a 1-minute average of 1-second data instead of the typical 1-hour average. The operation point on the *I–V* curve is estimated to quantify the loss due to the output restriction, using the module temperature, array output voltage, array output current, and solar irradiance. As a result, the loss due to output restriction is successfully quantified and the behavior of output restriction is clarified. © 2006 Wiley Periodicals, Inc. Electr Eng Jpn, 158(2): 9–19, 2007; Published online in Wiley InterScience (www.interscience.wiley.com). DOI 10.1002/eej.20452

Key words: photovoltaic; evaluation; output restriction; loss; quantitative analysis.

Contract grant sponsor: New Energy and Industrial Technology Development Organization (NEDO).

1. Introduction

Since the Kyoto Protocol came into force on February 2005, the introduction of renewable energy sources is becoming an increasingly important task for Japan to realize sustainable development and to reduce global warming gas emissions. Among renewable energy sources, photovoltaic (PV) systems are promising because they can generate electricity, which is one of the most useful energy forms, from the unlimited sunlight. However, when a few hundred residential PV systems are connected into the local power distribution network (i.e., "clustered"), reverse power flow from the PV systems may cause voltage rises more frequently than when a few PV systems are grid connected. To prevent overvoltage on the power distribution line, the power conditioning subsystems (PCS) of Japanese PV systems have a function to restrict output. As a result of this function, if the grid voltage reaches the upper limit of the control range, the PV system's output power will be restricted even though the PV modules are receiving enough sunlight to generate more electricity.

One way to avoid this output restriction is a battery-integrated PV system. A demonstration research project on clustered PV systems has been conducted since December 2002 by the New Energy and Industrial Technology Development Organization (NEDO) to investigate the behavior of "clustered" PV systems. This research is intended to clarify the issues of clustered PV systems, develop battery-integrated residential PV systems as output restriction avoidance systems, demonstrate their effect in the commercial power grid by installing a few hundred PV systems in the demonstration project area, and develop simulation models for potential issues [1]. This paper uses data from this demonstration project and develops a quantitative

method for the analysis of PV system performance and losses, including losses due to output restriction, in order to clarify the issues of clustered PV systems.

2. Output Restriction Function of PV System's PCS

In grid-connected residential PV systems, the generated electric power will be supplied to house loads and the excess power will be fed into the power distribution network. As a result of this reverse power flow, the voltage at the connecting point will be raised as shown in Fig. 1. The amount the voltage rise will become larger as the number of connected PV systems increases, and in the clustered case, the voltage may exceed the upper limit of the power distribution line, which is 101 ± 6 V or 202 ± 20 V in Japan. Thus, Japanese PCS are equipped with an output restriction function to prevent overvoltages. Output restriction functions can be classified into two types, reactive power control and active power control (regulation); however, since reactive power control is not sufficiently effective in lowering the voltage in power distribution lines, active power control is much more popular [1]. Examples of control methods in Japanese commercial PCS are summarized in Table 1. Phase advance reactive power control will shift the current phase and change the power factor between 1 and 0.85, and active power control will regulate the output current in order to reduce the output power. The PCS monitors its own output terminal voltage and uses it for the starting voltage of output restriction. However, there is a voltage drop between the PCS output terminal and the connection point due to the resistance of the drop wire, and thus the PCS may not need to start restriction at 107 V. This is one of the reasons why the starting voltages of output restriction are not exactly the same for all PCS. It has been pointed out that this kind of variation may cause the concentration of output restriction in particular PCS, while no restriction occurs in others; this variation should be minimized [1].

Table 1. Types of overvoltage protection for PCS

Types	Reactive power control	
	Default / Range	Speed
A	112V / 107V - 112V	PF=1 to 0.85 in 2 to 2.5sec
B	None	None
C	None	None
D	107V / 106.5V	PF=1 to 0.85 in 10sec

Types	Active power control (Regulation)	
	Default / Range	Speed
A	After PF reached 0.85	2A/sec, 100% to 0%=10sec
B	107V / 106V – 120V	43mA/4sec
C	109V / 107V – 110V	Immediately 0%
D	109V / 107.5V	100% to 0% in 4 to 10sec

PF: Power factor

3. Quantitative Analysis of Losses

3.1 Loss factors of PV systems

The input energy of the PV systems is solar irradiation. Solar irradiation will be converted to DC electric power in the solar cells and the DC power will be inverted to AC power in the PCS. Since deployed PV systems are not always operating under optimal conditions, there will be losses due to several factors [2]. Major loss factors of PV systems are summarized in Fig. 2. In the beginning of energy conversion, the incoming solar irradiance, the input energy, will be reduced by shading, reflection due to the angle of incidence, and dirt on the surface of PV modules

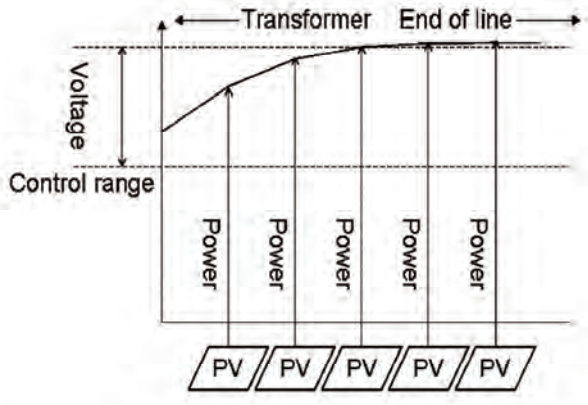

Fig. 1. Image of voltage rise due to the reverse power flow from PV systems.

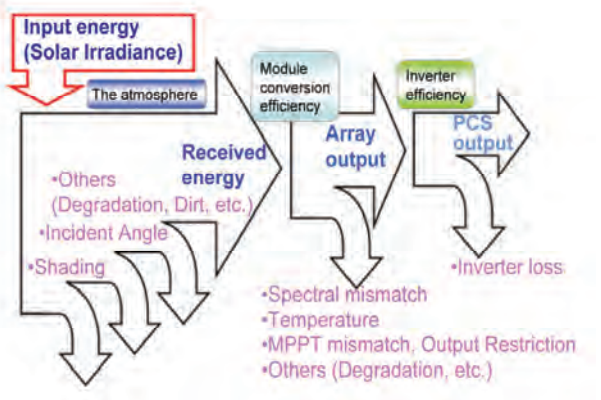

Fig. 2. Loss factors of PV systems.

before the energy reaches the solar cells. The next step is photovoltaic energy conversion. The energy received by the solar cells is used for photovoltaic conversion, but the conversion efficiency is defined for standard test conditions (STC) [3], so that the efficiency will be different under different conditions. For example, the solar cell temperature is defined as 25 °C under STC. If the cell temperature is higher than 25 °C, the typical crystalline silicon solar cell has a negative temperature coefficient; since the module temperature is usually higher than 25 °C under irradiation, there will be some output power loss due to the conversion efficiency reduction. Maximum power point (MPP) mismatch might also occur during this step. Additional loss will occur during current inversion in the PCS before we finally obtain AC electric power from the PV system.

3.2 Quantifiable loss factors

Since lost energy cannot be measured directly, the ideal output power with minimal losses must be determined for loss quantification. This paper uses the SV method [2] developed by Tokyo University of Agriculture and Technology as a base model for performance and loss analysis. The incoming irradiation and the PV array's peak power under the measured irradiance are used to calculate the ideal system output power, and the measured PV array output voltage and current and the AC output power from the PCS are used for loss quantification [4]. The new method can quantify the output energy loss for the following loss factors:

- PCS not operating
- PCS capacity shortage
- Output restriction
- Module temperature
- Fluctuation
- Inverter (PCS)

Besides the above loss factors, shading, reflection due to the angle of incidence, dirt on the module surface, and variations of the module peak power are considered in this method. Since these losses cannot be quantified directly, the proposed method takes a statistical approach, using about 1 month's data to quantify the loss due to dirt and module peak power variation. The effect of shading is excluded by selecting PV systems which do not have shading problems. The effect of reflection is included in miscellaneous losses because its effect is normally only a few percent of the performance ratio [5].

3.3 Overview of the quantitative analysis method

The input data of the new analysis method are the DC output voltage and the current from the PV array, the AC output voltage and the current from the PCS, the module temperature, the global irradiance, the direct irradiance, and the system specifications such as the array configuration, the type of module and so on. One-minute averages of 1-second measured data are used for the analysis. This is one of the unique characteristics of the new method. The standard SV method uses hourly data for the analysis, but the hourly data do not have enough resolution to quantify the output energy loss due to restriction.

In the beginning of the analysis, the incoming irradiance at the PV array's plane is calculated from the global irradiance and the direct irradiance, using the direct model for direct component, the Perez model [6] for the diffuse component, and the uniform reflection model for the reflected component. The system peak power under the calculated irradiance is calculated in the second step. All the input data are classified to loss factors using both theoretical and empirical models, and selected data under the minimal loss conditions are used to calculate the system's ideal output. The performance ratio and losses for each loss factor are quantitatively analyzed in the last step. This analysis flow is summarized in Fig. 3. Each step will be explained in the following sections.

3.4 Calculation of irradiance at the PV array plane and system peak power

Using the direct model for the direct component, the Perez model for the diffuse component, and the uniform reflection model for the reflected component, we calculate the incoming irradiation at the PV array plane and the system peak power under the calculated irradiance as follows:

$$E_{AS} = P_{AS} \cdot \frac{H_{Ag}}{G_S} \tag{1}$$

where

E_{AS} is the system output energy (kWh),
P_{AS} is the system rated power at STC (kW),

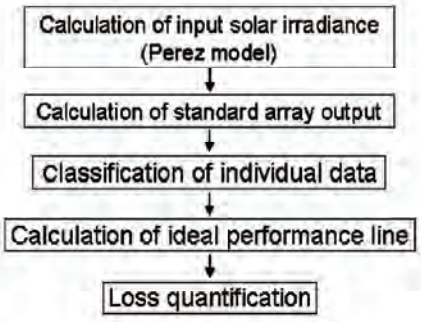

Fig. 3. Loss quantification flowchart.

G_S is the irradiance at STC = 1 (kW/m^2)
H_{Ag} is the irradiation at the PV array plane (kWh/m^2).

3.5 Classification of input data

(1) Detecting nonoperation of PCS

A typical commercial PCS uses the PV array output power for its control circuit. When the incoming irradiance is too weak to start the PCS, there will be no output power from the PCS even though the PV array is receiving irradiation. The new method classifies the energy loss due to this situation as a loss due to "PCS off". Intentional PCS off for maintenance purpose is also included in this loss. The criterion for judgment of PCS off is

$$ACIa_{PCS1} < 0.1 \text{ A} \quad \text{or} \quad ACIa_{PSC2} < 0.1 \text{ A} \qquad (2)$$

where

$ACIa_{PCS1}$ is the PCS AC output current of phase 1 (A)
$ACIa_{PCS2}$ is the PCS AC output current of phase 2 (A).

Since all the analyzed PV systems were residential PV systems and the capacity of the PCS is between 3 kW and 5 kW, 0.1 A is used in this paper. This figure might not be valid if a larger PCS capacity is used in the system.

(2) PCS capacity shortage case 1

The inversion efficiency of the PCS is normally higher in the vicinity of its rated output power and becomes worse along with decreasing input power. When the capacity of the PCS and that of the PV array are almost the same, the operation time at low input power will be relatively longer than for a smaller PCS. The initial cost of the larger-capacity PCS is also higher than that of the smaller one. Thus, a smaller-capacity PCS is sometimes used for residential PV systems [7]. In this case, there will be some energy loss due to PCS capacity shortage when the PV array is receiving enough irradiation to output the rated power. Equation (3) is used to separate this situation:

$$P_A > P_{PCS} \times 0.99 \text{ and } P_{AS} > P_{PCS} \qquad (3)$$

where

P_A is the array output power (kW), and
P_{PCS} is the PCS capacity (kW).

(3) Output restriction cases 1 & 2

The PCS tracks the MPP when the PCS output terminal voltage is in the control range. When the voltage exceeds the upper limit, the PCS will shift the operation point on the *I–V* curve toward the open circuit voltage (V_{OC}) of the PV array and regulate the input DC current to reduce its AC output power (see Fig. 4). To detect this output restriction, the PV array output voltage and array temperature are

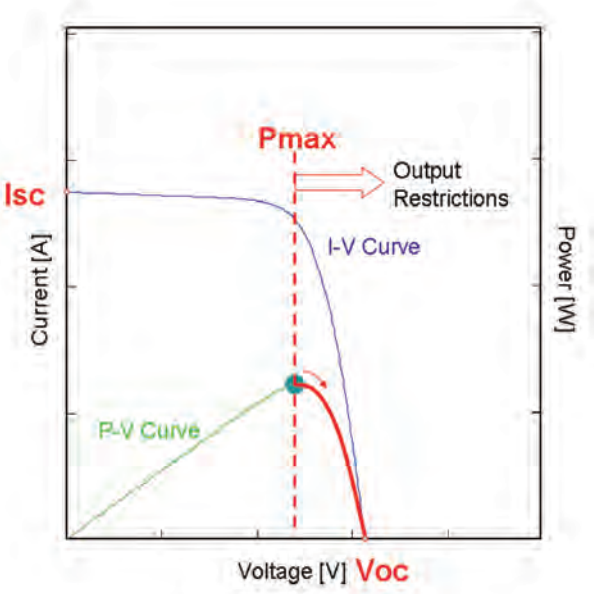

Fig. 4. Operation point during output restriction.

plotted on a scatter diagram as the *Y* axis and *X* axis, respectively, and data under the high-voltage condition are separated by using Eq. (4), which represents the locus of V_{Pmax}. The array output current and the irradiance at the array plane are also plotted on the scatter diagram as the *Y* axis and *X* axis, respectively. The data under current regulation are separated by using Eq. (5), which defines the range of I_{Pmax}. The data at voltages higher than V_{Pmax} and currents lower than I_{Pmax} are assumed to be data under restriction:

$$Y = V_{Pmax} \times N_{series} \times C + \beta_{Pmax} \times N_{series} \times (X - 25) \qquad (4)$$

where

Y is the PV array output voltage (V),
X is the PV array temperature (°C),
V_{Pmax} is the PV module's output voltage at MPP (V),
N_{series} is the number of series-connected PV modules,
β_{Pmax} is the temperature coefficient of the module output voltage (V/°C), and
C is a constant;

$$Y = I_{Pmax} \times N_{parallel} \times C_{loss} \times X \pm C_{range} \qquad (5)$$

where

Y is the PV array output current (A),
X is the irradiation at the PV array plane (kW/m^2),
I_{Pmax} is the PV module's output current at MPP (A),
$N_{parallel}$ is the number of parallel-connected PV modules (strings),
C_{loss} is a constant, and
C_{range} is a constant defining the range of I_{Pmax} (A).

Since the temperature coefficient of the ideal V_{Pmax} as a percentage is almost the same as V_{OC}, Eq. (4) describes the ideal V_{Pmax} for each array temperature. Excluding the data already assigned to the other loss factors, the remaining data are plotted on the scatter diagram shown in Fig. 5. The solid line in Fig. 5 is the locus of the ideal V_{Pmax}, and the data above the line can be assumed to be data for which the voltage is higher than the ideal output voltage.

The output current of the PV array is proportional to the incoming irradiance if there is no serious output power loss. If the current is significantly lower than the ideal output current, there must be some loss factors. Thus, the data outside the I_{Pmax} range can be assumed to be data for the restriction mode after the exclusion of data which have already been assigned to other loss factors. An example of a scatter plot of the array output current and irradiance is shown in Fig. 6.

In Eqs. (4) and (5), the constants C, C_{loss}, and C_{range} are used to improve the accuracy of the detection of restrictions. It is better to set these constants for each PV system, since they depend on the type of module, the array string configuration, and the system specification. However, C = 0.97 and C_{loss} = 0.95 are used in this paper as optimum constants derived from the analysis of eight systems. C_{range} is set to 1 A, which is 5% of the typical I_{Pmax} (= 20 A) of residential PV systems.

Using the above conditions, the data are assigned to restriction mode if the voltage is high and the current is low. They are assigned to output restriction case 1 if the PCS output terminal voltage is higher than 107 V, and otherwise to case 2. Case 1 is a typical output restriction to prevent overvoltage on the power grid. Case 2 includes the situation in which the temperature of the PCS increases and overtemperature protection reduces the output power.

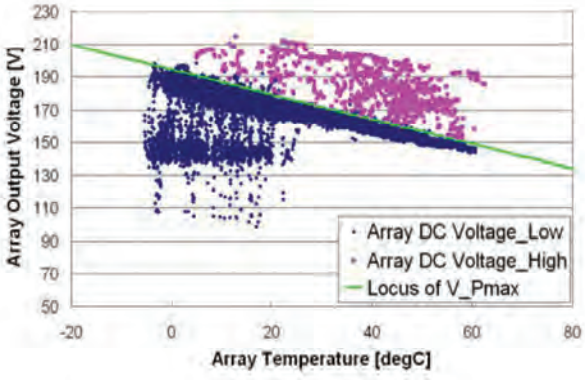

Fig. 5. Scatter diagram of array output voltage and array temperature.

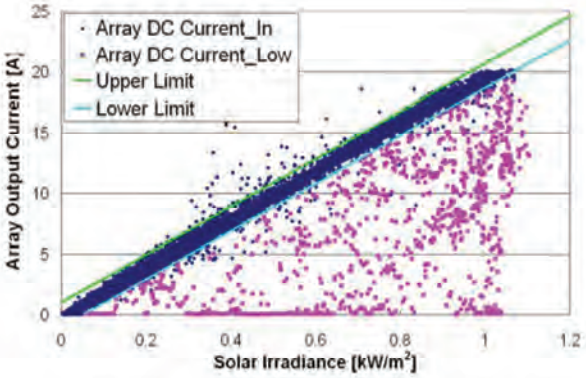

Fig. 6. Scatter diagram of array output current and solar irradiance.

(4) Temperature correction of array output power

After the above steps, remaining data which have not been assigned to any loss factors are temperature-corrected to STC temperature (= 25 °C) as follows:

$$P_{AT} = \frac{P_A}{1 + (\alpha_{P_{max}} \cdot (T_C - 25))} \quad (6)$$

where

P_{AT} is the temperature-corrected array output (kW),

α_{Pmax} is the temperature coefficient of P_{max} (1/°C), and

T_C is the PV module temperature (°C).

(5) PCS capacity shortage case 2

The PV module temperature at STC is 25 °C, but the module temperature is usually higher than 25 °C under irradiation in Japan. Due to the negative temperature coefficient of crystalline silicon PV modules, the temperature-corrected module output power (P_{AT}) will be higher than before. Thus, P_{AT} many exceed the PCS capacity. Equation (7) separates the data which may include a loss due to the PCS capacity shortage after temperature correction:

$$P_{AT} > P_{PSC} \times 0.99 \text{ and } P_{AS} > P_{PCS} \quad (7)$$

It should be noted that PCS capacity shortage case 1 represents an actual energy loss, but case 2 is only a calculated value which will be useful for system sizing and design.

(6) Fluctuations

Under fast fluctuation of the irradiance or PV output power, the data may be affected by moving clouds or other accidental shading. Since there is some distance between

the pyranometer and the PV systems, either the pyranometer or PV systems could be shaded when the fluctuation is too fast, and this situation will cause error in the results of analysis. On the other hand, MPP tracking sometimes takes a few seconds or minutes to find the MPP when the fluctuation is too fast. All of these errors or losses will occur in the presence of fast fluctuations; the following conditions are used to separate the data in the presence of fluctuations:

- Minute fluctuations of the PV array output power exceeding 3% (kW) of the PV array's peak power
- Minute fluctuations of the global irradiance exceeding 0.03 kW/m^2.

Equation (5) is also used to judge whether there is some output energy loss due to the fluctuation after separation. Only data below the range of $I_{P\max}$ are classified as including fluctuation losses.

3.6 Loss quantification

After the above steps, the remaining data which have not been assigned to any of the loss factors can be assumed to be data with minimal loss. Using these minimal loss data, the ideal output power during the evaluation period is calculated. After the calculation, the differences between the ideal power and actual output power are treated as losses. To calculate the ideal output power at each irradiance level, the ideal performance line (IPL) used in the SV method is employed. The output power of deployed PV systems is normally affected by dirt and by degradation or variation of the peak power, and thus the sum of the peak powers of the modules is not the same as the array's peak power. IPL represents this kind of characteristic. The IPL data are those in which the losses due to PCS off, PCS capacity shortage cases 1 & 2, output restriction cases 1 & 2, and fluctuations are minimal. All of the data which will be used for the IPL calculation have already been temperature corrected by Eq. (6). Since at least one data point with minimal loss for each irradiance level is needed in order to calculate the IPL, the evaluation period must be at least 3 weeks. The IPL is calculated using the following steps.

1. Select the minimal loss data (see Section 3.5).
2. Perform temperature correction [see Eq. (6)].
3. Select the data at an irradiance of more than 0.4 kW/m^2.
4. Plot the selected data on the scatter diagram of the array output as the Y axis with the irradiance as the X axis.
5. Calculate the regression line which will pass through the origin and the top 3% of the data.

The reason why we select the data at an irradiance of more than 0.4 kW/m^2 in step 3 is that most of the data on

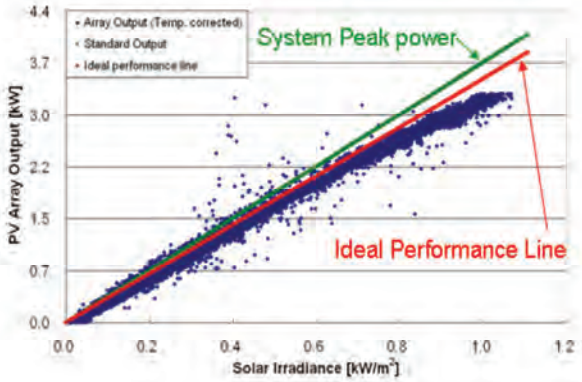

Fig. 7. Example of ideal performance line.

cloudy days and at peak reflection loss are usually observed when the irradiance is less than 0.4 kW/m^2. Figure 7 shows an example of the IPL calculation.

After the calculation of the IPL, the following equations are used to quantify the losses for each factor. All of the data have already been classified in Section 3.5. Equations (9), (10), (11), (12), (14), (15), (16), and (17) are used exclusively for the data rather than cumulatively:

$$l_{IPL} = E_{AS} - E_{IPL} \tag{8}$$

$$l_{PCO} = E_{IPL} \tag{9}$$

$$l_{PCC1} = E_{IPL} - E_A \tag{10}$$

$$l_{OR1} = E_{IPL} = E_A \tag{11}$$

$$l_{OR2} = E_{IPL} - E_A \tag{12}$$

$$l_T = E_{AT} - E_A \tag{13}$$

$$l_{PCC2} = E_{IPL} - P_{PCS} \cdot [\text{hour, min or sec}] \tag{14}$$

$$l_T = P_{PCS} \cdot [\text{hour, min or sec}] - E_A \tag{15}$$

$$l_F = E_{IPL} - E_{AT} \tag{16}$$

$$l_O = E_{IPL} - E_{AT} \tag{17}$$

$$l_{PCS} = E_{PCS} - P_A \cdot [\text{hour, min or sec}] \tag{18}$$

where

E_{IPL} is the output power on the ideal performance line (kWh),

E_A is the array output energy (kWh),

E_{AT} is the temperature-corrected array output energy (kWh),

l_{IPL} is the loss due to dirt and to degradation and variation of module peak power,

l_{PCO} is the loss due to PCS-off,

l_{PCC1} is the loss due to PCS capacity shortage case 1,

l_{OR1} is the loss due to output restriction case 1,

l_{OR2} is the loss due to output restriction case 2,

l_T is the loss due to temperature increase,

l_{PCC2} is the loss due to PCS capacity shortage case 2,
l_F is the loss due to fluctuation and MPP mismatch,
l_O is miscellaneous loss,
l_{PCS} is the PCS loss, and
E_{PCS} is the PCS output energy (kWh).

3.7 Calculating the performance ratio and losses

After loss quantification, the performance ratio and the relative sizes of the losses are calculated. The performance ratio uses the reference yield as the denominator and the system yield as the numerator. The reference yield is the time needed to supply the total input irradiation of the PV system from the STC irradiance. The system yield is the time needed to generate the total output energy from the system rated output power. The ratio of each loss to the reference yield is also calculated. It should be noted that a spectral mismatch between the STC irradiance and the actual irradiance may cause some loss, but it is included in miscellaneous losses in this method because of the difficulty of loss quantification for spectral mismatch.

4. Results and Discussion

4.1 Monthly analysis results

The evaluation periods used in this analysis were March 15 to April 25, June 1 to July 9, and August 10 to September 12, 2004. Eight PV systems with no shading were selected for the evaluation. Since each system had a few missing days of monitoring data, the total number of days for each analysis was about 30 days. Figures 8 and 9 show pie charts of the results of analysis. One hundred percent of the pie chart is the reference yield, and the performance ratio and the loss ratios are summarized in the

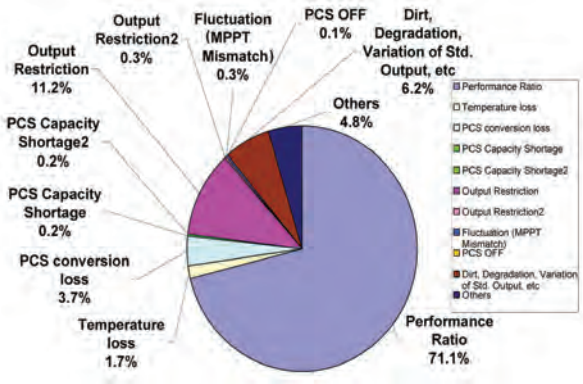

Fig. 8. Result, Site A, 2004/03/15–2004/04/25.

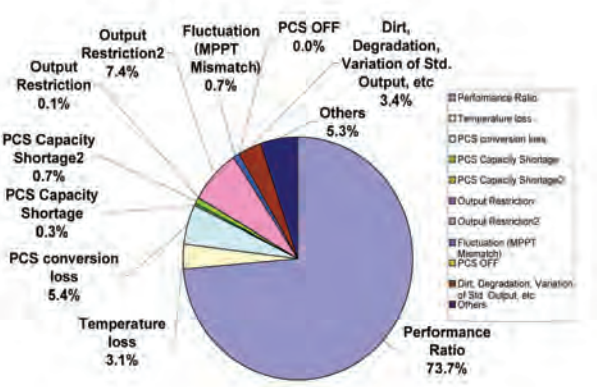

Fig. 9. Result, Site B, 2004/08/10–2004/09/12.

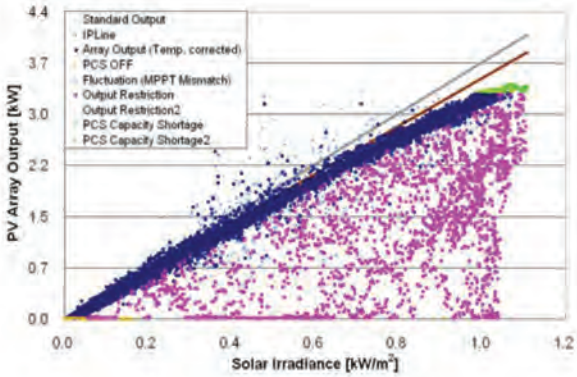

Fig. 10. Result, Site A, 2004/03/15–2004/04/25.

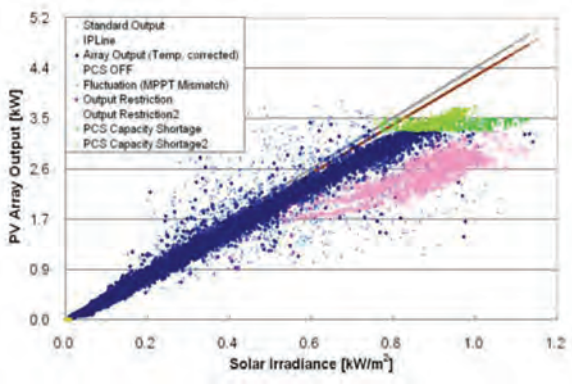

Fig. 11. Result, Site B, 2004/08/10–2004/09/12.

chart. Figure 8 represents one of the worst cases for output restriction case 1. Figure 9 represents one of the worst cases of output restriction case 2. Scatter plots of these results are also shown in Figs. 10 and 11. The data have already been assigned to loss factors and are plotted in different colors. The performance ratio of the result in Fig. 8 is 71.1%, which is equivalent to 306.9 kWh. It is clear that 11.2% of the possible energy output is lost due to output restriction case 1.

4.2 Daily analysis results

Daily analysis of the above two examples was also performed to investigate output restrictions in more detail. The results are shown in Figs. 12 and 13. The output restriction in Fig. 12 occurred on only a few specific days, and the rest of the days have few losses. In particular, on March 28, 2004, 73% of possible energy output was lost due to the grid voltage. On the other hand, output restriction case 2 in Fig. 13 occurred more frequently than case 1 in Fig. 12, but the daily losses are smaller than those of the worst case in case 1. In more detail, 1-minute data on the array output power, incoming irradiance, and PCS output terminal voltage are plotted in Figs. 14 and 15. The PV array output power increased along with the irradiance in the early morning in Fig. 14, but once the PCS terminal voltage reached about 107.5 V, which is the starting voltage of restriction, the output power was significantly restricted until around 6 pm. It is also shown in Fig. 14 that almost 100% of the possible energy output was lost due to over-voltage of the PCS output terminal at about 4 pm. The changes of the voltage and the PCS output power are not exactly matched because of the speed of the output restriction and reactive power control, but the change of the irradiance shows a clear-day pattern and no fast fluctuations were to be expected on this day. The significant loss can be

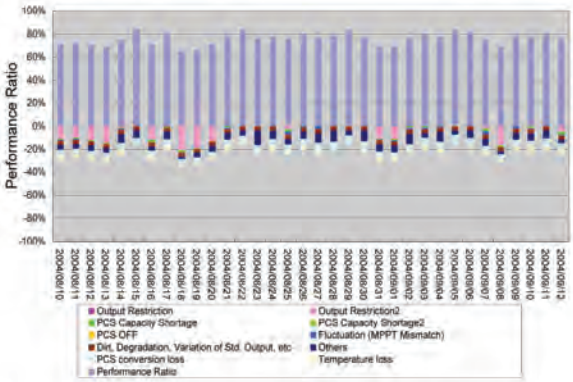

Fig. 13. Daily result, Site B, 2004/08/10–2004/09/12.

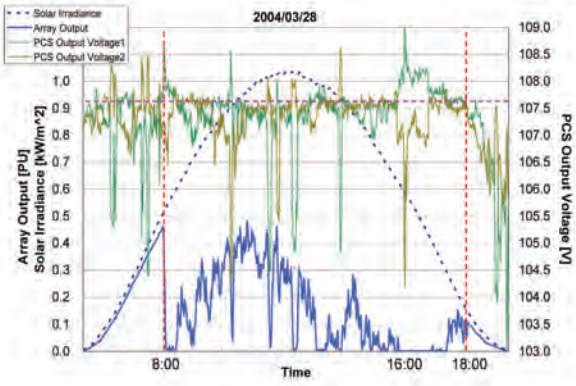

Fig. 14. Daily result, Site A, 2004/03/28.

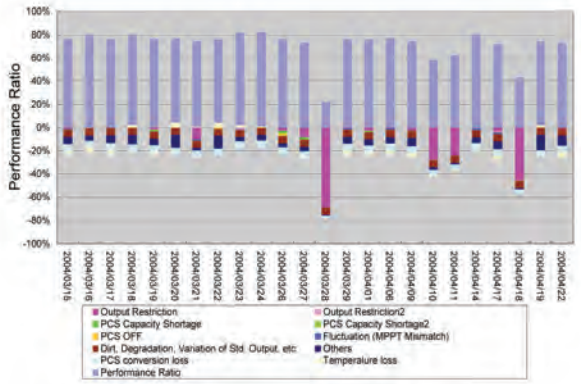

Fig. 12. Daily result, Site A, 2004/03/15–2004/04/25.

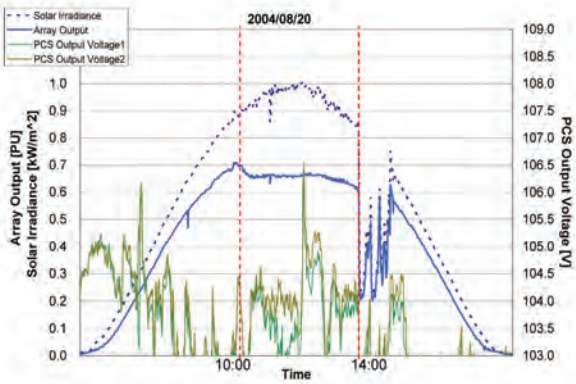

Fig. 15. Daily result, Site B, 2004/08/20.

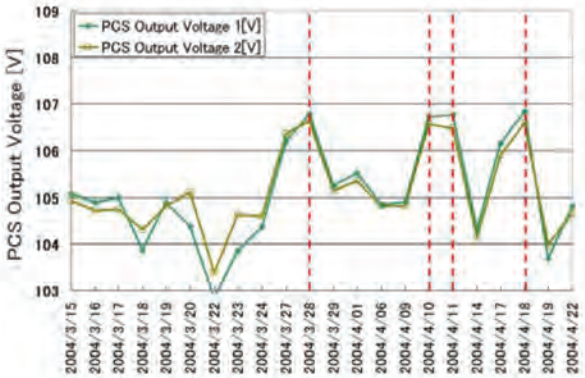

Fig. 16. PCS output voltage, Site A, 2004/03/15–2004/04/22.

assumed to be the loss due to output restriction case 1. Daily PCS output terminal voltages are also shown in Fig. 16. Higher voltages are observed on the days which have significant energy loss due to output restriction case 1 (see March 28, April 10, 11, and 18 in Figs. 12 and 16). From these results, it can be concluded that the method presented in this paper can accurately detect and quantify losses due to output restriction case 1, which prevents overvoltage on the power grid.

Since the PCS output terminal voltage on August 20 at PV site B (Fig. 15) did not exceed 107 V, these restrictions are assigned to case 2. Restriction started at about 10 am in Fig. 15 and continued until 2 pm, the time at which a shadow passed over the system. The fluctuation of the irradiance was not so fast during restriction. This kind of restriction appears to be associated with over-temperature protection, which is discussed in Section 3.5 (3). The

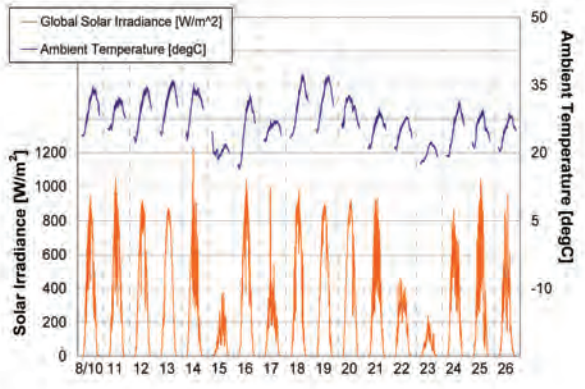

Fig. 17. Global solar irradiance and ambient temperature between 2004/08/10 and 2004/08/26.

changes of irradiation and ambient temperature are plotted in Fig. 17. The results indicate that restriction case 2 occurred on a clear day and that the ambient temperature was above 30 °C in most of cases. Although breakage of the PCS's cooling fan is reported in Ref. 8, no PCS breakage was found in this case. However, this system uses a 3.3 kW PCS for a 4.3 kW PV array, so that almost the maximum current is expected on sunny days in summer. Furthermore, this PCS is designed to be installed in a house but was actually installed in outdoor storage because of the requirements of the demonstration project, and thus temperature would be higher in this case. As a result, not only restriction due to the grid voltage but also restriction due to the over-temperature protection is successfully quantified in this method.

5. Conclusions

A quantitative method for analysis of the output energy loss of PV systems due to restriction to prevent overvoltage on the power grid is developed in this paper. The new method uses 1-minute averages of 1-second measured data instead of hourly data. The operation points on the *I–V* curves are successfully estimated in order to detect output restriction. It is confirmed that output restriction is strongly dependent on the PCS output terminal voltage, and the behavior of the output restriction function in the commercial power distribution system is also clarified. Another output restriction due to over-temperature protection of the PCS is also quantitatively analyzed. Using this new method, detailed system performance analysis of clustered PV systems becomes possible and the results of analysis can be applied to battery-integrated PV systems which will be installed in the near future.

Acknowledgments

This research was performed as part of the "Demonstration Research Project on Clustered PV Systems," which is a project of the New Energy and Industrial Technology Development Organization (NEDO). The authors acknowledge the financial support of NEDO and cooperative discussions with project members.

REFERENCES

1. Kandenko Co., Ltd. FY2002 NEDO report: Demonstration research project on clustered PV systems, 2003. (in Japanese)
2. Kurokawa K, Otani K, Sugiura T. Realistic PV performance values obtained by a number of grid-connected systems in Japan. Energy Congress VI, 2000.
3. Japanese Standards Association. JISC8910.

4. Ueda Y, Oozeki T, Kurokawa K, Itou T, Kitamura K, Miyamoto Y, Yokota M, Sugihara H. Evaluation method and data collection method of grid-connected clustered PV system's performance. 15th Annual Conference of Power & Energy Society, IEE Japan, 2004. (in Japanese)
5. Oozeki T, Izawa T, Otani K, Kurokawa K. An evaluation method of PV systems. Solar Energy Mater Solar Cells 2003;75:687.
6. Perez R et al. Modeling daylight availability and irradiance components from direct and global irradiance. Solar Energy 1990;44:271–289.
7. Nishikawa S. Optimum capacity of inverter in PV system with dispersed PV array. Proc JSES/JWEA Joint Conference, p 21–24, 2000.
8. Ransome SJ et al. Advanced analysis of PV system performance using normalized measurement data. 31st IEEE PVSC, 2005.

AUTHORS (from left to right)

Yuzuru Ueda (student member) received his B.S. degree from Shinshu University in 1995 and joined Applied Materials Japan, Inc. as a semiconductor wafer manufacturing process engineer. Since 2004, he has been a graduate student at Tokyo University of Agriculture and Technology. His main areas of interest are PV systems and their evaluation.

Takashi Oozeki (student member) received his bachelor's degree from Nagoya Institute of Technology in 1996 and M.E. degree from Tokyo University of Agriculture and Technology in 2002 and enrolled in the doctoral program. His main interests are PV systems and their evaluation. He is a member of the Japan Solar Energy Society and the Institute of Electrical Engineers of Japan.

Kosuke Kurokawa (member) received his bachelor's degree from Waseda University in 1965 and joined the Electrotechnical Laboratory, ETL, Ministry of International Trade and Industry, where he was engaged in research on energy system technology. Since 1996, he has been a professor at Tokyo University of Agriculture and Technology. His research interests include PV systems and energy systems. He holds a D.Eng. degree, and is a member of the Japan Solar Energy Society and the International Solar Energy Society.

Takamitsu Itou (member) received his M.E. degree from Niigata University in 1997 and joined Meidensha Corporation. He is engaged in power system analysis.

Kiyoyuki Kitamura (member) received his bachelor's degree from Waseda University in 1980 and joined Meidensha Corporation. He is currently engaged in the development of power system monitoring and control systems. He is a member of the Information Processing Society of Japan.

Yusuke Miyamoto (member) received his B.S. degree from Chuo University in 1996 and joined Kandenko Co., Ltd. He is engaged in research on PV systems.

AUTHORS (continued) (from left to right)

Masaharu Yokota (nonmember) received his M.E. degree from Tokyo University of Agriculture and Technology in 1996 and joined Kandenko Co., Ltd. He is engaged in research on PV systems.

Hiroyuki Sugihara (member) received his M.E. degree from Tokyo Denki University in 1976 and joined Kandenko Co., Ltd. He is engaged in research on PV systems. He holds a D.Eng. degree, and is a member of the Institute of Electrical Installation Engineers of Japan.

国際学会･招待講演

［2006 年～2007 年］

AUTONOMY-ENHANCED PV CLUSTER CONCEPT FOR SOLAR CITIES TO MEET THE JAPANESE PV2030 ROADMAP

Kosuke Kurokawa[1], Shinji Wakao[2], Yasuhiro Hayashi[3], Hiroshi Yamaguchi[4], Kenji Otani[4], Masahide Yamaguchi[5], Takafumi Ishii[6] And Yukiyoshi Ono[7]

[1]Tokyo University of Agriculture and Technology – TUAT, Naka-cho, Koganei, Tokyo, 184-8588 Japan email: kurochan@cc.tuat.ac.jp
[2]Waseda University, Okubo, Shinjuku-ku, Tokyo, 169-8555 Japan.
[3]University of Fukui, 3-9-1 Bunkyo, Fukui 910-8507 Japan.
[4]National Institute of Advanced Industrial Science Technology – AIST, Tshukuba, Ibaraki, 305-8568.
[5]Kyoto Head Office, GS Yuasa Corporation, Shimogyo-ku, Kyoto, 600-8007 Japan.
[6]Research & Development dept., Nippon Oil Corporation, Nishi-Shimbashi, Minato-ku, Tokyo 105-8412.
[7]Photovoltaic Power Generation Technology Research Association – PVTEC,.
2-7-19 Hamamatucho, Minato-ku Tokyo, 105-0013 Japan.

ABSTRACT: Japan set up the long-term R&D roadmap called "PV2030" in June 2004. In this article, a base-case scenario is showing that the mass deployment of 100GW PV aggregation will supply 10 % of national electricity up to year 2030. Around a half of this PV installation is assumed to be fulfilled by residential roof top applications. In such a state, PV penetration will reach 100 % or more in the majority of urban areas and might become unable to be harmonised with the conventional power grids beside these regions by ordinary grid-connected system approach allowing frequent and apparent reversal power flow from PVs. The authors propose new concepts to realise a less dependent PV aggregation on the existing power grids consisting of a large number of PV systems including power electronics and energy storages, which is to be called "autonomy-enhanced PV clusters" (AE-PVC). The authors composed a project proposal of feasibility study concerning the concepts of AE-PVC for 1 and a half year time frame and it was adopted by the New Energy and Industrial Technology Development Organisation (NEDO) at the end of August 2004. The aims of this preliminary research are to make R&D direction clear and a process for achieving the targets stated in "PV2030". Early results have already been obtained including conceptual definitions of autonomy-enhanced, community-base clustered PV systems and network simulation for some cases.

Keywords: Grid-connected, Interfaces, Inverter, PV system, Storage.

1 INTRODUCTION

Japan set up the long-term R&D roadmap titled "PV2030" in June 2004 as shown in Figures 1 and 2. In this article, a base-case scenario is showing that the mass deployment of 100GW PV aggregation will supply 10 % of national electricity up to year 2030. About a half of this PV installation is assumed to be brought from residential roof top applications. In such a state, PV penetration will reach almost 100 % in the majority of urban areas and might become unable to be harmonised with the conventional power grid beside these regions by ordinary grid-connected system approach allowing frequent and apparent reversal power flow from PVs. The authors have proposed new concepts to realise a less dependent PV aggregation on the existing power grids consisting of a large number of PV systems including power electronics and energy storages, which is to be called "Autonomy-Enhanced PV Clusters" or AE-PVC. [1], [2]

The authors composed a project proposal of feasibility study concerning the concepts of AE-PVC for one and a half year time frame and it was adopted by the New Energy and Industrial Technology Development Organisation (NEDO) at the end of August 2004, as one of five different categories covering thin-film silicon solar cells, crystalline silicon solar cells, compound types of solar cells, dye-sensitized solar cells, and PV power generation system technology. The aims of these preliminary researches are to make clear R&D direction and a process for achieving the targets stated in "PV2030".

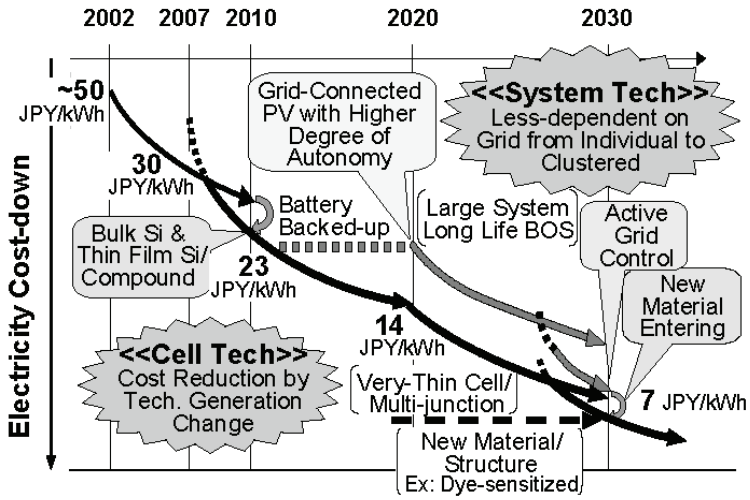

Figure 1: Japanese "PV2030 Roadmap" scenario

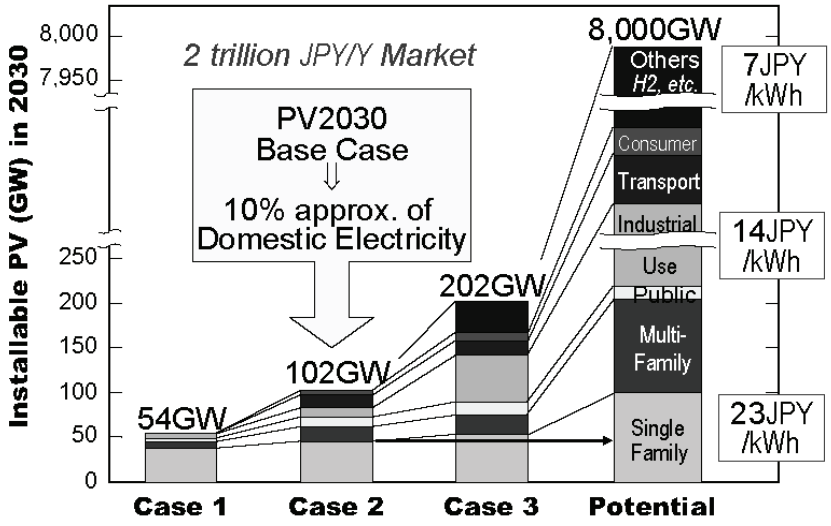

Case 1: Business as usual
Case 2: R&D and Market according PV2030 Base Case
Case 3: Accelerated R&D and Market with large–scale industrial use
Potential: Physical Limit by residential, public, industrial, unused land, etc.

Figure 2: PV roadmap and potential study by the Japanese PV2030

New system technology for the mass deployment of PV systems is being studied in this project. The major concept of this study is to enhance PV system "autonomy", which means a community-base PV clusters less-dependent on external utilities. Feasibility studies are being made on total system concept by simulation and some other key components such as battery station, power electronics for active network control and individual inverters, etc..

2. NECESSITY OF AUTONOMY-ENHANCED PV CLUSTERS:

In Case 2 in **Figure 2**, as the base case for the PV2030, around 40% out of 100 GW PV installation is assumed to be brought from single-family roof-top residential PVs. Therefore, this means almost 100 % PV penetration may be necessary in the majority of urban communities. It is supposed that these kinds of state may produce technical problems to formulate community network as described in **Table 1**.

In addition, the authors believe that the higher degree of the autonomy of the community network, which means less-dependent PV clusters, will give the higher bargaining power to a utility operating the network against external utility company.

Table 1: Possible grid concerns arising from highly-aggregated PV systems and distributed generators

Items	Description	Remarks
Voltage Problem	Unexpected voltage distribution caused by reversal power flow from PVs	the more notable for the larger clusters.
Harmonic Distortion	Multiple Effect of Harmonic Distortion from power conditioners	
EMI	Multiple Effect of EMI from power conditioners	
Grid Protection	· Short circuit capacity increase fed by DGs · Short circuit fault detection failure by DG's UV relay · Islanding chance increased by multiple interaction · Ground fault clearance difficulty by islanding chance increase	negligible for PVs.

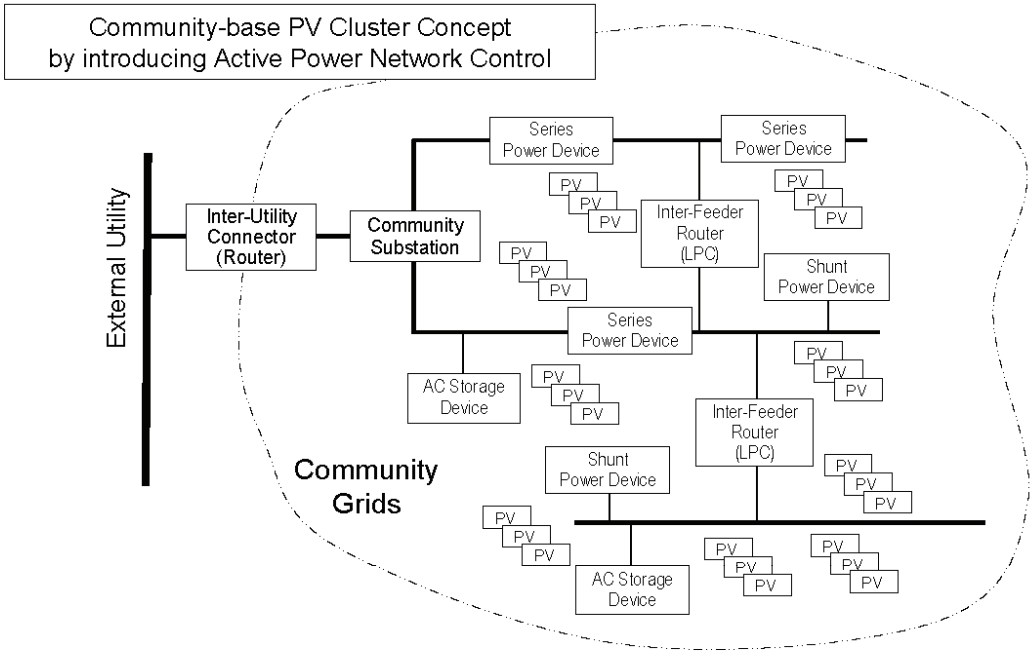

Figure 3: A basic network image of "Autonomy-Enhanced PV Clusters" by utilising power electronic devices and battery storage stations

Figure 3 illustrates a basic image of "Autonomy-Enhanced PV Clusters by utilising power electronic devices and battery storage stations. The former power electronic facilities will bring network control functions to improve grid parameters along the community internal grids by utilizing shunt/serial active components, meshed network, loop power controller (LPC) and so on. The existence of storage devices mainly gives higher degree of autonomy by the following control functions:

- Reversal power flow suppression,
- Demand/supply gap compensation with forecasting functions,
- Suppression of fluctuating power flow from PVs and loads exceeding the governor speed level of outer grids.

By formulating a kind of R&D consortium as show in **Figure 4**, the authors proposed a new

project to NEDO in summer, 2004. This is originally planned as a preliminary stage, with the time frame of 1.5 years, for going to the next stage of more extended R&D as shown in **Figure 5**.

The main objective of this feasibility study stage is planned for one and a half year time frame: *i.e.*,

- Illustrate possible scenarios and technological options toward 2030,
- Study new concepts of total network,
- Develop technological seeds newly required.

To realise this new technological challenge, a research group headed by Prof. K. Kurokawa has been formed under the supervision of the Photovoltaic Power Generation Technology Research Association – PVTEC, consisting of researchers from universities, national laboratory and industries: i.e., TUAT, Waseda Univ., Univ. of Fukui, AIST, GS Yuasa Corp., Nippon Oil Corp. and other institutional cooperation. The authors have already started basic investigations: i.e., conceptual definition of "autonomy-enhanced PV clusters"; extraction of possible technical options, selected case studies for network formations by simulation; key component developments such as SiC devices/conditioners, EDLCs (electric double layer capacitors), battery storage station, power electronic ICs.

The present study has been initiated in October 2004 as the Phase I after the Japanese PV2030 roadmap was published and will be continued until March 2006. The authors are intending that the Phase II of this project will be also proposed to NEDO to be started in FY2006 hopefully for the next 5 year R&D term as shown in **Figure 5**.

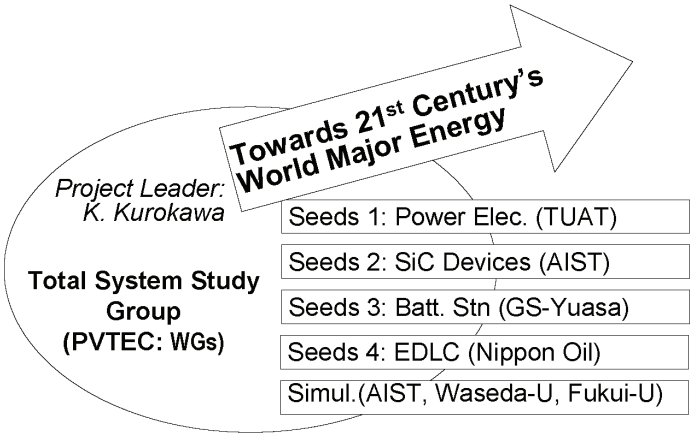

Figure 4: Study group for AE-PVC feasibilty

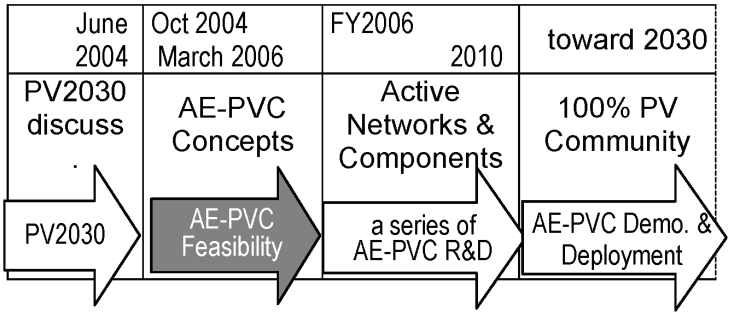

Figure 5: Present project status and possible future plan

3. DEFINITION OF AUTONOMY-ENHANCED PV CLUSTERS:

To achieve highly aggregated residential PV community expected by PV2030, AE-PVC is to be defined as described in Tables 2 and 3. Such PV aggregation can supply sufficient annual energy at the same range of or more than total, regional energy demand. A large number of PV systems are distributed and melted into community grids among scattered residential loads.

There are various strategies to accommodate a large number of (residential) PV systems into urban power networks: e.g.,

Table 2: Basic Definition of Autonomy-Enhanced PV Clusters

Items	Descriptions
Basic Recognition	Residential application is still one of major sectors according to PV2030.
Highly aggregated	Highly aggregated residential community where the annual energy production is at the same range of or more than total, regional energy demand.
Power direction	Downward and upward power flow along the community network.
Less-dependent	A self-controlled unit from the view point of external grids: no reversal power flow outward; no disturbance by internal faults; autonomous power/energy management as far as possible including planned purchase from external utility or IP.
Optimisation	Total optimisation on blank sheet in prospect of future technology advances free from present regulations.

Table 3: Detailed technological mission/definition for Autonomy-Enhanced PV Cluster concept

Studied Cases	· Major cases to meet "PV2030" roadmap scenario. · Residential community-based PV integration. · Technology optimised for 100% PV penetration or more.
Object Loads	· All the residential loads aggregated in a community network.
Reversal Power Flow Occurrence	· Designed for no reversal power flow outward to external utility grids · Community grid connected with inter-grid router in principle. · Battery storage stations provided for internal power and energy management.
Islanding Prevention	· Inter-grid router isolates community grids during external utility grid outage. · Continuing service without internal interruption. · No interference flown outwards during internal faults.
Battery Storage	· Reversal power flow suppression. · Gap compensation between demand & supply. · Forecasting functions of solar input & demands. · Suppression of power flow fluctuation homeward faster than governor control among outer grids.
Active Network Control	· Power electronics such as shunt/serial active components, meshed network, loop power controller (LPC). · Storage devices. · Low voltage grid formation as a unit bunch.
Interactions to and from external utility grids	· On occasion of external utility interruption, community network can continue its service after immediate isolation by an inter-utility router. · Community grids provide means for establishing its own voltage and frequency.

- Consider an appropriate number of PV systems individually connected to utility grids with reversal power flow following an allowable distribution voltage window,
- Divide power flow directions as one from a utility substation to individual residential loads and another from distributed PV systems to the substation respectively,
- Separate a community network entirely from the existing utility grids by providing a certain power electronics and storages for compensating voltage distribution and other grid parameters.

At least in Japan, most of presently existing projects in network issues with distributed

generators are considering the first 2 categories. The authors are now dealing with the third category on a long-term basis seeking for future technical capability apart from present regulatory restrictions.

4. AN EXAMPLE OF EARLY RESULTS

As shown in **Figure 4**, 5 research groups have started their sub-items respectively and been obtaining initial results. PVTEC has also been organising the study group meeting 3 times every month averagely to integrate these results for formulating total concepts. By using these initial results "First Workshop of the Feasibility Study Project on Autonomy-Enhanced PV Clusters was held in Tokyo, May 2005. [3]

Figure 5 shows a typical example among these initial results. In this case study, maximum possible size of low-voltage distribution has been studied. Japanese standard low voltage is specified 100 volt with the voltage window of 101±6 V. It is assumed that 5 kW PV systems is installed for each houses, which has its internal load of 3 kW. A number of PV houses are distributed along 200 V, 3 wire distribution lines as illustrated in the figure. [4]

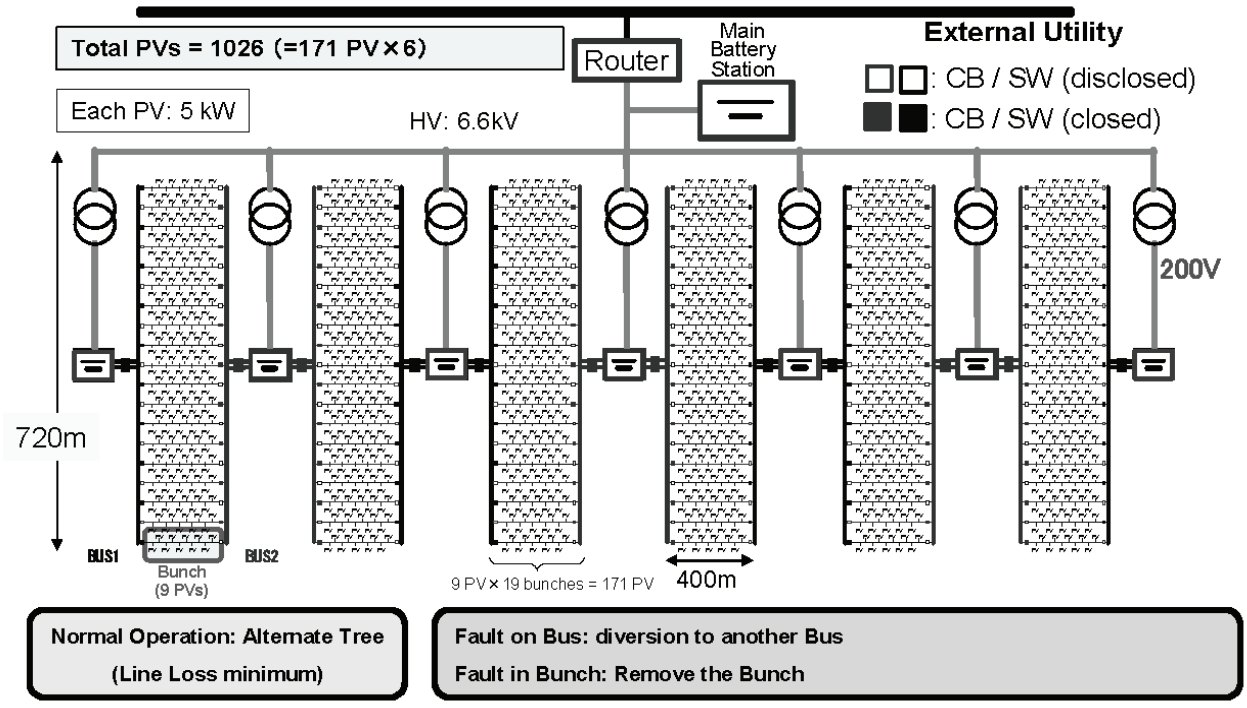

Figure 6:
One of typical example of alternate-Tree concept for AE-PVC community grids

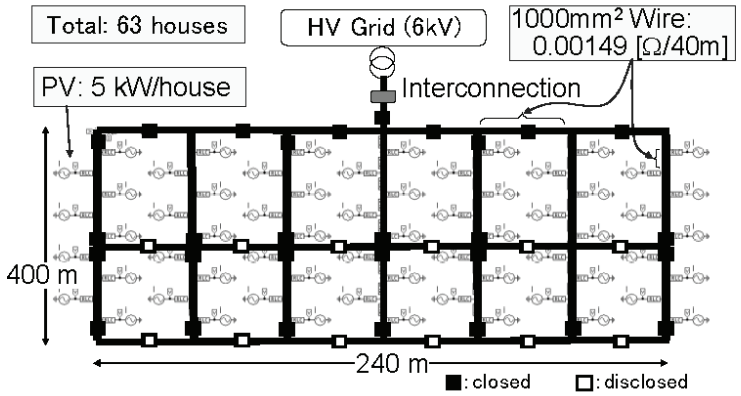

Figure 5: Simulation for low-voltage distribution - most reliable Case

By applying average hourly irradiation data and residential load profile, the direction and amount of power flows are calculated according to different line allocation patterns. The case indicated above is corresponding to most reliable cases, *i.e.*, voltage distribution kept inside the voltage window at any time of irradiation and load profiles under normal operation conditions, distributed line switch utilised for minimising power interruption under line fault condition at a certain point along any lines. Line resistances are assumed as indicated in the figure. Allowable number of PV houses is calculated 63 houses with one low-voltage line.

Maximum line losses for this case are estimated as 4.1 kW corresponding to 1.3 % of total line capacity. The number of interrupted house is suppressed to 5 houses with total loss-of-load of 15 kW.

This low-voltage distribution line is utilised as a unit cluster to integrate a residential community network as illustrated in Figure 6. This is a typical example of our present conceptual studies.

In this figure, a main battery station is provided at the point of utility interconnecting utility, which may be an actively controlled power electronic router. A number of distributed, smaller battery sub-stations may be necessary for improving utilisation factor of distribution line. Small battery or capacitor for each PV power conditioner might also be useful to raise the value of PV system by suppressing flicker arising from residential loads.

4. CONCLUSIONS

The authors have initiated their research works for a new type of system technology for the mass deployment of PV systems is being studied toward PV2030. Early results of them have already been obtained including conceptual definitions of autonomy-enhanced, community–base clustered PV systems and network simulation for some cases. This work is being supported by NEDO under the Ministry of Economy, Trade and Industry.

References

[1] K. Kurokawa & F. Aratani: perceived technical issues accompanying large PV development and Japanese "PV2030", EU-PVSEC, Paris, June 2004, 6DP2.5.

[2] K. Kurokawa: Photovoltaic technology direction - Japanese "PV2030", 31st IEEE-PVSC, Orlando, 3-7 Jan. 2005, Keynote Session 2.

[3] K. Kurokawa, Key note, 1st Workshop of the Feasibility Study Project on Autonomy-Enhanced PV Clusters, Takanawa Prince Hotel, Tokyo, 25 May 2005. (in Japanese)

[4] S. Wakao: Preliminary case studies for autonomy-enhanced PV clusters, 1st Workshop of the Feasibility Study Project on Autonomy-Enhanced PV Clusters, Takanawa Prince Hotel, Tokyo, 25 May 2005. (in Japanese)

[5] K. Kurokawa, et al: Conceptual study on Autonomy-Enhanced PV Clusters for urban community to meet the Japanese PV2030 requirements, EU-PVSEC, Barcelona, June 2005.

[6] Shinji WAKAO, et al: Investigation of the Configuration of Autonomy-Enhanced PV Clusters for Urban Community, PVSEC-15, Shanghai, 10-14 Oct. 2005, PV0654-O5.

[7] Masahide Yamaguchi, et al: Investigation of Battery Storage Station of Autonomy-Enhanced PV Clusters for Urban Community, PVSEC-15, Shanghai, 10-14 Oct. 2005.

A CONCEPTUAL STUDY ON SOLAR PV CITIES FOR 21ST CENTURY

Kosuke Kurokawa
Tokyo University of Agriculture and Technology - TUAT
Naka-cho, Koganei, Tokyo, 184-8588 Japan

ABSTRACT

According to Japan's R&D roadmap "PV2030", a base-case scenario is showing that the mass deployment of 100GW PV aggregation will supply 10 % of national electricity up to 2030. About a half of this PV installation is assumed to be brought still from residential roof-top applications. In such a state, PV penetration will reach almost 100 % in the majority of urban areas. Since the classical grid formation approach does not seems to be a good solution to deal with this issue, the author has already proposed "Autonomy-Enhanced PV Clusters (AE-PVC)" to realize a less dependent PV aggregation on the existing power grids in conjunction with grid power electronics and battery stations. Main contents are: (i) Case studies for residential towns and cities, (ii) Town grids mainly composed of massive residential PVs by considering fluctuating supply and demand; bidirectional power flows; daily cycle and irregular components; autonomous and distributed control of town grid; necessity of battery stations or controllable power sources; own frequency and voltage, (iii) Inter-grid coordination by autonomous and distributed principle: interconnection through national grids with power producers; inter-town interconnections; asynchronous power routers and so on

INTRODUCTION

Japan set up the long-term R&D roadmap titled "PV2030" in June 2004 [1]. A base-case scenario is showing that the mass deployment of 100GW PV aggregation will supply 10 % of national electricity up to year 2030. As shown in Table 1, about a half of this PV installation is assumed to be brought from residential roof top applications. In such a state, PV penetration will reach almost 100 % in the majority of urban areas and might become unable to be harmonized with the conventional power grid beside these regions by ordinary grid-connected system approach allowing frequent and apparent reversal power flow from PVs. The authors have proposed new concepts to realize a less dependent PV aggregation on the existing power grids consisting of a large number of PV systems including power electronics and energy storages, which is to be called "Autonomy-Enhanced PV Clusters" or AE-PVC. [1], [2]

A project of feasibility study was proposed concerning the concepts of AE-PVC for one and a half year time frame to by the New Energy and Industrial Technology Development Organization (NEDO) in August 2004, as one of five different categories covering thin-film silicon solar cells, crystalline silicon solar cells, compound types of solar cells, dye-sensitized solar cells, and PV power generation system technology.

Table 1. Fractions of single family houses

Positions	Potential (P)	PV2030 (C2)	P/C2
Single Family	1.3 %	44.6 %	45.0 %
Multi Family	1.3 %	16.2 %	15.6 %
Public	0.2 %	10.2 %	74.3 %
Industry	3.6 %	10.0 %	3.5 %
Road/Rail	0.7 %	14.5 %	26.9 %
Business	0.4 %	4.5 %	14.4 %
Unused Space	92.5 %	0.0 %	0.0 %
Total	7,985 GW	102 GW	1.3 %

New system technology for the mass deployment of PV systems is being studied in this project. The major concept of this study is to enhance "PV system autonomy", which means a community-base PV clusters less-dependent on external utilities. Such concepts can be realized by advanced distribution grids including some key components such as battery station, power electronics for active network control and individual inverters, etc..

CASE STUDIES FOR RESIDENTIAL COMMUNITY

In Case 2 in Fig. 1 and Table 1, as the base case for the PV2030, around 44.6% out of 102 GW PV installation is assumed to be brought from single-family roof-top residential PVs. It also corresponds to 45% the existing single-family houses over the nation.

Table 2 summarizes a statistics of residential areas per 1 km^2 block size. There are 11,654 blocks accommodating more than 1000 households over Japan. It is found that blocks mainly composed of single family houses corresponds to 8,3535. If these houses are all covered by 5 kW roof-top PV, it makes 42.7 GW in total.

Table 2. A case study of single-family house aggregation

Number of households exceeding 1000	Extracted blocks = 11,654
Residential neighborhood blocks corresponding to 1 km^2	
Roof-top PV installable blocks	8,535
Potential: 5 kW-PV x 1000 houses x 8,536 blocks	42.7 GW

1-4244-0016-3/06/$20.00 ©2006 IEEE

Fig. 1 An example of residential neighborhood unit – Seibu-Kitanodai, Hachioji, Tokyo

Figure 1 shows a typical case for representing residential neighborhood unit consisting of single-family houses, which is Seibu-Kitanodai located in the western suburb of Tokyo. Table 3 gives a case study to clarify a fundamental capability of such an area. Total south-facing, PV-installable area of 132,710 m2 can provide 23.9 MW PV-roofs. This can generate 23.9 GW/Y by assuming 1000 h/Y yield. A single family may consume 6,530 kWh/Y in the case of a fully-electrified house as described later. It is estimated this residential town consumes 21.4 GWh/Y by all houses in total, self-contained factor of which corresponds to 112 %. This is considered meaningful very much.

Table 3. Case study for Seibu-Kitanodai

Number of Houses (single family)	3,280 houses
South-facing Roofs	132,710 m^2
Installable PV by η =18%	23.9 MW
Producible Electricity	23.9 GWh/Y
Energy Consumption*/households	6,540 kWh/Y
Total Consumption	21.4 GWh/Y
Self-contained Factor	112 %

* Fully-electrified case assumed

NECESSITY OF AUTONOMY-ENHANCED PV CLUSTERS

Therefore, this means almost 100 % PV deployment may be necessary in the majority of urban communities. It is supposed that these kinds of state may produce technical problems to formulate community network.

In addition, the authors believe that the higher degree of the autonomy of the community network, which means less-dependent PV clusters, will give the higher bargaining power to a utility operating the network against external utility company.

Fig. 2 illustrates a basic image of "Autonomy-Enhanced PV Clusters by utilizing power electronic devices and battery storage stations. The former power electronic facilities will bring network control functions to improve grid parameters along the community internal grids by utilizing

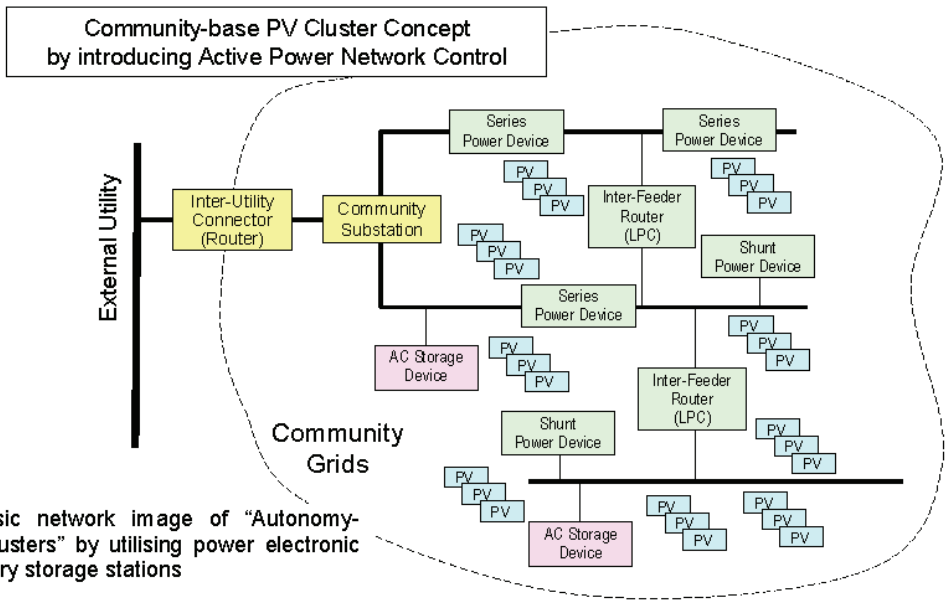

Fig. 2. A basic network image of "Autonomy-Enhanced PV Clusters" by utilising power electronic devices and battery storage stations

shunt/serial active components, meshed network, loop power controller (LPC) and so on. The existence of storage devices mainly gives higher degree of autonomy by the following control functions:

- 100 % reversal power flow from individual PVs permitted inside the community .
- Fluctuating reversal power flow suppression from the community to external grids,
- Orderly demand/supply gap compensation with forecasting functions,

For the first issues above, Fig. 3 gives a concept how to control voltage distribution on distribution grids inside the community. Power electronics adjusts the voltage to be fixed to middle value of allowable voltage window.

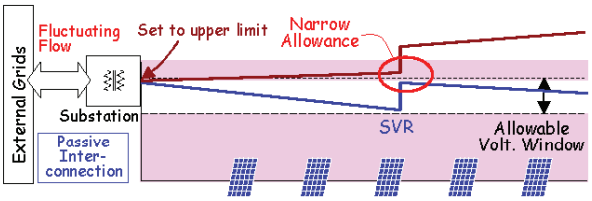

(a) Present approach according to existing regulations

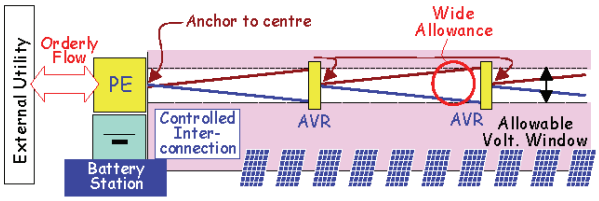

(b) Advanced approach which accept 100 % reversal power flow from PVs

Fig. 3. 2 types of concept of voltage distribution along the grids

The author proposed a new project to NEDO in summer, 2004. This is originally planned as a preliminary stage, with the time frame of 1.5 years, for going to the next stage of more extended R&D.

To realize this new technological challenge, a research group headed by the author has been formed under the supervision of the Photovoltaic Power Generation Technology Research Association – PVTEC, consisting of researchers from universities, national laboratory and industries: i.e., TUAT, Waseda Univ., Univ. of Fukui, AIST, GS Yuasa Corp., Nippon Oil Corp. and other institutional cooperation[4], [5]. They have already completed this feasibility study stage: i.e., conceptual definition of "autonomy-enhanced PV clusters"; extraction of possible technical options, selected case studies for network formations by simulation; key component developments such as SiC devices/conditioners, EDLCs (electric double layer capacitors), battery storage station, power electronic ICs. The research group is intending that the Phase II of this project will be also proposed to NEDO to be started in FY2006 hopefully for the next 4 year R&D term.

Table 4. Basic Definition of Autonomy-Enhanced PV Clusters

Items	Descriptions
Basic Recognition	Residential application is still one of major sectors according to PV2030.
Highly aggregated	Highly aggregated residential community where the annual energy production is at the same range of or more than total, regional energy demand.
Power direction	Downward and upward power flow along the community network.
Less-dependent	A self-controlled unit from the view point of external grids: no reversal power flow outward; no disturbance by internal faults; autonomous power/energy management as far as possible including planned purchase from external utility or IP.
Optimization	Total optimization on blank sheet in prospect of future technology advances free from present regulations.

Table 5. Detailed technological mission/definition for Autonomy-Enhanced PV Cluster concept

Studied Cases	· Major cases to meet "PV2030" roadmap scenario. · Residential community-based PV integration. · Technology optimized for 100% PV penetration or more.
Object Loads	· All the residential loads aggregated in a community network.
Reversal Power Flow Occurrence	· Designed for no reversal power flow outward to external utility grids. · Community grid connected with inter-grid router in principle. · Battery storage stations provided for internal power and energy management.
Islanding Prevention	· Inter-grid router isolates community grids during external utility grid outage. · Continuing service without internal interruption. · No interference flown outwards during internal faults.
Battery Storage	· Reversal power flow suppression. · Gap compensation between demand & supply. · Forecasting functions of solar input & demands. · Suppression of power flow fluctuation homeward faster than governor control among outer grids.
Active Network Control	· Power electronics such as shunt/serial active components, meshed network, loop power controller (LPC). · Storage devices. · Low voltage grid formation as a unit bunch.
Interactions to and from external utility grids	· On occasion of external utility interruption, community network can continue its service after immediate isolation by an inter-utility router. · Community grids provide means for establishing its own voltage and frequency.

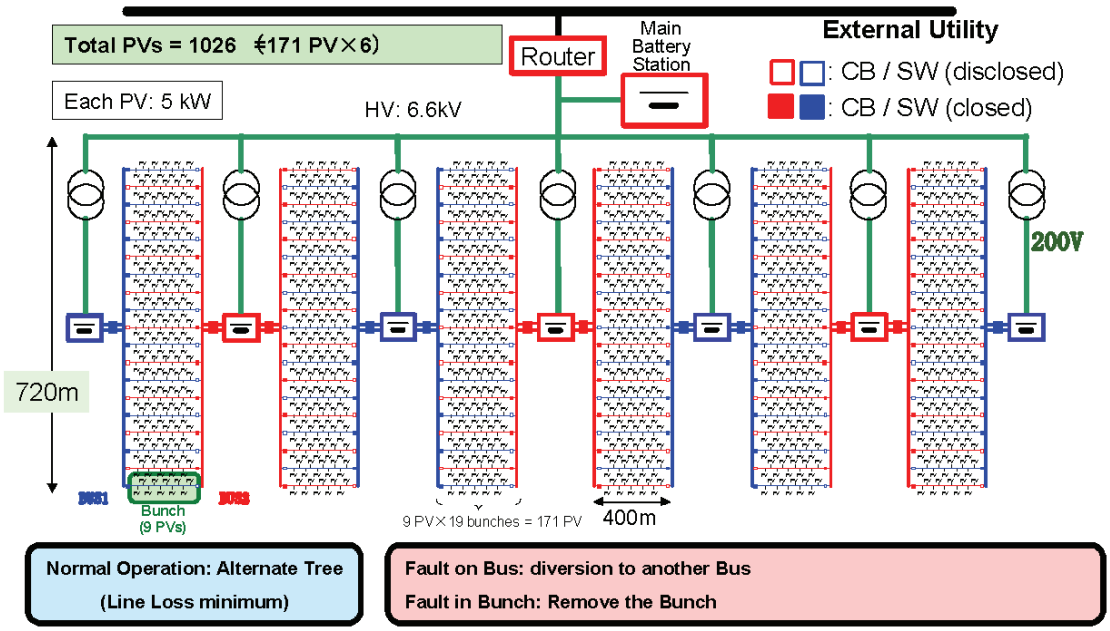

Fig. 4. One of typical example of alternate-Tree concept for AE-PVC community grids

DEFINITION OF AUTONOMY-ENHANCED PV CLUSTERS

To achieve highly aggregated residential PV community expected by PV2030, AE-PVC is to be defined as described in Tables 34and 5. Such PV aggregation can supply sufficient annual energy at the same range of or more than total, regional energy demand. A large number of PV systems are distributed and melted into community grids among scattered residential loads.

There are various strategies to accommodate a large number of (residential) PV systems into urban power networks: e.g.,

- Consider an appropriate number of PV systems individually connected to utility grids with reversal power flow following an allowable distribution voltage window,
- Divide power flow directions as one from a utility substation to individual residential loads and another from distributed PV systems to the substation respectively,
- Separate a community network entirely from the existing utility grids by providing a certain power electronics and storages for compensating voltage distribution and other grid parameters.

At least in Japan, most of presently existing projects in network issues with distributed generators are considering the first 2 categories. The authors are now dealing with the third category on a long-term basis seeking for future technical capability apart from present regulatory restrictions.

STUDIED EXAMPLS ON LOW VOLTAGE GRIDS

While 5 research sub-groups studied their sub-items respectively, PVTEC organized the study group meeting 3 times every month averagely to integrate these results for formulating total concepts. By using these initial results "First Workshop of the Feasibility Study Project on Autonomy-Enhanced PV Clusters was held in Tokyo, May 2005. [3]

Fig. 4 shows a typical example of proposed low voltage distribution grids. In this case study, maximum possible size of low-voltage distribution has been studied. Japanese standard low voltage is specified 100 volt with the voltage window of 101±6 V. It is assumed that 5 kW PV systems is installed for each houses, which has its internal load of 3 kW. A number of PV houses are distributed along 200 V, 3 wire distribution lines as illustrated in the figure. [5],[6]

By applying average hourly irradiation data and residential load profile, the direction and amount of power flows are calculated according to different line allocation patterns. The case indicated above is corresponding to most reliable cases, *i.e.*, voltage distribution kept inside the voltage window at any time of irradiation and load profiles under normal operation conditions, distributed line switch utilized for minimizing power interruption under line fault condition at a certain point along any lines. Line resistances are assumed as indicated in the figure. Allowable number of PV houses is calculated 63 houses with one low-voltage line.

Maximum line losses for this case are estimated as 4.1

kW corresponding to 1.3 % of total line capacity. The number of interrupted house is suppressed to 5 houses with total loss-of-load of 15 kW.

This low-voltage distribution line is utilized as a unit cluster to integrate a residential community network as illustrated in Fig. 5. This is a typical example of our present conceptual studies.
In this figure, a main battery station is provided at the point of utility interconnecting utility, which may be an actively controlled power electronic router. A number of distributed, smaller battery sub-stations may be necessary for improving utilization factor of distribution line. Small battery or capacitor for each PV power conditioner might also be useful to raise the value of PV system by suppressing flicker arising from residential loads.

RESULTS ON BATTERY STATION

Figure 5 shows a configuration of the battery storage station, which consists of bi-directional converter and secondary batteries. The batteries charge the surplus PVs the generated power and provide it to the loads during less generation period or nighttime. Bi-directional converter controls charge/discharge of the batteries to suppress reversal power flow and keep receiving power from utility line as small as possible. Moreover, the converter detects AE-PVC distribution lines current, compensating harmonic current and reactive power from loads. [7]

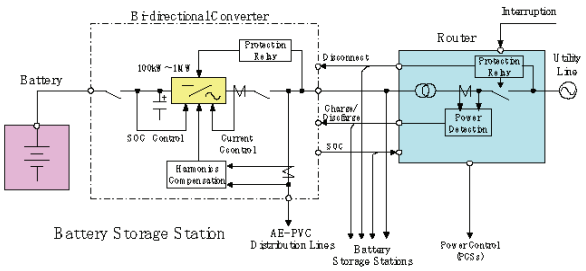

Fig. 5. Configuration of battery storage station

Figure 7 shows the data for day of maximum generation obtained with 5kW PV system in Tokyo, calculated from METPV[8]. Similarly, Fig. 7 shows the residential demand power data of west Japan area calculated by Jyukankyo Research Institute Inc. From these data, the capacity of converter and battery of the battery storage station can be obtained.

As shown in Fig. 7 and Table 6, residential energy consumption is typically given for fully-electrified home for these evaluations. According to pre-study .for identifying necessary PV system output, PV system capacity is specified 7 kW for this home.

Figure 8 shows an annual battery operation profile according to various storage capacities. The calculation of surplus power during daytime and demand power during nighttime from the generated energy and demand. The battery storage station is required to charge surplus power during daytime and supply demand power during nighttime. The capacity of these powers significantly varies depending on month. For example, while a large capacity of surplus power is generated due to plenty of solar radiation in May, the demand increases due to low temperature in February. Thus, it is necessary to store approximately 21 kWh of the surplus power per day in May (21 MWh for 1000 PVs). A typical annual profile of battery operation is given in Fig. 9.

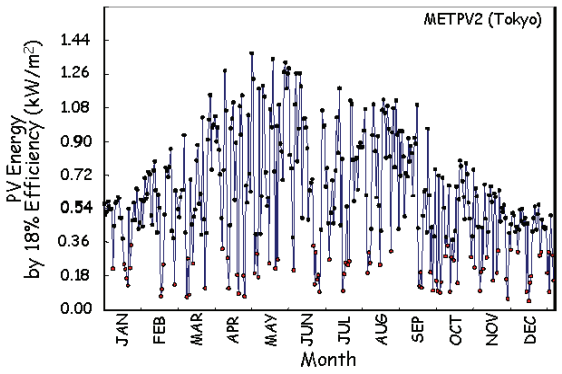

Fig. 6. Hourly generated PV energy for standard irradiation year in Tokyo

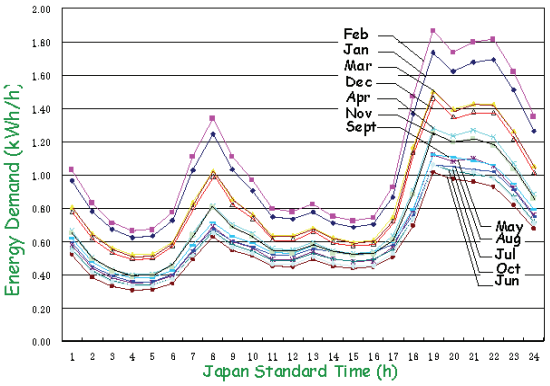

Fig. 7. Monthly-averaged, hourly domestic energy consumption by a fully electrified home in western Japan area

Table 6. Annual domestic energy consumption by a fully electrified home

	MJ/Home/ Year	kWh/Home/Year	Fraction for kWh
Space Heating	2955	821	13 %
Space Cooling	488	135	2 %
Hot Water	4,224	1,173	18 %
Cooking	1,914	532	8 %
Light/Appliances	1,3964	3,879	59 %
Total	2,3545	6,540	100 %

Notes: Thermal energy supplied by electrically driven heat pumps; Cooking by electromagnetic cooker.

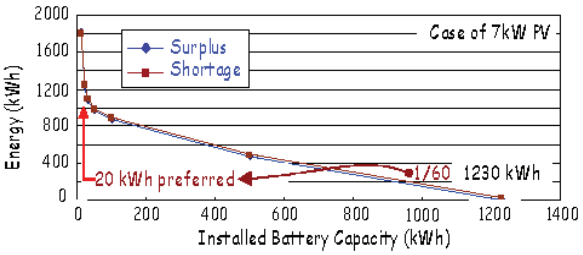

Fig. 8. Annual Battery shortage and PV energy surplus by installed battery capacity

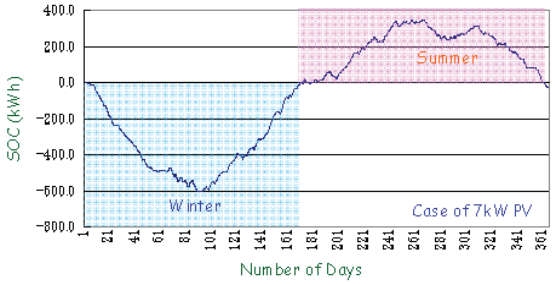

Fig. 9. Annual battery operation profile

INTER-GRID AND INTER-COMMUNITY COORDINATION

Figure 10 shows an image of autonomously interconnected community PV aggregation in order to form a regional electrical network. Town grids are mainly composed of massive residential PVs by considering fluctuating supply and demand; bidirectional power flows; daily cycle and irregular components; autonomous and distributed control of town grid; necessity of battery stations or controllable power sources; own frequency and voltage.

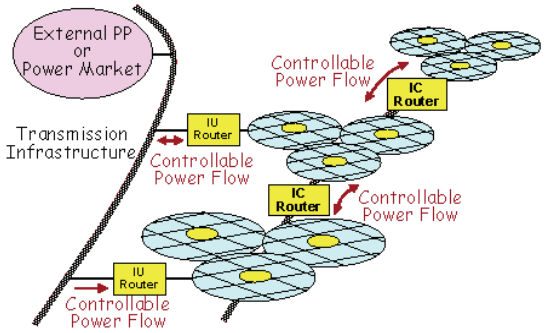

Fig. 10 A future image of "Energy Internet"

In this case, any centralized control units are not preferred to realize real distributed system like internet in the field of telecommunication network. Key technical requirements for this concept of "energy Internet" may be illustrated as follows:

- A synchronous router for inter-community and inter-utility interconnection to allow operating under different frequency.
- Distributed control strategy, which controls the frequency, P/Q flow and voltage of own terminal according to operational information at own terminals only.
- Pre-specified orderly inter-flow given by battery station control and forecasted PV total output.
- Routers and battery station varies system frequency according to their burden share of output power.
- From the existing external power network, the whole community grids to be treated as one system controlled in orderly manner.

CONCLUSIONS

The author has initiated their research works for a new type of system technology for the mass deployment of PV systems is being studied toward PV2030. Some results of them are presented including conceptual definitions of autonomy-enhanced, community–base clustered PV systems and network simulation for some cases and so on. This work is being supported by NEDO under the Ministry of Economy, Trade and Industry.

REFERENCES

[1] K. Kurokawa & F. Aratani: perceived technical issues accompanying large PV development and Japanese "PV2030", EU-PVSEC, Paris, June 2004, 6DP2.5.

[2] K. Kurokawa: Photovoltaic technology direction - Japanese "PV2030", 31st IEEE-PVSC, Orlando, 3-7 Jan. 2005, Keynote Session 2.

[3] K. Kurokawa, Key note, 1st Workshop of the Feasibility Study Project on Autonomy-Enhanced PV Clusters, Takanawa Prince Hotel, Tokyo, 25 May 2005. (In Japanese)

[4] K. Kurokawa, S. Wakao, Y. Hayashi, I. Ishii & K. Otani, M. Yamaguchi, T. Ishii, Y. Ono: Conceptual Study on Autonomy-Enhanced PV Clusters for Urban Community to Meet the Japanese PV2030 Requirements, 20th EU-PVSEC, Barcelona, 2005.6.6-10, 6DP.2.3.

[5] S. Wakao: Preliminary case studies for autonomy-enhanced PV clusters, 1st Workshop of the Feasibility Study Project on Autonomy-Enhanced PV Clusters, Takanawa Prince Hotel, Tokyo, 25 May 2005. (In Japanese)

[6] S. Wakao, y. Hayashi, n. Ueda, a. Onoyama, k. Kurokawa, m. Yamaguchi, k. Otani, y. Ono: Investigation of the Configuration of Autonomy-Enhanced PV Clusters for Urban Community, PVSEC-15, Shanghai, 10-14 Oct. 2005, PV0654-O5.

[7] M. Yamaguchi, T. Kawamatsu, T. Takuma, K. Kurokawa, K. Otani, S. Wakao, Y. Hayashi, Y. Ono: Investigation of Battery Storage Station of Autonomy-Enhanced PV Clusters for Urban Community, PVSEC-15, Shanghai, 10-14 Oct. 2005.

[8] A. Itagaki, H. Okamura, and M. Yamada: Preparation of meteorological data set throughout Japan for suitable design of PV systems, WCPEC-3, Osaka, May 2003.

A SENSITIVITY ANALYSIS OF VERY LARGE-SCALE PHOTOVOLTAIC POWER GENERATION (VLS-PV) SYSTEMS IN DESERTS

Masakazu Ito[1], Kazuhiko Kato[2], Keiichi Komoto[3], Tetsuo Kichimi[4], Kosuke Kurokawa[5]

[1]Tokyo Institute of Technology
[2]National Institute of Advanced Industrial Science and Technology (AIST)
[3]Mizuho Information & Research Institute (MHIR)
[4]Resources Total System (RTS)
[5]Tokyo University of Agriculture and Technology (TUAT)

ABSTRACT

A preliminary study on potential of Very Large Scale Photovoltaic Power Generation Systems (VLS-PV) in deserts from economical and environmental view points has been studied. However, the data in the studies depend on site, country, price and so on. Therefore, a sensitivity analysis of the studies should be obtained. In this paper, five case studies of sensitivity analysis of VLS-PV systems were evaluated from economical and environmental view points. Case studies were set five cases; (1) PV module efficiency, (2) PV module degradation, (3) interest ratio and depreciation period, (4) labor cost and (5) cable.

In summary, generation cost was affected by degradation, interest ratio, depreciation period and labor cost. Required energy and CO_2 emission were affected by PV module efficiency and degradation ratio.

BACKGROUND AND OBJECTIVE

A preliminary study on potential of Very Large Scale Photovoltaic Power Generation (VLS-PV) Systems in deserts from economical and environmental view points has been studied [1]. This is a part of study of IEA/PVPS Task 8. Authors focus on desert land area where there are rich sunshine and huge land, and have proposed a combination of the desert and Very Large-Scale Photovoltaic Power Generation Systems which are connected to power transmission lines. The VLS-PV systems have been evaluated payability, environmental impacts, transmission losses and so on. In addition, author have been showed the possibility to contribute to energy resource saving and mitigation of environmental problems, and propose practical systems to accelerate utilization of very large scale photovoltaic systems.

In order to evaluate VLS-PV systems, Life-Cycle Analysis (LCA) has been employed. It is a major tool to evaluate environmental impacts of products. As a result, energy payback time has been obtained as 2-3 years, and the CO_2 emission rate has been obtained as 11-20 g-C/kWh. Generation cost has been approximately 11 UScent/kWh using 2 USD/W PV modules, and 7 UScent/kWh using 1 USD/W PV modules.

However, the data in the studies depend on site, country, price and so on. Therefore, a sensitivity analysis of the studies should be obtained. In this paper, authors studied 5 sensitivity analyses, which are PV module efficiency, PV module degradation, interest ratio, depreciation period, labor cost and cable.

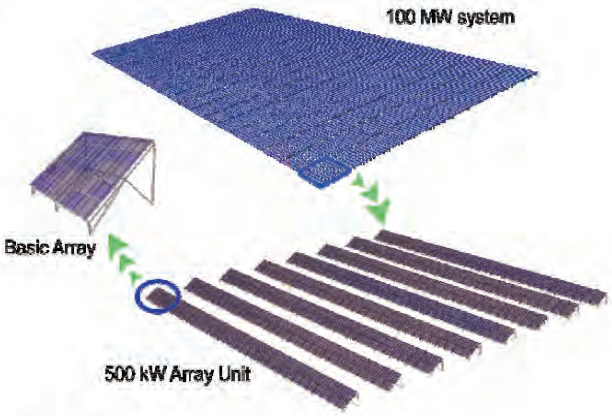

Fig.1 An image of a VLS-PV system

APPROACHES AND RESULTS

At first, we set "Base case" which is evaluated by LCA method. It is same evaluation way as our studies before [2]. Assumptions of the base case are; PV module is 15.8 efficiency multi-crystalline silicon, interest ratio is 3 percent and depreciation time is 30 years.

1) A sensitivity analysis for PV module efficiency

To evaluate sensitivity of PV module efficiency for VLS-PV systems, we set six case studies. They are about (1) generation cost as shown in the Fig. 2 , (2) energy pay-back time and CO_2 emissions rate in Fig. 3, (3) amount of steel and foundation for PV system arrays in Fig. 4, (4) number of labors in Fig. 5, (5) annual cost in Fig. 6, (6) energy requirement and CO_2 emissions in Fig. 7. For each case study, five module efficiencies which are 6, 10, 15.8, 20 and 30 percent were set and evaluated.

1-4244-0016-3/06/$20.00 ©2006 IEEE

As a result, in case of same module price for a VLS-PV system, module efficiency affected generation cost a little as shown in Fig. 2. High efficiency module reduced array support structures, foundations and labors as shown in Fig. 4 and 5. However steel and concrete cost was small as shown in Fig. 6. However, they reduced much energy and make much CO_2 emissions as shown in Fig. 7. Therefore high efficiency module reduced EPT and CO_2 emission rate as shown in Fig. 3, and was effective for environmental issue.

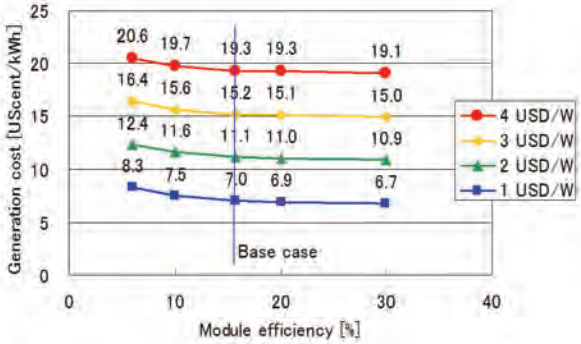

Fig. 2 Effect of module efficiency to generation cost

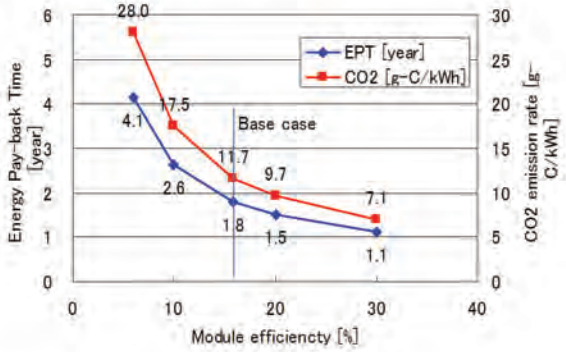

Fig. 3 Effect of module efficiency to Energy pay-back time and CO2 emissions rate

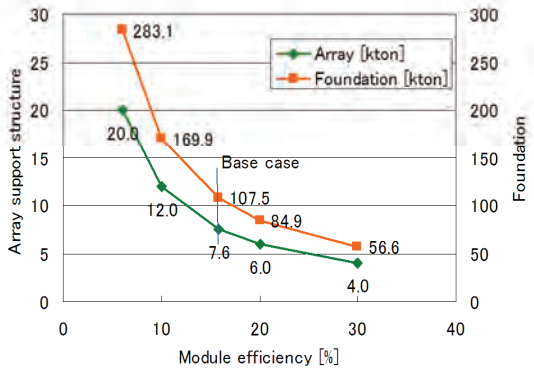

Fig. 4 Effect of module efficiency to amount of steel and concrete

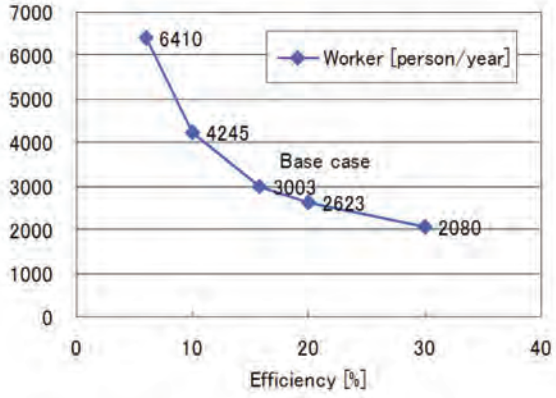

Fig. 5 Effect of module efficiency to labor

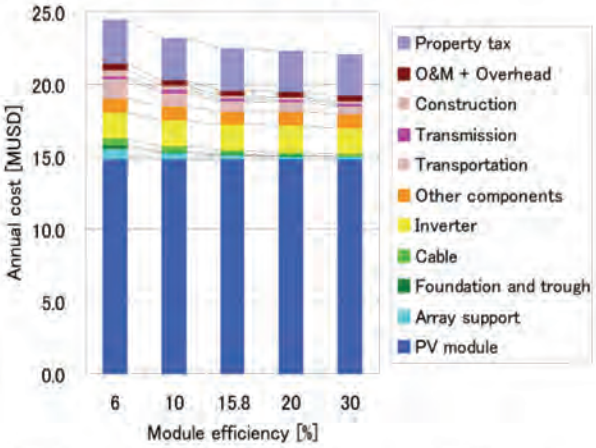

Fig. 6 Effect of module efficiency to annual cost (except for 3 USD/W module cost)

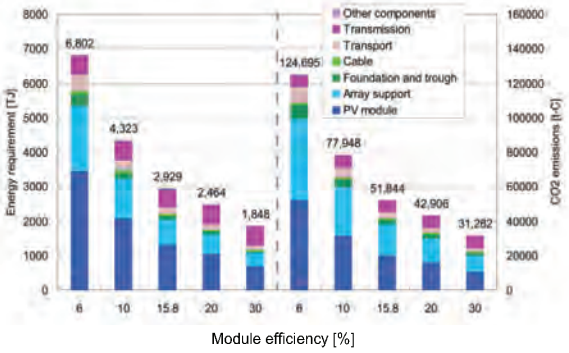

Fig. 7 Effect of module efficiency to Energy requirement and CO_2 emissions

2) A sensitivity analysis for PV module degradation ratio

0.5, 1.0 and 1.5 percent per year degradation ratios were set for the analysis. Increase of 0.5 % degradation ratio caused 7 to 8 percent increase of generation cost,

energy pay-back time and CO_2 emissions rate as shown in Fig. 8. Degradation ratio affected them directly.

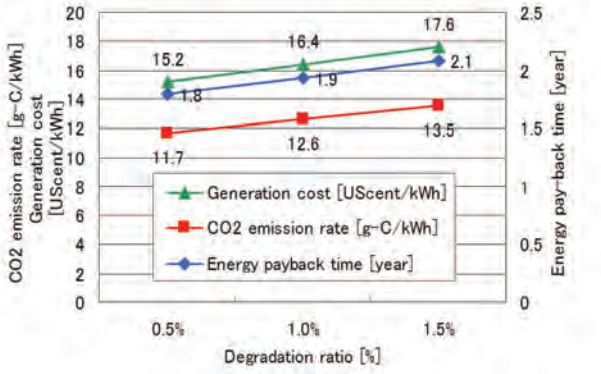

Fig. 8 Effect of degradation ratio to cost, energy and CO2

3) A sensitivity analysis for interest ratio and depreciation time

Interest ratio was set 1.0, 2.0, 3.0 and 6.0. Depreciation time was set 30 and 20 years. If interest ratio decrease from 3.0 to 1.0 percent, generation cost become 70 percent. 20 years depreciation time increased 20 to 30 percent of generation cost of 30 years case.

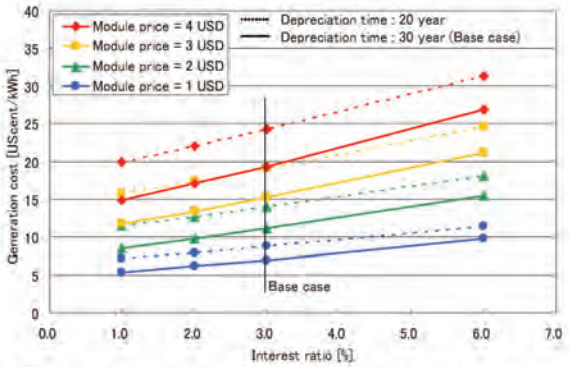

Fig. 9 Effect of interest ratio to generation cost

4) A sensitivity analysis for labor cost

Wage is very different between countries, and it affects construction cost strongly. However, in case of 4 USD/W PV module price, the effect was not very big. But in case of 1 USD/W PV module price, highest country's generation cost was twice as lowest country.

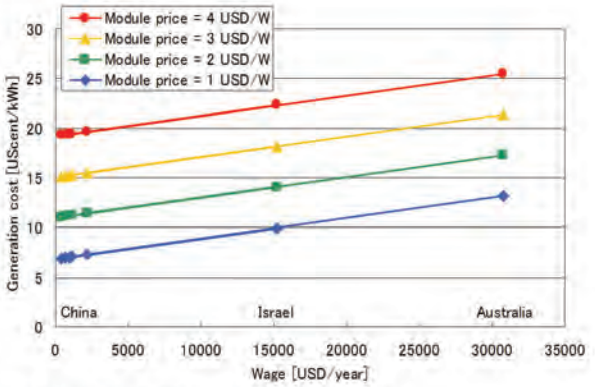

Fig. 10 Effect of wage to generation cost

5) A sensitivity analysis for cable

All cables are faced with compliance standards [3]. However, cable should be selected by consideration of cable cost and electricity loss. In this analysis, three kinds of cables for three DC sections were evaluated to investigate suitable cables. Fig. 11 is a result of the cable cost. In the left part of the figure, cable from module to first junction box was changed from 2 sq to 5.5 sq. In central part, cable from first junction box to second junction box was changed form 5.5 sq to 14 sq. In right part, cable from second junction box to inverter was changed from 150 sq to 250 sq. Cable cost of left and right part of the Fig. 11 was changed. However, differences of generation cost between cables were very small as shown in Fig. 12. In addition, increase of cable cost did not effect to EPT and CO_2 emission rate as shown in Fig. 13.

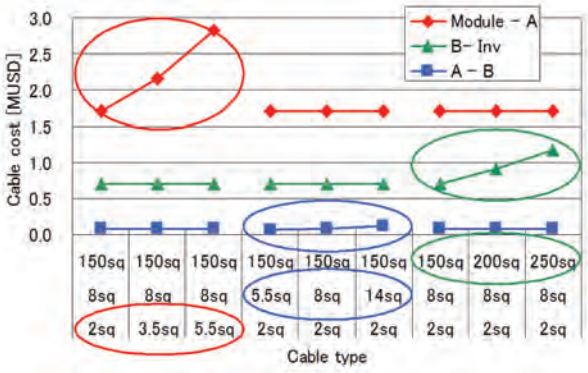

Fig. 11 Effect of cable type to cable cost

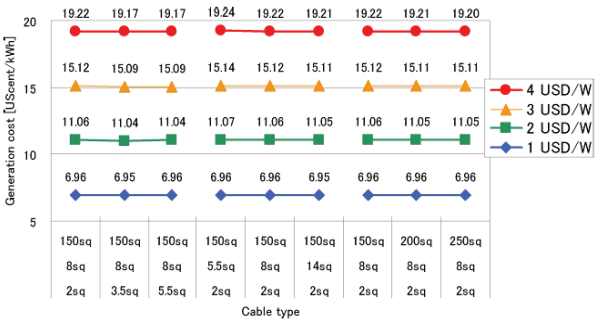

Fig. 12 Effect of cable type to generation cost

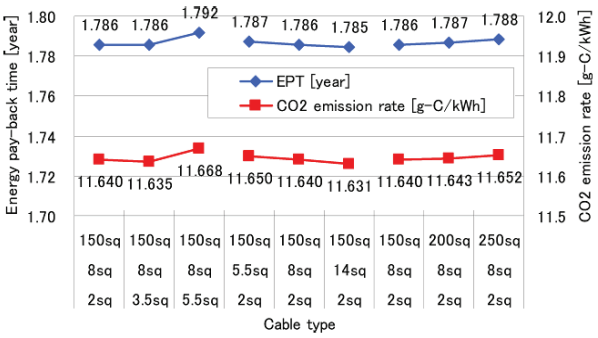

Fig. 13 Effect of cable type to EPT and CO_2 emission rate

CONCLUSION

In this paper, five case studies of sensitivity analysis of VLS-PV systems were evaluated from economical and environmental view points. Five case studies were; (1) PV module efficiency, (2) PV module degradation, (3) interest ratio and depreciation period, (4) labor cost and (5) cable.

From case study (1), PV module efficiency affected generation cost little. This result might be affected by module price which was set same price (USD/W) for all efficiency modules in this study. However, module efficiency affected energy and CO_2 emissions strongly. The reason was that change of module efficiency caused big change of amount of array support and foundation which require much energy and emit CO_2 emissions.

Degradation ratio in case study (2) affected economic and environmental points. Because it affected electricity output directly.

Interest ratio, depreciation period and labor cost in case study (3) and (4) affected generation cost strongly. Change of cable in case study (5) did not effect generation cost, energy requirement and CO_2 emissions even allowing electricity loss. Because cable did not take big part of cost, energy requirement and CO_2 emissions.

In summary, generation cost was affected by degradation, interest ratio, depreciation period and labor cost. Required energy and CO_2 emission were affected by PV module efficiency and degradation ratio.

REFERENCES

[1] M. Ito et al., "Comparative Study of m-Si, a-Si and CdTe System of Very Large-Scale PV (VLS-PV) Systems in Desert", *20th EU-PVSEC*, 2005, pp. 2178-2181.
[2] K. Kurokawa et al., "*Energy from the Desert*", James and James, 2003
[3] "*Electric wire manual*", Fujikura co., Ltd. (in Japanese)

VOLTAGE SAG/SWELL CONTROLLER BY MEANS OF D-UPFC IN THE DISTRIBUTION SYSTEM

Kyungsoo Lee, Hirotaka Koizumi, Kosuke Kurokawa
Tokyo University of Agriculture and Technology, 2-24-16 Naka-cho, Koganei, Tokyo 184-8588, Japan

ABSTRACT

A power quality issue, especially, voltage problem is the vital concern in most distribution system today. So far, the voltage problem is mainly from under-voltage (voltage sag) condition due to a short circuit or fault. Recently, renewable energy such as photovoltaic (PV) system affects over-voltage (voltage swell) condition caused by its reverse power flow at daylight.

In this paper, proposed Distribution-Unified Power Flow Controller (D-UPFC) for preventing both voltage sag and swell conditions is discussed. The proposed scheme consists of an AC chopper, a switch and a series transformer. The AC chopper generates compensation power when voltage sag or swell condition happens. The secondary and tertiary parts of a series transformer connect with switches for controlling voltage sag or swell. D-UPFC does not need any energy storage devices such as large capacitors or inductors and it provides fast compensation.Simulation results show D-UPFC controls voltage concerns in the distribution system.

INTRODUCTION

Power quality in the distribution system is the important issue for industrial, commercial and residential applications today. The voltage problem is mainly considered from under-voltage (voltage sag) condition caused by short circuit or fault somewhere in the distribution system. Preventing voltage sag condition, many researches have been implemented.

Among the most common are tap-changing transformers, which are the types of voltage regulators used in today's distribution system. However, these methods have significant shortcomings. For instance, the tap-changing transformer requires a large number of thyristors, which results in highly complex operation for fast response. Furthermore, it has very poor transient voltage rejection, and only has an average response time [1].

Recently, renewable energy such as photovoltaic (PV) system is installed in many places. Although PV system has many advantages for future view, a lot of PV systems which are installed in the residential areas together can cause over-voltage (voltage swell) condition due to their reverse power flows. Like tap changing transformer from existing technology, SVR (Step Voltage Regulator) which consists of autotransformer with line drop compensator controls voltage swell as well as voltage sag. Even though SVR controls distribution system's voltage, SVR can not install in every pole transformer place, because we should consider the price of the product. Also, future distribution system will be changed to increasing the installation of renewable energy, especially PV system. Thus, future distribution system might be more complex and there are occuring many problems than today. To solve voltage variations, voltage sag and swell, the author proposes Distribution-Unified Power Flow Controller (D-UPFC) in the distribution system. D-UPFC concept and its function shows in Figure 1.

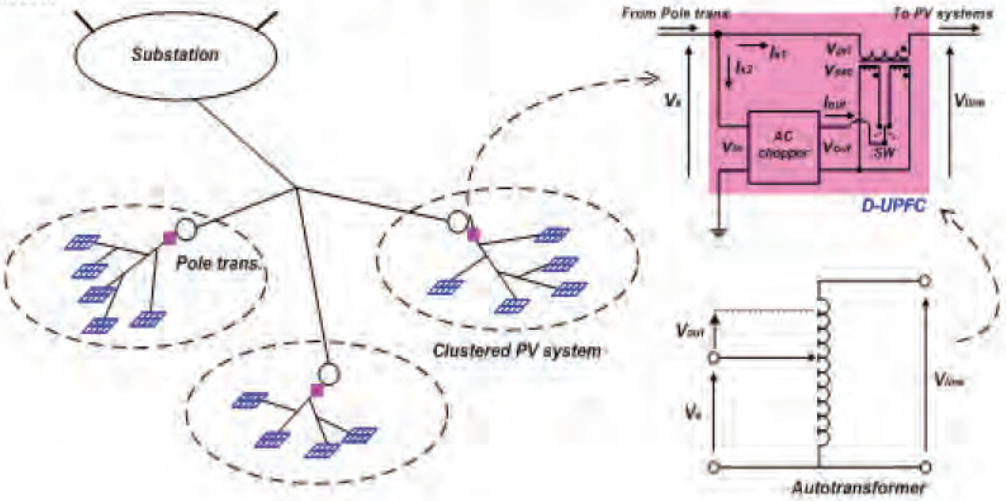

1-4244-0016-3/06/$20.00 ©2006 IEEE

Fig. 1. D-UPFC concept and its function in the distribution system.

It consists of an AC chopper with a series transformer. It places after pole transformer and it controls voltage sag and swell. D-UPFC is also regared as a transformer and thus, pole transformer with D-UPFC function is the same as autotransformer.

This paper discusses the proposed D-UPFC concept and shows distribution voltage control using simulation tool. An AC chopper generates control voltage when voltage sag or swell occurs and a switch connected series transformer selects voltage compensation or regulation. D-UPFC does not use any large energy storage, such as large capcitor or inductor and it fast controls distribution system voltage.

PROPOSED CONCEPT

The concept of D-UPFC is to control distribution system voltage during voltage sag or swell condition. D-UPFC equivalent circuit in order to control voltage effectively is shown in Fig. 2.

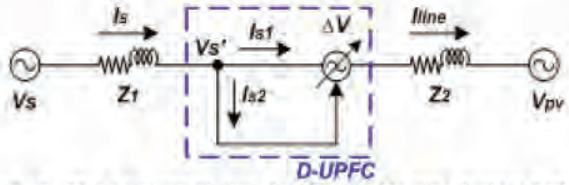

Fig. 2. The equivalent circuit of D-UPFC with clustered PV system.

When voltage variation ΔV happens due to voltage sag or swell in the D-UPFC, the D-UPFC output ΔP is given,

$$\Delta P = \Delta V \times I_{s1} \quad (1)$$

Also, D-UPFC input current I_{s2} due to voltage variation is,

$$I_{s2} = (\frac{\Delta V}{V_s'}) I_{s1} \quad (2)$$

Using Kirchhoff's current law, pole trans. current I_s is given,

$$I_s = I_{s1} + I_{s2} = (1 + \frac{\Delta V}{V_s'}) I_{s1} \quad (3)$$

D-UPFC input voltage V_s' is given,

$$V_s' = V_s - (Z_1 \times I_s) = V_s - Z_1 (1 + \frac{\Delta V}{V_s'}) I_{s1} \quad (4)$$

where, V_s is pole tr. Voltage, V_{pv} is clustered PV system voltage, Z_1 and Z_2 are line impedances (however, Z_1 is very small because D-UPFC connects with pole trans. voltage V_s in the same pole)

Through eq. (1) to (4), the effective D-UPFC control should agree with eq. (5).

$$\left|\Delta V_s'\right| \le \left|\Delta V\right| \quad (5)$$

where, $\Delta V_s'$ is the variation value of V_s'

D-UPFC SCHEME AND CONTROL

D-UPFC scheme

D-UPFC topology and normal state operation show in Fig. 3. D-UPFC consists of an AC chopper, a series transformer and a switch. D-UPFC does not generate power when distribution voltage is at normal state. Switch S_2 and S_3 of AC chopper are ON and also SW_1 always connects with a series transformer. Also, AC chopper operates with Pulse Width Modulation (PWM) control.

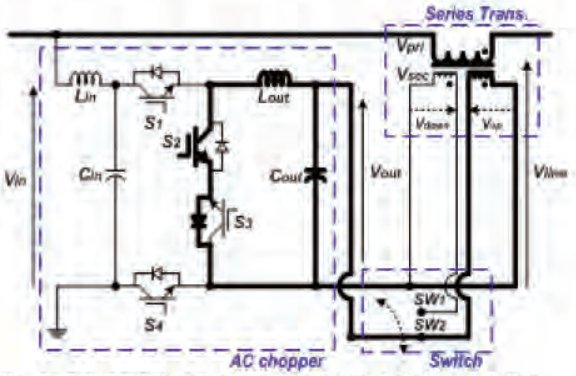

Fig. 3. D-UPFC topology and its normal state operation.

When voltage sag or swell condition happens, D-UPFC performs to generate voltage in order to regulate distribution system voltage. AC chopper output voltage V_{out} is always less than the input voltage V_{in}.

$$V_{out} \le V_{in} \times D \quad (6)$$

where, D is duty ratio

Table 1 shows D-UPFC switches operation during voltage control state.

Table 1. D-UPFC switches operation during voltage control state

** means current flows through reverse diode of the switch*

Mode	Phase	AC chopper				Series trans.	
		S1	S2	S3	S4	SW1	SW2
Voltage UP	+	ON	OFF	OFF	*ON	OFF	ON
		OFF	*ON	ON	OFF	OFF	ON
	-	*ON	OFF	OFF	ON	OFF	ON
		OFF	ON	*ON	OFF	OFF	ON
Voltage DOWN	+	ON	OFF	OFF	*ON	ON	OFF
		OFF	*ON	ON	OFF	ON	OFF
	-	*ON	OFF	OFF	ON	ON	OFF
		OFF	ON	*ON	OFF	ON	OFF

D-UPFC control

D-UPFC senses input voltage, line voltage and line current. Input voltage is the reference voltage because it connects with pole trans. voltage V_s. Line voltage and current represent the D-UPFC output voltage and output current, respectively. Figure 4 shows D-UPFC control in the distribution system. Input voltage V_{in} and line voltage with line impedance V_{line_sum} for controlling PCC (here, PCC is the next pole apart from the pole transformer) voltage and line current I_{line} are sensed and change to Direct Current (DC) values through Root-Mean-Square (RMS) function.

Next, V_{in} and V_{line} are compared each other and then voltage error V_{error} is calculated. V_{error} then changes to reference voltage V_{ref} through propotional (P) control. In the PWM control, V_{ref} and triangle voltage V_{tri} are compared and then this control supplys switching signals to the AC chopper. Also, SW_1 and SW_2, which decide voltage up or down during compensation mode operation using D-UPFC control. D-UPFC uses the voltage margin in order to control distribution voltage flexibly. Pole transformer's secondary voltage range of Japan is 101±6 [V,rms]. If V_{error} is less than 2[V] of voltage margin, D-UPFC does not operate. Voltage margin equation is shown in eq. (7).

$$\left|V_{in} - V_{line\_sum}\right| < 2[V] \quad (7)$$

where, V_{line_sum} means V_{line} plus line impedance Z_2 voltage V_{z2}

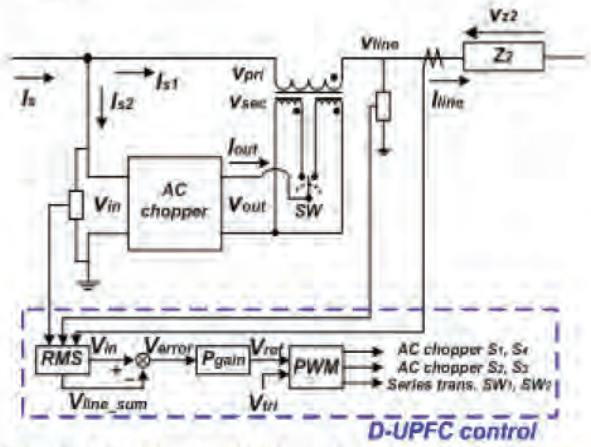

Fig. 4. D-UPFC control in the distribution system.

SIMULATION MODEL AND PARAMETERS

Simulation model

Grid connected D-UPFC simulation model is considered a simple condition. Figure 5 shows the D-UPFC simulation model. This model is analyzed from substation to load area. D-UPFC is installed at the back of pole transformer. Load and clustered PV system are simply fixed after PCC. However, the actual load conditions quiet complicate.

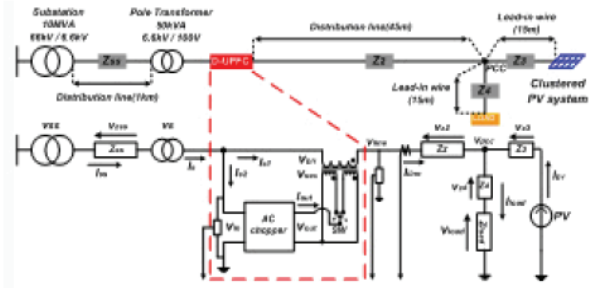

Fig. 5. D-UPFC simulation model.

Simulation model parameters of D-UPFC are shown in Table 2. Line impedance parameters refer to electric company information of Japan. A series transformer turns ratio for compensating voltage sag or swell condition refers to [1], [2]. Input and output filters should reduce the switching frequency harmonics present in the input current i_{s2}, output voltage V_{out}, respectively [3]. In the simulation model, the distance from substation to pole transformer is 1[km]. From pole transformer to PCC is 45[m]. PCC connects with load and the clustered PV system. The lead-in wire distance is 15[m].

Table 2. D-UPFC simulation parameters

V_{ss}	6600[V,rms]
V_s	100[V,rms]
Z_{ss}	0.25+j0.34[Ω/1km]
Z_2	0.011+j0.013[Ω/45m]
Z_3,Z_4	0.00345+j0.00015[Ω/15m]
Z_{load}	10+0.01[Ω]
Substation Tr. [N_{pri}/N_{sec}]	66:1
Distribution Tr. [N_{pri}/N_{sec}]	1:1
Series Tr. [N_{pri}/N_{sec}]	1:3
Input filter	50[μH], 20[μF]
Output filter	75[μH], 30[μF]
Switching frequency	10[kHz]
V_{sag}	0 ~ 4[V,rms]
PV source (I_{pv})	0 ~ 300[A,rms]

RESULTS AND DISCUSSIONS

The purpose of D-UPFC control is that the load area voltages, such as V_{pcc}, V_{load} which are shown in Fig. 5 should be controlled from voltage sag or swell. As mentioned, D-UPFC senses V_{line} and calculates V_{line_sum} using line impedance Z_2. So, V_{line_sum} can be written as eq. (8).

$$V_{line\_sum} = V_{pcc} + (I_{line} \times Z_2) \quad (8)$$

However, Eq. (8) can be only used when power flow is from substation to load area. When reverse power flow occurs eq. (8) changes to eq. (9).

$$V_{line\_sum} = V_{pcc} - (I_{line} \times Z_2) \quad (9)$$

Simulation performs considering both voltage sag and swell conditions. Table 1 shows the simulation result when voltage sag happens. Voltage sag V_{sag} from 0[V,rms] to 4[V,rms] was simulated in the distribution system. V_{in} is the D-UPFC input voltage, V_{line} is the D-UPFC output voltage, and V_{line_sum} is the compensatated D-UPFC output voltage to control V_{pcc}. D-UPFC controls V_{pcc} voltage to 98.6[V,rms] when V_{sag} is 3[V,rms]. V_{sag} voltage from 0[V,rms] to 2[V,rms] does not control V_{pcc} voltage because of voltage margin, which shows eq. (7). However, V_{pcc} was not controlled when V_{sag} was 4[V,rms].

Table 3. Voltage sag result

* All parameters indicate RMS value, '-' means unstable voltage.

Vsag	No D-UPFC control				D-UPFC Control		
	Vin	Vline	Vpcc	Vline_sum	Vline	Vline_sum	Vpcc
0	99.5	99.4	99.3	99.6	99.4	99.4	99.3
1	99.5	98.4	98.33	98.6	98.4	98.4	98.3
2	99.5	97.48	97.37	97.6	97.5	97.5	97.4
3	99.5	96.53	96.42	96.5	***98.8***	***98.8***	***98.6***
4	99.5	95.6	95.5	95.6	-	-	-

In the voltage swell simulation, clustered PV system regarded as the current source. Thus, I_{pv} means clustered

PV system. Voltage swell condition is considered the reverse power flow so that I_{pv} increases from 0[A,rms] to 300 [A,rms]. The same as voltage sag condition, D-UPFC controls V_{pcc} voltage after eq. (7) is implemented. When I_{pv} changed from 150[A,rms] to 300[A,rms], V_{pcc} voltage controlled from 100.1[V,rms] to 102.4[V,rms].

Table 4. Voltage swell result

* All parameters indicate RMS value.

Ipv	No D-UPFC control				D-UPFC Control		
	Vin	Vline	Vpcc	Vline_sum	Vline	Vline_sum	Vpcc
0	99.5	99.4	99.3	99.6	99.4	99.4	99.3
50	99.5	99.5	99.9	100.2	99.5	100.2	99.9
100	99.5	99.6	100.7	101.1	99.6	101.1	100.7
150	99.5	99.9	101.6	102.3	***98.6***	***100.1***	***100.3***
200	99.5	100.3	102.6	103.5	***98.5***	***101.8***	***100.9***
250	99.5	100.7	103.8	104.8	***98.5***	***102.6***	***101.6***
300	99.5	101.3	105.1	106.2	***98.6***	***103.5***	***102.4***

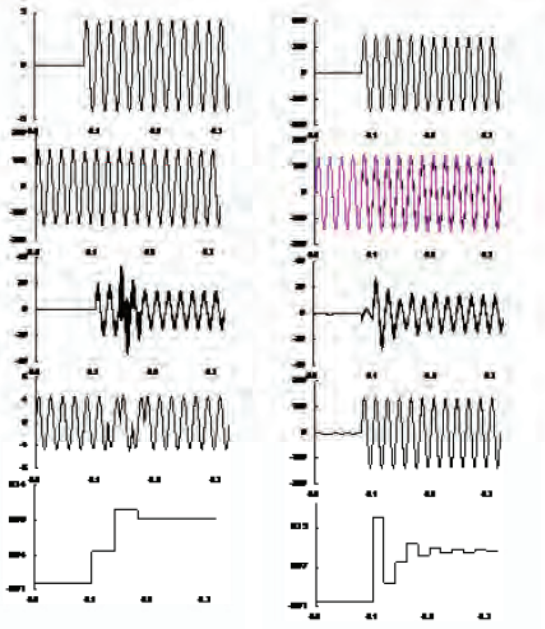

Fig. 6. Voltage sag and swell simulation waveforms (The left graph shows voltage sag 3[V,rms] from 0.08[s], the right graph indicates voltage swell 300[A,rms] from 0.08[s]).

The left of Fig. 6 shows when voltage sag 3[V,rms] occurs at 0.08[s]. The right of Fig. 6 shows when voltage swell I_{pv} 300[A,rms] happens at 0.08[s]. X axis shows simulation time from 0[s] to 0.3[s]. Two simulation results are already shown in Table 3 and 4, respectively. Fig. 6 shows the waveforms of voltage sag and voltage swell simulation. The left-top waveform shows the V_{sag} waveform, input voltage V_{in} and pcc voltage V_{pcc} are shown in the below waveform. Next, the third and fourth waveforms show AC chopper output voltage and current, respectively. Finally, the bottom waveform indicates PWM signal of D-UPFC is shown. Although V_{sag} occurs at 0.08[s], the steady-state condition of PCC voltage becomes steady-state after 0.2[s].

The top-right waveform shows the voltage swell with increasing reverse current I_{pv} from 0.08[s]. In the second graph, V_{in} and V_{pcc} increase instantaneously as I_{pv} increases. In the third waveform, AC chopper output voltage operates from 0.1[s]. However, voltage angle changed because of reverse power flow. The fourth waveform shows AC chopper output current also get effect from I_{pv}. The bottom waveform shows PWM signal of D-UPFC and also the steady-state condition starts after 0.3[s].

Although the author proposes D-UPFC in the distribution system, simulation problems occurred. Also, future study should be needed. Firstly, When voltage sag increases to 4[V,rms], D-UPFC control voltages are unstable. Control gain is not valid to D-UPFC. Secondly, when voltage swell happens, the voltage difference between V_{line_sum} and V_{pcc} occurs and it is shown in Table 4. The reason is that D-UPFC output voltage V_{line} is changed when reverse power flow happens. In the future study, D-UPFC capacity is necessary in order to install with the pole transformer. The difference of D-UPFC output voltage and current angle when power flow changes are essential to research.

CONCLUSIONS

For the reliable voltage control of the future distribution system, D-UPFC proposes in this paper. In this paper, D-UPFC concept and topology show. The basic D-UPFC switching operation mentioned. Voltage margin and voltage compensation method using line impedance introduced. D-UPFC simulation model is used to prove voltage control during voltage sag and swell condition. However, a few problems occur during voltage sag and swell simulations. More study is needed in order to use D-UPFC in the distibution system.

ACKNOWLEDGEMENT

This research has been carried as a part of "Autonomy-Enhanced PV Cluster" project and special thanks for financial support of New Energy and Industrial Technology Development Organization.

REFERENCES

[1] S. M. Hietpas and M. Nedan, "Automatic Voltage Regulator Using an AC Voltage-Voltage Converter", *IEEE Trans. Ind. Appli.*, vol. 36, No. 1, 2000, pp. 33-38.

[2] J. Pérez, V. Cárdenas, H. Miranda, and R. Álvarez, "Compensation of Voltage Sags and Swells using a Single-Phase AC-AC Converter", *The 30th Annual Conference of the IEEE industrial Electronics Society*, 2004, pp. 1611-1616.

[3] E. C. Aeloíza, P. N. Enjeti, L A Morán, O. C. Montero-Hernandez, and S. Kim, "Analysis and Design of a New Voltage Sag Compensator for Critical Loads in Electrical Power Distribution Systems", *IEEE trans. Ind. Appli., vol 39, No. 4, 2003, pp. 1143-1150.*

MODELING THE PERFORMANCE OF SEVERAL PHOTOVOLTAIC MODULES

Jun Tsutsui, Yusuke Sato, Kosuke Kurokawa
Tokyo University of Agriculture and Technology, 2-24-16 Naka-cho, Koganei, Tokyo 184-8588, Japan

ABSTRACT

The model equations to estimate the photovoltaic module performance for outdoor were proposed by many institutions. This work proposes the new model, which is the high predictive accuracy on low irradiance, combines the model proposed by National Renewable Energy Laboratory (NREL) and the model proposed by Joint Research Centre (JRC); meanwhile, we estimate the photovoltaic module performance using the linear interpolation method, which is being deliberated at the conference that International Electro technical Commission (IEC) sponsor. This paper describes the new model, and a result of comparing both models which adopted several photovoltaic modules; a crystalline silicon module (c-Si), a polycrystalline silicon module (poly-Si), and a cupper-indium-diselenide module (CIS).

INTRODUCTION

The outdoor maximum power (P_{max}) of solar module differs from the indoor P_{max} which is evaluated on Standard test condition (STC). For example, the junction temperature of solar cell reaches almost 50 ºC at 1kW/m^2, moreover, are influenced by the ambient temperature. And the solar spectrum changes during a day because of the aerosol and water vapor, therefore it is rare to fit the air mass 1.5 (AM1.5) means the standard spectrum. Consequently, to estimate the module performance, our proposal models need to take the module temperature, the solar irradiance and the solar spectrum into account.

This work proposes the new model which combines the model proposed by NREL and JRC.[1][2] Using the model of NREL, open-circuit voltage (V_{oc}), and short-circuit current (I_{sc}) of module are estimated, plus using the model of JRC, fill factor (FF) is estimated. Crossing the calculated value (V_{oc}, I_{sc}, and FF), arbitrary maximum power is obtained. On the other hand, as another model, we estimate the performance using the linear interpolation method which is deliberated as the energy rating. [3][4]

MODEL OF V_{oc} and I_{sc}

According to NREL, V_{oc} and I_{sc} are shown by equation (1), (2). V_{oc}, I_{sc} on STC are expressed by subscript zero.

$$I_{sc} = \frac{E}{E_0} I_{sc(0)} \left[1 + \alpha (T - T_0)\right] \qquad (1)$$

$$V_{oc} = V_{oc(0)} \left[1 + \beta (T - T_0)\right] \left[1 + \delta \ln\left(\frac{E}{E_0}\right)\right] \qquad (2)$$

Where:
E=irradiance [kW/m^2]; E_0 = 1kW/m^2
T=PV module temperature [ºC]; T_0 = 25 ºC
α=I_{sc} correction factor for PV module temperature
β=V_{oc} correction factor for PV module temperature
δ=V_{oc} correction for irradiance

MODEL OF FF

According to JRC, FF is shown by equation (3). The feature of this model is to obtain coefficient a, b, c, d, and e by the regression. Therefore, FF on STC is not needed to decide arbitrary FF. In addition, the regression coefficients are able to decide from I-V curve data a day.

$$FF = a + \frac{bE + c}{\ln E} + T(d + eE) \qquad (3)$$

Where:
E=irradiance [W/m^2];
T=PV module temperature [K]
a,b,c,d,e=regression coefficient

The result of our verifying predictive accuracy, we found the equation (3) model was not good to predict in low irradiance area. The reason is that third section of equation (3) expresses the temperature coefficient of FF is linear to the irradiance. But, according to the outdoor result, the temperature coefficient becomes smaller while the irradiance decreases. Fig.1 shows the irradiance dependency of the temperature coefficient of FF. Therefore, we proposed to add the new regression coefficient "f", which works so that the temperature coefficient becomes smaller. Equation (4) is our proposed equation.

$$FF = a + \frac{bE + c}{\ln E} + T\left(d + eE + \frac{f}{E}\right) \qquad (4)$$

Fig.2 shows the comparison of modeled value by Equation (3) and (4), and measured value of outdoor result. Depending on a new regression coefficient, modeled value by equation (4) is coincided with the measured value in low irradiance area, which is from 0.1kW/m^2 to 0.3kW/m^2.

1-4244-0016-3/06/$20.00 ©2006 IEEE

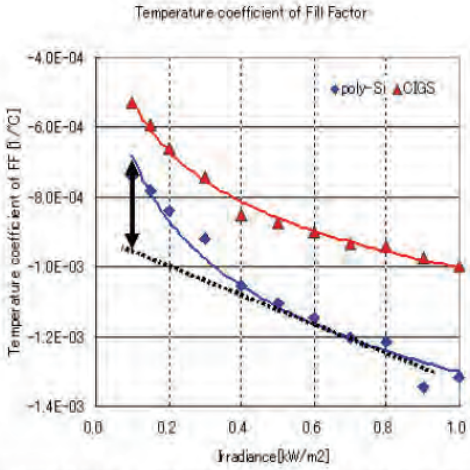

Fig.1 Irradiance dependency of the temperature coefficient

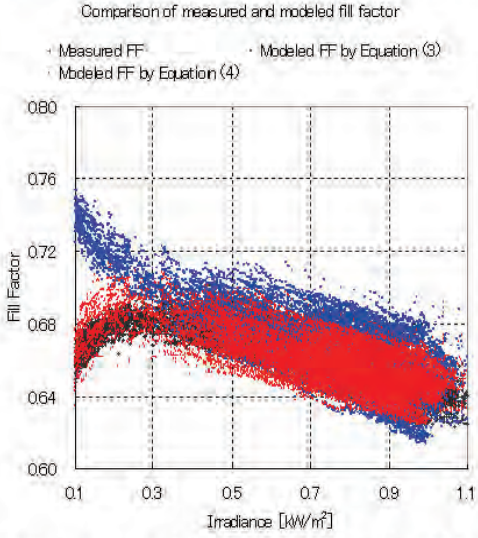

Fig.2 Comparison of measured and modeled fill factor

MODEL OF P_{max}

P_{max} is calculated by equation (5), using V_{oc} and I_{sc} by equation (1), (2), and FF by equation (4).

$$P_{max} = V_{oc} \cdot I_{sc} \cdot FF \qquad (5)$$

THE LINEAR INTERPOLATION METHOD

The linear interpolation method is estimated by using the I-V curve under four different environments; High irradiance & Low temperature (HILT), High Irradiance & High temperature (HIHT), Low irradiance & Low temperature (LILT), Low irradiance & High temperature (LIHT). The characteristic of this method doesn't need to calculate the series resistance (R_s) and the curve correction factor (K), which is included by conventional equation in IEC 60891. Following is the equation of the linear interpolation method. Equation (6) indicates the temperature interpolation; meanwhile equation (7) indicates the irradiance interpolation. (See Fig.3, Fig.4)

$$V_{T3}(I) = V_{T1}(I) + \frac{T_3 - T_1}{T_2 - T_1} \cdot (V_{T2}(I) - V_{T1}(I)) \qquad (6)$$

$$I_{E3}(V) = I_{E1}(V) + \frac{E_3 - E_1}{E_2 - E_1} \cdot (I_{E2}(V) - I_{E1}(V)) \qquad (7)$$

Where:
$V_T(I)$ =V-I curve points on arbitrary temperature
$I_E(V)$ =I-V curve points on arbitrary irradiance
T_1=High temperature, E_1=High irradiance
T_2=Low temperature, E_2= Low irradiance
T_3, E_3=temperature and irradiance on wanted I-V curve

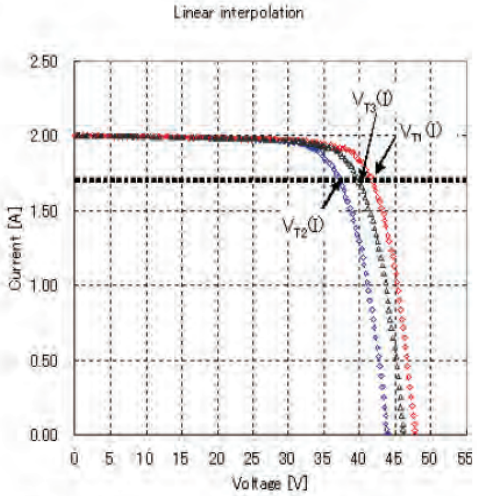

Fig.3 Linear interpolation of the temperature

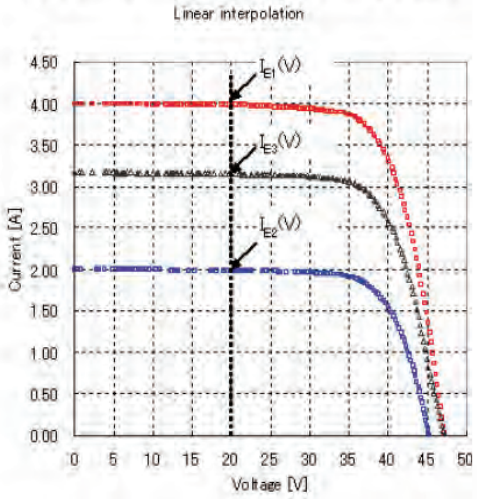

Fig.4 Linear interpolation of the irradiance

The input parameter necessary for the estimate is four I-V curves and arbitrary temperature and irradiance measured by the pyranometer. But the irradiance contains a slight error, for example there is a spectrum mismatch of

the solar module and the pyranometer. And when the solar altitude is low, incident angle loss occurs to the module. Hence we estimated by using the I_{sc} instead of the irradiance this time, that is to say, equation (7) was replaced by equation (8).

$$I_{E3}(V) = I_{E1}(V) + \frac{I_{sc3} - I_{sc1}}{I_{sc2} - I_{sc1}} \cdot (I_{E2}(V) - I_{E1}(V)) \quad (8)$$

DEFINITION OF THE ERROR

Before the estimated accuracy is indicated, we introduce the expression that shows the error as follows.

$$\text{Error}[\%] = \frac{\text{Calculated value} - \text{Measured value}}{\text{Each Parameter on STC}} \quad (9)$$

Equation (9) shows the error which is the absolute error divided by P_{max} on STC. In this paper, we defined this as the error.

RESULT

= Confirmation of calculation accuracy of V_{oc}, I_{sc} =

According to the equation (1), (2), the temperature coefficient α, β and δ expressed V_{oc} correction for irradiance as a function is necessary to calculate the arbitrary V_{oc}, I_{sc}. In this study, these coefficients were calculated by outdoor result. β and δ were able to calculate by high decision coefficient (R^2), which was more than 0.98. (See Table 1) On the other hand, α was not accurate because of slight inclination. Therefore we valued α at 0.05%/ºC on a temporary basis.

Table 1 Results of β, δ

Mod.	β	R^2	δ	R^2
c-Si	-0.29	0.98	5.27	1.00
poly-Si	-0.31	0.99	4.96	0.98
CIGS	-0.29	0.99	6.30	0.99
UNIT	%/ºC	-	%	-

Next, using the result of β, δ, we calculated V_{oc}, I_{sc} from equation (1), (2). Table 2 shows the calculation accuracy of them. According to table 2, the calculation accuracy of V_{oc} is high, that is the calculated value corresponded with the measured value. On the other hand, the calculation accuracy of I_{sc} is not better than V_{oc}, as the standard deviation is over 1.0%. In this case, we didn't consider the influence of the solar spectrum; so that it might enlarge the error of calculated I_{sc} and measured I_{sc} which is influenced by the outdoor solar spectrum.

Table 2 Confirmation of calculation accuracy

Mod.	Error			
	V_{oc}		I_{sc}	
	AVE.	SD.	AVE.	SD.
c-Si	-0.02%	0.35%	0.12%	1.07%
poly-Si	-0.67%	0.28%	-0.62%	1.21%
CIGS	0.11%	0.27%	0.50%	1.09%

= Confirmation of calculation accuracy of FF, P_{max}=

Table 3 shows the view of several regression coefficients from "a" to "f". These coefficients are calculated from I-V curve data a day after removing the measurement error, and adapted to the estimate of FF a year. The point that should be noted in the calculation of the regression coefficient is to include the sufficient data around the low irradiance which is from 100 W/m^2 to 300 W/m^2 a day. It's because an inclination of FF versus the solar irradiance changes from minus to plus prominently. (See Fig.2) Additionally, coefficient "f" definitely needs to become a minus figure.

Table 3 View of the regression coefficients

	c-Si	poly-Si	CIGS
a	7.32E-01	6.84E-01	6.89E-01
b	1.62E-03	5.89E-03	2.64E-03
c	8.72E-01	8.51E-01	8.54E-01
d	-3.98E-04	-4.53E-04	-5.44E-04
e	-7.20E-07	-2.51E-06	-1.15E-06
f	-2.06E-02	-1.74E-02	-2.60E-02

Using the regression coefficient, estimated FF of each module is calculated. Table 4 shows the confirmation of calculation accuracy of FF and P_{max}. The average error of the estimated FF is possible to calculate within 1% as well as the V_{oc}. Fig.5, 6 compares the measured and estimated FF or P_{max} on c-Si module.

Table 4 Confirmation of calculation accuracy

Mod.	Error			
	FF		P_{max}	
	AVE.	SD.	AVE.	SD.
c-Si	0.06%	0.46%	0.15%	1.08%
poly-Si	0.23%	1.64%	-0.99%	1.54%
CIGS	-0.17%	0.86%	0.37%	1.10%

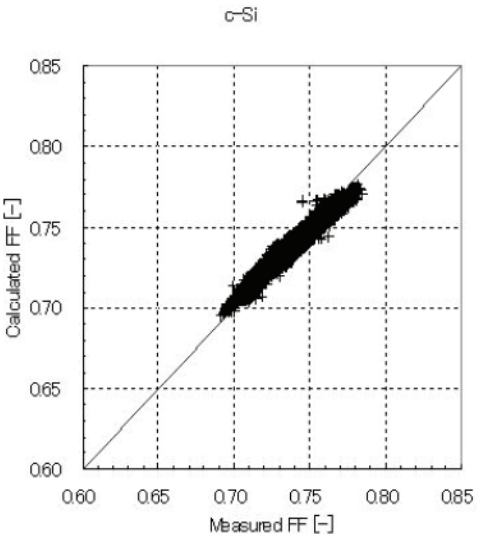

Fig.5 Comparison of measured FF vs. calculated FF

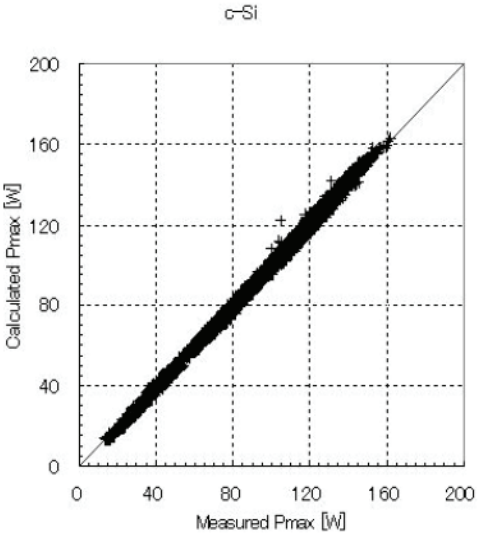

Fig.6 Comparison of measured P_{max} vs. calculated P_{max}

= Confirmation of calculation accuracy = of the linear interpolation method

Table 5 shows the result calculated by equation (6), (8).

Table 5 Confirmation of calculation accuracy

Mod.	Error of P_{max}	
	AVE.	SD.
c-Si	-0.11%	0.46%
poly-Si	-0.09%	0.36%
CIGS	-0.39%	0.41%

Comparing to table 4, table 5 indicates the average and standard deviation of the error was slight at all modules. Therefore, the estimated P_{max} doesn't depend on the kind of module. We establish the linear interpolation method is the superior estimated equation. However, in this estimate, we ignore the spectral mismatch parameter and the dependence of the solar angle of incidence, because the module's I_{sc} is used. Hence, as the next task, the linear interpolation method is improved to include their influences.

CONCLUSION

We have compared two kinds of model equations for the P_{max} of a c-Si, poly-Si, and CIGS module respectively. One model is to combine the conventional equations to calculate V_{oc}, I_{sc} and the new equation of FF improved around the low irradiance, so that the standard deviation of the error has become within about 1.5%. The other model is the linear interpolation method, which accuracy is within about 0.5%. Hence, the linear interpolation method is the accurate model that it is possible to adapt to the various modules.

REFERENCE

[1] B. Marion, "A Method for Modeling the Current-Voltage Curve of a PV Module for Outdoor Conditions", *Prog. Photovolt: Res. Appl.* 2002; 10:pp. 205-214.

[2] D. Anderson, G. Agostinelli, T. Sample and E. Dunlop, "Modeling Outdoor *Behavior of Fill Factor in Thin Modules*", *17th EU PVSEC*, *Munich*, *Germany*, 2001.

[3] B. Marion, S. Rummel and A. Anderberg, "Current–Voltage Curve Translation by Bilinear Interpolation", *Prog. Photovolt: Res. Appl.* 2004; 12:pp. 593-607.

[4] Y. Tsuno, Y. Hishikawa, K. Kurokawa, "Temperature and Irradiance Dependence of the I-V Curves of Various kinds of Solar Cells", *15th PVSEC*, *Shanghai*, *China*, 2005.

PERFORMANCE RATIO AND YIELD ANALYSIS OF GRID CONNECTED CLUSTERED PV SYSTEMS IN JAPAN

Yuzuru Ueda[1], Kosuke Kurokawa[1], Takamitsu Itou[2], Kiyoyuki Kitamura[2], Yusuke Miyamoto[3], Masaharu Yokota[3], Hiroyuki Sugihara[3]
[1] Tokyo University of Agriculture and Technology, 2-24-16 Naka-cho,Koganei,Tokyo 184-8588, Japan
[2] MEIDENSHA CORPORATION, Riverside Building, 36-2, Nihonbashi Hakozakicho, Chuo-Ku, Tokyo 103-8515, Japan
[3] Kandenko co., ltd., 4-8-33 Shibaura Minato-ku Tokyo 108-8533, Japan

ABSTRACT

It is becoming more important to evaluate the installed PV system's performance and loss factors to enhance the system's efficiency and pull more electric power from the systems. This paper describes the evaluation method of PV systems and summarizes the results of annual performance and loss analysis. Grid voltage and snow coverage are two major serious loss factors for PV systems, optimized array configuration results more system yield on roof mounted residential PV systems.

INTRODUCTION

In the case that many of grid-connected residential photovoltaic (PV) systems are installed in the small area and connected to the same power distribution network, this situation called "Clustered", voltage raise of power distribution line due to the reverse power flow from the PV systems would be the problem. To prevent the overvoltage of the power distribution line, Japanese PV system's power conditioning subsystems (PCS) is monitoring its own output voltage, and if it is higher than the specification of the voltage, PCS will automatically reduce its output power. Because of this function, PV system's output will be restricted even though PV array is receiving enough solar irradiance if the grid voltage is too high [1] To investigate the issues which may happen in the clustered PV systems, "Demonstrative research on clustered PV systems" is being conducted from December, 2002 by NEDO. Approximately 550 PV systems will be installed on the roofs of houses and connected to the commercial power grid in the demonstrative research area in Oota, Japan. [2]

ANALYSIS METHOD

Loss factors

Input energy of PV systems is irradiation. Pyranometer is commonly used to measure the irradiation, however, pyranometer cannot cover the whole area of the PV array so shading on the PV array may occur in some systems. Incident angle dependence, spectral sensitivity and other characteristics of pyranometer are also different from the characteristics of PV modules. Because of these differences, there is a difference between the irradiation that measured by the pyranometer and the irradiation that PV array actually received. Dirt on the surface of the modules or degradation of EVA layer may reduce the input energy too. The following loss factors are considered as a factor to reduce the input energy in this method.

1. Shading
2. Regular loss (Dirt, Degradation)
3. Incident Angle / Reflection

The next step is photoelectric conversion. During the energy conversion, increasing of the modules temperature will lower the conversion efficiency especially in the c-Si based PV modules. Operation point on the I-V curve is also very important to pull the maximum power from the systems. The reasons of the maximum power point (MPP) mismatch have a lot of variations. PCS sometimes intentionally shifts the operation point from MPP to the bad operation point (normally towered the open circuit voltage (V_{OC}) so the voltage will be higher than the maximum power voltage (V_{Pmax})) to reduce its output current in order to prevent the over voltage of the power distribution line. PCS sometimes can not find the MPP due to the stepped I-V curve which is observed in the partially shaded PV array. In the case that the capacity of the PCS is smaller than that of the PV array's, output current will be restricted around the PCS's maximum output. PCS will not track the MPP and keeps constant voltage if the irradiance is very low. The following loss factors are considered as a factor to lower the conversion efficiency.

4. Module Temperature
5. Output restriction (over voltage)
6. PCS capacity shortage
7. MPP mismatch (high voltage side)

Among the MPP mismatch loss factors, MPP mismatch in higher voltage side are mainly considered in this analysis and lower voltage side are included in the miscellaneous loss because the amount of the loss are limited. There would be a regular conversion efficiency loss due to the mismatch of modules. The photocurrent of one string will be restricted by the worst module so the actual photocurrent will be lower than the value which is calculated by the input irradiance and module's rated output current. This loss is included in the regular loss.

In addition to these seven loss factors, the following loss factors are also considered in this method.

8. DC resistance
9. Inverter

1-4244-0016-3/06/$20.00 ©2006 IEEE

10. PCS Off / PCS Standby
11. Fluctuation

During the DC power transmission from the PV array to the PCS, there will be some voltage drop and energy loss due to the resistance of the cable and voltage drop at the blocking diode. This loss is calculated using the formula of

$$I_A = \sum (0.6 \times DCI + 0.2 \times DCI^2) \quad (1)$$

Where
I_A: Loss due to the DC circuit [Wh]
DCI: PV array output current [A].

0.6[V] represents the voltage drop at the blocking diode and 0.2[ohm] is the resistance of the cable that is calculated using 20[m] of CV cable (2[mm^2]), the most frequently used cable within the evaluated systems.

Inverter loss simply means the loss at the PCS. PCS off / standby means there is no output from the PCS even with the irradiation including the maintenance purpose.

Fluctuation means the loss during the fast fluctuation of irradiance. Since we are measuring irradiance at the metrological stations and there is some distance between the pyranometer and the PV array, ether pyranometer or PV array may shaded by clouds if the fluctuation of the irradiance is too fast. Fluctuation loss includes this kind of measurement error.

Shading analysis

The definition of "shading" in this paper is the situation that the pyranometer does not have any shading but PV array has. Only the static sunlight-blocking objects are considered, moving clouds or other accidental shadings are not included. The maximum shading losses are calculated for each solar height angle and solar azimuth in increments of 5 degree. [3]

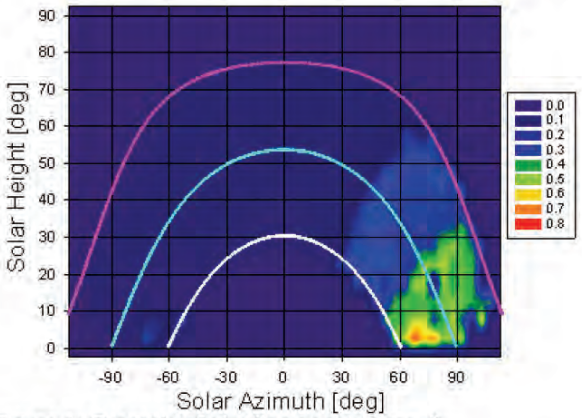

Figure 1: Example of shading analysis result

Example of the result is shown in Figure 1. Three arcs in this graph are the sun's path on the summer solstice, the equinox and the winter solstice from top to bottom respectively. Shading loss is observed when the sun is in west during evening time. This is because of the stepped roof as shown in Figure 2. Higher side of the roof is making the shadow on the lower side when the sun is in west.

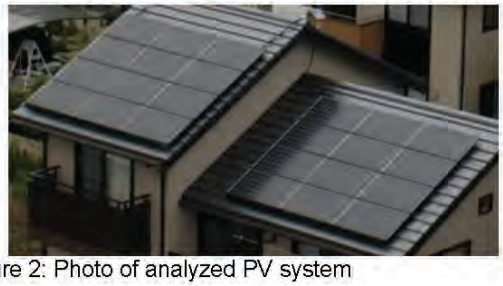

Figure 2: Photo of analyzed PV system

Reflection loss calculation

Output energy loss due to the reflection of the incoming irradiance at the PV module's surface is calculated using geometrical optics theory. [4] Cover grass, EVA and anti reflective coating are assumed as a single layer and the effective refractive index n_E is used for the calculation.

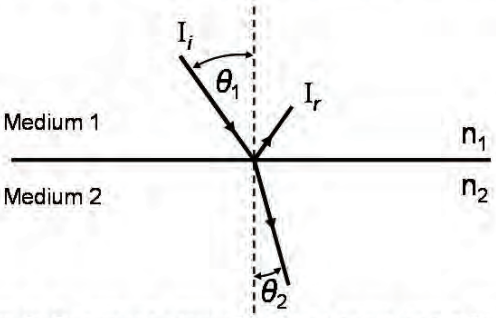

Figure 3: Schematic view of incident angle and refractive angle.

Figure 3 describes the schematic view of incident angle and refractive angle. The relationship of these two angles can be described using Snell's low;

$$n_1 \cdot \sin\theta_1 = n_2 \cdot \sin\theta_2 \quad (2)$$

where
n_1: Refractive index of medium 1
n_2: Refractive index of medium 2.

Reflectance can be expressed using the equation of;

$$r = \frac{I_r}{I_i} = \frac{1}{2}(r_\perp + r_\parallel) \quad (3)$$

where

$$r_\perp = \frac{\sin^2(\theta_2 - \theta_1)}{\sin^2(\theta_2 + \theta_1)} \quad (4)$$

$$r_\parallel = \frac{\tan^2(\theta_2 - \theta_1)}{\tan^2(\theta_2 + \theta_1)} \quad (5).$$

Assuming the incident angle = 0[deg] at the STC, reflection loss is calculated using the effective refractive index n_E of 1.8 which is obtained from a preliminary experiment.

RESULTS AND DISCUSSIONS

One-minute averages of secondly measured data are used for this analysis. Evaluation period is from Oct. 2004 to Sep. 2005. More than 300 PV systems were already installed in the demonstrative research area. Total capacity was nearly 1 [MW]. All the PV systems are connected to the same power distribution network. 104 systems out of more than 300 systems are used for the analysis due to the data availability. Performance and losses are quantified for every 30days because at least one sunny day is needed to quantify the shading loss and regular loss.

Annual performance and loss analysis

Annual performance analysis result is summarized in Figure 4. Average performance ratio was 79.3[%]. Even through these PV systems are clustered, loss due to the grid voltage was only 0.3[%] in average. However, this is demonstrative research and the grid condition is managed better than the conventional local power distribution networks, it could be worse in other cases.

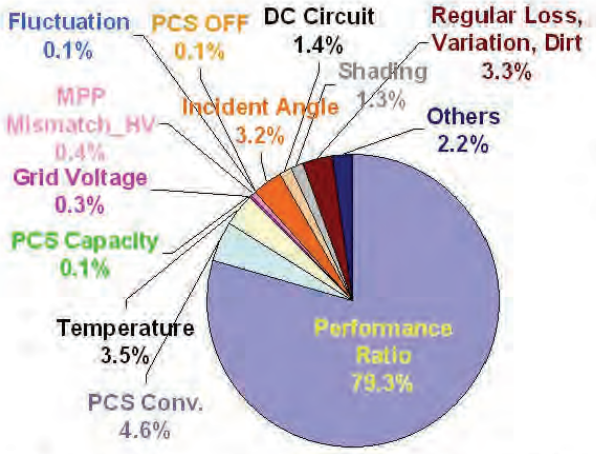

Figure 4: Annual performance analysis result of 104 PV systems.

Daily performance and loss analysis

Daily performance and loss analysis results are summarized in Figure 5,6,7,8. Each data point represents daily performance ratio of one system and 30days results are plotted in one box. The lower boundary of the box indicates the 25th percentile, a line within the box marks the median, dotted red line the average and the upper boundary of the box indicates the 75th percentile. Whiskers above and below the box indicate the 90th and 10th percentiles respectively. Data with more than 5[%] daily losses due to the PCS off are excluded from these results.

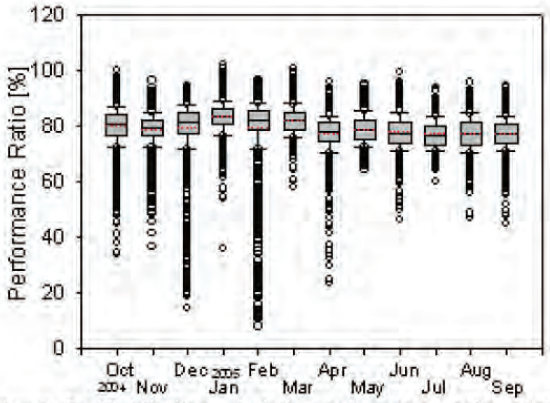

Figure 5: Distribution of daily performance ratio of 104 systems.

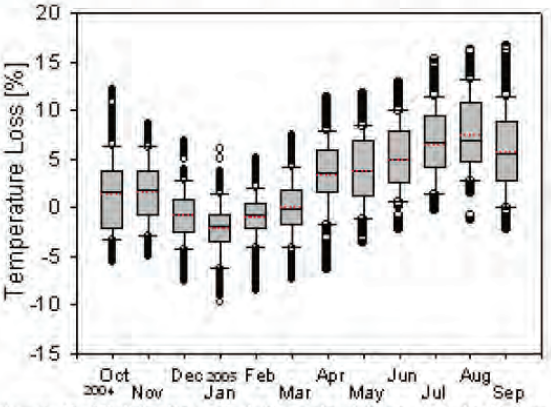

Figure 6: Distribution of daily output loss due to the module temperature.

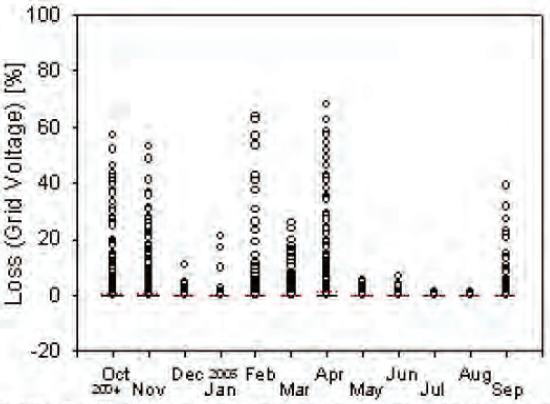

Figure 7: Distribution of daily output loss due to the grid voltage.

Averages of performance ratio are better in winter and lower in summer as shown in Figure 5. This is mainly because of the module temperature which loss is shown in Figure 6. Although the frequency is less than 10[%], less than 50[%] of performance ratio are observed through the year. The causes of these serious performance losses are grid voltage and snow coverage. Losses due to the grid

voltage are shown in Figure 7, more than 50[%] of loss are resulted in Oct. and Nov. 2004, Feb. and Apr. 2005. Figure 8 shows the results of miscellaneous loss. More than 50[%] of loss are resulted in Dec. 2004 and Feb. 2005. The reason of these losses was snow coverage. Since we are measuring the irradiation by pyranometer, there was a situation that snow on the pyranometer melted but PV array still covered by snow. Except these two loss factors, other loss factors showed predictable range of loss through the year.

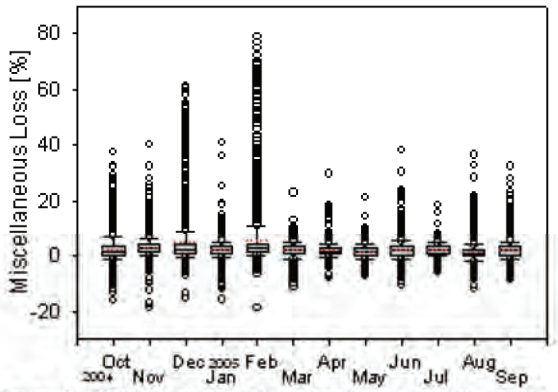

Figure 8: Distribution of daily miscellaneous output loss.

Comparison of array configuration

Since the design of the roof is not always optimized for PV system, some of the PV modules are installed on the roofs which have an orientation of east or west with non optimized tilt angles. To compare all the different configuration, all systems are classified according to the array configuration, i.e. single array oriented south as type1, multiple arrays oriented south and/or east and/or west as type2 and array(s) not oriented south as type3. Performance ratio and system yield are summarized in Figure 9.

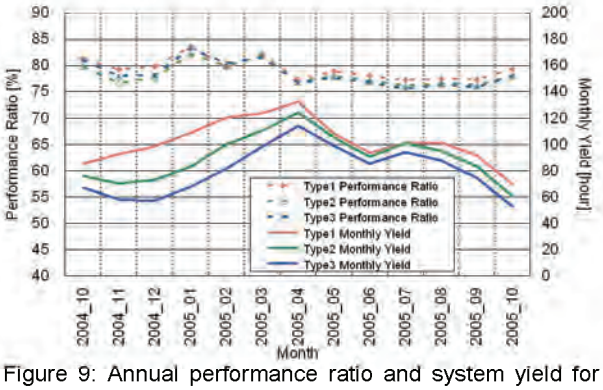

Figure 9: Annual performance ratio and system yield for three array configurations.

Performance ratio for all types are almost the same through the year but type1 has about 30[%] more system yield compare with type3. Type3 has more reflection loss especially in winter but less temperature increasing in winter compare with the type1. Detailed numbers are summarized in Table1.

Table 1: Analysis results of three array configurations.

	Type1	Type2	Type3
Annual system yield [h]	1330	1175	1039
Annual P.R. [%]	78.0	77.8	78.4
Loss (Temperature) [%]	2.8	2.5	1.8
Reflection loss [%]	3.3	4.5	4.9
Number of systems	74	17	5

CONCLUSIONS

Detailed performance analysis results of clustered PV systems are summarized in this paper. Characteristics of 12 loss factors including snow coverage are clarified. Results indicate that grid voltage and snow coverage caused serious performance loss in some cases. Different array configurations are also compared. Difference of the performance ratio between south oriented PV systems and others is only a few percent but approximately 30[%] of the system yield difference is observed.

ACKNOWLEDGEMENT

Demonstrative research on clustered PV systems is a project of New Energy and Industrial Technology Development Organization (NEDO). Authors would like to acknowledge the financial support of NEDO and cooperative discussions with project members.

REFERENCES

[1] Y.Ueda, T.Oozeki, K.Kurokawa, T.Itou, K.Kitamura, Y.Miyamoto, M.Yokota, H.Sugihara, S.Nishikawa, "ANALYTICAL RESULTS OF OUTPUT RESTRICTION DUE TO THE VOLTAGE INCREASING OF POWER DISTRIBUTION LINE IN GRID-CONNECTED CLUSTERED PV SYSTEMS", *31st IEEE Photovoltaic Specialists Conference*, pp1631 (2005)

[2] Shogo Nishikawa, Kazuhiko Kato, "DEMONSTRATIVE RESEARCH ON GRID-INTERCONNECTION OF CLUSTERED PHOTOVOLTAIC POWER GENERATION SYSTEMS", *3rd World Conference on Photovoltaic Energy Conversion*, 2003, 8LN-C-03

[3] Y.Ueda, T.Oozeki, K.Kurokawa, T.Itou, K.Kitamura, Y.Miyamoto, M.Yokota, H.Sugihara, "Advanced analysis of shading effect using minutely based measured data for PV systems" *15th International Photovoltaic Science and Engineering Conference*, TECHNICAL DIGEST pp.444-445 (2005)

[4] T Yamada, H Nakamura, T Sugiura, K Sakuta, K Kurokawa, "Refection loss analysis by optical modeling of PV module" *Solar Energy Materials & Solar Cells*, Vol.67 pp.405-413 (2001)

TRANSLATION EQUATIONS FOR TEMPERATURE AND IRRADIANCE OF THE I-V CURVES OF VARIOUS PV CELLS AND MODULES

Yuki Tsuno[1, 2], Yoshihiro Hishikawa[1] and Kosuke Kurokawa[2]
[1] National Institute of Advanced Industrial Science and Technology (AIST), Research Center for Photovoltaics
Central 2, 1-1-1 Umezono, Tsukuba, Ibaraki, 305-8568, Japan
[2] Tokyo University of Agriculture and Technology (TUAT), 2-24-16 Naka-cho, Koganei, Tokyo, 184-0012, Japan

ABSTRACT

A new practical formulation for the linear interpolation/extrapolation is proposed in order to translate the I-V curves to target conditions of irradiance (G) and PV device temperature (T). The accuracy of the method is investigated based on the experimental I-V curves of various kinds of PV cells and modules. By utilizing this method, four or three I-V curves measured at any G and T can be used as the reference I-V curves. This makes practical translation procedure much easier. The calculated I-V curves over a wide range of G and T well agree with measured results for various kinds of PV cells and modules. The difference between the calculated and measured P_{max} was 0.5% or less for indoor experiments, and 1.0% or less for outdoor experiments. These results indicate that the translation of the I-V curve based on the method is effective for estimating the performance of various PV devices under various climatic conditions.

INTRODUCTION

It is useful to understand the effect of the irradiance and temperature on the photovoltaic (PV) cell and module performance, in order to estimate their I-V curves under various climate conditions for power rating and energy rating. Although translation equations based on "shifted approximation" are employed on irradiance dependence in some current standards [1, 2], those equations can deviate from experiments when the variation in the irradiance and/or temperature is large. Also some equations are applicable only for limited kinds of PV devices. Translation of the I-V curves for G was discussed by Hishikawa et al. originally for a-Si solar cells [3] and incorporated in JIS standards. Recently, the linear interpolation method of the I-V curves by a linear interpolation for both G and T was proposed based on experimental (indoor and outdoor) data on various kinds of PV cells and modules by Marion et al.[4]. The method can accurately estimate the performance of various kinds of PV cells and modules for a wide range of irradiance (G) and temperature (T) [4, 5]. It requires that G (I_{sc}) or T of the reference I-V curves is the same. However, it is not always possible to obtain such reference I-V curves, especially under outdoor conditions. In this study a new practical formation for the linear interpolation/extrapolation is proposed. The accuracy of the method based on the experimental I-V curves of various kinds of PV cells and modules is investigated.

LINEAR INTERPOLATION/EXTRAPOLATION METHOD

The procedure of the linear interpolation/extrapolation of the present study is as follows. The measured current-voltage characteristics are corrected to target G and T values by equations (1) and (2).

$$V_3 = V_1 + a \cdot (V_2 - V_1) \quad (1)$$

$$I_3 = I_1 + a \cdot (I_2 - I_1) \quad (2)$$

Here, I_1 and V_1 are the current and voltage of the reference I-V curve measured at an irradiance G_1 and temperature T_1. I_2 and V_2 are the current and voltage of the reference I-V curve measured at G_2 and T_2. I_3 and V_3 are current and voltage of the I-V curve at G_3 and T_3. which is the target of the translation. The (I_1,V_1) and (I_2,V_2) shold be chosen so that $I_2 = I_1 + (I_{sc2} - I_{sc1})$. Here, I_{sc1} and I_{sc2} are the short circuit current of the refrence I-V curves. a is an arbitary constant (See Fig. 1). When $0< a <1$, the procedure is interpolation, When $a <0$ or $1> a$, the procedure is extrapolation.

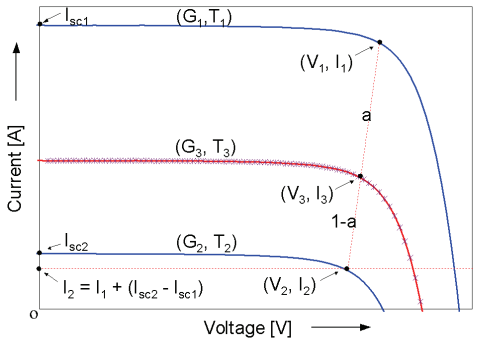

Fig.1 Schematic procedure for the calculations based on Eqs. (1)-(4). I-V curves measured at the irradiance and temperature of (G_1, T_1) and (G_2, T_2), shown by blue lines, are translated into the I-V curve at (G_3, T_3), shown by the red line. Measured I-V curve at (G_3, T_3) is also shown by crosses, which is in good agreement with the calculation.

1-4244-0016-3/06/$20.00 ©2006 IEEE

The G_3 and T_3 cannot be chosen independently, and are determined from T_1, G_1, T_2, G_2 and a from equations (3) and (4).

$$G_3 = G_1 + a \cdot (G_2 - G_1) \quad (3)$$

$$T_3 = T_1 + a \cdot (T_2 - T_1) \quad (4)$$

Equation (5) is also valid, as the present procedure assumes linear devices.

$$I_{sc3} = I_{sc1} + a \cdot (I_{sc2} - I_{sc1}) \quad (5)$$

Here, I_{sc3} is the short circuit current of the target I-V curves.

INDOOR RESULTS

Typical single-crystalline Si, polycrystalline Si, amorphous Si and a-Si/thin-film crystalline Si tandem cells were used as samples. Their sizes ranged 2-10 cm^2. They were attached on metal plates, whose temperature was stabilized at 20°C, 30°C, 40°C, and 50°C by a flow of temperature controlled water. The temperature was controlled within a nominal accuracy of ±0.2 °C. A solar simulator was used as the light source of 100 mW/cm^2. Irradiance was controlled by metallic thin film neutral density filters. For each solar cell, four reference I-V curves with irradiance of 0 and 100 mW/cm^2 and temperatures of 20°C and 50°C.

The I-V curves at various irradiances and temperatures were calculated by using equations (1) and (2) from the reference I-V curves. The calculated I-V curves well agree with the experiment for all the samples measured in the present study. For example, Fig. 2 shows the results for a polycrystalline Si cell. Measured and calculated I-V curve parameters I_{sc}, V_{oc}, maximum power (P_{max}) and fill factor FF excellently agreed, as shown in Figs. 3 and 4. Root mean square error (RMSE) between measured and calculated P_{max} for all the samples was <0.5%.

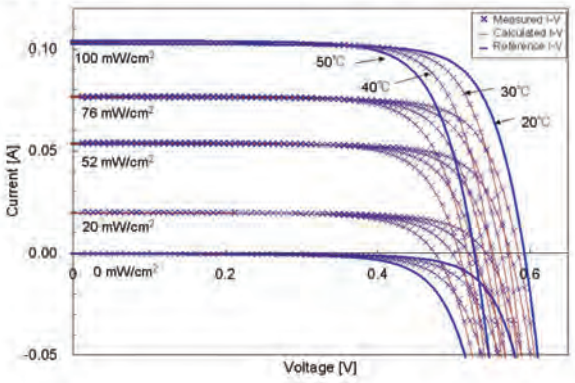

Fig.2 Measured (circles) and calculated (lines) I-V curves of a polycrystalline Si solar cell. I-V curves measured at G=0 and 100 mW/cm^2 and T = 20°C and 50°C were used for the reference I-V curves.

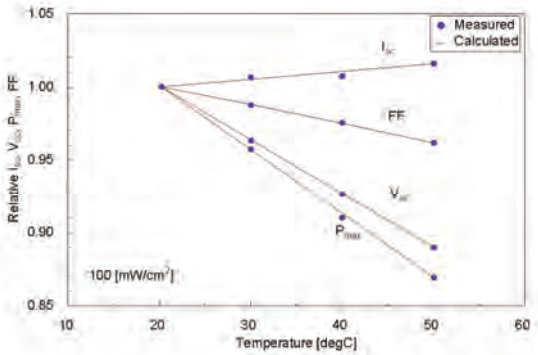

Fig.3 Measured (circles) and calculated (lines) I_{sc}, V_{oc}, P_{max}, FF for the polycrystalline Si cell shown in Fig. 1 as functions of the temperature T. The irradiance G is 100 [mW/cm^2]. The parameters are normalized to the value at T=20°C. The measured and calculated results agree within the RMSE of 0.1%.

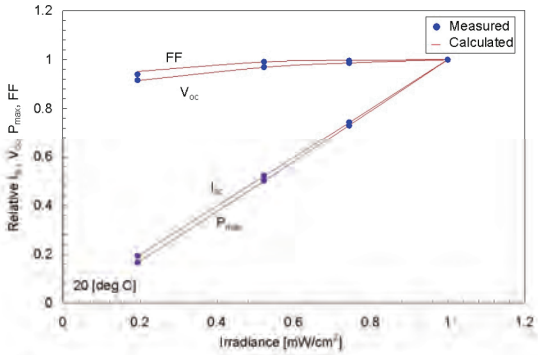

Fig.4 Measured (circles) and calculated (lines) I_{sc}, V_{oc}, P_{max}, FF for the polycrystalline Si cell shown in Fig. 1 as functions of the irradiance G. The temperature T is 20 °C. The parameters are normalized to the value at G=100 [mW/cm^2]. The measured and calculated results agree within the RMSE of 0.5%.

The present method does not restrict the G and T of the reference I-V's, and can simultaneously translate the I-V curves for G and T. Fig. 5 shows the example that the I-V curves at (100 mW/cm^2, 25°C) and (20 mW/cm^2, 50°C) are successfully translated into the I-V curve at (52 mW/cm^2, 40°C). The error of measured and calculated P_{max} was -0.1%. By utilizing present procedure (Eqs. (1) – (4)), the I-V curves at wide range of G and T can be calculated from only three or four reference I-V curves measured indoor or outdoor.

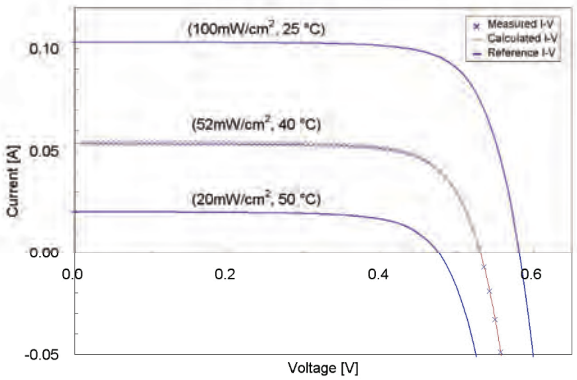

Fig.5 Measured (symbol) and calculated (line) I-V curves of polycrystalline solar cell. The I-V curves at (100 mW/cm^2, 25°C) and (20 mW/cm^2, 50°C) is successfully translated into the I-V curve at (52 mW/cm^2, 40°C). Blue lines are two reference I-V curves measured at different irradiance and temperature. I-V curve measured at (52 mW/cm^2, 40°C) is also shown by crosses, which is in good agreement with the calculation.

Fig. 6 shows the example of the linear interpolation/extrapolation based on four reference I-V curves into the target I-V curve by the following procedure (1)-(3). Points denoted as 1-4 represents the reference I-V curves. The point denoted as 7 is the target I-V curve.

(1) I-V curve 5 is calculated by I-V curves 1 and 2.
(2) I-V curve 6 is calculated by I-V curves 3 and 4.
(3) I-V curve 7 is calculated by I-V curves 5 and 6.

It is noted that other order of the calculation is also possible. At least three reference I-V curves can calculate the I-V curves at wide range of G and T as will be demonstrated in Fig. 10.

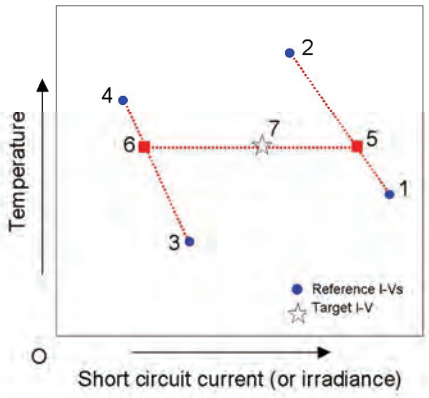

Fig.6 Example of the linear interpolation/extrapolation of four reference I-V curves into the target I-V curve. 1-4 are reference I-V curves. 7 is the target I-V curve.

OUTDOOR RESULTS

Single crystalline and polycrystalline silicon modules, CIS and hetero-junction module were investigated at outdoor conditions. Data measured for about a year were used for the present study. The total number of I-V curves was about 86000 for each module. The module temperature was measured by thermocouples attached to the backside of each module simultaneously with the I-V curve.

In this experience, I_{sc} was used instead of G (equation (5)), because irradiance measured by pyranometer is not proportional to I_{sc} due to spectral effects. Fig.8 shows typical example of experimental and calculated results for c-Si modules. This figure demonstrates that the calculated I-V curves agree with the experimental curves very well, also for modules. These resulting I-V curves in this figure do not include data near V_{oc} because measurement data points of reference I-V curves were measured from I_{sc} to I=0. If data near V_{oc} is desired, reference I-V curves shall be measured down to near $-I_{sc}$.

Comparisons of calculated and measured I-V curves were made using RMSE between measured and calculated P_{max}. Fig.9 shows RMSE of P_{max} for c-Si module, plotted versus the short circuit current I_{sc} and module temperature T. Each point includes data from 30-600 I-V curves. RMSE for wide range of G (0.1-1.0mW/cm^2) and T (5 -70°C) is less than 1.5%. This result indicates that the present method can calculate the I-V curves of the PV modules for the whole range of G and T of the outdoor conditions of the present study, based on only four reference I-V curves. It should be noted that the number of the reference I-V curves may be further reduced in some cases. Fig.10 also shows plot of RMSE of P_{max} for c-Si module. The number of the reference I-V curves is three, as shown by the open circles in the figure. RMSE at most of the conditions is less than 1.5%.

Table 1 shows average and standard deviation of the difference between measured and calculated P_{max} of each module. This result indicates that the linear interpolation method is applicable for various kinds of PV modules under various climatic conditions.

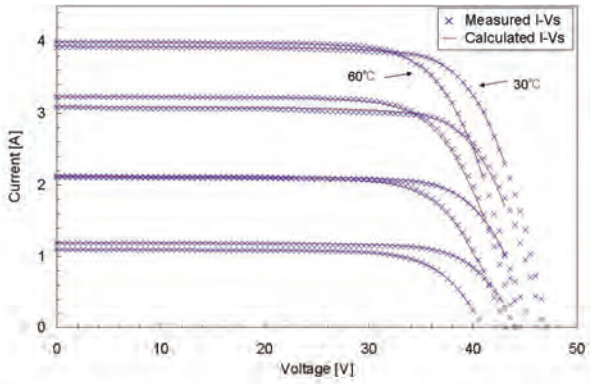

Fig 8. Measured (symbols) and calculated (lines) I-V curves of single crystalline PV module.

Although both the interpolation and extrapolation are possible by the present procedure, interpolation usually results in better agreement with the experiments than extrapolation. Therefore, choice of the reference I-V's is important for calculating the I-V's in a wide-range of G and T, as shown in Figs. 9 and 10.

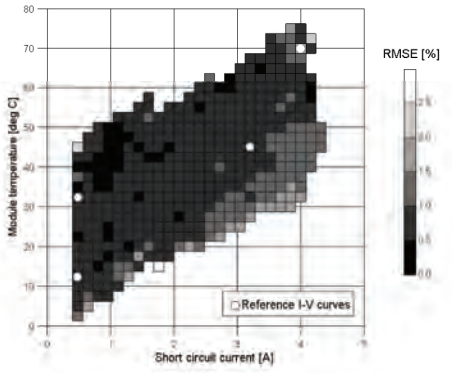

Fig 9 RMSE between measured and calculated P_{max} for a single crystalline silicon module, plotted versus the short circuit current I_{sc} and module temperature T. Circles represent the conditions of reference I-V curves.

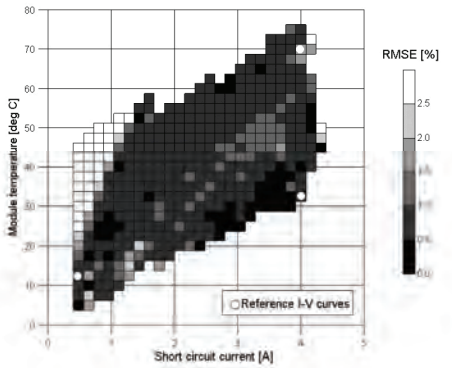

Fig.10 RMSE between measured and calculated P_{max} for a single crystalline silicon module, plotted versus the short circuit current I_{sc} and module temperature T. Circles represent the conditions of reference I-V curves.

Table 1 Average and standard deviation of the difference between measured and calculated maximum power of each module.

Module	Ave [%]	SD [%]
c-Si	0.1	0.8
c-Si (3 references)	0.4	2.1
pc-Si	0.2	0.8
Hetero-junction	0.1	1.0
CIS	0.4	0.8

CONCLUSIONS

A new practical formulation for the linear interpolation/extrapolation is proposed, in order to translate the I-V curves for the irradiance G and temperature T. The accuracy of the translation is investigated based on the experimental indoor and outdoor I-V curves of various kinds of PV cells and modules. By utilizing this method, four or three I-V curves measured at any G and T can be used as the reference I-V curves. This makes practical translation procedure much easier. The results over a wide range of G and T well agree with measured maximum power for various kinds of PV cells and modules. For indoor experiments, root mean square error (RMSE) between the measured and calculated P_{max} for four kinds of PV cells was <0.5%. For outdoor experiments, standard deviation of the measured and calculated maximum power of four kinds of PV modules was within 1% for wide range of G and T.

The present method is expected to be very useful for the energy rating and power rating of the PV devices.

ACKNOWLEDGEMENTS

This work was supported in part by NEDO under the Ministry of Economy, Trade and Industry.

REFERENCES

[1] IEC 60891, 1987.

[2] JIS C 8913, 1998.

[3] Y. Hishikawa , Y. Imura and T. Oshoro.," Irradiance -Dependence and Translation of the I-V Characteristics of Crystalline Silicon Solar Cells" Proceedings of the 28th IEEE PV Specialists Conference, 2000; 1464-1467.

[4] B. Marion, S. Rummel and A, Anderberg, "Current-Voltage Curve Translation by Bilinear Interpolation" Prog. Photovolt: Res. Appl. 2004; **12**:593-607.

[5] Y. Tsuno, Y. Hishikawa and K. Kurokawa, "Temperature and Irradiance Dependence of the I-V Curves of Various Kinds of Solar Cells" Technical Digest of the PVSEC 15, Shanghai, 2005. 422-423.

[6] TUV Rheinland, "Current-Voltage translation Procedure for PV Generators in the German 1000 Roofs-Programme" EUROSUN conference, Freiburg, 1996.

RESULT OF REVIEW BY ELECTRIC ENERGY AMOUNT COMPARISON WITH RESONANCE LOAD TURNED TO MOTOR LOAD STANDARDIZATION

Hironobu Igarashi[1] and Takanori Sato [1] and Hiromu Kobayashi [2] and Izumi Tuda [3] and Kosuke Kurokawa [4]
[1] Japan Electrical Safety & Environment Technology Laboratories, Research Division, －JET
5-14-12 Yoyogi, Sibuya-ku, Tokyo 151-8545, JAPAN,
[2] Central Research Institute of Electric Power Industry. －CRIEEPI
2-11-1 Iwado Kita, Komae-shi, Tokyo 201-8511 JAPAN
[3] National institute of Advanced Industrial Science and Technology.－ AIST
1-1-1 Umezono, Tukuba 305-8568 JAPAN
[4] Tokyo University of Agriculture and Technology － TUAT
2-24-16 Naka-cho, Koganei-shi, Tokyo, 184-8588, JAPAN
e-mail: Igarashi_H@jet.or.jp

ABSTRACT: The islanding phenomena of PV inverter are obviously influenced by the regenerative loads such as motor load and resonance circuit. In Japanese situation, the motor loads of 1KW or less are used in the certification test and evaluated in order to test the islanding detection device in a severer case from the viewpoint of safety. However, the motor load is not very clear in the specification of a standard motor to use for the examination so that there are diverse and unspecified kinds. Accordingly, it is certainly not easy to standardize the motor load for certification test around the world. On the other hand, in IEEE929-2000 and IEC62109CD2 standard, resonance circuit is used instead of motor load for the examination with consideration of regenerative load characteristic. Therefore, It is necessary to confirm whether the resonance circuit can simulate the motor load properly under the islanding condition.

Keywords: Motor load, Resonance load, Islanding, Grid-Connected, PV System,

INTRODUCTION

The islanding phenomena of PV inverter are obviously influenced by the regenerative loads such as motor load and resonance circuit. From the safety point of view, the regenerative load is generally used in the islanding prevention test to obtain more severe case for islanding detection. Less than 1kW grinder load, which has comparatively large inertia, is adopted in Japanese certification test of islanding[(1)] prevention function for PV inverter connected to low voltage(200V) distribution line. The grinder load is not so popular, but actually used by the low voltage customers such as small factory and so on. As we have to take the worst case into account for ensuring safety, we are using the grinder load in the certification test as a general worst case for islanding detection.

It is certainly not easy to standardize the motor load for certification test around the world. On the other hand, resonance circuit is standardized in some IEC standards in stead of motor load with consideration of regenerative load characteristic. Therefore, it is necessary to confirm whether the resonance circuit can simulate the motor load properly under the islanding condition.

The objectives of the study are to confirm the application of motor load on the "Testing Procedure of Islanding Prevention Measures for Utility Interactive PV Inverter" by experiment. The experiments practiced for this study are as followed.

1) The experiment concerning similarity and difference of islanding characteristic between using motor load and using resonance circuit as regenerative load.
2) The experiment concerning the possibility of standardization of motor load in the islanding prevention test.

Measuring the electric energy

Islanding phenomena tend to depend on the regenerative energy of motor load and/or resonance circuit.

From this point of view, we tried to evaluate the regenerative energy of several sampled motor loads and resonance circuit as the beginning of the study.

In the JET attestation system, the motor load is used in order to imitate the motor loads that actually exist on the electric power line and in order to imitate the situation that both a lot of PV generation systems and the motor dynamos drive parallel.

Moreover, the motor load that runs without electric power becomes a pilot of the voltage and the frequency of the electric power lines, imitates the situation in which many PV generation systems including the voltage control type are connected in parallel extremely well, and operates as an ideal motor load type dynamo that does not supply the active power.[(2)]

In addition, because it turns out that the motor load supplies and absorbs an reactive electric power in the past study results, it is used in the JET attestation examinations as the severest load condition for the inverters that try to change the frequency. However, the detail of the specification in the capacity and moment of intarsia of the motor load used for the examination have not be clarified currently; the influence to Islanding detection differs depending on the size of capacity, moment of inertia,

and so on that affect the islanding detection time as a result. Therefore, it was assumed that the characteristics of electric energy of an individual motor loads were clarified by measuring the electric energy of various motor loads.

Measuring the electric energy of the motor load

Four types of commercialized inductive grinder motor load connected 200V line are used.

The rated capacity and the moment of inertia of each load are shown in Table 1.

The electric energy of the motor loads was measured by timing for the resistance load to consume about 10% (20V) of the rating voltage (200V) of the electric energy remained in the motor in the condition that a motor load and a resistance load were connected in parallel to the AC utility power simulator.

1. Increase the electric power consumed by resistance load connected to the motor load from 0 to 4000W by 100W.
2. Separate both motor load and resistance load from the AC utility power simulator by opening the switch (SW_{CB}) when the timing is t=0.
3. Observe the voltage V_2between lines of the motor load of resistance load connected in parallel and measure the time delta X (Sec) while the voltage attenuate to about 10% (20V)of rated voltage (200V).
4. In the same way above, measure the time delta X (Sec) using different motor load in table 1.

Fig.1 shows the circuit chart to measure the electric energy of the motor load.

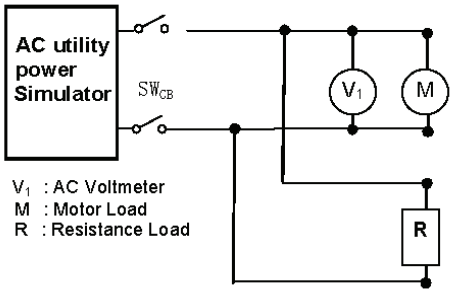

Fig.1.Measurement circuit of electric energy of motor load

Measuring the electric energy of the resonance load

In IEC standard, the inductivity load of the resonance load is defined by the formula (1) that is power conditioner ratings active effective output capacity

To execute our experiment, we had to decide the power conditioner output capacity. We examined the ratings output capacities of the certified power conditioners by JET authentication system in recent years.

As a result, since the majority of the power conditioners were 4kW of the rated output capacity, we decided the rated output capacity for the experiment was 4kW.

It is same as measuring the amount of electric energy of the motor load, amount of electric energy in resonant circuit is measured timing for the resistance load to consume about 10% (20V) of the rating voltage (200V) of the electric energy remained in the condition that a resistance load and a inductive and capacitive load were connected in parallel to the AC utility power simulator.

Moreover, the amount of inductive load was 2.6kVar, which was calculated with formula (1), and the same amount of capacitive load, 2.6kVar, was inserted.

$$P_{qL} = Q_f \times P_{EUT} \quad \cdots\cdots\cdots\cdots\cdots\cdots \quad (1)$$

P_{EUT}: Power conditioner ratings output

Q_f: 0.65

1. The resistance load connected with the resonance load parallel increases the electric power consumed by the resistance load from 0 to 4000W by 100W.
2. Switch (SW_{CB}) is opened according to the timing of t=0, and the motor load and the resistance load are separated from AC utility power Simulator.
3. The voltage between lines of the resistance load of each resistance load connected parallel that can be put is measured, and even about 10%(20V) of 200V in the ratings voltage measures delta X(Sec) until attenuating.

Fig.2 shows the circuit chart to measure the electric energy of the resonance load.

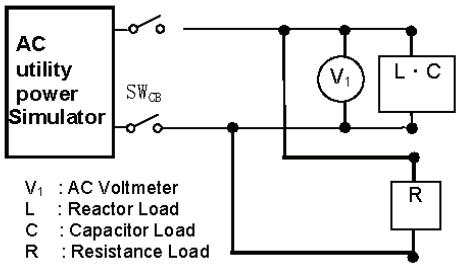

Fig.2.Measurement circuit of electric energy of resonance load

Table 1. Specifications of grinder motor loads (100V single phase)

Type	Rated capacity	Moment of inertia	Real power*)	Reactive power*)	rpm
Motor A	170 W	0.03 N-m^2	67 W	170 Var	3000 rpm
Motor B	365 W	0.03 N-m^2	80 W	270 Var	2970 rpm
Motor C	620 W	0.06 N-m^2	80 W	280 Var	2970 rpm
Motor D	645 W	0.06 N-m^2	95 W	175 Var	2960 rpm

*) in case of no load

Measurement result of electric energy

Fig.3 shows an experimental result concerning regenerative energy of motor loads and resonance circuit defined in IEC standards.

The EUT is disconnected from the experimental circuit in all cases. The relationships between the lapse of time from separation of SW_{CB} to the time when remaining voltage of load reaches 20V (see Fig.4 and Fig.5 as references), which is 10% of rated AC voltage(V_1) , and consumption of resistance load (AR) are indicated in Fig.3.

The lapse of time decreases according to the increase of consumption of resistance load because the consumption rate of the regenerative energy becomes faster.

The results reveal that motor C and D have almost the same regenerative energy, and the value of regenerative energy of motor A is close to the value of motor B. Besides, it is also clear that the value of the resonance circuit is almost equal to the value of motor A. Namely, it is judged that the resonance circuit and motor A is almost equivalent to the regenerative energy of the resonance circuit.

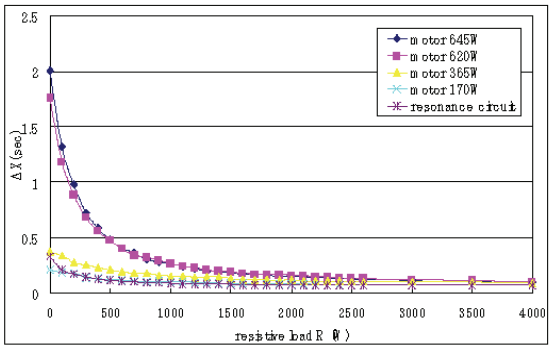

Fig.3. Measurement result of electric energy

However, because the result of above experiment is the length of time that it takes for the resistance load to consume the electric energy accumulated in each load, it is not clarified yet that whether the actual power conditioner would result in islanding by the influence of electric energy that was examined in this experiment.

Confirming the effectiveness of the motor load and resonance load by islanding experiment

The Islanding characteristics of motor A and the resonance circuit are the most similar in the regenerative energy. The 4kW PV inverter described above is used as a EUT in all islanding test below.

Fig.4 and Fig.5 show the relationship between islanding detection time, which means the time islanding continues (run on time), and imbalance condition of P and Q when both of the passive detection measure (PDM) and the active detection measure (ADM) in the inverter for islanding detection are masked.

Namely, islanding is detected only by voltage and frequency relays of the inverter in the cases.

In all figures, positive P means that load consumption is lager than real power of inverter just before SW_{CB} opened, and positive Q means that the system is in inductive condition just before SW_{CB} opened.

Table 2 and 3 also show frequency values of 0.3 sec. after S1 opened.

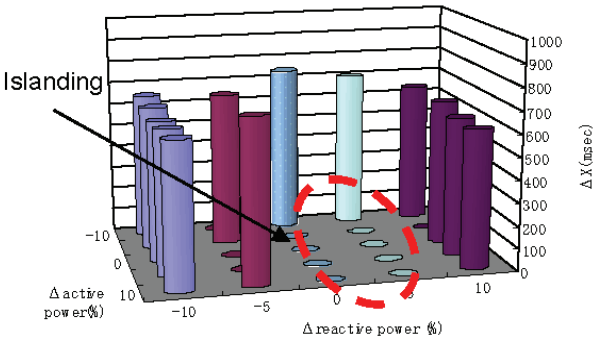

Fig.4 Islanding detection time limit by motor load

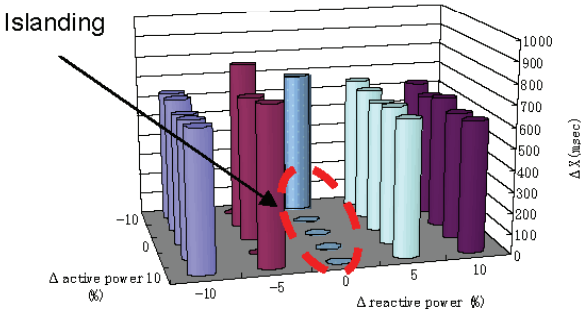

Fig.5 Islanding detection time limit by resonance load

It is shown that each characteristic of both resonance circuit case and motor load case is similar when P=0%, Q = 0% and P = 0%, Q = 5%.

Summary

By the experiment in which the electric energy of the motor loads and resonance load examined in IEC standard were measured, it was confirmed that, when the resonance coefficient was Qf=0.65, the amount of the electric energy of the resonance load had was almost equal to the amount of electric energy of the 170W motor load.

However, we cannot tell whether the influence by both loads on the islanding detection device of an actual power conditioner would be the same only by the evaluation of the electric energy that each load had.

Therefore, the islanding experiment was performed respectively of the resonance load and the 170W motor load with a real power conditioner.

It was confirmed that using either the resonance load or the 170W motor load, it resulted in islanding when the active power and the reactive electric power were in the state of equilibrium

In the same time, it was confirmed that, when the reactive electric power of both of the loads were in the state of equilibrium, it takes about 600ms for

Table 2. Frequency analysis result after 0.3 seconds after it blacks out (motor load 170W)

		Reactive power (Var)				
		-10%	-5%	0%	+5%	+10%
Active power (W)	-10%	45.45Hz	49.99Hz	50.51Hz	52.09Hz	55.24Hz
	-5%	45.84Hz	47.14Hz	50.05Hz	49.99Hz	50.00Hz
	0%	45.62Hz	50.05Hz	50.02Hz	50.04Hz	53.27Hz
	+5%	43.37Hz	49.96Hz	49.96Hz	49.99Hz	53.31Hz
	+10%	45.61Hz	48.51Hz	49.96Hz	49.97Hz	54.92Hz

Table 3. Frequency analysis result after 0.3 seconds after it blacks out (resonance load).

		Reactive power (Var)				
		-10%	-5%	0%	+5%	+10%
Active power (W)	-10%	46.75Hz	48.43 Hz	52.37 Hz	53.53 Hz	54.14 Hz
	-5%	46.47 Hz	48.25 Hz	50.21 Hz	53.12 Hz	54.46 Hz
	0%	46.88 Hz	48.05 Hz	50.59 Hz	52.09 Hz	54.03 Hz
	+5%	46.82 Hz	48.47 Hz	48.51 Hz	52.74 Hz	54.08 Hz
	+10%	46.78 Hz	48.35 Hz	48.81 Hz	52.12 Hz	54.39 Hz

the power conditioner to detect islanding and stop its operation even when the active power is increased and decreased.

From these results, it was shown that the resonance load and the 170W motor load have a similar characteristic in the influence given to the islanding detection device.

However, it also turns out from the result that the motor load cause islanding in wider range of load condition than the resonance load.

Therefore, we focused on the result of the frequency analysis after the black out considering the frequency would be the reason that the motor load caused islanding in wider range of load condition.

As a result, it was confirmed that in the load condition to cause the islanding phenomenon the frequency change after a black out is significant with the resonance load where the frequency barely changed with the motor load.

It is assumed that with the motor load the islanding phenomenon was caused in a wider-ranged load condition because the motor load maintained the frequency before blackout by absorbing and supplying the reactive electric power after the black out.

In the meanwhile, it is confirmed that the motor loads radically increases and decreases the frequency far more than the resonance loads in the other load conditions than that what causes islanding.

It is assumed that there is a possibility that the motor load increased the degree of the frequency change affected by the other inductive loads or capacitive loads.

The result of the experiment shows that there is similarity between both loads since the power conditioner resulted in islanding in the same load condition with either resonance load or the 170W motor load.

For the future study, the load condition to cause the islanding phenomenon will be confirmed by using other motor loads, the similarity between the 170W motor load and other loads will be verified, it will be confirmed whether a motor load absorb or supply reactive electric power after black out, and other influences by inductive loads and capacitive loads conditions will be clarified.

(1) October,2002 Electrical Safety & Environment Technology Laboratories"Test Procedure for Grid-connected Protective "Equipment, etc. for Photovoltaic Power Generation Systems

(2) 'New Sunshine project New Energy and Industrial Technology Development Organization (NEDO) consignment business result report' (PV) systems practical use technology development "Research and development of photovoltaic use system evaluation technology" and (research and development of technological in surrounding evaluation system) in 1994 fiscal year'

PERFORMANCE AND RELIABILITY OF 1 MW PHOTOVOLTAIC POWER FACILITIES IN AIST

Kenji OTANI[1], Takumi TAKASHIMA[1] and Kosuke KUROKAWA[2]
[1] National Institute of Advanced Industrial Science and Technology (AIST), Tsukuba, Ibaraki 305-8568, Japan
[2] Tokyo University of Agriculture and Technology (TUAT), Koganei, Tokyo, 184-8588 Japan

ABSTRACTS

The AIST 1MW PV facilities consist of a total of 211 inverters of the 4-kW type designed principally for residential uses, and tens of inverters of the 10-kW unit designed principally for industrial uses. These inverters are connected to low-voltage (200V) distribution line in AIST. There are 13 kinds of PV modules from 5 different technologies and tens kind of PV inverter from several manufactures. Benchmarking these PV components reveals the differences of the performance and reliability among other PV components under actual conditions.

During the first two years, there were several failures in the system components, mainly caused by improper installation works. But the PV facilities showed proper performance ratio (around 70%) and perfect availability in total. The mean time of failure was 7.9 times. More than 64% of individual PV systems had no failures. The mean time to repair was only 3.3 days.

INTRODUCTIONS

One of Japan's largest installations of megawatt-class solar photovoltaic (PV) systems was completed at AIST Tsukuba in April 2004 [1]. The main specifications of the facilities are indicated in Table 1.

The biggest characteristics of the facilities are the complexes of many numbers of systems (inverters) and of many series of PV components manufactured by many main PV companies, such as Sharp, Kyocera, Sanyo, MELCO, Shell Solar Japan, MSK, MHI, OMRON and etc. The configurations of PV component, newly introduced in spring 2004, are listed in Table 2. 78 of these 211 PV systems were monitored every one minutes with our special data-logger, and the rest were checked by human inspections.

The PV systems are located both at ground and on the rooftop of AIST buildings. The orientations of the arrays were set at the angle which the buildings faced towards, while the tilt angles were typically set at 15 degree optimized for summer season. A surrounding environment (shadings and etc.) varies significantly in the place. Therefore the treatment of the surrounding environment is important for benchmarking the PV systems. The location map of the PV systems is shown in Fig. 7 and the specifications are listed in Table 4.

Table 1. Main specifications of AIST 1MW System

Location	Tsukuba (Japan) 36°3' N – 140°8' E
Total capacity	1 MWp (869 kWp in FY2003)
Annual production	1 million kWh per year
CO_2 emission reduction	300 tons per year
PV module area	6,500m^2 (0.7% in AIST Tsukuba)
Investment	800 million Yen in FY2003
PV modules	5,600 PV modules 5 different technologies, 13 kinds of modules
Tilt angle:	15° (typical)
Grid-connected inverters	211(4kW), 14(10kW) and etc.
Monitoring systems	6 seconds and 1 minutes sampling intervals
Production:	2 000 MWh since Apr. 2004

Table 2. Configurations of PV components newly installed in April 2004

PV Module		Inverter (4 kW Unit)	
Sharp	NT-132BJ	Sharp	JH-L304
Sharp	ND-150AM	Sharp	JH-M303
Kyocera	SPG167	Kyocera	PVN-402
MELCO	PSOM-126F	MELCO	PV-PS05C2
Sanyo	HIP-180B2	Sanyo	SS-TL40A2
Shell Solar J	RK148/Λ HP	MHI	SPV400
MHI	MA100J1-YF	OMRON	KP40F
MSK	LPS125-180JH	OMRON	KP40F

PERFORMANCE ANALYSIS

Performance indices

For comparing the performance of energy conversion with different configurations of PV systems, three of the IEC standard 61724 performance parameters were used in this study. These parameters are the final system yield Y_f, reference yield Y_r, and performance ratio PR, and calculated by the equations below [2];

1-4244-0016-3/06/$20.00 ©2006 IEEE

$$Y_f = \frac{E}{P_0} \quad \text{[kWh/kWp] or [hour]} \quad (1)$$

$$Y_r = \frac{H}{G_0} \quad \text{[hour]} \quad (2)$$

$$PR = \frac{Y_f}{Y_r} \quad (3)$$

Where E: Net energy output during a certain period, P_0: Nominal DC power of the installed array, H: Total in-plane irradiation during a certain period, and G_0: Reference irradiance (i.e. 1 kW/m^2)

Macro analysis of the performance

Total power outputs fed into certain buildings have been monitored every 6 seconds or 1 minute. The performance indices calculated from these values may be helpful for knowing general evaluations of the facilities, such as the effect of energy saves and electricity demand power leveling. Since April 2004, the total amount of output energy has been more than 2 000 MWh, which value was almost equivalent to 1% of total electricity consumption in AIST Tsukuba during the same period.

Monthly trends of the final system yield and of the performance ratio are shown in Fig. 1. Annual final system yield was 985 hours and performance ratio was 0.70 in 2005. These values are almost equal to the average of ones for residential PV systems in Japan. The facilities may realize a smaller scale of large introduction of PV systems in Japan.

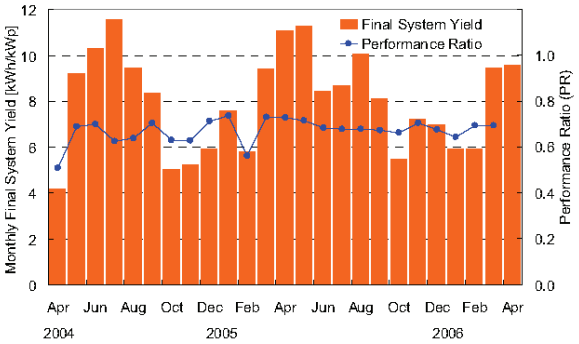

Fig. 1. Monthly Energy Yield since April 2004

Micro (Site) analysis of the performance

The range of the final system yield and of the performance ratio for each PV system was very wide because of wide variety of the specifications and configurations of PV systems in the facilities. Fig. 2 shows the frequency distributions of the final system yield obtained from 78 systems during a year (Aug. 2004 to Jul. 2005). There are appreciable differences of the distribution of the performance between ground and rooftop installed PV systems. The main reason of the differences was shadings.

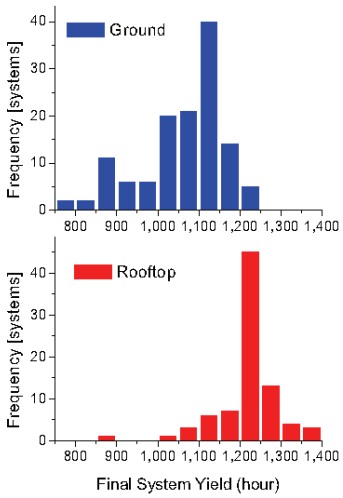

Fig. 2. Frequency distributions of the final system yield obtained from 78 systems

Long-term reliability of a PV system

The earliest PV system in AIST Tsukuba "Sakura-kan" was completed in the beginning in 1995 and has never encountered significant troubles and failures during continuous operation time. The visible defect (browning) of the surface of PV modules were found for almost half of PV modules on the arrays like a brown and black checkered pattern. This browning phenomenon seems to be caused by partial shadings on arrays by high pine trees on the south.

However, the performance decrease could not be found after ten years' operation in spite of the browning surface modules. Fig.3 indicates the scatter graph of the final system yield versus the reference yield during the initial three years and last three years.

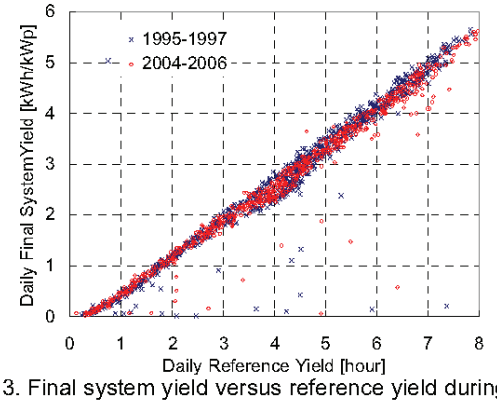

Fig. 3. Final system yield versus reference yield during the initial and last three years (after 10 years' operation)

Statistics of the reliability of PV systems and failures

By using 78 PV systems of 211 distributed PV systems completed in spring 2004, the evaluation of the statistics of the reliability of PV systems, such as mean

time between failure (MTBF) and mean time to repair (MTTR), has been done. The failures were found both by human inspections and by the performance diagnostic tool using our simulation technology.

There were no failures found from 50 PV systems during the last 20 months in the initial stage. Most of failures are concentrated on the worst three systems, and they decreased their MTBF values significantly. The frequency distributions of MTBF and of MTTR are shown in Fig. 4 and 5. Higher availabilities A, calculated by eq(4), were obtained as shown in Fig.6.

$$A = \frac{MTTR}{MTBF + MTTR} \qquad (4)$$

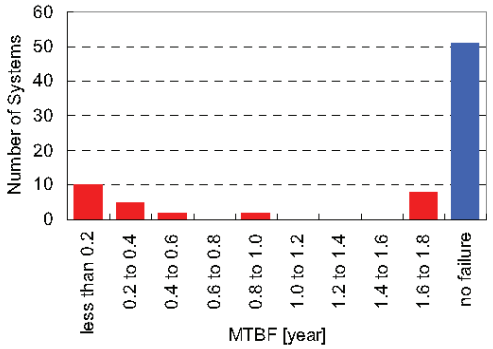

Fig.4. Frequency distribution of MTBF from 78 PV systems

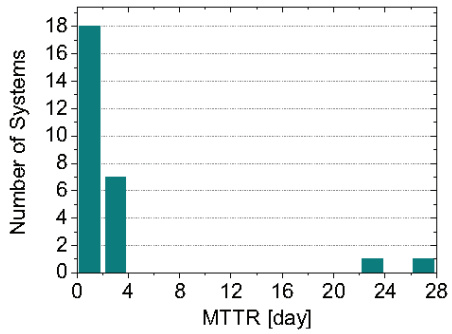

Fig.5. Frequency distribution of MTTR from 78 PV systems

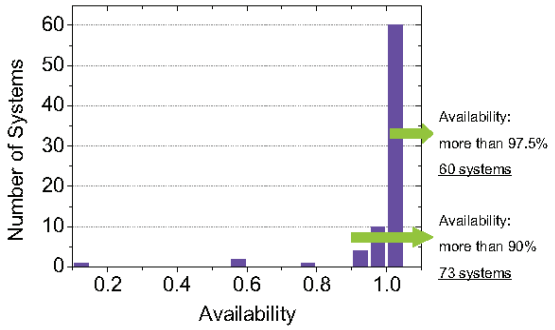

Fig.6. Frequency distribution of availability from 78 PV systems

Many numbers of minor failures were reported and repaired. The failure most frequently found was damaged back sheet of PV modules scratched in the installation works. These minor failures had little effect on the performance. The history of minor failures and monitoring errors are listed in Table 3.

Table 3. History of failure, replacement and repair (half-tone dot meshed rows indicate failures in PV components, and white-colored ones indicate failures in monitoring)

No.	Term	Location	Failure
1	Oct-2004	AIST 7-5	Inverter Replace
2	Oct-2004	AIST 3-5	Monitoring error
3	Dec-2004	AIST 3-5	EMCCB trip
4	Dec-2004	AIST 3-5	Intermittent inverter operation
5	Dec-2004	AIST 3-5	Broken module glass
6	Jan-2005	Energy Center	Wrong wiring
7	Feb-2005	Energy Center	Broken module glass
8	Mar-2005	Display	Monitoring error
9	Apr-2005	Parking	Damaged back sheet
10	May-2005	AIST3-5	Strike through
11	May-2005	AIST 3 & Energy Center	Damaged & colored back sheet
12	May-2005	Parking 7-6	Flooded terminal box
13	Jul-2005	AIST 2-12	Colored & burnt back sheet
14	Jul-2005	AIST 2-12	Inverter replacement
16	Sep-2005	AIST 3	Monitoring error

CONCLUSIONS

This paper describes field experiences from one of the largest PV facilities in Japan. The performance indices and reliability statistics were calculated for the first twenty months. The annual final system yield was 985 hours and the performance ratio was 0.70 in 2005. By using our performance diagnosis tool, failures in the operation were checked for 78 PV systems in order to evaluate the reliability of PV systems. The degradation of the performance was not found from our earliest PV system after ten years' operation.

REFERENCES

[1] K. Otani et al., "The Japan's largest introduction of photovoltaic systems reached one-megawatt for the assessment of the performance and reliability of grid-connected PV systems", 19th European Photovoltaic Solar Energy Conference, 2004.
[2] B. Marion et al., "Performance Parameters for Grid-Connected PV Systems", 31st IEEE PVSC, 2005, pp.1601-1606.

Fig.7. Location Map of Photovoltaic Systems in AIST Tsukuba

Table 4. Specifications of each PV System

No.	Location	PV Cell Type	PV Module Manufacture	Peak Power [kWp]	Buil d Year
	Solar Photovoltaic Monument				
1	AIST Tsukuba Center Bus Stop	multicrystal Si	Fuji Sash	4.0	2004
	Building-Integrated Photovoltaic System				
3	Tsukuba Headquarters and Information Technology Collaborative Research Center	monocrystal Si	Matsushita Ecology Systems	41.0	2004
4	Central 2-12 "OSL" Annex	monocrystal Si	Fuji Sash	12.0	2001
	Solar Photovoltaic Pavilion				
7	Central 3-5	monocrystal Si	Sharp	17.0	2004
8		multicrystal Si	Kyocera	16.0	
9		multicrystal Si	Mitsubishi Electric	16.0	
10		multicrystal Si	Shell Solar Japan	16.0	
11		heterojunction Si	Sanyo	17.0	
12		amorphous Si	Mitsubishi Heavy industries	16.0	
	Solar Photovoltaic Parking				
13	Central 3-5 Parking	monocrystal Si	MSK	86.0	2004
15	Central 2 Peripheral Road Parking	monocrystal Si	MSK	104.0	2004
24	Central 7-5 Parking	monocrystal Si	MSK	39.0	2004
	AIST Central Energy Center				
16	Eastern Hillside	multicrystal Si	Kyocera	8.0	2004
17	Southern Hillside	multicrystal Si	Kyocera	44.0	
18	Western Hillside	multicrystal Si	Kyocera	52.0	
19	Rooftop	multicrystal Si	Kyocera	36.0	
20	Ground	monocrystal Si	Sharp	68.0	
		multicrystal Si	Shell Solar Japan	24.0	
	Solar Photovoltaic System on Roof				
2	Central 1-1	heterojunction Si	Sanyo	34.6	2004
5	Central 2-12 "OSL" Annex	multicrystal Si	Sharp	162.0	2004
6	Central 2-7	monocrystal Si	Sharp	4.0	2002
14	Central 3-9	multicrystal Si	Shell Solar Japan	20.0	2004
21	Central 7-3	multicrystal Si	Mitsubishi Electric	36.3	2004
22	Central 7-4	multicrystal Si	Mitsubishi Electric	12.1	2004
23	Central 7-5	multicrystal Si	Mitsubishi Electric	12.1	2004
24	Central 7-6	multicrystal Si	Mitsubishi Electric	28.2	2004
25	Keyaki-Kan	multicrystal Si	Sharp	21.0	1997
26	Sakura-Kan	multicrystal Si	Sharp	72.0	1995

A Comparison of Output Envelope Waveforms of The Delta-Sigma Modulated Class D Series Resonant Inverter

Hirotaka Koizumi and Kosuke Kurokawa
Dept. of Elec. and Electronic Eng.
Tokyo Univ. of Agriculture and Tech.
Koganei, Tokyo 184-8588, Japan
Email: (koizumih,kurochan)@cc.tuat.ac.jp

Shinsaku Mori
Dept. of Elec. and Electronics Eng.
Nippon Institute of Technology
Miyashiro, Minamisaitama,
Saitama 345-8501, Japan

***Abstract*— The output envelope waveforms of the delta-sigma modulated Class D series resonant inverter is analyzed, compared, and discussed based on the simulation results with Matlab Simulink simulator. The Class D inverter operating at 200 kHz generates 50 Hz envelope waveform through the additional switching legs. Firstly, the relationship between the feed-back gain of the delta-sigma modulator and the output envelope waveforms is clarified. Secondly, the variable parameters are expanded to the loaded Q-factor Q_L. For Q_L= 10 to 10000, the output waveforms are analyzed. The simulation results show that THD is held under 3 % from Q_L = 50 to 100. The obtained envelope waveform is highly qualified as an ac power source.**

I. Introduction

Class D inverter [1]–[5] is one of the high-frequency high-efficiency resonant power sources, which can be applied to dc/dc resonant converters, radio transmitters, electronic ballasts for fluorescent lamps [2], and wireless communications [3]. The theoretically zero-current/zero-voltage switching (ZCS/ZVS) enables its operation at several hundred kHz (ZCS) to several hundred MHz (ZVS) with maintaining the high dc/ac power conversion efficiency.

The output power of Class D inverter is usually controlled with the operating frequency modulation (FM control). On the other hand, control methods without changing frequency are also proposed to maintain the ZVS/ZCS operation. In [4], irregular driving patterns are given to the gate drives to regulate the output power. In a full-bridge series resonant inverter, Pulse-Density Modulation (PDM) which controls the average output power by changing the driving-pulse density is proposed and applied to an induction melting [6]. However, in these types of regulation methods, harmonics and low frequency components are concerned.

Contrary to the above, the authors proposed to use the low frequency components actively [5]. The output envelope waveform of 50 Hz, which can be applied to an ac power supply, is formed with a Class D series resonant inverter driven at 200 kHz. With the 1-bit delta-sigma modulator [7], instead of a periodical-long-switching pattern for a 50 Hz sinusoidal waveform, the 1/0 driving pattern is easily and continuously generated based on the 50 Hz sinusoidal signal. That prevents the increasing of the driving-pattern digits leading up to the longer calculation time or the need of a higher performance micro-computer. The 1-bit signal keeps the constant frequency, which maintains the inverter operation with ZCS/ZVS.

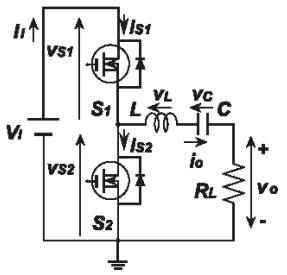

Fig. 1. Class D voltage-switching series resonant inverter.

In the previous research [5], the modulation process and the additional circuits to obtain a 50 Hz sinusoidal output envelope were shown. Those were tested with Matlab Simulink Simulator. The output waveforms with different feed-back gain G of the delta-sigma modulator were visually compared under the condition of the loaded Q-factor Q_L = 20. In the optimum case, its total harmonic distortion (THD) was 6.24 %. Further reduction of THD and discussion about the appropriate Q_L were the outstanding issues.

This paper firstly focuses on the relationship between the feed-back gain of the delta-sigma modulator and the output envelope waveforms. The flat peak and a small jump at the zero-crossing point of the envelope waveform can be improved by the feed-back gain.

Secondly, the variable parameters are expanded to the loaded Q-factor Q_L. The damping which strongly affects the envelope is characterized by the Q_L. The output waveforms and the total circuit operation are simulated by the Matlab Simulink simulator with Q_L from 10 to 10000. The output waveforms of the Class D series resonant inverter in steady state are confirmed by the numerically calculated waveforms. The obtained results are analyzed and discussed. The simulation results show that THD is no more than 3 % from Q_L = 50 to 100. The obtained envelope waveform is highly qualified as an ac power source.

II. Delta-Sigma Modulated Class D Series Resonant Inverter

A Class D voltage-switching series resonant inverter [1] is shown in Fig.1. It is composed of two switch devices S_1,

0-7803-9390-2/06/$20.00 ©2006 IEEE

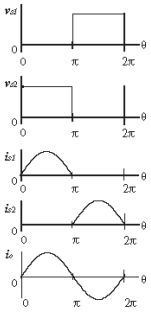

Fig. 2. Theoretical waveforms in Class D voltage-switching series resonant inverter with infinite Q_L in regular operation.

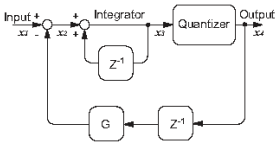

Fig. 3. 1st order delta-sigma modulator.

S_2, a band pass filter (BPF) L-C, and a load resistance R_L. The pair of switch devices performs as one switch which alternately connects with the dc voltage source V_I and an earth with keeping 0.5 duty ratio at the switching frequency f_s; i.e. while one device is ON the other is OFF in a half period $T/2 = 1/2f_s$. In the regular operation, it keeps alternate operation by a half period, which generates a square waveform v_{S2} at the input terminal of the BPF. Assuming an ideal BPF at the operating frequency, only the fundamental component of the square waveform flows to the load resistance in ideal. The output current i_o becomes sinusoidal and it flows through each switch by a half period. As shown in Fig. 2, while the switch current i_{S1} or i_{S2} is flowing through one switch, the voltage across the switch device v_{S1} or v_{S2} is zero, and the switching transition occurs at the zero current point, therefore the 100-percent power conversion efficiency can be achieved.

The 1st order delta-sigma modulator is shown in Fig. 3. If an ac signal with frequency f, $x_0 = \sin(2\pi ft)$, is directly given, the inverter output voltage waveform v_o becomes like Fig. 4 (a) [5]. The area painted over is filled with the

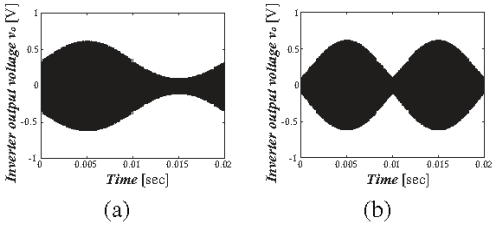

(a) (b)

Fig. 4. Calculated waveform v_o [5]. (a) The original input signal $x_0(t) = \sin(100\pi t)$ is given, and (b) the converted input signal $x_1(t) = |\sin(100\pi t)| - 0.5$; f_s = 200 kHz, G=0.6.

sinusoidal waveform with f_s. Sinusoidal envelopes appear in both the positive and negative edges with dc bias. To obtain a sinusoidal output envelope, the input signal x_0 is converted to the waveform having its absolute value, and shifted down to the half of the original amplitude. Finally, the ac signal x_0 is converted to x_1=$|\sin(2\pi ft)|$-0.5, which is shown in Fig. 5 (a). The range of x_1 is -0.5 to 0.5 V. The input signal to the integrator x_2 is x_1-G to x_1+G, because the output value of the quantizer x_4 is -1 for a negative value, 1 for a positive value, and 0 for 0. When x_4 = 1 the driving code becomes '1', otherwise '0'. While the code '1' is given to the inverter, S_1 and S_2 repeat the regular cycle; if the code '0' is given, the driving pulse of S_1 keeps 0 during the term. When the code '1' is continuously given, the amplitude of the output waveform increases and approaches $0.64V_I$ which is the theoretical amplitude in the regular operation. On the other hand, when the code '0' is given in series, the amplitude decreases and approaches 0. Giving x_1 to the modulator, the Class D series resonant inverter generates the output voltage v_o like Fig. 4 (b). To obtain the envelope waveform from v_o, additional circuit (Fig. 6) is needed [5]. The circuit is composed of two full-bridge switching legs. At the first stage, the RF waveform v_o is rectified by the full-bridge rectifier. At the second stage, the rectified waveform V_r is inverted by half cycle of the frequency f synchronized with the input signal. Through the LPF, the envelope v_e is obtained. All the switches maintain ZCS.

III. Simulation and Numerical Analysis

Before the simulation and calculation, the parameters have to be given. The input voltage and the load resistance are given as V_I = 1 V, and R_L = 1 Ω for generalization of the analysis [8]. The switching frequency f_s=200 kHz and the loaded quality factor of the series resonant circuit Q_L are given. The resonant inductance and capacitance are $L = Q_L R_L/\omega_s$, and $C = 1/\omega_s^2 L = 1/\omega_s Q_L R_L$, where $\omega_s = 2\pi f_s$. The low pass filter L_f-C_f is designed to reduce the switching frequency component and to be a resistive impedance as far as f_s, which is important to keep ZCS. Giving the C_f, L_f=$R_L^2 C_f/\{(1 + (2\pi f_s C_f R_L)^2\}$.

In the numerical analysis, all the elements including switch devices are assumed to be ideal. The driving pattern is generated following the process of Fig. 3. In the numerical analysis, the LPF of the additional circuit is not covered. Waveforms are numerically calculated from the differential equations. In the circuit of Fig. 1, the equations are

$$C\frac{dv_C}{dt} = i_o, \tag{1}$$

$$L\frac{di_o}{dt} = -v_C - R_L i_o + v_{S2}, \tag{2}$$

where v_C and v_L are voltages across the capacitance C and the inductance L as depicted in Fig. 1. In (2), v_{S2} takes V_I and 0 according to the drive pattern; thus, there exist two states. When the driving code '1' is given, each state is maintained by a half period. When '0' is given, v_{S2} maintains 0 during

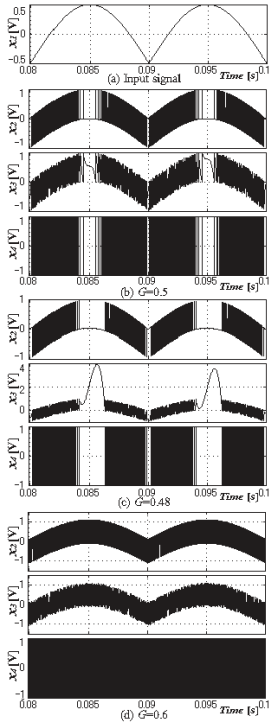

Fig. 5. Signal waveforms of the 1st order delta-sigma modulator. (a) Input signal to the modulator x_1. Input waveform to the integrator x_2, input waveform to the quantizer x_3, and the output waveform x_4 with the feed-back gain (b) G=0.5, (c) G=0.48, and (d) G=0.6.

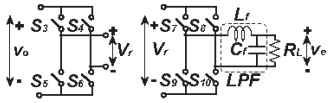

Fig. 6. Additional circuit.

one period. According to the continuity of inductor current and capacitor voltage, the initial values of i_o and v_C in a half period take the final values in the previous half period. In steady state, the last value should be equal to the initial value in one total cycle. Using this condition, the circuit equations (1) and (2) are numerically solved with Runge-Kutta formula.

In the simulation, a total system composed of the 1-bit delta-sigma modulator, Class D series resonant inverter, and switching legs is built as a simulation model. The values of the circuit elements and parameters are given as functions which conform to the numerical analysis. The switching leg composed of S_1 and S_2 is replaced by a controlled voltage source which generates a voltage pattern based on the modulated code. The switches S_3 to S_6 are substituted with ideal diode models; and S_7 to S_{10} are synchronized with the analog ac signal. For LPF, C_f = 10 μF is given. In all the simulation, ode15s solver is used because of the calculation time. The relative torelance is set to e^{-9} with considering strict ZCS transition.

TABLE I
OBSERVED THD WITH SIMULINK SIMULATION

Q_L	THD	G
10	0.0748–0.0754	0.6
20	0.0620–0.0624	0.6
10	0.0525–0.0531	0.5
20	0.0313–0.0322	0.5
50	0.0220–0.0227	0.5
60	0.0219–0.0226	0.5
65	0.0218–0.0227	0.5
70	0.0222–0.0229	0.5
100	0.0251–0.0257	0.5
150	0.0344–0.0350	0.5
500	0.1464–0.1472	0.5
1000	0.2875–0.2880	0.5
10000	0.475–0.485	0.5

IV. FEED-BACK GAIN OF THE DELTA-SIGMA MODULATOR

As shown in Fig. 3, the feed-back gain G is from the quantizer output signal x_4 which takes ± 1 and 0. As is clear from the block diagram, x_2 takes a value from x_1-G to x_1+G, which is integrated as x_3. The output value of the quantizer x_4 is determined by x_3. Assuming that the input signal is x_1=$|\sin(2\pi ft)|$-0.5, according to the above process, the modulator should generate the modulated code which causes a full-scale waveform, when G=0.5. The signal waveforms obtained by simulation are shown in Fig. 5 (b). Figure 7 (c) with Q_L=20, for example, shows the inverter output waveform. The sinusoidal envelope with the amplitude of $0.64V_I$ is confirmed. Around the peaks of x_1, x_4 keeps '1' which causes the flat top of the output envelope. If $G < 0.5$, x_3 increases near the peaks of x_1 as shown in Fig. 5 (c), which enlarges the flat part of the envelope. On the other hand, x_4 keeps '0' near the bottom peak of x_1, which causes a 'wide' zero-crossing point in the envelope. Increasing of G is a solution to the problems. As shown in Fig. 5 (d), the signals are continuously changing with G = 0.6. However, another problem occurs. Around the bottom peak of x_1, x_4 takes frequently '1', which causes small voltage at the zero-crossing point. As shown in Fig. 4 (b), the minimum amplitude is not reduced down to 0. In addition, x_4 often takes '0' around the peak of x_1. That is effective against the flat top, however reduces the amplitude of the output envelope. Both the flat top and small jump at the zero-cross cause THD. For G = 0.5, and 0.6, with Q_L = 10, and 20, THD are calculated by the simulation. These results are shown in the top 4 lines of Table I. Judging from the results, G=0.5, which keeps the zero-crossing point, is more suitable for low THD. Higher G than 0.6 causes larger jump; and lower G than 0.5 causes flat top and wide zero-crossing point.

V. OUTPUT ENVELOPE WAVEFORMS UNDER VARIOUS Q-FACTORS

The damping which strongly affects the envelope is characterized by Q_L. To find the appropriate Q-factor, the output waveforms and the total circuit operation were simulated by the Matlab Simulink simulation from Q_L=10 to 10000. The

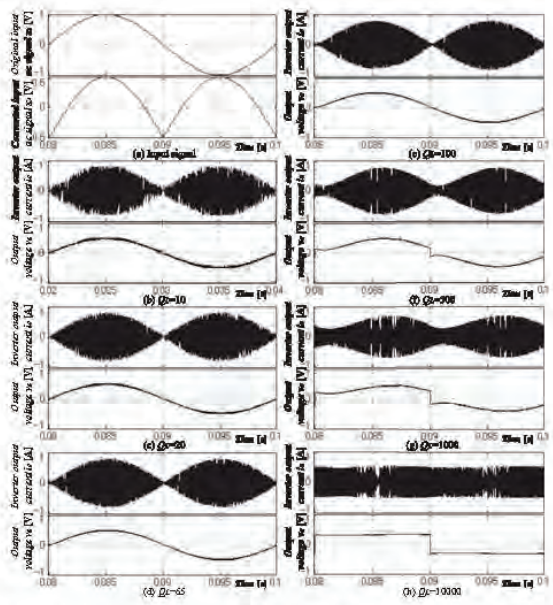

Fig. 7. Observed waveforms under different Q-factor conditions. (a) Original input signal x_0 (top) and the converted signal x_1 (bottom). From (b) to (h), the output current of Class D series resonant inverter i_o (top), and the output voltage v_e (bottom) for Q_L = 10, 20, 65, 100, 500, 1000, and 10000.

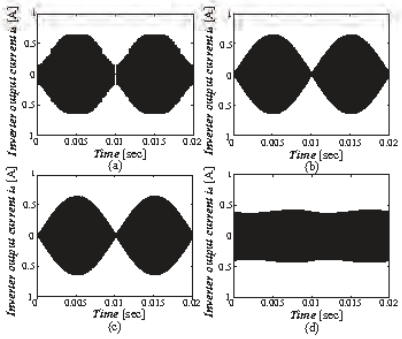

Fig. 8. Calculated waveform i_o in steady state; f_s = 200 kHz, G=0.5. (a) Q_L=10, (b) Q_L=65, (c) Q_L=100, and (d) Q_L=10000.

feed-back gain G was set to 0.5. Considering the calculation time and the performance of the computer, the simulation time was set less than 0.1 sec. The output current i_o of the Class D series resonant inverter and the envelope output voltage v_e are shown in Fig. 7. As is clear from Fig. 7, as Q_L becomes large, i_o becomes flat, the amplitude becomes smaller, and v_e becomes close to the square waveform. The time constant of the envelope τ is given by $\tau = 2L/R_L = 2Q/\omega_s$ [6]. In case of Q_L=10, τ=0.016 ms; and Q_L=10000, τ=15.9 ms which is longer than a half period of 50Hz. The small τ enables the quick response of the inverter; therefore i_o keeps the characteristic of x_4. Basically the quick response is preferable, however, rapid increase or decrease causes the flat top or the wide zero-cross as shown in Fig. 7 (b). On the other hand, large τ delays the response, which performs like a LPF. The slow increase cuts down the peak amplitude; and the slow decrease fills the zero-crossing point. Furthermore, as shown in Fig. 7 (f) and (g), the peak and zero-crossing are delayed. The waveforms shown in Fig. 7 (c), (d) and (e) corresponding to Q_L=20, 65, and 100 are visually preferable to the others. The waveform with Q_L=20 has a slightly flat top. Small phase-delay can be seen in the waveform with Q_L=100. Using the measurement tool of the simulator, THD was measured for various Q_L. Those are shown in Table I. Between Q_L=20 to 100, THD is less than 3 %. The minimum THD is measured around Q_L=65. In this case τ=0.103 ms, which is 0.5% of the 50 Hz envelope cycle. The waveforms of i_o in steady-state are confirmed by the numerical analysis. Some of them are shown in Fig. 8. Those agree well with the simulation results.

VI. Conclusion

The output envelope waveforms of the delta-sigma modulated Class D series resonant inverter have been compared based on the simulation results with Matlab Simulink simulator. The waveforms well agree with the numerical analysis.

The relationship between the feed-back gain of the delta-sigma modulator and the output envelope waveforms has been clarified. The flat peak and a small jump at the zero-crossing point of the envelope waveform can be regulated by the feed-back gain.

The output waveforms with Q_L= 10 to 10000 are compared based on the simulation results. The relationship between Q factor and the output waveforms have been discussed and analyzed. The appropriate Q_L is found based on the simulation results. From Q_L = 50 to 100, THD is held under 3 % . The obtained envelope waveform is highly qualified as an ac power source.

Acknowledgment

This work was supported in part by Grant-in-Aid for Scientific Research from the Ministry of Education, Science, Sports, and Culture, Japan.

References

[1] P. J. Baxandall, "Transistor sine-wave LC oscillators, some general considerations and new developments," *Proc. IEE*, vol. 106, pt. B, suppl. 16, pp. 748–758, May 1959.

[2] M. K. Kazimierczuk and W. Szaraniec, "Electronic ballast for fluorescent lamps," *IEEE Trans. Power Elec.*, vol. 8, No. 4 pp. 386–395, Oct. 1993.

[3] H. Kobayashi, J. M. Hinrichs, and P. M. Asbeck, "Current-mode Class-D power amplifiers for high-efficiency RF applications," *IEEE Trans. Microwave Theory Tech.*, vol. 49, No. 12 pp. 2480–2485, Dec. 2001.

[4] H. Koizumi, K. Kurokawa, and S. Mori, "Analysis of Class D inverter with irregular driving patterns," Proc. *IEEE Int'l Symposium on Circuits and Systems 2004*, vol.V, pp. 868-871, May 2004.

[5] H. Koizumi, K. Kurokawa, and S. Mori, "Thinned-out controlled Class D inverter with delta-sigma modulated 1-bit driving pulses," Proc. *IEEE Int'l Symposium on Circuits and Systems 2005*, pp. 1322-1325, May 2005.

[6] H. Fujita, and H. Akagi, "Pulse-density-modulated power control of a 4 kW, 450kHz voltage-source inverter for induction melting application," *IEEE Trans. Ind. Appl.*, vol. 32, No. 2 pp. 279–286, Mar./Apr. 1996.

[7] K. Masuda, T. Hayase, S. Satoh, "1 bit audio," *Sharp Tech. Report*, vol. 77, pp. 67-72, Aug. 2000 (in Japanese).

[8] M. Albulet, "An exact analysis of Class-DE amplifier at any output Q" *IEEE Trans. Circuits Syst. I*, vol. CAS-46, No. 10 pp. 1228-1239, Oct. 1999.

37th IEEE Power Electronics Specialists Conference / June 18 - 22, 2006, Jeju, Korea

Voltage Control of D-UPFC between a Clustered PV System and Distribution System

Kyungsoo LEE, Hirotaka KOIZUMI, and Kosuke KUROKAWA
Tokyo University of Agriculture & Technology
Graduate School of Technology
2-24-16, Naka-cho, Koganei, Tokyo, 154-8588
Email: (onnuri, koizumih, kurochan)@cc.tuat.ac.jp

Abstract—This paper proposes distribution-unified power flow controller (D-UPFC) in the distribution system. D-UPFC controls distribution system voltage during voltage *sags* and *swells*. A single-phase ac-ac converter in a matrix arrangement and a series transformer are the components of D-UPFC. Ac-ac converter generates power using switching pattern when voltage variation occurs. The series transformer compensates voltage to the loads. Voltage swell condition is considered when reverse power flows from the clustered photovoltaic (PV) system. D-UPFC simulations show the possibility of controlling distribution system voltage when voltage *sags* and *swells* occur.

I. INTRODUCTION

Nowadays, it is common to find disturbances in the amplitude or waveform shape of current and voltage in the electric systems. These conditions could produce fails in the equipments, raising the possibility of an energy interruption. The voltage fast variations that appear in the AC mains during 10 seconds or less are commonly known as voltage *sags* and *swells*. These variations are produced by normal operation of high power loads as well as theirs connection and disconnection; the voltage fast variation effects are function of the amplitude and the duration of the event. Some studies show that 92% of all disturbances in the electrical power distribution systems are produced by voltage *sags*.

Dynamic voltage restorer (DVR) and uninterrupted power supply (UPS) systems had been researched and developed along the last decades and they are capable to compensate voltage *sags* and *swells*. However, they depend on devices to store energy, like large capacitors or battery bank. If the power increases, the size of the devices will increase [1].

One of other options is to compensate voltage sags using PWM ac-ac converter with autotransformer. This system can compensate until 50% voltages *sags* and *swells*. It can continuously shape the output voltage to be sinusoidal (low THD) even when the input voltage is distorted [2]. The other option is step voltage regulator (SVR), which is based on autotransformer with line drop compensator. However, the autotransformer drives all the load power due to it is connected between the load and the AC mains [1].

Recently, voltage *swells* are occured not only heavy load condition but also reverse power flow from distributed system (DG) like PV systems. If a large number of PV power generation systems are connected to distribution lines, the voltage at the customer's terminals may increase because of reverse power flow. This increase will depend upon the relative sizes of the load and the power generation. Since the sending voltage on the secondary side of the distribution transformer is typically set at a value higher than the standard voltage under current operating procedures, the voltage at the end of a distribution line could exceed the upper limit even with slight reverse power flow, possibly created by the PV system during light-load hours in the daytime [3].

Thus, this paper proposes D-UPFC in order to control voltage *swells* as well as *sags*. Figure 1 shows the D-UPFC concept in the distribution system.

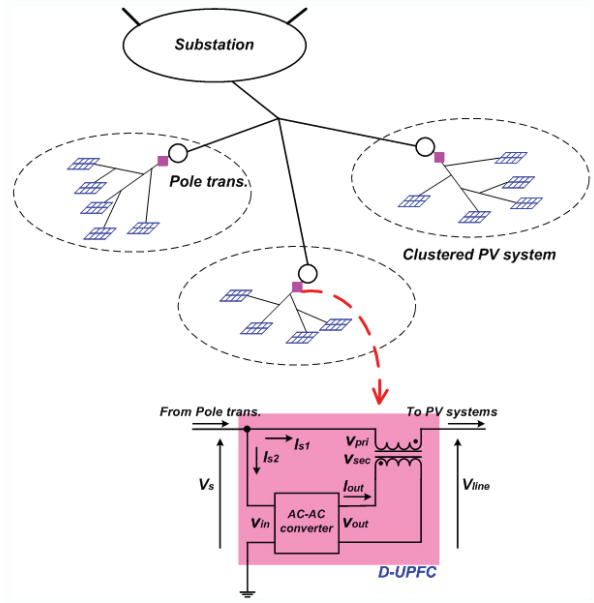

Fig. 1: D-UPFC concept in the distribution system

D-UPFC is installed at the back of pole transformer and it connects with load side. Also, D-UPFC is applied in the radial power system. D-UPFC consists of single-phase ac-ac converter in a matix arrangement and a series transformer. Ac-ac converter generates power using matrix arrangement and a series transformer compensates voltage to the load. D-UPFC does not need any energy storage device and it fast compensates load voltage during voltage *sags* and *swells*.

The remainder of this paper explains more specified D-UPFC concept, operation and control method. Finally, voltage *sag* and *swell* simulation results are discussed.

1-4244-9717-7/06/$20.00 ©2006 IEEE.

II. D-UPFC SCHEME

A. *Specified D-UPFC concept*

D-UPFC controls distribution voltage like autotransformer. Figure 2 shows the role of D-UPFC compared with normal autotransformer.

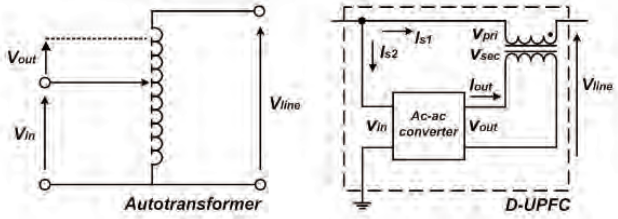

Fig. 2: D-UPFC role as an autotransformer

When input voltage V_{in} is in normal condition, ac-ac converter of D-UPFC does not generate voltage. However, when voltage *sags* or *swells* occur, D-UPFC generates output voltage V_{out} and then distribution line voltage V_{line} is controlled.

D-UPFC should control the distribution voltage when voltage *sags* and *swells* occur. Thus, effective control condition is necessary. Figure 3 shows D-UPFC equivalent circuit.

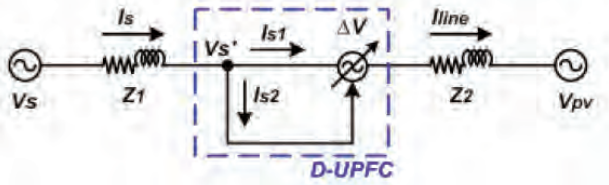

Fig. 3: D-UPFC equivalent circuit in the distribution system

When voltage variation ΔV occurs due to voltage *sags* or *swells* in the distribution, the D-UPFC output ΔP is given,

$$\Delta P = \Delta V \times I_{s1} \tag{1}$$

D-UPFC input current I_{s2} due to voltage variation is,

$$I_{s2} = (\frac{\Delta V}{V_s'}) I_{s1} \tag{2}$$

Using Kirchhoff's current law, pole transformer current I_s is given,

$$I_s = I_{s1} + I_{s2} = (1 + \frac{\Delta V}{V_s'}) I_{s1} \tag{3}$$

D-UPFC input voltage V_s' is induced,

$$V_s' = V_s - (Z_1 \times I_s) = V_s - Z_1 (1 + \frac{\Delta V}{V_s'}) I_{s1} \tag{4}$$

where, V_s is pole transformer voltage, V_s' is the D-UPFC input voltage. V_{pv} is the clustered PV system voltage, Z_1 and Z_2 are line impedances (however, Z_1 is very small because D-UPFC connects with pole trans. voltage V_s in the same pole)

Through the eq. (1) to (4), the effective D-UPFC control should comply with eq. (5).

$$\left|\Delta V_s'\right| \le \left|\Delta V\right| \tag{5}$$

where, $\Delta V_s'$ is the variation value of V_s'

B. *D-UPFC operation*

Ac-ac converter consists of four bi-directional switches and input/output filters. When there is no voltage variation, D-UPFC operation is shown in Fig. 4.

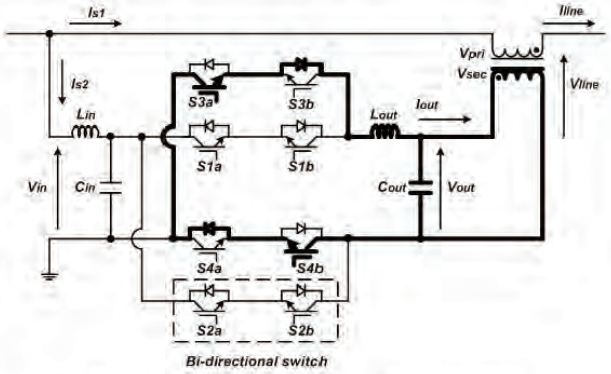

Fig. 4: D-UPFC circuit operation during normal mode

In the D-UPFC normal condition, bi-directional switch S_3 and S_4 are closed (or S_1 and S_2) and the output voltage is equal to zero.

When voltage *sags* happen, the switch S_4 is closed, and S_1 and S_3 are operated with a duty cycle D, generating a V_{out} for compensation. When voltage *swells* caused by reverse power from clustered PV system occur, the switch S_3 is closed and S_2 and S_4 generate V_{out} for voltage regulation. Bi-directional switches S_1-S_3 and S_2-S_4 never should be closed at the same time in order to avoid short-circuit in the ac-ac converter [1], [4].

C. *Voltage control method*

D-UPFC senses input voltage V_{in} , line voltage V_{line} and line current I_{line}. Input voltage is the reference voltage because it connects with pole transformer voltage V_s. Line voltage and current represent the D-UPFC output voltage and output current, respectively. Figure 5 shows D-UPFC control in the distribution system.

Input voltage V_{in}, line voltage V_{line} and line current I_{line} are sensed and change to dc values through root-mean-square (RMS) function for controlling ac-ac converter. Next, V_{in} and V_{line_sum} are compared each other and then voltage error V_{error} is calculated. Here, V_{line_sum} means line voltage V_{line} with line impedance Z_2. V_{line_sum} is used to control PCC (here, PCC indicates the next pole apart from the pole transformer) voltage. V_{error} changes to reference voltage V_{ref} through propotional (P) control. In the PWM control, V_{ref} and triangle voltage V_{tri} are compared and then this control supplies switching signals to the ac-ac converter. D-UPFC uses the voltage margin in order to control distribution voltage

flexibly. Pole transformer's secondary voltage range of Japan is 101±6[V,rms]. If the value of v_{error} is larger than 2[V] of voltage margin, D-UPFC performs.

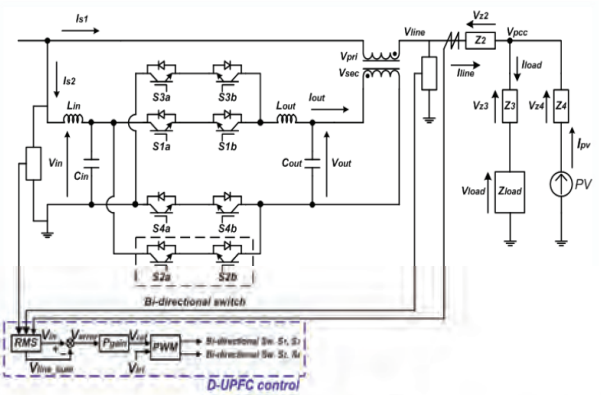

Fig. 5: D-UPFC control circuit

As mentioned, D-UPFC senses V_{line} and calculates V_{line_sum} with line impedance Z_2. So, V_{line_sum} can be written as eq. (6).

$$V_{line\_sum} = V_{pcc} + (I_{line} \times Z_2) \quad (6)$$

However, eq (6) can be only used when power flow is from substation to the load area. When reverse power flow occurs from PV systems eq. (6) changes to eq. (7).

$$V_{line\_sum} = V_{pcc} - (I_{line} \times Z_2) \quad (7)$$

Voltage margin equation is shown in eq. (8).

$$\left| V_{in} - V_{line\_sum} \right| < 2 \quad (8)$$

Thus, D-UPFC performs when voltage difference between V_{in} and V_{line_sum} is larger than 2[V,rms].

III. SIMULATION RESULTS AND DISCUSSION

A. Simulation model

A simple case of D-UPFC simulation model is considered. Figure 6 shows the D-UPFC simulation model.

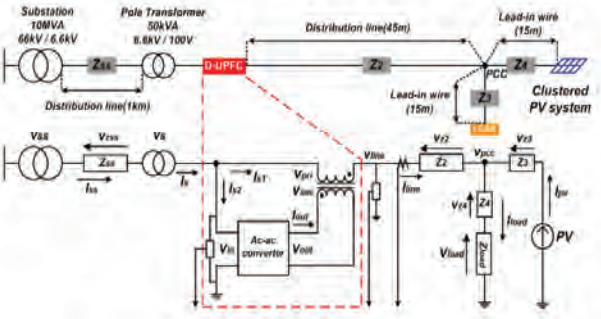

Fig. 6: D-UPFC simulation model

This model analyzed from the substation to the load areas. D-UPFC is installed at the back of pole transformer. Load and clustered PV system are simply fixed. The distance from substation to pole transformer is 1[km]. From pole transformer to PCC is 45[m]. PCC connects with load and the clustered PV system. The lead-in wire is 15[m] between PCC and loads with clustered PV system.

Simulation model parameters of D-UPFC are shown in Table 1. Line impedance parameters refer to electric company information of Japan. A series transformer turns ratio for compensating the maximum voltage sag or swell condition refer to [1], [5]. Input and output filters should reduce the switching frequency harmonics present in the input current I_{s2}, output voltage V_{out}, respectively. It refers in [6].

TABLE I
D-UPFC SIMULATION PARAMETERS

V_{ss}	6600[V,rms]
V_s	100[V,rms]
Z_{ss}	0.25+j0.34[Ω/km]
Z_2	0.011+j0.013[Ω/km]
Z_3,Z_4	3.45m+j0.15m[Ω/km]
Z_{load}	10+0.01[Ω]
Substation trans.[N_{pri}:N_{sec}]	66:1
Pole trans.[N_{pri}:N_{sec}]	1:1
Series trans.[N_{pri}:N_{sec}]	1:3
Input filter	50[μH], 20[μF]
Output filter	75[μH], 30[μH]
Switching freq.	10[kHz]
Voltage sag (V_{sag})	0-5[V,rms]
PV source (I_{pv})	0 - 300[A,rms]

Simulation performs considering both voltage *sags* and *swells*. Table II shows the simulation result when voltage sag happens.

TABLE II
VOLTAGE SAG SIMULATION RESULT

V_{sag}	No D-UPFC control			D-UPFC control	
	V_{in}	V_{line}	V_{line_sum}	V_{line}	V_{line_sum}
0	99.7	99.7	99.5	99.7	99.8
1	99.7	99.7	99.5	99.8	100.5
*2	99.7	99.7	97.5	***99.4**	***99.3**
*3	99.7	96.7	96.5	***99.2**	***99.0**
*4	99.7	95.7	95.5	***98.9**	***98.8**
*5	99.7	94.7	94.5	***98.7**	***98.7**

All parameters show in rms value, '*' means controlled value

Voltage sag was simulated from 0[V,rms] to 5[V,rms] in AC main. V_{in} is the input voltage, V_{line} is the D-UPFC output voltage, and V_{line_sum} shows the PCC voltage. Especially, V_{line_sum} calculates PCC voltage using eq. (6) and thus, it can control load area voltage. In the D-UPFC control, V_{sag} was controlled from 2[V,rms] to 5[V,rms]because it uses voltage margin as shown eq. (8).

In the voltage swell simulation, clustered PV system regarded as the current source. Thus, I_{pv} indicates reverse current from clustered PV system. Table III shows voltage swell simulation result.

I_{pv} increases from 0[A,rms] to 300[A,rms]. The same as voltage sag simulation, voltage margin was applied to the simulation. When I_{pv} was from 150[A,rms] to 300[A,rms], V_{line_sum} changed from 101.4[V,rms] to 104.1[V,rms]. In the simulation results, D-UPFC does not control V_{line_sum} voltage

in *swells* condition.

Figure 7 shows voltage sag simulation waveforms.

TABLE III
VOLTAGE SWELL SIMULATION RESULT

I_{pv}	No D-UPFC control			D-UPFC control	
	V_{in}	V_{line}	V_{line_sum}	V_{line}	V_{line_sum}
0	99.7	99.7	99.8	99.7	99.8
50	99.7	99.7	99.8	99.8	100.5
100	99.7	99.7	99.8	100	101.6
150	99.7	100.4	102.8	***99.1***	***101.4***
200	99.7	100.9	104.1	***99.0***	***102.3***
250	99.7	101.4	105.5	***99.1***	***103.1***
300	99.7	102.1	107	***99.2***	***104.1***

All parameters show in rms value, '*' means controlled value

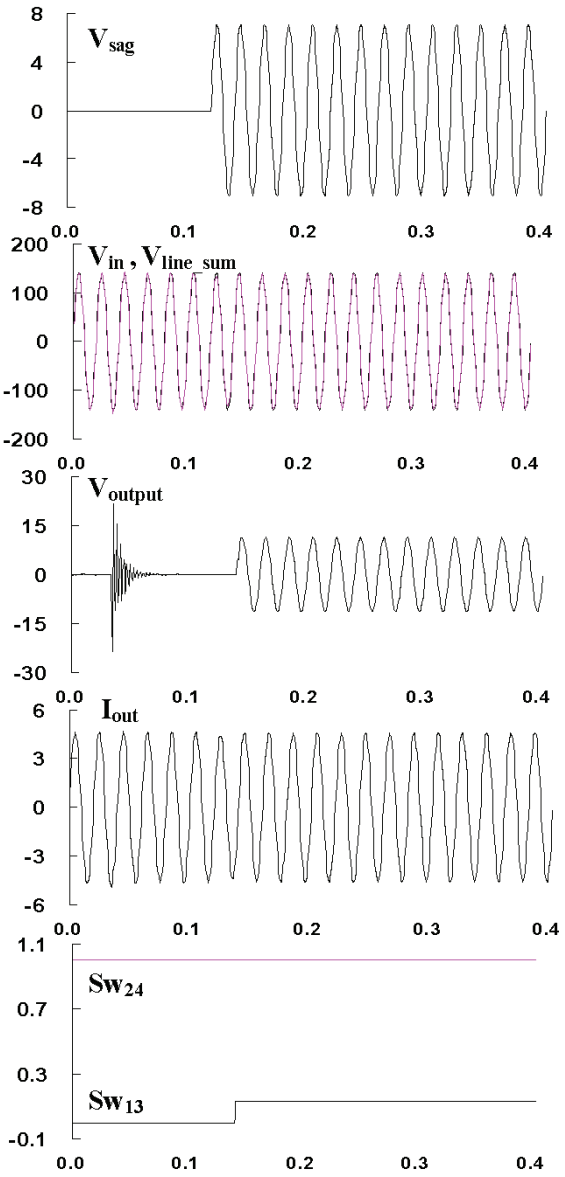

Fig. 7: Voltage sag simulation (V_{sag} 5[V, rms] at 0.12[s])

All the waveforms were simulated from 0[s] to 0.4[s]. The top waveform shows V_{sag} 5[V,rms] at 0.12[s]. The second waveforms indicate V_{in} and V_{line_sum}. The third and fourth waveforms show ac-ac converter output voltage and current, respectively. The bottom waveforms show switch 1, 3 and switch 2, 4 reference signals. When V_{sag} 5[V,rms] happens at 0.12[s], ac-ac converter operates from 0.14[s] because it uses rms function. Also, switch 1 and 3 perform pwm control. Switch 2 is opened, switch 4 is closed. After V_{sag} starts 0.12[s], the transient-state condition continued for two cycles and then it becomes the steady-state condition.

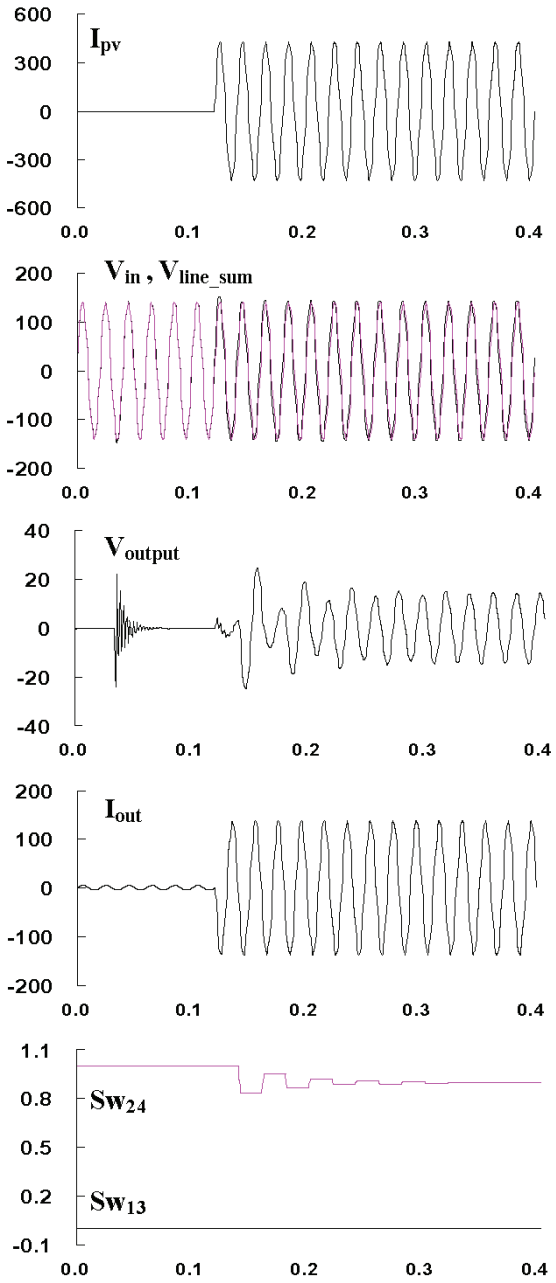

Fig. 8: Voltage swell simulation (V_{swell} 300[A, rms] at 0.12[s])

Voltage swell simulation waveforms are shown in Fig. 8. The top parameter shows reverse power I_{pv}. This simulation implemented from 0[s] to 0.4[s]. I_{pv} inputs 300[A,rms] from 0.12[s]. When reverse power flows from I_{pv} to the grid, V_{line_sum} increases to 107[V,rms]. Ac-ac converter operated from 0.14[s] due to using rms function. Under the voltage swell condition, bi-directional switch S_3 is closed and S_1 is openned. Also, S_2 and S_4 implemented pwm control. Through the reverse power flow simulation, PCC voltage is controlled from 0.32[s]. D-UPFC couldn't control distribution voltage. Also, the phase of ac-ac converter output voltage and current is changed.

In this research, D-UPFC capacity and the phase angle variation during reverse power flow were not considered fully.

IV. CONCLUSION

This paper proposed D-UPFC in the distribution system. D-UPFC scheme, operation and control method are shown. D-UPFC works as an autotransformer and consists of ac-ac converter and a series transformer. Voltage margin and load voltage compensation methods are introduced. Simulation model is used in voltage sag and swell test. Through the simulations, D-UPFC shows the possibility of controlling distribution voltage when voltage *sags* and *swells* occur.

ACKNOWLEDGMENT

This research has been carried as a part of "Autonomy-Enhanced PV Cluster" project and special thanks for financial support of New Energy and Industrial Technology Development Organization.

REFERENCES

[1] J. Pérez, V. Cárdenas, H. Míranda, and R. Álvarez, "Compensation of Voltage Sags and Swells using a Single-Phase Ac-Ac Converter," *The 30th Annual Conference of the IEEE Industrial Electronics Society,* Busan, Korea, November 2004, pp. 1611-1616.

[2] E. C. Aeloiza, P. N. Enjeti, L.A. Morán, and I. Pital, "Next Generation Distribution Transformer: To Address Power Quality for Cirtical Loads," *Power Electronics Specialists Conference PESC 2003*, Vol. 3, June 2003, pp. 1266-1271.

[3] Bas Verhoeven, Utility aspects of grid connected photovoltaic power system, Task V, Report IEA PVPS T5-01, December 1998.

[4] P. W. Wheeler, J. Rodríguez, J. C. Clare L. Empringham, and A. Weinstein, "Matrix Converters: A Technology Review," IEEE Trans. Ind. Elec., Vol 49, No. 2, April 2002, pp. 276-288.

[5] S. M. Hietpas and M. Nedan, "Automatic Voltage Regulator using an Ac Voltage-Voltage Converter," *IEEE Trans. Ind. Appli.*, Vol. 36, No. 1, January/Febuary 2000, pp. 33-38.

[6] E. C Aeloíza, P. N. Enjeti, L. A. Morán, O. C. Montero-Hernandez, and S. Kim, "Analysis and Design of a New Voltage Sag Compensator for Critical Loads in Electrical Power Distribution Systems," *IEEE Trans. Ind. Appli.*, Vol 39, No. 4, July/August 2003, pp. 1143-1150.

IEEE ISIE 2006, July 9-12, 2006, Montréal, Québec, Canada

A Single-Phase Grid-Connected Inverter by Utilizing Ready-Made PWM Power IC

Kentaro Hayashi, Hirotaka Koizumi, Yasuo Ohashi, Kosuke Kurokawa
Department of Electrical and Electronic Engineering
Tokyo University of Aguriculture and Technology
2-24-16, Naka-cho Koganei city, Tokyo, Japan
Phone: +81-42-388-7445 FAX: +81-42-388-7445
E-mail: kentaro-@cc.tuat.ac.jp

***Abstract*- For popularization of photovoltaic (PV) systems, it is important not only approach to cost reduction, but also approach to mass production. As one of the approaches, this paper presents the inverter by utilizing ready-made power integrated circuit. The integrated circuit (IC), Audio Power Amplifier, has been developed and mass-produced with the PWM switching technique recently. Most of photovoltaic (PV) inverters are based on the PWM technique. The proposed inverter has possibility of the dramatically cost reduction and mass production. Availability of the application of the IC to the PV inverter is shown by experimental results.**

I. Introduction

During the last few years, there has been a growing market demand for photovoltaic systems. In Japan, the long-term R&D roadmap titled "PV2030" was set up in May 2004, in which 100 GW of total domestic installation of PV systems are expected. When 20 GW/y PV market is considered to exist in 2030, the level of their need is considered adaptable enough for automated assembly lines and power ICs [1]. On the other hand, power ICs, for example audio power amplifiers, have been developed and mass-produced with PWM techniques often called "class-D audio amplifier." A typical class-D audio amplifier consists of a modulator that converts an analog or digital audio signal into a high-frequency PWM signal, followed by a half bridge or full bridge power switch. The circuit configuration can be found in the main circuit of photovoltaic (PV) inverters. Therefore, if the IC is used in place of the main circuit of the PV inverter, a lot of discrete elements of the inverter can be reduced. That increases productivity of PV inverter.

In this paper, a stereo class-D audio IC was tested with bridge-tide -load (BTL) configuration.

II. Ready-Made PWM ICs for Audio Power Amplifier

There are many kinds of class-D audio ICs available. For monaural one, the amplifier consists of an audio input channel,

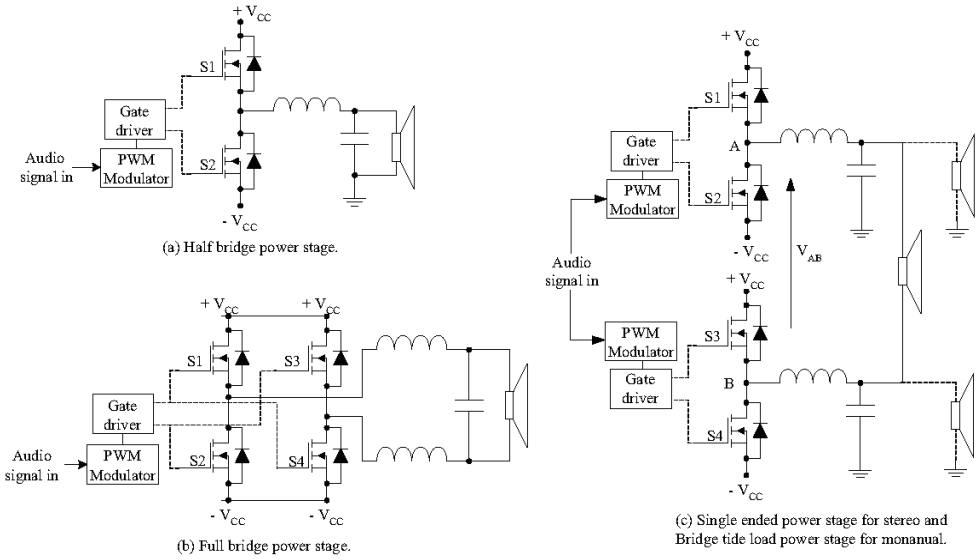

Fig. 1. Power stage of class-D audio amplifier.

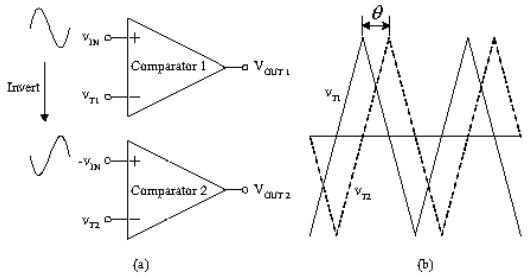

Fig. 2. Input stage of BTL configuration (a) and relationship of phase difference between two carrier signals (b).

a PWM modulator, a half bridge power stage as shown in Fig. 1 (a) or a full bridge power stage as shown in Fig. 1 (b). For stereo one, the amplifier consists of two audio input channels, two PWM modulators, two half bridge power stages or two full bridge power stages. In addition, the stereo amplifier makes single-ended (SE) as well as bridge-tied-load (BTL) operation possible as shown in Fig. 1 (c).

In the BTL application, two audio input channels receive an audio signal 'v_{IN}' but the phase of one of the channels should be inverted '$-v_{IN}$' as shown in Fig. 2. In this case an approximately four times higher output power can be obtained with the same loudspeaker impedance. In some of the ICs, the switching patterns for the two channels are not synchronized by the phase difference θ between the two carrier waves.

III. Application of Grid-connected System

Fig. 3 shows the circuit model of grid-connected system with a class-D audio IC. The particular parameters for the system are shown in Table I. In this circuit, a stereo class-D audio IC "TDA7490 (STMicroelectronics) [2]" was used as a main

TABLE I
System Parameters

Parameter	Value
L_1, L_2	31 μH
C_O	1 μF
R_L	15.6 Ω
v_S	14.26 V
Z_{S1}, Z_{S2}	51 mΩ + 2 μH
V_{dc1}, V_{dc2}	22 V
C_{i1}, C_{i2}	2200 μF

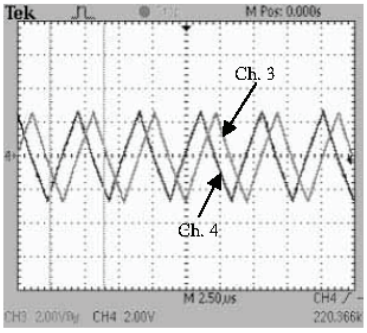

Fig. 4. Carrier waveforms of TDA7490 for PWM stage 1 (Ch. 3), and PWM stage 2 (Ch. 4). Horizontal: 2.5 μs/div., channel 3, 4: 2.0 V/div.

circuit of this system. The TDA7490 consists of two preamplifiers has a constant gain $G = 2.5$, two integrators, two PWM stages containing of a half bridge and a common section which contains an oscillator and some protection circuit. These components are designed optimally in the IC. In this circuit, the two integrators are treated the same as OP amplifier and the integrator 1 operates as a voltage follower, and the integrator 2 operates as an inverting amplifier for the BTL configuration. The two switching carriers have the phase difference about 90

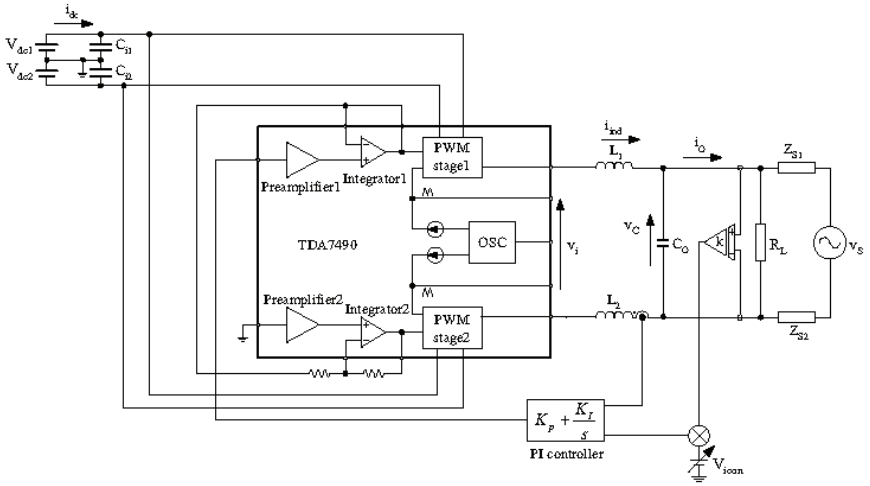

Fig. 3. Circuit configuration

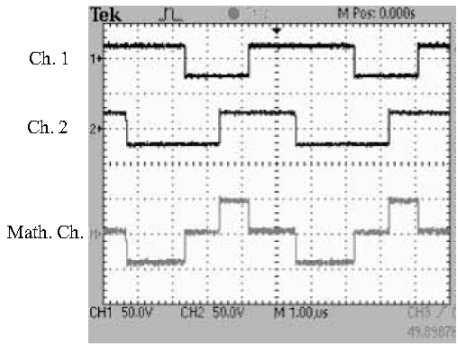

Fig. 5. Output voltage from PWM stage 1 (Ch. 1), PWM stage 2 (Ch. 2) and v_i (Math. ch.). Time base: 1.0 µs/div., channel 1, 2: 50 V/div., math channel: 50 V/div.

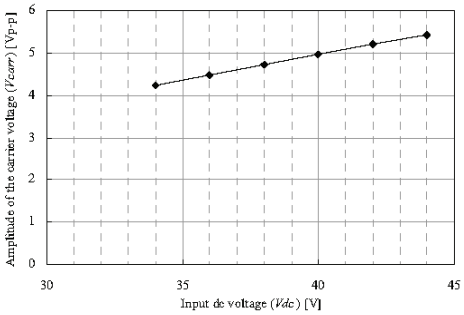

Fig. 6. Relationship between input dc supply voltage (V_{dc}) and carrier voltage (v_{carr}).

degrees at 200 kHz as shown in Fig. 4 and output voltage from PWM stage 1, PWM stage 2 and v_i is shown in Fig. 5. The inverter has constant gain K given by

$$K = \frac{V_{CC}}{v_{carr}} \times 2.5 \cdot \quad (1)$$

The carrier voltage v_{carr} changes proportionally inside of the IC with dc supply voltage V_{dc} (= V_{dc1}+ V_{dc2}) as shown in Fig. 6. Therefore the value of the inverter gain K is approximately 40 calculated using (1). In this system, the inverter uses one current sensor to sense inductor current i_{ind} for current control by a PI controller consisted of the analog circuit. The transfer function of the PI controller is given by

$$C(s) = K_P + \frac{K_I}{s} \cdot \quad (2)$$

The complementary sensitivity function is given by

$$T(s) = \frac{K(sK_P + K_I)}{s^2 L + K(sK_P + K_I)} \cdot \quad (3)$$

The angular frequency ω_O and resonant frequency f_{con} of this controller are:

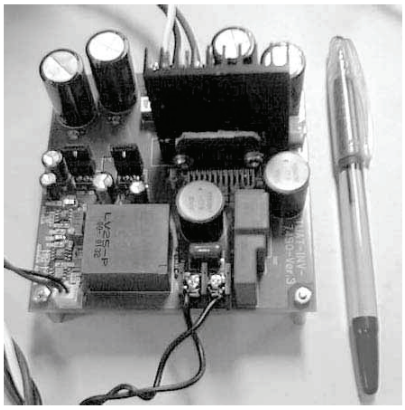

Fig. 7. Printed circuit board (PCB). Scale: 100 mm × 100 mm

$$\omega_O = \sqrt{\frac{KK_P}{L}}, \quad (4)$$

$$f_{con} = \frac{\omega_O}{2\pi} \cdot \quad (5)$$

The value of proportional gain K_P = 0.47 VA^{-1} and integral gain K_I = 1000 $VA^{-1}s^{-1}$ are selected for the current feedback. From these values, this system is free of the influence of the resonant frequency (f_Z) between inverter filter capacitor (C_O) and grid impedance (Z_{S1} and Z_{S2}) because the resonant frequency of the control f_{con} (≈ 4 kHz) is lower than f_Z (≈ 113 kHz). Therefore, the controller responds quickly to the target frequency of this system (50Hz) with stability.

Synchronization of the inverter output current (i_O) to the capacitor voltage (v_C) is achieved by the analog multiplier implemented for the regulation of the current reference by multiplication of the sensed capacitor voltage ($k_{sense}v_C$) and the regulated dc voltage as the current control level (V_{icon}). The sensor gain (k_{sense}) is adjusted constant gain level about 0.015.

IV. Experimental and Simulation Results

An experimental circuit based on Fig. 3 was designed and built on the 100 mm × 100 mm printed circuit board (PCB) as shown in Fig. 7. A stabilized dc power supply was used as a dc link voltage. Since of class-D audio IC has the limited input dc link voltage within ± 25 V, this system cannot output the grid voltage in fact. For this approach, it's possible to convert the voltage level with a transformer. However, it isn't necessary to use a transformer if an appropriate power IC which withstands the voltage level of the grid voltage. In the experiment, the 4 quadrants bipolar power supply (KIKUSUI: PBX40-10, output impedance $Z_{OUT} \approx 0$ [Ω]) and function generator (KENWOOD: FG273A) was used as the simulated grid voltage to connect the circuit without low frequency (LF) transformer. The voltage of the simulated grid v_S was assumed to be 14.6 V and maintain

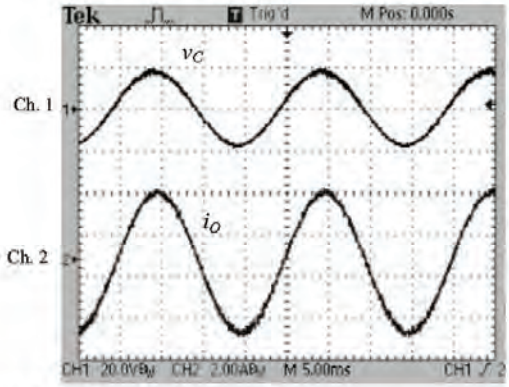

Fig. 8. Capacitor voltage (v_C) and inverter output current (i_O) in steady-state condition. Time base: 5 ms/div., channel 1: capacitor voltage 20 V/div., channel 2: inverter output current 2 A/div.

of the voltage. Although it is likely to connect the class-D audio IC to the real grid with LF transformer, it is enough to check the operation whether the inverter using the IC can be connected to the distribution grid or not with this scale downed system.

Fig. 8 shows the observed waveforms of the capacitor voltage v_C and the inverter output current i_O when the system output power is 28.7 W in steady state. In this condition, the multiplied current control level V_{icon} was constant.

Fig. 9 shows the simulated and measured waveforms of the capacitor voltage and inverter output current before and after a step change of the control level V_{icon}. These waveforms show the consistency between the predicated and the experimental results. From these results, it is clarified that this system operates stably in the gird-connected condition.

The Fig. 10 shows the measured power conversion efficiencies and power factors of the class-D audio IC in the grid-connected condition. This result was measured with a power analyzer (PZ4000: YOKOGAWA). The efficiency η is calculated within PZ4000 with:

$$\eta = \frac{P_{ac} = \frac{1}{T}\int_0^T v_C(t) i_O(t)\,dt}{P_{dc} = \frac{1}{T}\int_0^T V_{dc}(t)\, I_i(t)\,dt}, \qquad (6)$$

and the power factor λ is calculated with:

$$\lambda = \frac{P_{ac} = \frac{1}{T}\int_0^T v_C(t) i_O(t)\,dt}{V_{rms}\, I_{rms}}. \qquad (7)$$

The maximum value of the efficiency is 76.6 % and power factor is 0.9828 at 20.1 W, and that of the power factor is 0.9882 and efficiency is 73.9 % at 29.4 W. From the datasheet [2], the power conversion efficiency of the power IC is 89 % at

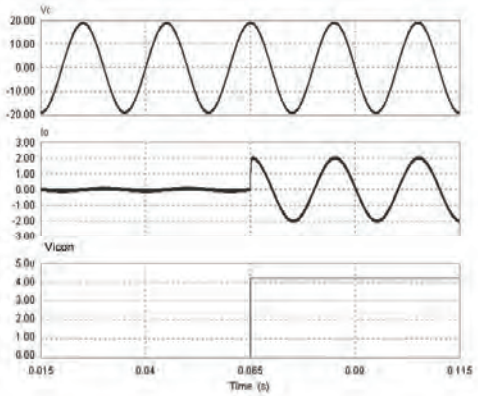

(a) Simulation results (Time base: 25 ms/div., capacitor voltage (v_C): 10 V/div., inverter output current (i_O) :1A/div., current regulation level (V_{icon}) : 1 V/div.)

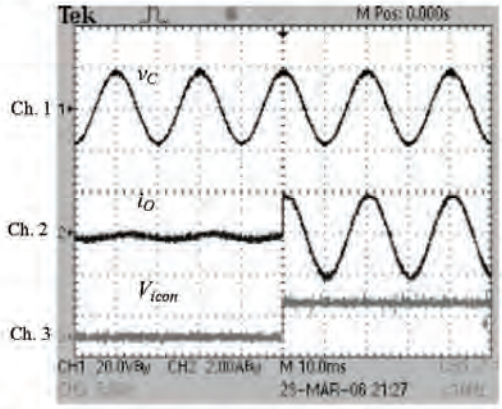

(b) Observed waveforms in circuit experiments (Time base: 10 ms/div., channel 1: capacitor voltage (v_C) 20 V/div., channel 2: inverter output current (i_O) 2 A/div., channel 3: current regulation level (V_{icon}) 5 V/div.)

Fig. 9. Comparison of simulated (a) and experimentally obtained (b) capacitor voltage (v_C) and inverter output current (i_O).

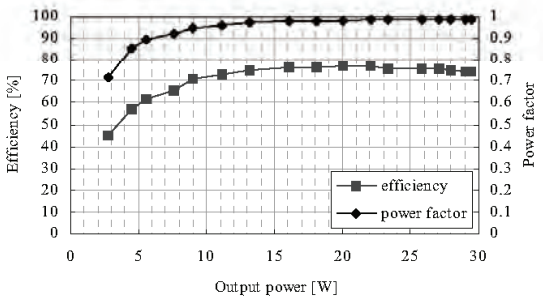

Fig. 10. Measured power factor and power conversion efficiency of the class-D audio IC in the grid-connected condition.

25 W + 25 W output power for each speaker in stereo audio configuration when 1 kHz audio signal is given. These results also cannot be made an easy comparison each other from the standpoint such as difference of the circuit configuration, the load impedance and power factor. However, this system operates in the grid-connoted condition with marinating more than 70 % of the power conversion efficiency in the range of 8.95 W to 29.47 W. Additional selection of the power device may increase the efficiency.

V. Conclusion

This paper has presented a prototype of grid-connected inverter utilizing ready-made ICs for class-D audio power amplifier. Simulation results and hardware measurements have demonstrated the feasibility of the proposed system in scale-downed grid-connected condition. There remains a few challenges, for example withstand voltage. However, the implementation ready-made IC will make a large contribution to the mass-production with the reduction of discrete elements in the system and the simplification of the production process.

Acknowledgment

This study has been carried out as a part of "Autonomy-Enhanced PV Cluster" project funded by New Energy and Industrial Technology Organization (NEDO).

References

[1] K. Kurokawa, "Mass Production Scale of PV Modules and Components in 2030s and beyond," *in Proc. 15th International Photovoltaic Science & Engineering Conference (PVSEC-15)*., Shanghai, 2005, pp.272-274.

[2] STMicroelectronics. "TDA7490 25W + 25W STEREO CLASS-D AMPLIFIER 50W MONO IN BTL," Product review Dec. 1999.

[3] Marco Berkhout., "An Integrated 200-W Class-D Audio Amplifier," *IEEE Journal of Solid-State Circuits*, vol. 38, No. 7, JULY 2003.

[4] T. Abeyasekera, C. Mark Johnson, D. J. Atkinson, and M. Armstrong, "Suppression of Line Voltage Related Distortion in Current Grid Connected Inverters," *IEEE Trans. Power Electronics*, vol. 20, no. 6, pp. 1393-1401, Nov. 2005.

[5] M. Liserre, R. Teodorescu, F. Blaabjerg, "Stability of Grid-Connected PV Inverters with Large Grid Impedance Variation," in Proc. IEEE Power Electronics Specialist Conference, 2004, pp.4773-4779.

IEEE ISIE 2006, July 9-12, 2006, Montréal, Québec, Canada

Plane Division Maximum Power Point Tracking Method for PV Module Integrated Converter

Hirotaka Koizumi and Kosuke Kurokawa

Department of Electrical and Electronic Engineering
Tokyo University of Agriculture and Technology
2-24-16 Naka-cho, Koganei, Tokyo, 184-8588, JAPAN
(koizumih, kurochan)@cc.tuat.ac.jp

Abstract— Solar cells have a current-voltage (I-V) characteristic affected by the radiation and temperature. To obtain the maximum electricity from solar cells, the power converters for PV (photovoltaic) modules have a function called MPPT (Maximum Power Point Tracking). Under the various conditions, the dc input voltage or current is controlled to track the maximum power point (MPP) where the PV modules feed the maximum output power. A module integrated converter (MIC) is individually installed behind of a PV module. In this type, manufacturers can obtain the basic characteristics of the PV module in the manufacturing process. Therefore, the domain of MPP can be predicted.

The plane division (PD) MPPT method takes full advantage of the known I-V characteristic. The I-V plane is divided into two domains by a PD function. One includes MPPs and the other one doesn't. Using the PD function, the operating point can rapidly approach the MPP.

In this paper, a combination of two or three linear functions is proposed and tested. In circuit experiments, the measured approaching time to the MPPs is reduced from 87.0 % to 65.0 % for the combination of three linear functions compared to the IncCond algorithm. Based on the measured data, the proposed functions are also compared to the previous PD functions. Consequently, the square root function and the combination of three linear functions are superior to the others. The PD-MPPT, which can be easily added to various MPPT algorithms, is effective to accelerate the MPPT operation of the MIC.

I. Introduction

Photovoltaic (PV) system, which is one of the important renewable energy sources, has been increasing world wide. Solar cells are semiconductor devices, therefore they have a current-voltage (I-V) characteristic which is affected by the radiation and temperature. Most of the photovoltaic solar energy systems are combined with the power converters in accordance with the application. To obtain the maximum electricity from the solar cells, the power converters for photovoltaic (PV) system have a function called MPPT (Maximum Power Point Tracking) which controls the dc voltage or current at the primary side to track the operating point where the PV modules feed the maximum output power. Usually, the solar power system for residential use is composed of many modules and a central PV inverter. Each PV module has own characteristic by the condition, therefore the PV modules connected in series and parallel sometimes suppress their output power each other and form a complex I-V characteristic which makes it difficult for the MPPT to seek the maximum power point (MPP).

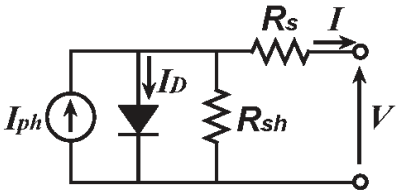

Fig. 1. An equivalent circuit of a solar cell.

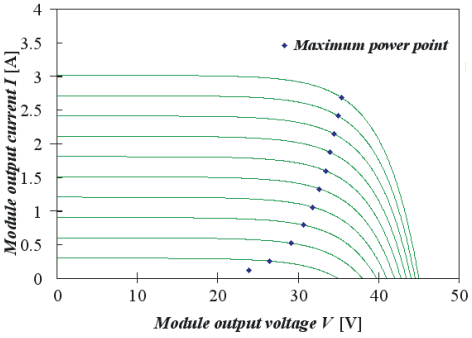

Fig. 2. $I-V$ characteristics of the PV module: $T = 25$ °C, $FF = 0.7$, from the top, radiation = 1.0 kW/m^2 with $P_{MAX} = 94.0$ W to the bottom, radiation 0.1 kW/m^2 with $P_{MAX} = 6.86$ W, every 0.1 kW/m^2 of radiation.

On the other hand, the module integrated converter (MIC), which is installed by each PV module, tracks MPP by one module and feeds dc or ac power depending on the system [1] [2]. In this type, even if some modules are shaded, the others can independently continue the operation at the MPP. AC module, which is composed of one PV module and one interconnected inverter, has been in the market [2]. The output port is directly connected with the ac wiring.

In AC module, different from the central inverter system, a PV module and a MIC are combined in a factory. Therefore the manufacturer can know the basic characteristics of the PV module before combining the PV module with a MIC. Based on the known data, the distribution of MPPs can be approximately predicted. The I-V plane division (PD) MPPT method takes full advantage of the

known I-V characteristic. The I-V plane is divided into two domains; that is, one includes MPPs and the other one doesn't. The operating point can rapidly approach the MPP passing quickly the domain without MPPs. Around the MPP, the algorithm is switched to the IncCond method [3]. The PD-MPPT can be easily applied to various MPPT algorithms. In case of DSP based controller, only several additional program lines are required.

The authors have proposed two PD-MPPT methods for the module-integrated converter [4] [5]. The first one divides the I-V plane by a linear function. The measured approaching time was dramatically reduced. However, there was a limitation of the linear function; that is, when the slope is adjusted to MPPs in high radiation conditions, it is not always effective for low radiations, and vice versa. Against the limitation, the second one used a square root function instead of a linear function. A square root function well follows the MPPs from low radiation to high radiation condition; i.e. it is effective for wide range of radiation. The range of rapid approach is expanded more than that with linear function. However there remains a disadvantage; i.e. the calculation process of square root function may need high-performance calculator.

In this paper, in addition to the above PD functions, a combination of two or three linear functions is proposed and tested. Linear functions are switched by the operating range. The combination of linear functions should be able to cover the MPPs in wider range than the single linear function with lighter calculation process than square root function. In circuit experiments with a 100 W class inverter and a Solar cell array simulator (Kernel) [6], the measured approaching time to the MPP is reduced from 86.9 % to 2.5 % for the combination of two linear functions and from 87.0 % to 65.0 % for the combination of three linear functions compared to the IncCond algorithm. Those results and characteristics are also compared with the previously proposed PD functions in advantages and disadvantages.

II. Maximum Power Point Tracking

An equivalent circuit of a solar cell can be given as Fig. 1, which provides an equation for I-V characteristic of a solar cell,

$$I = I_{ph} - I_D = I_{ph} - I_o \left[\exp\left(\frac{q(V + R_s I)}{A k_B T} \right) - 1 \right] - \frac{V + R_s I}{R_{sh}}, \quad (1)$$

where V(V) is the PV output voltage, I(A) the PV output current, I_{ph}(A) the photocurrent, I_D(A) the diode current, I_o(A) the saturation current, A the ideally factor, q(C) the electronic charge, k_B(JK^{-1}) Boltzmann's gas constant, T(K) the junction temperature, R_S(Ω) the series resistance, and R_{sh}(Ω) the shunt resistance [7]. Fig. 2 shows simulated I-V characteristics of a PV module under the condition of T = 25°C, FF = 0.7, from radiation = 0.1 kW/m^2 with P_{MAX} = 6.86 W to radiation = 1.0 kW/m^2 with P_{MAX} = 94.0 W by 0.1 kW/m^2. The fill factor FF is defined as $FF = I_{MAX}V_{MAX}/I_{sc}V_{oc}$, where

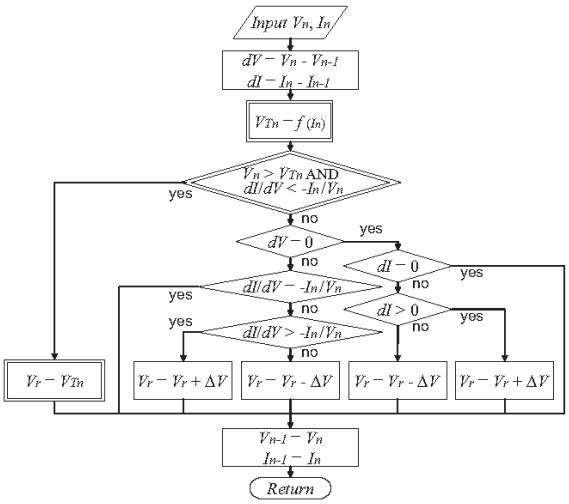

Fig. 3. Flow chart of PD-MPPT algorithm added to the IncCond algorithm.

I_{MAX} and V_{MAX} are the current and voltage at MPP, and I_{sc} and V_{oc} are short-circuit current and open-circuit voltage of the PV module. P_{MAX} means the PV output power at MPP, which is equal to $I_{MAX}V_{MAX}$. Substituting V = 0 into (1), the I_{sc} can be obtained, which is considered equivalent to the I_{ph}, i.e. proportional to the radiation. Substituting I = 0 into (1), the V_{oc} can be obtained, which increases logarithmically with increasing radiation level [7]. The MPP of each I-V characteristic is shown in Fig. 2. To seek the MPP, various algorithms have been proposed. The Perturb and Observe (P&O) algorithm and Incremental conductance (IncCond) algorithm are widely used because of the simple structure and the few measured parameters. The P&O algorithm finds the MPP by periodically perturbing the PV output voltage V and comparing the PV output power P_n with the previous one P_{n-1}. The perturbing operation at the MPP and the instability against rapidly changing atmospheric conditions are problem in the P&O algorithm. The IncCond algorithm requires the same measured parameters to the P&O algorithm and obtains dP/dV using

$$\frac{dP}{dV} = \frac{d(IV)}{dV} = I + V\frac{dI}{dV}. \quad (2)$$

Thus, by measuring the incremental and instantaneous PV module conductance i.e. dI/dV and I/V, the direction of the MPP can be known [3]. When $dP/dV = 0$, the operating point is at the MPP. If $dP/dV > 0$, the operating point is to the left of MPP. If $dP/dV < 0$, the operating point is to the right of MPP. This algorithm keeps the stability at the MPP and can follow it against rapidly changing atmospheric conditions [3]. A flow chart shown in Fig. 3 is mainly with the IncCond algorithm because the PD-MPPT algorithm is added to the IncCond algorithm as the items enclosed with double line.

III. Principle of PD-MPPT

The MPP is changing following the I-V characteristic with radiation and temperature changing. With increasing of radiation, the I_{sc} proportionally increases and the V_{oc} logarithmically increases. Also, the V_{oc} decreases linearly with an increase in junction temperature T [7]. However, as shown in Fig. 2, the domain where MPP can exist is limited. The highest radiation and the lowest temperature give the limitations for I_{sc}, and V_{oc} under the climate condition in a region. The I_{MAX}, and V_{MAX} are also given under the condition. Assuming that the locus of rhombic plots in Fig. 4 shows the right-side limitation of the MPP existing area under the climate condition, the right side of the locus never includes MPPs. If the operating point passes through the area quickly, the MPP can be sought and tracked efficiently. An idea proposed in our study is to give the plane-division function which divides the I-V plane into two; thus, one includes MPPs and the other one doesn't. In case of AC module, the PV module and the MIC are connected one-on-one. Therefore, the manufacturer can reflect the characteristics of the PV module on the MPPT algorithm for the MIC.

A. PD-MPPT Using Linear Functions

A flow chart of the PD-MPPT algorithm added to the IncCond algorithm is shown in Fig. 3. A linear function is given as a PD function $f(I)$. As shown in Fig 4 (a), the linear function doesn't cross the MPP existing area. Assuming that an operating point is presently at (V_n, I_n) in Fig 4 (a). The next targeted voltage V_{Tn} of the operating point is calculated with $f(I)$ using the measured current I_n. If $V_n > V_{Tn}$, the operating point is out of the MPP existing area. Considering the rapidly changing atmospheric condition, only when $V_n > V_{Tn}$ and $dP/dV < 0$ are satisfied, the V_{Tn} is returned to the main algorithm as the targeted voltage V_r following the flow chart shown in Fig. 3. Aiming at the V_r, the MIC increases the output power. Consequently the operating point moves to (V_{n+1}, I_{n+1}). The next targeted voltage V_{Tn+1} is calculated with I_{n+1}. The same process is repeated toward the crossing point X of I-V characteristic and the linear function. Over the crossing point X, the targeted voltage is given following the conventional IncCond algorithm. The difference between V_{Tn} and V_n is far larger than ΔV, therefore the operating point moves quickly toward the proper direction. As shown in Fig. 3, the PD-MPPT method is so simple that it can be expressed by just additional three items enclosed with double line, which are also easily applied to P&O algorithm or the others.

B. PD-MPPT Using Square Root Functions

As shown in Fig. 2, the distribution of MPPs is not linear. Therefore, the linear function cannot follow whole the range. The difference between the linear function and MPPs in low radiation conditions is large when the slope of the function is adjusted to MPPs in high radiation conditions, and vise versa. As a solution, the square root function is applied as $f(I)$ instead of a linear function. The given function shown in Fig. 4 (b) seems a quadric function, however the targeted voltage V_{Tn} is calculated from I_n with the square root function. As shown in Fig. 4 (b), the curve of the square root function well follows the distribution of MPPs from low radiation to high radiation. The square root function expands the range following the PD-MPPT algorithm.

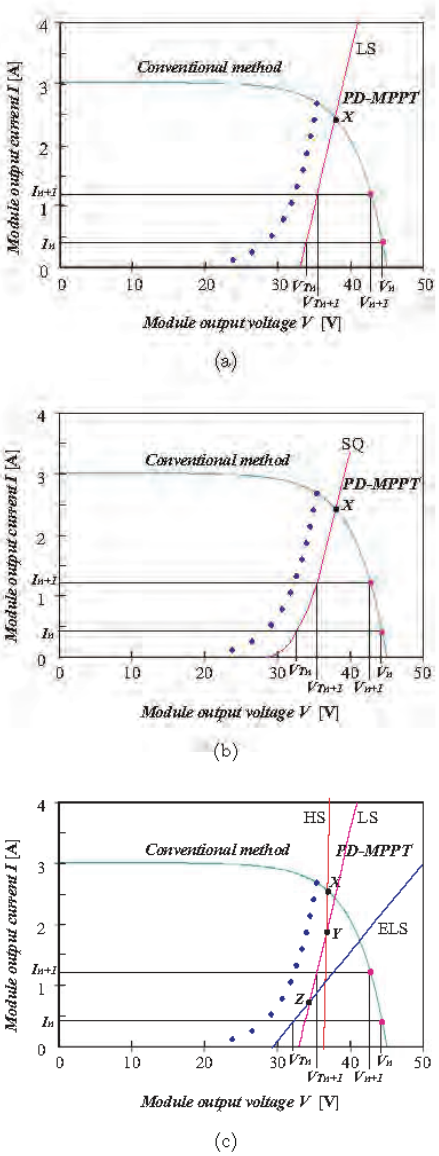

Fig. 4. Transition of the operating point with (a) a linear function, (b) a square root function, and (c) a combination of linear functions.

C. PD-MPPT Using Combination of Linear Functions

The square root function remains a short coming; that is, the calculation process of the square root function itself

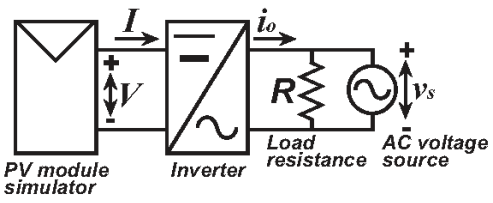

Fig. 5. Experimental circuit.

may need a high-performance CPU. To follow the MPPs in wide range, in this paper, combination of linear functions is proposed and tested. As shown in Fig. 4 (c), linear functions are switched at the crossing points Y and Z based on the current I. The combination of linear functions and 'if branch' is lighter than square root function in the calculation process. The short coming of the single linear function is improved by using the combination of linear functions.

IV. PV Module Conditions and PD Functions

Two types of PV module are performed by a Solar cell array simulator (Kernel) [6]. One has the I-V characteristics shown in Fig. 2 under the condition of $T = 25^oC$, $FF = 0.7$, from radiation = 0.1 kW/m^2 with P_{MAX} = 6.86 W to radiation = 1.0 kW/m^2 with P_{MAX} = 94.0 W. For the other one, $T = 25^oC$, $FF = 0.8$, from radiation = 0.1 kW/m^2 with P_{MAX} = 8.05 W to radiation = 1.0 kW/m^2 with P_{MAX} = 94.5 W. The high slope linear functions (HS) are decided based on the linear approximation using the 6 coordinates of the MPPs with the radiation from 0.5 kW/m^2 to 1.0 kW/m^2 by 0.1 kW/m^2. For the I-V characteristics with FF=0.7, (a) $I = 5V - 182$ which is drawn in Fig. 4; for those with FF=0.8, (b) $I = 7.7V - 303$ are respectively given. The PD functions should be shown as functions of I, however only for linear functions, their inverse function is shown with considering the visual impression corresponding to the expressions of 'high' and 'low' slope. The low slope linear functions (LS) have a slope of 1/10 of the above slopes; thus, (c) $I = 0.5V - 16.2$ for $FF = 0.7$, and (d) $I = 0.77V - 29$ for $FF = 0.8$ are given. Those are obtained and used in [4].

In this paper, combinations of the high slope and low slope linear functions (C2) are also tested. The crossing points Y are $(V, I) = (36.60, 1.8)$, and $(39.48, 1.4)$ for FF = 0.7, and 0.8 respectively. The voltage at the crossing point calculated with high slope functions is slightly ($\leq$ 0.16) larger than the voltage obtained by low slope functions to prevent rapid reduction of the target voltage. In addition to the above, another lower slope function is added in consideration of low radiation condition. The extra low slope linear functions (ELS) are obtained based on the linear approximation using the 4 coordinates of the MPPs with the radiation of from 0.1 kW/m^2 to 0.4 kW/m^2 by 0.1 kW/m^2. For FF=0.7, (e) $I = 0.146V - 4.3$, for FF=0.8, (f) $I = 0.225V - 8.05$ are respectively obtained. The crossing points Z between LS and ELS are (34.46, 0.7316), and (38.44, 0.6) for FF = 0.7, and 0.8 respectively. The ELS is used in the combination of three linear functions (C3) as shown in Fig. 4 (c).

The square root functions (SQ) are calculated based on the approximation using the 11 coordinates of the MPPs with the radiation from 0.05 kW/m^2 to 1.0 kW/m^2 and shifted to place the apex on the V axis. For the I-V characteristics with $FF = 0.7$, (g) $V_{Tn} = \sqrt{(I_n/0.0256)} + 28.55$ which is drawn in Fig. 4 (b), and for $FF = 0.8$, (h) $V_{Tn} = \sqrt{(I_n/0.0662)} + 35.0$ are respectively given. Those are obtained and used in [5].

All the functions are close to the MPP existing domain but never touch nor cross it; the constant term in each function is chosen to keep that condition. The margin between the MPP and each function is experimentally searched to prevent that the operating point falls into the short current position by the error of sensing.

V. Experimental Results

The PD-MPPT algorithms are respectively installed into a PV inverter for the circuit experiments. The PV inverter was designed for 100 W class AC module in a past project. It is composed of a controller board [8] and a fly back inverter which is a prototype of [9]. A PD-MPPT program is installed into the ROM of the controller board. The experimental circuit is shown in Fig. 5. The primary side is connected with the Solar cell array simulator, and the secondary side is connected with AC power source (P-Station, NF corporation). The load resistance $R = 60\,\Omega$, the system voltage v_s = 100 V$_{rms}$ at 50 Hz. The radiation parameter of the PV module simulator was given from 0.1 kW/m^2 to 1.0 kW/m^2 by 0.1 kW/m^2 for FF = 0.7 and 0.8 respectively. The module output voltage V, module output current I, inverter output current i_o, and the system voltage v_s are observed with the digital scope (DL716 YOKOGAWA). Examples of the observed waveforms are shown in Fig. 6, which are under the condition of the radiation 0.5 kW/m^2 with $FF = 0.7$. The top half shows the long-term variation, and the bottom half shows the enlarged waveforms on the black vertical line shown in the top half. The output current i_o is observed through a low pass filter of the DL716 to filter out the noise. At first, the solar cell array simulator is turned on, then, the module output voltage V goes to V_{oc} level and gradually reduces. The module output current I rises slowly from 0 A toward the I_{MAX}. The arrival to the MPP is measured by comparing with the values of V and I in steady-state.

The measured time taken for the approach from the MPPT starting to the MPP at radiation of 1.0 kW/m^2, 0.5 kW/m^2, and 0.3 kW/m^2 are shown in Table I, where IncCond, linear functions with high slope (HS) and low slope (LS), square root functions (SQ), combinations of two linear functions (C2), and of three linear functions (C3) mean the installed MPPT functions. For 1.0 kW/m^2 and 0.5 kW/m^2, the test results with IncCond, HS, LS, and SQ are reported in [5]. However the same tests were repeated with the emphasis on the relative relation between the measured values under the same condition and at the same time. Generally the measured time for those is shorter than that

TABLE I
MEASURED TIME TAKEN FOR THE APPROACH FROM THE TRACKING START TO THE MPP.

FF, *Radiation*	IncCond	HS	LS	SQ	C2	C3
0.7, 1.0 kW/m^2	108.1 s	38.2 s	(38.9) s	*36.5* s	37.8 s	37.8 s
0.7, 0.5 kW/m^2	159.5 s	91.89[17.0] s	*20.3* s	21.1 s	20.8 s	20.7 s
0.7, 0.3 kW/m^2	(291.9) s	170.8[12.4] s	14.1 s	16.2 s	*14.6* s	16.5 s
0.8, 1.0 kW/m^2	112.4 s	34.1 s	73.5[36.5] s	34.6 s	*31.9* s	35.7 s
0.8, 0.5 kW/m^2	86.5 s	84.3[14.1] s	16.8 s	17.8 s	*15.1* s	17.3 s
0.8, 0.3 kW/m^2	93.0 s	68.6[10.8] s	149.2[12.0] s	*11.9* s	84.3[12.7] s	13.2 s

TABLE II
MEASURED TIME FROM THE TRACKING START TO THE MPP NORMALIZED BY THE APPROACHING TIME WITH INCCOND METHOD.

FF, *Radiation*	HS	LS	SQ	C2	C3
0.7, 1.0 kW/m^2	35.3 %	(36.0) %	*33.8* %	35.0 %	35.0 %
0.7, 0.5 kW/m^2	57.6[10.7] %	*12.7* %	13.2 %	13.1 %	13.0 %
0.7, 0.3 kW/m^2	(58.5[4.3]) %	(4.8) %	(5.5) %	(*5.0*) %	(5.6) %
0.8, 1.0 kW/m^2	30.3 %	65.4[32.5] %	30.8 %	*28.4* %	31.7 %
0.8, 0.5 kW/m^2	97.5[16.3] %	19.4 %	20.6 %	*17.5* %	20.0 %
0.8, 0.3 kW/m^2	79.4[12.5] %	172.5[13.9] %	*13.8* %	97.5[14.7] %	15.3 %

of [5], especially for IncCond in $FF = 0.8$, though the inclination is quite similar. The brackets "[ ]" means the time for which the MPPT operation was following a PD function. For example, as shown in Fig. 6 (b), from the MPPT starting to 17 sec (at the second grid), I rises rapidly and V decreases; during this period HS is used. After the period, I continues increasing and V decreasing slowly following the IncCond algorithm. The numbers in the brackets "( )" include ambiguity. It was too slight change to find the term following IncCond in the test with LS under the radiation 1.0 kW/m^2 with $FF = 0.7$. In the test with IncCond under the radiation 0.3 kW/m^2 with $FF = 0.7$, the beginning of MPPT operation was unstable, therefore it took a long time. For a comparison, the measured times normalized with the approaching time with IncCond are shown in Table II. The italic number means the minimum value under the condition. Judging from the Tables, the HS and the LS have their appropriate range in high radiation and low (middle) radiation respectively. Under the condition of 0.3 kW/m^2 with $FF = 0.8$, the LS extends its approaching time contrary to the purpose. That can be caused by the nearness of current I at MPP and the point X which divides the IncCond and PD-MPPT. The C2, which has both the advantages of HS and LS, shows good results except 0.3 kW/m^2 with $FF = 0.8$. The C3, which has extra low slope linear function (ELS), compensates the lack of C2. Based on the Table II, comparing to the IncCond, the C2 and the C3 respectively reduce their approaching time from 86.9 % to 2.5 %, and from 87.0 % to 65.0 % with ignoring 0.3 kW/m^2 with $FF = 0.7$. Depending on the choice of linear functions, the characteristics of C2 can be improved. The SQ reduces its approaching time from 86.8 % to 66.2 %, which efficiently follows MPPs in wide range. The characteristic of the C3 is rather close to the SQ than the HS or the LS. If the calculation time of square root function becomes longer by the choice of CPU, the C3 may exceed the SQ in the approaching time.

Consequently, the SQ and the C3 are superior to the others. The choice depends on the CPU. The C2 is also effective if low radiation conditions can be ignored. The C2 and the C3 can be more improved by means of the choice of functions. The linear functions should be used as a combination, not a single function.

Against 0.1 kW/m^2 rapid radiation increase and reduction, the inverter response was tested with each algorithm. With the condition of radiation between 0.7 kW/m^2 and 1.0 kW/m^2, sometimes inverter restart was observed in all cases. However, in less than 0.7 kW/m^2, inverter followed the change without stopping or fault. The response time is varied but within the same level to the IncCond because the IncCond algorithm, which can keep tracking the MPP against rapidly changing atmospheric conditions, mainly controlled the operation around the MPP also in the PD-MPPT programs.

VI. CONCLUSIONS

The PD-MPPT method for the module-integrated converter has been introduced. The PD-MPPT takes full advantage of the known PV module characteristic. Identifying the domain without MPP, the operating point can rapidly approach the MPP using a PD function. In the neighborhood of the MPP, the algorithm is switched to a conventional IncCond method. Circuit experiments have been carried out with the 100 W class inverter using the proposed algorithm. In addition to the linear function and square root function, the combination of linear functions are proposed and tested. In case of the combination of three linear functions, the measured time taken for the approach to the MPP is reduced from 87.0 % to 65.0 % compared to the IncCond algorithm. Its performance is

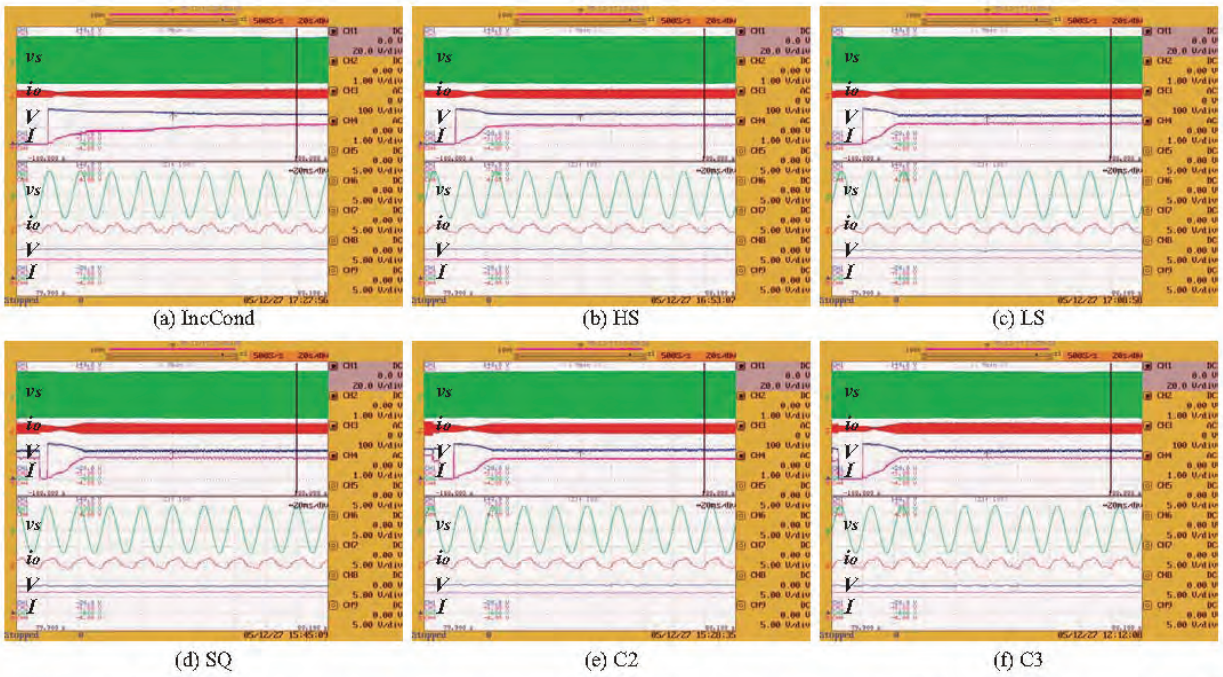

Fig. 6. Observed voltage and current waveforms under the condition of the PV characteristics with $FF = 0.7$, $Radiation = 0.5$ kW/m^2; (a) using the conventional IncCond algorithm, (b) using PD function HS, (c) LS, (d) SQ, (e) C1, and (d) C2; vertical: ch1: V, 20 V/div, ch2: I, 1 A/div, ch3: v_s, 100 V/div, ch4: i_o, 1 A/div, and horizontal: 20 s/div (top), 20 ms/div (bottom).

close to that with square root function. The characteristics of the PD functions have been compared based on the test results and summarized. Against rapid radiation reduction of 0.1 kW/m^2, the inverter maintains its operation with each algorithm under the radiation of 0.7 kW/m^2 and below. The response time is kept about the same to the IncCond algorithm. The PD-MPPT is quite simple so that it can be easily applied to not only IncCond method but also various MPPT algorithms. The PD-MPPT is effective to accelerate the MPPT operation of MIC.

References

[1] E. Roman, P. Ibanez, S. Elorduizapatarietxe , R. Alonso, D. Goitia, and I. Martinez de Alegia "Intelligent PV module for grid-connected PV systems," in *Proc. IEEE 30th Annual Conference of the IEEE Industrial Electronics Society*, pp. 3082–3087, Nov. 2004.

[2] C.P.M. Dunselman, T.C.J. van der Weiden, S.W.H. de Hann, F. ter Heide, R.J.C. van Zolingen, "Feasibility development of PV module with integrated inverter: AC modules," in *Proc. 12th European Photovoltaic Solar Energy Conference*, vol. 1, pp. 313–315, Apr. 1994.

[3] K. H. Hussein, "Maximum photovoltaic power tracking: an algorithm for rapidly changing atmospheric conditions," *IEE Proc. Transm. Distrib.*, Vol. 142, No. 1, pp. 59–64, Jan. 1995.

[4] H. Koizumi, and K. Kurokawa, "A novel maximum power point tracking method for PV module integrated converter," in Proc. *IEEE 36th Annual Power Electronics Specialists Conference*, pp. 2081–2086, June 2005.

[5] H. Koizumi, and K. Kurokawa, "A novel maximum power point tracking method for PV module integrated converter using square root functions," in Proc. *The 31th Annual Conference of the IEEE Industrial Electronics Society*, pp. 2511–2516, Nov. 2005.

[6] http://www.kernel-sys.co.jp/cell-h.pdf (in Japanese and English).

[7] A. Lasnier and T. G. Ang, "Photovoltaic engineering handbook," *Adam Hilger Bristol and New York*, pp. 69–97, Jan. 1990.

[8] H. Koizumi, K. Nagasaka, K. Kurokawa, N. Goshima, M. Kawasaki, Y. Yamashita, A. Hashimoto, "Interconnecting micro controller for PV systems in Japan," in *Proc. 3rd World Conference on Photovoltaic Energy Conversion*, pp. 2031-2034, May 2003.

[9] T. Shimizu, K. Wada, N. Nakamura, "A flyback-type single phase utility interactive inverter with low-frequency ripple current reduction on the DC input for an AC photovoltaic module system," in *Proc. IEEE 33rd Annual Power Electronics Specialists Conference*, vol. 3, pp. 1483-1488, June 2002.

21st European Photovoltaic Solar Energy Conference, 4-8 September 2006, Dresden, Germany

A NEW KNOWLEDGE HOW TO MAKE THE VERY LARGE SCALE PVS HAPPEN ON THE DESERT!

Kosuke Kurokawa[1], Keiichi Komoto[2], Peter van der Vleuten[3], David Faiman[*4]
[1]TUAT - Tokyo University of Agriculture & Technology, Koganei,Tokyo,184-8588 Japan. (kurochan@cc.tuat.ac.jp)
[2]Mizuho Information & Research Institute (MHIR), Takebashi Square, Kanda-Nishiki-cho, Chiyoda-ku, Tokyo, 101-8443.
[3]Free Energy International BV, P.O. BOX 9564, 5602 LN Eindhoven, the Netherlands.
[4]Ben-Grion University of Negev , Sede Boquer Campus, 84990 Israel.

ABSTRACT: In 2003, IEA PVPS Task8 published their report titled "Energy from the Desert" concerning Very Large Scale Photovoltaic Power Generation (VLS-PV) Systems on deserts. Through their 5 year really international, collaborative works, the book showed that VLS-PV, ranging from several mega watts to giga watts, is not a simple dream story but becomes realistic in near future. For the past 3 years since then, specialists in the task have studied and proposed more detailed, practical, demonstrative R&D approaches toward the realization of VLS-PV in different regions in the world deserts: e.g., the Mediterranean region, the Middle East, Asia and Oceania. These new works will be published soon as the Second Phase Report of Task VIII titled "Energy from the Desert - Practical Proposals for Very Large Scale Photovoltaic Systems" and their essences are to be released at the conference right before the publication.
Keywords: Large Grid-connected PV system, Sustainable, Desert, VLS-PV

1 INTRODUCTION

In 2003, IEA PVPS Task8 published their report titled "Energy from the Desert" concerning Very Large Scale Photovoltaic Power Generation (VLS-PV) Systems on deserts. Through their 5 year real, collaborative works, the book showed that VLS-PV, ranging from several megawatts to gig watts, is not a simple dream story but becomes realistic in near future. For the past 3 years since then, specialists in the task have studied and proposed more detailed, practical, demonstrative R&D approaches toward the realization of VLS-PV in different regions in the world deserts: e.g., the Mediterranean region, the Middle East, Asia and Oceania. These new works will be published soon as the Second Phase Report of Task VIII and their essences are to be released at the conference right before the publication.

A series of these international works have been activated as the Second Phase of IEA PVPS Task VIII among 10 countries and 2 observer countries: Japan (OA), Canada, Germany, Israel, Italy, Korea, the Netherlands, Spain, U.S.A., Australia, Mongolia (obs.) and China (obs.). It is well known that the team of this Task has been studying on a wide range of scope by really mutual-collaborative approaches as a whole.

The major studies have been made as follows:

(1) The Mediterranean region studies include 8 cases in 4 countries, i.e., Morocco, Tunisia, Portugal and Spain.

(2) In the of Middle East, 4 types of technologies, which are fixed tilt array, 1-axis tracking, 2-axis tracking and concentrated PV, have been examined for 17 countries: Bahrain, Cyprus, Egypt, Iran, Iraq, Israel, Jordan, Kuwait, Lebanon, Oman, Qatar, Saudi Arabia, Syria, Turkey, UAE and Yemen.

(3) In Asian region, the Gobi desert in both Mongolian and Chinese territories, LCA models have been formulated for cost, energy payback and CO2 emission. 2 type of arrays, fixed and one-axis, are designed assuming m-Si, a-Si, CdTe and CIS modules. Power transmission cost has also been estimated for the distance of 100 km.

(4) More detailed study was made for 8 MW pilot stage at Dunhuang in the Gansu Gobi of China. Gansu Gobi can accept nearly 500 GW VLS-PV.

(5) Step-by-step sustainable approach was taken to evaluate the possibility of VLS-PV at Perenjori in western Australian desert. Up to around 2020, 1 GW PV aggregate will be realised gradually from multi-megawatt scale to 200 MW annual installations approximately.

(6) Another consideration of socio-economic model has been given for villages around the Gobi. It includes various kinds of flows into and out of villages, e.g., energy delivery, physical distribution and money to make the whole social system sustainable.

(7) Remote sensing technology by utilizing satellite images has clarified actually utilisable land area on world deserts. Sand dunes, mountains, forest and water surface are all omitted from the surface of deserts by their nature of morphology and spectroscopy. Only stiff and flat lands are selected as appropriate VLS-PV site candidates as summarised in the table.

2 DEFINITION AND ADVANTAGES OF VLS-PV

The definition of VLS-PV may be summarized as follows:

- The size of a VLS-PV system may range from 10 MW to 1 or several GW, consisting of one plant, or an aggregation of plural units distributed in the same district operating in harmony with each other.
- The amount of electricity generated by VLS-PV can be considered significant for people in the district, nation or region.
- VLS-PV systems can be classified according to the following concepts, based on their locations:
  - land based (arid to semi-arid deserts);
  - water based (lakes, coastal and international waters);
  - locality options: developing countries (lower-, middle- or higher-income countries; large or small countries) and Organisation for Economic Co-operation and Development (OECD) countries).
- It is very easy to find land in or around deserts appropriate for large energy production with PV systems.
- Deserts and semi-arid lands are normally high insolation areas.

- The estimated potential of such areas can easily supply the estimated world energy needs by the middle of the 21st century.
- When large-capacity PV installations are constructed, step-by-step development is possible through utilizing the modularity of PV systems. According to regional energy needs, plant capacity can be increased gradually. It is an easier approach for developing areas.
- Even very large installations are quickly attainable in order to meet existing energy needs.
- Remarkable contributions to the global environment can be expected.
- When VLS-PV is introduced to some regions, other types of positive socio-economic impacts may be induced, such as technology transfer to regional PV

3 MEDITERRANEAN REGION CASE STUDIES

The economic conditions for VLS-PV systems in the Mediterranean region were examined. Originally focusing on the Sahara Desert-bordering countries of Morocco and Tunisia, Portugal and Spain were also included in order to compare the impact of recently approved PV feed-in tariffs with the less-supportive framework environments in Northern Africa. Two sites were selected for each country, one more affected by marine climate influences with lower irradiation, and one representing a higher irradiated desert-like location.

The study was performed from a professional project developer's perspective by determining PV electricity generation cost and potential revenues from electricity sales from VLS-PV systems to customers, either to consumers on a standard electricity price level or to grid-operating entities on a feed-in tariff basis.

As taken from experience with already realized MW systems, a stationary (non-tracking, flat-plate) large scale PV installation can, to date, be realized at around 4 010 Euros/kW. The value serves as a fair approximation for the following calculations, including a limited overhead cost of 8 %. Note that this overhead does not yet include a further 6 to 8 % capital acquisition cost, which is typically required if the project is sold to private or fund investors, a frequently encountered way of project financing at present. Three-quarters of the system cost amounts to the PV modules, the module prices thus being the main parameter for future cost reduction. For annual cost, 20 years' linear depreciation and 100 % loan financing at a 5 % interest rate serve as model parameters, which, of course, need to be adapted for concrete project proposals. No investment for land was considered here, and the estimated land rental cost is included in the 2 % annual operation and maintenance cost. The total annual cost per kW was assumed to be equal to 480 Euros/kW at all locations.

PV electricity generation costs in the analysed Mediterranean countries are between 30,2 and 47,6 Euro-cents/kWh, as shown in Table 1. As expected, the generation cost for PV calculated is distinctly higher than the price level of conventional electricity drawn from the grid in all places. In this context, it is important to note that the assumed 100 % loan financing makes up a substantial proportion of the generation cost. Generation costs below 20 Euro-cents/kWh result for almost all sites, without including the financing cost and the 7 % safety reduction in the annual energy yield. This confirms that PV generation costs are not too far above the conventional price line and could reach or even fall below this line after a price decrease of PV modules, which is already anticipated by foreseeable advances in technology and economy of scale with increasing mass production.

Although the lowest generation cost of 30,2 Eurocents/ kWh is reached in Quarzazate, this is not low enough to become attractive for a buyback scheme in Morocco, even considering that the general electricity price level is comparatively high there. Tunisia has a centralized electricity industry with a low price level, making the situation for PV even more difficult.

Morocco and Tunisia have no specific legal framework to support PV electricity generation and no existing feed-in tariff. Therefore, the economic feasibility for VLS-PV is low in these Northern African countries if based on achieving income from electricity sales to consumers or on the grid alone – that is, not considering any investment subsidies.

Portugal and Spain also have much lower prices for conventional electricity than the calculated PV electricity-electricity-generation cost. In these countries, however, smaller systems appear to be economically feasible with the available feed-in tariffs in higher irradiation sites. The exciting question for VLS-PV is whether large systems can also be economically operated under special circumstances. Answering this question requires a closer look at the conditions in these Southern European countries.

In summary, we expect the best conditions for VLSPV to develop in Spain on an intermediate time scale of 2 to 5 years, even though there are now several larger projects proposed in Portugal. Concrete realisation

Table 1: Solar irradiation, energy yield and PV electricity-generation cost data compared with the conventional electricity price level and local feed-in tariff rates for stationary systems at two representative sites in four Mediterranean countries

Country	Site	Annual global irradiation ($kWh/m^2/y^{-1}$)	Annual energy yield ($kWh/kW/y^{-1}$)	Generation cost for PV (Euro-cents/kWh)	Conventional grid electricity price level (Euro-cents/kWh)	Feed-in tariff rate (Euro-cents/kWh)
Morocco	Casablanca	1 772	1 337	35,9	~8–12	None
	Quarzazate	2 144	1 589	30,2		
Tunisia	Tunis	1 646	1 219	39,4	~2–5	None
	Gafsa	1 793	1 339	35,8		
Portugal	Porto	1 644	1 312	36,6	~12	~55 <5 kW
	Faro	1 807	1 360	35,3		~31–37 >5 kW
Spain	Oviedo	1 214	1 008	47,6	~9	41,44 <100 kW
	Almeria	1 787	1 372	35,0		21,62 >100 kW

of VLS-PV projects depends upon successful negotiation between project developers, PV and electricity industries, and politicians with regard to acceptance, sustainability and incentives in every single project.

4 MIDDLE EAST REGION CASE STUDIES

A top-down approach to providing solar electricity to any given region must address the following five questions:

- How much land area is available for the harvest of sunshine, and how much electricity could this resource provide?
- How much electricity is required?
- What kind of technology should be used, and how much of it would be needed for the task?
- At what rate should the technology be introduced?
- What monetary resources would be required and how could these resources be provided?

This study provides a set of answers for the principal electricity-consuming countries in the Middle East.

First, we studied the current electricity requirements and land availability of all countries in the region as shown in Table 2, with the specific aim of being able to provide some 80 % of their total electricity needs with solar energy within 36 years. For all of the major electricity-producing countries, it was concluded that land area considerations should present no obstacles to such aims.

Second, we studied existing concentrator photovoltaic (CPV) technology at the system component level, considering the expected costs involved in their mass production. These costs included the VLS-PV plants and the necessary mass production facilities for their manufacture. It was concluded that, in Israel, VLSPV plants would cost no more than US$850/kW, and that production facilities, capable of an annual throughput of 1,5 GW collectors and 0,5 GW storage, would cost approximately US$1 170 million.

Third, we studied the kind of investment that would be necessary to create a production facility in four years, the first VLS-PV during the fifth year, and one successive new VLS-PV plant every year thereafter.

Assuming an open credit line being made available by the government (or investors) at a 3 % real rate of interest, it was concluded that, in the Israeli case as shown in Table 3:

- the credit line would reach its maximum value in the 13th year;
- the maximum required credit would be equal to the cost of approximately ten fossil-fuelled plants;
- the credit-line plus interest would be fully paid off by electricity revenues after 21 years;
- by that time, revenues would be sufficiently high to enable both the continued annual production of VLS-PV plants with no further investment, and the decommissioning and replacement of old plants after 30 years of service.

It is important to point out that after the initial investment has been paid off, the price of electricity no longer depends upon any factors related to its generation. It becomes a purely arbitrary figure that can be fixed at any desired level. For our examples, we arbitrarily fixed it at 5,5 US cents/kWh. However, if it is deemed desirable to continue installing VLS-PV plants at the rate of one per year, then the price of electricity can be lowered to a figure enabling the annual net revenue from sales to precisely cover the cost of one new VLS-PV plant.

Similarly, if it becomes necessary to replace old plants after 30 years of service, it is sufficient to fix the electricity price during the 29th year at a level covering the cost of constructing two new VLS-PV plants the following year, etc. Simple arithmetic shows that in both of these examples, the required electricity price will be less than the 9 US cents/kWh that we have adopted for our calculations.

Table 3 Expected economic benefits to Israel of VLS-PV plant introduction during the first 36 years

Interest rate	3	% y–1
Yearly added solar power	1,5	GW
Yearly added six-hour storage power	0,5	GW
Credit line capacity required for the entire project	9 781	US$ million
Interest paid	3 397	US$ million
Loan repaid after	21	years
Total solar power installed	46,5	GW
Total storage power installed	15,5	GW
Electricity price after five years, when solar electricity sales start	9	US cents/kWh
Electricity price after 22 years, when all debts are paid off	5,5	US cents/kWh
Land area required for installation	558	km^2
Fraction of total national land area	2,7	%
Yearly manpower requirements for solar production	4 500	jobs
Yearly manpower requirements for solar operation	11 625	jobs
Yearly manpower requirements for storage production	1 500	jobs
Yearly manpower requirements for storage operation	3 875	jobs
Headquarters and engineering	1 395	jobs
Total number of jobs after 36 years	22 895	jobs

In the fourth part of this study, we repeated the Israeli calculations for the other major electricity producers in the region, making certain simplifying assumptions that were specified in each case. Given uncertainties yield electricity at costs fully competitive with fossil fuel. Second, one may think in terms of typically 80 % of a country's entire electricity requirements coming from solar energy within a period of 30 to 40 years.

Third, VLS-PV plants turn out to be triply renewable. In addition to the normal sense in which solar is deemed to be a renewable energy, the revenues from this topdown approach would be sufficient to completely finance the continued annual construction of VLS-PV plants and the replacement of 30-year-old VLS-PV plants with new ones without the need for any further

Table 4 Proposed projects for VLS-PV development in Mongolia

	Location	Capacity	Demands
First stage: R&D/pilot phase	Sainshand	1 MW	Households and public welfare (significant level compared to the peak demand and electricity usage in Sainshand city)
Second stage: demonstration phase	Four sites along the railway: 1 Sainshand 2 Zumiin Uud 3 Choir 4 Bor-Undur	10 MW/site (total: 40 MW)	Industry (surpasses the peak demand and almost equivalent to electricity usage around these locations)
Third stage: deployment phase	Five sites along the railway: 1 Sainshand 2 Zumiin Uud 3 Choir 4 Bor-Undur 5 Mandalgobi One site between Oyu–Tolgoi and Tsagaansuvrage	100 MW/site (sub-total: 500 MW) and 500 MW (total: 1 GW)	Power supply (almost double the peak demand and significant level compared to electricity usage in Mongolia)

investment, surrounding local electricity prices, labour costs, and production/consumption growth rates, our results for these countries should be regarded as indicative rather than definitive.

5 VLS-PV PROJECT ON THE GOBI DESERT

5.1 Demonstrative Research Project for VLS-PV in the Gobi Desert of Mongolia

Mongolia has the vast Gobi Desert area in the southern and south-east parts. There are two types of electricity users in Mongolia, nomadic families and users of the electricity network. While electrification using PV for nomadic families has occurred, an existing electricity network supports Mongolian economic activity.

The electricity networks (transmission lines) have been constructed only in specific regions, such as those centring on Ulaanbaatar, the capital of Mongolia. The transmission lines have basically been constructed along a railway connecting Atlanbulug with Zumiin Uud through Ulaanbaatar – the borders in the north and south-east. The railway is playing a very important role in Mongolian economic activity. Therefore, these areas along the railway and transmission lines are expected to further develop in the future. However, electricity for the areas is generated by coal at Ulaanbaatar, worsening the atmospheric environment around Ulaanbaatar. As a result, installing large scale carbon-free renewable electricity such as the VLS-PV system may contribute both to protecting against air pollution and supporting regional development.

The VLS-PV scheme is a project that has not been carried out before. In order to achieve VLS-PV, a sustainable development scheme will be required. There are many technical and non-technical aspects that should be considered. Therefore, we will propose a demonstrative research project in the areas along the railway and discuss a future possibility for VLS-PV in the Gobi Desert, in Mongolia. The proposed project will include three phases as follows (see Table 4). The potential sites in the Gobi Desert area along the railway were identified using long-term meteorological observation data conducted over the last 30 years. Grid access, as well as favourable market, economic, climatic and weather conditions, prevail in southern Mongolia – hence the choice of the candidate sites for the development of the VLS-PV system in the Gobi.

It is expected that the first phase will take four to five years. The project site will be Sainshand and the capacity of the PV system will be 1 MW. The assumed demands are households and public welfare needs in the region. The project has benefits beyond electricity.

Apart from the creation of jobs and employment, the tourism industry will also benefit. In the second phase, 10 MW PV systems will be installed in Sainshand, Zumiin Uud, Choir and Bor-Undur, where they are located along the railway lines. These sites are important cities and the scale is classified as medium-large scale in Mongolia. The total capacity of PV systems installed will reach 40 MW, and the demands assumed are to supply industry sectors, such as mining, located in the sites' neighbourhoods. The project will then be shifted to the third phase, which is the deployment phase. In this stage, 10 MW PV systems will be enhanced to 100 MW VLS-PV systems, and one new 100 MW system will be constructed in Mandalgobi.

Besides these 100 MW VLS-PV systems, another 500 MW VLS-PV system will be constructed in between Oyu Tolgoi and Tsagaansuvraga, which are located in Umnugobi and Dornogobi provinces.

Renewable energy development is a promising way for social development and is one of the most important policies in Mongolia. Two documents, the Law for the Promotion of Renewable Energy and a proposal for a Utilization and National Renewable Energy Programme, have recently been drafted and submitted to the government for the approval of parliament. Final approval of these two documents will positively affect taxes and other funding that will assist in the development of VLS-PV systems.

4.2 Feasibility Study on 8 MW Large Scale PV System in Dunhuang, China

Energy shortages and environmental pollution have become the bottleneck of social and economic development in China. Improving the current structure of energy supply and promoting utilization of renewable energy are effective solutions for these problems. The photovoltaic power generation system involves clean energy without greenhouse gas emissions. In China, there are huge lands in the Gobi Desert and elsewhere that provide the possibility of large scale PV systems on very large scale applications. Only when PV is used for large

scale applications can costs be reduced to the level of those associated with traditional electric power.

The Gobi area in Gansu is about 18 000 km2. This area can be used to build 500 GW VLS-PV, which is more than the whole power capacity in China today. The targeted place for 8 MW large scale photovoltaic power generation (LS-PV) in the Gobi Desert is at Qiliying, 13 km from Dunhuang city. The latitude is N-40° 39', with a longitude of E-94° 31' and an elevation 1 200 m. It is only 5 km from Qiliying to the 6 000 kVA/35 kV transformer station, so it will be not cost that much to build a high voltage transmission line.

The 8 MW PV system will be divided into eight substations of 1 MW each. Each 1 MW sub-station will feed the generated electricity to a high voltage grid (35 000 V) through a 1 000 kVA transformer. Each 1 MW sub-station will be divided into five channels with 200 kW each, Each 200 kW PV channel will be equipped with a grid-connected inverter to convert the DC power from the PV into three-phase AC power for the primary of the 1 000 kVA transformer.

Each 1 MW sub-station and each 200 kW channel will be independent. Such design offers the advantages of being easier for troubleshooting and maintenance, being flexible for potential investors, and allowing various types of PV systems to be installed and compared.

The system efficiency is assumed to be 0,77. Using the efficiency and the annual in-plain irradiation facing south with a 40° tilted angle, the annual output is calculated to be 13 761 MWh/year.

Table 5 Capital investment for 8 MW LS-PV system (1 yuan = approximately USD0.12)

	Investment (million yuan)	Share (percentage)
Equipment	277,02	85,91
PV module	236,8	73,43
Inverter	34,2	10,61
Transformer	3,52	1,09
Test and monitoring	2,5	0,78
Civil construction	15,56	4,83
Transportation and installation	7,35	2,34
Feasibility study and preliminary investment	7,0	2,17
Miscellaneous	15,36	4,65
Total	322,4	7 100

Total capital investment is 322,47 million Chinese yuan (approximately 38.7 MUSD), and 86 % of total investment is for PV system equipment, such as PV modules, inverters and transformers, as shown in Table 5. However, it is expected that 96,74 million yuan (30 % of the total capital) will be a grant provided by the central government of China, and the real required capital will be 225,73 million yuan. The Gansu grid company will guarantee 1,683 yuan/kWh as the feed-in tariff and the annual income for the PV system will be 23,16 million yuan: 13,761 MWh/year × 1,683 yuan/kWh. The tariff purchased by the grid company will be added on to all the electricity consumed in Gansu Province and the electricity consumption in Gansu Province was 340×10^8 kWh in 2002. Therefore, the additional tariff will be 0,006 8 yuan/kWh: 23,16 million yuan/340×10^8 kWh. For a family consuming 2 kWh/day, the annual consumption will be 730 kWh, and they will only need to pay 5 yuan/year in addition.

The proposed 8 MW LS-PV plant in Dunhuang city is considered the first pilot project in China with the Great Desert Solar PV Programme proposed by the World Wide Fund for Nature (WWF) and an expert group. The development of further large scale PV systems in other regions is also being discussed. It has been proposed that 30 GW of solar PV power generation capacity could be developed by 2020 if government incentive policies are developed and are in place. This could enable China to become a leading country in solar power development in the world.

6 OCEANIAN CASE STUDY

Perenjori is a small township approximately 350 km north-east of Perth in the wheat belt of Western Australia and situated at E-116,2° longitude and S-29° latitude. The required land to set up a VLS-PV power generation project can be obtained at a reasonably low price or leased for 30 to 50 years from local farmers. The land is flat and suitable for mounting the structure or installing solar PV power generation projects.

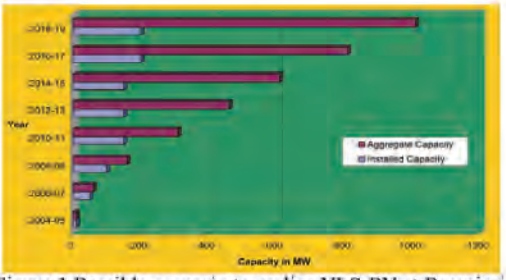

Figure 1 Possible scenario to realise VLS-PV at Perenjori

Several issues arise in terms of achieving a very large scale solar photovoltaic power generation project at Perenjori. Although the Great Sandy Desert receives more solar radiation than Perenjori, the overall economy of setting up the project and generation costs will be less at Perenjori due to its location to enough loads and the availability of the local grid.

At present, the load is almost negligible; but there is a strong interest in promoting the mining industry in the region provided that sufficient and good quality power is available for mining activities. A number of mining companies have also shown interest in setting up their mining operations in the Perenjori regions, and there will be a load of the order of 1 GW over the next 10 to 15 years.

The size of a VLS-PV system may range from 10 MW (pilot) to 1 or several GW (commercial), consisting of one plant or an aggregation of a number of units, distributed in the same region and operating in harmony with one another. Figure 1 gives a rough idea how a VLS-PV project can be realized in a circular distance of 100 km of Perenjori over the next 15 years, aggregating to a capacity of over 1 GW.

What will be feasible is to install several stand-alone solar PV systems as per the load requirement of each individual mining operation in the region. Then, when three to four projects have been set up in the region, they can be interconnected by creating a small local grid.

Table 6 Estimated project cost for 10 MW PV power generating system (Aus$1 = approximately US$0.76)

Components	Unit cost	Total cost (Aus$)
PV modules	4,4 Aus$/W	44 000 000
Mounting structure with single-axis tracking	10 % of modules	4 400 000
Inverter(s)	125 000	5 000 000
Transformers and cabling	4 % of modules	1 760 000
Installation and commissioning	7 % of modules	3 080 000
Land	Lump sum	500 000
Miscellaneous, including transportation to site	Lump sum	1 260 000
Total		60 000 000

A project for installing a 10 MW pilot power generation system will be proposed as the first step for a VLS-PV system at Perenjori. The estimated project cost of a 10 MW PV power generation project at Perenjori will be of the order of Aus$60 million, with the following cost breakdowns as shown in Table 6. Almost 70 % of the project cost comprises PV modules only. The generation cost of the pilot project of 10 MW, after availing of a 50 % subsidy from the government, will be approximately 14 Australian cents/kWh under the Mandatory Renewable Energy Target (MRET) of the federal government of Australia, which is very much comparable with the cost of power generation from a diesel power project. At a price of 36 cents/litre, diesel fuel is available to the mining companies in Perenjori; the cost of power generation from diesel power projects comes to about 12 cents/kWh. Therefore, the mining companies would be interested in purchasing power from the proposed pilot project of 10 MW, and the installation of a diesel-based power project as a backup has been suggested.

Prior to setting up the pilot project, arrangements must be made by the project developers to sell the power to the mining operators. The power purchase agreements (PPAs) should be signed for the whole lifetime of the project. The Shire of Perenjori and Mid West Development Commission would play an important role in negotiating the terms and conditions of the PPAs, and their assistance would be necessary to attract project developers for this project, as well as for other projects to be installed later on.

7 DESERT COMMUNITY DEVELOPMENT

A region, where the VLS-PV is introduced, should also be sustainable as well in socioeconomic issues. By the Phase I studies [1], sustainable scenario was developed in order to maintain sustainable economical effects to the regional society year by year by introducing local PV module assembly factory lines and by supplying most of modules to VLS-PV constantly every year. This approach assures local job creation and income by purchasing electricity. Some part of electricity can be also utilised for agricultural development in the desert area. Especially, the presence of electricity in agricultural field seems to be a new kind of motif and this approach can provide useful means for agricultural people, for instance, in order to avoid soil property deterioration caused by careless irrigation.

Figure 2 illustrates a desert community development that aims to achieve an ideal community. Agriculture and tree planting can be facilitated with plentiful renewable energy. The electricity can also be fed to neighbouring communities. The modelling for the desert community

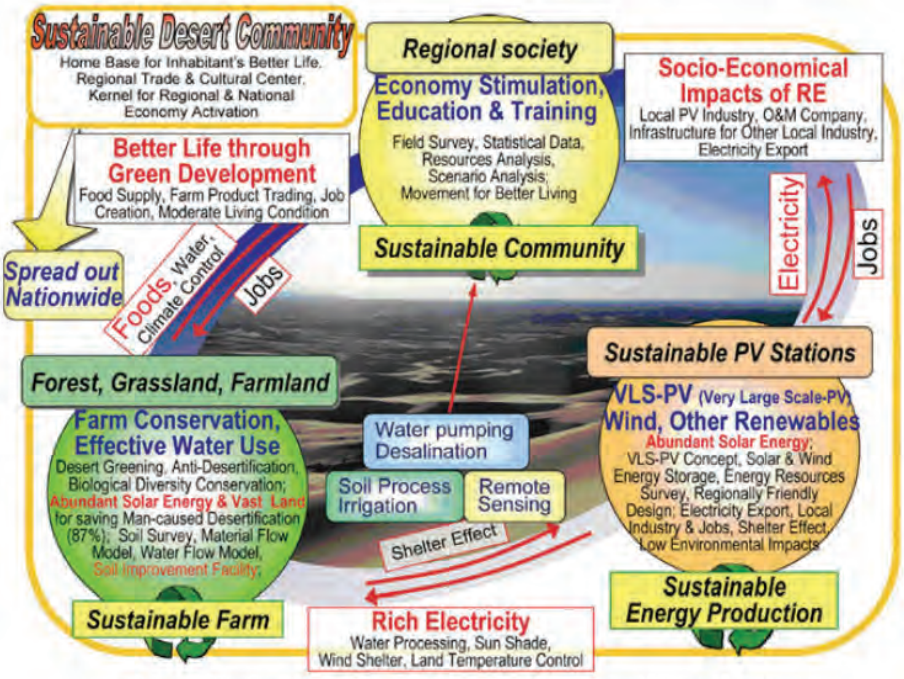

Figure 2 Framework of desert community development and research topic

has been discussed and a fundamental structure has been formulated in terms of a specific village in the Mongolian Gobi by considering the following items:

- *Sustainable energy production by sustainable PV stations.* Here, the VLS-PV system is the main feature. Other renewable energy source can also be utilised such as wind, biomass, etc.. Battery storage is essential for service during night.
- *Sustainable farming.* Utilising soil and water conservation technology, we will conserve and rehabilitate the environment of a desert area. This may be relatively easy to achieve with PV support.
- *Sustainable community.* Statistical and scenario analyses are used to develop an ideal community. In order to sustain regional society, education and training are also considered in addition to the facilities and technology needed.
- *Remote sensing.* It can be utilised find out suitable places where to implement VLS-PV and wind power systems. It can also bring data on soil and water required for sustainable agricultural production.
- *Desalination.* PV power can drive a desalination plant, which will supply enough amount of drinking and irrigation water.
- *Effect of PV station on local agriculture.* Proper operation of a water pump and desalination system can remove salt from the groundwater to provide good quality water. This can enhance crop yields and reduce the use of fuel wood. PV-driven greenhouse can produce agriculture product of high quality and yields.
- *Effect of PV station on the local community.* PV stations including a local module factory can create more employment. This would also increase local incomes through selling electricity.

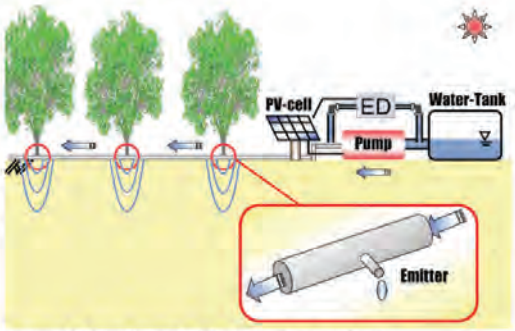

Figure 3 Desalinised drip irrigation system

- *Technology.* Implementing a subsurface drainage system may save groundwater quality, and desalination equipment protects soil from damage due to salinisation. Considerable amounts of low saline water will be available when PV system can drive a desalination system, such as reverse osmosis (RO) or electro-dialysis (ED). Figure 3 shows an example of a drip irrigation system with a desalination system.

8 CONCLUSIONS

It is strongly indicated that VLS-PV could directly compete with fossil fuel as the principal source of electricity and with existing technology for any country that has desert areas. This could be accomplished by finding an investment scheme and by getting institutional and organizational support for its implementation. The proposals developed in this study may motivate expected stakeholders to realize VLS-PV project in the near future. Moreover, a series of these practical project proposals from different viewpoints and directions will enable us to provide essential knowledge or detailed practical instructions in order to realize the sustainable implementation of VLS-PV development in the future.

- Discuss and evaluate future technical options for VLS-PV, including electricity network, storage and grid management issues, as well as global renewable energy systems.
- Analyse local, regional and global environmental and socio-economic effects induced by VLS-PV systems from the viewpoint of the whole life cycle.
- Clarify critical success factors for VLS-PV projects, on both technical and non-technical aspects, based on experts' experiences in the field of PV and large scale renewable technology, including industry, project developers, investors and policy-makers.
- Develop available financial, institutional and organizational scenarios, and general instruction for practical project proposals to realize VLS-PV systems.
- The International Energy Agency (IEA) PVPS community will continue Task 8 activities. Experts from the fields of grid planning and operation, desert environments, agriculture, finance and investment should be involved.
- The IEA PVPS community welcomes non-member countries to discuss the possibility of international collaboration in IEA PVPS activities.

ACKNOWLEDGEMENT

This study has been carried out under the activities of IEA/PVPS Task 8, "Study on Very Large-Scale Photovoltaic power generation (VLS-PV) systems". The latest results will be published in September 2006 [2]. Task 8 Operating Agent has been supported by New Energy and Industrial Technology Development Organization as their contract research.

REFERENCES

[1] Kosuke Kurokawa, Energy from the Desert, James & James Ltd., London, 2003.
[2] Keiichi Komoto, Peter van der Vleuten, David Faiman and Kosuke Kurokawa, Energy from the Desert: Practical Proposals for Very Large Scale Photovoltaic Systems (to be published by James & James Ltd., London, 2006).

21st European Photovoltaic Solar Energy Conference, 4-8 September 2006, Dresden, Germany

PERFORMANCE ANALYSES OF BATTERY INTEGRATED GRID-CONNECTED RESIDENTIAL PV SYSTEMS

Yuzuru Ueda[1], Kosuke Kurokawa[1], Takamitsu Itou[2], Kiyoyuki Kitamura[2], Katsumi Akanuma[3], Masaharu Yokota[3], Hiroyuki Sugihara[3], Atsushi Morimoto[4]
1 Tokyo University of Agriculture and Technology, 2-24-16 Naka-cho, Koganei, Tokyo 184-8588, Japan
email: yzrueda@cc.tuat.ac.jp
2 MEIDENSHA CORPORATION, Riverside Building, 36-2 Nihonbashi Hakozakicho, Chuo-Ku, Tokyo 103-8515, Japan
3 Kandenko Co., Ltd., 4-8-33 Shibaura, Minato-ku, Tokyo 108-8533, Japan
4 Matsushita Ecology Systems Co., Ltd., 4017 Shimonakata Takaki-cho, Kasugai-city, Aichi 486-8522, Japan

ABSTRACT: Grid connected PV systems will feed electric power to the power distribution network. Voltage at the connecting point to the grid will become higher along with the reverse power flow increasing. PCS output power is restricted by the grid voltage so the significant amount of the possible energy output will be lost if the grid voltage is too high. To avoid this output energy loss due to the high grid voltage, battery integrated PV systems are developed in the "Demonstrative research on clustered PV systems." More than 550 residential PV systems are installed in the demonstrative research area. Annual performance analysis results of commercial PV systems without battery and battery integrated systems are summarized in this paper. Variation of the output energy loss due to the grid voltage is observed in commercial PV systems due to the difference of the regulating method. Approximately 8% of additional performance loss is observed in battery integrated PV systems. Active power regulations due to the high grid voltage are successfully avoided in some cases.
Keywords: Grid-Connected, PV System, Performance

1 INTRODUCTION

Grid connected-residential photovoltaic (PV) systems such as roof mounted PV systems feed electric power to the power distribution line. Since radial power distribution system is designed for a power flow from the high voltage (HV) side to the low voltage (LV) side, reverse power flow from the end of LV side may cause voltage rise of LV line. [1](see Figure 1) To prevent the over voltage of the power distribution line, Japanese PV system's power conditioning subsystems (PCS) have a function to regulate output power when the voltage of the grid is too high. Because of this function, significant amount of electric power will be lost. [2]

"Demonstrative research on clustered PV systems" is being conducted from December, 2002 by NEDO to investigate about the voltage problem and other potential issues of grid-connected PV systems. Approximately 550 PV systems are installed on the roofs of houses and connected to the commercial power grid in the demonstrative research area in Oota, Japan. A total of nominal system power is more than 2[MW] and all the systems are connected to the same power distribution network. [3]

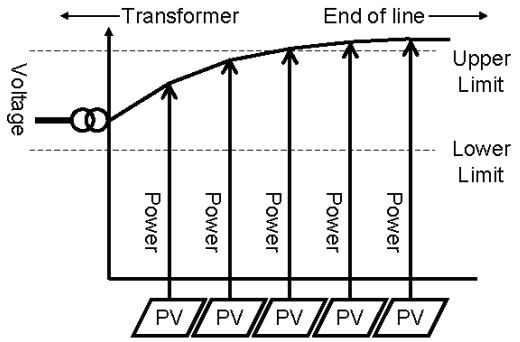

Figure 1: Voltage rising of power distribution line

2 BATTERY INTEGRATED PV SYSTEMS

2.1 Overview of battery integrated PV system

To minimize the output energy loss due to the high grid voltage and maintain the power quality of the grid, battery integrated PV systems are developed in the demonstrative research. Lead acid battery with a capacity of 49 [Ah] for single cell are used for the systems, 96 cells are series connected and installed in the outdoor storage box for each PV systems. Two types of charge controller are developed in the demonstrative research. One is the unified PCS for PV and battery and the other is the additional charge controller for commercial PV systems. Installation of the unified PCS is started from January, 2005. Additional charge controllers for the installed commercial PV systems are started in a year later.

2.2 Unified PCS for PV and battery

The unified PCS is composed of a DC/DC booster, DC/DC charge controller and DC/AC inverter. Figure 2 shows a schematic view of the battery integrated PV system with the unified PCS.

Only the power from the PV array will be charged to the battery, the charged power will be used in the in-house load. Unified PCS monitors a power flow at the connecting point, more than 150[W] of forward power flow are required for discharging in order to prevent the reverse power flow from the battery to the grid.

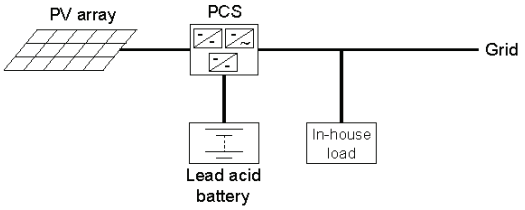

Figure 2: Schematic view of the battery integrated PV system with the unified PCS

3 ANALYSIS METHOD

One-minute averages of secondly measured data are used for the analysis. System yield [kWh/kW] and performance ratio are employed for the overall system performance analysis. In addition to these indexes, detailed loss analyses are performed to clarify the benefit of the battery integration.

Deployed PV systems performance is highly depending on the various loss factors, i.e. temperature, shading, array configuration, grid voltage and so on. Expected output power which would be generated in the normal grid voltage condition and lost energy under the high voltage condition need to be quantified in order to quantify the energy which is saved by the battery. Some of the losses occur exclusively but some of them occur simultaneously, the following loss factors are considered and separately quantified in this paper.

1. Shading
2. Regular loss (Soil, Degradation, Array config.)
3. Incident Angle / Reflection
4. Module Temperature
5. Output restriction (over voltage)
6. PCS capacity shortage
7. MPP mismatch (high voltage side)
8. DC resistance
9. Inverter
10. PCS Off / PCS Standby
11. Fluctuation

Input energy of the PV systems is irradiation. Irradiation is measured at the meteorological stations using pyranometer in this research. Shading, soil, degradation and incident angle are treated as factors to reduce the input irradiation of the PV array. Received irradiation will be used for the photovoltaic energy conversion. Module temperature, operation point on the I-V curve and array configuration are treated as factors to change the conversion efficiency of the PV array. Grid voltage, PCS capacity and MPP mismatch are considered as factors to determine the operation point on the I-V curve of the PV array.

Loss due to the incident angle and DC circuit resistance are calculated using theoretical model. [4][5] Loss due to the module temperature and inverter are directly calculated using measured module temperature, PV array's output power and inverter's output power. Other losses are quantified for each factor using empirical models. [5][6][7]

4 RESULTS AND DISCUSSIONS

4.1 System yield and performance ratio

Monthly averages of daily reference yield, daily system yield and daily fed power are summarized in Figure 3. Monthly performance ratios are also plotted in this figure as a right y-axis. In general, April has a longest reference yield but peak of the performance ratio is in winter. Performance ratio in summer is slightly lower because of the efficiency drop due to the module temperature increasing. PV systems with battery always result approximately 8% lower performance ratio due to the additional energy loss at the charge controller and battery. 30% of generated power is once charged in the battery for battery integrated systems. As a result, fed power is less than half of the non battery integrated systems.

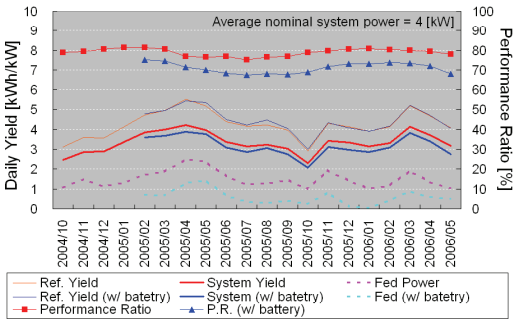

Figure 3: Reference yield, system yield, fed power and performance ratio for commercial and battery integrated PV systems

4.2 Annual system performance

Annual system performance and loss analysis results of commercial PV systems and those of battery integrated PV systems are shown in Figures 4 and 5 respectively. Data collected from March, 2005 to February, 2006 are used in these results. Numbers of PV systems used in these graphs are gradually increased during the evaluation period, numbers of commercial (non battery integrated) PV systems in March, 2005 are 134 and 140 in February, 2006. On the other hand, numbers of battery integrated PV systems are 19 in March and 197 in February. Both energy losses at the inverter and charge controller are included in a loss due to the unified PCS. Additional energy consumption of the measurement system and control system are also included.

Looking at the results, all the loss factors showed almost the same values and seasonal trend except the loss due to the battery and PCS. Since commercial PCS and unified PCS have almost the same DC/AC conversion efficiency, 4.7% of the expected energy can be assumed as a loss at the charge controller of unified PCS and other additional losses. 3.3% of the expected power is also lost in the battery itself so that the total performance ratio is around 8% lower in the battery integrated systems.

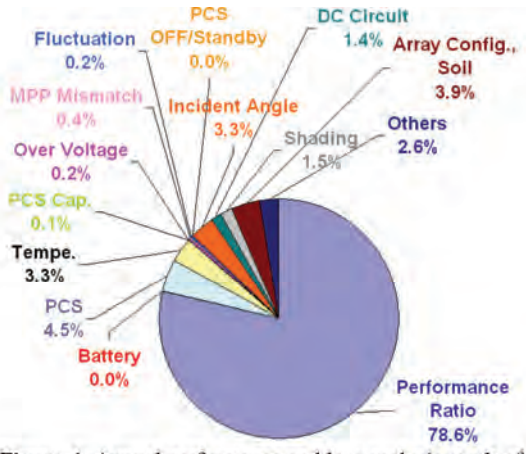

Figure 4: Annual performance and loss analysis result of commercial (non battery integrated) PV systems

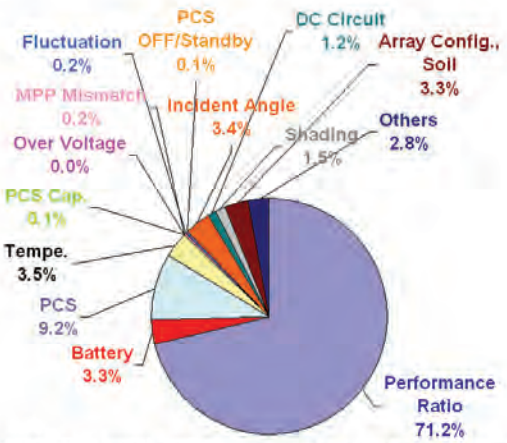

Figure 5: Annual performance and loss analysis result of battery integrated PV systems

It should be noted that charged energy have to go through the charge controller twice. When the generated electricity is being stored in the battery, current will go through DC/DC booster and DC/DC charge controller. During the discharging, current will go through DC/DC charge controller again and DC/AC inverter. Charging DC current are not the constant current but follow the PV array output, this is not the best way to charge the battery in terms of the efficiency stand point but necessary in the battery integrated PV systems.

4.3 Loss due to the grid voltage

The voltage at the power distribution line needs to be controlled within 101V +- 6V or 202V +- 20V in Japan. Flowing current and line impedance are two major factors to determine the voltage at the connecting point. If the sending voltage of the transformer substation and tap positions are the same but different current in the same line impedance, more current cause more voltage drop in forward power flow case but results voltage increasing in reverse power flow case at the end of LV line. Thus reducing the feeding power to the grid is necessary to avoid the over voltage for the distributed generator such as grid connected PV systems. Battery integration is one of the options for PV systems to minimize the risk of over voltage without sacrificing the output energy by mean of storing the electricity in the battery.

So far, energy loss due to the grid voltage is not so severe even in the non battery integrated PV systems. Percentage of the loss due to the grid voltage is less than 1% in annual average as shown in Figure 4. This is probably because of the good voltage control of the power grid. However, there are a few systems which tend to have more energy loss due to the grid voltage and amount of lost energy is sometimes more than 50% of the expected energy out. Figure 6 shows analysis result of the loss due to the grid voltage for commercial PV systems. Each data point represents the daily loss of one system and more than 3000 data are plotted in each month. Although most of the data are on the 0% line, some of the systems result significant energy loss on particular days. Most of these bad days are weekends and clear sunny days as shown in Figure 7. The results suggest that the reduced load (reducing forward current) in the power distribution network in weekends and more reverse power flow (increasing reverse current) in clear sunny days caused higher grid voltage.

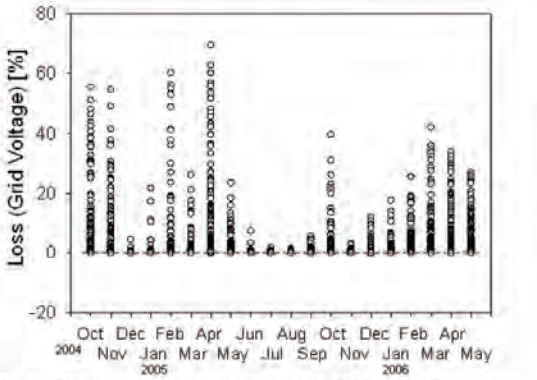

Figure 6: Daily loss ratio due to the high grid voltage for commercial (non battery integrated) PV systems

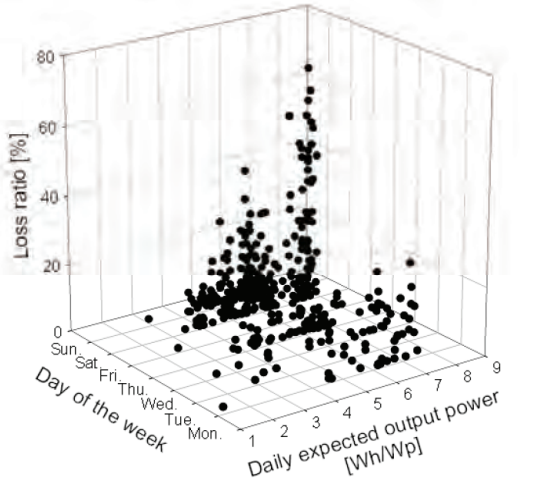

Figure 7: Loss ratios due to the grid voltage as a function of the day of the week and daily expected output power

Another factor to differentiate the amount of energy loss due to the grid voltage among the systems is the starting voltage of output regulation. Examples of the regulation methods, starting voltage and regulating speed are summarized in Table 1. Phase advance reactive power control will shift the phase of current and change the power factor between 1 and 0.85, active power control will regulate the output current in order to reduce the output power by shifting the operation point from MPP to the open circuit voltage. Since PCS is not monitoring the voltage at the connecting point but its own output terminal voltage and there is a voltage drop between PCS output terminal and connecting point due to the resistance of the drop wire, voltage at the connecting point might be lower than that at the PCS output terminal. Thus PCS may not need to start the regulation from 107V but can start from slightly higher voltage. This is one of the reasons why starting voltages of output regulation are not exactly the same among all the PCS. However, it is pointed out that this kind of variation may cause the concentration of output restriction in particular PCS so this variation should be minimized. [8]

PCS Types	Starting Voltage	Speed
Reactive power control		
1	112V	PF=1 to 0.85 in 2.5sec
2	None	None
3	None	None
4	107V	PF=1 to 0.85 in 10sec
Active power control (Regulation)		
1	After PF reached 0.85	2A/sec, 100% to 0%−10sec
2	107V	43mA/4sec
3	109V	Immediately 0%
4	109V	100% to 0% in 4 to 10sec

Table 1: Examples of output regulation method

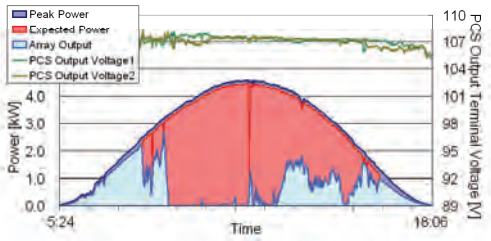

Figure 8: Example of output regulation due to the high grid voltage. System #1 with commercial PCS type A

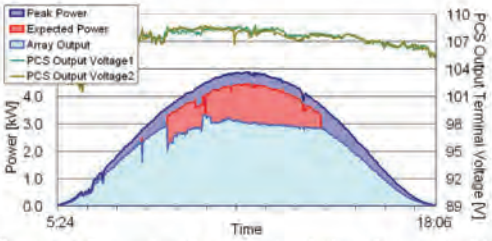

Figure 9: Example of output regulation due to the high grid voltage. System #2 with commercial PCS type B

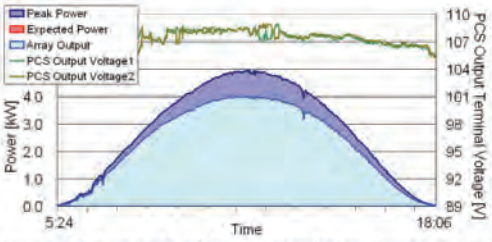

Figure 10: Example of output regulation due to the high grid voltage. System #3 with commercial PCS type C

Figures 8, 9 and 10 are examples of the output regulations due to the high grid voltage for three different commercial PCS. All the systems are connected under the same pole transformer, no battery are installed in these systems. Data are collected on April 9, 2005, Saturday. Peak power means expected system output power under the measured irradiation at the module temperature of 25 degree Celsius. Array output means actual output power from the PV array under the actual module temperature. Red area means lost energy mainly because of the restriction of the output power due to the high grid voltage. PCS output voltage1 and 2 are measured voltage at the single-phase three-wire PCS output terminals. Starting voltage of the active power regulation for system #1's PCS is around 107.5[V]. On the other hand, that of system #2's is around 109[V] and 110[V] for system #3's PCS. As a result, around 69% of the expected power was lost due to the high grid voltage in system #1 while system #2 lost around 15% and no loss was observed in system #3. PCS output terminal voltages of system #3 are slightly higher than those of the others because #3 has more reverse power flow to the grid. However, this result does not mean that system #3 was in over voltage condition because these voltages are not the voltages at the connecting point.

4.4 Effect of battery

Battery can be used as an output restriction avoidance system in grid connected PV systems. Charging battery with generated electricity can minimize the power fed to the grid in the daytime. Stored electricity will be used in the in-house load during the nighttime. Figures 11 and 12 are examples of the results how the battery worked as an output restriction avoidance system. Data are collected on March 25, 2006, Saturday. In addition to the data showed in Figures 8, 9 and 10, feeding power to the grid and charged power to the battery are plotted in these figures. Negative power of the feeding power means forward power flow from the grid to the in-house load, negative power of the battery power means charging battery. Bottom side of Figure 12 shows state of charge. (SOC)

System #4 in Figure 11 resulted out put energy loss due to the high grid voltage in afternoon and lost energy was approximately 20% of the daily expected energy out. On the other hand, system #5 started charging battery around 10 a.m. so there is no fed power when the voltage is high in the afternoon. As a result, no electric power was lost due to the high grid voltage.

Another example of battery integrated system is shown in Figure 13. The system started charging battery when the PV array started generation of electricity. Then battery was fully charged around noon so there was no more room to store the electric power when the voltage became high in the afternoon. The capacity of the battery should be minimized from the installation cost point of view, however, less capacity requires more intelligent method for charging and discharging battery. Further study will be continued to optimize the control pattern of the battery.

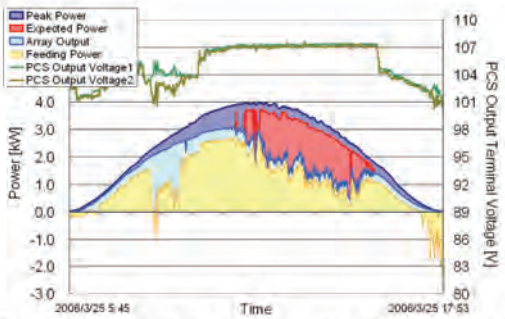

Figure 11: Example of output regulation due to the high grid voltage. System #4 with commercial PCS type A

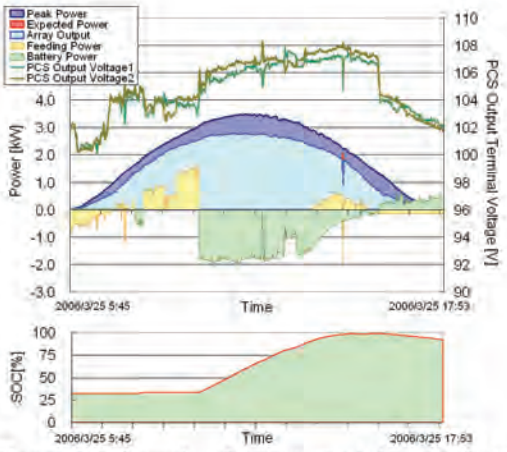

Figure 12: Example of output restriction avoidance. System #5 with unified PCS with battery

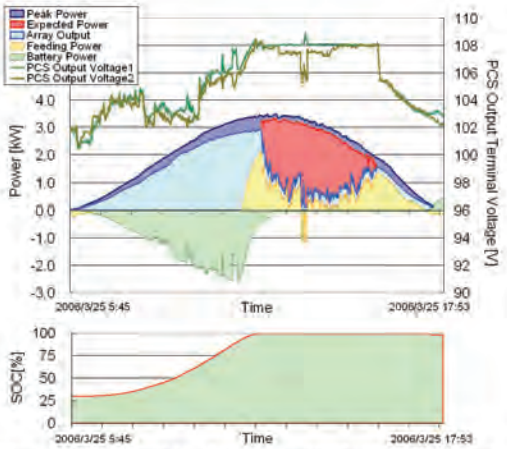

Figure 13: Example of the failure of output restriction avoidance. System #6 with unified PCS with battery

5 CONCLUSIONS

Output energy loss due to the high grid voltage is analyzed in this paper. Without the battery, PV system's output energy is restricted by the grid voltage. Since the reverse power flow from the PV system to the grid is one of the causes of high grid voltage, battery integration is one of the options to reduce the risk of over voltage and minimize the energy loss due to the high grid voltage for PV system's user side.

Although the frequency of the occurrence of active power regulation due to the high grid voltage is very low, some of the systems had significant amount of output energy loss in fewer load / more electricity generation condition such as weekend and sunny clear day. Different PCS have different starting voltage of the active power regulation so the amount of the lost energy is not the same among all the PCS. If the battery is appropriately operated, battery integrated PV system can avoid the output energy loss under the high grid voltage situation. However, battery integration results additional energy loss due to the charge controller and battery, saved energy should be larger than the additional loss in order to maximize the merit of PV system user. Amount of saved energy will be affected by the grid condition and battery operation. Further research will be continued in the "Demonstrative research on clustered PV systems."

ACKNOWLEDGEMENT

"Demonstrative research on clustered PV systems" is a project of New Energy and Industrial Technology Development Organization (NEDO). Authors would like to acknowledge the financial support of NEDO and cooperative discussions with project members.

REFERENCES :

[1] A F POVLSEN, "Impacts of Power Penetration from Photovoltaic Power Systems in Distribution Networks", Report IEA PVPS T5-10 (2002)

[2] Y.Ueda, T.Oozeki, K.Kurokawa, T.Itou, K.Kitamura, Y.Miyamoto, M.Yokota, H.Sugihara, S.Nishikawa, "ANALYTICAL RESULTS OF OUTPUT RESTRICTION DUE TO THE VOLTAGE INCREASING OF POWER DISTRIBUTION LINE IN GRID-CONNECTED CLUSTERED PV SYSTEMS", 31st IEEE Photovoltaic Specialists Conference (2005) pp1631

[3] S.Nishikawa, K.Kato, "DEMONSTRATIVE RESEARCH ON GRID-INTERCONNECTION OF CLUSTERED PHOTOVOLTAIC POWER GENERATION SYSTEMS", 3rd World Conference on Photovoltaic Energy Conversion (2003) 8LN-C-03

[4] T Yamada, H Nakamura, T Sugiura, K Sakuta, K Kurokawa, "Refection loss analysis by optical modeling of PV module" Solar Energy Materials & Solar Cells, Vol.67 pp.405-413 (2001)

[5] Y.Ueda, K.Kurokawa, T.Itou, K.Kitamura, Y.Miyamoto, M.Yokota, H.Sugihara, "PERFORMANCE RATIO AND YIELD ANALYSIS OF GRID CONNECTED CLUSTERED PV SYSTEMS IN JAPAN", 4th World Conference on Photovoltaic Energy Conversion (2006)

[6] Y.Ueda, T.Oozeki, K.Kurokawa, T.Itou, K.Kitamura, Y.Miyamoto, M.Yokota, H.Sugihara, "Quantitative Analysis Method of Output Loss due to Restriction for Grid-connected PV Systems", IEE Japan Vol.125-B, No.12, pp1317-1326 (2005-12)

[7] Y.Ueda, T.Oozeki, K.Kurokawa, T.Itou, K.Kitamura, Y.Miyamoto, M.Yokota, H.Sugihara, "Advanced analysis of shading effect using minutely based measured data for PV systems", 15th International Photovoltaic Science and Engineering Conference, TECHNICAL DIGEST pp.444-445 (2005)

[8] Kandenko Co., Ltd., FY2002 NEDO report "Demonstrative research on clustered PV systems" (2003) (in Japanese)

THE STATUS REPORT OF THE PV SYSTEM REAM INTER-CONNECTED GUIDELINE IN 5 COUNTRIES OF ASIA

Hironobu Igarashi[1] and Hiroyoshi Tasai[2] Kousuke Kurokawa[3]

[1] Japan Electrical Safety & Environment Technology Laboratories.5-14-12, Yoyogi, Shibuyaku, Tokyo 151-8545 Japan
[2] Japan Electrical Safety & Environment Technology Laboratories.5-14-12, Yoyogi, Shibuyaku, Tokyo 151-854
[3] Tokyo University of Agriculture and Technology. 2-24-16 Naka－cho , Koganei 184-8588 Japan

The investigation about the status of the PV standards such as industrial standards for equipment of PV system, certification of equipment, regulations (guideline) of grid connection in China, Korea, Taiwan, Thailand and Malaysia.

The Renewable Energy Law was effective from January 1st in 2006. Renewable Energy such as PV, Wind, Hydro attracts attention. There are expected spreader installations. There are making original standards for PV in china. They are introduction of Japanese Standards and Certification program in other to be export to Japanese market for their equipments. The stage of PV market is aggressive installation period in Korea and Taiwan. The person, who is expert in PV, makes a planning to install of PV by National Projects in Thailand and Malaysia.

Keywords: PV system, certification of PV system, PV standards, regulations, guideline, Asia

FOREWORD

General

The introduction of Asian major power's including Japan PV system is active now. As for Japan, the standard and the guideline are maintained for the operation of the PV system. It is thought that the thing to investigate the PV operation of another country is very advantageous information when Japan of the future approaches another country. The investigation about the status of the PV standards such as industrial standards for equipment of PV system, certification of equipment, regulations (guideline) of grid connection in China, Korea, Taiwan, Thailand and Malaysia.

The following turned out by the investigation that we had executed. The Renewable Energy Law was effective from January 1st in 2006. Renewable Energy such as PV, Wind, and Hydro attracts attention. There are expected spreader installations. There are making original standards for PV. Korea and Taiwan are introduction of Japanese Standards and Certification program in other to be export to Japanese market for their equipments. The stage of PV market is aggressive installation period. Korea, and Taiwan are introduction of Japanese Standards and Certification program in other to be export to Japanese market for their equipments. The stage of PV market is aggressive installation period.

This study is part of the Investigation concerning maintenance situation of standard etc. related to PV in cooperation base business China, South Korea, Taiwan, Thailand, and Malaysia like measures business of international energy use rationalization etc. international energy consumption efficiency improvement etc. etc.," project we conducted under contract to the New Energy and Industrial Technology Development Organization (NEDO).

MAINTENANCE SITUATION OF STANDARD IN EACH COUNTRY

National standardization conservancy Standardization Administration of China has jurisdiction, and standards in China are maintained as People's Republic of China national standard (GB). China has the standard of 39. China is quoting the IEC standard as a standard in the country. A lot of standards are the one of the characteristic of the solar sells. However, the equipment such as PV systems and the power conditioners is not standardized.

KS: Korean Industrial Standards that is the national standard of Korea is what a technological standard academy of the Korea industrial resource part enacts it. A technological standard academy of the Korea industrial resource part and a Korea standard society can retrieve standards of Korea from the managed site. Korea is quoting an IEC standard and Japanese JIS standard as a standard in the country. Korea was a country where standardization and the attestation system were maintained most in five countries that had been investigated this time.

CNS:Chinese National Standards that is the national standard of Taiwan is what Bureau of Standards, Metrology and Inspection (BSMI) enacts it. Taiwan has the standard of 10.

It investigated in Department of Alternative DEDE: Energy Development and Efficiency and NSTDA: National Science and Technology Development Agency. If the standard that relates to the solar battery in a Thai country conforms to the standard of IEC, it is a current state in the problem in a domestic procedure it not is. Moreover, it is expected for original standards to be made by groups of Wattanapong Ratkwichian professors of the Dr. Porponth Sichanugrist and Naresuan University of the science and technology ministry, and to be promulgated from TISI: Thailand Industrial Standard Institute though a detailed content is uncertain.

It conforms from the result of the survey in PTM: Pusat Tenaga Malaysia and UKM: University Kebangsaan Malaysia to the standard of IEC about the standard related to the solar bsells in a Thai similar country in Malaysia, and it is a current state in the problem in a domestic procedure it not is. The business that sets up the photovoltaic generation system in the roof top type for the house is begun as a national project of Malaysia according to the Malaysian energy center in fiscal year 2006. I hear that the standard by which a ream system requirement to the low-pressure supply of electric power system was recorded referring to the standard of IEC was enacted as MS1837 along with this.

ABOUT THE CERTIFICATION SYSTEM RELATED TO PV SYSTEM THAT EACH COUNTRY

In China and Thailand and Malaysia, there was no certification system concerning the photovoltaic generation system.

The authentication system of the power conditioner in Korea quotes the system that JET of Japan executes and has gone. Moreover, the attestation examination standard also similarly used the same one as Japan, and part had been changed to a demand regulated in Korea. Korea is executing the test of the power conditioner with Korea Institute of Energy Research: KIER and Korea Testing Laboratory: KTL. The investigation of the factory that manufactures the equipment is a system where the attestation of the equipment can be taken after Korea Energy Management Cooperation: KEMCO executes, and the examination result of the power conditioner and the examination result of the factory pass.

In Taiwan, there were neither solar modules nor an certification system concerning the PV inverter. The subsidy is delivered to those who set it up about the photovoltaic generation system as a government's position now. Therefore, a positive introduction of the Grid connects type photovoltaic generation system will be expected in the future. t is thought that the attestation system will be needed from such a background in the future.

ABOUT THE STANDARD CONCERNING THE PHOTOVOLTAIC GENERATION SYSTEM INSTALLATION

There were no standards of the photovoltaic generation system in China when constructing it the design. However, many books that relate to the design and the construction, etc. of the photovoltaic generation system are published in 2005. The case with the photovoltaic generation is introduced to these books besides the principle of the solar battery, the inverter, and the storage battery is technically recorded, and the view will be described in the future. Moreover, there is a description concerning the independent type photovoltaic generation system, and the capacity of the storage battery is selected and the number of sheets of the solar battery module is calculated about the design approach. Neither the design nor the economy of the Grid connect type photovoltaic generation system are discussed.

I hear that the application permission was necessary to confirm the bearing force in the building when standards made an express statement were not found when the photovoltaic generation system is designed, and constructed, and photovoltaic generation system was set up from the rooftop side in the rooftop in the building as a law in the country by the height of 1.5m or more.

There were no standards of the photovoltaic generation system when designing, and constructing it in Korea and Thailand.

There were no standards of the photovoltaic generation system when designing, and constructing it in Korea and Thailand and Malaysia.

CURRENT STATE OF GRID CONNECT GUIDELINE

China is recorded to enact the standard of a Grid connect guideline and a technological requirement, and to promulgate it in "People's Republic of China acceptable reproduction Nou source method" of the renewable energy method enforced about the guideline that lies a Grid connect in the power generation field by renewable energy on January 1, 2006, so-called Article 11,

Korea Electric Power Company: KEPCO issued "Decentralized power supply of electric power Grid connect technological standard" to the guideline related to the Grid connect system in Korea in 2005. It follows Korea Electric Power Corporation's standard though this is a technological standard concerning all of not only the photovoltaic generation but also the decentralized power supply of electric power Grid connects of the cogeneration and other renewable energy power generations, etc. and no national standard.

The technological standard related to the Grid connects system of Taiwan is "Cogeneration Grid connect technological points." intended for the general cogeneration power generation that the government enacted in 1989(the fourth revision in 1999). Moreover, "Taiwanese electric power company renewable energy power generation Grid connect technological points" was promulgated as a technological standard to the renewable energy power generation by Taiwanese Economic Department in 2002. The revision work to add a more concrete standard is proceeded, and "Photovoltaic generation Grid connect type inverter Grid connect technological standard" is expected to be enacted as a technological standard of the inverter now.

A technological requirement for ream system is provided and Thailand executed to the system of dynamo of the power generation output 1MW or less. MEA: Metropolitan Electricity Authority from May, 2002 and PEA: Provincial Electricity Authority.

A Malaysian government made the start in May, 2001 to SREP: Small Renewable Energy Power Programme: SREP public. It is being advanced by the government so that SREP may promote the use of renewable energy in the power generation field. The dynamo in this program should confer directly with the electric power company where Grid connects and the

contractor relate in the supply of electric power system.

SUMMARY

The photovoltaic generation industry might be immature, Korea was excluded, and the attestation system was not maintained.

However, the contribution of our country for the establishment of the solar sells market is possible in the future by increasing the chance to introduce the system of Japan to the object country and the region from the viewpoint etc. of the simplification of the ream system conference on the quality securing of the composition equipment and the electric power company because of the expectation of the spread of the photovoltaic sells, and sharing the finding in these regions.

Concretely, the symposium and the lecture meeting are held for an electrical engineering laboratory (China), Taiwanese Agency of Industrial Science and Technology (Taiwan), the science and technology ministry, the alternative energy development efficiency improvement bureau (Thailand), and the energy commission and the energy centers (Malaysia). It is thought that it is possible to contribute to the spread of the photovoltaic generation technology including the attestation system by sharing information.

There is a project for the roof top PV systems for house in Malaysia. The future can be expected that the introduction number of Grid connect photovoltaic generation systems increases. When the PV system is set up, inefficiency needing the attendance of the electric power company whenever setting it up, and the execution of the test of various of relay on the site. Therefore, it is thought that it maintains and it is introducing necessary of the inverter attestation system.

Thus, maintenance and smooth operation of inside and these attestation systems from which the Grid connect type photovoltaic generation system is expected to be introduced by centering on the national policy become keys to the introduction of the photovoltaic generation system of a private base and the spread..

References

[1] “Investigation concerning maintenance situation of standard etc. related to PV in cooperation base business China, South Korea, Taiwan, Thailand, and Malaysia like measures business of international energy use rationalization etc. international energy consumption efficiency improvement etc. etc. “, report by NEDO

RENEWABLE ENERGY 2006 Proceedings

ABOUT THE EXAMINATION OF AN ALTERNATIVE TECHNIQUE OF THE MOTOR LOAD ACCORDING TO THE RESONANCE LOAD

Hironobu Igarashi[1] and Takanori Sato[1] Kousuke Kurokawa[2]

[1] Japan Electrical Safety & Environment Technology Laboratories.5-14-12, Yoyogi, Shibuyaku, Tokyo 151-8545 Japan

[2] Tokyo University of Agriculture and Technology. 2-24-16 Naka－cho , Koganei 184-8588 Japan

The islanding phenomenon is generated by the load with the resurrection energy. The kind of the resurrection load has the resonance load and the motor load, etc. It turns out that the load that generates a lot of islanding phenomena is a motor load in those a lot of kinds of loads from our experiment result. To confirm we were loads where the characteristic of the motor load being able to generate the islanding phenomenon most in this experiments, the characteristic of the motor load was replaced with a linear load and it verified it to a linear load like the resonance load. Moreover, it was assumed that the inductivity load characteristic of the motor load was substituted and it matched and it examined it.

Keywords: Islanding, islanding phenomenon, motor load, resonance load

FOREWORD

General

Recently, the concern for global environmental concerns such as global warming has spread between general people.

Therefore, the photovoltaic generation system for the house is paid to attention as a clean energy source from which CO_2 is not exhausted to the power generation of the electric power. The Grid connect type is most popular photovoltaic generation system.

The Grid connect system is a system that can do the selling of electricity to a power company of the remainder of the electric power used at the power generation electric power and home to the general electric utility. It is necessary to set up the islanding detection device to the selling of electricity to a power company situation the general electric utility of the electric power in which electricity is generated in the photovoltaic generation system. Because it is necessary to detect the power failure due to the accident that occurs in the power line in the electric power company, to stop the power generation of the photovoltaic generation system, and to prevent the electric shock.

However, it is rugged and it might be difficult to detect the power failure of the electric power company the islanding detection device by the influence of the load with the resurrection energy.

Authors were confirmed the motor load was generated of the state of the islanding from the resonance load and verified whether to obtain the comparable result when the inductivity load of a linear load substituted[(1)] and the motor load this time.

STUDY OF RESONANCE LOAD AND MOTOR LOAD

Resonance load by IEC standard

The resonance load by the IEC standard is a resonance load in which an inductivity load, a capacitive load, and the resistance load are connected in parallel. The size of the inductivity load of the resonance load is requested by the expression (1). Moreover, a capacitive load equal with the inductivity load is prepared. To consume the active power that the power conditioner outputs, the same resistance load as the declared power is connected. Therefore, amount PqL of the inductivity load becomes 2.6kVar obtained from the expression (1).

$$P_{qL} = Q_f \times P_{EUT} \quad (1)$$

P_{qL} : inductive load [VARL]

P_{EUT} : Rated power of power conditioner

Q_f : 0.65

Comparative study of resonance load and motor load

The resonance load and the motor load have a regenerative energy. The islanding detection device generates the islanding phenomenon by the influence of the energy discharged from the resurrection load. Therefore, it is necessary to clarify the energy of the resonance load and the motor load. Moreover, it is necessary to measure the load it with the same amount of the resurrection energy to prove the influence of the regenerative energy given to the islanding detection device and to prove. Therefore, the energy discharge time was measured by the following methods by using the circuit chart shown in Fig. 1 and 2.

1. Parallel resistance load (R) is increased from 0 to 4000W at the time of each carving 100W, and it is assumed the following procedures of ② -④ and repeats.
2. Switch SW_{CB} is opened according to the timing of t=0.
3. Voltage V1 between lines measures time ΔX(Sec)

that decreases up to 20V.

4. The electric energy amount consumed by the parallel resistance load is requested.

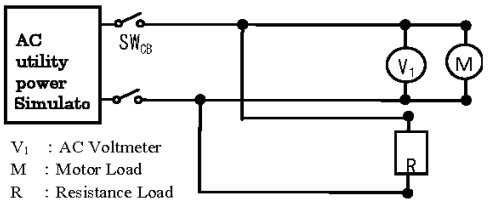

Fig. 1.Measurement circuit at energy discharge time motor load

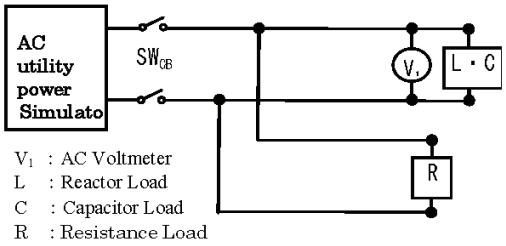

Fig. 2.Measurement circuit at energy discharge time resonance load

Result of measurement

The measurement result at the energy discharge time became a result as shown in Figure 3.

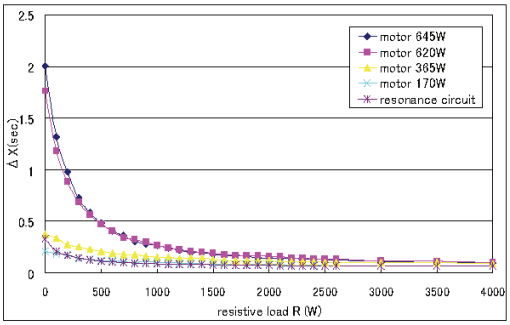

Fig. 3 Measurement result at energy consumption time.

It turned out the measurement result that the rotation machine load 170W was the same as the energy discharge time of the resonance load. However, it was assumed that the amount of energy was requested by the expression (2) from equal uncertain even if the energy discharge time was the same the amount of energy.

$$J = \mathrm{R} \times \int \mathrm{i}^2 \mathrm{dt} \qquad (2)$$

J : Amount of electric energy [J]

R : Resistance [Ω]

i : Current A that flows to resistance [A]

The energy discharge characteristic was shown that it became a result as shown in Figure 4 and the resonance load was equal to the motor load 170W, and result the same as the measurement result of the energy discharge time. Moreover, the difference of the energy discharge characteristic that was not able to be confirmed at the energy discharge time was able to be confirmed from the point where the parallel resistance load had exceeded 1000W. As for this phenomenon, the one that the current that flowed to parallel resistance increased is thought as a factor by the resonance of parallel resistance and each load.

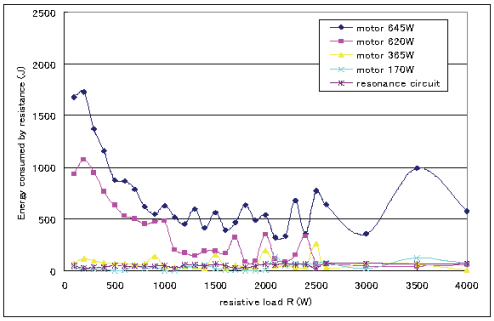

Fig. 4 Calculation result of amount of energy discharge.

Alternative examination of motor load by linear load

The motor load is thought to be the same characteristic as the inductivity load when driving under no load. Therefore, the current and the voltage of the characteristic of the motor load of 170W were measured and arithmetic was done from the measurement result to the amount of the inductivity load. As a result, it turned out that the motor load of 170W had the reactive power of 180Var. The load in which the inductivity load for 180Var was added to the resonance load and the motor load of 170W respectively was made. The islanding test used the load in which the inductivity load for 180Var was added to each load. Fig.5 shows the islanding test circuit.

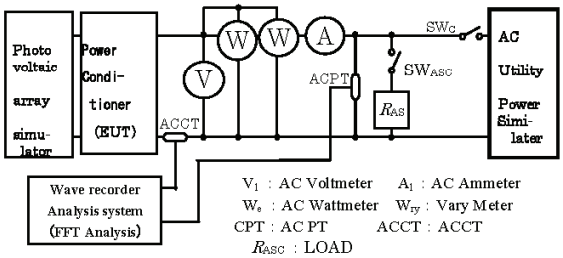

Fig.5 Islanding test circuit.

Result of islanding test

It was able to be confirmed to the experiment result the generation of the islanding phenomenon in this load balance condition of both loads. Table 1 is an islanding experiment result of adding the inductivity load of 180Var to the resonance load. The value is time until stopping detecting the islanding phenomenon. Moreover, when the detection value of the islanding phenomenon has stopped exceeding one second, it judges as an islanding and the numerical value is not filled in. Table 2 is an experiment result of adding the inductivity load of 180Var to the motor load.

Table 1. Islanding detection time of resonance load plus 180Var inductivity load.

Unit [mS]		Reactive power (Var)				
		-10%	-5%	0%	+5%	+10%
Active power (W)	-10%	663.3	Islanding	676.9	640.8	646.2
	-5%	627.9	Islanding	Islanding	639.8	616.8
	0%	633.7	Islanding	Islanding	667.0	619.1
	+5%	672.2	Islanding	Islanding	670.0	632.7
	+10%	690.1	798.1	Islanding	675.1	649.5

Table 2. Islanding detection time of motor load plus 180Var inductivity load.

Unit [mS]		Reactive power (Var)				
		-10%	-5%	0%	+5%	+10%
Active power (W)	-10%	618.0	Islanding	Islanding	Islanding	626.0
	-5%	665.0	702.0	686.0	691.0	647.0
	0%	628.0	Islanding	Islanding	719.0	626.0
	+5%	675.00	Islanding	Islanding	688.0	601.0
	+10%	649.0	Islanding	Islanding	649.0	623.0

However, we show the islanding experiment result of doing in the past only by the motor load in Table 3.

Table 3. Islanding detection time limit by motor load (170W)

Unit [mS]		Reactive power (Var)				
		-10%	-5%	0%	+5%	+10%
Active power (W)	-10%	655.0	Islanding	743.0	702.8	637.8
	-5%	644.6	684.8	Islanding	Islanding	Islanding
	0%	628.3	Islanding	Islanding	Islanding	650.8
	+5%	641.6	Islanding	Islanding	Islanding	621.6
	+10%	647.6	726.6	Islanding	Islanding	619.6

Only the motor load is generated when the experiment results of doing only by the motor load in experiment result and Table 3 where the resonance load in Table 2 was combined with the motor load are compared and more islanding phenomena are generated. islanding detection time of resonance load plus 180Var inductivity load. When the factor to generate the islanding phenomenon that is the characteristic of the motor load that the influence by the resonance loads originally has been erased, this test result is surmisable.

Summary

This result of reviews were compared by adding the amount of the inductivity load of equal to the motor load amount to the resonance load, and experimenting on the islanding prevention with resonance load 2.6kVar as an alternative load of the motor load.

As a result, even if the inductivity capacity of the motor load was able to be shown simply as a linear load of the inductivity load because a lot of islanding phenomena were generated in the case only of the rotation machine load, it turned out to differ from the factor to generate the islanding phenomenon though the thing that almost the same islanding phenomenon as both load condition is generated was confirmed.

References

[1] Hironobu Igarashi: "The tests of islanding have an influence on motor", Proc for 2005 National Convention Record IEE Japan, No.6-192, p.341~342 (2005)

Analysis Results of Maximum Power Point Mismatch on Grid-connected PV Systems

Yuzuru Ueda[1], Kosuke Kurokawa[1], Takamitsu Itou[2], Kiyoyuki Kitamura[2], Katsumi Akanuma[3], Masaharu Yokota[3] and Hiroyuki Sugihara[3]

[1]Tokyo University of Agriculture and Technology, 2-24-16 Naka-cho, Koganei, Tokyo, 184-8588, Japan
[2]MEIDENSHA CORPORATION, Riverside Building, 36-2 Nihonbashi Hakozakicho, Chuo-Ku, Tokyo, 103-8515, Japan
[3]Kandenko Co., Ltd., 4-8-33 Shibaura Minato-ku, Tokyo, 108-8533, Japan

This paper describes the method to estimate maximum power point of the PV systems under the measured irradiance and module temperature, reviews the error factors of the MPP estimation and summarizes the analysis results of the MPP mismatch analysis for grid-connected PV systems. Spectral mismatch is not always the loss factor but gain factor in cloudy condition. Regular loss including MPP tracking error is a major factor of MPP mismatch.

Keywords: PV systems, Maximum power point, loss, spectral mismatch

INTRODUCTION

Performance analysis of the PV systems normally uses irradiance data as an input energy and module temperature is used to estimate the ideal output energy and maximum power point (MPP) of the PV systems under the measured irradiance and module temperature. There are several factors which may affect the accuracy of the MPP estimation, some of them have non-linear characteristics for the irradiance and temperature. This research concentrates to analyze the loss of DC output energy using array output current and voltage. Simple MPP estimation methods are introduced and analysis results of MPP mismatch are summarized in this paper.

PV SYSTEMS AND MEASUREMENT

Data from "Demonstrative research on clustered PV systems" are used in this paper. "Demonstrative research on clustered PV systems" is a project of New Energy and Industrial Technology Development Organization and being conducted from December, 2002 to investigate about the potential issues of grid-connected PV systems.

One-minute averages of secondly measured data are used for the analysis. PV array's output current and output voltage are measured at the input terminal of the power conditioning subsystems (PCS). Global irradiance and direct irradiance are measured at the meteorological stations. Incoming irradiation at the PV array's plane is calculated using direct model for direct components, Perez model [1] for diffused components and uniform reflection model for reflected components. Module temperature is measured at the selected systems using thermocouple sensor.

More than 100 PV systems are initially evaluated and 80 PV systems which do not have shading loss are selected for this analysis. Orientations of the PV arrays are south, east or west. Some of the systems have single array but others have multiple arrays oriented different direction. Data from March 2005 to February 2006 are used in this study.

METHODS

Input data of the analysis are Irradiance [kW/m^2] on the PV array's plane, PV module temperature [degrees Celsius], PV array's output voltage [V] and output current [A]. Ratios of measured value to estimated MPP value for current, voltage and power are used for the MPP mismatch analysis.

Estimating maximum power points

Short circuit current (I_{SC}) and open circuit voltage (V_{OC}) under the measured irradiance at measured module temperature can be calculated using following equations.

$$I_{SC} = \frac{G}{G_0} I_{SC(0)} \left[1 + \alpha (T - T_0)\right] \quad (1)$$

$$V_{OC} = V_{OC(0)} \left[1 + \beta (T - T_0)\right] \quad (2)$$

Where
G : Irradiance [kW/m^2]
G_0 : Irradiance in STC (= 1[kW/m^2], AM 1.5G)
$I_{SC(0)}$: Short circuit current in STC [A]
α : Temperature coefficient of I_{SC} [degC^{-1}]
T : Module temperature [degC]
T_0 : Module temperature in STC (= 25[degC])
$V_{OC(0)}$: Open circuit voltage in STC [V]
β : Temperature coefficient of V_{OC} [degC^{-1}]

Ideal maximum power point current (I_{Pmax}) and

maximum power point voltage (V_{Pmax}) are calculated from the following equations using the results of equations (1) and (2).

$$I_{P\max} = I_{SC}\frac{I_{P\max(0)}}{I_{SC(0)}} \quad (3)$$

$$V_{P\max} = V_{OC}\frac{V_{P\max(0)}}{V_{OC(0)}} \quad (4)$$

Where
$I_{Pmax(0)}$: Maximum power point current in STC [A]
$V_{Pmax(0)}$: Maximum power point voltage in STC [V]

Error factors

Spectral mismatch is one of the known error factor for the I_{SC} estimation. Equation (1) dose not have a term to correct spectral mismatch because spectral data are not available in the data set. Thus spectral mismatch between G_0 and G might be an error factor for the I_{SC} estimation.

V_{OC} estimation also has a known error factor. Actual V_{OC} will become lower along with the G decreasing compared with the estimated V_{OC} from equation (2). [2] However, this behavior is not considered in equation (2) due to the lack of the data of characteristics for installed PV modules.

Change of the fill factor (FF) [2] [3] is another error factor in equations (3) and (4).

Incident angle correction

Incoming irradiance is measured by pyranometer and incident angle dependence of the pyranometer is less than 3[%]. However, PV module's surface is normally flat so there will be reflection loss due to the large incident angle. Simplified calculation method [4] of reflection loss is used to correct this effect. Effective refractive index of 1.8 is used for the correction. Figure 1 shows relative transmittance of the PV module (τ_{PV}) as a function of incident angle. Assuming the reflection loss will reduce the input irradiance G, ratio of measured output current (I) to I_{Pmax} is calculated using equation (5).

Fig. 1. Relative transmittance of the PV module as a function of incident angle.

$$R_I = \frac{I}{I_{P\max}\cdot\tau_{PV}} \quad (5)$$

Where
R_I : Ratio of I to estimated I_{Pmax}

DC voltage correction

During the DC power transmission from the PV array to the measurement point at the PCS input terminal, voltage becomes lower due to the resistance of the cable and blocking diode. This voltage drop (Δ_V) is calculated using following equation.

$$\Delta_V = 0.6 + 0.2\cdot I \quad (6)$$

0.6[V] represents the voltage drop at the blocking diode and 0.2[ohm] is the resistance of the cable that is calculated using 20[m] of CV cable (2[mm^2]), the most frequently used cable within the evaluated systems. Using the calculated Δ_V, ratio of measured output voltage (V) to V_{Pmax} is described as follow.

$$R_V = \frac{V}{V_{P\max} - \Delta_V} \quad (7)$$

Where
R_V : Ratio of V to estimated V_{Pmax}

Power calculation

The ratio of measured power (P) to estimated maximum power (P_{max}) is calculated using following equation.

$$R_P = \frac{I\cdot V}{(I_{P\max}\cdot\tau_{PV})(V_{P\max} - \Delta_V)} = R_I\cdot R_V \quad (8)$$

Where
R_P : Ratio of P to estimated P_{max}

Data filtering

To minimize the intentional MPP mismatch by PCS, data under the high grid voltage condition and PCS capacity shortage condition are excluded from the data set. The threshold voltage of high grid voltage is 107[V].

RESULTS AND DISCUSSIONS

Ratios of measured value to estimated MPP value for current, voltage and power are calculated for each one-minute data and its frequency are summarized for each irradiance level in an increment of 0.01[kW/m^2] . Results are shown in contour graphs of Figures 2, 3 and 4. Average ratios and standard deviations for each irradiance level are also shown in these figures.

As a result, both current and voltage showed lower R_I and R_V when the irradiance level is very low. Standard deviations at low irradiance level are larger in both current and voltage, one of the reasons is a small value of a denominator for the ratios calculation. R_I once have a peak around the irradiance level of 0.2 to 0.4 [kW/m^2]

then gradually go down but R_V have a peak at very high irradiance level. Higher voltage and lower current at the high irradiance level indicate that operation point is not on MPP but slightly shift toward V_{OC}.

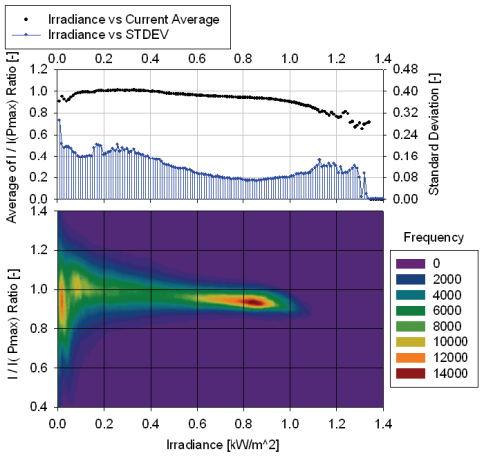

Fig. 2. R_I analysis results.

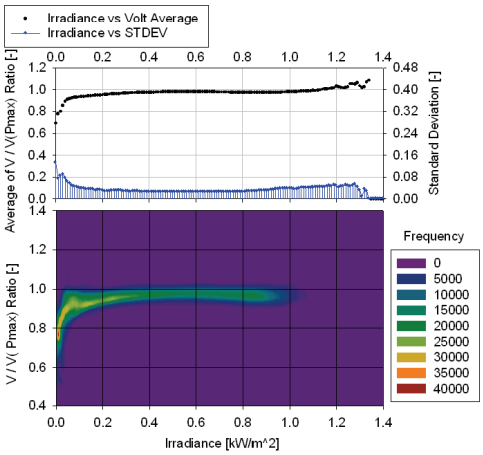

Fig. 3. R_V analysis results.

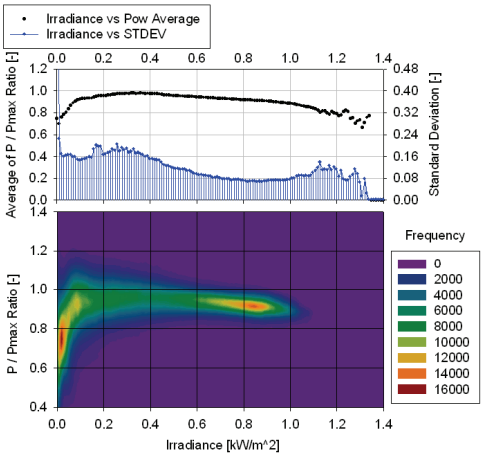

Fig. 4. R_P analysis results.

To analyze more detail about the results, all the data are classified into five conditions. The first condition is the irradiance level of less than 0.15[kW/m^2]. This category has lowest ratios and largest standard deviations. As it is mentioned before, voltage drop and change of FF are more severe in low irradiance level, thus this category can be assumed that estimated MPP values may have a lot of error. Generated power in this class is 6.2[%] of the total of generated power, loss in this class is 10[%] of the total loss. Generated energy and loss for each irradiance level and those cumulative percentages are summarized in figure 5.

The second condition is also the irradiance but more than 1.05[kW/m^2]. Data under this condition generate only 1[%] of the total so this category may have scatter. Loss in this class is 2.4[%] of the total loss.

After excluding these two conditions, rest of the data are classified to three weather conditions, i.e. clear, cloudy and other. The definition of the clear is the data which clearness index is more than 0.7, that of cloudy is the data which ratio of diffused light is more than 0.95. Classified results are summarized in table 1.

Table. 1. Analysis results for five conditions.

	Generated energy [kWh]	Loss [kWh]	Loss Ratio [%]	Average R_ρ	Standard deviation
≤0.15[kW/m^2]	19350.1	2365.1	0.70	0.802	0.280
≥1.05[kW/m^2]	3147.8	569.4	0.17	0.848	0.093
Irradiance: 0.15[kW/m^2] < G < 1.05[kW/m^2]					
Clear	111511.0	11034.8	3.27	0.912	0.063
Cloudy	29019.1	−46.8	−0.01	0.998	0.195
Other	151189.8	9722.0	2.88	0.941	0.123
All	314217.7	23644.5	7.00	0.905	0.179
Air Mass: 1.3–1.7, Irradiance: 0.15[kW/m^2] < G < 1.05[kW/m^2]					
Clear	22169.2	1929.9	0.57	0.922	0.034

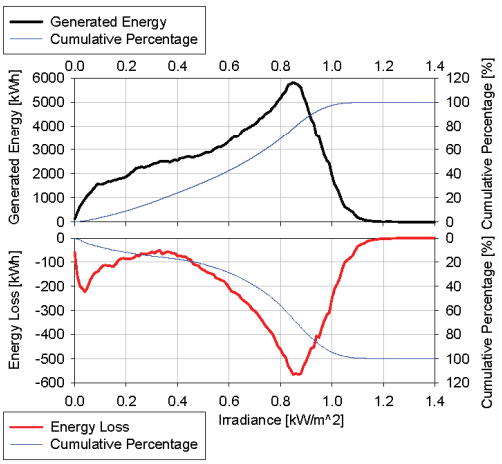

Fig. 5. Generated energy, loss and those cumulative percentages for each irradiance level.

As a result, clear and other condition have 46.7[%] and 41.1[%] of the total loss respectively but cloudy condition has 0.2[%] of gain. This gain can be explained as a spectral mismatch which is also mentioned before. Figures 6, 7 and 8 show the ratios R_I, R_V and R_P for each weather conditions. In addition to the above three weather conditions, air-mass of between 1.3 and 1.7 in clear condition are also plotted in these figures. As

shown in figure 6 and 8, only the cloudy condition results more than 1 of R_I and R_P because of the "matching" of the spectrum. Figure 9 describes the examples of the relative spectral response of c-Si solar cell and normalized spectral irradiances of AM 1.5G, clear and cloudy conditions. Cloudy condition have relatively blue rich spectrum and this will match with the spectral response of c-Si PV modules. [5] Thus actual output current is larger than the estimated I_{Pmax} in cloudy condition. On the other hand, clear condition sometimes have red rich spectrum compared with the AM 1.5G spectrum and this will reduce the output current of the c-Si PV module. This spectral mismatch can be seen in figure 6. R_I of all clear condition are lower than the results of AM 1.3 to 1.7 condition specially at the higher irradiance level.

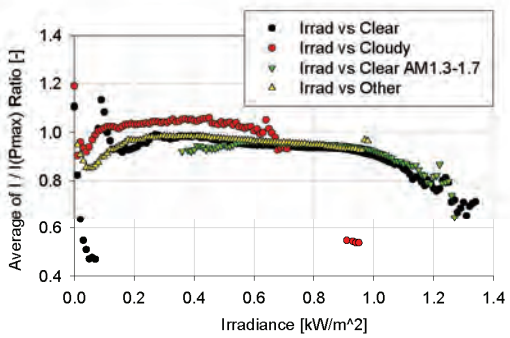

Fig. 6. Average R_I results for four weather conditions.

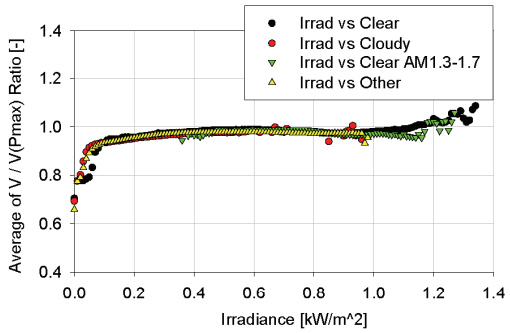

Fig. 7. Average R_V results for four weather conditions.

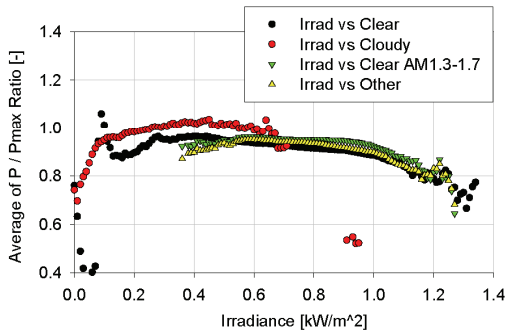

Fig. 8. Average R_P results for four weather conditions.

Another factor of MPP mismatch is the system configuration itself. Since these are not the results of PV modules but systems, array configurations and variations of the PV modules can cause mismatch of system peak power. Soiling and degradation are also the causes. To estimate this kind of regular loss, AM 1.3 to 1.7 clear condition is used because of its minimal standard deviation and better spectrum matching with the AM 1.5G. Considering the variation of the measurement error, average plus standard deviation is assumed as a regular loss. As a result, 62.9[%] of the loss are assumed as a regular loss including regular MPP tracking error, that is 4.4[%] of the expected energy out. Rest of them is assumed as spectral mismatch loss and gain, MPP tracking error and other non-identified loss factors, that is 1.7[%] of the expected energy out.

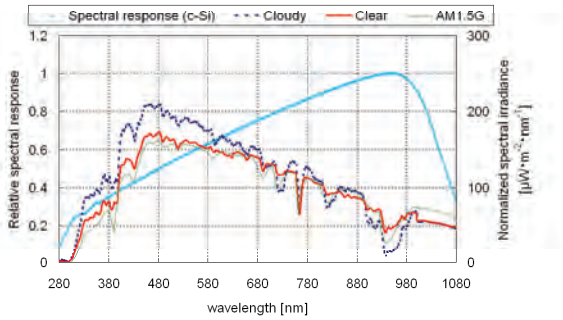

Fig. 9. Relative spectral response of c-Si and normalized spectral irradiance as a function of wavelength.

SUMMARY

Detailed analyses of MPP mismatch are performed in this paper. Results indicate the non-linearity of V_{Pmax} and FF are not the major error factor for MPP analysis because of the low irradiance level. Spectral mismatch is not always the loss factor but gain factor in cloudy condition. Regular loss including MPP tracking error was a major factor of MPP mismatch in this analysis.

"Demonstrative research on clustered PV systems" is a project of New Energy and Industrial Technology Development Organization (NEDO). Authors would like to acknowledge the financial support of NEDO and cooperative discussions with project members.

References

[1] R.Perez, R.Seals, P.Ineichen, R.Stewart, D.Menicucci, "A NEW SIMPLIFIED VERSION OF THE PEREZ DIFFUSE IRRADIANCE MODEL FOR TILTED SURFACES", *Solar Energy* Vol.39(3) pp.221-231 (1987)

[2] B. Marion, "A Method for Modeling the Current-Voltage Curve of a PV Module for Outdoor Conditions", *Prog. Photovolt: Res. Appl.* 2002; 10:pp. 205-214.

[3] D. Anderson, G. Agostinelli, T. Sample and E. Dunlop, "Modeling Outdoor *Behavior of Fill Factor in Thin Modules", 17th EU PVSEC, Munich, Germany,* 2001.

[4] Y Ueda, T Oozeki and K Kurokawa "Outdoor measurement and analysis of incident angle effect of PV module" *Proceedings of JSES/JWEA Joint Conference* pp51-54 (2005)

[5] K. Hirata, Y. Miyake, K. Nakamura, T. Kato and K. Kurokawa, "Spectral Error Analyses of Pyranometers Composed of Multiple Photodiodes", *RE2006 Proceedings*, 2006

SUITABLE VERY LARGE-SCALE PV (VLS-PV) SYSTEMS FOR DESERT REGIONS FROM FOUR TYPE CASE STUDIES BY USING LCA METHOD

Masakazu Ito[1], Kazuhiko Kato[2], Keiichi Komoto[3], Tetsuo Kichimi[4], Kosuke Kurokawa[5]

[1] Integrated Research Institute, Tokyo Institute of Technology, Tokyo 152-8550 Japan
[2] National Institute of Advanced Industrial Science and Technology (AIST), Tsukuba, 305-8568 Japan
[3] Mizuho Information & Research Institute (MHIR), Tokyo 101-0054 Japan
[4] Resources Total System (RTS), Tokyo, 104-0033 Japan
[5] Tokyo University of Agriculture and Technology (TUAT), Tokyo, 184-8588 Japan

To save the earth from environmental issue such as grovel warming and energy problem, the authors proposed combination of environmental friendly PV system and huge and shiny desert area, and evaluated the possibility of the systems by using LCA method. As a result, 1) It has potential to solve energy issue, 2) Slow down the speed of global worming, 3) Hope low price and high efficiency PV module, 4) Lower array structure reduces steel and foundation, 5) Highest module efficiency make the most suitable system, 6) In case of same transmission length, high irradiation area such as Sahara desert is suitable, 7) Interest rate and wage effect generation cost.

Keywords: VLS-PV, desert, LCA, energy payback time, CO_2 emissions rate

INTRODUCTION

Some organizations propose 'Sustainable development' with large photovoltaic system utilizations. Especially, German advisory council on global change (WBGU) [1] estimated that solar electricity is more than two-third of world energy demand in 2100 in a sustainable development scenario. The authors propose utilization of very large-scale photovoltaic power generation (VLS-PV) systems (Fig. 1.) in desert area toward PV days when large amount of PV energy is utilized as main energy in the world.

Background

The authors focus on combination of desert and PV systems. The reasons are; 1) Desert is not only sand desert but also gravel desert, soil desert, stone desert and salt desert. Especially, gravel desert has hard and flat land area which is suitable for PV system. 2) Desert has strong irradiation. 3) Desert has big potential. For example, if PV systems are installed in Gobi desert with 50 percent space factor, it can generate world energy demand in 2000. 4) If we put an electricity grid map and a desert map on a same map, we can see transmission lines reach desert areas. It means it is not difficult to connect large PV in desert to big demand such as city. 5) PV is clean and maintenance free. From these reasons, the authors have started to find a way to resolve energy problem and environmental problem by large-scale PV utilization with support of IEA/PVPS Task 8 members.

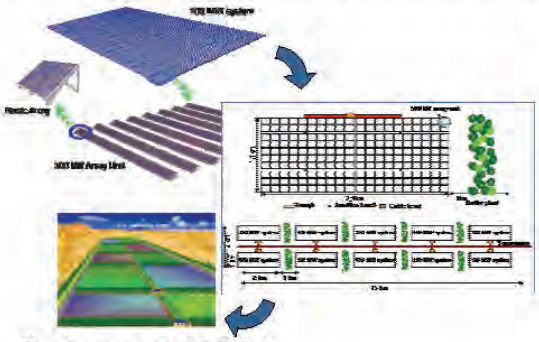

Fig. 1. Image of a VLS-PV

OBJECTIVE

This study is about possibility of combination of 'desert' which have strong irradiation and huge land area and very large scale photovoltaic power generation systems (VLS-PV). To find suitable system for desert area, four kinds of case studies were evaluated and compared.

APPROACH

A methodology of "Life-Cycle Assessment (LCA)" is a appropriate measure to evaluate the potential of VLS-PV systems in detail, because a purpose of this methodology is to evaluate its input and output from cradle to grave. In this study, generation cost, energy payback time (EPT), CO_2 emission rate of the VLS-PV system were calculated by the method. EPT means years to recover primary energy consumption throughout its life-cycle by its own energy production. CO_2 emission rate is a useful index to know how much the PV system is effective for the global warming.

Based on concept of LCA, VLS-PV system followed these steps. Estimation items are listed in Fig. 2.

1) Plan basic assumptions such as capacity, component, transport etc.
2) Calculate irradiations for static and tracking systems
3) Design module layout, array structures, foundations, transmissions and wires
4) Calculate all materials' price, maintenance, tax, wages etc., and generation costs, energy payback time and CO_2 emissions rate.

These approaches are applied for four kinds of case studies to compare the systems. Case studies are listing below.

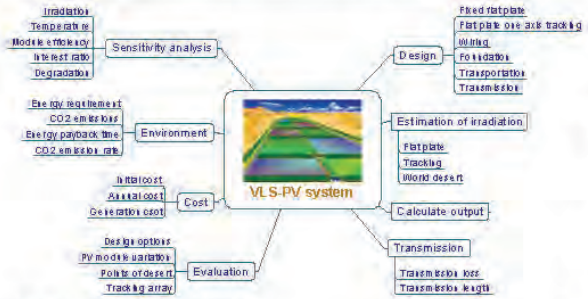

Fig. 2. Estimation items

- Case study A: Compare array structures
  Assume same system configuration and environment, evaluate three types array structures.
- Case study B: Compare module types (m-Si, a-Si, CdTe, CIS)
  Same system configuration and environment. Just change module types.
- Case study C: Compare desert regions (8 region in 6 world desert)
  Assume same system configuration, and compare environmental condition.
- Case study D: Compare fixed and tracking arrays
  Assume same environment and module, compare flat plate one axis tracking and fixed system.

INDICES

Generation cost

Generation cost concerned all components, maintenance cost and transmission losses. Annual expense of the VLS-PV [US cent/year] divided by Annual power generation [kWh/year] equal Generation cost [US cent/kWh]

Energy payback time (EPT)

EPT means years to recover primary energy consumption throughout its life-cycle by its own energy production. Total primary energy requirement of the VLS-PV throughout its life-cycle [GJ] divided by Annual primary energy reduction by using VLS-PV [GJ/year] equal EPT [year]

CO_2 emission rate

CO_2 emission rate shows amount of CO_2 produced by one kWh electricity. Total CO_2 emissions throughout its life-cycle per life-time [g-C/year] divided by Annual power generation [kWh/year].

ASSUMPTIONS

General assumptions

Economic data are shown in Table 2. The VLS-PV systems were assumed 3 %/year interest rate, 30 years life time and 1.6 %/year salvage value rate.

Table 2 Economic data used in this study

Item	Unit	Value
Salvage value rate	-	0.1
Interest rate	/year	0.03
Property tax rate	/year	0.016
Overhead expense rate	/year	0.05
Depreciation years	years	30
System lifetime	years	30

Both irradiation and ambient temperature data were referred to the World Irradiation Data Book [2]. In-plain irradiation data was calculated by using the r_b [3], Hey [4], and isotropic models [3]. Results of irradiation estimates are shown in Table 1.

An image of the VLS-PV system installed in a desert area is shown in Fig. 1. It shows an image of a basic array and a 500 kW array unit, which is about 100 m in length and width in the m-Si case. A 100 MW system consists of 200 sets of 500 kW array units.

200 sets of inverters, 208 sets of 6.6 kV circuit breakers, 5 sets of 30 MVA transformers, 18 sets of 110 kV GIS, 10 sets of 110 kV disconnecting SW, 2 sets of SVC (Static Var Compensator), and a common power board are installed in a 100 MW unit. Table 2 is information about the balance of systems (BOS) for a 100 MW system.

PV module

Four types of PV module were selected in this study. m-Si module-1 (Case study B) is 152 W, 15.8 % module efficiency and -0.49 %/°C coefficient of power. m-Si module-2 (Case study A, C, D) is 120 W, 12.8 % and -0.5 %/ °C. a-Si is 58 W, 6.9 % and -0.22 %/ °C. CdTe is 65 W, 9.0 % and -0.25 %/°C. CIS is 80 W, 11.0 % and -0.36 %/°C. PV module prices are given 4 USD/W to 1 USD/W.

Table 1. Geographic information for world deserts

Region	Sahara	Sahara	Negev	Thar	Sonoran	Great Sandy	Gobi	Gobi
Location	Nema 16°N 7°W	Ouarza-zate 31°N 6°W	Bet dagan 32°N 34°E	Jodhpur 26°N 73°E	Chihuahuan 28°N 106°W	Port headland 20°S 118°E	Hoh hot 40°N 111°E	Dalan-zadgad 43°N 104°E
Ambient temperature	30.2 [°C]	19.2	18.9	26.9	18.4	26.1	5.8	3.5
Global	2688	2042	1943	2173	1998	2345	1702	1570
Tilt angle=10°	2750	2159	2042	2301	2100	2418	1848	1736
Tilt angle=20°	2769	2235	2104	2381	2170	2451	1958	1865
Tilt angle=30°	2721	2254	2115	2407	2184	2422	2020	1949
Tilt angle=40°	2604	2221	2075	2374	2148	2334	2031	1985
Tracking (One axis flat plate)	3707	2882	2751	3007	2743	3324	2408	2350 [kWh·m^{-2}·yr^{-1}]

Array design

Fig. 3. shows the basic structures of array supports for a 30 degree tilt angle. It is assumed that array support is made of zinc-plated stainless steel (SS 400), and thickness of several types of steel material are chosen according to stress analysis assuming that the wind velocity is 42 m/s (based upon the design standard of structure steel by the Japanese Society of Architecture). Cubicle foundations made of concrete are applied. The rectangular solids are about 1.0 m each, considering the design standard of support structure for power transmission by the Institute of Electrical Engineering in Japan. Material composition of the concrete is determined in order to obtain 240 kg/cm^2 of concrete strength.

Fig. 4. shows image of tracking array system. The simplest one axis sun tracking PV systems consists of PV module mounted on horizontal axis that rotate from east to west in synchronization with the sun's position in the sky.

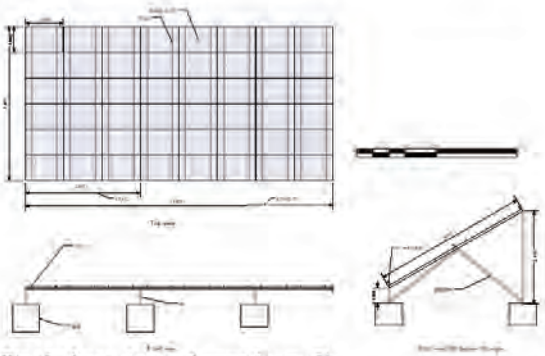

Fig. 3. Array design image for m-Si

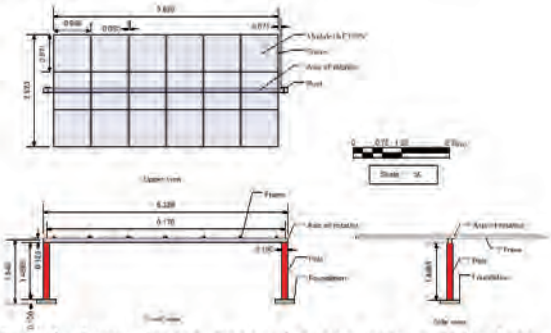

Fig. 4. Array design image for one axis sun tracking system

Wiring

The short and simple wiring is designed in order to prevent miswiring. The cable is considered current capacity to make the voltage drop less than 4%. It is determined from Japan Industrial Standards-JIS.

Transmission

The electric transmission system is assumed to be 100 km, 2 channels, and 110 kV for connecting to existing transmission. It consists of steel towers, foundations, cables, and ground wires. They consider a wind velocity 42 m/s. After calculations, transmission lines and ground wires are decided at TACSR 410 sq and AC 70 sq. An expert of utility company designed the transmission towers. 22.0 ton steel tower and 22.1 m^3 foundation are required for each 334 towers for 100 km transmission. Transmission loss is also considered. Details of transmission loss have been discussed in previous paper [5].

RESULT OF CASE STUDIES

Case study A

Three types of arrays which are high, moderate and low array structure were designed, and assumed to be installed in the Gobi desert in China. At the optimum tilt angle of generation cost (30 degree), generation cost of high array structure was 15.5 UScent/kWh (3 USD/W module price), EPT was 2.3 yeas and CO_2 emission rate was 15.1 g-C/kWh. Moderate was 15.5 UScent/kWh, 2.2 year and 15.0 g-C/kWh. Low array structure was 15.4 UScent/kWh, 2.2 year and 14.2 g-C/kWh. Therefore, in case of same tilt angle, lower array structure was suitable for VLS-PV system.

Case study B

Table 3 shows the results of generation cost of the 100 MW VLS-PV systems with 100 km transmission line in the Gobi desert in China. These results were obtained by dividing annual cost by power generation.

Table 3. Generation cost at 30 degree tilt angle [UScent/kWh]

	m-Si	a-Si	CdTe	CIS
Module price = 1 USD/W	7.0	8.2	7.9	7.6
Module price = 2 USD/W	11.1	12.3	12.1	11.7
Module price = 3 USD/W	15.2	16.4	16.2	15.8
Module price = 4 USD/W	19.3	20.6	20.4	19.9

Fig. 5. shows the required energy and energy payback time of each system. For the comparison, energy requirements were normalized at 100 MW. With multi crystalline silicon solar modules, the EPT was 1.8 years, 3.0 years of EPT were obtained for amorphous silicon solar modules, 2.4 year of EPT for CdTe PV modules, and 2.0 year of EPT for CIS PV modules.

Four kinds of PV modules were assumed for 100 MW VLS-PV systems, and their CO_2 emissions were estimated as shown in Fig. 6. It was 11.7 g-C/kWh for multi crystalline silicon, 20.2 for amorphous silicon, 17.5 for CdTe, and 14.0 for CIS module technology. The majority of all systems is the array support. High module efficiency can reduce CO_2 emissions rates because it can reduce array support structures and foundations that require much energy to produce.

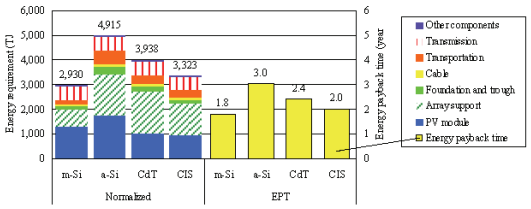

Fig. 5. Energy requirement and EPT

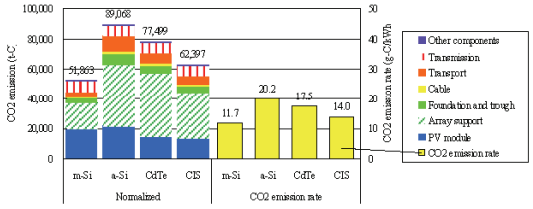

Fig. 6. CO_2 emission and CO_2 emission rate

Case study C

Case study C was studied for economic analysis. Fig. 7. that is a summary of generation cost of VLS-PV in the deserts suggests that the VLS-PV system is economically feasible for all the regions. Irradiation in Sahara is higher than Gobi, but generation cost is similar. Generation cost of Negev and Great sandy is higher than others. Because these country's wage is high.

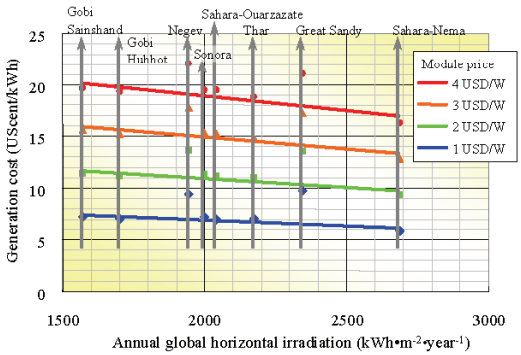

Fig. 7. Generation cost of VLS-PV in world desert

Case study D

Table 4 is a result of comparison between fixed flat plate system and one axis sun tracking system. Tracking system can reduce 10 to 15 % of generation cost, even though generation cost of tracking system include high maintenance cost which was referred to PV USA project [6]. EPT and CO_2 emission rate of tracking system is also smaller than fixed system. But difference is not big.

Table 4 Generation cost of fixed and tracking system

PV module	m-Si (Fixed)	m-Si (Tracking)
Module price		
1 USD/W	6.8	6.3
2 USD/W	11.3	9.8
3 USD/W	15.4	13.2
4 USD/W	19.5	16.7
EPT [year]	2.2	2.1
CO2 emissions rate [g-C/kWh]	14.8	13.3

CONCLUSIONS

The authors proposed combination of environmental friendly PV system and huge and shiny desert area to save the earth from environmental issues. And to know suitable system configuration, over twenty case studies were evaluated by using Life-cycle analysis.

From comparative studies. Most suitable system is;

- Lower array structure
  Lower array structure reduce steel and foundation. It is lower cost and lower environmental pollution in case of low land cost.
- Higher efficiency module
  Efficiency is dominant factor of cost, energy and CO_2 estimation.
- Install in higher irradiation area
  In case of same transmission length, high irradiation area such as Sahara desert is suitable
- A tracking system has a potential
  Tracking system generate much electricity than constructing the system.

From all case studies;

- It has potential to resolve environmental problem
  Energy requirement to produce the system is equal to power production in two to three years.
- Slow down the speed of global worming
  CO_2 emissions rate was estimated 10-20 g-C/kWh. It is much smaller than Oil fired plant (200 g-C/kWh)
- Hope low price and high efficiency PV module
  m-Si is the most suitable in this study. However, generation cost is still high (20 UScent/kWh) in case of present module price of 4 USD/W.

ACKNOWLEDGMENT

This work was supported in part under Grant-in-Aid for JSPS Fellows. The authors also would like to thank IEA/PVPS Task VIII members for discussing results.

REFERENCES

[1] World in Transition: Turning Energy Systems Towards Sustainability, WBGU, Mar 2003
[2] Japan Weather Association. *World Irradiation Data Book*. FY1991 NEDO Contract Report. (In Japanese)
[3] Japan Solar Energy Society. *Japan Solar Energy Utilization Handbook*. 2000, 26 pp.
[4] J. E. Hay. *A Study of Shortwave Radiation on Non – horizontal Surfaces*. Report No.79-12. Atmospheric Environment Service, Downsview, Ontario. 1979. 140 pp.
[5] M. Ito, K. Kato, K. Komoto, T. Kichimi, K. Kurokawa, et al. Analysis of transmission losses of Very Large-Scale Photovoltaic power generation systems (VLS-PV) in world desert. *Proceedings of 31st IEEE PVSC* 2005. 1706-1709 pp
[6] C.Jennings, A.B.Reyes & K.P.O'. Brien PVUSA utility-scale system capital and maintenance costs, *Proceedings of WCPEC-1*, Dec, 5-9, 1994, Hawaii.

A STUDY ON THE EVALUATION OF SOLAR HOME SYSTEM VIEWED BY USERS -A CASE OF NOMADIC FAMILIES IN MONGOLIA-

Amarbayar Adiyabat[1], Masahiro Nakajima[2], Kenji Otani[3], Enebish Namjil[4] and Kosuke Kurokawa[1]

[1] Faculty of Engineering, Tokyo University of Agriculture and Technology, Nakamachi 2-24-16, Koganei-shi, Tokyo, 184-8588 Japan

[2] Faculty of Agriculture, Tokyo University of Agriculture and Technology, Saiwai-cho 3-5-8, Fuchu, Tokyo, 183-8509 Japan

[3] National Institute of Advanced Industrial Science and Technology, Tsukuba, 305-8500 Japan

[4] National Renewable Energy Center of Mongolia, Ulaanbaatar, Mongolia

Here, we present the results of a questionnaire survey regarding Solar Home Systems (SHS) in nomadic families in Mongolia. The present study was performed to clarify user behavior, user satisfaction, problems, needs, and awareness of SHS by non-users. The survey was carried out in 67 nomadic families by the face-to-face questionnaire method, and 359 responses were received from nomadic families by the mail questionnaire survey method. From the results, most users indicated that they were satisfied with their SHS. They appreciated improvement in lighting and the ability to watch TV. It is shown that SHS is appropriate power system for nomadic lifestyle to compare with other type generation systems from the view point of users. The main problem for SHS users was a lack of after-sale service.

Keywords: Solar Home System, Electrification, Questionnaire Survey, Nomadic family

INTRODUCTION

By administration the Mongolia is divided in 21 aimags, which include 314 soums and the soums are divided in 1564 bags. About 43% of the total soums (about 135 soums) are not connected with the electricity transmission lines (off-grid soum). The national electrification ratio was indicated 67.3%, also nomadic family's electrification ratio was 17% in 2003. Power supply in the soums is at a considerably insufficient level in that diesel generators in the soums only allows 3 to 4 hour daily power supply because of difficulties in long distance fuel transportation due to bad roads and also because of instable, insufficient fuel supply to the soums due to shortage of funds to purchase fuel.

The government of Mongolia intends to improve supply power to off-grid soums by introducing sustainable and independent renewable energy with a focus on solar power in order to improve social services such as telecommunication, health care and education. As a part of this policy, the government is pushing forward with the "100,000 Solar Ger" Project to provide portable solar power systems (SHS) for nomads (Enebish, 2000) [1]. By this national project, 32,000 SHS sets introduced to nomadic families since 2000. On the other hand, actual condition of SHS use is less well understood in Mongolia and other countries (Nieuwenhout, 2001) [2].

In this study, the regional appropriateness of photovoltaic (PV) systems for nomadic families and villages in the arid and semi-arid land, were verified by the case study in Mongolia. As approach angle from technology, potential of solar energy resource, PV module performance by exposure test (Amarbayar, et al., 2006) [3], and the system performance of SHS (Amarbayar and Kurokawa, 2005) [4] based on 37 sites operation data in Mongolia, were evaluated.

From the social approach, we were investigated the questionnaire survey regarding SHS in nomadic families in Mongolia. This study is performed to clarify user behavior, user satisfaction, problems, needs, and awareness of SHS by non-users

ANALYSIS METHOD

The main purpose of the study was to collect information about users of the SHS, motivation for using the SHS, how SHS used, main problems occurring during the use of SHS, and service which is needed by users of SHS. The survey was carried out in 67 nomadic families by the face-to-face questionnaire method, and 359 responses were received from nomadic families by the mail questionnaire survey method.

Table 1. Category of questions

No	Questions category	Ques.Num
1	About the user of SHS	3
2	About motivation for using SHS	5
3	About the service of SHS	4
4	About the advantage of using SHS	2
5	Problem and demand	4
6	About satisfaction with SHS	2
7	SHS awareness of nonuser	4

The nomadic families from 6 prefectures (aimag) in the west, central, and southern regions (Khovd, Zavkhan, Bulgan, Dundgobi, Dornogobi, and Khentii prefecture) were chosen to be an investigation object of this research (Fig.1).

Fig.1. The object regions of questionnaire survey

Answers to questionnaire were collected 359 (Table 2). The response ratio of this survey was indicated low value (12%) to distributed numbers of questionnaire. Because, nomadic families move for pasture in every season, their location not undefined; this survey was costly and spend time, because the object were in special conditons. 359 answers are meaning in order to evaluate actual conditions and trend of user's consciousness.

Table 2. Responce conditions by the object regions

Province name	SHS user	Non SHS user
	by mail	face-to-face
Dornogobi	63	6
Dundgobi	27	-
Bulgan	45	37
Khentii	-	7
Khovd	117	-
Zavkhan	107	-
Total	359	50

Other hand, to examine the possibility of the introduction of SHS in the future, 7 items as the recognition extent of SHS and the purchase intention etc., were set to nonuser of SHS. The execution method was the face-to-face questionnaire survey method. The cooperation of the nomadic who was not using SHS was received from the nomad in the Bulgan province Khishigundur village (37 families), the Dornogobi province Sainshand villages (6 families), and Khentii province (7 families) in total 50 families (Table 2).

RESULTS OF ANALYSIS

Results of survey to SHS user

The ratio of four (28.7%) and five (25.7%) member's families are indicated high value (Table 7, Q1). As for the household income, ratios of 1 millionTg (94,000 yen) or less is high (Table 7, Q2). The nomadic families income of the this survey objects, is a low tendency compared with nationwide average annual income 1.24 million Tugrug (local currency, about 1,060US$) in the households in the rural area (NSO 2004) [5]. It is assumed that the reason for this tendency is that the households of the civil servant and the company employee with high cash earnings are included in the households in the rural area.

Also, livestock numbers are the main indices of nomad's property. Generally, the nomadic family that owns 50 head of cattle or less is made the poorest family segment of the population and 150-250 with the interlayer (Jargal et al. 2004) [6]. The ratio of the SHS owner families that corresponds more than the interlayer is higher than that of the distribution of the cattle ownership number of nomads in the whole country by Mongolian Statistics Bureau (NSO 2004) [5].

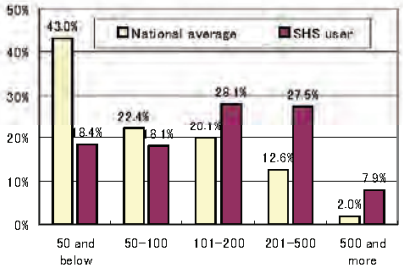

Fig.2. Number of cattle owned by SHS user

The price of the market for each single-unit of SHS is about 40,000 yen including 1 PV module (50W) and storage battery (12V, 75Ah) and the charge controller, etc. SHS is very large amount of money for the nomad whose average income during year is about 1.24 million Tugrug (NSO 2004) [5]. Therefore, the loan was executed for one interest-free year from 1999 in "100,000 Solar Ger" plan, and the subsidy of 50% of the delivery etc. was taken measures in 2003-2004. In the estimate of Mongolian Fuel and Energy Ministry, about 32,000 SHS has been introduced by April, 2005 (and by 2000 about 900 sets).

About motivation for using SHS

In the fig. 3 (Q4), 78% of the answer families bought SHS from "100,000 Solar Ger" project. The case bought from "Shop or market in the city" and "Door-to-door selling" was in total about 16%. The use period of SHS within 1 year, 2 years, and 3 years, more than 3years were indicated 30%, 41%, 24%, and 5%, respectively. From this result, it can say that the users with a little experience of SHS were the majority.

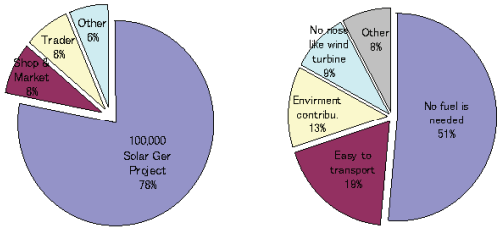

Fig. 3. Answers of the Q4 Where did you buy your SHS?, Q6 What was your motivation for using SHS?

The answers of not having used the power supply before use SHS, are 44%. Most of families (56%) have been used some power supply systems such as the gasoline generator, the wind power generation systems, and storage batteries, before using SHS, and their were

knows the convenience of electricity.

The motivation for introducing SHS were "It was using electrical appliances" (53.3%) in the meaning of demand to the convenience improvement of life, and next was "Neighbor used SHS" (21%). "The fuel was not needed" (51%) and "Easy to transport" (19%) became a hit to the reason to choose SHS from several types of power supply systems (Fig. 3, Q6). In the nomadic families that are uses the small gasoline generator, it is necessary to procure the gasoline fuel from a village center away on average at 60km regularly. Because the enormous expenditure needs in the fuel delivery to nomadic family, continuous use for the small gasoline generator is difficult and there is no delivery service.

Maintainance of SHS

From answers of Q10 "How many times did you have troubles?", 67 families (18.7%) experienced some troubles. The failure-prone parts of SHS are charge controller unit (32.2%), battery (29.7%) (Q11). When the SHS failured, users asks well known friend about electricity (54.6%) or repairs by themselves (29.4%)

Problems and needs of users

The main problem of SHS users it that there is no after sale service at all. First of all it because the "100000 SHS" project does not provide any service. As mentioned before about 70% of the families purchased their SHS from this project. For the private companies service will not be profitable because of the long distance and few customers.

Q15 Weak point of SHS? 1st: Expensive (48.9%), 2nd : Low power (22.7%). Q16 User needs for SHS? 1st: Repair shop in the soum center (39.1%), 2nd : Useful user manual for SHS (36.8%). Q18 About warranty and quality, 1st: To have long time warranty (61.0%), 2nd: Improvement of SHS parts (33.2%).

Main problem of SHS owners is lack of service. There is no service at all. They would like to have service shops in soum centers, shops where they can by spare parts for SHS, lamps and other small electrical equipment. At least they would like to have more information about SHS and introductions how to use and how to repair SHS. Many of them said that they would like to learn to repair SHS, so that they can help themselves and neighbors.

About the satisfaction with SHS

The most users (90%) indicated that they were satisfied with their SHS (Fig.4). They appreciated improvement in the ability to watch TV and lighting. Because, the answers of Q13 What is the advantage of using SHS were: 1st: The news, market info etc. on TV Broadcasting have been acquired instantly (53.3%), 2nd: The weather forecast is obtained in detail (22.9%). It is shown that SHS is appropriate power system for nomadic lifestyle to compare with other type generation systems from the view point of users.

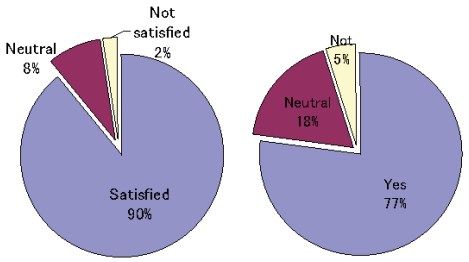

Fig. 4. The user satisfaction with SHS

Results of survey to non SHS user

In addition to this 50 families without SHS in Bulgan, Dornogobi and Khentii aimag were interviewed. 46% of them knows SHS well (Fig. 5, Q21) and 71% of them are going to buy SHS (Fig. 6, Q24). 31% of them would like to buy some power source, but they don't have cash (Fig. 5, Q23). Annual income and number of cattle of those 50 families is the same as the average of the 405 families below.

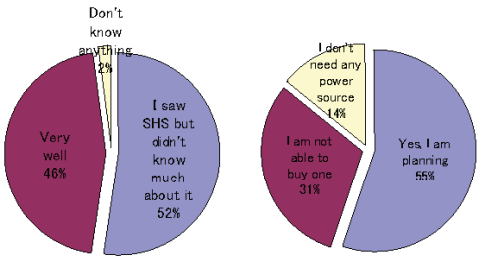

Fig. 5. Answers of the Q21 How well do you know SHS?, Q23 Are you going to buy some power source?

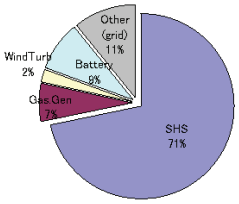

Fig. 6. Answers of the Q24 What kind of power source you would like to buy?

CONCLUSIONS

Here, we present the results of a questionnaire survey regarding Solar Home Systems (SHS) in nomadic families in Mongolia. This study was performed to clarify user behavior, user satisfaction, problems, needs, and awareness of SHS by non-users. The survey was carried out in 67 nomadic families by the face-to-face questionnaire method, and 359 responses were received from nomadic families by the mail questionnaire survey method.

From the results, most users indicated that they were satisfied with their SHS. They appreciated improvement in lighting and the ability to watch TV. It is shown that SHS is appropriate power system for nomadic lifestyle to compare with other type generation systems from the view point of users.

The electrification rate increased 18% at 5 years from 10.7% (in 2000), to 29% (estimation in Mart 2005) by implementation of the "100,000 Solar Ger" project. The main problem for SHS users was a lack of after-sale service. There is a requirement to establish service chains, review of preferential treatment for the sales and support system based on market principle.

References

[1] Enebish, N.(2000) National Photovoltaic Program " 100,000 Solar House (GER) in Mongolia" , 28th IEEE Photovoltaic Specialists Conference, September 15-22, 2000.

[2] Nieuwenhout, F.D.J. and Dijk, A.L. van, et al.(2001), Experience with solar home systems in developing countries: a review, Progress in Photovoltaics, Vol.9(DOI: 10.1002/pip.392)455-474pp.

[3] A.Amarbayar, K.Otani, et al.(2006) Evaluation of Solar Energy Potential and PV module Performance in the Gobi Desert of Mongolia, Progress in Photovoltaics, Vol.14 (DOI:10.1002/pip.692) pp.553-566.

[4] A. Amarbayar and K. Kurokawa (2005) Performance Analysis of Portable Photovoltaic Systems based on the Demonstrative Research Data in Mongolia, *Journal of JSES*, Vol.31 (168) No.4, pp.83-88.

[5] NSO:National Statistical Office of Mongolia (2004) Statistical Year Book 2003, 141-147pp.

[6] Jargal, G. and Y.Otgonbold, et al.(2004)Study Report " Bringing herders' assets into full economic and productive use" , UNDP/SIDA, Ulaanbaatar, 31-33pp.

[7] NEDO(1997) The New Energy and Industrial Technology Development Organization of Japan, "Demonstrative Research of Movable Type Photovoltaic Power Generation System" Overall Research Report, Kyocera Corporation, http://www.tech.nedo.go.jp/Index.htm

[8] NSO:National Statistical Office of Mongolia(2004b) Statistical Year Book 1989-2002: " Mongolia in a Market System" , 163-165pp.

[9] Nikolakaki, E.Krontiris(2001) "Problems and Prospects of Autonomous Power Plants with Small Scale Wind Turbines in Isolated Areas, Demonstration Project of Rural Electrification in Mongolia", International Conference Renewable Energies for Islands: Towards 100% RES Supply, Chania - Crete, Greece, 14-16 June 2001.

[9] The New Energy Foundation (NEF)(2005) Report of questionnaire survey about installation quality of PV systems for House

[10] Suzuki Yukio (2003) Actual condition of agriculture in Mongolia, Science Journal Kagaku, Vol.73 No.5, May 2003, 549-553pp.

[11] Tserendash, S. (2000) Some policy related issues for pasture management, Newsletter No. 6 (38), Mongolian Academy of Sciences, Ulaanbaatar.

[12] ADB(2002) Mongolia's Environment Implications for ADB's Operations, East and Central Asia Department of Asian Development Bank, PSNo.090602, ISBN 971-561-468-x.

An Evaluation of Area-dependency Equalization of Fluctuation Characteristics from Distributed PV Systems

Norihiro Kawasaki[1], Kiyoyuki Kitamura[2], Hiroyuki Sugihara[3], Shogo Nishikawa[4], Kosuke Kurokawa[1]

[1] Tokyo University of Agriculture and Technology, 2-24-16 Naka-cho, Koganei, Tokyo, 184-8588 Japan

[2] MEIDENSHA CORPORATION, Riverside Building, 36-2, Nihonbashi Hakozakicho, Chuo-Ku, Tokyo 103-8515, Japan

[3] Kandenko Co., Ltd., 4-8-33 Shibaura Minato-ku Tokyo 108-8533, Japan

[4] Nihon University, 1-8-14 Kanda Surugadai Chiyoda-ku Tokyo 101-8308, Japan

Short time fluctuations of solar irradiance will become an important issue with regard to future embedded photovoltaic (PV) systems. However, when a large number of systems introduce in certain area intensively, the output of the systems will be stable by the equalization of irradiance fluctuation. This phenomenon is called "the smoothing effect" by the authors. In this paper, the evaluation method of fluctuation of PV output is described. By using this evaluation method, frequency characteristics of PV output are evaluated. Moreover, relations between the smoothing effect and installation scale of PV systems are examined.

Keywords: fluctuation, the smoothing effect, Wavelet transform, clustered PV system

INTRODUCTION

An output of PV systems has a short-term fluctuation due to weather fluctuation. It may give undesirable effects on an individual power system, and it makes the capacity value (kW value) of the PV system lower. For resolution of those problems, authors have studied "the smoothing effect" which is smoothed total irradiance in the area. Fluctuation of output of a few PV systems is sensitive, but fluctuation of total output in clustering PV systems is not remarkable because there is the smoothing effect of irradiance in certain area. According to the smoothing effect, the capacity value of PV systems is increased, and problems for utility occurred by fluctuation of PV output power can be alleviated. Therefore, it is very important to quantify this effect and to develop the evaluation method. In this study, the evaluation method of smoothing effect of PV systems is proposed by frequency analysis: i.e. Wavelet transform. Frequency analysis is useful to identify fluctuation values of each time scales. Over the last few years, authors have developed this method [1], [2]. In this paper, by using this method, the evaluation result of fluctuation characteristics of PV output is described. Moreover, relations between the smoothing effect and installation scale of PV systems are examined.

MEASURED DATA

Irradiance and PV output data 553 PV systems clustered will be measured every second as the part of NEDO's project, "Demonstrative Research on clustered PV Systems" from March, 2004, to March 2008. Therefore, measured data has been recorded by one second sampling. PV array power was used for this analysis.

APPROACH

Fluctuation Analysis

In an evaluation of fluctuation characteristics of PV output, it is necessary to know the relation between speed of fluctuation and magnitude of fluctuation. Therefore, a new method is suggested to analyze the fluctuation (see Fig.1.).

First, analytical data is prepared, and the power spectrum (PS) is calculated from this data by using the Wavelet transform. Haar has been chosen as a wavelet function. Next, the peak of PS is detected for each range of fluctuation time (see Table.1.). An evaluation window is prepared centering on the peak of PS as shown in Fig. 2, and the difference between the maximum value and minimum value in the window is calculated. This difference is defined as Maximum magnitude of the fluctuation (MMF). MMF shows the biggest magnitude of fluctuation during a day for each range of fluctuation time. In other words, this is the worst case in the fluctuation.

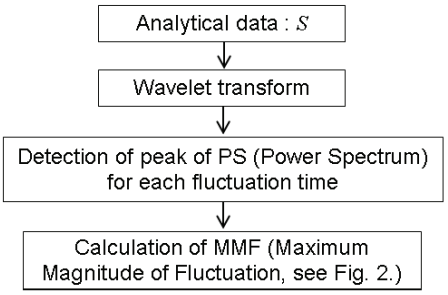

Fig. 1. Fluctuation analysis flow.

Table. 1. Range of fluctuation time.

Level j	Range of fluctuation time ($2^j \sim 2^{j+1}$) [sec]	Frequency [Hz]
1	2 ~ 4	0.5 ~ 0.25
2	4 ~ 8	0.25 ~ 0.125
3	8 ~ 16	0.125 ~ 0.0625
4	16 ~ 32	0.0625 ~ 0.03125
5	32 ~ 64	0.03125 ~ 0.01562
6	64 ~ 128	0.01562 ~ 0.00781
7	128 ~ 256	0.00781 ~ 0.00390
8	256 ~ 512	0.00390 ~ 0.00195
9	512 ~ 1024	0.00195 ~ 0.00097
10	1024 ~ 2048	0.00097 ~ 0.00048
11	2048 ~ 4096	0.00048 ~ 0.00024
12	4096 ~ 8192	0.00024 ~ 0.00012
13	8192 ~ 16384	0.00012 ~ 0.00006
14	16384 ~ 32768	0.00006 ~ 0.00003
15	32768 ~ 65536	0.00003 ~ 0.00001

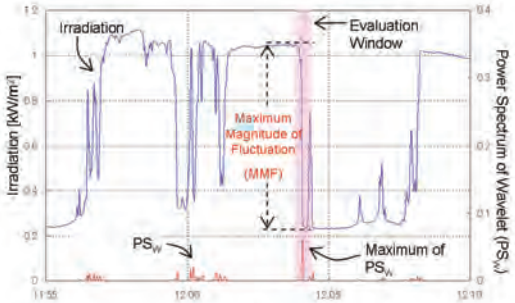

Fig. 2. Example of calculating MMF.

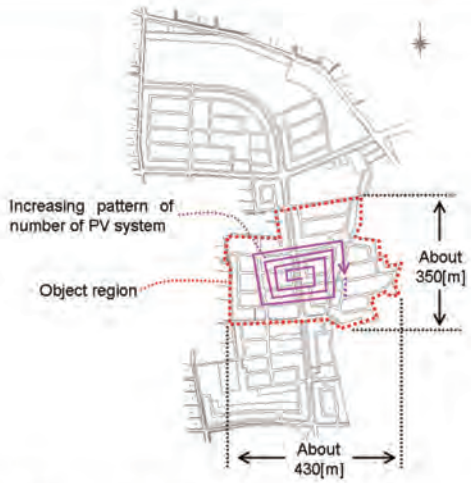

Fig. 3. Increasing pattern of number of PV systems.

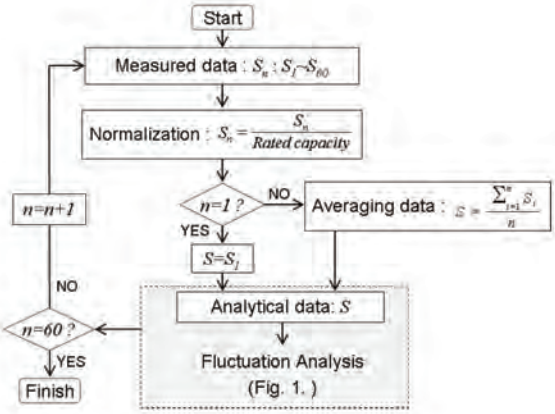

Fig. 4. An evaluation flow of the smoothing effect.

An evaluation method of the smoothing effect

The data of some PV systems are necessary to evaluate the smoothing effect. The data of 60 PV systems in red dotted line of Fig.3. was used this time. Moreover, increasing pattern of number PV systems becomes important in this evaluation. A swirling arrowed line in Fig.3. shows increasing pattern of number PV systems. In this analysis, number of PV systems is increased one-by-one by using this increasing pattern.

Fig.4. shows an evaluation flow of the smoothing effect. First, measured data of 60 PV systems are prepared. Next, measured data of PV array power is divided by rated capacity of PV array, and normalization. This reason is that capacity of PV array is different in each PV systems. Next, when n (number of PV systems) is two or more, those data is averaged. It is thought that the more n increases, the more the smoothing effect influences averaging data. This averaging data becomes an input data of the fluctuation analysis of Fig.1. Finally, these processes are repeated 60 times.

In the evaluation of the smoothing effect, number of installation of the PV system and installation area of the PV system is important. However, only number of installation of the PV system is discussed in this analysis. Note that the influence of installation area of the PV system is included.

RESULTS AND DISCUSSION

In this paper, fluctuation characteristics of three typical weathers (Fig.5, 8, and 11) are discussed. The weather was selected referring to reference [3]. Clearness Index (CI) 0.5 is fluctuation day, CI 0.39 is cloudy day, and CI 0.69 is clear day.

When the number of PV systems was increased from 1 system to about 60 systems, MMF was calculated each fluctuation time. Analyzed results are shown as follows. Fig.6, 9, and 12 show the relation between MMF and fluctuation time when the number of PV systems is 1, 10, 40 and 60. Fig. 7, 10, and 13 show the relation between MMF and number of PV systems when fluctuation time is from 2 to 128 seconds.

Fluctuation day (Clearness Index: 0.50)

As for the irradiance on this day, the fluctuation magnitude is large, and the fluctuation speed is fast. In Fig.6, short time fluctuation of output becomes small in 60 systems, though one system fluctuates wildly the output. This reason is that the fluctuation of each PV system for a short time has not synchronized. In Fig.7, it is seen that MMF tend to decrease in ranges of 2-32 seconds at fluctuation time as the number of PV systems increased. The characteristics of MMF showed a flat characteristic for 64 seconds or more the fluctuation cycle. Therefore, the smoothing effect was effective at 32 seconds or less.

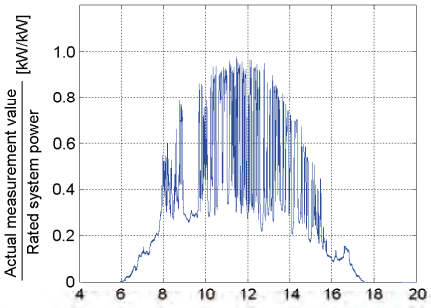

Fig. 5. Normalized PV array output power. (Clearness Index: 0.50, 14 May 2005)

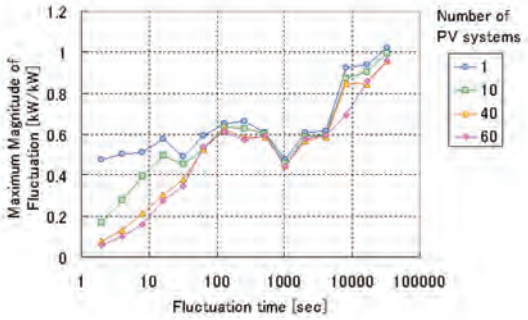

Fig. 6. Relation between MMF and fluctuation time. (Clearness Index: 0.50, 14 May 2005)

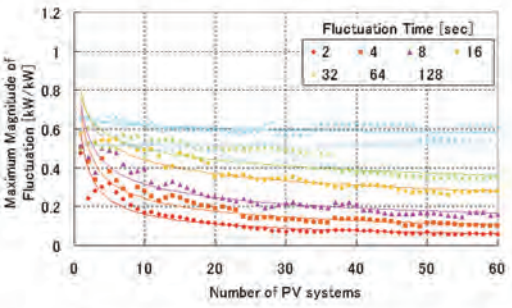

Fig. 7. Relation between MMF and number of PV systems. (Clearness Index: 0.50, 14 May 2005)

Cloudy day (Clearness Index: 0.39)

As for irradiance on this day, fluctuation is small and slower than the fluctuation day. In Fig.9, there is little difference of one system and 60 systems in fluctuation characteristic. This reason is that the fluctuation of each PV system has almost synchronized. In Fig.10, it seen to that MMF is constant regardless of number of PV systems. This means the smoothing effect has not occurred. However, the fluctuation for a short time will not become a problem any more than fluctuation day, because it is smaller than fluctuation day.

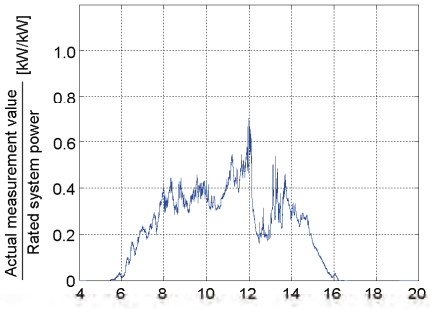

Fig. 8. Normalized PV array output power. (Clearness Index: 0.39, 1 May 2005)

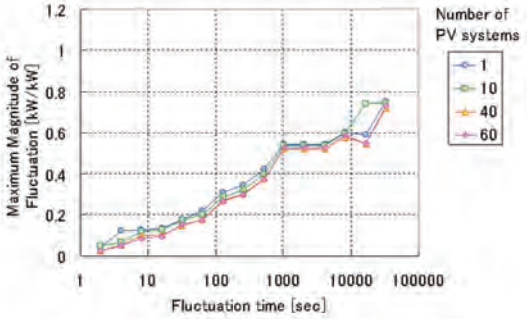

Fig. 9. Relation between MMF and fluctuation time. (Clearness Index: 0.39, 1 May 2005)

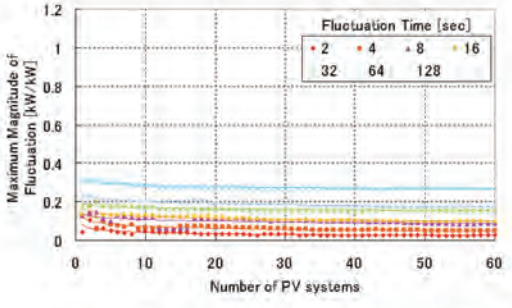

Fig. 10. Relation between MMF and number of PV systems. (Clearness Index: 0.39, 1 May 2005)

Clear day (Clearness Index: 0.69)

As for irradiance on this day, this irradiance is basic curve of irradiance, and has no fluctuation by the cloud. In Fig.12, there is no difference of one system and 60 systems in fluctuation characteristic. This reason is that the fluctuation of each PV system has synchronized. In Fig.13, it seen to that MMF is near 0 [kW/kW] regardless of number of PV systems. This means the smoothing effect has not occurred, too. However, the fluctuation for a short time will not become a problem as well as cloudy day.

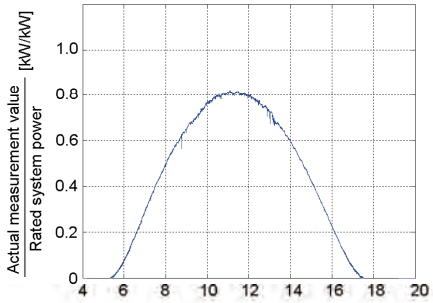

Fig. 11. Normalized PV array output power. (Clearness Index: 0.69, 4 May 2005)

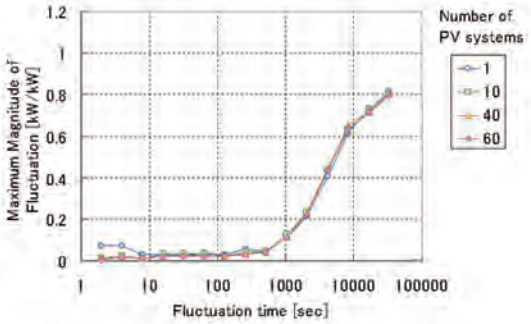

Fig. 12. Relation between MMF and fluctuation time. (Clearness Index: 0.69, 4 May 2005)

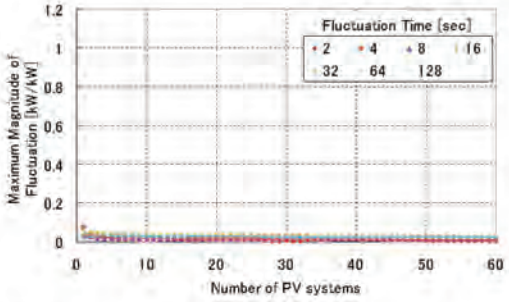

Fig. 13. Relation between MMF and number of PV systems. (Clearness Index: 0.69, 4 May 2005)

CONCLUSIONS

Maximum Magnitude of fluctuation was defined as an evaluation index of the fluctuation characteristic. From analysis results, it was quantitatively shown that the smoothing effect occurs on the day when a short time fluctuation is large. Therefore, the smoothing effect can be clarified by this evaluation method.

In the future, the smoothing effect will be modeled based on a long-term analytical result.

ACKNOWLEDGMENTS

This work was supported by New Energy and Industrial Technology Development Organization (NEDO) as a part of the “Demonstrative Research on Clustered PV Systems” under Ministry of Economy, Trade and Industry (METI).

Authors would like to acknowledge the financial support of NEDO and cooperative discussions with project members.

References

[1] K. Otani, J. Minowa, and K. Kurokawa, "Study on Areal Solar Irradiance for Analyzing Areally-Totalized PV Systems", *Solar Energy Materials and Solar Cells*, 47, pp.281-288, 1997

[2] N. Kawasaki, T. Oozeki, K. Otani and K. Kurokawa, “An evaluation method of the fluctuation characteristics of photovoltaic systems by using frequency analysis”, *Solar Energy Materials and Solar Cells*, Volume 90, Issues 18-19, pp. 2951-3480, 2006

[3] N. Kawasaki, T. Oozeki, K. Otani, K. Kitamura, H. Sugihara, S. Nishikawa, and K. Kurokawa, “An Evaluation Method of Area-dependency Equalization of Output Fluctuation from Distributed PV System by Using Frequency Analysis", *Proceedings of 15th PVSEC*, pp.393-395, 2005

[4] J. Tamura, K. Otani, K. Kurokawa, "Study of the instant separation into direct and scattered radiation using instant solar radiation", *Proceedings of JSES/JWEA Joint Conference*, 54, p.p. 225-228, 2002 (in Japanese)

D-UPFC as a Voltage Regulator in the Distribution System

Kyungsoo Lee, Kenichiro Yamaguchi, Hirotaka Koizumi, and Kosuke Kurokawa

Tokyo University of Agriculture and Technology, 2-24-16 Naka-cho, Koganei, Tokyo, 184-8588 Japan
(E-mail: onnuri@cc.tuat.ac.jp)

This paper proposes a voltage controller in order to control under-voltage and over-voltage condition in the distrubution system. The voltage controller, which are called distribution-unified power flow controller (D-UPFC), consists of ac-ac converter and the transformer. D-UPFC does not use any energy storage component or rectifier circuit, and it directly converts ac power to ac power. All pass filter and direct-quadrature (d-q) transformation functions are employed in the D-UPFC control. Also, D-UPFC is located in the pole transformer or any place in the distribution line. Simulation and experiment results show the possibility of controlling under-voltage and over-voltage conditions in the distribution system.

Keywords: distribution system, D-UPFC, ac-ac converter, all pass filter, d-q transformation

INTRODUCTION

In the present power system, the generated power is assumed to feed into the system at the high voltage level and the power is consumed at the low voltage level. Thus, the power direction through a transformer would always be from the high voltage level to the low voltage level [1]. The present power system is shown in Fig. 1.

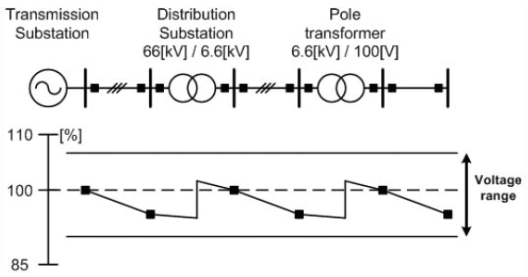

Fig. 1. The present power system.

However, when the clustered PV system connects with distribution system and reverse power flows, the distribution line voltage increases. The clustered PV system connected with distribution system is shown in Fig. 2.

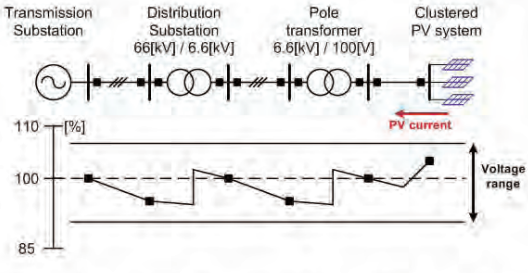

Fig. 2. Clustered PV system connected with distribution system.

So far, some distribution voltage controllers have been used in the distribution system. Dynamic voltage restorer (DVR) and uninterrupted power supply (UPS) systems have been researched and developed along the last decades. They are capable of compensating under-voltage and over-voltage conditions. However, they depend on devices in order to store energy, like large capacitors or battery bank. If the power increases, the size of the devices will increase [2].

This paper proposes D-UPFC in order to control under- and over-voltage conditions in the distribution system. D-UPFC consists of ac-ac converter and the transformer. The ac-ac converter uses four MOSFET switches, input and output LC filters. D-UPFC employs all pass filter and d-q transformation. D-UPFC does not need any energy storage components, such as large capacitor or inductor. Morever, D-UPFC does not use any rectifier circuit in order to convert ac power to ac power. However, it directly converts ac to ac conversion.

This paper begins by studying D-UPFC concept with clustered PV system. D-UPFC circuit analysis is performed. In the D-UPFC control, all pass filter and d-q transformation methods are used in order to control distrubution line voltage simultaneously. Switching patterns, which are considered power flow, reverse power flow, and inductive load conditions, are proved in the simulation. Under-voltage and over-voltage conditions are proved using simulation tool, which named PSIM ver. 6.1.

D-UPFC CONCEPT

D-UPFC can control under-voltage condition, which can happen during heavy load or short-circuit. Also, it can control over-voltage condition, which can occur during reverse power flow from clustered PV system. D-UPFC can be located at the back of the pole transformer or any place in the distribution line. The overview of D-UPFC installation is shown in Fig. 3. The higher power flows from the substation to the clustered PV system through the pole transformer.

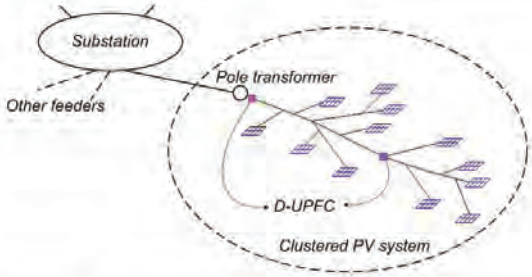

Fig. 3. Overview of D-UPFC installation.

D-UPFC CIRCUIT ANALYSIS

AC-AC converter consists of four MOSFET switches, input and output LC filters. Its topology is the similar with dc-dc buck converter, but the difference is that it converts ac power to ac power. AC-AC converter output voltage can be expressed,

$$V_{load} = D \times V_s \quad (1)$$

Where, V_s and V_{load} are input and output voltage, respectively. D is duty ratio.

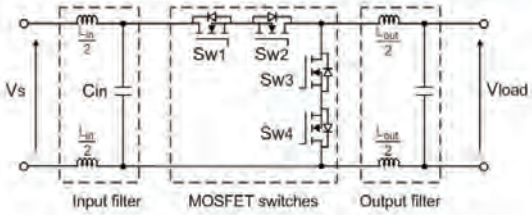

Fig. 4. AC-AC converter circuit.

Proposed D-UPFC topology is shown in Fig. 5. Here, the ac-ac converter controls distribution line voltage during under-voltage or over-voltage condition. D-UPFC output voltage is expressed,

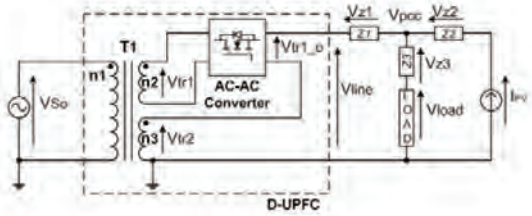

Fig. 5. Proposed D-UPFC topology.

$$V_{line} = \frac{n_2 + n_3}{n_1} \times V_{so} = V_{tr2} + V_{tr1\_o} = V_{tr2} + (D \times V_{tr1}) \quad (2)$$

Where, n_1 is the primary side and n_2, n_3 are secondary and tertiary sides of the transformer. V_{so} is the source voltage and V_{line} is distribution line voltage. V_{tr1} and V_{tr1_o} are the secondary input and output voltage, respectively. V_{tr2} is the tertiary voltage.

D-UPFC SWITCHING PATTERN ANALYSIS

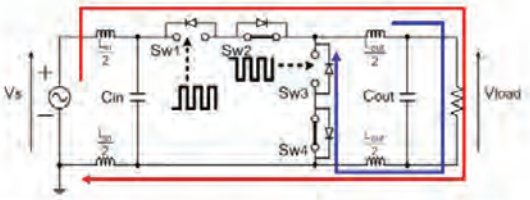

Fig. 6. AC-AC converter switching during power flow(Vs is plus polarity).

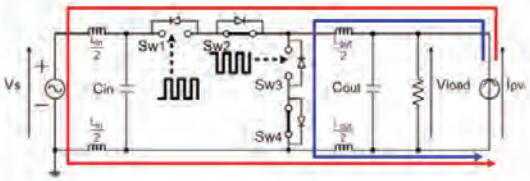

Fig. 7. AC-AC converter switching during reverse power flow(Ipv is plus polarity).

D-UPFC switching pattern can be considered in the three conditions. When the power flows from pole transformer to clustered PV system and Vs is plus polarity, ac-ac converter switches Sw1 and Sw3 are pwm and Sw2 and Sw4 are on. If Vs is minus polarity, Sw2 and Sw4 are pwm and Sw1 and Sw3 are on. Figure 6 shows the ac-ac converter switching pattern during power flow condition [3].

When the reverse power flow occurs from the clustered PV system to the distribution system and Ipv is plus polarity, Sw1 and Sw3 are pwm and Sw2 and Sw4 are on. If Ipv is minus polarity, Sw2 and Sw4 are pwm and Sw1 and Sw3 are on. Figure 7 shows the ac-ac converter switching pattern during reverse power flow condition [3].

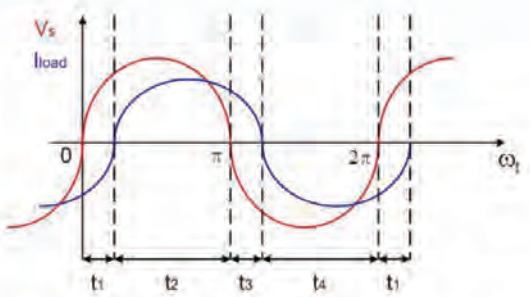

Fig. 8. Inductive load condition in the ac-ac converter.

When the inductive load connects with ac-ac converter, the output current is lag compared with input voltage. Thus, D-UPFC switching pattern should

consider the phase condition. AC-AC converter source voltage V_s and inductive output current I_{load} can be shown in Fig. 8. In order to control the phase difference between V_s and I_{load}, four periods of the switching pattern are shown in Table 1 [4].

Table 1. Switching pattern of inductive load.

Period	Sw1	Sw2	Sw3	Sw4
t_1	PWM	ON	PWM	ON
t_2	PWM	ON	PWM	ON
t_3	ON	PWM	ON	PWM
t_4	ON	PWM	ON	PWM

D-UPFC CONTROL

All pass filter and d-q transformation are used in the D-UPFC control. The d-q transformation changes fundamental frequency signals to dc components, allowing a fast transient response to control distribution line voltage. The all pass filter shifts fundamental sine waveform(real value) to 90 degree lead or lag(imaginary value) in order to employ d-q transformation. Figure 9 shows the phase shift concept.

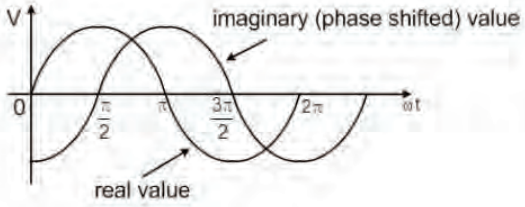

Fig. 9. Real and imaginary values in the all pass filter

Using the all pass filter concept, the real and imaginary values can be expressed,

$$V_r = b_1 sin(\omega t) \tag{3}$$

$$V_i = b_1 sin(\omega t - \frac{\pi}{2}) = -b_1 cos(\omega t) \tag{4}$$

Where, V_r and V_i mean real and imaginary values, respectively. b_1 is the instantaneous voltage magnitude. According to eq. (3) and (4), the single-phase d-q transformation is given by,

$$\mathbf{V}_{dq} = \mathbf{T}\mathbf{V}_{ri} \tag{5}$$

Where, $\mathbf{T} = \begin{bmatrix} sin\theta & -cos\theta \\ cos\theta & sin\theta \end{bmatrix}, \theta = \omega t$

Where, V_d and V_q indicate the real and imaginary voltages, respectively [5]. D-UPFC control block is shown in Fig. 10. The purpose of D-UPFC control is that D-UPFC output voltage V_{load} always follows the reference voltage V_{ref}. D-UPFC input voltage V_s, output voltage V_{load} and current I_{load} are sensed and change the original values to dc values using all pass filter and d-q transformation functions. The voltage error V_{error} is controlled using PI compensator and then it compares with carrier waveform in the PWM function. The final pwm signal inputs four switches considering phase angle between V_s and I_{load}.

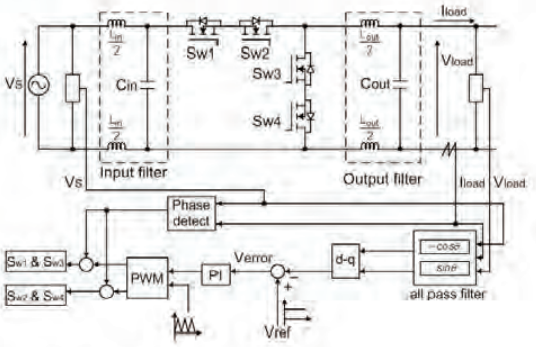

Fig. 10. D-UPFC control block.

D-UPFC SIMULATION & EXPERIMENT

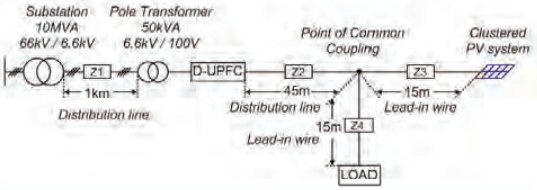

Fig. 11. D-UPFC simulation model.

D-UPFC simulation model is considered from the substation to the load and clustered PV system. The basic simulation model is shown in Fig. 11. D-UPFC locates behind the pole transformer. Considering line impedances in the distribution system, the distance between the substation and the pole transformer is 1[km], rom D-UPFC to the point of common coupling (PCC) is 45[m]. The distance between PCC and the load or clustered PV system is 15[m].

D-UPFC simulation model parameters are shown in Table 2. Also, ac-ac converter parameters are shown in Table 3.

Table 2. D-UPFC simulation model parameters.

Substation vol.(sec.)	6.6[kV, rms]
Pole trans. vol.(sec.)	100[V,rms]
Z_1	0.025+j0.034[Ω/1km]
Z_2	0.011+j0.013[Ω/45m]
Z_3 & Z_4	0.00345+j0.00015[Ω/15m]
Load	3.33[Ω]
I_{pv}	100[A,rms]
Max. output voltage	100[V,rms]
Max. output current	70[A,rms]
Max. power	7[kW]

Table 3. AC-AC converter parameters.

Max. output voltage	10[V,rms]
Max. output current	70[A,rms]
Max. power	700[W]
Input & Output L and C	176.75[μH], 15.94[μF]

Figure 12 shows the experimental result of the ac-ac converter switching pattern. The switching pattern S_{w1} depends on the source voltage V_s.

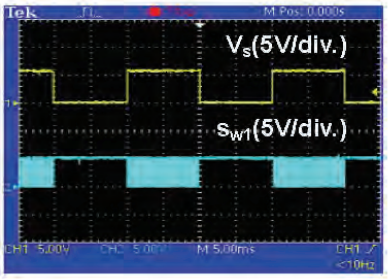

Fig. 12. AC-AC converter switching pattern.

The under-voltage simulation result is shown in Fig. 13. Here, D-UPFC control voltage is expressed,

$$V_{ref} - V_s > 2[V, rms] \quad (6)$$

Where, V_{ref} shows the D-UPFC reference voltage. In the simulation, D-UPFC refecence voltage V_{ref} is fixed to 101[V,rms]. The source voltage V_s changes 98[V,rms] to 93[V,rms], because the under-voltage affects the source voltage from 2[V,rms] to 6[V,rms]. V_{line} shows distribution line voltage and it is affected by under-voltage condition. $V_{line\text{-}controlled}$ means D-UPFC controlling voltage. $V_{line\text{-}controlled}$ is changed 100.4[V,rms] to 99.1[V,rms] when D-UPFC performed.

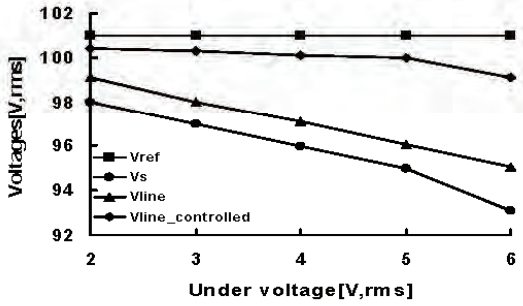

Fig. 13. D-UPFC control in the under-voltage condition.

The over-voltage simulation result is shown in Fig. 14. Here, D-UPFC control voltage expresses,

$$V_{line} - V_{ref} > 2[V, rms] \quad (7)$$

Where, V_{line} means the distribution line voltage. In the simulation, reverse power from clustered PV system flows from 70[A,rms] to 100[A,rms]. V_{ref} is the D-UPFC reference voltage. When the I_{pv} changes 70[A] to 100[A], V_{line} also changes 104.3[V,rms] to 107.2[V,rms]. D-UPFC controls voltage 102.2[V,rms] to 103.7[V,rms] during over-voltage condition.

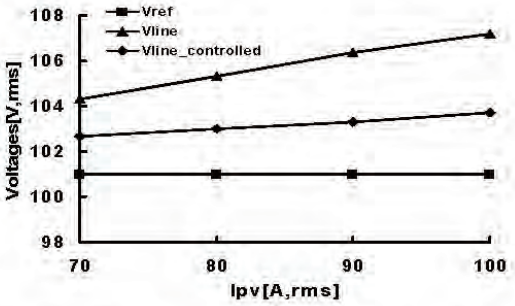

Fig. 14. D-UPFC control in the over-voltage condition.

CONCLUSION

Proposed D-UPFC is shown in this paper. D-UPFC controlled the distribution line voltage during under- and over-voltage conditions. D-UPFC concept, circuit, switching pattern, and control method are analyzed. The proposed D-UPFC proves the performance using simulation and experimental results. However, it needs more reliability tests during reverse power flow condition.

ACKNOWLEDGEMENT

This research has been carried as a part of "Autonomy-Enhanced PV Cluster" project and special thanks for financial support of NEDO.

References

[1] A. F. Povlsen, "Impacts of Power Penetration from Photovoltaic Power Systems in the Distribution Networks", *IEA PVPS T5-10*, 2002.

[2] J. Pérez, V. Cárdenas, Ho. Miranda, and R. Álvarez "Compensation of Voltage Sags and Swells using a Single-phase Ac-Ac Converter", *The 30th Annual Conference of the IEEE Industrial Electonics Society*, 2004, pp. 1611-1616.

[3] B. Kwon, B. Min, and J. Kim, "Novel topologies of AC choppers", *IEE Proc. –Electr. Power Appl., Vol. 143, No. 4, 1996*, pp. 323-330.

[4] S. Ben-Yaakov, Y. Hadad, and N. Diamantstein, "A Four Quadrants HF AC chopper with no Deadtime", *IEEE APEC 2006*, 2006, pp. 1461-1465.

[5] M. González, V. Cárdenas, and F. Pazos, "DQ Transformation Development for Single-Phase Systems to Compensate Harmonic Distortion and Reactive Power", *IEEE CIEP 04*, 2004, pp. 177-182.

TRANSLATION EQUATIONS FOR TEMPERATURE AND IRRADIANCE OF THE I-V CURVES OF VARIOUS PV CELLS AND MODULES BY LINEAR INTERPOLATION

Yuki Tsuno[1, 2], Yoshihiro Hishikawa[1] and Kosuke Kurokawa[2]

[1] National Institute of Advanced Industrial Science and Technology (AIST), Research Center for Photovoltaics, Central 2, 1-1-1 Umezono, Tsukuba, Ibaraki, 305-8568, Japan

[2] Tokyo University of Agriculture and Technology (TUAT), 2-24-16 Naka-cho, Koganei, Tokyo, 184-0012, Japan

Phone: +81-42-388-7445, FAX: +81-42-388-7445, E-mail: kanbai@cc.tuat.ac.jp

A new translation procedure based on the linear interpolation/extrapolation is proposed, in order to translate the I-V curves to target conditions of irradiance and temperature. The accuracy of the method is investigated, based on the indoor and outdoor I-V curves of various kinds of PV cells and modules. The calculated I-V curves over a wide range of irradiance and temperature well agree with experimental results for various kinds of PV cells and modules. These results indicate that the translation of the I-V curve based on the method is effective for estimating the performance of the PV devices under various climatic conditions.

Keywords: I-V curves, translation, temperature, irradiance

INTRODUCTION

It is useful to understand the effect of the irradiance and temperature on the photovoltaic (PV) cell and module performance, in order to estimate their I-V curves under various climate conditions for power rating and energy rating. Although translation equations based on "shifted approximation" are employed on irradiance dependence in some current standards [1], those equations can deviate from experiments when the variation in the irradiance and/or temperature is large. Also some equations are applicable for limited kinds of PV devices. Recently, the linear interpolation method for the I-V curves was proposed based on experimental (indoor and outdoor) data on various kinds of PV cells and modules [2-5]. This method can accurately estimate the performance of various kinds of PV cells and modules for a wide range of irradiance (G) and (T). This method requires that G or T of the reference I-V curves is the same. However, it is not always possible to obtain such reference I-V curves, especially under outdoor conditions. In this study a new practical formation for the linear interpolation/extrapolation is proposed. The accuracy of the method based on the experimental I-V curves of various kinds of PV cells and modules is investigated.

LINEAR INTERPOLATION METHOD

The present study demonstrates the new practical formulae [6, 7], which are extension of the equations and do not require adjustment of the reference I-V curves. The procedure of the linear interpolation/extrapolation of the present study is as follows. The measured current-voltage characteristics are corrected to target G and T values by equations (1) and (2).

$$V_3 = V_1 + a \cdot (V_2 - V_1) \quad (1)$$

$$I_3 = I_1 + a \cdot (I_2 - I_1) \quad (2)$$

Here, I_1 and V_1 are the current and voltage of the reference I-V curve measured at an irradiance G_1 and temperature T_1. I_2 and V_2 are the current and voltage of the reference I-V curve measured at G_2 and T_2. I_3 and V_3 are current and voltage of the I-V curve at G_3 and T_3. which is the target of the translation. The pair of (I_1,V_1) and (I_2, V_2) should be chosen so that $I_2 = I_1 + (I_{sc2} - I_{sc1})$. Here, I_{sc1} and I_{sc2} are the short circuit current of the reference I-V curves. a is a constant for the interpolation, which has the relation with the irradiance and temperature as shown in Eqs. (3) and (4) (Figs. 1-3). When $0 < a < 1$, the procedure is interpolation, When $a < 0$ or $a > 1$, the procedure is extrapolation.

$$G_3 = G_1 + a \cdot (G_2 - G_1). \quad (3)$$

$$T_3 = T_1 + a \cdot (T_2 - T_1). \quad (4)$$

Equation (5) is also applicable, when the I_{sc} of the device is linear with G. Here, I_{sc3} is the short circuit current of the target I-V curve.

$$I_{sc3} = I_{sc1} + a \cdot (I_{sc2} - I_{sc1}), \quad (5)$$

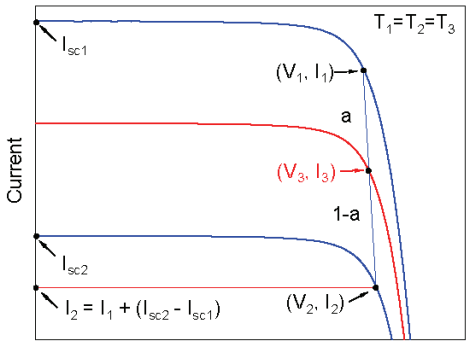

Fig.1 Schematic procedure for the calculations based on Eqs. (1)-(2); translation for G at constant T.

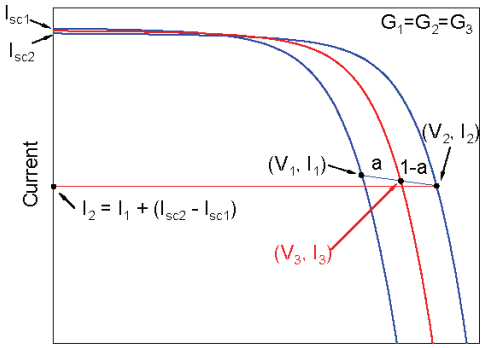

Fig.2 Schematic procedure for the calculations based on Eqs. (1)-(2); translation for T at constant G.

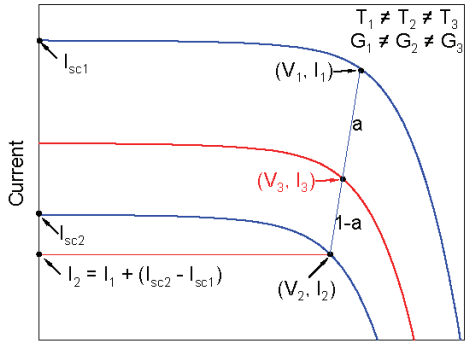

Fig. 3 Schematic procedure for the calculations based on Eqs. (1)-(2); simultaneous translation for G and T.

The primary advantage of the Eqs. (1), (2) is that there is no restriction for the I_{sc}(or G) and the T of the reference I-V curves. Therefore, any I-V curves can be used as the reference I-V curves without adjustment. Translation of the I-V curves for G at constant T (Fig. 1) and translation for T at constant G (Fig. 2) are possible by the same formulae. Furthermore, simultaneous translation for both G and T is possible within the relation of Eqs. (3) and (4).

By utilizing present procedure, I-V cures at wide range of G and T can be calculated from only three or four reference I-V curves measured at indoor or outdoor.

Fig. 4 shows the example of the linear interpolation/extrapolation of four reference I-V curves into the target I-V curve. 1-4 are reference I-V curves. 7 is the target I-V curve. First, I-V curves 5 under target temperature are calculated from I-V curves 1 and 2. Similarly, I-V curves 6 under target temperature are calculated from I-V curves 3 and 4. Then I-V curve 7 under target temperature and irradiance is calculated from I-V curves 5 and 6. It is noted that other order of the calculation is also possible. At least three reference I-V curves can calculate the I-V curves at wide range of G and T.

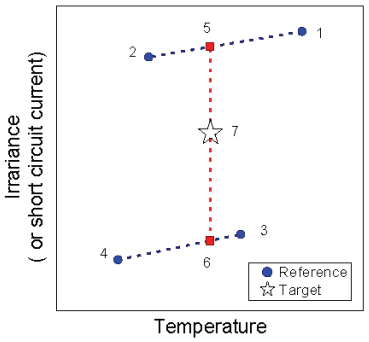

Fig.4 Example of the linear interpolation/extrapolation of four reference I-V curves into the target I-V curve. 1-4 are reference I-V curves. 7 is the target I-V curve.

TRANSLATION OF THE I-V CURVES

Indoor results

The I-V curves at various G and T were calculated by the present procedure using equations (3) and (4) from the experimental reference I-V curves. Typical single-crystalline Si, polycrystalline Si, amorphous Si and a-Si/thin-film crystalline Si tandem cells were used as samples. Their sizes ranged 2-10 cm^2. They were attached on metal plates, whose temperature was stabilized at 20°C, 30°C, 40°C, and 50°C by a flow of temperature controlled water. The temperature was controlled within a nominal accuracy of ±0.2 °C. A solar simulator was used as the light source of 100 mW/cm^2. Irradiance was controlled by metallic thin film neutral density filters. For each solar cell, four reference I-V curves with irradiance of 0 and 100 mW/cm^2 and temperatures of 20°C and 50°C.

The calculated I-V curves well agree with the experiment for all the samples measured in the present study. For example, Fig. 5 shows the results for a polycrystalline Si cell. Measured and calculated I-V curve parameters I_{sc}, V_{oc}, maximum power (P_{max}) and fill factor FF excellently agreed, as shown in Figs. 6 and 7. Root mean square error (RMSE) between measured and calculated P_{max} for all the samples was <0.5%.

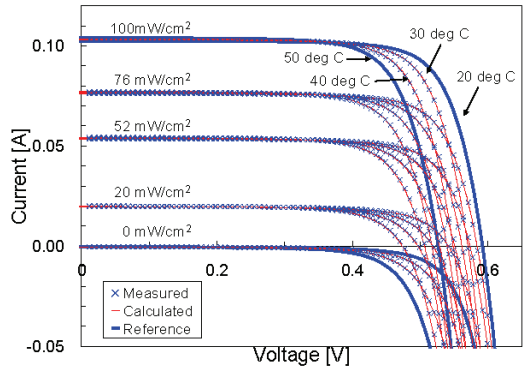

Fig. 5 Measured (circles) and calculated (lines) I-V curves of a polycrystalline Si solar cell. I-V curves measured at G = 0 and 100 mW/cm^2 and T = 20°C and 50°C were used for the reference I-V curves. Calculated results show very good agreement with the experiment.

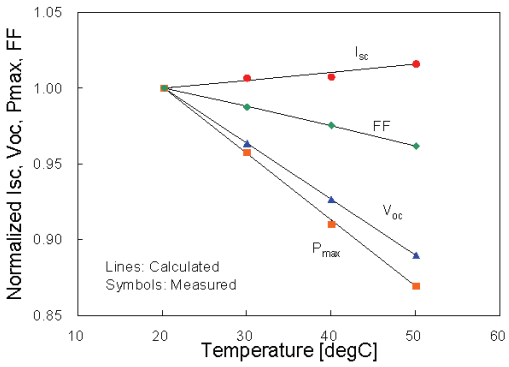

Fig. 6 Measured (circles) and calculated (lines) I_{sc}, V_{oc}, P_{max} and FF for the polycrystalline Si cell shown in Fig. 5 as functions of the temperature T. The irradiance G is 100 [mW/cm^2]. The parameters are normalized to the value at T=20°C. The measured and calculated results agree within the RMSE of 0.1%.

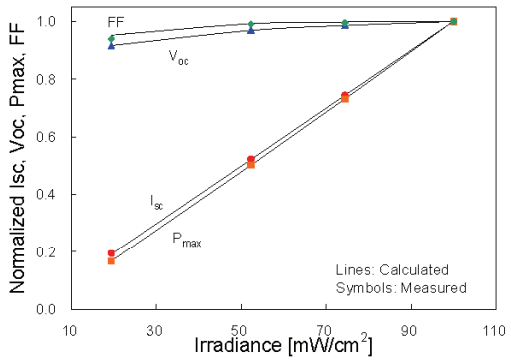

Fig. 7 Measured (circles) and calculated (lines) I_{sc}, V_{oc}, P_{max} and FF for the polycrystalline Si cell shown in Fig. 5 as functions of the irradiance G. The temperature T is 20 °C. The parameters are normalized to the value at G=100 [mW/cm^2]. The measured and calculated results agree within the RMSE of 0.5%.

The present method does not restrict the G and T of the reference I-V curves , and can simultaneously translate the I-V curves for G and T. Fig. 8 shows the example that the I-V curves at (100 mW/cm^2, 25°C) and (20 mW/cm^2, 50°C) is successfully translated into the I-V curve at (52 mW/cm^2, 40°C). The error of measured and calculated Pmax was -0.1%. By utilizing present procedure (Eqs. (1) – (5)), the I-V curves at wide range of G and T can be calculated from only three or four reference I-V curves measured indoor or outdoor.

Another feature of the present formulae is that the series resistance R_s of the PV devices need not be considered, because the effect of R_s in the translation for G is automatically cancelled by the procedure of Eqs. (1)-(5).

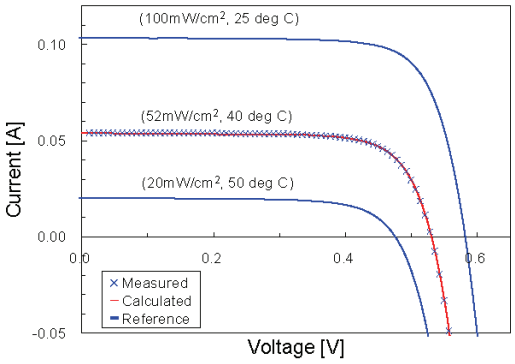

Fig. 8 Measured (symbol) and calculated (line) I-V curves of polycrystalline solar cell. The I-V curves at (100 mW/cm^2, 25°C) and (20 mW/cm^2, 50°C) were successfully translated into the I-V curve at (52 mW/cm^2, 40°C). Blue lines are two reference I-V curves measured at different irradiance and temperature.

Outdoor results

Translation of the I-V curves was also investigated by using the experimental I-V curves of the outdoor PV modules which are located in Tsukuba, Japan. Data were taken for about 3 months. The total number of the I-V curves used was about 15,000. The four I-V curves with the (I_{sc} and T) of (5.36A, 65.3°C), (5.01A, 49.0°C), (1.02A, 37.9°C) and (0.81A, 23.4°C), were used as the reference (Fig. 8). The I-V curves calculated by the reference I-V curves showed very good agreement with the experimental data (Fig. 9). For example, the standard deviation between the measured and calculated P_{max} was about 0.75% (Fig. 10), which demonstrates the accuracy and usefulness of the present procedure of the linear interpolation. Similar results for other PV technologies are also reported based on the outdoor data taken at different location in Japan [6].

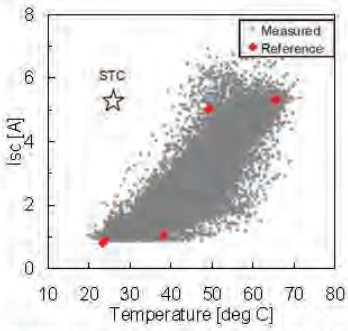

Fig. 9 Temperature and I_{sc} for the outdoor I-V curves investigated in the present study. Each "x" symbol corresponds to one I-V curve. Four reference I-V curves are shown by squares. It is noted that the I_{sc} and T of the reference I-V curves can be chosen without restriction.

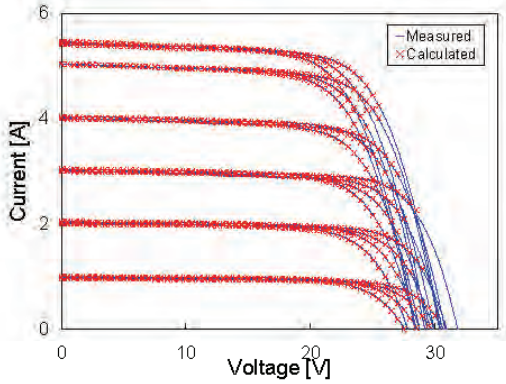

Fig. 10 Examples of measured (lines) and calculated (circles) I-V curves of a polycrystalline Si PV module. Calculated results show very good agreement with the experiment.

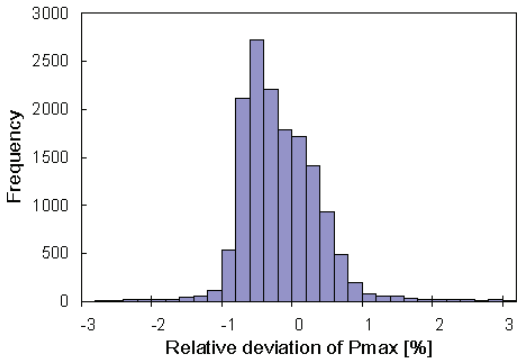

Fig. 11 Deviation of the measured and calculated P_{max} of the outdoor poly-Si modules shown in Fig. 8. Equations (3)-(5) were used for the calculation, based on the experimental four I-V curves, which are also shown in Fig 8.

CONCLUSION

A new practical formulation for the linear interpolation/extrapolation has been investigated, in order to translate the I-V curves of the PV devices for the irradiance G and temperature T. The accuracy of the translation has been investigated based on the experimental indoor and outdoor I-V curves of various kinds of PV cells and modules. By utilizing this method, four or three I-V curves measured at any G and T can be used as the reference I-V curves. This makes practical translation procedure much easier. The results over a wide range of G and T well agree with measured maximum power for various kinds of PV cells and modules. For indoor experiments, root mean square error (RMSE) between the measured and calculated P_{max} for four kinds of PV cells was <0.5%. For outdoor experiments, standard deviation of the measured and calculated maximum power of PV modules was within 1% for wide range of G and T. The present method is expected to be very useful for the energy rating and power rating of the PV devices.

ACKNOWLEDGEMENT

This work was supported in part by NEDO under the Ministry of Economy, Trade and Industry.

REFERNCES

[1] IEC 60891, 1987, JIS C8913,1998, etc.

[2] Y. Hishikawa, Y. Imura and T. Oshiro, "Irradiance - Dependence and Translation of the I-V Characteristics of Crystalline Silicon Solar Cells" Proceedings of the 28th IEEE PV Specialists Conference, (2000); 1464-1467.

[3] B. Marion, S. Rummel and A, Anderberg, "Current-Voltage Curve Translation by Bilinear Interpolation" Prog. Photovolt: Res. Appl. 12 (2004), 593-607.

[5] B. Marion, J. del Cueto and B. Seculic, "Modeling Current-Voltage Curves Using Bilinear Interpolation" Proceedings of the WREC VIII (2004), Denver

[5] Y. Tsuno, Y. Hishikawa and K. Kurokawa, "Temperature and Irradiance Dependence of the I-V Curves of Various Kinds of Solar Cells" Technical Digest of the PVSEC 15, Shanghai, (2005) 422-423.

[6] Y. Tsuno, Y. Hishikawa and K. Kurokawa, "Translation Equations for Temerature and Irradiance of the I-V curves of Various PV Cells and Modules" to be published in the Proceedings of the 4th WCPEC (2006) Waikoloa, Hawaii

[7] Y. Hishikawa, Y. Tsuno and K. Kurokawa, "Translation of the I-V curves of various solar cells by improved linear interpolation" , to be published in the Proceedings of the 21st EU PVSEC (2006) Dresden.

HIGH PRECISION SIMULATION MODEL OF BATTERY CHARACTERISTICS

Takae Shimada [1, 2], Kosuke Kurokawa [1]

[1] Kosuke Kurokawa Lab., Tokyo University of Agriculture and Technology,
2-24-16 Naka-cho, Koganei, Tokyo, 184-8588 JAPAN
[2] Power Supply Systems Unit, Hitachi Reserch Lab., Hitachi, Ltd.
7-1-1 Omika-cho, Hitachi, Ibaraki, 319-1292 JAPAN

This paper reports a simulation model of battery characteristics and its simulation/verification test results. Battery simulation model is necessary in order to simulate systems including batteries such as the grid-connected photovoltaic systems that less depends on the utility grid. The authors created the battery simulation model based on a new method. In this model, internal resistances depend on current, state of charge, and temperature. Verification test results show 0.5 % of power simulation error ratio, high precision was confirmed.

Keywords: AE-PV system, grid-connected PV, battery simulation, battery modeling

INTRODUCTION

Most of the photovoltaic (PV) systems for residences spreading rapidly are grid-connected type. Usually, since this system has no electricity storage, the difference between generated and used electric power is processed by electric power flow of the utility grid. In the future so that the PV systems may spread further, it is necessary to develop "Autonomy-Enhanced" PV (AE-PV) system technologies with electricity storage functions that less depends on the utility grid [1]. To design and evaluate the PV systems with battery storages shown in **Fig.1**, the battery simulation model is necessary [2].

A lot of battery models have been researched. The authors also have been researching it [3] [4]. This time, the authors propose high precision simulation model of battery characteristics.

MODELING

Model

Fig.2 shows the equivalent circuit of the battery model of proposal. Terminal voltage V is estimated by the following equation.

$$V = E - V_d + V_g \quad (1)$$

E is the electromotive force of appearance during charge or discharge. V_d is the voltage drop by current, and consists of resistance component and voltage saturation component. V_g is the voltage rise at final phase of charging, and has a characteristic that looks like the parallel connection of voltage saturation component and current saturation component.

These voltages depend on I, SOC, and T_{25}. I is the current. SOC is the state of charge, and means full charge when SOC = 1. T_{25} is the battery temperature based on 25 deg C.

E is calculated by the following equation which considers the Nernst equation.

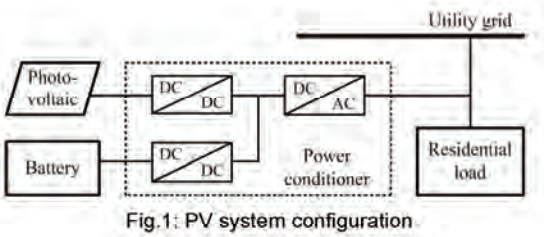

Fig.1: PV system configuration

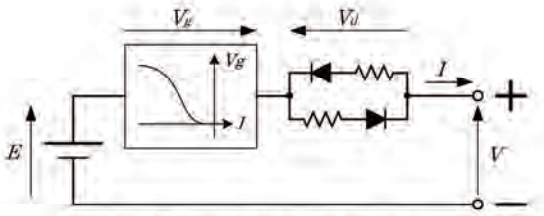

Fig.2: Equivalent circuit of battery

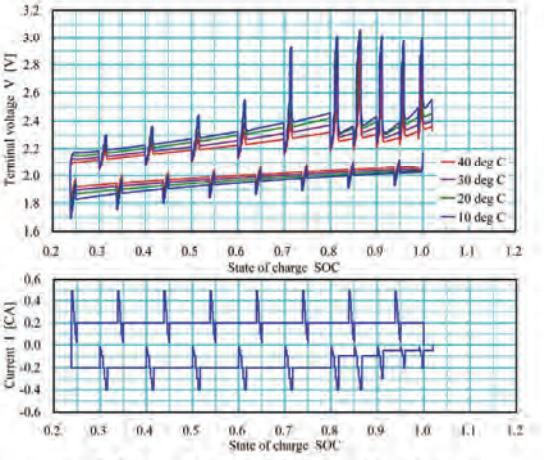

Fig.3: Measured characteristic of test battery

$$E = E_0 + E_1 \ln\left(1 - \frac{1 - SOC}{S_E}\right) \quad (2)$$

V_d is calculated by the following equation.

$$V_d = R\,I + V_a\left(1 - e^{-\frac{|I|}{I_a}}\right) \quad (3)$$

During discharge, R, V_a, and V_g are calculated by the following equations.

$$\textbf{Case}\,(I \geq 0)$$
$$R = R_0 + R_1 e^{-\frac{SOC}{S_R}} \quad (4)$$
$$V_a = V_{a0} + V_{a1} e^{-\frac{1-SOC}{S_a}} \quad (5)$$
$$V_g = 0 \quad (6)$$

During charge, R, V_a, and V_g are calculated by the following equations.

$$\textbf{Case}\,(I < 0,\ SOC < S_b)$$
$$R = R_0 + R_1 e^{-\frac{1-SOC}{S_R}} \quad (7)$$
$$V_a = V_{a0} + V_{a1} SOC \quad (8)$$
$$V_g = V_{ga} e^{\frac{SOC - S_b}{S_g}} \quad (9)$$

$$\textbf{Case}\,(I < 0,\ SOC \geq S_b)$$
$$R = R_0 + R_1 e^{-\frac{1-S_b}{S_R}} \quad (10)$$
$$V_a = V_{a0} + V_{a1} S_b \quad (11)$$
$$V_g = V_{ga}\left(2 - e^{\frac{S_b - SOC}{S_g}}\right) \quad (12)$$

$$S_b = S_{b0} - \beta_b |I| \quad (13)$$
$$S_g = S_{g0} + \beta_g |I| \quad (14)$$

Constants described above are calculated by the following equations.

$$E_0 = E_{00}\,(1 + \alpha_{E_0} T_{25}) \quad (15)$$
$$E_1 = E_{10}\,(1 + \alpha_{E_1} T_{25}) \quad (16)$$
$$S_E = S_{E0}\,(1 + \alpha_{S_E} T_{25}) \quad (17)$$
$$R_0 = R_{00}\,(1 + \alpha_{R_0} T_{25}) \quad (18)$$
$$R_1 = R_{10}\,(1 + \alpha_{R_1} T_{25}) \quad (19)$$
$$V_{a0} = V_{a00}\,(1 + \alpha_{V_{a0}} T_{25}) \quad (20)$$
$$S_{b0} = S_{b00}\,(1 + \alpha_{S_{b0}} T_{25}) \quad (21)$$
$$\beta_b = \beta_{b0}\,(1 + \alpha_{\beta_b} T_{25}) \quad (22)$$
$$S_{g0} = S_{g00}\,(1 + \alpha_{S_{g0}} T_{25}) \quad (23)$$

Table 1 shows these symbols and constants.

Constants

All constants shown in **Table 1** are calculated from only 4 cycles of charge-discharge measurement results shown in **Fig.3** by the least-squares method. The test battery is 70 Ah VRLA battery (SLC70 made by GS Yuasa Corporation).

First, the constants about electromotive force E are calculated from the measurement results of the part of step change.

The constants about voltage drop V_d are calculated from the measurement results of the same part and the relation between E and SOC and T_{25} calculated above.

The constants about voltage rise V_g are calculated from the measurement results during charge and E and V_d estimated from I, SOC, and T_{25}.

It is also possible to simulate without measurements if the constants are scaled by the scaling factor K.

$$K = \frac{C}{70\,[\mathrm{Ah}]} \quad (24)$$

C is the capacity of battery to simulate. **Table 1** shows scaling factors of constants.

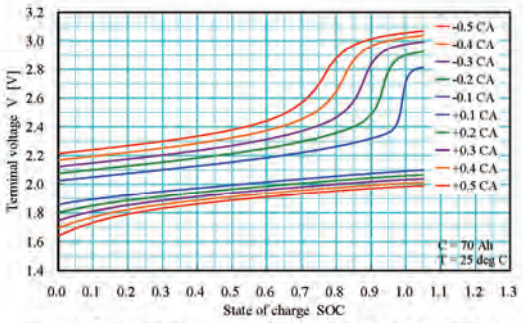

Fig.4: Simulation result from the model (V - SOC)

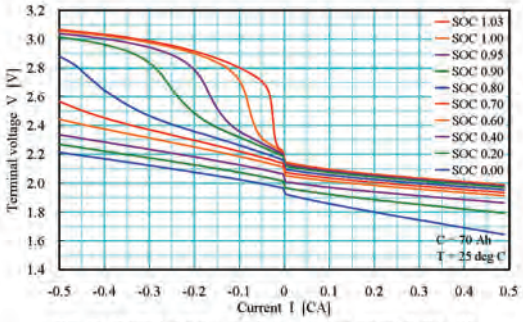

Fig.5: Simulation result from the model (V - I)

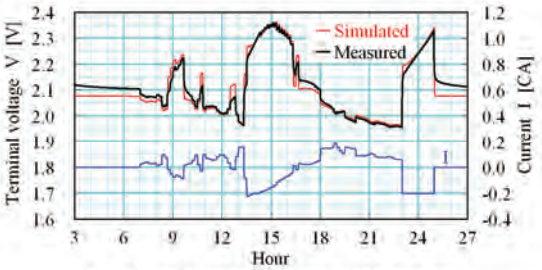

Fig.6: Verification test result (17 deg C)

SIMULATION RESULT

Simulation results from the model are shown in **Fig.4** and **Fig.5**. These results show natural curves. Terminal voltages in various conditions are calculated by a simple calculation of substitution.

VERIFICATION TEST RESULT

Fig.6 shows a verification test result at 17 deg C of battery temperature. At this point, the test pattern of battery current was decided by the PV system simulation based on the irradiance data and the residential electric power consumption data measured in Tokyo.

There are the voltage estimation errors. But the errors are in the small current area, so there are little estimation errors of power. Power estimation error ratio was 0.5 % at 17 deg C and 32 deg C of battery temperature. High precision was confirmed.

CONCLUSIONS

To simulate systems including batteries such as the grid-connected photovoltaic systems that less depends on the utility grid, the authors propose a new simulation model of battery characteristics. It can simulate a battery with high precision without complex handling.

The authors are defining detailed procedure for modeling in order to be more useful.

REFERENCES

[1] K. Kurokawa, S. Wakao, Y. Hayashi, I. Ishii, K. Otani, M. Yamaguchi, T. Ishii, Y. Ono, "Conceptual Study on Autonomy-Enhanced PV Clusters for Urban Community to meet the Japanese PV2030 Requirements", *20th European Photovoltaic Solar Energy Conference and Exhibition*, Barcelona SPAIN, 2005, 6DP.2.3. (Invited).

[2] T. Shimada, K. Kurokawa, "Grid-connected Photovoltaic Systems with Battery Storages Control based on Insolation Forecasting Using Weather Forecast", *Renewable Energy 2006*, Chiba JAPAN, 2006, O-Pv-6-1

[3] T. Shimada, K. Kurokawa, T. Yoshioka, "Grid-connected Photovoltaic System with Battery", *Proceedings of STORE Conference*, Aix-en-Provence FRANCE, 2003, Session 2.

[4] T. Shimada, K. Kurokawa, T. Yoshioka, "Highly Accurate Simulation Model of Battery Characteristics", *Proceedings of Annual Meeting Record I.E.E.JAPAN*, Tokushima JAPAN, 2005, Vol.7, pp.48-49.

Table 1: Symbols and constants of battery simulation model

Symbol	Discharge	Charge	Unit	Scaling	Remarks
V					Terminal voltage
E					Electromotive force of appearance
E_0					E at SOC = 1 (full charge)
E_1					SOC coefficient of E
S_E					SOC curvature of E
E_{00}	2133	2219	mV	1	E_0 at T = 25 deg C
α_{E0}	0.00016	-0.00032	1/℃	1	Temperature coefficient of E_0
E_{10}	589	705	mV	1	E_1 at T = 25 deg C
α_{E1}	0.0028	0.0038	1/℃	1	Temperature coefficient of E_1
S_{E0}	3.082		-	1	S_E at T = 25 deg C
α_{SE}	0.00687		1/℃	1	Temperature coefficient of S_E
V_d					Voltage drop by current
R					Resistance component of V_d
V_a					Maximum of saturation component of V_d
I_a	7.53	5.85	A	K	Current at 63% of saturation component of V_d
R_0					Constant component of R
R_1					SOC component coefficient of R
S_R	0.201	0.167	-	1	SOC shift at 2.7 times of SOC component of R
R_{00}	3.29	5.84	mΩ	1/K	R_0 at T = 25 deg C
α_{R0}	-0.008	-0.017	1/℃	1	Temperature coefficient of R_0
R_{10}	5.97	20.16	mΩ	1/K	R_1 at T = 25 deg C
α_{R1}	-0.039	-0.028	1/℃	1	Temperature coefficient of R_1
V_{a0}					Constant component of V_a
V_{a1}	23	-43	mV	1	SOC component coefficient of V_a
S_a	0.345	-	-	1	SOC shift at 37% of SOC component of V_a
V_{a00}	25	-22	mV	1	V_{a0} at T = 25 deg C
α_{Va0}	-0.029	-0.022	1/℃	1	Temperature coefficient of V_{a0}
V_g					Voltage rise at final phase of charging
V_{ga}	-	213	mV	1	Half of maximum of V_g
S_b					SOC at inflection point of V_g
S_g					SOC curvature of V_g
S_{b0}					Maximum of S_b
β_b					Current coefficient of S_b
S_{g0}					Minimum of S_g
β_g	-	0.00027	1/A	1/K	Current coefficient of S_g
S_{b00}	-	1.044	-	1	S_{b0} at T = 25 deg C
αS_{b0}	-	0.00067	1/℃	1	Temperature coefficient of S_{b0}
β_{b0}	-	0.01066	1/A	1/K	β_b at T = 25 deg C
$\alpha\beta_b$	-	-0.0177	1/℃	1	Temperature coefficient of β_b
S_{g00}	-	0.0146	-	1	S_{g0} at T = 25 deg C
αS_{g0}	-	-0.0272	1/℃	1	Temperature coefficient of S_{g0}

GRID-CONNECTED PHOTOVOLTAIC SYSTEMS WITH BATTERY STORAGES CONTROL BASED ON INSOLATION FORECASTING USING WEATHER FORECAST

Takae Shimada [1, 2], Kosuke Kurokawa [1]

[1] Kosuke Kurokawa Lab., Tokyo University of Agriculture and Technology,
2-24-16 Naka-cho, Koganei, Tokyo, 184-8588 JAPAN
[2] Power Supply Systems Unit, Hitachi Reserch Lab., Hitachi, Ltd.
7-1-1 Omika-cho, Hitachi, Ibaraki, 319-1292 JAPAN

This paper reports an insolation forecasting method and simulation results of a control method of grid-connected photovoltaic systems with battery storages. First, it predicts the global irradiance every one hour by using weather forecast every three hours, and corrects the prediction accuracy by 14 kinds of weather change patterns. Second, it estimates tomorrow's photovoltaic generated power from the insolation forecasting, and calculates the best amount of charge to the battery from the utility grid every night. Simulation results show that providing with battery and using weather forecast are effective in cost, energy efficiency, and dependence on the utility grid.

Keywords: AE-PV system, grid-connected, battery control, insolation forecasting

INTRODUCTION

Most of the photovoltaic (PV) systems for residences spreading rapidly are grid-connected type. Usually, since this system has no electricity storage, the difference between generated and used electric power is processed by electric power flow of the utility grid. In the future so that the PV systems may spread further, it is necessary to develop "Autonomy-Enhanced" PV (AE-PV) system technologies with electricity storage functions that less depends on the utility grid [1]. The authors propose new control method of grid-connected PV systems with battery storages.

OUTLINE OF CONTROL METHOD

The control method of proposal contains the technology of two steps in the PV system configuration shown in **Fig.1**. The technology of first step predicts insolation by using weather forecast announced by the Japan Meteorological Agency (JMA). The technology of second step controls battery storage charging or discharging based on the tomorrow's insolation forecasting.

INSOLATION FORECASTING

Weather and irradiance

The authors investigated the past weather (Fair, Cloudy, and Rain) every three hours of 10 years from 1994 through 2003 based on precipitation and cloud cover observed in the JMA Tokyo point.

The irradiance observed every one hour in the same 10 years and the same point are categorized by the weather, date, and time. And they are calculated the mean value at each category. Base estimation is defined as the calculated mean value of days moving average. **Fig.2** shows one example of the base estimation in the categories of time from 9 to 10 o'clock.

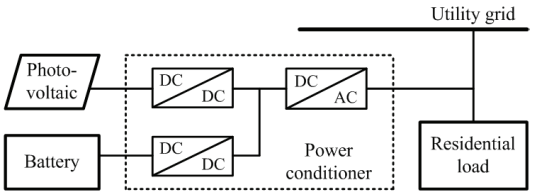

Fig.1: PV system configuration

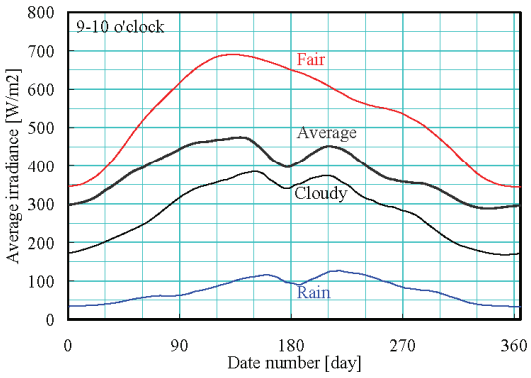

Fig.2: Base estimation (9-10 o'clock)

Weather change pattern

There must be difference between the cloudy close to fair and the cloudy close to rain. Then the observed irradiance are categorized by 14 kinds of weather change patterns, and calculated the mean values at each category. Weather change pattern correction factor is defined as the calculated mean value divided by the base estimation. **Table 1** shows the categories and the correction factors of the weather change patterns. The predicted global irradiance every one hour is estimated by the product of the base estimation and the correction factor.

Table 1: Weather change pattern categories and correction factor

Categories	Fair			Cloudy						Rain				
	1-1	1-2	1-3	2-1	2-2	2-3	2-4	2-5	2-6	3-1	3-2	3-3	3-4	3-5
Correction factor	1.054	1.016	0.884	1.467	1.343	1.224	0.937	0.714	0.598	1.341	1.195	0.983	0.793	0.768
Appearance frequency [times/10years]	14524	4511	6147	620	4173	2667	9794	1648	2676	611	975	958	1029	735
Contained weather change pattern Fair: 1 Cloudy: 2 Rain: 3	11111	11112	112	121	122	12221	12223	22223	123	131	331	133	13331	33333
		11113	113		221	12222	22222	32222	223	132	332	233	13332	
		21111	211			22221	32221	32223	321	231			13333	
		31111	311						322	232			23331	
		21112	212						323				23332	
		21113	213										23333	
		31112	312										33331	
		31113	313										33332	

Results

Insolation forecasting results are shown in **Fig.3** and **Fig.4**. Estimation error ratio (Err_{rat}) is defined as the following equation.

$$Err_{rat} = \frac{\sum_i |Irr_{est_i} - Irr_{msr_i}|}{\sum_i Irr_{msr_i}} \quad (1)$$

$Irr_{est\ i}$ is the predicted global irradiance. $Irr_{msr\ i}$ is the measured global irradiance. In **Fig.3** and **Fig.4**, the result of using weather forecast contains misses of weather forecast. The method of insolation forecasting decreases the prediction error to the half.

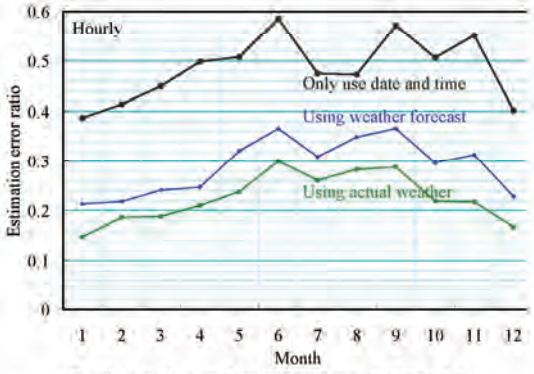

Fig.3: Insolation forecasting result (Hourly)

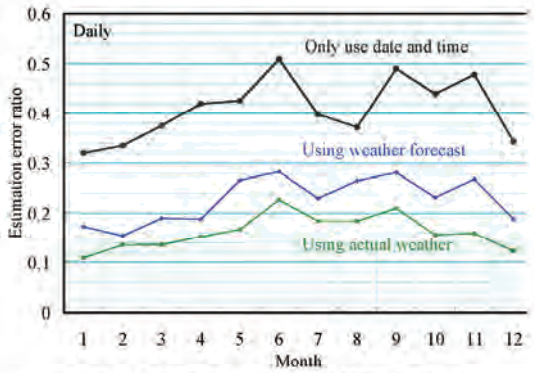

Fig.4: Insolation forecasting result (Daily)

BATTERY CONTROL

Control method

The battery control method calculates the best amount of charge from the utility grid every night. Charging during midnight has advantages in cost because midnight power is cheap. However, it is not good that the battery is charged full, because it has to compensate demand/supply power gap during day time. Then, the method calculates PV power by using insolation forecasting, and calculates demand/supply power gap by using demand forecasting. Therefore, it can calculate the best amount of charge.

The method also schedules equalizing charge plan based on the tomorrow's demand/supply power gap in order to keep the battery's health.

Simulation model

The effect of the control method of proposal is confirmed by the simulation.

- Solar cell model A standard I-V curve is made by the equation (2) based on the equivalent circuit of a solar cell. The curve is converted into various conditions by the following equations of (3) and (4) [2].

$$I = I_{ph} - I_0\left[\exp\left\{q\left(\frac{V + R_s \cdot I}{nkT}\right)\right\} - 1\right] - \frac{V + R_s \cdot I}{R_{sh}} \quad (2)$$

$$I_2 = I_1 + I_{sc}\left(\frac{E_2}{E_1} - 1\right) + \alpha(T_2 - T_1) \quad (3)$$

$$V_2 = V_1 + \beta(T_2 - T_1) - R_s(I_2 - I_1) - K \cdot I_2(T_2 - T_1) \quad (4)$$

- Battery model The authors also propose a battery simulation model shown in **Fig.5**. This model is reported in the references of [3].

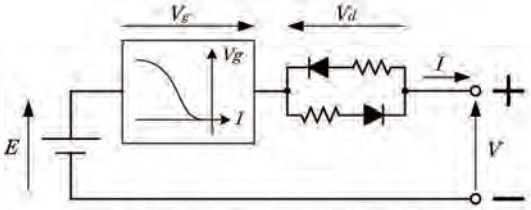

Fig.5: Equivalent circuit of battery

- Power conditioner model Electric power is lost with three converters shown in **Fig.1**. The input power of converter is shown by the quadratic expression of the output power.

Conditions

In this simulation, reverse power flow to the utility grid is limited in order to less depend on the utility grid. If the PV excess power is larger than the permissible reverse power when the battery is charged full, the excess power is summed up to the PV limiting loss.

Installed PV array rated power is decided as annual demand electric energy divided by 1000 hours. The battery capacity is variable.

The simulation uses the irradiance data and the residential power consumption data measured in Tokyo every minute during one year, and also uses the weather forecast announced every day by the JMA.

Results

The simulation results are shown in **Fig.6 to 9**. Battery capacity ratio is defined as the battery capacity divided by the average daily electric energy consumption. Reverse power limiting factor is defined as the permissible reverse power divided by the PV array rated power. PV limiting loss ratio is defined as the PV limiting loss divided by the PV ideal energy.

Fig.6 and **Fig.7** show that using forecast has advantages in both of PV limiting loss and electric bill. If the demand forecasting error will decrease by increasing number of demands such as AE-PV clusters [1], using forecast will have more advantages.

Fig.8 and **Fig.9** show that installing battery has advantages in hard limiting of reverse power. In addition, the effect of increasing battery capacity weakened when the battery capacity ratio exceeded the half.

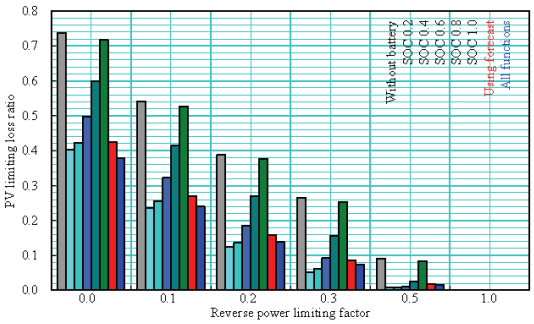

Fig.6: PV limiting loss ratio

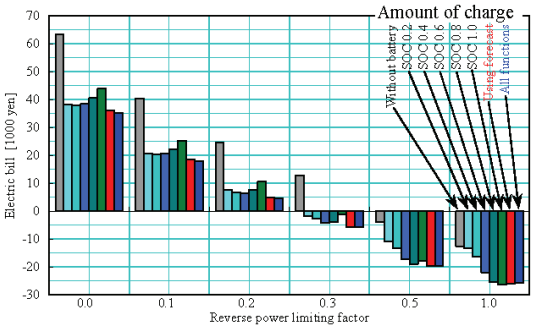

Fig.7: Electric bill

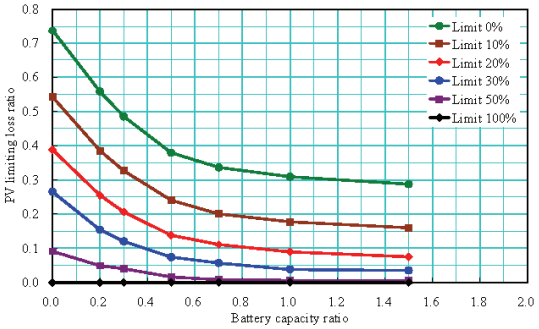

Fig.8: PV limiting loss ratio

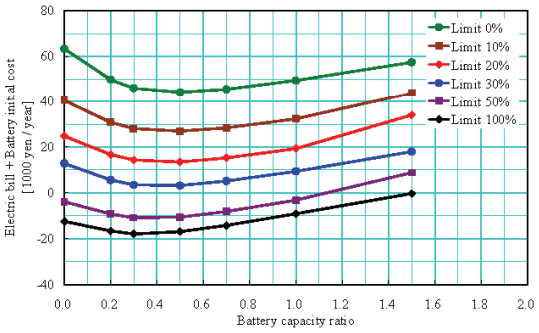

Fig.9: Electric bill added Battery initial cost

CONCLUSIONS

To develop AE-PV system that less depends on the utility grid, the authors propose the insolation forecasting method and the battery control method.

In the PV system limiting reverse power flow, it was confirmed that using weather forecast is effective. In addition, the effect of providing with battery weakened when the battery capacity exceeded the half of average daily electric energy consumption.

The authors are studying the battery control method based on the forecasting in the AE-PV clusters. This work is being supported by NEDO under the Ministry of Economy, Trade and Industry.

REFERENCES

[1] K. Kurokawa, S. Wakao, Y. Hayashi, I. Ishii, K. Otani, M. Yamaguchi, T. Ishii, Y. Ono, "Conceptual Study on Autonomy-Enhanced PV Clusters for Urban Community to meet the Japanese PV2030 Requirements", *20th European Photovoltaic Solar Energy Conference and Exhibition*, Barcelona SPAIN, 2005, 6DP.2.3. (Invited).

[2] Japanese industrial standards committee, "Measuring method of output power for crystalline solar cells", JIS C 8913, 1998.

[3] T. Shimada, K. Kurokawa, "High Precision Simulation Model of Battery Characteristics", *Renewable Energy 2006*, Chiba JAPAN, 2006, P-Pv-1.

CONSIDERATIONS ON POWER LINE ROUTER BY USING MATRIX CONVERTER

Teruo Kamakura[1] Kentaro Hayashi[1] Yasuo Ohashi[1] and Kosuke Kurokawa[1]

[1]Tokyo University of Agriculture and Technology, 2-24-16 Naka-cho, Koganei-shi, Tokyo, Japan

A power line router has been proposed the power flow control when clustered photovoltaic system (PV) is connected with utility. Back-to-Back (BTB that means AC/DC/AC converter) and matrix converter are thought as the power line router. This paper proposes a concept of power line router which is composed of a matrix converter. The matrix converter is based on direct power conversion without any intermediate DC power stage in order to obtain longer life and smaller size than conventional BTB system. Simulation with PSIM ver.6.1 shows active and reactive power flow is controlled independently by matrix converter.

Keywords: matrix converter, virtual indirect method, power line router, Autonomy-Enhanced PV Cluster

INTRODUCTION

The installation of PV has been expanding according to "PV2030 roadmap" in Japan. Generally, distribution voltage and fluctuation become large because of total installation of PV increase. Thus, it has been said that installation of conventional PV system connected with utility has upper limitation. For this matter, the project Autonomy-Enhanced PV clusters (AE-PVC) is proposed [1]. In AE-PVC, as the power flow is normally closed in the community, it is not necessary to synchronize with an external utility. AE-PVC configuration is shown in Fig.1. Electricity is generated by customer's PV, and the electricity that is not used is stored in the AC battery station. If PV could not generate power, the power is supplied by AC battery station. Voltage and frequency inside community are fixed. The electric power of the AC battery station is thought to be insufficient to long time insolation shortage or season change. It is necessary to supply the electric power only of the determine quantity and time from the external utility to prepare for such a low-speed change. At this time, internal community and external utility is asynchronous and it has possibility of different frequency. In addition, inter-community connection is needed when two or more communities are implemented as shown in Fig. 2. In this case, it is required that power flow direction is changed by the speed of PV system generation. In AE-PVC, power line router to supply the controllable electricity is proposed. Proposed power line router should satisfy the independent control of active power and reactive power flow in asynchronous and a different frequency at utility and community or inter-community.

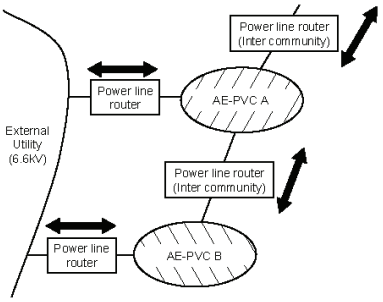

Fig. 2. Overview of AE-PVC.

POWER LINE ROUTER

BTB system and matrix converter using power electronics are considered as a power line router. BTB system needs intermediate DC link capacitors. On the contrary, matrix converter does not need any DC link capacitors and has some advantages such as longevity and miniaturization. Generally, matrix converter is used for driving motor load. In this study, matrix converter is proposed as a power line router from abovementioned reasons. Matrix converter circuit configuration is shown in Fig. 3.

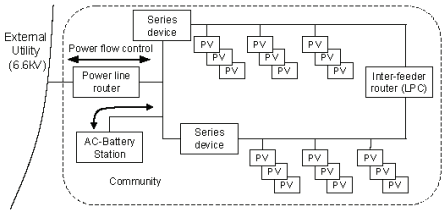

Fig. 1. Community image of AE-PVC.

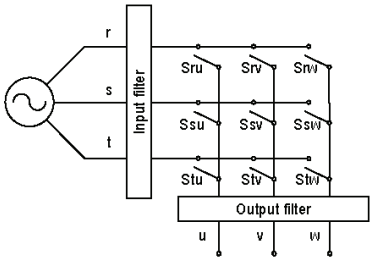

Fig. 3. Matrix converter circuit configuration.

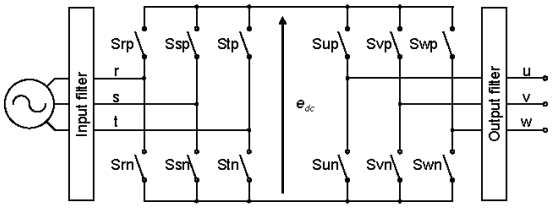

Fig. 4. BTB circuit.

MATRIX CONVERTER CONTROL METHOD

Matrix converter virtual indirect control

In Fig. 3, the relation between input voltage and output voltage can be expressed in eq. (1).

$$\begin{bmatrix} v_u \\ v_v \\ v_w \end{bmatrix} = \begin{bmatrix} s_{ru} & s_{su} & s_{tu} \\ s_{rv} & s_{sv} & s_{tv} \\ s_{rw} & s_{sw} & s_{tw} \end{bmatrix} \begin{bmatrix} v_r \\ v_s \\ v_t \end{bmatrix} \quad (1)$$

s_{mn} is the switching function of switch s_{mn}. The suffix m means r, s, t, and n means u, v, w, respectively. s_{mn} equals to "1" when switch s_{mn} turned on, and s_{mn} equals to "0" when s_{mn} turned off. In matrix converter, it must be $s_{mn} + s_{mn} + s_{mn} = 1$ to prevent short circuit of input voltage source and open circuit of output reactive load current. Fig. 4 shows the main circuit of BTB system (the left side six switches are PWM rectifier and right side six switches are PWM inverter). The same as eq. (1), the relation between input voltage and output voltage can be expressed in eq. (2).

$$\begin{bmatrix} v_u \\ v_v \\ v_w \end{bmatrix} = \begin{bmatrix} s_{up} & s_{un} \\ s_{vp} & s_{vn} \\ s_{wp} & s_{wn} \end{bmatrix} \begin{bmatrix} s_{rp} & s_{sp} & s_{tp} \\ s_{rn} & s_{sn} & s_{tn} \end{bmatrix} \begin{bmatrix} v_r \\ v_s \\ v_t \end{bmatrix} \quad (2)$$

Switching functions in eq. (2), it must be $s_{rk} + s_{sk} + s_{tk} = 1$ and $s_{kp} + s_{kn} = 1$ to prevent short circuit of input voltage source and open circuit of output reactive load current. The suffix k means p, n, in the rectifier side, u, v, w in the inverter side. Generally, if the ideal switching function can be obtained from different topology converters, the waveforms of the input current and the output voltage in different topology converters become exactly the same. Thus, it can be summarized that PWM pulses of the matrix converter is expressed in eq. (3).

$$\begin{bmatrix} s_{ru} & s_{su} & s_{tu} \\ s_{rv} & s_{sv} & s_{tv} \\ s_{rw} & s_{sw} & s_{tw} \end{bmatrix} = \begin{bmatrix} s_{up} & s_{un} \\ s_{vp} & s_{vn} \\ s_{wp} & s_{wn} \end{bmatrix} \begin{bmatrix} s_{rp} & s_{sp} & s_{tp} \\ s_{rn} & s_{sn} & s_{tn} \end{bmatrix} \quad (3)$$

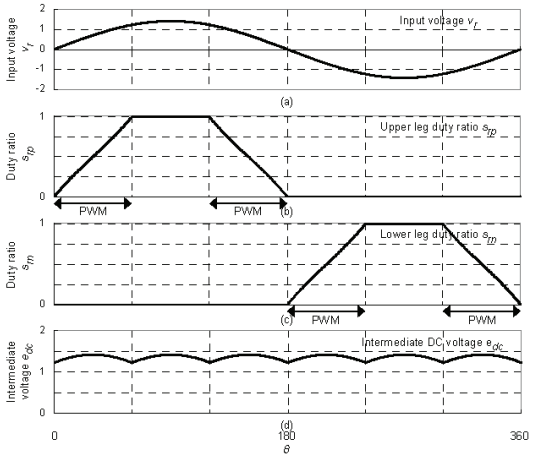

Fig.5 . Virtual current mode rectifier duty and e_{dc}.

The eq. (3) only consists of switching functions ("0" or "1"). Thus, it is easy to calculate by a digital logic hardware and it consists of "AND" gate and "OR" gate. This method consists of virtual rectifier control, virtual inverter control, and PWM pulse pattern conversion. Thus, it can be controlled complex matrix converter

Virtual rectifier control

Input voltage and the virtual rectifier PWM duty (r phase) are shown in Fig. 5. The virtual rectifier switches only operate 240 degree on one period as shown in Fig. 5 (b) and (c). In this rectifier pulse pattern, the intermediate DC voltage e_{dc} includes voltage ripple as shown in Fig. (d).

Virtual inverter control

Duty ratio is a percentage of on-time in triangle waveform period. Thus, numerical multiplication of duty ratio is not always equates to logical "AND" gate calculation. The logical multiplication result of inverter duty D=0.5 for rectifier pulse s_{rp} with the same triangle waveform is shown in Fig. 6.

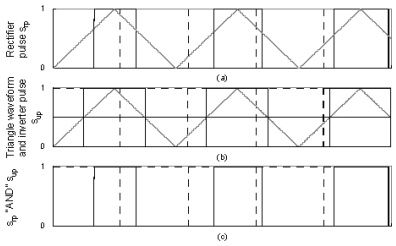

Fig.6 . Relation between rectifier and inverter pulse.

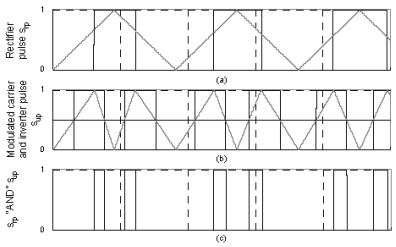

Fig. 7. Relation between rectifier and inverter pulse by using modulated triangle waveform.

It is confirmed that calculation result (c) doesn't become the half of (a). Thus, there is a special triangular modification to solve this problem [2]. In this method, the triangular carrier slope is controlled by converter duty ratio as shown in Fig.7. It is confirmed that calculation result (c) equals to the half of (a). The virtual inverter makes possible to control like the conventional inverter by using modulated triangle waveform.

CURRENT COMMUTATION

Fig.8 shows the circuit of two phase to single phase matrix converter, representing the first two switches in the matrix converter shown in Fig. 3. In steady state, both switch s_{A1} and s_{A2} are on state and both switch s_{B1} and s_{B2} are off. The next steady state switched s_B and switch s_A are off at the same time. Here, both s_A and s_B do not turn on or off simultaneously, open circuit and short circuit occur. In this study, "2-step swithing strategy" as a kind of several multi-step commutation strategies is used to solve this problem [3]. In this method, only the device which carries the current (switch s_{A1} and s_{B1} in this case) is gated at any given time. So, switch s_{A2} and s_{B2} are not used at above description. In this state, turn on of switch s_{B1} is delayed time t_0 from turn off of switch s_A, as shown in Fig. 9. The input voltage sources v_A and v_B are not open. Output current direction is needed in this method. Fortunately, input and output current are controlled in the proposed power line router system as shown in Fig. 10. The controller has output current feedback signal to control output current. Therefore, it doesn't occur any problem.

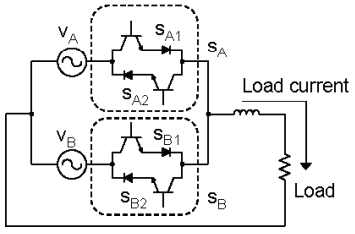

Fig. 8. Two-phase to single phase matrix converter.

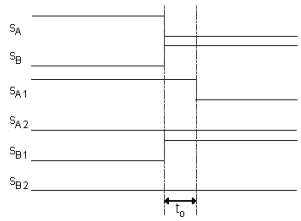

Fig. 9. Timing diagram of two-step commutation.

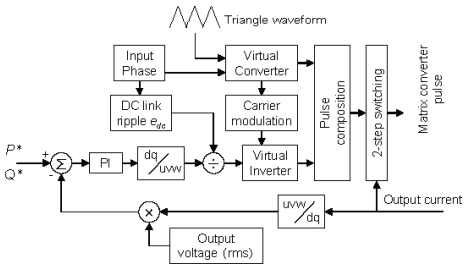

Fig. 10. Block diagram of power line router system.

Table 1. Circuit parameter for simulation

Line impedance	0.025+j0.339 Ohm	L3	600 uH
Triangle waveform	10.5 kHz	C1	10 uF
L1	35 uH	C2	4 uF
L2	250 uH		

SIMULATION AND RESULT

Fig.11 shows the router system configuration in AE-PVC. In this power line router simulation, voltage and frequency of the input community side A and the output community side B are fixed by the ideal AC battery station. Each community is simulated by three-phase voltage source and line impedance. Each frequency is different that two or more introductions of AE-PVC and extreme case are assumed. Therefore, this situation is asynchronous and the frequency is different. Circuit parameter is shown in Table.1.

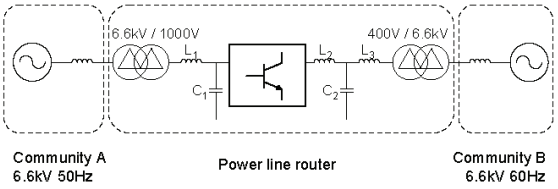

Fig. 11. Router system configuration.

Fig.12 shows the steady-state waveforms of each voltage and current at active power flow control P*=100kW and reactive power flow control Q*=0kVar with constant. It is verified that the power line router provides sinusoidal current with high power factor on different frequency connection. The reverse power flow case (P*=-100kW, Q*=0kVar) is shown in Fig.13. Waveforms (b) and (d) are anti-phase from both (a) and (c).

Fig. 14 shows the power flow direction changing from P=100 kW to -100 kW from 0.5 [s] to 1 [s], and reactive power flow is fixed to 0 kVar. Thus, power flow direction change is verified in this simulation.

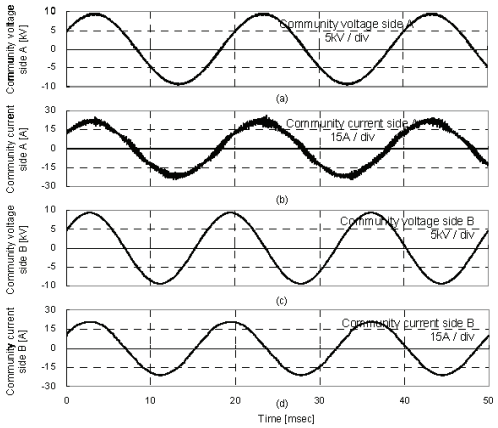

Fig. 12. Waveforms of forward power P*=100kW.

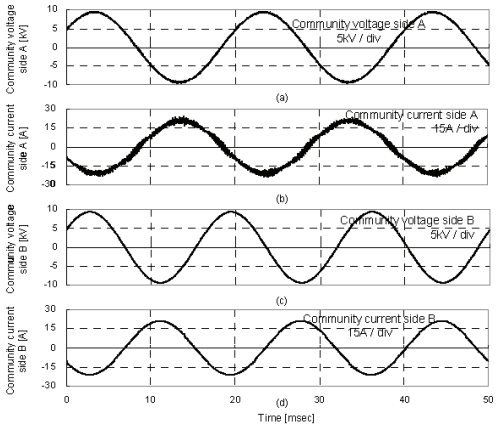

Fig. 13. Waveforms of reversal power P*= -100kW.

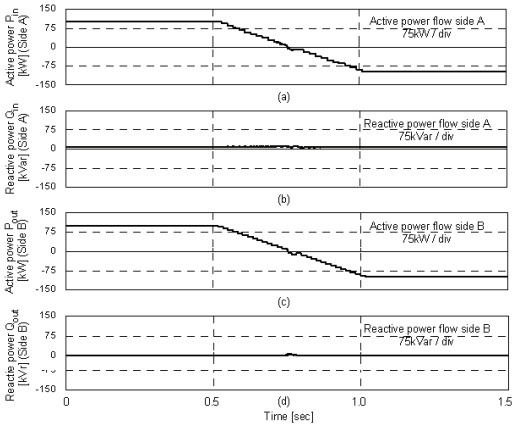

Fig. 14. Independent control of active and reactive power flow and power flow direction change.

CONCLUSION

This paper proposes application of matrix converter based on virtual indirect method to power line router on AE-PVC. An independent control of active and reactive power flow and power flow direction change are shown in the simulations. Thus, it is confirmed that the controls of power line router can be satisfied in the AE-PVC.

Acknowledgement

This study has been carried out as a part of "Autonomy-Enhanced PV Cluster" project founded by New Energy and Industrial Technology Organization (NEDO). The authors wish to thank them for their support.

References

[1] Kosuke. Kurokawa et al., "Conceptual study on autonomy-enhanced PV clusters for urban community to meet the Japanese PV2030 requirements", *20th european photovoltaic solar energy conference*, 2005, pp.2439-2443.

[2] Jun-ichi. Itoh et al., "A novel approach to practical matrix converter motor drive system with reverse blocking IGBT", *IEEE transactions on power electronics*, 2005, pp. 1356-1363.

[3] Patrick W. Wheeler et al., "Matrix converters: a technology review", *IEEE transactions on industrial electronics*, 2002, pp. 276-288.

A new type of scaled-down network simulator for testing PV inverters

Yusuke Nakamura[1], Hirotaka Koizumi[1], and Kosuke Kurokawa[1]
1. Tokyo University of Agriculture and Technology
2-24-16 Naka-cho, Koganei, Tokyo, 184-8588 Japan

This paper describes to design and build the ultra scaled-down network simulator. It is composed of the ultra scaled-down network simulator with electronic circuits and an active power interface (API). The component of the ultra scaled-down network simulator and its fundamental characteristics are described in detail. The simulator can imitate the distribution grid which a lot of distribution generators connected with. Islanding and voltage arising can be tested using the simulator.

Keywords: PV inverter, scaled-down network simulator, distribution generator

1. Introduction

Recently, a number of grid-connected photovoltaic (PV) systems have been rapidly increasing. Moreover, in view of diffusion PV system, a great number of PV systems will be connected to the distribution grid intensively. In addition, a lot of distribution generators as well as PV systems are connected. To test the functions of PV system in such a condition, it is necessary to enlarge experimental equipment, which leads to high construction cost and large space to install.

The purpose of this study is to develop a new scaled-down network simulator which has advantages in size and cost for expanding. In the previous study, the ultra scaled-down network simulator with electronic circuits and an Active Power Interface (API) [1] is proposed. That includes resistance, capacitance and inductance composed with electronic circuit. Using the API, it is possible to connect actual PV inverters to electronic circuit directly.

2. Ultra scaled-down network simulator

2.1 Basic design

An ultra scaled-down network simulator is composed of electronic circuits. The advantage is the flexibility in the expanding and the replacement. In addition, it makes the space and cost reduced. However, it is impossible to connect the actual PV inverters for grid connection with the electronic circuits, because there is a serious difference in the power levels between PV inverters and electronic circuits. A solution is inserting an API between a PV inverter and an ultra scaled-down network simulator.

A basic design of such a simulator is shown in Fig.1. It consists of the ultra scaled-down network simulator and the API. The most significant component in this system is the API, which makes it possible to be connected with actual scale power sources such as a PV inverter.

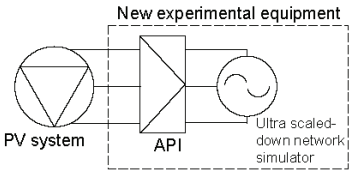

Fig.1.Composition of ultra scaled-down distribution grid simulator.

2.2 Composition of the proposed simulator

A model diagram of the ultra scaled-down network simulator is shown in Fig.2. It is based on the average distribution system in Japan. It is modeled on residential area; low voltage system is 100/200V, single-phase three wire type, and the capacity of transformer is 30kVA. To design a scaled-down model, the capacity and voltage of the distribution system are respectively reduced from 30kVA to 10VA and from 100/200V to 5/10V. Using these scale-factors, impedance, connected loads, and PV output power are calculated by the p.u. method.

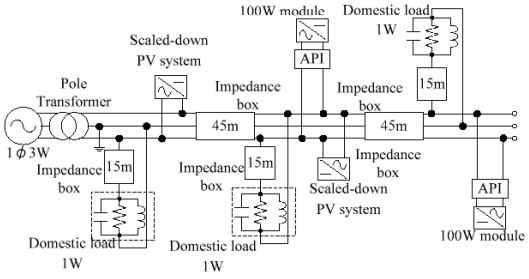

Fig.2. A model diagram of the ultra scaled-down network simulator.

The Ultra scaled-down network simulator includes an AC power supply, pole transformers, low voltage distribution lines, incoming lines, and low voltage loads. The AC power supply is a bipolar power supply which can absorb the reverse power flow from the PV systems. Pole transformer includes resistances and inductances. It is designed from an equivalent circuit of a transformer. Low voltage distribution line consists of resistance and inductance which are connected in series. The impedance is calculated from ACSR-OW120mm^2, and it is assumed up to 90m. Incoming line is consists of resistance and inductance which are connected in series. The impedance is calculated from 3DV3.2mm, and it is assumed 15m. Low voltage load consists of resistance, inductance and capacitance which are connected in parallel. The impedance can be changed by sequential change of the resistance and the inductance. The capacitance is changed in 1μF step. Active power and reactive power are able to be changed variously by adjusting the resistance and the inductance. The all inductances are included in the ultra scaled-down network simulator consist of electric circuit.

PV inverters are connected through the APIs. Instead of a real array, a PV array simulator is used [2]. Scaled-down PV systems will be the ac current sources which perform as PV inverters. They output higher harmonics like PV inverters and have islanding protections.

The view of the installed simulator in our laboratory is shown in Fig.3. The simulator can be set as arbitrary experimental circuits by wiring with jumper leads. The specifications of the ultra scaled-down network simulator compared with the actual scale [3] are shown in Table 1.

Fig.3. Installation situation of the simulator.

Table 1. Specifications of simulator and comparison with actual scale.

	Simulator	Actual scale
Capacity (VA)	10	30k
Voltage (V)	5/10	100/200
Low voltage distribution line (Ω/km)	1.87+j2.18	0.25+j0.29
Incoming line (Ω/km)	17+j0.77	2.3+j0.1
Maximum low voltage load (W)	2.5	7500

2.3 Expansion of ultra scaled-down network simulator

It is easy to expand the proposed simulator because it is composed the electronic circuits. At the present stage it is designed from pole transformer to low voltage loads. For the future, the simulator is to be expanded, which can be applied for various kinds of distribution generators. They may include wind turbines, gas generators, fuel cells etc. as well as PV systems. Those can be scaled down using the scale-factors described in chapter 2.2.

3. Fundamental characteristics of the API

The composition of the API is shown in Fig.4. Fundamental functions of the API are to transfer electrical properties, voltage and current from Terminal 1 to Terminal 2 and vice versa. These two Terminals have different power scale. A PV inverter is connected with Terminal 1, and the ultra scaled-down network simulator is connected with Terminal 2. The voltage V_1 and the current I_1 at Terminal 1 are transferred to Terminal 2 by multiplying factors of $1/n$ and $1/m$, respectively. At the same time, voltage V_2 and current I_2 at Terminal 2 are transferred to Terminal 1 by multiplying factors of n and m, respectively.

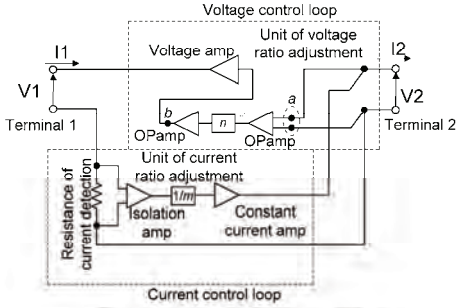

Fig.4. Composition of the API.

3.1 The accuracy of setting voltage ratio and current ratio

The accuracy which the voltage ratio is decided by is examined. An AC voltage source with $0.1V_{peak}$ is connected with Terminal 2. The voltage ratio n is set by the unit of voltage ratio adjustment. It is set from 1 to 60 discretely and the V_1 is measured. The two APIs, API 1 and API 2, are measured. The voltage ratio R_v is calculated from V_1/V_2, the calculation results are shown in Table 2. The error E_{rv} between n and R_v is calculated by $E_{rv}=(n- R_v)/n$. As the results of the calculation, the Erv is within 4.6%.

Table.2 The calculation results V_1/V_2.

Setting	1	2	5	10	20	50	60
API 1	1.0	2.0	5.0	10.0	19.9	47.7	59.6
API 2	1.0	2.0	5.0	10.0	20.0	49.9	59.9

The accuracy which the current ratio is decided is examined. An AC current source with $10mA_{peak}$ is connected with Terminal 1. The current ratio m is set by the unit of current ratio adjustment. It is set from 1 to 40

discretely and the I_2 is measured. The two APIs are measured. The current ratio R_i is calculated from I_1/I_2, and the calculation results are shown in Table 3. The error E_{ri} between m and R_i is calculated by $E_{ri}=(m-R_i)/m$. As the results of the calculation, the Eri is within 5.0%.

Table.3 The calculation results I_1/I_2.

Setting	1	2	5	10	20	40
API 1	1.0	2.0	4.9	9.9	20.0	40.0
API 2	1.0	1.9	5.0	10.0	20.0	40.0

3.2 Frequency characteristics

The frequency characteristics of the voltage control loop from the point *a* to the point *b* in the Fig.4 are measured. The measured results are shown in Fig.5. The gain characteristic is maintained constant gain up to 100kHz, and the phase characteristic is maintained constant phase up to 25kHz. However, if the voltage amplifier is connected, the frequency is limited to 20kHz because of the frequency limitation of the amplifier.

Therefore, the voltage fluctuation up to 20kHz is transferred between Terminal 1 and Terminal 2.

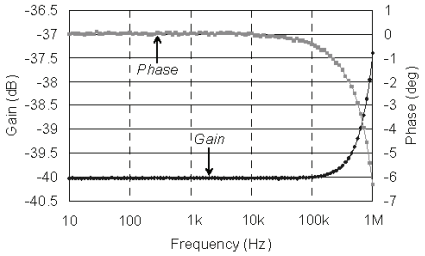

Fig5. The frequency characteristics of the voltage control loop from the point *a* to the point *b* in Fig.4.

The frequency characteristics of the current control loop are measured and the results are shown in Fig.6.

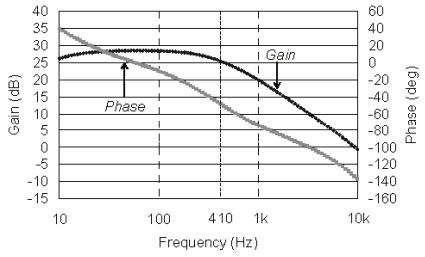

Fig.6 The frequency characteristics of current control loop.

The gain characteristic drops by 3dB at 410Hz. The gain characteristic keeps dropping over 410Hz, which is affected by a low pass filter. If a spike is generated at Terminal 2, the harmonic components flow into positive feedback by the voltage control loop and the current control loop. If an over voltage is output to Terminal 1, PV inverters may be broke down. Thus, the low pass filter is included in the current control loop. The spikes may be generated at turning off of a circuit breaker in islanding tests.

Therefore, the current fluctuation up to 410Hz is transferred between Terminal 1 and Terminal 2.

4. Fundamental characteristics of the inductance [4]

The resistance and the capacitance in the ultra scaled-down network simulator are passive elements. On the other hand, the inductance components are built as electronic circuits by using the Generalized Impedance Converter (GIC) circuit with OP amps. As shown in Fig.7, all inductances in the simulator are the floating inductance; thus neither terminal voltage is connected to ground. It is used for the components of the pole transformers, line impedances and loads.

The circuit diagram is shown in Fig.7 (a), and the equivalent circuit of Fig.7 (a) is shown in Fig.7 (b). The R_5 in Fig.7 (a) is behaved as a inductance L in Fig.7 (b), and given by $L=(C_4 \cdot R_1 \cdot R_3 \cdot R_5)/R_2$.

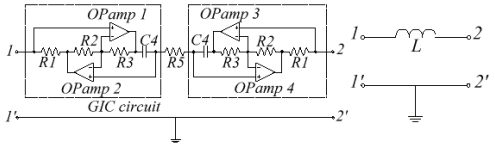

(a) The circuit diagram (b) Equivalent circuit

Fig.7 The floating inductance

The frequency characteristics of the inductance are measured at 1.59, 585, and 1000mH. The measured results are shown in Fig.8 to 10. The phase at 50Hz is 83.5deg, 89.6deg, 88.1deg. The gain characteristic is increased as the frequency is increased up to 400kHz, 18kHz, 3.2kHz. The phase characteristic is maintained 85deg or more up to 12.6kHz, 18kHz, 126Hz. It becomes 0deg at 400kHz, 18kHz, 12.6kHz.

As the results, the phase characteristic of each measured value is 83.5deg or more at 50Hz. And they are maintained 85deg or more up to 126Hz.

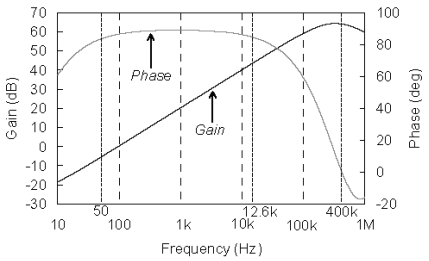

Fig.8 The frequency characteristics of the inductance at 1.59mH.

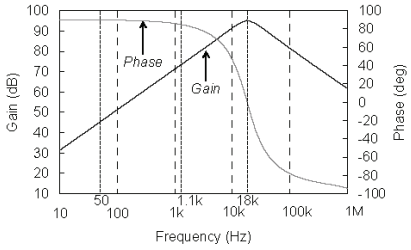

Fig.9 The frequency characteristics of the inductance at 585mH.

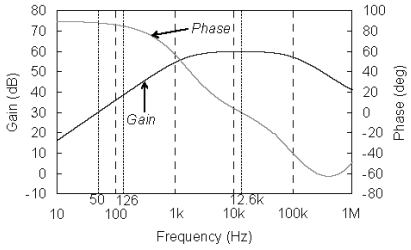

Fig.10 The frequency characteristics of the inductance at 1H.

5. Experimental Results of islanding test

An experimental circuit is shown in Fig.11. It is imitated a distribution system which is the single-phase two-wire type. The AC power supply outputs 5V, 50Hz. The line impedance is set to 0.1+j0.01Ω. The load is set to 0.31 W. The inductance is set to 0.27Var, the capacitance is set to 0.24Var, they are connected in parallel. PV inverters are European AC module (90W). In the both APIs, the voltage ratio is set to 1/46, and the current ratio is 1/20; thus the power ratio is 1/920. In this experiment, one PV inverter is considered as concentration of three PV inverters.

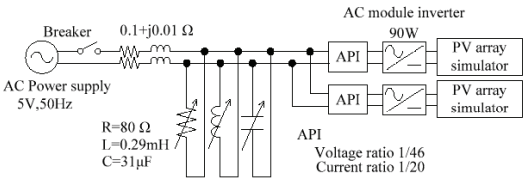

Fig.11 A circuit model for islanding tests.

The experimental wave forms are shown in Fig.12. The grid current is expanded to 10 times and displayed. The power supply from AC power supply stopped at the cutting off point. However, both the inverter 1 and the inverter 2 didn't stop. The islanding operation kept up to 8.5 seconds.

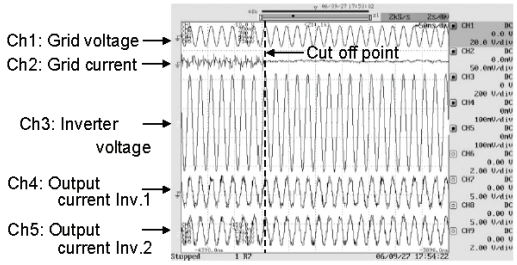

Fig.12 Observed waveforms in the islanding phenomenon. Horizontal: 50msec/div., Vertical: Ch1: 20V/div, Ch2: 500mA/div, Ch3: 200V/div, Ch4: 1A/div, Ch5: 1A/div

6. Conclusion

A new experimental equipment for PV inverters has been designed and built. Fundamental characteristics of the API and the inductance have been confirmed. Islanding phenomena have been observed with the proposed system. For the future, islanding and voltage arising will be tested in various experimental circuits. And the simulator is to be expanded, which can be applied for various kinds of distribution generators.

Acknowledgement

This study had been carried out as a part of "Autonomy-Enhanced PV Cluster" project funded by New Energy and Industrial Technology Organization (NEDO). The authors wish to thank them for their support.

Reference

[1] K. Takeuchi et al. "A new type of scaled-down network simulator composed of power electronics", in Proc. 3th World Conference and Exhibition on Photovoltaic Solar Energy Conversion, May 2003, pp.2039-2042 vol.2

[2] H. Matsukawa et al, "Dynamic evaluation of maximum power point tracking operation with PV array simulator", Solar Energy Materials & Solar Cells, 75, (2003) pp537-546

[3] Y. Nakamura, et al. "Development of test equipment for PV inverters with ultra scaled-down distribution grid" Proceedings of 17th Annual Conference of Power & Energy society IEE-J, No.182, pp.10.3-10.4.

[4] Y. Nakamura, et al. "Performance Assessment with Different Inductance Model in the ultra scaled-down distribution grid simulator", in Proc. 20th European Photovoltaic Solar Energy Conference and Exhibition, June 2005, pp.2798-2801

A FUNDAMENTAL EXPERIMENT OF SOLAR CELL'S I-V CHARACTERISTICS MEASURMENT USING LED SOLAR SIMULATOR

Jun Koyanagi[1] and Kosuke Kurokawa[1]

Tokyo University of Agriculture and Technology, 2-24-16 Naka-cho, Koganei-shi, Tokyo, 184-8588 Japan
Phone & Fax: +81-42-388-7445, E-mail: 50005645111@st.tuat.ac.jp

A solar simulator using LED (light-emitting diode) lamps can measure low-cost to current-voltage (I-V) characteristics compared with using Xenon lamp. Until now, we calculated the crystalline silicon's (c-Si) I-V characteristics under the standard test condition (STC) using two I-V characteristics measured under the different irradiance using white LED. However, calculated current is too small compared with using Xenon lamp. In this paper, we added new methods for calculating I-V characteristics of c-Si using dark current and absolute spectral responses. As the results, accuracy of the calculated I-V characteristic was improved compare with the previous method.

Keywords: LED, solar simulator, I-V measurement

INTRODUCTION

Current-voltage (I-V) characteristics under the standard test condition (STC) are important data to evaluate c-Si cell's performance. Normally, I-V characteristics are measured by 1-Sun solar simulator using Xenon lamp. However the cost of measurement is expensive because the facility is so large and electric power consumption is also large. Additionally, it has spectral mismatch because Xenon has characteristic spectrum in infrared band. Therefore, we have been proposed a solar simulator using LED (light-emitting diode) lamps which take advantage of its lifetime, electric power consumption and cost. Characteristics of LED ,for example spectrum and irradiance, are different from reference solar spectrum, so we also have been proposed calculation method that can calculate the c-Si's I-V characteristics under the STC by interpolation method using bilinear I-V characteristics measured with White LED or monochromatic LED irradiance source [2]. The method of I-V characteristic measurements using LED solar simulator is able to measure without spectral mismatch because it uses reference solar spectrum and monochromatic lights to calculate absolute spectral response [1]. However, irradiance of the White LED is very weak, so it was extrapolated to calculate 1-Sun I-V characteristic using bilinear I-V characteristics (approximately 1.5 and 1.0[mW/cm^2]). In other words, the difference of irradiance is so small (approximately 1/70 of the 1-Sun) that an error of measurement is too much expanded. It is also difficult to stabilize LED's irradiance and temperature during measurement of two I-V characteristics. Therefore, calculated 1-Sun I-V characteristic is smaller than nominal I-V characteristics. In this paper, we improve the accuracy of calculated I-V characteristic including spectral response using LED solar simulator by using I-V characteristics which measured with all LED and dark current. The irradiance of all LED is approximately 1/9 of the 1-Sun.

EXPERIMENTS

Spectral responses at discrete wavelength are derived by three monochromatic LED. Experimental discrete spectral responses are supplemented by a theoretical characteristic of photocurrent, and the whole spectral responses characteristic of the test cell is calculated. Total output power under the STC (calculated short circuit current (I_{sc})) is obtained in integrating spectral responses and reference solar spectral irradiance distribution. Flow chart to calculate I_{sc} is shown by figure 1.

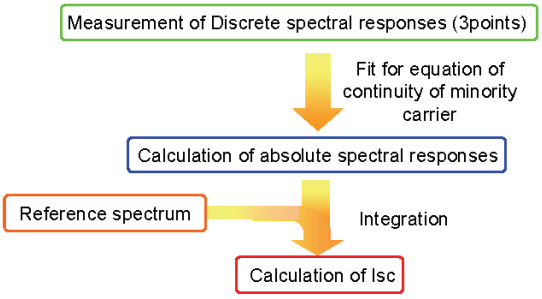

Fig.1. Flow chart to calculate I_{sc}.

I-V characteristic on STC (nominal I-V characteristic) is obtained from two I-V characteristics, which measured by LED solar simulator and dark current. Dark current and one I-V characteristic measured by 1/9 of the 1-Sun are used. To stabilize LED's irradiance and temperature is easier than using two measured I-V characteristics, which measured with different irradiance.

Experimental Details

The detail of experiment for measuring I-V characteristics of c-Si cell using LED solar simulator is shown in figure 2. C-Si cell that used experiment is packaged one. The cell size is 10×10 [cm^2]. Irradiance

is measured with an optical power meter, c-Si cell's back-surface temperature is measured with thermocouples and power supply is used bipolar DC source. Temperature of the cell is stabilized at 25 [deg. C] by airflow. It takes around one half hour to warm up LED solar simulator to stabilize irradiance.

LED solar simulator has 4colors of irradiance sources (Blue, Red, Infrared and White), which are designed for uniform power distribution. The detail of LED's property is shown in table 1.

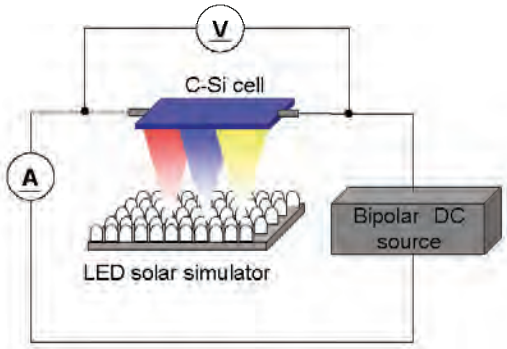

Fig 2. Configuration of measuring c-Si cell using LED solar simulator.

Table 1. The detail of LED's property.

	Blue	Red	Infrared	White
Peak wavelength [nm]	466	646	950	-
Irradiance [mW/cm^2]	3.0	2.5	4.0	1.5

RESULTS AND DISCUSSION

Spectral response

Figure 3 shows the packaged c-Si cell model. Packaged c-Si cell consist of grass, ethylene vinyl acetate (EVA) and Si. Spectral response which packaged c-Si cell is different from raw c-Si cell for ultraviolet (UV) absorber included in EVA, which absorbed UV band (>400nm). Hence, we made approximate expression from its characteristic and integrate it for improve calculation result of SR. Function of absorption feature $f(\lambda)$ is

$$f(\lambda) = 1 - \frac{1}{1 + e^{\frac{\lambda - \lambda_0}{a}}} \quad (1)$$

Here, a is rate of change and λ_0 is center of wavelength of absorption. These values are determined a is 2 and λ_0 is 395[nm] to fit the data sheet. Spectral response is calculated by integrating this function.

Figure 4 shows measurement of discrete spectral responses and comparison of integration result and previous result. At UV bands (<400nm), calculated spectral response is good at previous result. Additionally, discrete spectral responses are increased due to improve measuring device. The result of calculated I_{sc} is 3.41[A]. However, this result is smaller than nominal I_{sc} (3.76[A]). It is thought that spectral response at infrared band (>700nm) is underestimated.

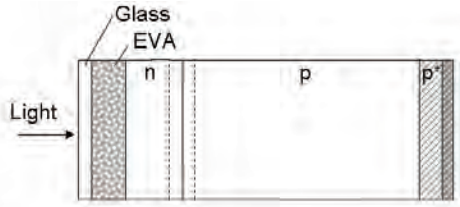

Fig. 3. Packaged c-Si cell's model.

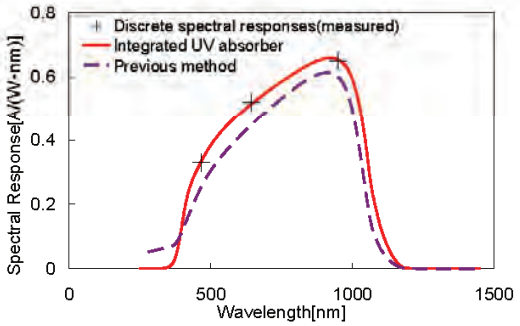

Fig. 4. Comparison of spectral responses between integration result and previous result.

I-V characteristics

Figure 5 shows measured I-V characteristics using white LED and the result of 1-Sun I-V characteristic calculation. The difference of two measured I-V characteristics is so small and close to zero that it can't measure using current meter. Thus, at higher bias voltages (>0.5[V]), the characteristics are need to supplement by theoretical characteristics of diode.

On the other hand, figure 6 shows measured I-V characteristic using all LED, dark current and the result of 1-Sun I-V characteristic calculation. Compared the result using white LED, the difference of two measured I-V characteristics is become clear. Calculated I-V characteristic doesn't become smooth line at higher bias

voltages (>0.5[V]). It caused by increasing of current in cell from bipolar DC source that generates heat in consequence of internal resistance. Temperature controlled within ±0.5 [deg. C] when I-V characteristics measured, although the error of measurement was expanded due to extrapolate calculate method.

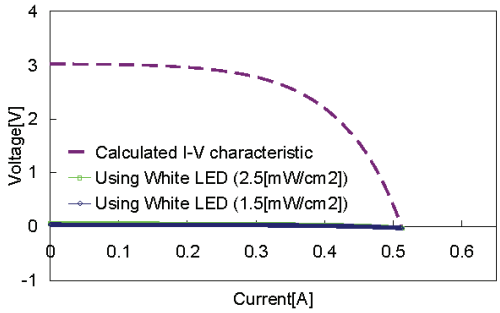

Fig. 5. Calculated I-V characteristic using different irradiance of White LED.

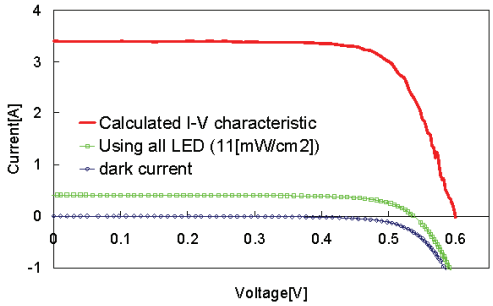

Fig. 6. Calculated I-V characteristic using dark current and all LED.

Table 2. Comparison of measured and calculated solar cell's property.

	Previous method	Calculated I-V characteristic	Nominal I-V characteristic
I_{sc} [A]	3.023	3.410	3.760
V_{oc} [V]	0.513	0.600	0.603
Maxmum Power (Pmax) [W]	0.907	1.535	1.554
Voltage at Pmax [V]	0.368	0.477	0.461
Current at Pmax [A]	2.467	3.219	3.370

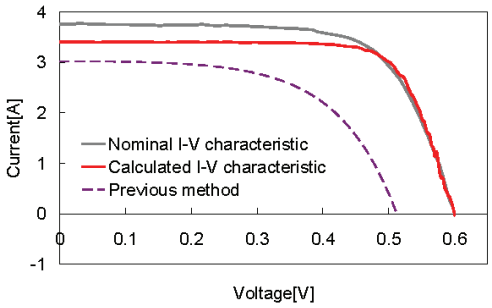

Fig. 7. I-V characteristics compared with measured by 1-Sun solar simulator and previous method data.

Figure 7 shows the comparison of I-V characteristics between calculated and nominal I-V characteristic. And the detail of I-V characteristics is shown by table 2. Calculated I-V characteristic is more approximate to the nominal I-V characteristic than previous method. Therefore, the value of Pmax is improved. However, calculated I-V characteristic is underestimated I_{sc} compared with the values that measured by 1-Sun solar simulator. Thus, fill factor was overestimated.

Verification using nominal I_{sc}

Accuracy of calculated I-V characteristics is verified by using nominal I_{sc}. Figure 8 shows the result of the I-V characteristic calculation. I-V characteristic which calculates previous method is underestimated at higher voltage. On the other hand, calculated I-V characteristic using all LED is improved compared with previous method. However, the I-V characteristic is overestimated near Pmax. Even though all LED used, its irradiance was much smaller than 1-Sun. Consequently, series resistance (R_s) might be ignored and the error of measurement was expanded.

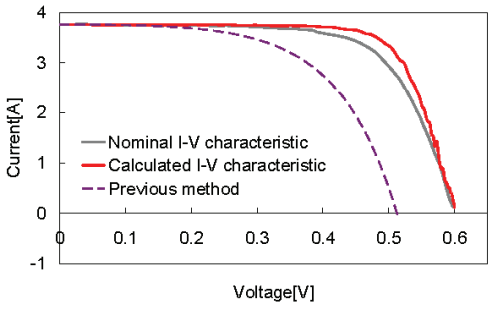

Fig.8. Comparison of nominal I-V characteristic and calculated I-V characteristics using nominal I_{sc}.

On this account, formula (2) is used for the correction of calculated I-V characteristic.

$$V_2 = V_1 - R_S(I_2 - I_1) \quad (2)$$

Here, V_1 and I_1 are voltage and current of the former value, respectively. V_2 and I_2 are corrected value. The value of R_s (=0.01[Ω]) was determined to best fit the experience. Figure 9 shows the result of I-V characteristics using nominal I_{sc} and correction formula using R_s. The corrected result is almost same as nominal I-V characteristic so that it is important to improve the accuracy of calculated I_{sc} and to consider R_s.

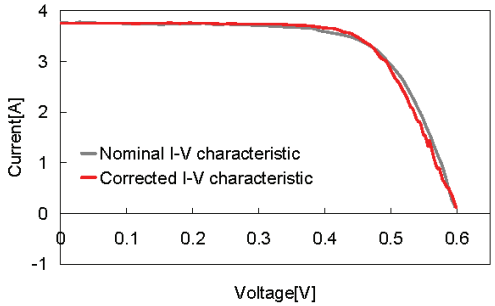

Fig.9. Comparison of corrected I-V and nominal I-V characteristics.

CONCLUSION

This paper describes calculation results with extrapolation method using LED solar simulator. Accuracy of the calculated I-V characteristic is improved using dark current and 1/9 of the 1-Sun irradiance compared with the previous method that is using two reference I-V characteristics measured with LED. It is obtained that the result using nominal I_{sc} and R_s correction is almost same to nominal I-V characteristic.

ACKNOWLEDGMENTS

This research was supported by the Ministry of Education, Science, Sports and Culture, Grant-in-Aid for Exploratory Research.

References

[1] Shogo Kohraku, Kosuke Kurokawa. "A fundamental experiment for discrete-wavelength LED solar simulator" 14th International Photovoltaic Science and Engineering Conference (2004)

[2] Hishikawa Y, Imura Y, Oshiro T. "Irradiance-dependence and translation of the I-V characteristics of crystalline silicon solar cells." Jpn. J. Appl. Phys. Part2, 39-7A (2000) L6

[3] F.J.Pern. "Factors That Affect The EVA Encapsulant Discoloration Rate Upon Accelerated Exposure", 1st WCPEC pp.897-900 (1994)

The Development of FPGA-based Digital Controller for PV Inverter

Yusuke Seo[1], Kosuke Kurokawa[1]
[1]Tokyo University of Agriculture and Technology, 2-24-6 Naka-cho, Koganei, Tokyo, 184-8588, Japan,
Phone: +81-42-388-7445, Fax: +81-42-388-7132, E-mail: 50005645118@st. tuat.ac.jp

The development of the FPGA based digital controller for the PV inverter with the typical full-bridge inverter is described. The authors have developed the current control function, the grid connected control function and the MPPT control function using the FPGA. As results of the experiments, the inverter was able to connect the grid in two current control methods. In addition, the MPPT control function was mounted on the FPGA and the stable operation was confirmed. It is presented that the lower control (waveform control etc.) and the higher control (MPPT control) can be controlled by only one FPGA.

Keywords: PV, inverter, digital controller, FPGA

Introduction

According to the Japanese PV2030 roadmap, 100GW cumulative Photovoltaic (PV) installation is expected up to 2030. Japanese domestic market size may be assumed 10 to 20GW/Y [1]. It is necessary that the PV module and the Power conditioner etc. will be mass processed by a production line. In this research, Field Programmable Gate Array (FPGA) which has been mass produced is used as the digital controller for the PV inverters. Now, the current control method for single phase inverter with FPGA has been developed [2], where control responsiveness and high speed calculation of FPGA are shown. However, this control method is not for only the PV inverter. So, the unique control functions for the PV inverter, for example Maximum Power Point Tracking (MPPT) and Islanding detection, have not included.

In this paper, the development of the FPGA based digital controller for the PV inverter with the typical full-bridge inverter is described. The authors have developed and tested the current control function, the grid connected control function and the MPPT control function using the FPGA. The circuit configuration and the experimental results are shown.

Field Programmable Gate Array

FPGA is a logical device that contains a matrix of reconfigurable gate array logic circuitry. Therefore, it is the device which holds the advantages of both, high-speed operation which is feature of the hardware and adaptability which is feature of the software. In addition, FPGA has a function of parallel processing. So, FPGA is possible to utilize in various applications.

Circuit Design within FPGA

As the FPGA controller for the PV inverter, two current control methods are designed. One is the “sensor type” which senses the current reference waveform from the grid voltage waveform. The other is the “data type” which previously stores the current reference waveform data in the FPGA.

Fig.1 shows the block diagram of the constant current control in the “sensor type”. The analog signal of the current reference and the inverter output current converted into digital signal are sent into the FPGA. In the FPGA, the inverter output current is controlled with P control method and the FPGA outputs the PWM signal. The advantage of this method is a high-speed response. The defect is that the distortion of the grid voltage waveform influences the inverter’s output current waveform.

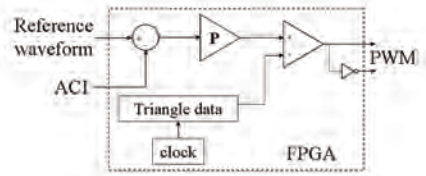

Fig.1.Block diagram of the “sensor type”.

Fig.2 shows the block diagram of the “data type”. Only phase information is extracted from the analog signal of the current reference, the cycle pulse which has the phase information of the grid was input into the FPGA. In synchronous control, the time cycle of the cycle pulse is counted by the counter. The counter outputs the count value which is the frequency information of the cycle pulse. And the frequency of the inverter’s output current is decided by the count value. The digital data is stored in the FPGA for the current reference. After synchronous control, constant current control is applied, and PWM signal is given to the gate-drive IC. The logic of constant current control is the same to the “sensor type”. The advantage of this method is that the inverter can maintain the clean output current waveform. The defect is the response of the output current delays one cycle because the Digital Phase Lock Loop (PLL) uses the frequency of the former period.

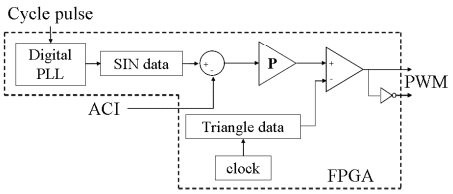

Fig.2.Block diagram of the "data type".

Fig.3 shows the circuit model. The particular parameters for the system are shown in Table I. The I_d shows the DC current. The i_o shows the inverter's output current and the i_g shows the current which flows into the R_L(load) from the grid. The ACI, the *ACV*, the *DCI* and the DCV show the signals which are detected from the main circuit. The ACI detects i_o and the *ACV* detects v_g. The *DCI* detects I_d and the *DCV* detects V_d. They are used for the inverter control. The *DCI* and the *DCV* are used for the MPPT.

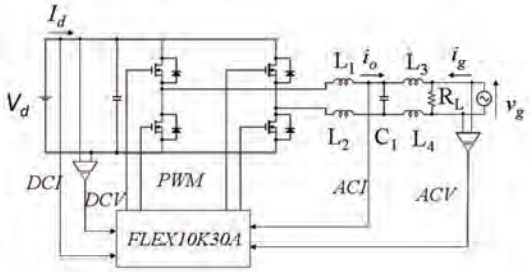

Fig.3.Circuit configuration.

Table 1.Circuit Parameters.

V_d 32V	v_g 40V_{P-P}
L_1, L_2, L_3, L_4 430μH	C_1 4.75μF
R_L 50Ω	Currier frequency 50kHz
FPGA *FLEX10K30A*	MOS-FET *IRF644*
Gate Driver *IR2108*	AD Converter *ADC0820*

Experimental condition

In the experiments of the constant current control, a DC voltage source was used. The current reference waveform was supplied by a function generator. The inverter was not under the grid-connected condition.

In the experiments under the grid connected condition, a DC voltage source was used. The scale-down grid voltage waveform which was a reduced grid voltage waveform with a transformer was used on AC side.

Constant current control

Fig. 4 and Fig. 5 show the observed waveforms of the current reference waveform v_{ref} and the inverter output current waveform i_o in the "sensor type" and the "data type". In this condition, the AC power source was disconnected. The $v_{ref}$was supplied by the function generator. From these results, both the "sensor type" and the "data type" operate stably in steady state.

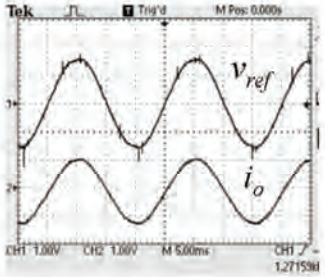

Fig.4.Observed waveforms of v_{ref} and i_o in the "sensor type". Horizontal: 5ms/div., Vertical: v_{ref}: 1V/div., i_o: 1A/div.

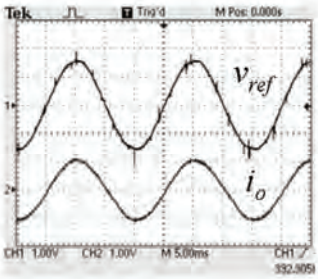

Fig.5.Observed waveforms of v_{ref} and i_o in the "data type". Horizontal: 5ms/div., Vertical: v_{ref}: 1V/div., i_o: 1A/div.

Fig. 6 and Fig. 7 show the step response of the inverter output waveforms in transient state. Fig 6 shows the result of the "sensor type". The inverter output the current waveform just as the step input. So it is confirmed that this method is possible to respond to high-speed. Fig 7 shows the result of "data type". The inverter outputs the current waveform one cycle lately from the step input, because the frequency is counted for the first cycle and the Digital PLL uses the counted value for the next output.

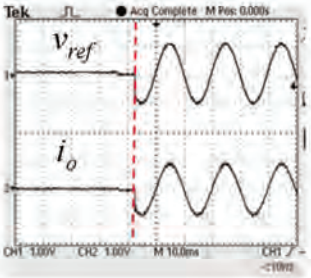

Fig.6.Observed waveforms of v_{ref} and i_o in transient state in the "data type". Horizontal: 10ms/div., Vertical: v_{ref}: 1V/div., i_o: 1A/div.

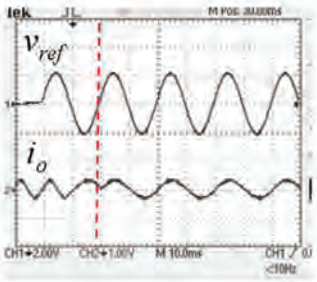

Fig.7.Observed waveforms of v_{ref} and i_o in transient state in the "data type". Horizontal: 10ms/div., Vertical: v_{ref}: 2V/div., i_o: 1A/div.

Experiments under the grid-connected condition

Fig. 8 and Fig. 9 show the observed waveforms of v_{ref}, i_o and the scale-down grid voltage v_g which is a reduced grid voltage waveform with a transformer. Fig. 8 shows the observed waveforms in the "sensor type" and Fig. 9 shows the result in the "data type". The i_o synchronized the v_g in both types. This result means that the inverter operates under the grid-connected condition in Power factor 1. It was confirmed that the inverter can output stably in both types.

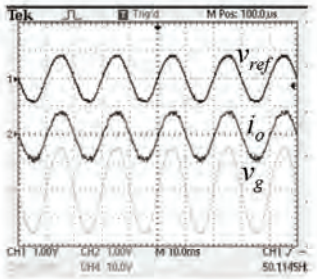

Fig.8.Observed waveforms of v_{ref}, i_o and v_g in the "sensor type". Horizontal: 10ms/div., Vertical: v_{ref}: 1V/div., i_o: 1A/div., v_g: 10V/div.

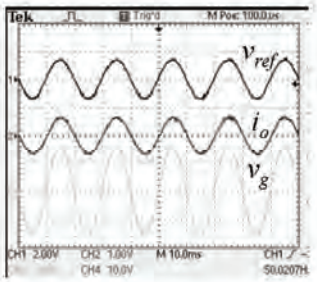

Fig.9.Observed waveforms of v_{ref}, i_o and v_g in the "data type". Horizontal: 10ms/div., Vertical: v_{ref}: 1V/div., i_o: 1A/div., v_g: 10V/div.

Fig. 10 and Fig. 11 show the results of analysis of the output current distortion under the grid-connected condition. Fig. 10 shows the result in the "sensor type". The 9th and 11th harmonics were more than 3%, and the Total Harmonics Distortion (THD) was 6.01%. In this cause, the influence of the transformer characteristic which was used is considered. THD of the scale-down grid voltage waveform was 1.97%. On the other hand, Fig. 11 is the result of the "data type". In this case, the harmonics of each degree were less than 3%, and The THD was 3.49%. The As the results, the "data type" satisfied the stipulation of the technical guide in Japan [3].

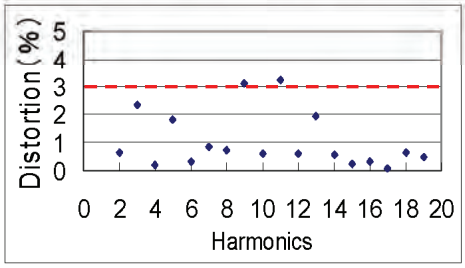

Fig.10. Distortion of output current in the "sensor type".

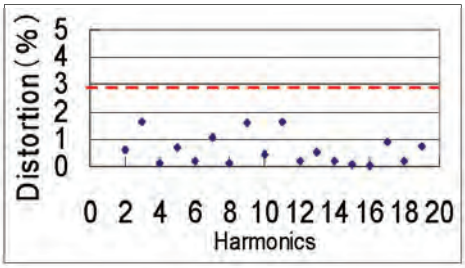

Fig.11. Distortion of output current in the "data type".

MPPT control using the FPGA

System configuration

The system was configured from a ready-made FPGA board, main board, AD converter board and voltage sensor board. The cement register (50Ω40W) was used as load. Instead of a PV module, a DC voltage source was used. In addition, the potentiometer was connected in series, so the I-V curve of PV was simulated. The bipolar power source which can operate in four quadrants was used on AC side.

MPPT control logic

Various MPPT control logics have been developed, in this paper, authors used the method that adjusting the

parameter k changes the i_o, therefore V_d and I_d are controlled by adjusting the parameter k [4]. The output of the MPPT loop is the parameter k that can control the output the inverter's output current. The inverter's output i_o is given by the following equation (1):

$$i_O = i_{O\_MAX} \times k \qquad (1)$$

where i_o shows the value of the inverter output current, i_{o_MAX} shows the value of rated current, and $k(0 \le k \le 1)$ shows the parameter of the inverter operation.

To decide the maximum power point, the P&O method [5] is used. Fig 12 shows the block diagram in the FPGA. The high-speed loop (constant current control and PWM control) was configured by the"data type". In the FPGA, this high-speed loop and the MPPT loop was designed in parallel. The MPPT loop outputs the parameter k, and the high-speed loop receives this value. Therefore, the inverter changes control its power toward the MPP.

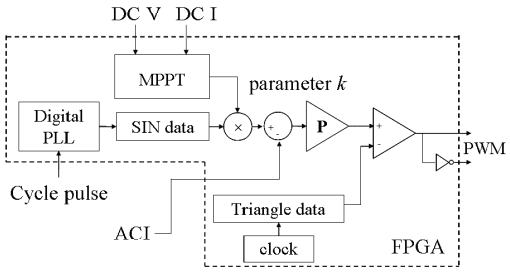

Fig.12. Block diagram of the FPGA mounting the MPPT.

Experimental results of MPPT function

Fig. 13 shows the observed waveforms. The DC current waveform I_d and the inverter's output current waveform i_o increase gradually, and the DC voltage waveform V_d decreases. On the other hand, the grid voltage waveform v_g is constant. The waveforms show that the inverter increases its output power, so the MPPT control operates normally. Additionally, the AC current waveform i_g increases. The reverse current from the inverter flows into the grid in this condition, so the phase of the i_o is in reverse compared to the v_g.

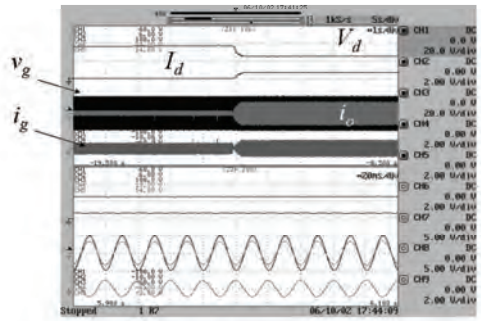

Fig.13. Observed waveforms of V_d, I_d, v_g, i_o and i_g in the MPPT operation. Horizontal: (up): 1s/div., (down): 20ms/div., Vertical: V_d: 20v/div., I_d: 2A/div., v_g: 20v/div., i_o: 2A/div., i_g: 2A/div.

Conclusion

This paper has presented a prototype of the digital controller based on FPGA for PV inverter. The experiments were carried out utilizing FLEX10K30A FPGA (ALTERA Corp.). The "sensor type" and the "data type" have been developed, and the inverter is able to be connected to the grid in both types. In addition, the MPPT control function is mounted on the FPGA and the stable operation has been confirmed. The lower control (waveform control etc.) and the higher control (MPPT control) are realized by only the FPGA.

Acknowledgement

This study had been carried out as a part of "Autonomy-Enhanced PV Cluster" project funded by New Energy and Industrial Technology Organization (NEDO). The authors wish to thank them for their support.

References

[1] K. Kurokawa, "Mass Production Scale of PV Modules and Components in 2030s and beyond" *in Proc. 15th International Photovoltaic Science & Engineering Conference (PVSEC-15)*, pp272-274, Shanghai, China, Oct 11-15, 2005.

[2] T. Komiyama et al., "Current Control Method Using Voltage Deadbeat Control for Single Phase Utility Interactive Inverter with FPGA based Hardware Controller", *in proc. The 30th Annual Conference of the IEEE Industrial Electronics Society*, Busan, Korea, November 2-6, 2004.

[3] Japan Electric Association., "Grid interconnection code", 2006

[4] T. Kaito et al., "Development of MPPT Algorithm for a Digital controlled PV inverter", *in proc. 14th International Photovoltaic Science & Engineering Conference (PVSEC-14), Bangkok, Thailand,* January 27-30, 2004.

[5] D. P. Hohm et al., "Comparative Study of Maximum Power Point Tracking Algorithm Using an Experimental, Programmable, Maximum Power Point Tracking Test Bed", *in proc 28th IEEE Photovoltaic Specialists Conference(PVPC-28)*, pp1699-1702, Anchorage, Alaska, September, 2000

Spectral Error Analyses of Pyranometers Composed of Multiple Photodiodes

Keiji Hirata[1], Yukiharu Miyake[2], Kouzou Nakamura[2], Tadashi Kato[2] and Kosuke Kurokawa[1]

[1] Tokyo University of Agriculture and Technology, 2-24-6 Naka-cho, Koganei, Tokyo, 184-8588, Japan

[2] EKO Instruments Co., Ltd., 2-1-6 Sasazuka Shibuya-ku Tokyo 151-0073, Japan

In order to develop a cheap, stable, and high performance pyranometer, we propose the dual sensor pyranometer which measures the irradiance based on the outputs from two kinds of photodiodes. The first photodiode detects the short wavelength range of the irradiance, and the other detects the long wavelength range of the irradiance. To evaluate only the spectral error in pyranometer composed of photodiodes, the method to calculate outputs from each photodiode was developed. As the result, the spectral error in "Si+InGaAs" of the dual sensor pyranometer was smaller than that in the single Si pyranometer.

Keywords: Irradiance, Pyranometer, Spectral Response, Sensitivity Factor, Spectral Error

INTRODUCTION

In order to evaluate the Photovoltaic (PV) system and estimate the amount of power generation, the irradiance data is the most important factor. Thus, it is necessary to measure it precisely. So far, thermopile-based pyranometer is widely used in the PV field. However, since a thermopile-based pyranometer is very expensive as well known and its sensitivity degrades somewhat with time, it is inappropriate for a long time measurement and applying for large number of sites or modules. In order to solve these problems, the pyranometer which is installed a silicon photodiode (single Si pyranometer) has been used. Its spectral response, however, strongly depends on wavelength and does not cover whole solar spectrum. Therefore, the single Si pyranometer cannot measure the irradiance precisely like the thermopile-based pyranometer because a spectral miss match error arises strongly. In consequence, the development of a cheap, stable, and high performance pyranometer base on the new idea is required greatly now, particularly in PV Field.

The purpose of this study aims to the development of the dual sensor pyranometer which is composed of two kinds of photodiodes, which are for both short- and long- wavelength range measurements.

At the present day, the required data has been collected in the open air. However, output voltages from each photodiode measured in the open air muddle directional, temperature, spectral error and the others at same time. Therefore, only the spectral error of the dual sensor pyranometer cannot be evaluated precisely. In this study, the irradiances are estimated by the using output voltages from each photodiode. They are calculated by multiplying the spectral irradiances, absolute spectral response, receiving area of each photodiode and a shunt resistance. Then, the method to evaluate only the spectral error and the result calculated the spectral error independently are described in this paper.

THE DUAL SENSOR PYRANOMETER

Construction

The purposed dual sensor pyranometer produces the irradiance on the outputs from both Si Photodiode that responses from 300 nm to 1100 nm of wavelength and InGaAs Photodiode that responses from 900 nm to 1700 nm of wavelength. In our new dual sensor pyranometer, it is necessary to achieve measurement error within ± 0.01 kW/m^2 compared with the thermopile-based pyranometer. Moreover, GaAsP Photodiode, which responses in the short wavelength range, is introduced instead of the Si photodiode because the maximum of spectral sensitivity for the GaAsP photodiode is closer to that of solar spectrum. That is two combinations, which are "Si+InGaAs" and "GaAsP+InGaAs" for comparison.

Fig. 1 shows relative spectral responses of the Si, InGaAs and GaAsP photodiode compared to Reference Solar Radiation.

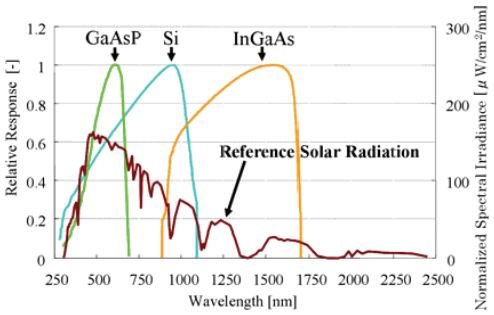

Fig. 1. Relative spectral responses of the Si, InGaAs and GaAsP photodiode and Reference Solar Radiation.

Irradiance and Sensitivity factor

The irradiance obtained from the dual sensor pyranometer is calculated by

$$G_{Dual} = \mathrm{K}_{\mathrm{Si}} \times E_{Si} + \mathrm{K1}_{\mathrm{InGaAs}} \times E_{InGaAs} \quad (1)$$

or

$$G_{Dual} = \mathrm{K}_{\mathrm{GaAsP}} \times E_{GaAsP} + \mathrm{K2}_{\mathrm{InGaAs}} \times E_{InGaAs}, \quad (2)$$

where G_{Dual} [kW/m^2] represents the global irradiance, K_{Si}, K_{GaAsP}, $K1_{InGaAs}$ and $K2_{InGaAs}$ [kW/m^2/mV] represent the sensitivity factors to transfer from the output voltage to the irradiance. Moreover, E_{Si}, E_{GaAsP} and E_{InGaAs} [mV] represent the output voltages from each photodiode. They are usually measured in open air and used as data.

In the next place, the calibration method to determine the sensitivity factors is the following explanation. It is to determine them based on spectral irradiance measured by spectroradiometer [1]. In fact, the sensitivity factors are calculated by equation (3), (4), (5) and (6) from the data measured on one clear day.

• Si+InGaAs

$$K_{Si} = \frac{\left\{\sum_{300}^{1000}(I_\lambda \times \Delta\lambda)\right\}}{E_{Si}} \quad (3)$$

$$K1_{InGaAs} = \frac{\left\{\sum_{1000}^{2500}(I_\lambda \times \Delta\lambda)\right\}}{E_{InGaAs}} \quad (4)$$

• GaAsP+InGaAs

$$K_{GaAsP} = \frac{\left\{\sum_{300}^{680}(I_\lambda \times \Delta\lambda)\right\}}{E_{GaAsP}} \quad (5)$$

$$K2_{InGaAs} = \frac{\left\{\sum_{680}^{2500}(I_\lambda \times \Delta\lambda)\right\}}{E_{InGaAs}} \quad (6)$$

Where: I_λ [μW/cm^2/nm] represents the spectral irradiance measured by the spectroradiometer; Δλ [nm] represents one nanometer interval. Therefore, the numerators for each equation represent the wavelength ranges of the spectral irradiance coverd by each photodiode.

METHOD

Problems for measurement in the open air and its improvement

An advantage of the dual sensor pyranometer is decreasing the spectral error caused by the non-flat spectral response compared with single Si pyranometer. This idea results in that more precise measurement is possible.

However, the spectral error analysis for each pyranometer is very difficult because irradiances are calculated by using the output voltages which include directional, temperature, spectral error and the others at same time in the open air as shown Fig. 2 [2].

Therefore, we proposed a method that irradiances are estimated by using the output voltages from each photodiode which are calculated by multiplying the spectral irradiances, absolute spectral response, receiving area of each photodiode and a shunt resistance as equation (7). The main error in the calculated irradiances is only spectral error caused by the spectral miss match. Then, the spectral error analysis for each pyranometer is possible independently compared with the reference value of the thermopile-based pyranometer [3].

$$E_{estimate} = \left\{\sum_{\lambda 1}^{\lambda 2}(I_\lambda \times \Delta\lambda)\right\} \times S \times R \quad (7)$$

Where: $E_{estimate}$ [mV] represents the calculated output voltage from each photodiode based on spectral irradiance measured by spectroradiometer; λ1 [nm] represents the starting wavelength of spectral response for each photodiode; λ2 [nm] represents the ending wavelength of spectral response for each photodiode; S [mm^2] represents receiving area of each photodiode; R [Ω] represents a shunt resistance.

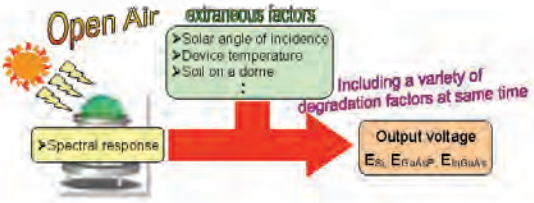

Fig. 2. Including a variety degradation factors in open air.

Spectral Error Analysis

In order to evaluate the spectral error in the pyranometer, the estimated output voltages from each photodiode ($E_{estimate}$) were calculated by equation (7) on the data of both typical cloudless five days and three

cloudy days as shown in Table 1. The irradiances which are from single Si pyranometer and two prepared dual sensor pyranometers were calculated by applying the obtained output voltages to the equation (1), (2) and (3). In this regard, however the Sensitivity factors of each pyranometer shown in Table 2 are determined from the data measured on clear day, April 6, 2005. Mean Bias Error (MBE) in a unit of W/m^2, Root Mean Square Error (RMSE) in a unit of W/m^2 and the improvement rate (IR) from single Si pyranometer in a unit of % are calculated by equation (8), (9) and (10) as the index.

Table 1. Used data for evaluating the spectral error in the pyranometer.

	Year/month/day
Fine day	2003/4/22, 2004/10/1, 2004/12/16, 2005/3/31, 2005/4/6
Cloudy day	2003/7/22, 2003/8/28, 2005/5/20

Table 2. Sensitivity factors for each pyranometer.

			K [kW/m^2/mV]
Dual Sensor Pyranometer	Si+InGaAs	Si	0.572
		InGaAs	0.071
	GaAsP+InGaAs	GaAsP	0.889
		InGsAs	0.156
Single Si Pyranometer			0.762

$$MBE = \frac{1}{N}\sum_{i=1}^{N}\left(G - G_{ref}\right) \quad (8)$$

$$RMSE = \sqrt{\frac{1}{N}\sum_{i=1}^{N}\left(G - G_{ref}\right)^2} \quad (9)$$

Where: G represents the global irradiance of the single Si pyranometer or the dual sensor pyranometer; G_{ref} represents the global irradiance of thermopile-based pyranometer; N represents the number of data.

$$IR = \frac{RMSE_{Si} - RMSE_{Dual}}{RMSE_{Si}} \times 100 \quad (10)$$

Where: $RMSE_{Si}$ and $RMSE_{Dual}$ represent the values for the calculated RMSE of the single Si pyranometer and the dual sensor pyranometer, respectively.

EVALUATION RESULTS

Fig. 3 shows the spectral error distribution from the thermopile-based pyranometer in each pyranometer on five clear days. As time is running out during the day, the error distribution doesn't change, excluding a solar angle dependent error in irradiance measurements. Therefore, only the spectral error in the pyranometer is extracted by the proposed method.

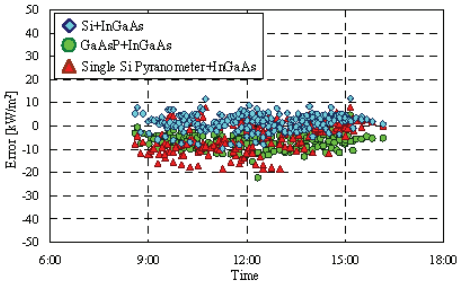

Fig. 3. Spectral error distribution of each pyranometer on five clear and three cloudy days.

Table 3. Value of evaluation index for each pyranometer on five clear and three cloudy days.

		MBE [W/m^2]	3σ [W/m^2]	RMSE [W/m^2]
Si+InGaAs	Fine	2.0	11.0	4.0
	Cloudy	-3.0	20.0	7.0
GaAsP+InGaAs	Fine	-7.0	10.0	7.0
	Cloudy	-14.0	15.0	15.0
Si Pyranometer	Fine	-4.0	20.0	8.0
	Cloudy	17.0	27.0	19.0

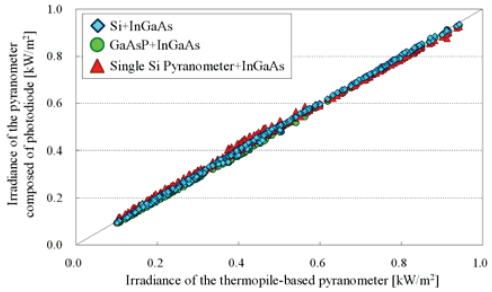

Fig. 4. Correlation of irradiances between the thermopile-based pyranometer and each pyranometer on five clear and three cloudy days.

Table 3 shows MBE, 3σ and RMSE for each pyranometer, then Fig. 4 shows the correlation of irradiances measured by the thermopile-based

pyranometer and each pyranometer on five clear and three cloudy days.

As a result, the spectral error of cloudless days was improved 49 % for "Si+InGaAs" compared with the single Si pyranometer. Moreover, that of the cloudy days was improved 62 % for "Si+InGaAs" compared with the single Si pyranometer. The spectral errors calculated as absolute value are 7.0 W/m^2 per 1000 W/m^2 of the irradiance in the cloudless days and 13.0 W/m^2 per 500 W/m^2 in cloudy days and suggest the spectral errors in "Si+InGaAs" are small relatively.

In the next place, same analysis was conducted for more data than those used in the Table 1. Table 4 shows MBE, 3σ and RMSE for each pyranometer. Then, Fig. 5 shows the correlation of irradiances measured by the thermopile-based pyranometer and each pyranometer on more clear and cloudy days.

Table 4. Value of evaluation index for each pyranometer on more clear and cloudy days.

		MBE [W/m^2]	3σ [W/m^2]	RMSE [W/m^2]
Si+InGaAs	Fine	1.0	24.0	8.0
	Cloudy	2.0	21.0	7.0
GaAsP+InGaAs	Fine	-9.0	19.0	11.0
	Cloudy	-14.0	16.0	15.0
Si Pyranometer	Fine	-4.0	22.0	8.0
	Cloudy	19.0	27.0	21.0

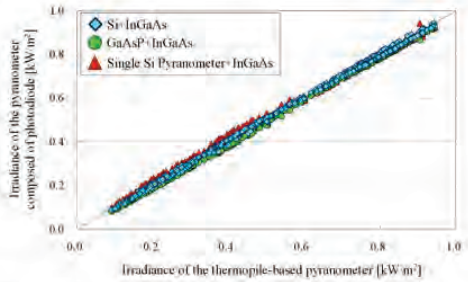

Fig. 5. Correlation of irradiances between the thermopile-based pyranometer and each pyranometer on more clear and cloudy days.

Consequently, the spectral error of cloudless days wasn't improved for "Si+InGaAs" compared with the single Si pyranometer as well as results in Table 1. However, that of the cloudy days was also improved 65% for "Si+InGaAs" compared with the single Si pyranometer as well as results in Table 1. Alternatively, the spectral error in the single Si pyranometer is big for either clear or cloudy day if its sensitivity factor is fixed.

On the other hand, the spectral error in "GaAsP+InGaAs" was a small improvement or not a improvement compared with the single Si pyranometer in both the cloudless and the cloudy days. This reason is considered that both photodiodes in this dual pyranometer has no sensitive wavelength range in between 680 nm and 900 nm.

CONCLUSION

In order to evaluate only the spectral errors in pyranometer composed of photodiode, we proposed a method that irradiances are estimated by using the output voltages from each photodiode which are calculated by multiplying the spectral irradiances, absolute spectral response, receiving area of each photodiode and a shunt resistance.

When the developed method is applied to five clear and three cloudy days, the spectral error in "Si+InGaAs" was improved 49 % for five cloudless days and 62 % for three cloudy days respectively compared with the single Si pyranometer. On the other hand, the spectral error in "GaAsP+InGaAs" was a small improvement on five clear and three cloudy days. This reason is considered that both photodiodes in this dual pyranometer has no sensitive wavelength range in between 680 nm and 900 nm.

Fig. 6. Picture of experimental equipments for the development of the dual sensor pyranometer

ACKNOWLEDGEMENTS

The authors would like to thank everyone Kurokawa Laboratory and EKO Instruments Co., Ltd for their help.

References

[1] K. Hirata et al., "Development of a Reliable, Long Life Pyranometer Composed of Multiple Photosensors", *Proceeding of the 15th International Photovoltaic Science and Engineering Conference*, October 2005, pp. 832-833.

[2] D. L. King, W. E. Boyson et al., "Oprational Characteristics and Improved Calibration Procedures for LI-COR LI-200 Silicon-Photodiode Pyranometers".

[3] K. Hirata et al., "Development of Analysis Method of Spectral Error on A New Pyranometer Composed of Multiple Photosensors", *the institute of Electrical Engineers of Japan*, September 2006.

国内学会

[2006 年～2007 年]

平成 18 年電気学会電力・エネルギー部門大会

159

共振負荷による回転機負荷の代替検討について

正　員　五十嵐　広宣（財団法人　電気安全環境研究所　研究部）

非会員　佐藤　孝則（財団法人　電気安全環境研究所　研究部）

正　員　黒川　浩助（東京農工大）

About an alternative examination of the motor load according to the resonance load

Hironobu Igarashi, member, Takanori Sato, Non-member, Kousuke Kurokawa member,
(Research Division, Japan Electrical Safety & Environment Technology Laboratories)
(Tokyo University of Agriculture and Technology.)

1.　まえがき

近年，地球温暖化対策などの地球環境問題に対する関心が一般の人々の間にも広まり，電力の発電に CO_2 が排出されないクリーンなエネルギー源として住宅用太陽光発電システムが注目されている。現在の住宅用太陽光発電システムは，発電電力と家庭内で使用する電力の差を余剰電力として一般電気事業者へ売電できる系統連系型太陽光発電システムが主流である。

発電電力を一般電気事業者へ売電する場合には，配電線等で発生した事故等による停電状態を検出し，発電を停止させる単独運転防止が重要である。この単独運転検出装置は，回生エネルギーを持つ負荷の影響により，単独運転を防止することが困難な場合がある。

今回著者らは，回転機負荷が共振負荷よりも単独運転状態を発生させることが確認されているが[1]，回転機負荷を線形負荷の誘導性負荷とて代替をした場合にも同様の結果が得られるかの検証を行なった。

2.　共振負荷と回転機負荷の検討

〈2･1〉 IEC 共振負荷　IEC 共振負荷は，(1) 式によって誘導性負荷量を求め，それと同等の容量性負荷とパワーコンディショナの定格出力を消費する抵抗負荷を並列に接続し共振回路を構成している。本検討に用いた誘導性負荷量は，定格出力 4kW パワーコンディショナを用いたので，(1)式より P_{qL} は 2.6kVar となる。

$$P_{qL} = Q_f \times P_{EUT} \quad \cdots\cdots(1)$$

P_{qL}　：誘導性負荷［VAR_L］
P_{EUT} ：パワーコンディショナ定格出力
Q_f　：0.65

〈2･2〉 共振負荷と回転機負荷の比較　IEC 規格において定められている共振負荷と数種類の回転機負荷は，回生エネルギーを持つ負荷であることから，各負荷が持つ電気的エネルギー量の測定を行い比較することにより，共振負荷と同等の電気的エネルギー量を持つ回転機負荷を確認した。共振負荷と回転機負荷の電気的エネルギー量の測定結果を図 1 に示す。

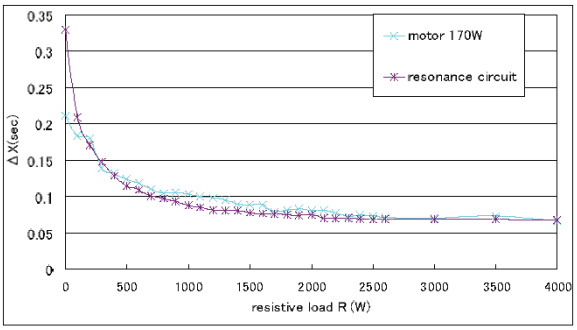

図 1 電気的エネルギー量の測定結果

Fig.1. Measurement result of amount of electric energy

〈2･3〉 単独運転試験結果　各負荷が，単独運転検出装置へ与える影響について検証を行なうため，実際のパワーコンディショナを用いて単独運転防止試験の実験を行なった。負荷条件は，共振負荷が誘導性負荷を 2.6kVar に固定し，抵抗負荷及び容量性負荷の増減によって負荷バランスを調整した。また，回転機負荷条件は，回転機負荷 170W を固定とし，抵抗負荷及び容量性負荷の増減によって負荷バランスを調整した。その結果，共振負荷よりも回転機負荷 170W の場合のほうがより多くの範囲で単独運転現象を発生させることが確認された。

表 1　共振負荷による単独運転検出時限
Table 1. Islanding detection time limit by resonance load.

		Reactive power (Var)				
		-10%	-5%	0%	+5%	+10%
Active power (W)	-10%	663.3mS	Islanding	676.9mS	640.8mS	646.2mS
	-5%	627.9mS	Islanding	Islanding	639.8mS	616.8mS
	0%	633.7mS	Islanding	Islanding	667.0mS	619.1mS
	+5%	672.2mS	Islanding	Islanding	670.0mS	632.7mS
	+10%	690.1mS	798.1mS	Islanding	675.1mS	649.5mS

表 2　共振負荷＋回転機負荷 170W による単独運転検出時限
Table 2. Islanding detection time limit by resonance load + motor load (170W).

		Reactive power (Var)				
		-10%	-5%	0%	+5%	+10%
Active power (W)	-10%	618.0mS	Islanding	Islanding	Islanding	626.0mS
	-5%	665.0mS	702.0mS	686.0mS	691.0mS	647.0mS
	0%	628.0mS	Islanding	Islanding	719.0mS	626.0mS
	+5%	675.00mS	Islanding	Islanding	688.0mS	601.0mS
	+10%	649.0mS	Islanding	Islanding	649.0mS	623.0mS

表 3　回転機負荷（170W）による単独運転検出時限
Table 3. Islanding detection time limit by motor load (170W).

		Reactive power (Var)				
		-10%	-5%	0%	+5%	+10%
Active power (W)	-10%	655.00mS	Islanding	743.00mS	702.80mS	637.80mS
	-5%	644.60mS	684.80mS	Islanding	Islanding	Islanding
	0%	628.30mS	Islanding	Islanding	Islanding	650.82mS
	+5%	641.60mS	Islanding	Islanding	Islanding	621.60mS
	+10%	647.60mS	726.60mS	Islanding	Islanding	619.60mS

〈2･4〉 回転機負荷の代替検討　回転機負荷が通常運転を行なっている時は，誘導性負荷として存在していることから，回転機負荷の電流・電圧の計測結果から誘導性負荷量へ算術を行い，共振負荷 2.6kVar に回転機負荷分の誘導性負荷量を追加とした。また，比較検討を行なう負荷条件は，共振負荷 2.6kVar に回転機負荷 170W を並列に接続をした条件である。それぞれの負荷条件において，単独運転防止の実験を行なった。単独運転防止実験結果の共振負荷 2.6kVar に回転機負荷分の誘導性負荷量を加えた結果を表 1 に，共振負荷 2.6kVar に回転機負荷 170W を並列に接続をした結果を 2 に示す。

〈2･5〉 回転機負荷の代替試験結果　実験結果は，両負荷条件にいて同等の単独運転現象が発生していることが確認できた。しかし，2.3 項に記載した回転機負荷 170W と調整用の誘導性・容量性負荷のみで構成された共振負荷の場合の表 3 に示す単独運転実験結果は，代替検討を行なった負荷条件よりも多くに範囲で単独運転現象が発生していることが分かる。これらの結果から共振負荷量が少ない場合において単独運転現象が発生することを考慮した場合は，回転機負荷の誘導性容量を単純に誘導性負荷の線形負荷として表すことが出来ても，単独運転現象を発生させる要因とは異なることが判明した。

3．まとめ

今回の検討結果は，回転機負荷の代替負荷として回転機負荷の同等量の誘導性負荷量を共振負荷に加え，共振負荷 2.6kVar との単独運転防止の実験を行なうことにより比較を行なった。その結果，両負荷条件ともほぼ同じ単独運転現象が発生した事が確認されたが，回転機負荷のみの場合のほうが，多くの単独運転現象が発生していることから，回転機負荷の誘導性容量を単純に誘導性負荷の線形負荷として表すことが出来ても，単独運転現象を発生させる要因とは異なることが判明した。

文　献

(1) Hironobu Igarashi: “The tests of islanding have an influence on motor”, Proc for 2005 National Convention Record IEE Japan,No.6-192, p.341~342 (2005)
五十嵐広宣:「単独運転防止試験時の回転機負荷影響について」,平成17 年度電気学会全国大会, No.6-192, p.341～342 (2005)

平成 18 年電気学会電力・エネルギー部門大会

188

太陽光発電システム出力変動の検出時間別発生確率分布を用いた変動特性定量化手法

学生員 川崎 憲広（東京農工大学） 学生員 植田 譲（東京農工大学）
正 員 北村 清之（明電舎） 正 員 杉原 裕征（関電工）
正 員 西川 省吾（日本大学） 正 員 黒川 浩助（東京農工大学）

Evaluation method of PV system's output fluctuation using time dependent probability distribution

Norihiro Kawasaki, Yuzuru Ueda, student member, Kosuke Kurokawa, member, (Tokyo University Agriculture and Technology),
Kiyoyuki Kitamura, member, (MEIDENSHA CORPORATION), Hiroyuki Sugihara, member, (Kandenko co., ltd.),
Shogo Nishikawa, member, (Nihon University)

1. はじめに

太陽光発電（PV）や風力発電のような自然エネルギーを利用した発電方式は，二酸化炭素の削減効果等の環境的メリットを有することから導入目標が設定され，普及が進んでいる。しかし，その発電出力は天候により変動するので，系統連系する際に周波数変動等の悪影響が懸念されている。そのため，変動特性を把握し，系統への影響を評価することが重要な課題である。

これまでに発電出力の変動に関していくつかの研究が行われてきた[(1)-(5)]。これらの研究では，周波数解析[(1)]や統計的な方法[(2)-(5)]で最大の変動幅を抽出したり，変動の分布を把握したりしている。本稿では，新たに開発した変動の検出時間別の発生確率分布を用いて，これらの変動の特徴を 1 つの値に集約する評価手法について述べる。

2. 変動特性定量化手法

変動特性を把握するための手法として「出力変動幅[(2)(4)]」と出力変動幅の検出時間別出現頻度から求まる「発生確率」を用いた。

〈2･1〉 出力変動幅 変動の大きさを検出するため，任意に検出時間を変更できる検出窓を準備し，その検出窓内の最大値と最小値の差を「出力変動幅」とした（図 1）。

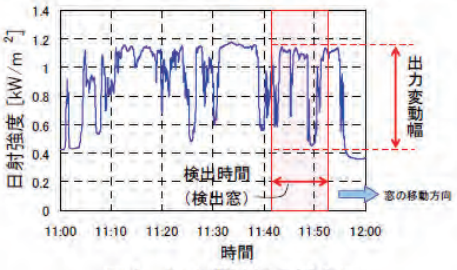

図 1 出力変動幅の概念図
Fig. 1. Image of output magnitude of fluctuation.

〈2･2〉 検出時間の選定 短周期から長周期までの領域に関して評価を行うために，ある値の累乗となるような検出時間の間隔を決定した。この方法は対数軸上で等間隔になり，あらゆる領域を満遍なく見ることができるという特徴を有している。今回は 1.5 の累乗を用いた。検出窓の幅は最大で解析範囲約 16 時間のおよそ半分である 7 時間（1.5^{25} ≒25251[sec]）としたので，25 パターンの検出窓で解析した。

〈2･3〉 解析範囲 本手法は変動の発生確率を用いているため，日射強度が 0[kW/m²]のときを解析してしまうとその値に偏ってしまう。そのため，大気外日射強度の値が 0[kW/m²]より大きい値のときのみを解析範囲とした（図 2）。

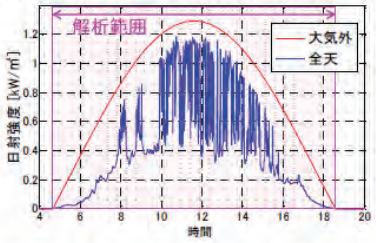

図 2 水平面大気外日射強度と水平面全天日射強度
Fig. 2. Extra-atmospheric irradiance and global irradiance.

〈2･4〉 出力変動幅の検出時間別発生確率分布 解析には 1 秒値を用いている。そのため，検出窓は 1 秒毎にスライドさせ，解析範囲内で検出した出力変動幅の度数分布を作成し，発生確率を算出した。これを各検出時間に対して行うことで検出時間別の発生確率分布を作成することができる。図 3 にはその例を示しており，縦軸(y)が出力変動幅，横軸(x)が検出時間，面(z)が発生確率を表している。ここで，(a)は変動の激しい日，(b)はスパイクのような変動を含む曇天日，(c)は曇天日，(d)は快晴日の代表的な日射パターンであり，各グラフ内の左上に示した。また，検出時間毎の出力変動幅の最大値を「最大出力変動幅」とよび，実線で示した。これらの分布をみることで，変動の様子が視覚的にイメージし易くなっている。

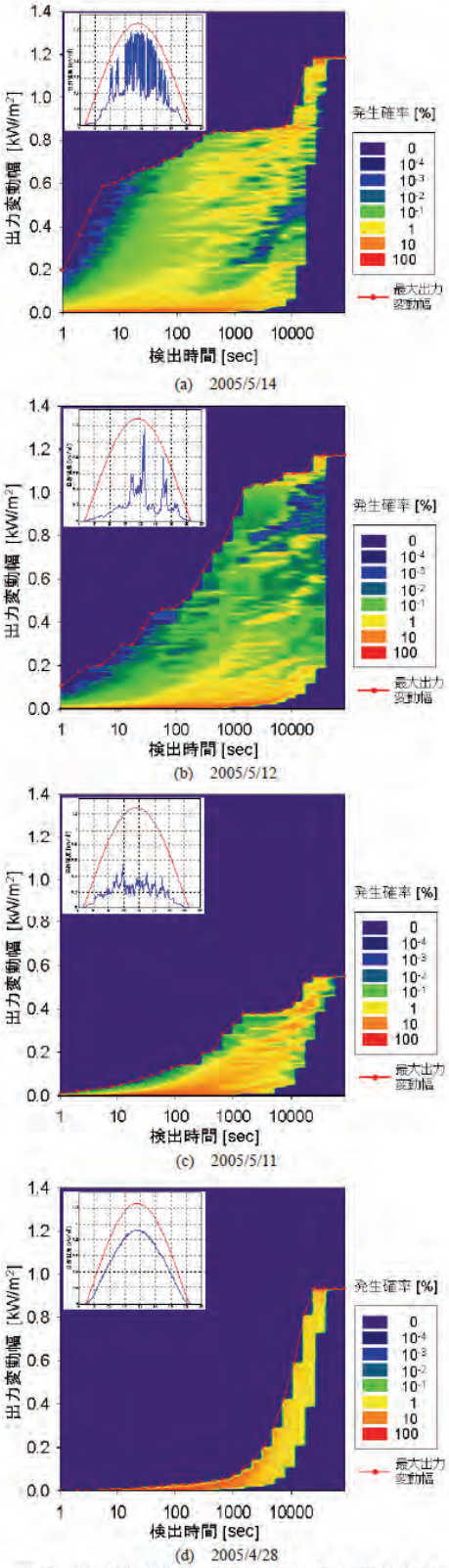

図 3 出力変動幅の検出時間別発生確率分布
Fig. 3. Time dependent probability distribution of output magnitude of fluctuation.

〈2･5〉 出力変動指数　出力変動幅の発生確率分布は変動特性をイメージし易いが情報量が多いので，長期間の解析結果を処理する際にはこの分布を 1 日で 1 つの値に集約させることができれば便利である。そこで発生確率分布を利用し，変動の発生確率が高く，出力変動幅が大きいほどに大きな値を示す指標を提案する。その算出方法は，出力変動幅と検出時間の全ての組み合わせに対して，発生確率と出力変動幅の積を求め，それらの総和を算出するものである。これを出力変動指数（OFI : Output Fluctuation Index）と定義し，次式で示す。

$$OFI = \sum_{i=1}^{M}\sum_{j=1}^{N}\left(y_j z_{i,j} \right) \quad \cdots\cdots (1)$$

ここで，y：出力変動幅，z：発生確率，x：検出時間，
M：x の分割数，N：y の分割数

OFI を算出する領域は検出時間 x の分割数 M によって決定する。今回の場合，検出時間が 1 秒から 1.5^M 秒までの領域の間で M を変更すれば，対象とする変動の速さに応じた OFI を算出することが可能である。**表 1** には算出する領域を 85 秒から 7 時間まで変化させた場合の OFI の値を示した。ここから各領域で OFI を相対的に比較すると，日射パターン(a)と(b)はそれぞれ順位が固定されているが，(c)と(d)に関しては算出する領域が 7 時間のときは(d)のほうが大きく，2 時間以下では(c)のほうが大きく評価された。これは(d)の日射の日周期による長周期変動の絶対値の大きさが影響している。通常，PV システムの評価では変動と扱わないが，系統に対しては変動とみなされるので，対象とする変動の速さによっては評価する必要性が出てくると考えられる。なお，表 1 の晴天指数は天候を判断する際に一般的に用いられる指標であり，参考として示した。

表 1 算出する領域毎の出力変動指数
Table 1. Output Fluctuation Index each calculation domain.

日射パターン	晴天指数 CI	出力変動指数 OFI			
		7h	2h	16min	85s
(a)	0.500	655.6	400.9	175.9	37.48
(b)	0.228	363.8	164.3	39.44	5.527
(c)	0.231	228.1	117.2	32.15	3.456
(d)	0.661	263.2	89.63	14.32	1.442

※ 7h, 2h, 16min, 85s は算出する領域である

3. まとめと今後の展望

出力変動幅の検出時間別発生確率分布を用い，出力変動指数を定義することで対象とする変動に対して，1 日の変動特性を 1 つの値で定量化することができた。今後は，日射変動の平滑化効果（ならし効果）の評価へ応用させていく。

謝　辞

本研究は，（独）新エネルギー・産業技術総合開発機構（NEDO 技術開発機構）の「集中連系型太陽光発電システム実証研究」の一環として行っている。関係者各位に感謝の意を表する。

文　献

（1） 川崎，大関，大谷，北村，杉原，西川，黒川：「面的広がりを考慮した太陽光発電変動特性の分析」，平成 17 年度 電気学会 電力･エネルギー部門大会，No.272 (2005)
（2） NEDO 技術開発機構：「風力発電電力系統安定化等調査」，平成 13 年度調査報告書 (2002)
（3） 村田，山口：「太陽光発電出力変動の統計的な一性質」，平成 17 年度 電気学会 電力･エネルギー部門大会，No. 273 (2005)
（4） 村田：「電力貯蔵による分散電源の出力変動抑制」，第 2 回 分散型エネルギーシンポジウム，p.43-48 (2005)
（5） 箕輪・大谷・津田・作田・黒川：「地域面平均日射の推定による太陽光発電システムの kW 価値分析」，太陽／風力エネルギー講演論文集 1998，p.17-20 (1998)

平成 18 年電気学会電力・エネルギー部門大会

183

二種類のフォトセンサを持つ新型日射計における スペクトル誤差の解析手法の開発

学生員 平田 啓二　正 員 黒川 浩助（東京農工大学）
非会員 三宅 行美　非会員 加藤 正　非会員 中村 幸三（英弘精機株式会社）

Development of Analysis Method of Spectral Error on A New Pyranometer Composed of Multiple Photosensors

Keiji Hirata, Student-member, Kosuke Kurokawa, member, (Tokyo University of Agriculture and Technology)
Yukiharu Miyake, Non-member, Tadashi Kato, Non-member, Kouzou Nakamura, Non-member, (EKO INSTRUMENTS Co., Ltd.)

1. はじめに

太陽光発電システムの発電量推定や評価を行う上で，日射量は重要な要素である。本研究では，安価で長期安定性に優れた半導体素子を二種類用いることで，従来の Si 日射計の弱点であるスペクトル誤差を改善し，高精度な日射の計測を可能とするデュアルセンサ型日射計（Dual 日射計）の開発を目的としている。

現在，データの収集は屋外計測にて行っている。しかし，得られる出力電圧には，スペクトル誤差の他，温度特性や角度特性による誤差が同時に存在するため，Dual 日射計のスペクトル誤差のみを評価することが困難であった。

本稿では，分光放射強度と各センサの絶対分光感度を用いて，各々の理論出力電圧を推定することで，Dual 日射計が持つ角度特性および各センサが持つ温度特性の影響を受けずに，スペクトル誤差のみを評価する手法を開発した。

2. デュアルセンサ型日射計

Dual 日射計は，Si センサ（分光感度域：300～1100nm）および GaAsP センサ（分光感度域：300～680nm）で補うことができない日射の長波長域に分光感度を持つ InGaAs センサ（分光感度域：900～1700nm）を追加することで，二種類のセンサから得られる出力電圧により，正確な日射強度が計測できる。図 1 に，計測に用いた各センサの相対分光感度特性および基準太陽光スペクトルを示す。

図 1 に示すように，Dual 日射計の組合せは，Si+InGaAs と GaAsP+InGaAs の二通りが考えられる。

また，Dual 日射計の日射強度は，次式から求められる[1]。

$$=(2-C)\times K_1\times {}_1+C\times K_2\times {}_2 \quad \cdots\cdots\cdots\cdots\cdots\cdots (1)$$

ここで，　：全天日射強度，　，　：各センサの出力電圧，K_1，K_2：感度定数，C：感度定数を最適化するための補正係数とする。

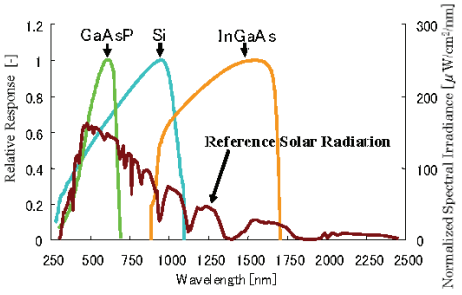

図 1　各センサの相対分光感度と基準太陽光スペクトル
Fig. 1.　Relative Spectral Response and Reference Solar Spectrum.

3. スペクトル誤差の解析手法

〈3･1〉　問題点および解析手法

Dual 日射計は，Si 日射計では感知することができない長波長域の日射を捉えることで，スペクトル誤差を減少させ，より高精度な日射計測が可能になると考えられる。

しかし，日射の屋外計測においては，各センサの出力電圧にスペクトル誤差の他，温度特性，日射計の角度特性による誤差が同時に存在するため，Dual 日射計のスペクトル誤差のみを評価することが困難であった。

そこで，本稿では分光器（MSR-7000/00，オプトリサーチ）を用いて，実測した分光放射強度と各センサの絶対分光感度から各センサの理論出力電圧を推定することで，日射計の角度特性および各センサの温度特性の影響を受けずに，Si+InGaAs および GaAsP+InGaAs，Si 日射計のスペクトル誤差のみを評価する手法を開発した。

〈3･2〉　理論出力電圧の算出手法

各センサの理論出力電圧は，分光放射強度を　，各センサの絶対分光感度を　とすると，次式で求められる。

$$E=\left(\sum_{\lambda 1}^{\lambda 2} I_{\lambda}\times K_{\lambda}\right)\times S\times R \quad \cdots\cdots(2)$$

ここで，S：各センサの受光面積，R：検出抵抗値，$\lambda 1$：各センサの感度波長域における始点波長，$\lambda 2$：各センサの感度波長域における終点波長とする。

任意の快晴日 1 日を検定日と定め，分光放射強度と推定した理論出力電圧から各センサの感度定数を決定する(1)。得られた感度定数を用いて，天候別の理論出力電圧を回帰式（1）に適用し，Dual 日射計の日射強度を求め，精密日射計（MS-801，EKO）で計測された日射強度を基準値とし、その値と比較することより，Dual 日射計である Si+InGaAs および GaAsP+InGaAs のスペクトル誤差の評価を行う。また、Dual 日射計が持つスペクトル誤差の比較対象として、Si 日射計の日射強度に関しても、同様に本手法を用いて求める。

4. 解析結果

表 1 に示す快晴日 216 データ，曇天日 192 データの分光放射強度から各センサの出力電圧を式（2）より推定した。そして，2005/04/06 を検定日と定め，各センサの感度定数を決定し(1)，式（1）より各日射計の日射強度を算出した。

基準値は精密日射計で計測された日射強度を用い，式 (3) より Si+InGaAs および GaAsP+InGaAs，Si 日射計における基準値からの誤差を算出した。

図 2 に快晴日，図 3 に曇天日の結果をそれぞれ示す。また，評価指数として用いた MBE および 1σ，RMSE の結果を表 2 に示す。

$$Error = G_s - G \quad \cdots\cdots(3)$$

ここで，G_s：各日射計の日射強度，G：精密日射計の日射強度とする。

表 1　検証に使用したデータ

Table 1.　Using data for the verification.

	年月日
Fine day	2003/4/22, 2004/10/1, 2004/12/16, 2005/3/31, 2005/4/6
Cloudy day	2003/7/22, 2003/8/28, 2005/5/20, 2006/4/14, 2006/4/19

快晴日における誤差分布は，時間変化に伴う影響を受けておらず，ほぼ一定の誤差分布を示していることがわかる。つまり，求められた日射強度に関しては，日射計の角度特性および各センサの温度特性による影響を受けていないと考えられる。（図 2，表 1 参照）

また，曇天日における誤差分布からは，Si 日射計において誤差が大きく，且つ基準の日射強度よりも大きい日射強度が出力されていることがわかる。これは，天候の違いから相対的な太陽光スペクトルが変化し，その結果 Si 日射計のスペクトル誤差が大きくなるという特徴(2)と類似した結果を表しており，この点からも本稿で提案した手法を用いることで，スペクトル誤差のみを抽出できていると考えられる。（図 3，表 1 参照）

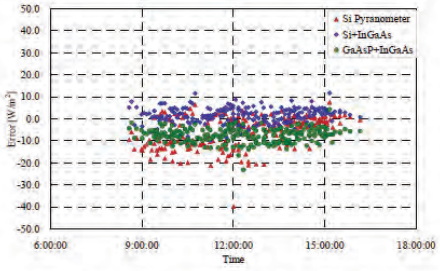

図 2　快晴日における誤差分布

Fig. 2.　Error distribution in fine days.

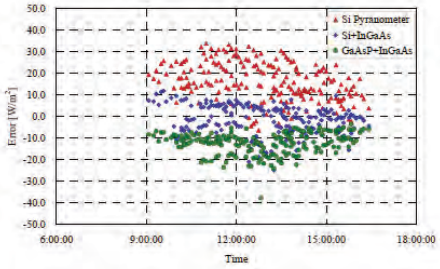

図 3　曇天日における誤差分布

Fig. 3.　Error distribution in cloudy days.

表 2　各日射計における評価指数

Table 2.　Characteristic of evaluation for each pyranometer.

	weather	MBE [W/m²]	1σ [W/m²]	RMSE [W/m²]
Si+InGaAs	Fine	2.0	4.0	4.0
	Cloudy	-1.0	7.0	7.0
GaAsP+InGaAs	Fine	-8.0	3.0	8.0
	Cloudy	-12.0	5.0	13.0
Si Pyranometer	Fine	-6.0	7.0	9.0
	Cloudy	16.0	9.0	18.0

5. まとめ

日射計のスペクトル誤差のみを評価するために，分光放射強度と絶対分光感度から理論出力電圧を推測し，評価する手法を新たに開発した。そして，この手法から推測した天候別の理論出力電圧を用いることで，日射計の角度特性および各センサの温度特性による影響を受けずに，日射計のスペクトル誤差のみを評価することが可能であることを示した。今後は，年間を通じてのデータ数を収集することで，Dual 日射計の精度や組み合わせを含めた検証を目指す。

文　献

（1）K.Hirata, Y.Miyake, T.Kato, K.Nakamura and K.Kurokawa: "Development of a Reliable, Long Life Pyranometer Compsed of Multiple photo sensors", Proceeding of the 15th International Photovoltaic Science and Engineering Conference, pp.832-833, October 2005.

（2）井上・三宅・中村・加藤・黒川「デュアルセンサ型日射計の開発」，平成 15 年電気学会電力･エネルギー部門大会論文集 pp.567～568

超縮小模擬配電系統を用いたＰＶインバータ試験装置の開発

学生員 中村 祐介（東京農工大学） 非会員 小泉 裕孝（東京農工大学）
正員 黒川 浩助（東京農工大学）

Development of test equipment for PV inverters with ultra scaled-down distribution grid

Yusuke Nakamura, Student Member, (TUAT), Hirotaka Koizumi, Non-member, (TUAT),
Kosuke Kurokawa, Member, (TUAT)

1. まえがき

近年、一般家庭を中心に系統連系される太陽光発電(以下, PV)システムが急速に普及しており，将来的には一本の配電線に PV システムが多数台連系される可能性がある。PV システムを電力系統に接続する場合，設置前に単独運転防止機能や電力系統保護機能などの安全機能を試験する必要がある。直接的な試験としては実規模の独立した模擬配電系統を用いればよいが、これは大規模な設備になるため大学や研究機関の実験室に設置することは現実的でない。このため当研究室では配電系統をインピーダンス変換によって縮小した等価回路を，受動素子で置き換えたシミュレータを開発した[1]。しかしこのシミュレータも設置面積が大きく、コストも高額である。また、多数台連系試験に適応するために試験装置を拡張させると設置面積が数十 m^2 程度にもなり、拡張することは容易でない。そこで当研究室では，シミュレータを電子回路で構成することにより，大きさやコスト，拡張性にメリットがある新しい配電系統シミュレータの開発を行ってきた[2]。

本稿では超縮小模擬配電系統シミュレータのモデルを提案し、試作を行ったので報告する。

2. 超縮小模擬配電系統シミュレータ

<2･1> 構成 シミュレータの構成を図 1 に示す。

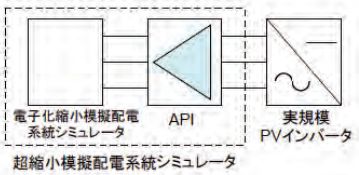

図 1 超縮小模擬配電系統シミュレータの基本構成
Fig 1. Composition of ultra scaled-down distribution grid simulator.

提案したシミュレータは電子回路で作成された電子化縮小模擬配電系統シミュレータと API から構成され，API の片端に実規模の PV インバータが接続される構成とする。電子化縮小模擬配電系統シミュレータは配電系統をインピーダンス変換によって縮小し、抵抗成分と容量成分は受動素子によって置き換える。誘導成分は特性が複雑であるため、オペアンプなどの電子回路によって模擬する[3]。

<2･2> モデル 図 2 に超縮小模擬配電系統のモデルを示す。日本の平均的な配電線の線路定数等のデータ[4]を使用し、柱上変圧器から低圧需要家までをモデル化する。

モデルは 30kVA の柱上変圧器を 10VA に縮小し，電圧を単相 3 線式 100/200V から 5/10V に縮小した。このスケーリングファクターに基づいて、変圧器容量、線路や負荷のインピーダンス、PV システム容量を決定する。

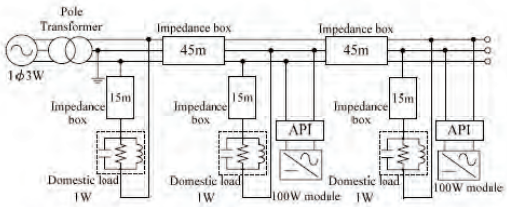

図 2 超縮小模擬配電系統シミュレータのモデル図
Fig 2. The model of ultra scaled-down distribution grid simulator.

<2･3> API API のブロック図を図 3 に示し、仕様を表 1 に示す。API (Active Power interface)[5]は，電力レベルの異なる機器の等価的な接続を可能にするインターフェースである。API はインバータ側(端子 2 側)の電流，電圧を忠実に 1/M，1/N 倍させた電流，電圧を系統側(端子 1 側)の電流，電圧とし，これと同時にインバータ側の電流，電圧を忠実に M，N 倍した電流，電圧を系統側の電流，電圧とする。

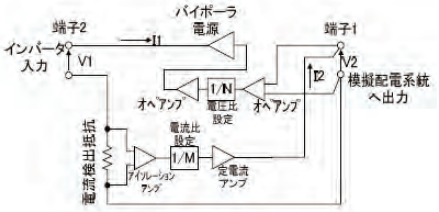

図3 APIのブロック図
Fig. 3 Composition of API.

表 1.API の仕様
Table.1 Specifications of API

電圧比	電流比	電力比	最大インバータ電圧	最大容量
1/60～1	1/40～1	1/2400～1	230V	約120W

3. 試作

<3･1>　超縮小模擬配電系統シミュレータ　超縮小模擬配電系統シミュレータの試作を行った。シミュレータの仕様を表 2 に示し、設置状況を図 4 に示す。シミュレータ内の各模擬装置はそれぞれユニットとして構成されているため、自由に結線することができ、任意の試験回路を構成できる。API は 2 ユニット試作し、最大 2 台の PV インバータの並列試験が可能である。ただし API の容量は 120W 程度であるため、供試インバータは AC モジュール用 PV インバータとする。模擬負荷は抵抗負荷、誘導性負荷、容量性負荷の組み合わせにより、有効電力と無効電力を様々に変化させることができる。

表 2.シミュレータの仕様
Table.2 Specifications of simulator.

		シミュレータ	実スケール	備考	
最大電圧		10V	200V		
低圧配電線	抵抗成分	0.1～1 [Ω]	0.25+j0.29 [Ω]	0.1[Ω]ステップで可変	最大100m相当
	誘導成分	0.01～1 [Ω]		0.01[Ω]ステップで可変	
引込み線		0.3+j0.01 [Ω]	2.3+j0.10 [Ω]	15m相当	
負荷レンジ	抵抗負荷	10～1.1k [Ω]	1.3～147 [Ω]	連続可変	
	誘導性負荷	0.05～20 [H]	6.67～2667 [mH]	連続可変	
	容量性負荷	1～150 [μF]	7.5～1125 [μF]	1μFステップで可変	
最大消費有効電力		2.5 [W]	7500 [W]		
最大消費無効電力		6.5 [Var]	19500 [Var]		
力率		遅れ0.53～進み0.42			

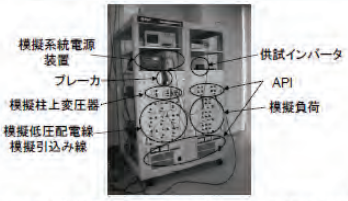

図 4. 超縮小模擬配電系統シミュレータの設置状況
Fig .4 Installation situation of experiment equipment.

<3･2>　PV インバータの単独運転実験　試作したシミュレータにより、PV インバータの単独運転を発生させる実験を行った。実験回路を図 5 に示す。

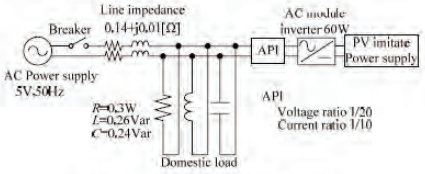

図 5. 単独運転試験回路図
Fig.5 The circuit of islanding test.

実験はブレーカを開放することで系統の停電を模擬し、インバータの挙動を観測した。単独運転時の波形を図 6 に示す。ブレーカを開放した直後に系統から負荷に流れる電流が停止し、停電が模擬されていることがわかる。しかしインバータは停止することなく動作し続け、単独運転状態となっている。

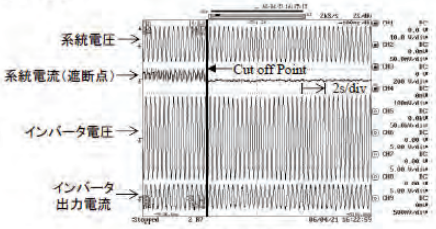

図 6 単独運転波形
Fig.6 Behavior of inverter in islanding.

4. まとめ

PV システムの多数台連系試験を目的とした、超縮小模擬配電系統シミュレータを電子回路によって構成し、試作を行った。設計したシミュレータの利点を以下に挙げる。

- 従来の試験装置より安価で省スペースである
- 試験装置の拡張が容易である
- 一定条件下における繰り返し実験が可能である
- 任意の試験回路を構成できる

今後は API の高周波特性等を慎重に検証した後、多数台システムへの拡張を計る。

なお、本研究は新エネルギー・産業技術総合開発機構（NEDO）の革新次世代太陽光発電システム研究開発，自律度向上型太陽光発電システム先導研究開発の一環として実施された。

文　献

(1) Y.Noda et al. “The deployment of a scaled-down simulator for distribution grid and its application for verifying interference behavior among a number of module integrated converters(MIC)”, 29th IEEE PVSC, May 2002, pp.1545-1548
(2) K.Takeuchi et al. “Development of ultra scaled down network simulator for testing PV inverters”, 14th PVSEC, Jan. 2004, pp.799-800
(3) Y. Nakamura et al. “Performance Assessment with Different Inductance Model in the ultra scaled-down distribution grid simulator”, 20th EU PVSEC, June 2005, pp.2798-2801
(4) 平成 9 年度新エネルギー・産業技術総合開発機構委託業務成果報告書「太陽光発電システム実用化技術開発(高密度連系技術の研究)」(1998)
(5) K.Takeuchi, et al. “A new type of scaled-down network simulator composed of power electronics”, in Proc. WCPEC-3, May 2003, pp.2039-2042 vol.2

平成 18 年電気学会電力・エネルギー部門大会

185

マトリックスコンバータを用いた系統連系用ルータ機器の開発

学生員 鎌倉 輝男（東京農工大学） 非会員 林 健太郎（東京農工大学）
会 員 黒川 浩助（東京農工大学）

Development of Power Line Router based on Matrix Converter

Teruo Kamakura, student-member, (TUAT), Kentaro Hayashi, Non-member, (TUAT)
Kosuke Kurokawa, member, (TUAT)

1. はじめに

電力系統の調整余力を前提としている現在の太陽光発電（PV）システムは，連系される PV の総量が増加すれば系統への負担が増加し，導入量には限界があると考えられる。この問題に対し，さらに大量の PV が導入されたコミュニティにおいて基本的に潮流をコミュニティ内部で完結し，外部系統にじょう乱を波及させない自律度向上型太陽光発電システム（Autonomy-Enhanced PV Clusters : AE-PVC）が提案されている[1]。AE-PVC では需要家 PV による逆潮流はコミュニティ内で完結し，余剰電力はコミュニティ内で AC 蓄電ステーションに貯蔵される。基本的にコミュニティでの需用電力は PV 及び AC 蓄電ステーションで賄われ，外部系統との電力の融通は極力少なくなるが，季節変動など緩やかな変動に対しては外部系統との電力の融通を行う。基本的に独立する AE-PVC においては外部系統と同期をとる必要のない非同期連系がのぞましい。また，このようなコミュニティが複数存在し，隣接した場合は異周波間での連系も考えられる。外部系統と内部コミュニティとの電力の融通にはパワーエレクトロニクスによる系統間ルータ機器を用いることが提案されている[1]。外部系統，コミュニティとルータのイメージを図 1 に示す。

本論文では，AE-PVC にマトリックスコンバータを用いたルータを適用した場合の電力潮流についてのシミュレーション結果を示す。

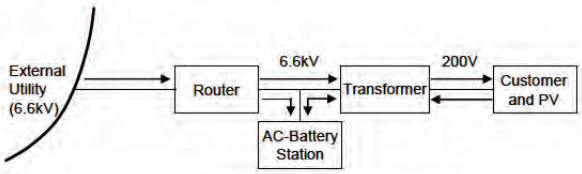

図 1 AE-PVC

Fig. 1. Figure image of internal community.

2. 系統間ルータ回路方式

パワーエレクトロニクスを用いた系統間ルータ機器の構成としては，AC/DC/AC 変換による BTB（Back-to-Back）方式とマトリックスコンバータ方式が考えられる。図 2 に示すマトリックスコンバータ方式は，BTB 方式において中間部に存在する直流リンクコンデンサを省略することができ，また直接変換方式であることから機器の小型化，長寿命化，導通損失低減が見込めるなど有利な点が多いと考える。

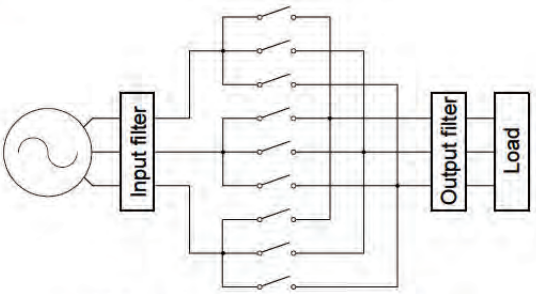

図 2 マトリックスコンバータ回路

Fig. 2. Matrix converter circuit.

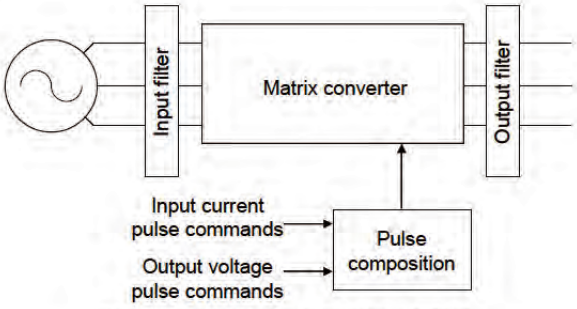

図 3 仮想 AC/DC/AC 方式による制御

Fig. 3. Configuration of virtual AC/DC/AC method.

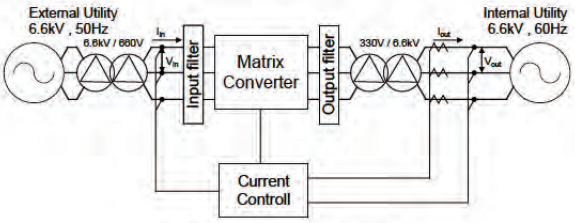

図 4　ルータシステム構成

Fig. 4.　Configuration of router system.

3.　系統間ルータの制御法

〈3･1〉　マトリックスコンバータの制御法

マトリックスコンバータの制御法の一つに仮想 AC/DC/AC 方式がある。この方式ではマトリックスコンバータを仮想的に AC/DC/AC 回路と見て間接的に制御する方式である。この方式では入力電流指令と出力電流指令を独立に考えることができるため，従来の BTB 方式での制御方式が応用でき，系統用ルータ機器としての制御を行いやすい。仮想 AC/DC/AC 方式の制御ブロックを図 3 に示す。

〈3･2〉　系統間ルータ

図 4 に AE-PVC におけるシミュレーションに用いた系統間ルータのシステム構成を示す。一般的なマトリックスコンバータは図 2 に示すように負荷が接続されるが，ルータの場合では出力端の電圧はコミュニティ内の需要家 PV, AC 蓄電ステーションにより固定される。従って，コミュニティ内部の位相情報よりコミュニティ内部に対し電流を流し込む必要がある。PV, AC 蓄電ステーションにより電圧が固定されるコミュニティ内部は 3 相電圧源により模擬する。本シミュレーションでは外部系統 50Hz，コミュニティ内部 60Hz の異周波連系を仮定する。

4.　シミュレーション結果

有効電力指令 P=200kW，無効電力指令 Q=0kVar としたときの外部系統，コミュニティでの電圧,電流を図 5 に示す。

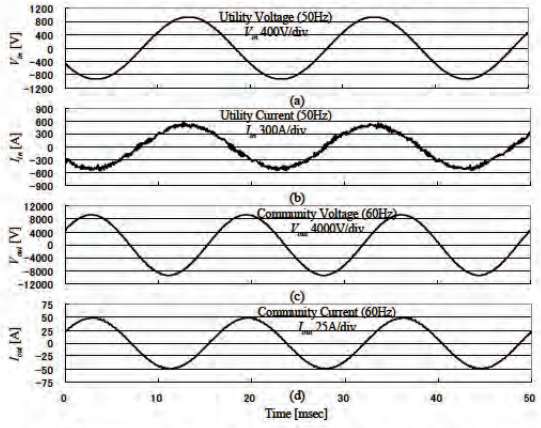

図 5　系統/コミュニティ電圧とルータ出力波形

Fig. 5.　Waveforms of utility voltage/current and router output voltage/current.

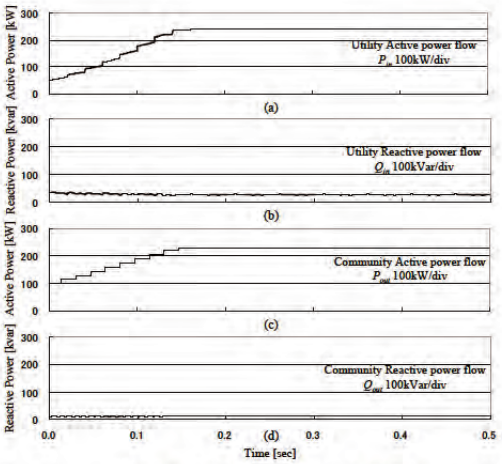

図 6　有効/無効電力の独立制御

Fig. 6.　Independent control of active and reactive power flow .

この結果より，外部系統，コミュニティ間において系統間ルータがコミュニティに電流を供給していることが判る

また，時間 t=0 から 0.15 秒において有効電力指令 P=100 から 250kW，無効電力指令 Q=0kVar 固定としたときのシミュレーション結果を図 6 に示す。シミュレーション結果より，異周波連系状態において外部系統，コミュニティ間で有効電力，無効電力の独立制御が可能であることが判る。

5.　まとめ

本論文では AE-PVC において必要とされる系統間ルータ機器に仮想 AC/DC/AC 方式のマトリックスコンバータを適用することの検討を行った。シミュレーション結果より，有効電力，無効電力の独立制御が可能であり，系統間ルータ機器に適用可能であることを明らかにした。今後は AE-PVC における複数のコミュニティ間に発展したコミュニティ間ルータについて検討を行う予定である。

6.　謝辞

本研究は New Energy and Technology Organization（NEDO）による受託研究，自律度向上型太陽光発電システム（AE-PVC）の一部として実施されてものであり，関係者各位に感謝する。

文　　献

（1）Kosuke Kurokawa, Shinji Wakao, Yasuhiro Hayashi, Itaru Ishii, Kenji Otani, Masahide Ymaguchi, Takafumi Ishii, and Yukiyoshi Ono : "Conceptual study on Autonomy-enhanced PV clusters for urban community to meet the Japanese PV2030 requirements", 20th European PV Solar Energy Conf., pp.2439-2443, 6-10 2005, Barcelona, Spain.

（2）伊東　淳一，佐藤　以久也，大口　英樹，佐藤　和久，小高　章弘，江口　直也：「キャリア比較方式を用いた仮想 AC/DC/AC 変換方式によるマトリックスコンバータの制御法」，電学論 D，Vol.124，No.5 pp.457-463 (2004).

平成 18 年電気学会電力・エネルギー部門大会

197

FPGA を用いた PV インバータ用デジタルコントローラの開発

学生員 瀬尾 祐介（東京農工大学） 正員 黒川 浩助（東京農工大学）

The Development of FPGA-based Digital Controller on for PV Inverter

Yusuke Seo, Student Member, (TUAT), Kosuke Kurokawa, Member, (TUAT)

1. まえがき

2001 年に示された「PV2030」では，2030 年までに総量 100GW の導入を目指しており，そのためには年産 10～20GW の自動生産ラインによる大量生産が必要となる。これには，太陽電池モジュールはもちろんインバータについても革新的な技術が必要とされる [1]。

本稿では，市販されている低価格な評価用 FPGA ボードをコントローラとして用いた太陽光発電用インバータの開発を行い，その試験結果を報告する。また，地域新生コンソーシアム研究開発事業によって開発されたデジタルコントローラ [2] との組み合わせ試験を行い，その結果についても報告する。

2. システム構成概要

本研究で用いたデジタルインバータの構成図を図 1 に示す。本システムは，FPGA ボードとインバータ本体が一つになったFPGAインバータと既存のデジタルコントローラの2つからなっている。インバータの回路パラメータを表 1 に示す。

表 1 システムパラメータ

Table 1. System Parameters.

L_1, L_2	438 μ H	C_1	4.75 μ F
R_L	10 Ω	*Carrier Frequency*	50kHz
MOS-FET	IRF644	FPGA	FLEX10K30A
最大入力電圧	36V	出力電力	20W

FPGA インバータには，交流電圧波形をレベルダウンした電流指令波形 v_{ref}，インバータ出力電流波形 i_o が A/D コンバータによって取り込まれ、定電流制御が行われる。

デジタルコントローラでは、主にインバータの起動，MPPT 制御，単独運転検出が行われており，インバータ運転指令値である出力電流定数（電流定数 k）の増減計算を行いインバータ本体へ出力している。電流定数は以下の(1)式を満たす。

$$i_o = i_{o\_max} \times k \quad \cdots(1)$$

ただし，i_{o_max}:インバータ定格出力電流

(1)式より，k の調整により交流出力電流が変化し，その結果直流入力電圧，電流の調整が可能である [3]。

図中，①はインバータの運転可否信号，②はインバータ起動信号，③は電流定数 k を表している。

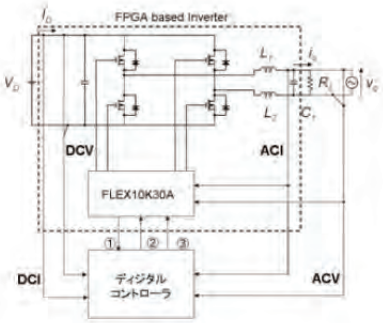

(a) 概要図

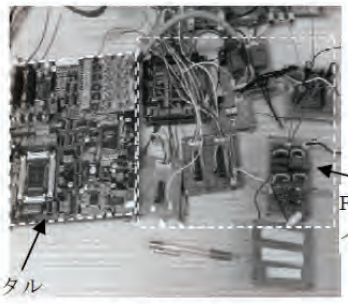

(b) 実回路

図 1 システム構成図

Fig. 1. System Configuration.

3. FPGA デザイン

図 2 に FPGA の内部構成を示す。電流指令波形 v_{ref} からサイクル信号のみを取り出し，PLL にて内部に格納された正弦波データと系統との同期制御を行う。系統と同期した正弦波データに，デジタルコントローラから出力された電流係数 k を乗算し，定電流制御をかけ PWM 信号を出力する。

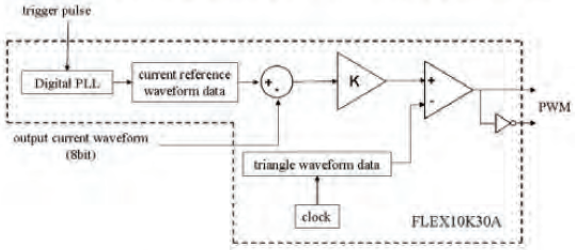

図 2　FPGA 内部構成図
Fig. 2.　Internal Configuration of FPGA.

4. FPGA based Inverter 基本動作試験

図 3 に系統連系時における定電流制御の結果を示す。系統側には実際の系統波形をトランスによって降圧したものを使用した。ここでは，デジタルコントローラボードは使用せず,電流定数 k は一定としている。

電流指令波形 v_{ref} からは系統波形のサイクル信号を取り出している。図 4 に各次の電流歪率の計算結果を示す。また，その計算結果より総合電流歪率の計算を行ったところ，3.48%となった。これより，出力電流の歪率は電気技術指針[4] で述べられている総合歪率 5%，各次歪率 3%以内の規定内であった。

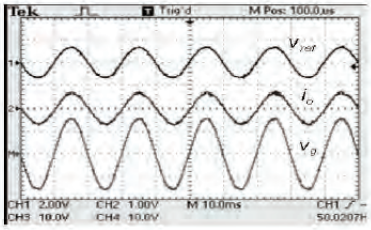

図 3　定電流制御時の波形
Fig. 3.　Waveforms at Current Control.

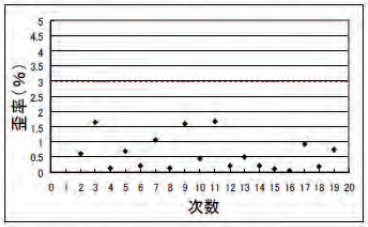

図 4　各次における歪率
Fig. 4.　Harmonic Distortion.

5. デジタルコントローラとの組み合わせ試験

デジタルコントローラの動作を確認するために，AC バイポーラ電源を系統として模擬した縮小実験を行った。

試験結果を図 5 に示す。インバータはデジタルコントローラの起動条件をクリアした後に運転を開始する。コントローラはインバータの運転状態を確認して MPPT 制御に移る。

図 5 では直流安定電源を模擬的につなぎ試験を行った。電流定数 k の増加に伴ってインバータ出力電流波形の振幅が増加している。また，k 値が急変した際も電流はその変化に追従できている。この結果よりインバータ，デジタルコントローラが正常に起動し動作していることが示された。

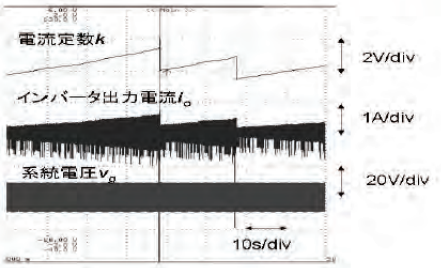

図 5　MPPT 制御時の波形
Fig. 5.　Waveforms at MPPT Control.

6. まとめ

本稿では，FPGA ボードをコントローラとして用いた FPGA インバータの開発ならびに，既存のデジタルコントローラボードとの組み合わせ試験を行い，オールデジタルのコントローラとしての動作を確認した。試験により，FPGA ボードとデジタルコントローラボートとの協調を取ることができ，静特性における安定性を確認することができた。

本研究は，新エネルギー・産業技術総合開発機構（NEDO）の革新次世代太陽光発電システム研究開発，自律度向上型太陽光発電システム先導研究開発の一環として実施された。

文　献

(1) K. Kurokawa, "Mass Production Scale of PV Modules and Components in 2030s and beyond" *in Proc. 15th International Photovoltaic Science & Engineering Conference (PVSEC-15)*, pp272-274, Shanghai, China, Oct 11-15, 2005.
(2)平成 13 年度　地域新生コンソーシアム研究開発事業「地域新生コンソーシアムエネルギー研究開発分野」「太陽光発電用分散型パワーコンディショナの研究開発」（第 2 年度）成果報告書
(3) 皆藤　貴志他:「太陽光発電用インバータ向けディジタル MPPT 法の開発」，電気学会全国大会，NO.7-131，pp201-202 東北学院大学，2003.3.17-19，
(4) 分散型電源系統連系技術指針（電気技術指針分散型電源系統連系編），社団法人　日本電気協会，2001

平成 18 年電気学会電力・エネルギー部門大会

184

LED ソーラシミュレータを用いた IV 特性測定の改良基礎実験

学生員 小柳 淳　　正 員 黒川 浩助（東京農工大学）

An Improved Fundamental Experiment of Solar Cell's I-V Characteristics Measurement Using LED Solar Simulator

Jun Koyanagi, student-member, Kosuke Kurokawa, member, (Tokyo University of Agriculture and Technology)

1. はじめに

太陽電池の定格出力評価はシステム設計や価格決定において非常に重要である。一般的に，出力評価にはキセノンランプを光源としたソーラシミュレータを用いるが，キセノンランプは赤外域で特有の輝線スペクトルを持ち，連続した基準太陽光スペクトルの模擬が難しいという問題がある。現在，赤外域の補正を行ったソーラシミュレータが開発されているが，装置が高価で，ランプの寿命が短く消費電力が大きいため，測定コストがかさむなどの問題点を抱えている。本研究では，小型，長寿命で省電力な LED を光源としたソーラシミュレータを試作し，青，赤，赤外 LED の持つスペクトルにより測定した，３つの波長における分光感度から（以下，離散分光感度と称す），全体の分光感度を推定する評価手法，および低照度で測定した IV カーブから 1-Sun における IV 特性の推定を行い，離散光源による太陽電池の評価手法の検討を行ってきた[(1)]。

本論文では，これまでの評価手法を改良し，これらを用い算出した太陽電池セルの出力精度を検証する。

2. 分光感度の推定手法の改良

〈2･1〉 分光感度推定手法　LED ソーラシミュレータを用い，結晶 Si 太陽電池の n 層，空乏層，p 層それぞれに感度がある離散光（青，赤，赤外）をそれぞれ照射し，３つの離散分光感度を得る。この離散分光感度を少数キャリア連続の方程式にフィッティングすることにより，全体の分光感度を推定する（式１，式２，式３）。フィッティングは表面再結合速度，少数キャリア濃度，表面反射率を変数として，最小二乗法を用いる。

〈2･2〉 推定手法の改良　これまでは半導体そのものの出力を推定していたが，実際にはパッケージ化された太陽電池セルの出力評価を行う。このため，セルの封止材（EVA），テクスチャ構造や BSF（Back Surface Reflector）構造などを反映させ分光感度推定を行った。具体的には EVA による紫外線吸収を考慮し掛け合わせた[(2)]。また，これまで p 層と裏面金属電極間の再結合速度を∞[cm/s]として計算していたものを，BSF 構造により p^+層があることから 10～100[cm/s]とし，光閉じ込め効果により屈折・反射し長波長の光路長が増大するため，p 層の膜厚を３倍とし算出した。また，フィッティング後離散点とずれが生じている場合，濃度や p^+層の影響により空乏層の幅にばらつきが生じると仮定し，空乏層の膜厚を変数とし再度フィッティングを行った。

$$\frac{J_p}{I_0(\lambda)}=\left(\frac{e(1-R)\frac{\lambda}{e\times hc}\alpha(\lambda)L_p}{\alpha(\lambda)^2L_p^2-1}\right)\times\left[\frac{\frac{S_pL_p}{D_p}+\alpha(\lambda)L_p-\exp(-\alpha(\lambda)x_j)\left(\frac{S_pL_p}{D_p}\cosh\left(\frac{x_j}{L_p}\right)+\sinh\left(\frac{x_j}{L_p}\right)\right)}{\frac{S_pL_p}{D_p}\sinh\left(\frac{x_j}{L_p}\right)+\cosh\left(\frac{x_j}{L_p}\right)}\right] \quad \cdots\cdots(1)$$

$$\frac{J_{dr}}{I_0(\lambda)}=e(1-R)\frac{\lambda}{e\times hc}\exp(-\alpha(\lambda)x_j)\{1-\exp(-\alpha(\lambda)W)\} \quad \cdots\cdots(2)$$

$$\frac{J_e}{I_0(\lambda)}=\left(\frac{e(1-R)\frac{\lambda}{e\times hc}\alpha(\lambda)L_e}{\alpha(\lambda)^2L_e^2-1}\right)\exp\{-\alpha(\lambda)(x_j+W)\}\times\left[\alpha(\lambda)L_e-\frac{\frac{S_eL_e}{D_e}\left(\cosh\left(\frac{H'}{L_e}\right)-\exp(-\alpha(\lambda)H')\right)+\sinh\left(\frac{H'}{L_e}\right)+\alpha(\lambda)L_e\exp(-\alpha(\lambda)H')}{\frac{S_eL_e}{D_e}\sinh\left(\frac{H'}{L_e}\right)+\cosh\left(\frac{H'}{L_e}\right)}\right] \quad (3)$$

J：電流密度	[A/m^2]
I_0：入射光強度	[W/m^2]
R：表面反射率（任意パラメータ）	[-]
h：プランク定数（=6.626×10^{-34}）	[J・s]
c：光速（=2.998×10^8）	[m/s]
λ：波長	[μm]
e：電荷（=1.602×10^{-19}）	[C]
α：吸収係数	[1/cm]
Lp：少数キャリア拡散長（=232）	[μm]
Le：少数キャリア拡散長（任意パラメータ）	[μm]
Sp：表面再結合速度（任意パラメータ）	[μm]
Se：表面再結合速度（=∞）	[μm]
Dp：拡散係数（=36）	[cm/s]
De：拡散係数（=1.295）	[cm/s]
x_j：空乏層までの深さ（=0.5）	[μm]
W：空乏層の厚さ（=0.93）	[μm]
H：セルの厚さ（=450）	[μm]
H'：$H'=H-(xj+W)$	[μm]

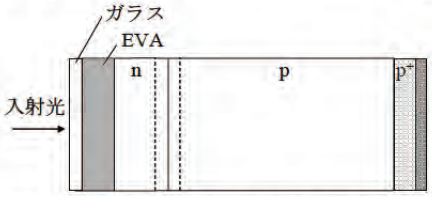

図１　分光感度の推定に用いたセルのモデル
Fig. 1.　Model of packaging solar cell.

〈2･3〉 **理想離散値による推定結果** フィッティング結果を図 2 に示す。300[nm]付近の大きく推定していた値を実測した分光感度値に近づくことがわかった。

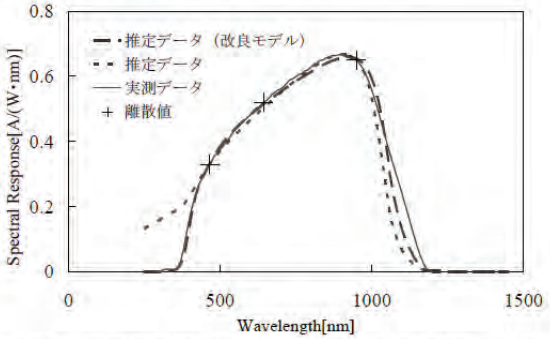

図 2 理想離散値を用いた分光感度の推定結果の比較

Fig. 2. Comparison of measured and estimated spectral response using ideal discrete spectral response.

〈2･4〉 **実測離散値による推定結果** LED に定格電流および定格電流の半分を流し，同色 LED の放射照度を変えたときの放射照度および電流値を実測し，差分より離散分光感度を求め全体を推定した。結果および実測に用いた LED のスペクトル分布を図 3 に示す。

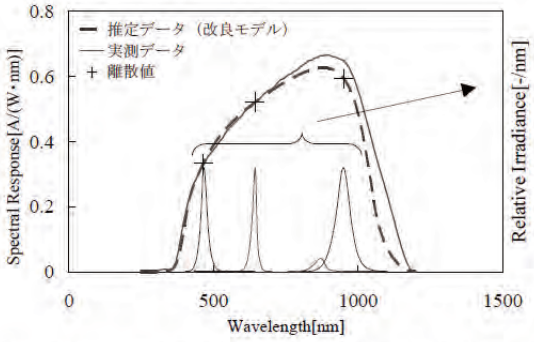

図3 実測離散分光感度より求めた分光感度推定値および測定に用いた LED のスペクトル分布

Fig. 3. Calculated spectral response and wavelength characteristics of LED.

3. 実測離散分光感度値による IV 特性推定

これまで，直線補間法[3]を外挿に用い，異なる照度で測定した IV 特性を標準試験状態における IV 特性を推定していたが，今回青色 LED を照射し測定した IV 特性と暗電流を用い，2 つの IV 特性の照度差を広げ推定精度の改善を図った。実測離散分光感度より算出した短絡電流値を用い，外挿した結果を表 1 および図 4 に示す。

4. まとめ

これまでの手法に紫外吸収，光閉じ込め効果などを考慮することでパッケージ化されたセルの分光感度を推定できることがわかった。また，推定した分光感度より求めた短絡電流値を用い，青色 LED と暗電流から直線補間法により算出した IV 特性はこれまでの手法に比べ実測値に近づくことがわかった。特に最大電力点は改善が見られた。

表 1 実測結果と算出した結果の比較

Table 1. Comparison of measured and calculated solar cell's property.

	算出	実測
短絡電流[A]	3.410	3.760
開放電圧[V]	0.571	0.603
最大電力点[W]	1.535	1.554
最大電力点電流[A]	0.477	0.461
最大電力点電圧[V]	3.219	3.370

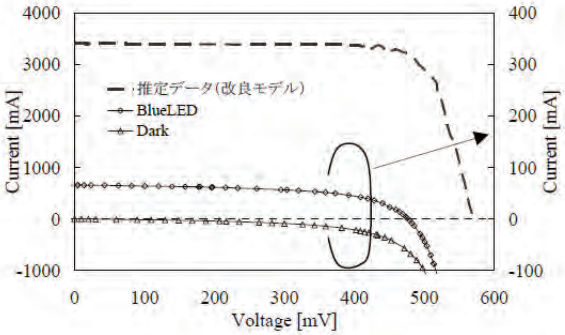

(a) 推定に用いた 2 つの IV 特性と推定 IV 特性

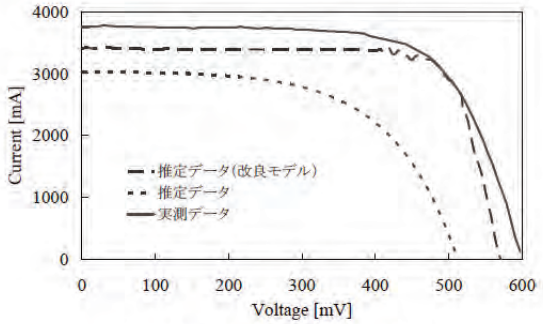

(b) 実測 IV 特性と推定 IV 特性の比較

図 4 暗電流を用いた IV 特性の推定結果

Fig. 4. Calculated I-V curve using dark current and blue LED.

5. 謝辞

データ計測など多大な協力を頂いた英弘精機株式会社に感謝の意を表する。本研究は文部科学省科学研究費萌芽研究の補助を受けた。

文 献

（1） Shogo Kohraku, Kosuke Kurokawa : "A fundamental experiment for discrete-wavelength LED solar simulator", 14th International Photovoltic Science and Engineering Conference (2004)

（2） F.J.Pern : "Factors That Affect The EVA Encapsulant Discoloration Rate Upon Accelerated Exposure", 1st WCPEC pp.897-900 (1994)

（3） 菱川善博，井村好宏，関本 巧，大城壽光：「各種太陽電池の IV 特性における放射照度依存性及び補正の検討」，電気学会論文誌，Vol.122-B，No.1，pp.26-32. (2002)

シンポジウム・解説

［2006 年～2007 年］

第 23 回太陽光発電システムシンポジウム
2006 年 6 月 14～16 日，朝日ホール

太陽光発電システム研究開発の方向性と再生可能エネルギー2006 国際会議

東京農工大学大学院
黒川浩助

1．まえがき

平成 17 年度には，総合科学技術会議において，第３期科学技術基本計画が制定された。この中で，第二期計画で重点推進分野としてライフサイエンス，情報通信，環境，ナノテクノロジー・材料の４分野が抽出されていたが，さらに推進４分野の，エネルギー，ものづくり技術，社会基盤，フロンティアが追加されたことは，太陽光発電システム技術分野の推進の背景として大きな進展と評価される。太陽光発電は重点推進分野の環境分野に含まれるところではあるが，エネルギーとして見える形で示されたことは心強い。

また，これらの基本計画の制定に加えて，分野ごとの超長期のロードマップが「技術戦略マップ」という形で示された。エネルギー技術戦略マップでは，エネルギー政策では言及されてこなかった 2100 年までの長いスパンでの複数のケースタディが実施されたことは特筆に値する。これらのケーススタディでは，化石燃料重点ケースおよび原子力重点ケースに加えて，再生可能エネルギー重点ケースが示されたことも喜ばしいことである。

太陽光発電技術開発のロードマップである「PV2030」では，目標としている 100GW 導入において，競合コストの点から依然として個人住宅分野が全体の半分近くを占めるとしている。住宅地域においてこのような高い普及率を目指すには，ある地域の配電系統で，分散した家庭負荷と太陽光発電が融合したような系統構成を実現することが必要と考えられる。すなわち。現在の配電系統のように変電所側を上流側とする概念ではなく，配電系統での電力フローを両方向に自由に流通する（すなわち 100%の逆潮流を許容）基本デザインが望まれる。

また，「PV2030」が目標とする太陽電池の高効率化により，ある地域が太陽光発電のみで系統内負荷とバランスすることができる（年ベースで自給可能）という想定に立つと，外部系統とのインターラクションは，現在のように太陽光発電電力の変動を無計画に吸収することを前提とすることは，電力システムのトータルシステム最適化の観点からは望ましいとはいえない。むしろ，地域の中での平準化を図りながら，外部系統とのやりとりを計画的に行い，外部系統から見れば，連系点において制御されたひとつの電源または負荷のように運用できれば，連系運用契約上の付加価値は数等高まると予想される。

このようなコミュニティでは，それが持つ太陽光発電ポテンシャルを地域のために 100%活かすことが可能となる。これはまさしく「ソーラーシティ」と呼ぶことができる。このような基本概念を具体的なイメージに深めるために，平成 17 年度末までに NEDO 技術開発機構委託研究「自律度向上型太陽光発電システム」のフィージビリティ研究が１年半にわたって実施されてきた。

太陽光発電システムをよく知るものは，きっと誰しも太陽光発電が環境に優しいと深く信じているであろう。しかし，そう思いこんではいけない。本当に「環境に優しい」ことをみずからデータを示しながら，社会に向かって示していかなければならない。このようなチャンスがやってきた。エコマーク制度に，住宅用太陽光発電の［システム］，「太陽電池モジュール」，「パワーコンディショナ」が指定製品に加えられた。初めての制定なので，少し注意深く製造された製品・システムであれば，指定を受けることはそう困難ではないはずと思う。本来であれば，製品ごとのＬＣＡデータを出さなければならない時代であるが，今はそうなっていない。

京都議定書制定の際の日本は，2008～2012 年までの CO_2 削減目標の 1990 年比－6%の達成は，

現状で+6%レベルまで増加している現状で，実質 12%台の削減を目指すことと同義であり極めて苦しい立場にある。またさらに，世界の目は次の期間である 2020 年を目指した議論も行われるようになってきており，日本としても，上記 METI ビジョンでも示された，省エネ・新エネにおいて得意な技術力を活かすことが提唱されてきている。このような状況を座視することなく，積極的なメッセージを世界へ向けて発信する一つの機会として，「再生可能エネルギー2006 国際会議 Renewable Energy 2006」が 2006 年 10 月に幕張メッセにおいて開催されようとしている。同国際会議では 10 大再生可能エネルギー分野の技術発表に加えて，これらの産業力を示すための，「新エネルギー世界展示会」が併設され，多くの耳目を集めようとしている。

2．第３期科学技術基本計画（平成 18～22 年度）の概要[1]

2.1　第３期科学技術基本計画の基本理念

（１）基本姿勢

①　社会・国民に支持され，成果を還元する科学技術を目指し，絶え間なく科学水準の向上を図りながら，知的・文化的価値を創出していく。また，研究開発の成果をイノベーションを通じて，社会・国民に還元していき，社会的・経済的価値の創出につなげていく。

②　このために，人材育成と競争的環境を重視する。

（２）科学技術の政策目標の明確化

政府研究開発投資が何を目指すのかを明確にするため，3 つの基本理念の下で目指すべき具体的な政策目標を設定する。その大目標は以下の通りである。

①　飛躍知の発見・発明
②　科学技術の限界突破
③　環境と経済の両立
④　イノベーター日本
⑤　生涯はつらつ生活
⑥　安全が誇りとなる国

（３）政府研究開発投資

政府研究開発投資の総額規模を約 25 兆円とする。（計画期間中の対 GDP 比 1%，GDP 名目成長率 3．1%を前提）

2.2　科学技術の戦略的重点化

（１）基礎研究の推進

①　研究者の自由な発想に基づく研究を推進し，多様性の苗床を形成していく。これらは，政策課題対応型研究とは明確に区分する。また，ビッグサイエンスは国としても優先度を含めた判断を行い取り組む。

②　政策に基づき将来の応用を目指す基礎研究を推進し，非連続的なイノベーションの源泉となる知識を創出していく。

（２）政策課題対応型研究開発における重点化

①　政策課題対応型研究開発における重点化について，第２期基本計画における重点推進４分野に加えて，推進４分野を進める。第３期基本計画で推進４分野が追加され，エネルギー分野が明示されることとなった。（歓迎！）

重点推進　４分野	推進　４分野
ライフサイエンス	**エネルギー**
情報通信	ものづくり技術
環境	社会基盤
ナノテクノロジー・材料	フロンティア

②　分野別推進戦略

第３期期間中に重点投資する対象として，戦略重点科学技術を選定し，選択と集中を図る。①社会・国民ニーズ（安全・安心等），②国際的な科学技術競争，③国家基幹技術（スーパーコンピュータ，宇宙輸送システム等）。また，新興領域・融合領域へ対応していく。さらに，第３期期間中であっても，必要に応じて分野別推進戦略の変更・改訂を柔軟に行う（「活きた戦略」の実現）。

2.3　科学技術システム改革

科学技術システム改革として，①人材の育成・確保・活躍の促進，②科学の発展と絶えざるイノベーションの創出，③科学技術振興のための基盤の強化，④国際活動の戦略的推進，⑤社会・国民に支持される科学技術，⑥総合科学技術会議の役割があげられており，若手・女性・外国人研究者の育成，大学の競争力強化，地域イノベーション，研究教育基盤強化，アジア諸国との協力などのキーワードが見えるが，詳細は割愛する。

３．エネルギー技術戦略マップ・超長期ビジョン[(2)]

3.1　ビジョン策定をとりまく背景

第３期科学技術基本計画を受けて，各分野での技術戦略ロードマップ策定審議が経済産業省産業技術環境局において進められたが，エネルギー分野においては，同省資源エネルギー庁がエネルギー技術戦略マップを策定した。この際の前提として，地球環境問題についてはポスト京都議定書が議論されるようになっていること，エネルギー長期的ビジョンにおいて環境制約およびエネルギーセキュリティの両面の可能性を論じたいことなどから，化石燃料重点，原子力重点，再生可能エネルギー重点の３つの極端ケースについて可能なシナリオを検討した。

3.2　超長期ビジョン策定のアプローチ

今回の超長期ビジョン策定のアプローチは，図１に示すように，まず，西暦 2100 年時点に資源制約・環境制約を乗り越えるために求められる「将来の技術の姿」を想定した。次に，この将来の姿へ到達するための道筋や技術スペックを「技術戦略マップ」としてまとめたこと，すなわちバックキャストのアプローチを採用したことが一大特徴である。そのために，エネルギー転換，運輸，民生，産業のニーズ側からの議論を優先し，技術分野ごとの積み上げ議論を避けたことも特徴といえる。

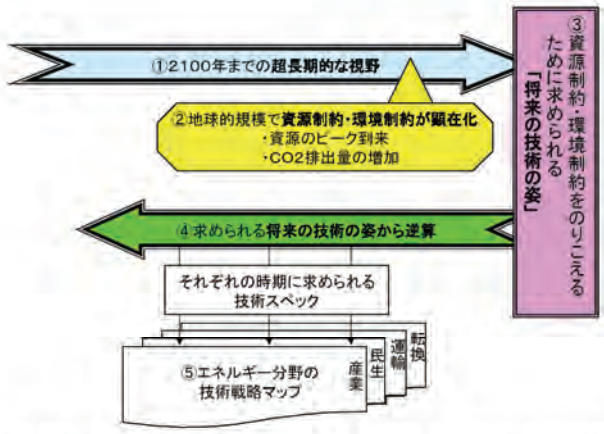

図１　エネルギー技術戦略策定のためのバックキャスト・アプローチ

検討の前提は以下の通りである。

① 水素社会，分散型エネルギー社会，バイオマス社会といった絵姿を前提としない。
② エネルギーにかかわる種々の制約を構成する連鎖構造を断ち切るとの観点から技術を検討。
③ 極端シナリオを想定して技術の備えを検討。バックキャストと既存のフォアキャストによるシナリオ・ロードマップのギャップを同定する。
④ 長期エネルギー需給見通しや既存のロードマップなどに制約されない。

3.3 ３つの極端ケース

以下に３つの極端ケースについての検討結果をまとめる。西暦 2100 年の日本の姿を**表１**のよう想定した上で，

① ケースＡ（化石資源＋CO2 回収・隔離）
② ケースＢ （原子力でほぼ供給）
③ ケースＣ：（2100 年には全量再生可能エネルギーで供給）

の極端化した場合のケーススタディを実施した。**表２～表４**にこれらをまとめた。**図２**にこれらのケースの相互の位置づけを示した。これらの中のどのアプローチが選択肢であるといっているわけではないが，再生可能エネルギーと（究極の）省エネルギーによって 2100 年ニーズを全量まかなうシナリオを描きだしていることの意味は大きい。この方向はわが国が工業力によって世界のエネルギー市場での存在感を示せる選択肢の一つである。**図３**にケースＣの試算結果を参考に載せる。

表１ ケーススタディの全体の考え方

全 体 の 考 え 方	
需要分野	・得られる「効用（経済活動，生活の質など）」は，GDP に比例して増大する。 ・その上で，連鎖脱却に向け，必要エネルギー量（＝転換分野からの供給エネルギー）の原単位を最小化する等の必要な技術的備えを行う。
GDP（日本）	・2050 年で 1.5 倍，2100 年で２倍程度と想定。

西暦 2100 年という超長期のシナリオ検討が経済産業省や資源エネルギー庁の土俵にあがったということの意味はもっと大きい。これからのわが国の将来を占っていく場合に，このように将来を見通す視点が不可欠であり，今回のビジョンを参照することで道が拓けたと考える。

これらの検討の中で 2100 年の地球温暖化を考える上でも，ＧＤＰ当たりの排出量という考え方をとっているが，欧州などで見られる人口当たり排出量との考え方の差は大きく，今後の大きな争点となることが予感させる。しかし，京都議定書でとられている単純な 1990 年基準の排出量論議はいかにも客観性を欠くところから，このような議論は大いに仕掛けていただきたいところである。

表２ 極端ケースＡの考え方

ケースＡ （化石資源＋CO2 回収・隔離）	
転換分野	・発電・水素量：現状総発電量の約８倍：石炭火力＋CCS を主体，他
産業分野	・化石資源消費時には，８割以上を CO2 回収・隔離 ・CO2 回収・隔離が困難な設備では電化・水素化を進める
運輸分野・民生分野	・電気と水素で 100%を供給する〔ＣＯ２回収・隔離付きの石炭火力等で供給〕
主な仮定	・発電・水素製造設備の設備稼働率は，80%と想定。 ・エネルギー需要が 2.1 倍に増加するとともに，電化・水素化率の上昇によって，発電・水素量は，現状の約８倍と算出。 ・転換分野から 95%，産業分野から 80%の CO2 を回収・隔離する前提で算出。 ・CO2 回収・隔離のために追加的に必要となるエネルギーは含まない。 ・運輸分野において，飛行機等を除く。 ・転換・産業分野で CO2 の隔離総量は約 40 億 t-CO2/年になる。

CCS: CO2 Capture and Storage

表３　極端ケースＢの考え方

ケースＢ　（原子力）	
転換分野	・発電・水素量：現状総発電量の約８倍：原子力でほぼ供給
産業分野	・原材料以外は，全て電気と水素でまかなう。
運輸分野・民生分野	・電気と水素で 100%を供給する。
主な仮定	・省エネ等に大きく依存できない場合を想定。 ・電気・水素化率の上昇を加味し，原子力設備（発電・水素製造）の利用率は，90%を想定。 ・エネルギー需要が 2.1 倍に増加するとともに，電化・水素化率の上昇によって，発電・水素量は，現状の約８倍と算出。 ・運輸分野において，飛行機等を除く。

表４　極端ケースＣの考え方

ケースＣ　（再生可能エネルギー＋究極の省エネルギー）	
転換分野	・発電・水素量：現状総発電量の約２倍：2100 年には全量再生可能エネルギーで供給
産業分野	・エネルギー需要を 70%低減：①製造エネルギー原単位を 50%低減 ②物質エネルギー再生を 80%に　③高機能化（強度等）を４倍に ・発電・水素量・バイオマスで供給
運輸分野	・省エネルギー，燃料転換により：エネルギー需要を 70%低減 ・自動車では 80%低減
民生分野	・省エネルギー，創エネルギーにより，エネルギー需要を 80%低減
主な仮定	・「効用」が 2.1 倍に増大する中で，各需要分野での省エネ等を最大限に引き出してもなお転換分野において供給することが必要となる量を再生可能エネルギーで賄うものとして算出。

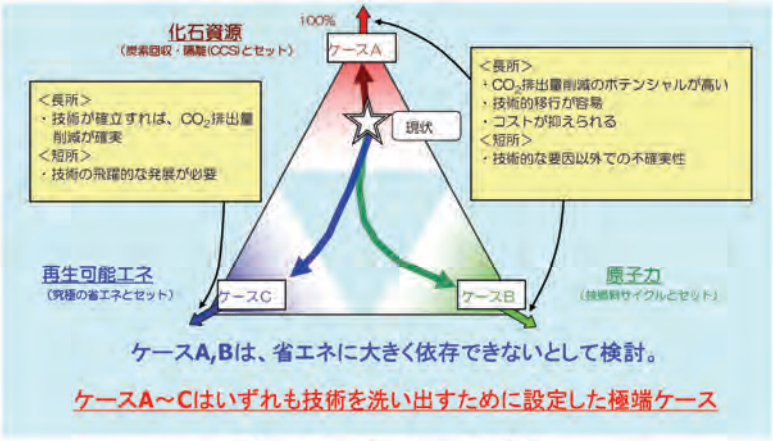

図２　３つの極端ケースの設定

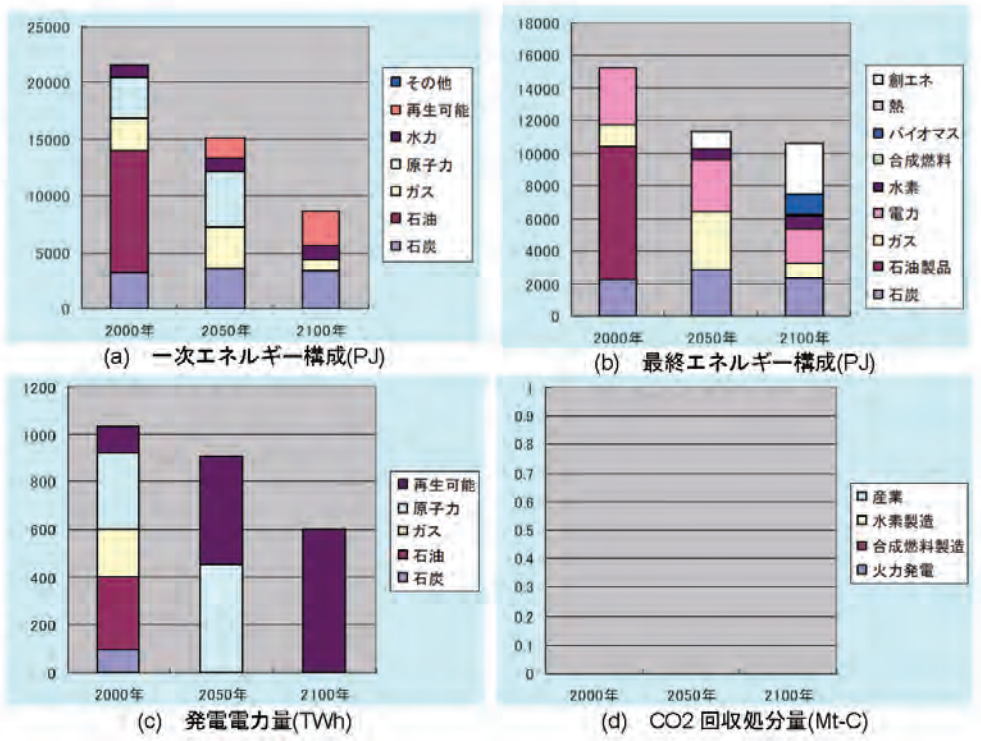

図３　再生可能エネルギー極端ケースの試算結果

４．自律度向上型太陽光発電システムの概念[4]～[8]

4.1　自律度向上システムの必要性

図４に示す「PV2030」のケース２は技術開発で加速した，2030 年次展のシステム導入形態を示している。ココでは総導入量 100GW のうち，40%以上が個人住宅の屋根上発電を想定している。これは，他の適用分野に比べて電力の競合コストの展で個人住宅が比較有利になることによる。これは国内の個人住宅の総量の半分近くに相当するレベルである。全国平均でこのような普及を目指すということは，太陽光発電普及率が 100%に達するコミュニティが多数出現すると考えるのが自然である。

また，太陽光発電出力は，日射変動にほぼ比例した出力となり，日射の変動による出力変動が生ずる。このため，現状では電力系統の調整余力でカバーされ，運用上の問題は顕在化してはいないが，太陽光発電導入率は高まるに連れ，系統運用上の導入制約が問題になる可能性がある。また，このことにより，外部への余剰電力送電や，外部系統からの応援電力の単価が現状枠組みとは変わってくる可能性があるので，太陽光発電の採算性向上の障害となる問題点も予想される。

このような諸課題を可能な限り回避するために，高度集中した太陽光発電集合を主体にした新しいコミュニティシステム概念を「自律度向上型太陽光発電システム」と名付けて，フィージビリティ研究を提案し，平成１６～１７年度に研究実施した。

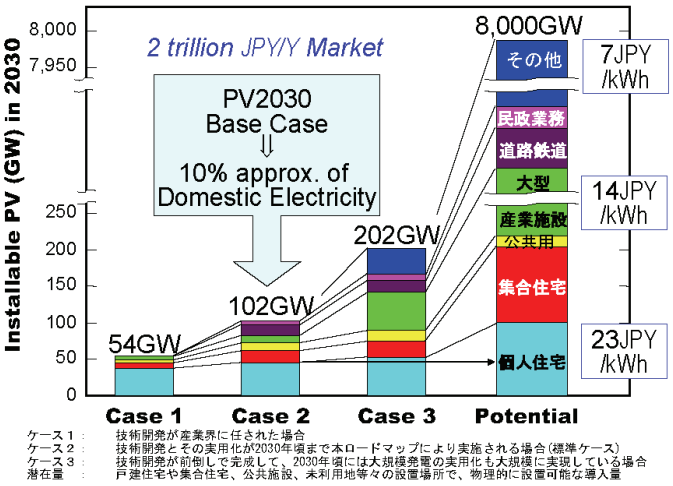

図４　PV2030 ロードマップにおける個人住宅割合の想定

4.2　自律度向上型太陽光発電システムの定義

図５に自律度向上型太陽光発電システムのイメージを示す。ここでは，以下のような基本的な諸点を考慮してイメージ図を作成した。

(i)　外部系統への不規則な逆潮流（場合によっては系統内の逆潮流）を抑制しがら，地域内全体の太陽光発電電力の有効利用を図り，また計画的な電力購入も可能とするために，蓄電池ステーション（集中配置・分散配置など）を設置する。

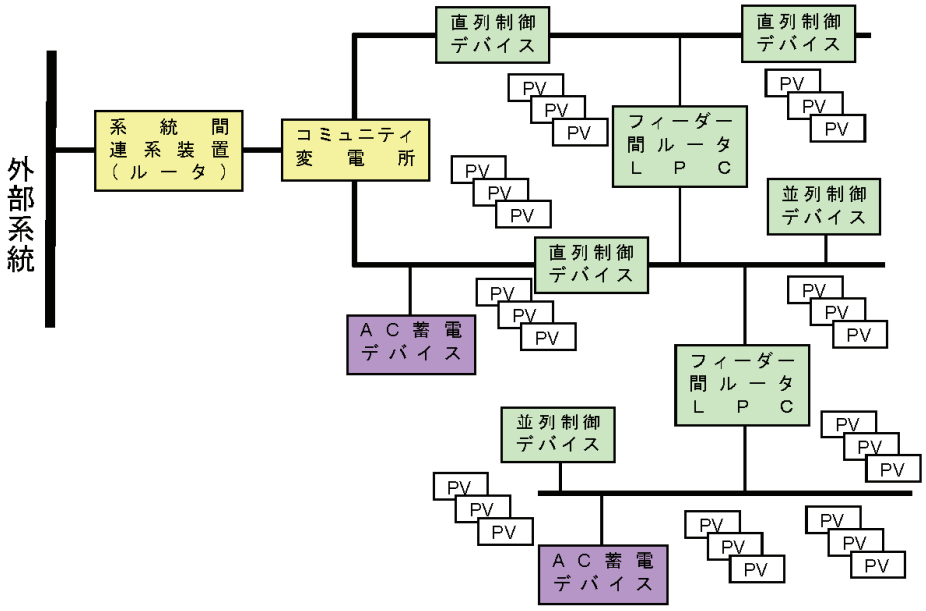

図５　アクティブ・ネットワーク概念を導入した自律度向上型太陽光発電システムのイメージ

(ii)　外部系統との相互のやりとりを制御されたものとするための外部系統連系ルータ機能を連系点に具備する。また，系統内部のフィーダ間や他のコミュニティ系統との間のコミュニティ間ルータも発展系として考慮できる。ルータ機能はパワーデバイス技術の進展に伴い，BTB やマトリックスコンバータを構成する。地域系統内の事故や，あるいは外部系統での事故が互いに波及しないように制御・保護することも可能になる。

(iii)　100%の PV 導入状態において自由に逆潮流させ，地域系統配電線全体の電圧問題や配電系統設備の稼働率向上・最適潮流制御を解決する手段としてのパワーエレクトロニクスを導入したアクティブ・ネットワーク技術を導入する。

また，本研究の進展により，

(iv)　おおむね 100 軒以上の小住区を対象として配電方式として，高圧系を並行して引き回さない低圧系統の可能性を，この概念に追加した。

(iv)項のイメージとして，**図 6** を掲げる。図中，楕円の格子状部分が低圧配電小住区を示している。

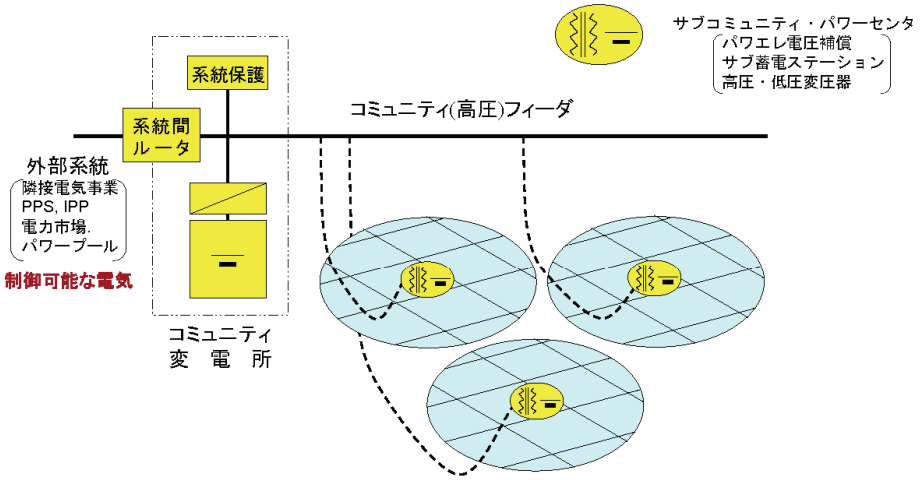

図６　低圧配電によるおおむね 100 軒以上の小住区を単位とした
自律度向上コミュニティ系統のイメージ

4.3　自律度向上型太陽光発電システムのトータルシステム考察

（１）　既存電力系統の存在を前提

(a)　前述の考え方に基づき，当面わが国での大量普及を考え，既存商用電力系統とのやりとりを最小化していくことを自律度向上策の方向とするが，最小限度といえども既存商用系統の存在は第一前提としている。（独立型システムを目指すものとは質的に異なる）

(b)　しかし，2030 年を目指して長期の可能性として，最適なコミュニティ電力供給（配電）ネットワーク構成を考えるに当たっては，既存形態にとらわれずに，自由な形態へ展開していくことを主要な検討項目の一つとして考えていく。（マイクログリッドプロジェクトの視点との大きな違い）

(c)　なお，地球エネルギー問題を考えれば，独立型のシステム開発も大命題であるが，本提案のような技術開発が成功裏に進めば，その波及効果として途上国の村落電化や，さらには砂漠などの未利用地における大規模太陽光発電システム(VLS-PV)への適用は応用問題として扱うことが可能となろう。

（２） 想定する自律度向上型システムの基本機能

系統連系された太陽光発電システムの系統への依存度を低下する基本戦略としては次のようなアプローチを考察した。

① 外部系統への依存度合い（自律度）に差を付けた単体あるいは集合としての太陽光発電システムを構築・運用する方策。

② オプションとして家庭内や地域内負荷の機能や利用状態と協調をとって，総体として自律度を高める方策。

③ 自律度 100%を仮想的な状態を参照ケースとした概念を考察。

④ 隣接するコミュニティ間で分散自律的に互いの需給を補完運用するインター・コミュニティ・ルータ機能の構築。

以上の①～④の程度や組み合せによって，自律度のレベルを０～Ⅴまで想定・分類し，要求される主な基本機能を**表５**に示した。

表５ 自律度向上のための各種基本機能（仮想的なケースを含む）

自律度	主要な機能	PV の連系
レベル０	双方向潮流	個別 PV 連系 従来型配電系統
レベルⅠ	双方向潮流 電圧上昇抑制用個別内部蓄電池	個別 PV 連系 従来型配電系統
レベルⅡ	双方向潮流 配電線制御・蓄電最適化	個別 PV 連系 従来型配電系統
レベルⅢ	片方向（または双方向）潮流連系 非常時電力融通(潮流制御された相互連系) 蓄電ステーション・アクティブ内部系統	コミュニティ系統
レベルⅣ	完全自律・連系潮流常時時は０ 非常時電力融通(潮流制御された相互連系) 蓄電ステーション・アクティブ内部系統	コミュニティ系統
レベルⅤ	コミュニティー間相互連系に発展 潮流制御された自律分散相互連系（常時） 蓄電ステーション・アクティブ内部系統	コミュニティ系統

（３）自律分散型ソーラーシティー概念への発展

コミュニティ内の主力電源が太陽光発電であるケースは地域新エネルギーふそん量からいって 2030 年に向かって非常に多く見込まれる。太陽光発電サイドの制御機能を生かしたコミュニティシステムの検討は欠かせない。レベルⅢはこのようなケースを含んでいると考える。

上述③では利用機器がわの使用量の制御機能やエネルギー貯蔵機能の利用を想定している。たとえば，昼間の太陽光発電電力によりヒートポンプを駆動するシステムでは，夏期冷房期には冷水の貯蔵タンクを設けて夕方ピーク冷房需要もまかない，冬季には温水貯蔵に切り替えて，夕方ピーク暖房に回すことが可能である。このような方策により，ＰＶを主体としたオール電化住宅の実現も夢ではない。現状では，住宅屋根の形状制約から思ったほどの設置面積が得られず，自

給度が低いのが現状であるが，2030 年に向かって，例えば 22%程度の高効率モジュールが実現すれば，80%程度の住宅で自給度 100%が実現できる可能性がある。

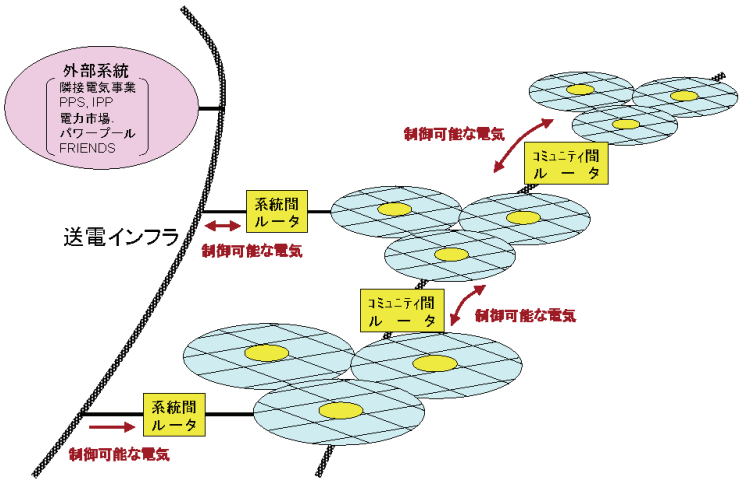

図７　自律度向上型太陽光発電コミュニティによる広域展開のイメージ

また，レベルⅤは，隣接し合った自律度向上型太陽光発電系統が自律・分散的に相互連系していく，分散自律広域ネットワークへの展開を想定している。自律度向上型ネットワーク概念で考察している系統間ルータ機能を発展させることにより，**図７**のような広域ネットワークの構築が示現できよう。ルータ機能の持つ，自分の系統にとって負担あるいは受け入れ可能な範囲内の電力潮流に制限して相互運用することで，自律分散的な広域連系することが基本的要件と判断される。全体システムをあらかじめ設計し，中央コンピュータにより制御しようとすることは，このように自律分散的に発展していくネットワークでは非常に困難が伴うであろう。

（４）　外部系統との連系機能

以下の３種類を定義する。

①　抑えた量の電力量の双方向のやりとり　（卸売電力レベル）
②　片方向のやりとり　（制御された買電のみ：将来卸売り電力として購入したい）
③　非常時予備力　（事故や定期点検時の応援電力：非常電力契約が必要）

（５）　系統間連系の方式

(a)　同期連系

①　隣接系統と同期連系するので周波数は相手側に従属
②　連系点の電圧制御は，P・Q 制御により可能となる。
③　P 制御は，コミュニティ系統内の蓄電システムや個別電源のパワー調整により実現。
④　Q制御は，連系点における，アクティブ移相機，VAR 調整，SVC，あるいは各電源の位相調整などにより実現。
⑤　全体的な制御ロジックを開発するには，系統間連系を含むトータルシステムのシミュレーションが必要である。
⑥　蓄電システムとの協調運用・制御システム開発は必須。

(b)　非同期連系

①　２台の双方向交直変換装置を組み合わせた DC リンク方式 BTB 変換装置やマトリックスコンバータによる非同期連系装置を開発する。
②　制御方式：自端情報にもとづくＰ潮流制御；各端でのQ制御；コミュニティＰＶ系統の周波数制御・電圧制御，コミュニティ系統の事故に対する保護
③　シミュレーション研究の必要性
④　分布された蓄電池ステーション群の自律分散制御やコミュニティ間の負荷分担を自律的

に可能とする周波数垂下あるいは電圧垂下制御方式の導入の可能性

5．　住宅用太陽光発電システム・エコマーク制定[9]

5.1　エコマーク製品可否の一般条件

住宅用太陽光発電システムを含めたエコマーク認定基準が 2006 年 3 月 15 日制定施行された。

エコマークは，「ちきゅうにやさしい」という言葉とともに，母親の手のようにやさしく，しっかり抱きしめている地球を表している。この地球の環境をみんなで大事にしようというマークであり，（財）日本環境協会によって運営されている。また，国際的な活動としての広がりを持ち，エコマークの付いた商品を使うことで地球全体の環境を守ることになる。

毎日の生活の中で人々はいろいろな製品に対し，次のような基本的なポイントでエコマーク可否が製品群ごとに判断される。

(1)　製造段階で環境に注意しているか。
(2)　使用する場合に，資源やエネルギーが節約されているか。
(3)　廃棄するとき，簡単に処理ができ，公害にならない。
(4)　品質や安全性などが基準に合っている。

地球環境にやさしいと認められた製品は，平成元年で 46 商品だったが，現在では 54 類型，5,646 商品（2004 年 3 月現在）と幅が広がり，文房具をはじめ，せっけん，タイル，ブロック，インク，ゴム手袋などの日用品からプリンター，建築用のマット，パソコンなど工業用材料や事務機器・電気製品などさまざまをカバーしている。

5.2　住宅用太陽光発電システムを対象としたエコマークの概要

(a)太陽光発電システム

(b)太陽電池モジュール

(c)太陽光発電用パワーコンディショナ

図８　新しく制定されるエコマーク

図８は，新しく制定される「太陽電池を使用した製品」に対して用意されたエコマークのロゴ（予定）である。こんかいの制定では，エコマークとしては異例の大型商品である住宅用太陽光発電システムを含めたことである。また，住宅用とに使用される，太陽電池モジュールやパワーコンディショナも要素機器として個別に申請ことができるのも特徴である。今回の認定基準策定で，住宅用太陽光発電システムを含めた考え方などを以下に記す。

5.2.1　製品類型　No.135「太陽電池を使用した製品 Ver１」

（１）区分 A「住宅用太陽光発電システム」

1973 年の第一次石油危機を契機として発足したサンシャイン計画技術開発は 30 年の地道な努力の積み上げとして，　2004 年累積導入量で 110 万 kW(約 20 万戸)を達成し，2010 年の政府目標 482 万 kW(約 100 万戸）へ向かって，今後の発展が大きく期待されている。

この大きな可能性に向かって，急速に技術が発展し，産業振興がおこっていると現状を認識し，様々な方向性の開発の芽を摘まないように配慮する必要がある。このため，環境サイドからニーズの高い個別製品の環境影響評価について，現時点では必要なデータベース等の整備がともなわず LCA 評価の個別詳細な方法論は確立していないことから，今回は製品群としての総体的な定量評価に注目した。

しかしながら，エコマークとしてのシンボを記すために，企業に一歩進んだ努力を以下の点について求め，商品開発によりよい影響力を及ぼしていくことを配慮した。すなわち，フレームや

支持体に再生アルミ使用を使用すること，パワーコンディショナ長寿命設計，施工品質の維持のためのマニュアル整備や工事作業者の研修制度，品質保証基準の明確化やユーザーへの提示太陽電池モジュール 90%以上の出力保証などである。

一般家庭に設置する電機機器である「住宅用太陽光発電システム」を対象として明文化したことは，エコマーク制度としてエポックメーキングなことである。

（２）住宅用太陽光発電システム

太陽電池モジュール・パワーコンディショナなどの要素機器や，接続コード・取り付け用の支持体などから構成される。これらを，ユーザーの要望や住宅の立地条件や構造上の条件によって，柔軟にまた適切に組み合わせ，電気工事や設置工事を施す。

(i) 太陽光発電システムのマクロ的評価として EPT（エネルギーペイバックタイム），CO_2PT（CO_2ペイバックタイム）は 2 年程度であるが，現在の太陽光発電システムの寿命は 20 年程度以上と考えられている（パワーコンディショナは取替えが必要となる）。

(ii) 長期間にわたって発電能力が高水準で維持されれば累積的な環境負荷低減効果が高くなり，またユーザが安心して使用できる。

(iii) 「住宅用太陽光発電システム」が正常に機能し，長期にわたって当初の高水準のレベルを維持して発電するために以下のような認定基準を策定した。

各要素機器の正常な作動	要素機器の JIS 規格などへの適合に加え， ・太陽電池モジュールの出力保証(当初の効率の 90%以上 10 年間) ・パワーコンディショナの長寿命設計
適正な設計	・適切な施工マニュアルを有していること *太陽電池モジュールの設置(取りつけ位置・方向・間隔と配列) *取り付け方法(配線工事，金具，強度の確保，防水処理) *施工時の安全性確保(高所作業，配線工事) *解体時の安全性確保(感電等の防止)
適正な施工（設計どおりの設置・配線）	・施工作業員が施工マニュアルを理解するための技術指導制度
保守点検や修理体制の整備	・保守点検や修理などの受託体制の整備
ユーザへの周知	・ユーザへの情報提供

6． 再生可能エネルギー2006 国際会議

図９ 再生可能エネルギー２００６国際会議の１０大分野

5.1 日本から国際社会へ向けて情報発信する

地球の地下に埋蔵される化石燃料は何億年といわれる長い年月をかけて動植物の生態系と太陽エネルギーの恵みによってできた。しかしながら，このような化石燃料は産業革命以降ここ 100 年強の短期間で猛烈な勢いで使うことによって，経済発展に象徴される先進諸国を築き上げた。

画期的な発展によって近代国家ができ経済成長が進み文明が発展した。それは素晴らしいことであった。反面，地球温暖化に代表される環境問題，国家間の経済格差，そして化石燃料既得をめぐる戦争という負の遺産も背負ってしまった。

生きとし生けるものすべてが永続的，持続的に存続していくためには，負の遺産の責任者である先進諸国が先ず力を合わせ，プラスに転換させるべく革新的技術に向けた知恵と工夫を出し合い，行動を起こさなければならない。先進国の一員としてわが国も積極的に取組む必要がある。国の発展，産業の発展，経済の発展は，これら取組みと同義語である。

2006 年 10 月に計画する「再生可能エネルギー2006 国際会議」は，まさに，この趣旨に沿い，わが国がイニシアティブをもって世界に呼びかけ，先進的，先端的技術を共有し広め合う地球持続性希求の国際エネルギー会議である。学産官が一体になりわが国一般市民にも広く参加を呼びかけていく。”Renewable Energy 2006”は日本の旗印である。

本国際会議には「新エネルギー世界展示会」が併設される。会場は幕張メッセを予定している。会議期間は，再生可能エネルギー2006 国際会議については，2006 年 10 月 9 日（月）～13 日（金），新エネルギー世界展示会については，2006 年 10 月 11 日（水）～13 日（金）としている。国際会議は論文数 800 件，参加者 1200 人を見込んでいる。展示会には 40 カ国から 250 社程度の参加と 4 万 5000 人規模の来場を期待している。

5.2 21 世紀は再生可能エネルギーの世紀

これらからの世界のエネルギー供給は 2020 年頃から再生可能エネルギー中心の構造への移行が始まり，2100 年には世界の一次エネルギー供給の過半が再生可能エネルギーによってまかなわれるシナリオが真実みを帯びつつある。この共通認識の下に，再生可能エネルギー技術の進歩に対する先進工業国の持てる知識を集合するような機会の実現が強く望まれている。このような時に，日本から国際社会へ向けて情報発信する機会を持つことは，京都議定書議長国であり，また，多くの再生可能エネルギー分野で世界第一級のレベルにある日本にとって，これから飛躍していくための有意義なスタート台である。

5.3 再生可能エネルギー技術面にフォーカス・１０大分野をカバーする

プログラムすべてを貫くのは *"Advanced Technology Paths to Global Sustainability"* である。「先進的，先端的技術を通して，地球の持続性（道しるべ）を探求しよう」という会議である。過去，現在を定量的に直視し，それを踏まえた 21 世紀の環境，エネルギー，社会経済を持続的に満たす先端技術の開発が急務となっており，この会議を通じて参加者それぞれが世界の最先端技術や動向を知り自分の専門分野に生かし，持続的地球環境の人の輪が広げられるようなそのような会議になることを目指す。そのためにもできるだけ多くの方々の参加が得られるよう産官学すべてをカバーする多様なプログラムを構成する。

会議のメインテーマは，①再生可能エネルギー政策課題，②太陽光発電，③太陽熱利用，④省エネルギー建築，⑤風力，⑥バイオマス，⑦水素・燃料電池，⑧海洋エネルギー，⑨地熱，⑩新電力システム他，の 10 大分野である。

21 世紀人類の共通の課題となる再生可能エネルギー技術について，その技術解決にかかわる各国の産官学における専門家・研究者が一同に集まり，21 世紀中葉を見つめた技術の方向性を明らかにしていく世界第一級の国際会議を実現していきたい。そのためにも会議に併行し，「新エネルギー世界展示会」や各種のイベントを大々的に計画する。

5.4 わが国の関連機関の総力を結集した再生可能エネルギー国際会議

このような状況に鑑み，国内の再生可能エネルギーに携わるすべての研究者・専門家・事業者の支持による事業主体（再生可能エネルギー2006 国際会議組織委員会）を組織し，同会議を関連の 9 共催機関・団体とともに開催しようとしているところである。また，このような活動に対しすでに，関連 35 団体に協賛いただき，経済産業省，環境省，国土交通省，文部科学省，農林水産省，千葉県の後援をいただく。

会場は国際会議・併設展示会ともに幕張メッセを予定し，表 1 に示したように再生可能エネルギー2006 国際会議については，2006 年 10 月 9 日（月）～13 日（金），新エネルギー世界展示会については，2006 年 10 月 11 日（水）～13 日（金）としている。国際会議の参加者は 1200 人（論文数 800 件），展示会には 40 カ国から 250 社程度の参加と数万人規模の来場を期待している。

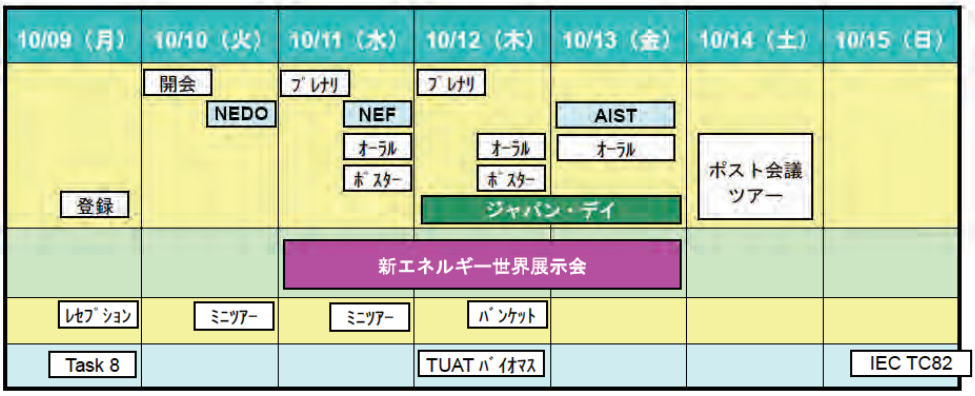

図 10　再生可能エネルギー２００６国際会議概略日程

5.5　豊富なプログラム

（1）プレナリーセッションと招待講演

再生可能エネルギーの各々の技術分野で国際的にも著名な専門家を海外主体に招待し，21 世紀の先端技術の紹介を依頼するとともに，世界の主要各国の中長期政策に関する講演も企画している。すでにその選考・依頼作業は進みつつある。

（2）特別セッション

独立行政法人新エネルギー・産業技術開発機構(NEDO)，財団法人新エネルギー財団(NEF)，独立行政法人産業技術総合研究所(AIST)が会期中にそれぞれ特別セッションを企画している。これは招待後援者によるそれぞれ異なる性格付けの講演会形式である。NEDO 技術開発機構は技術開発プロジェクトの成果を中心に，NEF は新エネルギー各分野における産業界の導入・普及への取組み，AIST は新エネルギーネットワークをはじめとした最先端研究開発や技術の紹介，など特徴あるプログラムを展開する予定である。

（3）分野別研究・開発・技術発表

会議の主体となる一般等好論文はプログラム委員会で精査し，採用可否を決定する。採用された論文はプログラムに合わせて口頭一般講演とポスター発表に分けられる。分野としてはプログラム委員会の分科会に相当する 10 分野であるが，発表セッションとしては 7～8 分類になる予定である。発表後の質疑応答にも時間を割き十分に討論ができるよう配慮する。一般投稿論文数は国内外を合わせて 700 件以上を目標とする。併せて，特定の分野のテーマに対して，招待後援者も交えたシンポジウムの設定を呼びかけていきたい。

（4）ジャパン・デー

毎年秋季に開催されている日本太陽エネルギー学会(JSES)と日本風力エネ協会(JWEA)共催の「太陽・風力エネルギー合同研究発表会」を，2006 年度は本国際会議の中に組込み，日本語で行なうジャパン・デーとして実施する予定である。ジャパン・デーの参加者は一定の追加費用で国際会議にも参加でき，一方，国際会議参加者はジャパン・デーセッションに自由に参加できるようにするなど，できるだけ多くの方々が気軽に参加できるよう工夫している。

（5）ソーシャルプログラム

テクニカルツアーとバンケットが予定されている。

テクニカルツアーとしては，会議後の土曜日に１日かけて実施されるポスト会議ツアーが目玉である。わが国の先端分野の一つである，集中連系や新電力ネットワーク技術を見学できるように折衝をすすめている。現在のところ，NEDO/集中連系プロジェクト（㈱関電工受託）による群馬県太田市パルタウン（PV 住宅約 500 件）および電力中央研究所赤城試験センターの需要地系統ハイブリッド実証試験設備を有力候補として検討している。赤城試験センターにおいては，集中連系プロジェクトの多数台インバータ（60 台）連系模擬試験設備見学についても見学に含めるよう願いしている。

また，会議期間中にも会議場近郊でのミニテクニカルツアーを計画している。会議参加者の同伴者のための一般ツアーの案内も忘れられない。バンケットは参加者全員が自由に交流を深められる場であり，かつ海外からの参加者にとってはわが国の文化を経験する最良の機会であることから，楽しい雰囲気は盛り上げられるよう計画中である。

（6）各種のサイドイベント

再生可能エネルギーや新エネルギーの普及促進も当会議の大きな目的の一つであることから，その目的に即した多くのサイドイベントを実施する予定である。現在企画が進められている主なものを例記する。

10 月 9 日（月）午後には国際エネルギー機関（IEA）太陽光発電国際共同研究プログラム・タスク 8 国際シンポジウム，同タスク 9 専門家会合（日程未定），次週における IEC TC82 東京大会，10 月 12 日（木）全日予定のバイオマスサミット（東京農工大学生存科学 COE 主催），市民団体を中心にした再生可能エネルギー市民フォーラム（日程未定）など。各種ワークショップも含めて，今後の新企画も歓迎していきたい。

世界展示会においても，体験実習，実演，市民講座，レースイベントなどのサイドイベントが同様に企画されている。開催地自治体や地元を包含したプログラムも企画される。これらも併せて，日本から世界へ向けて再生可能エネルギー産業・専門家の結集を呼びかけていく盛大な「フェスタル・プラザ"Renewable Energy 2006 Festal Plaza"」を実現していきたい

5.6 新エネルギー世界展示会

「新エネルギー世界展示会」は，再生可能エネルギー産業界を横断結集し，「見て！触れて！明日を拓く新エネルギー」という統一テーマを掲げている。公開日程は 2006 年 10 月 11 日（水）～13 日（金）の３日間である。以下に現在計画が進められている概要を紹介する。

（1）展示コンセプト

下記のような分野を網羅し，これに沿ったゾーニングを計画している。

A　日本の新エネルギー政策
B　燃料電池・ソーラーカーなど近未来社会の演出
C　新エネルギー産業の素材から商品開発
D　住宅・ゼネコン・施工・販売等流通
E　電力エネルギー関連の取組
F　自治体・研究・大学・NPO/NGO・書籍など

（2）出展内容・規模（予定）

国際会議の１０大分野にあわせて，下記のような分野を設定し，総計で 250 社・団体，550 ブースを予定している。そのうち海外からは，約３割の参加を見込んでいる。2003 年大阪での太陽光発電世界会議と同様なハイレベルの展示会の再現が大いに期待される。また，現在の産業の実態からみれば太陽光発電産業が主力であり，全体の４割程度に達するのではないかと観測している。各社の積極的な出展に期待したいところである。

- □ 政策課題：日本の各省政策パネル展示
- □ 太陽光発電：日本初から現在と将来に向けた商品
- □ 太陽熱利用：PV ハイブリット高効率と省エネ
- □ ローエナジー建築：省エネ建築など
- □ 風力：大型から小型まで現状の実績と新開発
- □ バイオマス：発電の仕組みと実用性
- □ 水素･燃料電池：燃料電池発電，燃料電池車
- □ 海洋エネルギー：海洋発電実用機と仕組み
- □ 地熱：現在の実用化状況と開発状況
- □ 新電力システム他：高効率ガス・エネ等
- □ 官・NEDO・NEF・自治体・大学・書籍など
- □ 新エネ関連団体

（3）世界展示会関係サイドイベント

展示会場内・近傍に設けた会議場で以下の企画の実現を計画している。国際会議側のサイドイベントも併せて，日本から世界へ向けて再生可能エネルギー産業・専門家の結集を呼びかけていく盛大な「フェスタル・プラザ "Renewable Energy 2006 Festal Plaza"」を実現していきたい。

日米欧インダストリデー

日米欧の産業代表者が情報交換と発展施策のディスカッション：経営者・専門技術者向け（100 人程度）

新エネルギー講座

誰でも解る新エネルギー講座・太陽光発電・風力・燃料電池・バイオマス発電など：一般向け（300 人程度）

地域の新エネ取組み講座

積極的な新エネルギー取組事例の紹介と効果：地方自治体中心に官庁関係向け（200 人程度）

環境経営セミナー

21 世紀環境経営の将来性：産業界経営者向け（300 人程度）

自治体物産展

新エネルギー観光とふるさと物産展・10 ヶ所程度：官庁・自治体及び産業界・一般向け

実感コーナー

ソーラーカー・燃料自動車・風力などデモ機の運転：一般向け・児童向け

× × × × × × × × × ×

再生可能エネルギー２００６国際会議及び第１回新エネルギー世界展示会を通じて 21 世紀のための新たらしい環境ビジネスの事業機会につながると信じている。また，光輝く「再生可能エネルギー」の旗印のもとに次代をになう若い人材が結集してくるきっかけとなれば大変うれしい。是非，この機会に多くの方々の参加を期待している。

そのためにも，このような国際会議や展示会を持続的に開く道を模索していきたい。多くの関係者の積極的なご提案をお待ちしたい。

参考文献

(1) http://www.mext.go.jp/a_menu/kagaku/kihon/06032816/001.pdf
(2) 赤井誠：METI 超長期エネルギー技術ビジョン，「温暖化研究最前線：気候変動と温暖化対策研究への日本の取組」公開シンポジウム，三田共用会議所，2005 年 11 月 11 日
(3) K. Kurokawa, S. Wakao, Y. Hayashi, I. Ishii & K. Otani, M. Yamaguchi, T. Ishii, Y. Ono: Conceptual Study on Autonomy-Enhanced PV Clusters for Urban Community to Meet the Japanese PV2030 Requirements, 20th EU-PVSEC, Barcelona, 2005.6.6-10, 6DP.2.3.

(4) Shinji WAKAO, Yasuhiro HAYASHI, Naoki UEDA, Akitaka ONOYAMA, Kosuke KUROKAWA, Masahide YAMAGUCHI, Kenji OTANI, Yukiyoshi ONO: Investigation of the Configuration of Autonomy-Enhanced PV Clusters for Urban Community, PVSEC-15, Shanghai, 10-14 Oct. 2005, PV0654-O5.
(5) Masahide Yamaguchi, Tatsuya Kawamatsu, Takafumi Takuma, Kosuke Kurokawa, Kenji Otani, Shinji Wakao, Yasuhiro Hayashi, Yukiyoshi Ono: Investigation of Battery Storage Station of Autonomy-Enhanced PV Clusters for Urban Community, PVSEC-15, Shanghai, 10-14 Oct. 2005.
(6) K. Kurokawa, Shinji Wakao, Yasuhiro Hayashi, Hiroshi Yamaguchi, Kenji Otani, Masahide Yamaguchi, Takafumi Ishii6 and Yukiyoshi Ono: Autonomy-Enhanced, PV Cluster Concept for Solar Cities to Meet the Japanese PV2030 Roadmap, 2nd International Solar Cities Congress, Oxford UK, 3-6 April 2006, 7E.2.
(7) 山口 雅英, 詫間 隆史, 川松 達弥, 黒川 浩助, 大谷 謙仁, 若尾 真治, 林 泰弘, 小野 之良：自律度向上型太陽光発電システムにおける蓄電ステーションの検討, パワーエレクトロニクス学会 162 回定例研究会, 2006.4.22, JIPE-32-5.
(8) K. Kurokawa: A Conceptual Study on Solar PV Towns and Cities for 21st Century, WCPEC-4, Hawaii, May 8-12, 2006.
(9) エコマーク商品類型Ｎｏ.１３５「太陽電池を使用した製品 Version１」の認定基準の制定について, 日環協 News Release, №05-015, 2006.3.15.

[付録：WCPEC-4 速報]

米国の太陽光発電 R&D 次年度予算要求について, 米国 DOE キング氏から以下のような発表があった。2007 年度予算要求課程で当初 75.1 百万ドルであったものが, 現在では, ほぼ倍増し, 役 140 万ドルとなった経過が報告された。1980 年から予算推移が示され, カーター政権時代に匹敵する予算規模であることを示した。［注：153 億円　(1USD=110JPY)］

開会プレナリで基調講演した同氏は壇上でシャンペン祝杯のパフォーマンスを演じた。

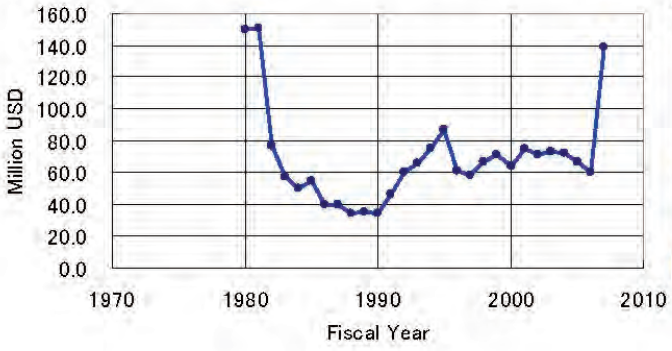

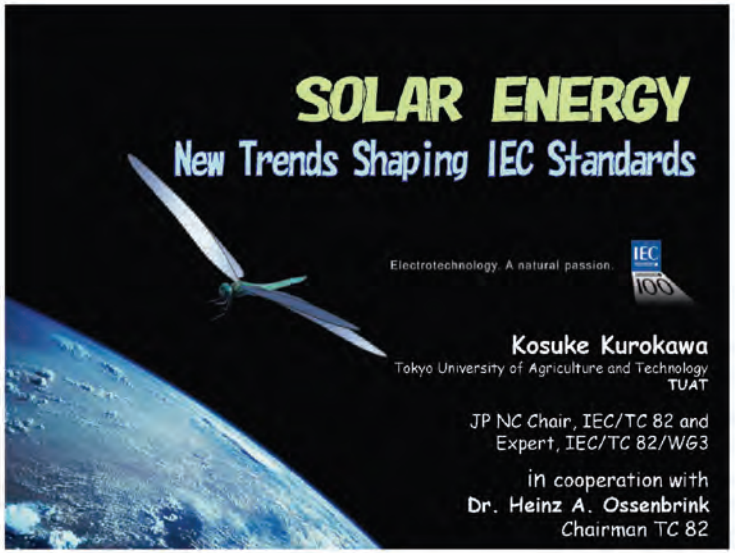
SOLAR ENERGY
New Trends Shaping IEC Standards
Electrotechnology. A natural passion.
IEC 100
Kosuke Kurokawa
Tokyo University of Agriculture and Technology
TUAT
JP NC Chair, IEC/TC 82 and
Expert, IEC/TC 82/WG3
in cooperation with
Dr. Heinz A. Ossenbrink
Chairman TC 82


50th Anniversary of Bell Labs Solar Cell Discovery
Calvin S. Fuller
Gerald Pearson
Daryl M. Chapin
Still Works!
Source: Larry Kazmerski

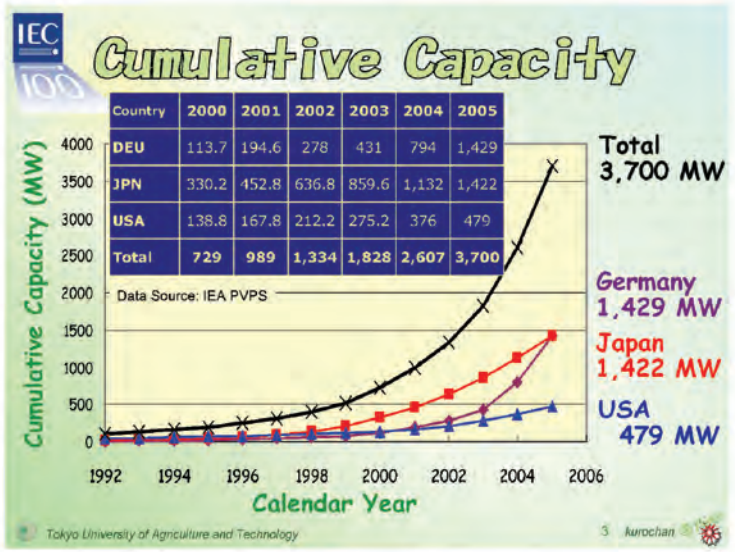
IEC 100
Cumulative Capacity
Country | 2000 | 2001 | 2002 | 2003 | 2004 | 2005
DEU | 113.7 | 194.6 | 278 | 431 | 794 | 1,429
JPN | 330.2 | 452.8 | 636.8 | 859.6 | 1,132 | 1,422
USA | 138.8 | 167.8 | 212.2 | 275.2 | 376 | 479
Total | 729 | 989 | 1,334 | 1,828 | 2,607 | 3,700
Data Source: IEA PVPS
Cumulative Capacity (MW)
4000
3500
3000
2500
2000
1500
1000
500
0
1992 1994 1996 1998 2000 2002 2004 2006
Calendar Year
Total 3,700 MW
Germany 1,429 MW
Japan 1,422 MW
USA 479 MW
Tokyo University of Agriculture and Technology
3 kurochan

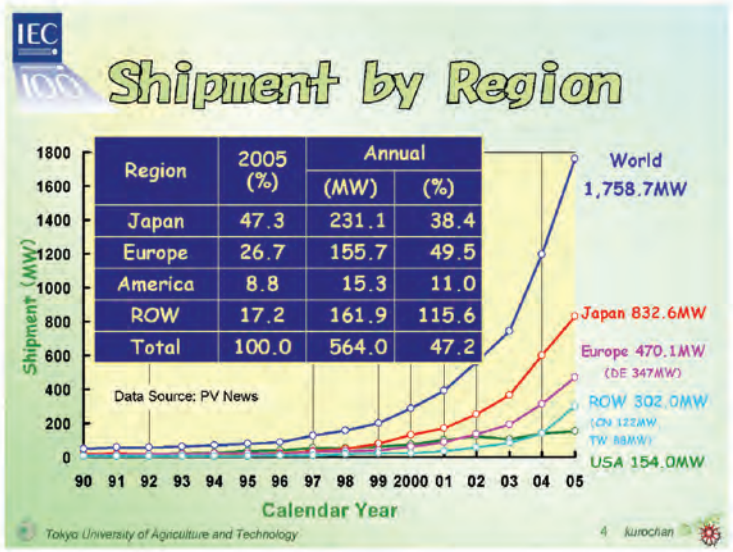
IEC 100
Shipment by Region
Region | 2005 (%) | Annual (MW) | Annual (%)
Japan | 47.3 | 231.1 | 38.4
Europe | 26.7 | 155.7 | 49.5
America | 8.8 | 15.3 | 11.0
ROW | 17.2 | 161.9 | 115.6
Total | 100.0 | 564.0 | 47.2
Data Source: PV News
Shipment (MW)
1800
1600
1400
1200
1000
800
600
400
200
0
90 91 92 93 94 95 96 97 98 99 2000 01 02 03 04 05
Calendar Year
World 1,758.7MW
Japan 832.6MW
Europe 470.1MW
(DE 347MW)
ROW 302.0MW
(ON 122MW
TW 88MW)
USA 154.0MW
Tokyo University of Agriculture and Technology
4 kurochan

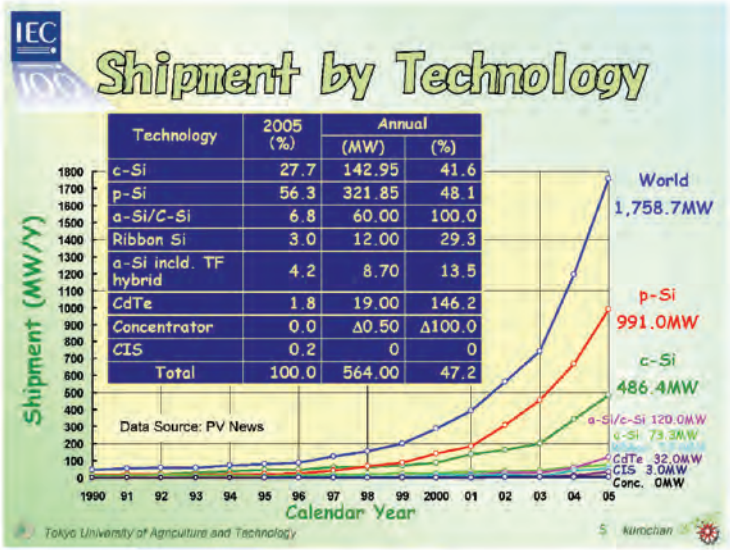
Shipment by Technology
Technology | 2005 (%) | Annual (MW) | Annual (%)
c-Si | 27.7 | 142.95 | 41.6
p-Si | 56.3 | 321.85 | 48.1
a-Si/C-Si | 6.8 | 60.00 | 100.0
Ribbon Si | 3.0 | 12.00 | 29.3
a-Si incld. TF hybrid | 4.2 | 8.70 | 13.5
CdTe | 1.8 | 19.00 | 146.2
Concentrator | 0.0 | Δ0.50 | Δ100.0
CIS | 0.2 | 0 | 0
Total | 100.0 | 564.00 | 47.2
Shipment (MW/Y)
Calendar Year
Data Source: PV News
World 1,758.7MW
p-Si 991.0MW
c-Si 486.4MW
a-Si/c-Si 120.0MW
a-Si 73.3MW
CdTe 32.0MW
CIS 3.0MW
Conc. 0MW
Tokyo University of Agriculture and Technology
5
kurochan

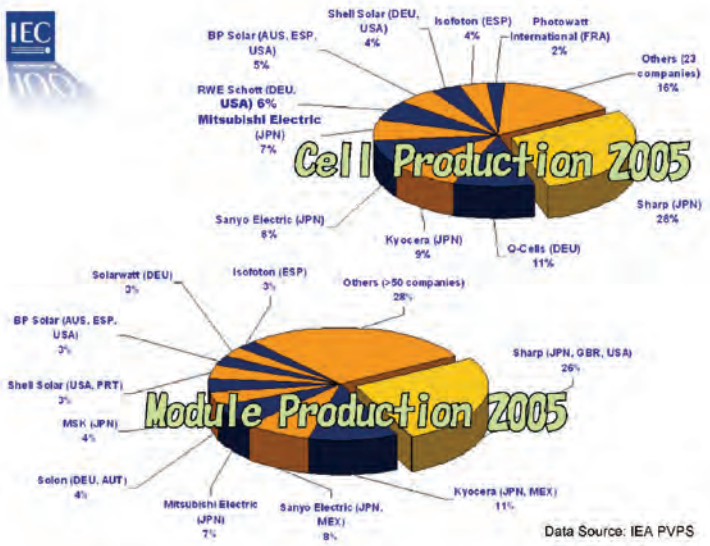
Cell Production 2005
Shell Solar (DEU, USA) 4%
Isofoton (ESP) 4%
Photowatt International (FRA) 2%
BP Solar (AUS, ESP, USA) 5%
Others (23 companies) 16%
RWE Schott (DEU, USA) 6%
Mitsubishi Electric (JPN) 7%
Sanyo Electric (JPN) 8%
Kyocera (JPN) 9%
Q-Cells (DEU) 11%
Sharp (JPN) 26%
Module Production 2005
Solarwatt (DEU) 3%
Isofoton (ESP) 3%
Others (>50 companies) 28%
BP Solar (AUS, ESP, USA) 3%
Sharp (JPN, GBR, USA) 26%
Shell Solar (USA, PRT) 3%
MSK (JPN) 4%
Solon (DEU, AUT) 4%
Mitsubishi Electric (JPN) 7%
Sanyo Electric (JPN, MEX) 8%
Kyocera (JPN, MEX) 11%
Data Source: IEA PVPS

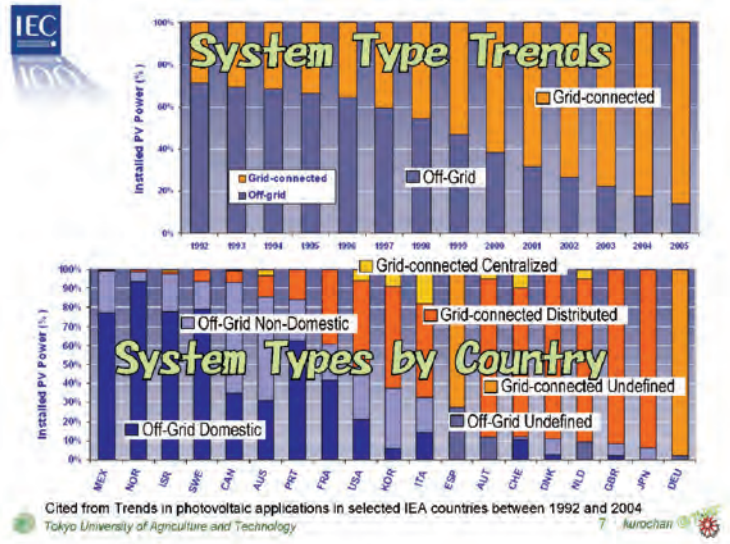
System Type Trends
Grid-connected
Off-Grid
Installed PV Power (%)
System Types by Country
Grid-connected Centralized
Off-Grid Non-Domestic
Grid-connected Distributed
Grid-connected Undefined
Off-Grid Undefined
Off-Grid Domestic
MEX NOR ISR SWE CAN AUS PRT FRA USA KOR ITA ESP AUT CHE DNK NLD GBR JPN DEU
Cited from Trends in photovoltaic applications in selected IEA countries between 1992 and 2004
Tokyo University of Agriculture and Technology
7
kurochan


25 Years TC82
Technical Committee 82
Solar Photovoltaic Energy Systems
Established 1981. Japan joined 1983.
WG1: Terminology, WG2: Cell/Module, WG3: System
WG4: PV Storage
WG5: Quality/Certification, WG6: BOS, -WG4
-WG5, WG7: Concentrator
JWG 1: JCG TC 82/TC 88/TC 21/SC 21A
23 P-members, 13 O-members
61 Standards Published (2.5 per year)
Tokyo University of Agriculture and Technology
8
kurochan

25 Years TC82

1981:

- 18 MW/Y
- 30 MW Total
- 25 $\$_{2002}$ / W or more

2006:

- 2000 MW/y (~30%/Y_ave)
- 5000 MW Total
- 5 $\$_{2002}$/ W or less (-6.5 %/Y)

Heinz Ossenbrink

Basic Measurement Requirements

- IEC 60891: Inter- & Extrapolation
  - PV cells → non-linear devices
- IEC 60904 series -1 to -10
  - STC: sensitive to 25°C-cell, AM 1.5, 1000 W/cm²

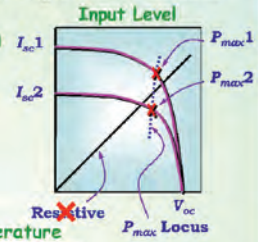

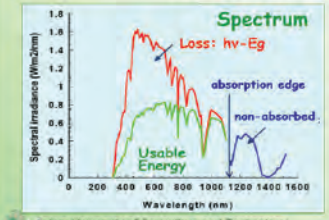

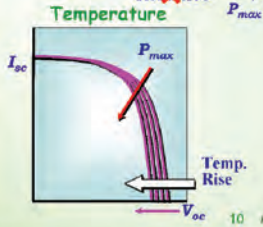

Basic Measurement Requirements

Solar Simulator – Key Equipment

Working Group 2

- **Basic Measurement Requirements:**
  - **IEC 60904** -1 to -10:
    I-V characteristics: reference cells; equivalent cell temp.; reference modules; spectral mismatch error; solar simulator; linearity measurement
- **Initial emphasis was on modules:**
  - **IEC 61215 Ed. 2** Design qualification and type approval for crystalline modules
  - **IEC 61646** for thin film modules
- **Module Safety qualification standards:**
  - **IEC 61730-1** Requirements for construction
  - **IEC 61730-2** Requirements for testing
- *Others*
  - **IEC 61345** UV test; **IEC 61701** Salt mist corrosion test

Working Group 3

- **WG 3 Systems has published the following:**
  - **IEC 61724** PV system performance monitoring--Guidelines for measurement, data exchange and analysis
  - **IEC 61727** PV Systems--Characteristic of the utility interface
  - **IEC 61829** Crystalline silicon PV array--On site measurement of I-V characteristics
  - **IEC 62124** PV stand alone systems--Design verification

Working Group 6

- **WG 6 Balance of Systems components is working on:**
  - **IEC 62109-1** Safety of power converters for use in PV power systems--Part 1--General requirements
  - **IEC 62116** Test procedure of islanding prevention measures for utility-interconnected PV inverters

Working Group 7

- **WG 7 Concentrator modules:**
  - **IEC 62108** Concentrator Photovoltaic (CPV) Modules and Assemblies - Design Qualification and Type Approval (should be published in 2007)
  - Tracker standard is under initial draft (publish in 2009?)

Requirements for Modules

- **Protect active layers from long-term exposure to climatic conditions:** heat cycles, rain fall, humidity, UV, etc.
- Provide front sheet of **maximum transparency**
- **Mechanical Stability:** wind load, snow, hail ...
- Isolate outer surfaces from **high internal voltage**
- **Electrical contacts for cabling**
- Protection against **partial shading** (hot spot)
- Resistance against **fire**

IEC 61215 & 61646

- Today's IEC 61215 (and 61646) Address:
  - Climatic Exposure
    - To include 1000 hours of Damp Heat, 200 Temperature Cycles, 10 Humidity Freeze cycles
  - Mechanical Stress
  - Electrical Insulation
  - Partial Shadowing (Hot Spot Test)
  - Performance measurements

Typical Test Equipments:

- Damp heat chamber (85°C,85%RH)
- Temperature and humidity cycling chamber (-40 to 85°C,85%RH)
- Long pulsed solar simulator
- Hail impact test equipment
- Mechanical load tester
- Light soaking equipment
- Tester for robustness of termination
- Wet leakage current tester
- Twist tester
- Impulse voltage tester
- Fire test equipment
- Bypass diode thermal tester

Hail Impact Test Equipment (23m/s, 25mmφ Ice ball)

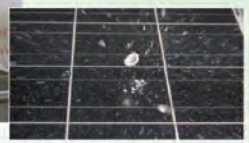

A photo of broken ice ball in testing

Hot Spot Test Equipment

IECEE PV Scheme Conformity Assessment

- IEC
  - Central Office
  - Standard Management Board
    - TC82
      - WG2 flat plate
      - WG3 System
      - WG6 BOS
      - WG7 CPV
    - Other TCs
  - Conformity Assessment Board
    - IECEE
      - CTL
        - ETF-9
      - NCB
        - CBTL
    - IECQ
    - IECEx
- ISO
- ITU

IECEE PV Scheme Participation Coutries

Country	Member Body	NCB	CBTL
France	LCIE by delegation from UTE	LCIE	
Germany	Deutsches Komitee der IEC	VDE TÜV Rh	VDE TÜV RH PS GmbH
India	BIS	STOC	ETDC NERDC
Japan	JISC	JET	JET Yokahama
The Netherlands	Netherlands National Committee of the IEC	KEMA	KEMA Quality B.V
Spain	AENOR	AENOR	CIEMAT Fundacion Cener-CIEMAT
USA	US National Committee of the IECEE	UL Inc.	UL Inc. ASU

Qualification testing

in accordance with **IEC 61215 Ed. 2 (2005)**

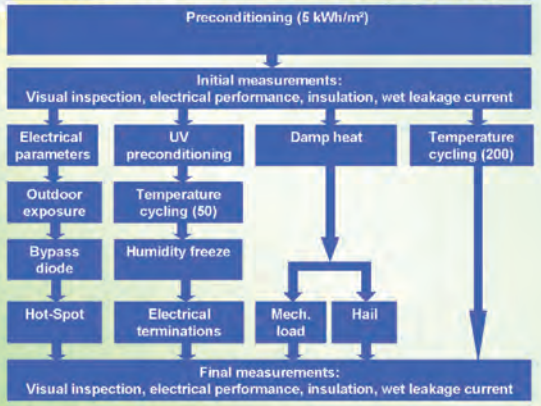

Safety Qualification testing

in accordance with **IEC 61730-2 Ed. 1**

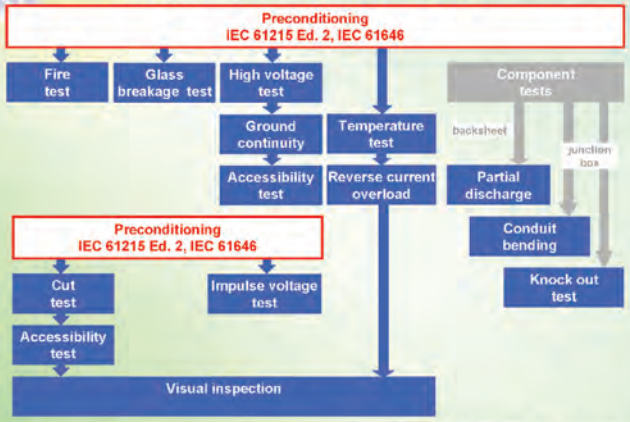

Fire Test by 61730-2

Fire Brand Test according to fire class B

Building Integrated PV Modules
BIPV

- Roof tiles and shingles
- Custom made façade modules
- Transparency important for building elements
- Flexible "Roll-out" modules
- but: often custom design and expensive
- not commonly standardized yet

Source: H. Ossenbrink
Tokyo University of Agriculture and Technology
25 kurochan

MuHi Values Added
Color Cells for BIPV

Aesthetic Values Rather than PV Performance
Tokyo University of Agriculture and Technology
27 kurochan

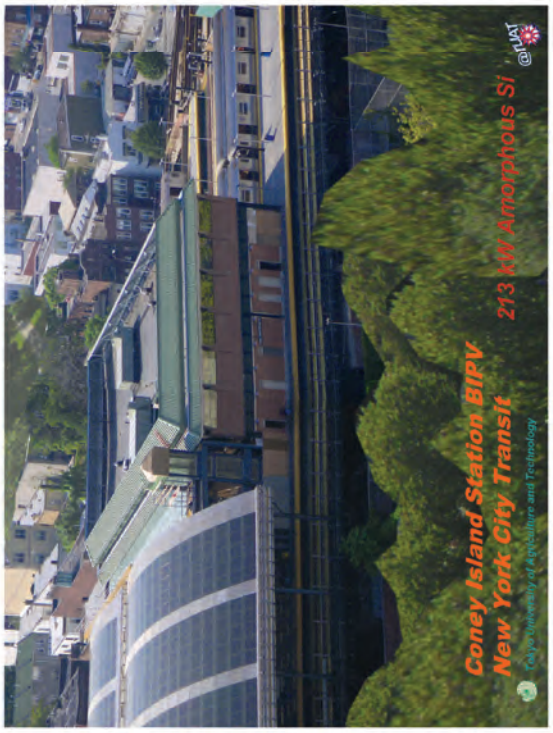
Coney Island Station BIPV
New York City Transit
213 kW Amorphous Si
@TUAT
Tokyo University of Agriculture and Technology


Courtesy of Sanyo


HERNE ROOF PV 1 MW
@TUAT

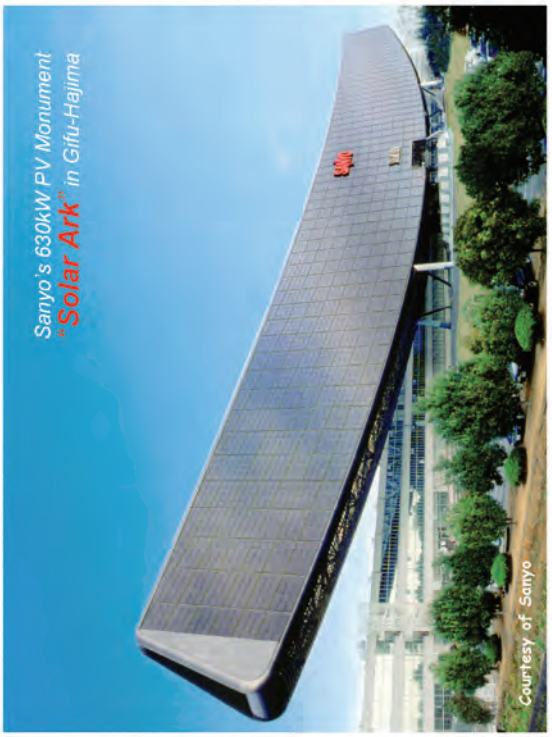
Sanyo's 630kW PV Monument
"Solar Ark" in Gifu-Hajima
Courtesy of Sanyo

Power Conditioning Systems

- MIC: AC module integrated conditioners
- SHS: Battery chargers
- String inverters (distributed)
- Residential inverters (single; clustered)
- Medium size inverters
  - central; - distributed
- Large size inverters
- Multi Megawatts Class inverters

PCS Architectures

Sharp Kameyama LCD Factory 5.22 MW Roof-top PV

Power Conditioning Systems

- Charge Controller
  Morningstar: Prostar-12
  12 A-PV, 8 A-Load
  12 V or 24 V
- MIC for AC module
  OKE4: 24~50 V-DC, 0~130 W
  230 V-AC, 50 Hz

Distributed Medium-Size PCS
XANTREX
trace TECHNOLOGIES
35 kVA
APS Prescott Airport 5MW PV Project 11 Jan 2005

21st EU-PVSEC
Dresden, 4-8 Sept. 2006
SINAMICS
Siemens Solar
700 kVA PCS

Distributed String Inverters
School Project by Schoenau/Sanyo/Sunny Boy
2 Nov. 2003

Modular Container Concept
PCU
1.2 MVA
MSS 400 kVA each
5 MW Leipzigerland Plant completed 2004

Solar Lanterns(Typical SHS)

Nowadays
Misawa Home Co.Ltd.

SHS to VLS-PV
SHS: Solar Home System
- Domestic; tens watt to hundreds watt
Mini Grid: Village Electrification
- tens kilowatt to hundreds kilowatt
isolated
Residential Rooftop
distributed, grid-connected
- several kilowatt to 20 kilowatt
PV Micro Grid: Solar PV Community
- Unit Community Size: 1000 houses;
1 km by 1 km; ~10 mega watt
LS-PV: Large Scale PV System
central
- Multi megawatt to tens megawatt
VLS-PV: Very Large Scale PV System
- 100 megawatt to 1 giga watt
- Desert Community Development
Tokyo University of Agriculture and Technology
41
kurokawa

Residential PV
NEDO established in 1980

NEDO's Clustered
PV PROJECT
City of Ota, Gumma
~1km×0.5km
~550 PVs

Future PV Directions
Rancho Seco PV Plant
3.9 MW

Residential PV & Grid Connection
Islanding Phenomena identified by
the Rokko Island Facility
1985~1990

Power Conditioning Systems
20 units of PCS tested in parallel for
studying multiple islanding issues.

SOLON P.T. Inverter
Cabinets
Leipziger Land: 32.727 modules = 5 MW

4.6 MW Springerville PV Plant, AZ
Tucson Electric Power
fixed, south facing with 34° tilt
http://greenwatts.com/pages/SolarStats/SolarTech.html

An Old Coal Mine Refurnished to 5MW PV Plant
Leipziger Land: 5 MW by Shell Solar
Google

12 MW Solarpark Gut Erlassen

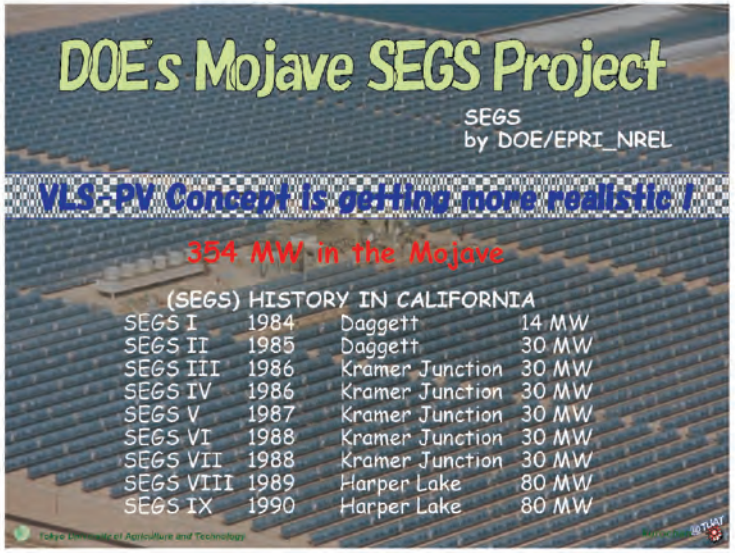
DOE's Mojave SEGS Project
SEGS
by DOE/EPRI_NREL
VLS-PV Concept is getting more realistic !
354 MW in the Mojave
(SEGS) HISTORY IN CALIFORNIA
SEGS I 1984 Daggett 14 MW
SEGS II 1985 Daggett 30 MW
SEGS III 1986 Kramer Junction 30 MW
SEGS IV 1986 Kramer Junction 30 MW
SEGS V 1987 Kramer Junction 30 MW
SEGS VI 1988 Kramer Junction 30 MW
SEGS VII 1988 Kramer Junction 30 MW
SEGS VIII 1989 Harper Lake 80 MW
SEGS IX 1990 Harper Lake 80 MW

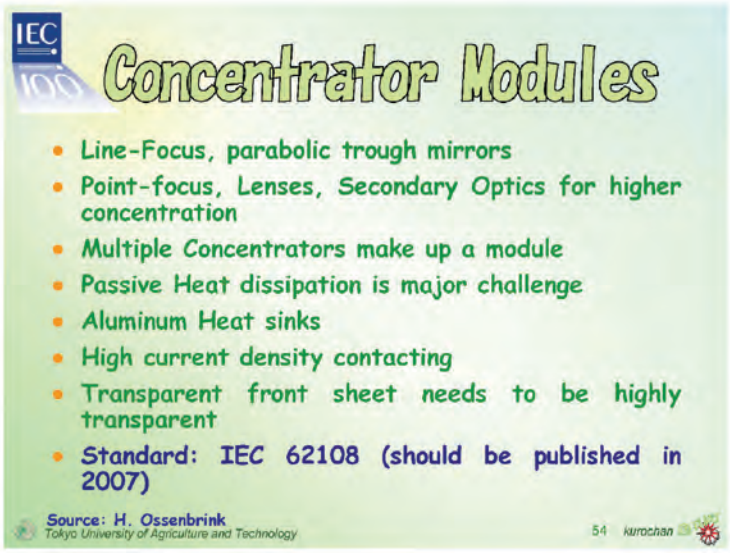
IEC
Concentrator Modules
Line-Focus, parabolic trough mirrors
Point-focus, Lenses, Secondary Optics for higher concentration
Multiple Concentrators make up a module
Passive Heat dissipation is major challenge
Aluminum Heat sinks
High current density contacting
Transparent front sheet needs to be highly transparent
Standard: IEC 62108 (should be published in 2007)
Source: H. Ossenbrink
Tokyo University of Agriculture and Technology
54 kurochan

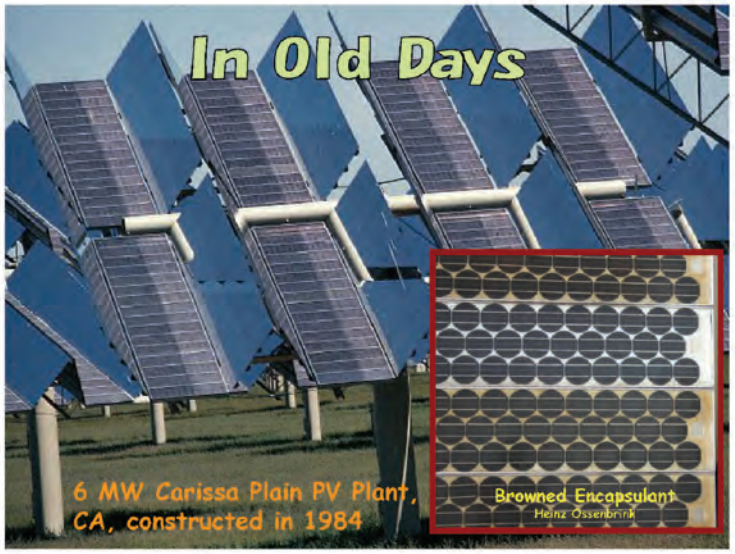
In Old Days
6 MW Carissa Plain PV Plant, CA, constructed in 1984
Browned Encapsulant
Heinz Ossenbrink


Amonix 250X 35 kW concentrator system at Arizona Public Service STAR facility

Suggested Requirements

- **Lifetime Energy Production**
  - How many years to pay back investment?
- **Reliable Electricity Delivery in Rural Regions**
  - How to Design Complex Hybrids?
- **Reduce Costs of Building Integration**
  - How to avoid the trap of labor costs?
- **Meet Environmental Standards**
  - How to meet the expectations for clean energy?

Source: H. Ossenbrink

Villedge Electrification(Mini-grid)

TC82 & the PV Future

- 2010: 10 GWp / yr (40%/yr)
- 2020: 100 GWp / yr (26%/yr)

- **Major Markets:**
  - Professional Grid for Peak Demand
  - Urban Residential Clusters
  - Rural Electrification
- **Global Deployment toward world major**

Lifetime Energy Production

Global Market Value of Calibration:

- ± 2% equivalent to ± 500 M$ revenue in 2010, when 10 GW are produced
- STC Power (± 2%) 'Module Calibration'
- Annual Yield (± 10%) 'Energy Rating'
- Equivalent Lifetime (± 30%) 'EOL testing'?

Source: H. Ossenbrink

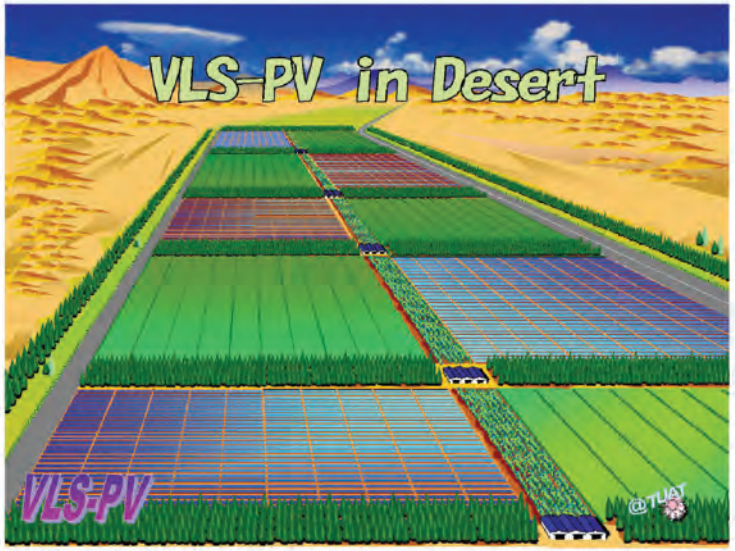
VLS-PV in Desert
VLS-PV
@TUAT

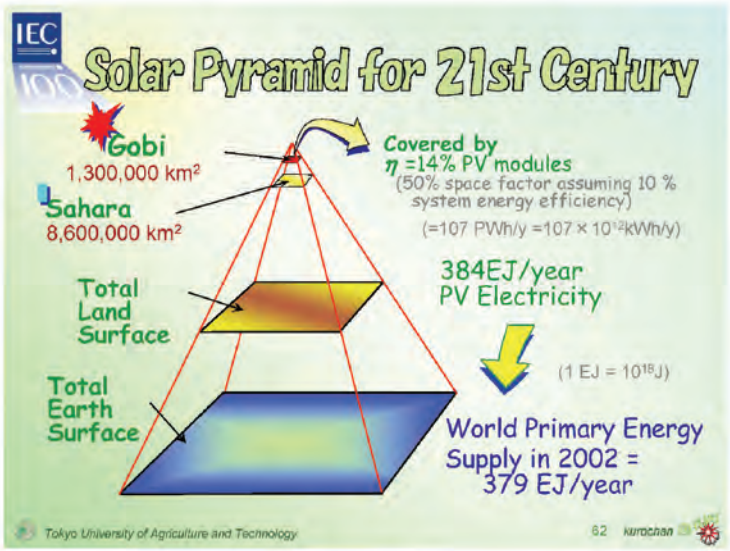
IEC
Solar Pyramid for 21st Century
Gobi
1,300,000 km²
Sahara
8,600,000 km²
Covered by
η =14% PV modules
(50% space factor assuming 10 % system energy efficiency)
(=107 PWh/y =107 × 10¹²kWh/y)
384EJ/year
PV Electricity
(1 EJ = 10¹⁸J)
Total Land Surface
Total Earth Surface
World Primary Energy Supply in 2002 = 379 EJ/year
Tokyo University of Agriculture and Technology
62
kurochan

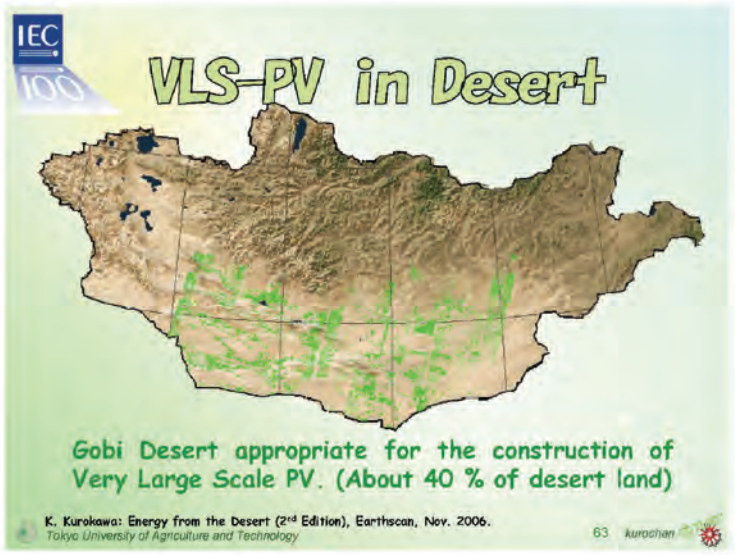
IEC
VLS-PV in Desert
Gobi Desert appropriate for the construction of Very Large Scale PV. (About 40 % of desert land)
K. Kurokawa: Energy from the Desert (2nd Edition), Earthscan, Nov. 2006.
Tokyo University of Agriculture and Technology
63
kurochan

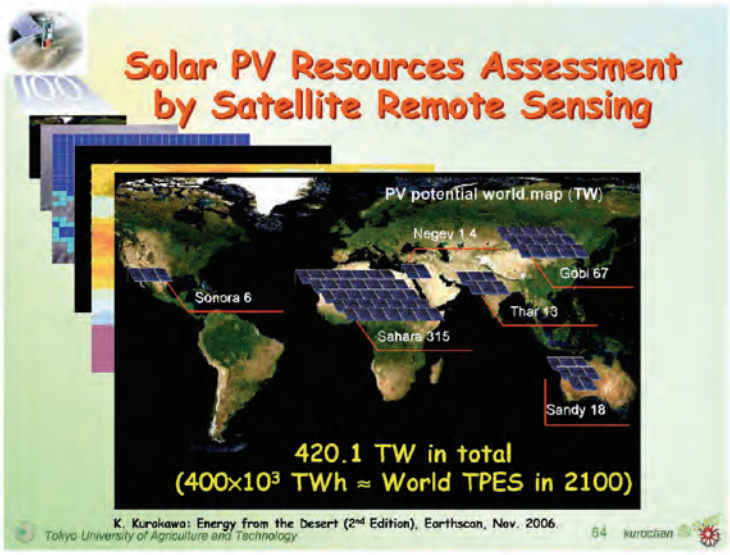
Solar PV Resources Assessment by Satellite Remote Sensing
PV potential world map (TW)
Negev 1.4
Gobi 67
Sonora 6
Thar 13
Sahara 315
Sandy 18
420.1 TW in total
(400×10³ TWh ≈ World TPES in 2100)
K. Kurokawa: Energy from the Desert (2nd Edition), Earthscan, Nov. 2006.
Tokyo University of Agriculture and Technology
64
kurochan

WBGU's World Energy Vision 2100
WBGU: German Advisory Council on Global Change
Primary Energy Supply [EJ/Y]
YEAR
Geothermal
Other REs
Solar heat
Solar electricity
Wind
Biomass adv
Biomass trad
Hydro-PW
Nuclear PW
Gas
Coal
Oil
Tokyo University of Agriculture and Technology
Kurochan

Long Term Sustainable PV Scenario
GW_PV equivalent = 1000 GWh
TPES in GW-pve
IEA-2050
400TW
WBGU
Global Installation toward sustainable 2100
133TW
Stabilized Installation
Sustainable PV Production-pa
Old PV Replacement-pa
1GW/line
Stabilized Production = Stabilized Installation
Life Time
4,400GW/Y
10GW/line
30 Year Life
Kurochan

Fixed Light
Energy Poverty
1.6 billion population without access to electricity!
http://earthobservatory.nasa.gov/Newsroom/

IEA's World Energy Forecast
Primary Energy Supply (EJ)
Other REs
Biomass
Nuclear
Gas
Oil
Coal
[IEA-2050/SD Vision]+[IPCC-2100-A1T_modified]
Tokyo University of Agriculture and Technology
Kurochan

The Module of Tomorrow: Challenges

- 2010..... 2020 ~ :
  Module Factories toward 1 GW ~ annual Capacity!
- New processes and module designs required for:
- 1GW/Y → 700W module of 1.8m□ every 18 seconds
- 4.4 cells/sec (200mm□)
- 15,200 m² / day

Kurokawa: PVSEC-15, Shanghai, Oct. 2005
Tokyo University of Agriculture and Technology 69 kurochan

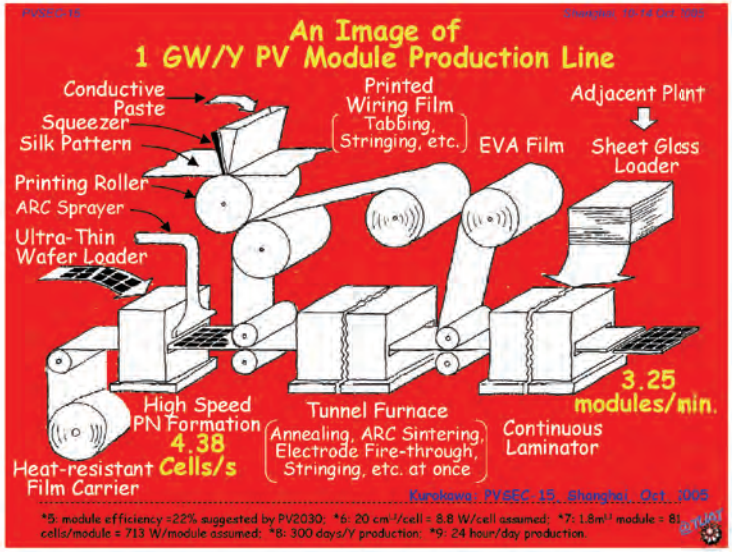

Future Standards Work?

- Cells or wafers?
- Organic cell technology
- Third Generation

- Solar PV Community or Solar PV City
  - Urban Community Renewal
- VLS-PV: Very Large Scale PV System
  - Global Deployment Scenario

Tokyo University of Agriculture and Technology 71 kurochan

One Common Stadards or Regional?

- Global Markets:
  - Wafers, Cells, Modules, BOS, Systems
- Technical Differences Do Exist:
  - Inverters (2006 sales: ~ 600 M$)
  - Grid interface
  - Safety
  - EMC, Recycling/ Disposal, Env. Friendly Material
  - Project Management / Design Quality
- But, PV installation be harmonized with its surroundings/culture. Some parts provided by Regional Business/Industries: Nature of distributed system.
- Balance: one common standard / regionality

Tokyo University of Agriculture and Technology 72 kurochan

100 GW ~
100 TW~
giga-watts
mega-watts
kilo-watts
NASA Helios
IEC

Conclusions
Over the years, surprising Convergence of module designs.
We believe global standards played an important role in module design qualification.
Quality very high, lifetime > 20 years.
Still, " useful energy for lifetime" almost unknown
Real Building Integration did NOT take off yet.
Revival of Concentrator modules, mainly in dry climate.
Large capacity module factories will drive new design concepts.
Global Scale Deployment throughout 21st Century seeking for real sustainability in energy.
IEC
73
Tokyo University of Agriculture and Technology

特集 解説

これが世界一！日本の技術力

世界のトップを走る太陽光発電*

Japan, Running the Top in the Photovoltaic Power Generation Industry

大谷 謙仁**
Kenji OHTANI

Key words photovoltaic systems, solar cell, energy, silicon, grid-connected, IEA, Feed-in Tariff

1. はじめに

太陽光発電システムの普及は，日本が世界を牽引している．太陽電池生産量は，世界市場のほぼ半分を占め，6割以上が欧米に輸出されている．太陽光発電の累積導入量は約4割で，日本とドイツの両国だけで8割にもなる．本稿では，2000年以降の太陽光発電システムの普及状況を概説し，わが国が太陽光発電産業において先頭を走る理由と今後の普及策について展望を述べる．

2. 太陽光発電システムの普及状況

2.1 太陽電池の利用形態

太陽光発電システムは，太陽電池を用いて太陽エネルギーを電気に変換する発電装置である．太陽電池から発生する電力は，電力変換器を介して電気機器（負荷）に供給される．太陽光発電システムは，商用電力系統とつながっているのか否かで，系統連系形システム（GCS）と独立形システム（SAS）とに大別することができる．

太陽電池が発明されてから数年後の1958年には人工衛星に搭載されるなど，初期の太陽光発電では，宇宙や山岳・海洋・離島などの電源供給が困難な場所において独立形システムとして使われることが一般的であった．現在でも，発展途上国等において村落電化のための一手段として利用されることは多い．基本的には，独立形システムは電力貯蔵装置やその他の発電機（ディーゼル発電機等）を組み合わせて，特定の負荷に対する電力供給手段として用いられる．

一方で，昨今の太陽電池価格の低下や地球環境の保護意識の高まりと共に，商用電力系統の発達した都市部においても，太陽光発電システムが利用されるようになってきた．この場合には，太陽光発電システムは既存の電力系統と接続し，電力需要のピークに対応した補助電源として利用する他，系統停電時におけるバックアップ電源として利用することが可能である．

なお，系統連系形システムと独立形システムの利用比率は，国際エネルギー機関（IEA）に加盟するOECD諸国においては8：2であり，わが国においては図1に示すように9：1と，現在では系統連系形システムの利用が圧倒的に多くなっている[1]．

2.2 世界の太陽電池生産量

太陽電池の代表的な種類としては，シリコン結晶から切り出したシリコン基板を用いた結晶シリコン太陽電池や，ガラス等の基板上に蒸着等で形成されたアモルファスシリコン太陽電池等がある．硫化カドミウムやひ化ガリウムなどの化合物半導体を利用することもある．図2に太陽電池の主な種類の分類を示した．

現在市場に出回っている太陽電池は主に結晶シリコン形（単結晶シリコン形と多結晶シリコン形）であり，世界市場で結晶シリコン形が84.7%のシェアを占めている[2]．そのうち多結晶シリコン形が56.3%であり，半分以上のシェ

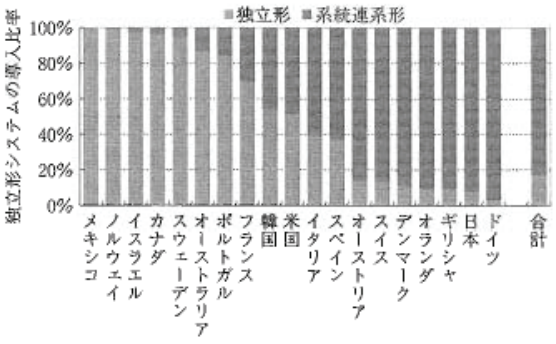

図1 OECD諸国における太陽光発電の利用形態（2004年時点のシェア）

*原稿受付 平成18年11月28日
**独立行政法人産業技術総合研究所太陽光発電研究センター（茨城県つくば市梅園1-1-1 中央第2）
大谷謙仁
1995年，東京農工大学大学院修士課程修了．同年，通産省工業技術院電子技術総合研究所に入所．現在，独立行政法人産業技術総合研究所太陽光発電研究センターに所属し，太陽光発電システムの実環境における運転性能の分析や，最適設計法の研究を実施．

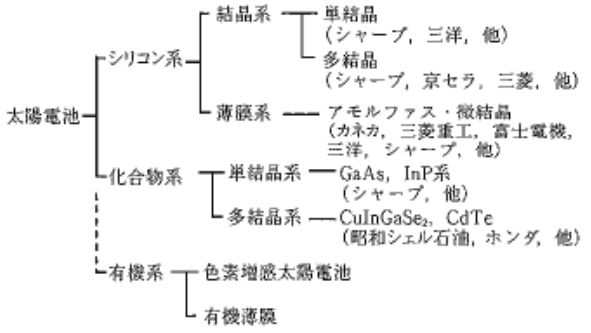

図2　太陽電池の種類と主な国内メーカ

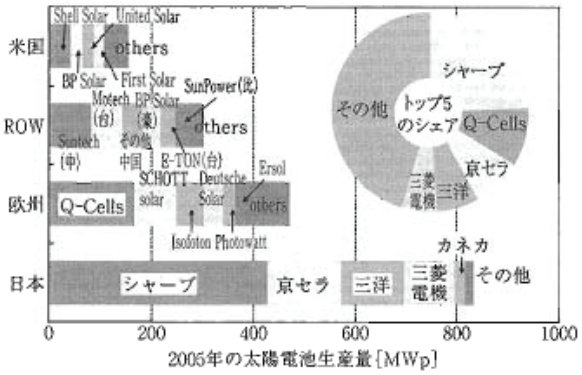

図3　2005年における地域別の太陽電池生産量

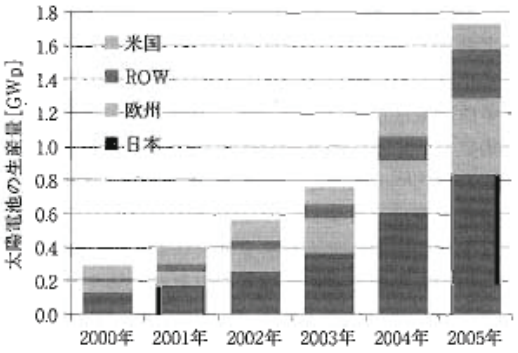

図4　太陽電池導入量の年推移

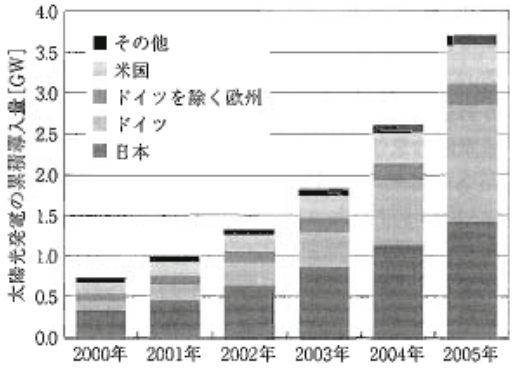

図5　太陽光発電累積設備量の年推移（IEA加盟国）

アをもち，単結晶シリコン形は28.3%である．残りは，アモルファスシリコン形が3.4%，リボンシリコン形が3.0%と続き，ほとんど（98%）がシリコンを材料としている．

2005年の太陽電池生産量は世界全体で1758.7 MWであり[2]，その地域別のメーカシェアを図3に示す．日本企業は世界上位5社中に4社が食い込んでおり，約半分に当たる832.6 MWを出荷している（シャープ：427.6 MW，京セラ：142 MW，三洋：125 MW，三菱：100 MW他）．そこに欧州が470 MWと続き，日米欧を除く他の国（ROW）が289 MWと第3勢力に，米国が154 MWとなっている．

太陽電池生産量の近年の伸びは著しく，この2000年からの6年間では毎年30～50%の拡大を続け，生産量は2000年時点と比べて約6倍にもなった．2004年度における日本の太陽電池生産量は658.1 MWであったが，そのうち，約6割は欧米に輸出された[3]．特に，ドイツを中心とした欧州市場への輸出が牽引となり，輸出量は対前年度比で110%と飛躍的に拡大し，日本は世界最大の生産基地となった．しかし，ここ数年は中国・台湾・インド等のROWのシェアが急拡大しており，今夏に中国のSuntech社が日本の太陽電池パネル製造会社のMSKを買収したというM&Aのニュースは記憶に新しい．日本がトップの座を守るにはうかうかしていられないのが現状である．

2.3　世界の太陽光発電導入状況

近年，原油価格の上昇が石油依存への警鐘を鳴らし，地球環境保全の意識の高まりと相まって，再生可能エネルギー利用の拡大が続いている．太陽光発電は，各国の普及推進政策の後押しもあり，設置容量は年々着実に増加している．図5に太陽光発電の累積設備容量の年推移[2]を示すように，世界全体で年率40%もの増加が見られる．

中でも日本とドイツは太陽光発電システムの導入量が際立って大きい国である．IEAの統計によると，2005年末におけるわが国の太陽光発電設備量は1422 MWに上ったものの，1997年から守り続けた世界第一位の座を初めてドイツ（1429 MW）に譲り渡している．ドイツと日本の太陽光発電導入量は世界全体の約8割にも達し，両国が太陽光発電の世界市場を牽引しているといえる．

2.4　わが国における太陽光発電導入状況

2004年度における日本の太陽電池出荷量は658.1 MWであったが，そのうち，約4割が国内需要である[3]．用途別では，住宅向けの一般電力用途が246 MWで9割を占めた．残りがその他の一般電力用途で7.5%，電卓・時計等の電気機器や照明・標識等の電力応用商品用途が2.5%であった．住宅向けでは，新築住宅に設置するケースが8割と多い．

太陽光発電システムの設置価格は市場拡大と共に着実に低下し，1994年度には1 kW当たり平均200万円であった設置価格が，2005年度には平均66万円と約3分の1にまで低下した．この支援策は太陽光発電システムの導入拡

大と設置価格の低減という一定の成果を上げたため，2005年度で終了している．図6にNEFから補助金交付を受けた住宅用太陽光発電システムの設置価格の推移を示す．ここ数年は設置価格がほとんど低減していないが，太陽電池の市場拡大による需給逼迫が主要因と思われる．

2.5 メガワット級大型システム（メガソーラ）の導入

太陽光発電は，数メガワット級の大規模システムから数十ワット級システムの小規模まで，ユニット化された太陽光発電パネルの総出力を調整することによって自在に設計できるのが特徴である．わが国では先述のように住宅向けの小規模（4 kW級）分散利用がほとんどである．これとは対称的に，ドイツ・米国などでは大規模システムを集中設置する事例が多い．

ドイツでは，フィードインタリフ（Feed-in Tariff）という制度によって，急速に大規模太陽光発電の普及が進んでいる．フィードインタリフでは，太陽光発電や風力発電などからの電気を固定的な買い取り価格で一定期間買い上げることが約束される．その買い取りの原資は，17.2ユーロセントの電気単価から2%が充てられ，2004年の総費用は22億ユーロであった．買い取り価格は，その再生可能エネルギー発電が既存の化石燃料発電と競争力をもてるようなプレミアムを上乗せして決められるため，発電コストを出来るだけ下げて，一層の利益拡大を目指そうとするインセンティブが働くようになっている．2005年には，屋根置き形の30 kW以下の太陽光発電システムに対して，発電量1 kWh当たり54.53ユーロセントが買い取り価格とされた．太陽光発電の場合は燃料が必要なく，保守費用もほとんどかからないことから変動費が小さく，固定費をいかに小さくするかが損益分岐点を早める最大のポイントとなる．このために，太陽光発電システムの大型化と集中化によって設置コストと運用コストを低減する方策が採られることが多い．

わが国においても，新エネルギー・産業技術総合開発機構（NEDO）の「大規模電力供給用太陽光発電系統安定化等実証研究」や環境省の「メガソーラ共同利用モデル事業」によって太陽光発電の大規模・集中導入を目指す動きが活発化してきた．現在の国内最大の太陽光発電は，シャープの亀山工場屋上に設置された5 MWの太陽光発電システムで，建物の屋上に設置されたものとしては世界一の規模を誇る．独立行政法人産業技術総合研究所つくばセンターでは，住宅用のユニットを多数台並べてメガワット級太陽光発電設備を実現した．ここでは，わが国が世界最大の太陽光発電の普及国かつ生産国であることを記念するかのように国内主要各社の太陽光発電システムを2004年に211台導入した．図7に示す太陽光発電パビリオンでは，6社6仕様の太陽光発電システムが4台ずつ合計96 kWが導入され，発電性能のベンチマークが行えるようになっている．

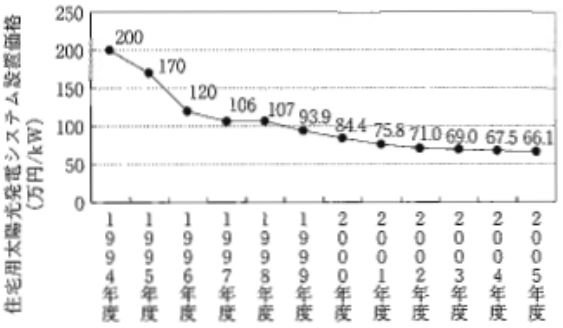

図6 国内住宅用太陽光発電システムの設置価格の推移

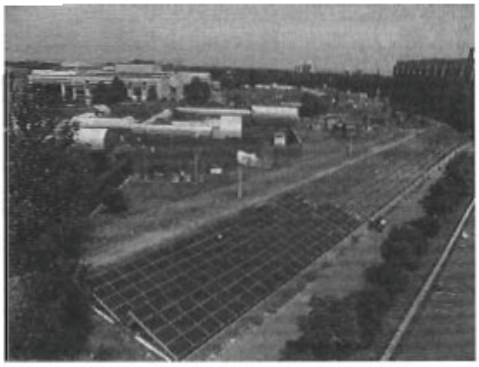

図7 産業技術総合研究所つくばセンター太陽光発電パビリオンの鳥瞰写真

3. わが国の太陽光発電大国化の理由

わが国では，太陽光発電システムの事業および普及が世界に先駆けて進んでいる．その理由として確実にいえることは，政府・自治体による導入促進政策が功を奏したということである．1992年度からNEDOによる太陽光発電フィールドテスト事業，1994年度から財団法人新エネルギー財団（NEF）による住宅用太陽光発電システムモニター事業が実施され，太陽光発電システムが一般家庭や公共建物等に最も普及した再生可能エネルギーとなった．NEDOフィールドテスト事業では，2005年度までに約1800件（約53 MW）[6]の太陽光発電システム，NEFの導入基盤整備事業では2005年度までに25万件以上（約932 MW）[4]の住宅用太陽光発電システムが実現された．2006年度に住宅用太陽光発電システムの設置支援策を有する自治体は319市町村ある．

当然のことながら，単に財政的支援のみが太陽光発電の普及を促したわけではない．通商産業省（当時）のサンシャイン計画からニューサンシャイン計画へと引き継がれた連続的な研究開発の実績が下地にある．メーカ各社が高効率で耐久性のある太陽電池を開発し，国内市場の拡大をバネとして，世界市場に進出できる高品質の太陽電池パネルの製造技術を立ち上げたことが大きい．住宅や建材メーカ等とタイアップして，建材一体型太陽電池パネルの開発に

もいち早く取り組んでいた．

太陽電池パネルだけでなく，電力変換器（パワーコンディショナ）などのシステム開発にも他国に先んじるものがあった．電力各社による余剰電力購入サポートにより，わが国の住宅用太陽光発電システムは電力会社の配電ネットワークに連系し，余剰電力を逆潮流させることが可能となった．日本の高い電力品質を保持するためには，太陽電池の直流電力を交流電力に変換し，安全に連系するためのパワーコンディショナの高性能化が不可欠である．太陽電池から最大の電力を引き出すための最大電力追尾（MPPT）制御や高い変換効率，さらに，パワーコンディショナは室内に置かれることもあるので静穏・小型化が必要であった．これら全てのハードルをクリアしたパワーコンディショナ製品が，国内市場の信頼を勝ち得ている．

また，実際に太陽光発電システムを購入し，小さな発電所長となった個人ユーザの数が，世界的に見て圧倒的に多い．25 万世帯もの個人ユーザが目を光らせている国内市場は，アフターセールの点でメーカにとって最も厳しい市場であるといえるかもしれない．このため，各社は 10 年保証などのメンテナンスサービスを充実させてきた．個人ユーザ側からも，自身が所有する太陽光発電システムの健全性の評価のために，互恵グループを発足する等の工夫を試みてきた．自然エネルギー推進市民フォーラム（REPP）やクリーンエネルギーライフクラブ（CELC）によるモニタリング活動や，太陽光発電所ネットワーク（PV-Net）による PV 健康診断等の活動が挙げられる．PV 健康診断では，産業技術総合研究所が NEDO からの受託研究によって開発した発電量シミュレーション技術[5]を用い，会員の申告する発電量実績値と推定値を比較し，乖離度を基にシステムの故障診断を行っている．

4. さらなる普及拡大のために

わが国で NEF による住宅用太陽光発電システムの設置補助が終了した只今，欧州を中心にフィードインタリフが太陽光発電普及の切り札として注目を浴びており，お隣の韓国でも導入されたばかりである．それでは，わが国でもフィードインタリフを導入することが太陽光発電普及にとってハッピーかというと，そうとはいい切れないと思う．もちろん，太陽光発電を大規模に導入する即効薬としては期待できるのであるが，太陽光発電が電気収入を得るための道具と化して，地球環境保全という錦の御旗を掲げながら私利追求の場となってしまう傾向があるからである．ドイツでは既にファンドや投資家らがメガソーラの担い手であると聞く．日本は，住宅向け市場が主戦場であり，さらに共同出資による市民共同発電所の建設などの良い事例があるため，街づくりや村おこしと協調した独自の普及形態が模索できると思う．

ただ，市民共同発電所や街づくり・村おこしでの太陽光発電導入計画では，作ることが目的と化してモニュメントとしては意味をなすものの，長期運用成績では発電量や稼働率が見劣りする可能性がある．発電所として好成績をあげる上ではフィードインタリフのようなインセンティブは効果的であるので，同様の長期モニタリングの仕組みを組み合わせると良いだろう．

個人ユーザが自身の太陽光発電の健全性を判断するのは実は難しい．太陽光発電の性能に影響する気象（特に日射量）の変化が日々大きいことや，太陽光発電装置に対する知識不足などが原因である．(財)電気安全環境研究所が産業技術総合研究所と共同で実施した太陽光発電ユーザの不具合事例意識調査の結果[5]からは，約 4 割のユーザが自身の太陽光発電の発電量が適切であるかを判断できていないことが分かった．発電量が多い（普通）と感じていても実際は標準より 10% 以上も少ない発電量しか得られていなかった楽観的なユーザに対しては，毎月の運転履歴を検査し，故障の有無を自動診断する仕組みがいる．発電量が少ないと感じていても実際は標準以上に得られていた悲観的なユーザに対しては，太陽電池パネルの物理的解説が必要かもしれない．後者の「発電量が期待よりも出ていない」という悲観的ユーザは結構多く，期待値が高く設定されていることに原因があると思われる．これは，太陽電池パネルの銘板定格出力が結晶シリコン系太陽電池にとってほぼ最良の環境条件で規定されていることをほとんど知らされておらず，実環境において定格出力より小さい出力しか表示されないことが不満として現れたものと考えられる．

太陽電池パネルの銘板表示を出力（ワット）定格から発電量（ワット時）定格で補完するという国際規格（IEC 61853）策定の動きが進行中であり，このような一般消費者の誤解を解く一助となるであろう．さらに，発電量定格の策定は，真に発電性能の優れた太陽電池を引き立てるため，諸外国に急追されるわが国の太陽電池産業にとって，得意とする高効率太陽電池の開発推進の追い風となるであろう．

参 考 文 献

1) IEA International Energy Agency, Trends in Photovoltaic Applications, Report IEA-PVPS T1-15 : 2006, (2006).
2) Photovoltaic News, Vol. 25, No. 4, The Prometheus Institute, (2006).
3) 光産業技術振興協会，オプトニューズ，153 号，(2006).
4) 新エネルギー財団（NEF）ホームページ：http://www.nef.or.jp
5) 電気安全環境研究所，産業技術総合研究所，NEDO 平成 16～17 年度研究報告書「太陽光発電システム評価技術の研究開発」，(2006).
6) 太陽光発電協会，第 23 回太陽光発電システムシンポジウム，2006 年，他からの著者集計．

IEC E-TECH ONLINE NEWS

IEC E-TECH ARCHIVES

November 2006 edition

- NEWS
  - IEC present at CEATEC – Japan's hi-tech tradeshow
  - WTO workshop in Tunis
  - IEC at March 2007 Geneva Motor Show – "The fully networked car"
  - US National Committee celebrates IEC centenary
  - London hosts dependability seminar
  - Renewable Energy 2006 Conference held in Japan
  - Renewable energies in Japan
- INTERVIEW
- SPOTLIGHT
- FOCUS
- PRODUCTS / SERVICES
- CONTACTS

ARCHIVES INDEX

Year: Section:

2007
2006
2005
2004
2003
2002
2001
2000

or
|< Current edition

- Email alert service! subscribe now...
- RSS feed service

Subscribe and get the latest iec e-tech headlines delivered to your desktop. (RSS guide)

SEARCH THE SITE

OK

WEBSTORE

- Search & buy standards
- Download area
- Customer Service Centre

Articles back | next

Renewable Energy 2006 Conference held in Chiba, Japan

Professor Kosuke Kurokawa

The General Chairperson at the 2006 conference on renewable energies, which took place at the beginning of October, was TC82 *(Solar photovoltaic energy systems)* member Kosuke Kurokawa of Japan. The week-long conference, attended by over 1 000 specialists from 64 countries, was organized in conjunction with the International Solar Energy Society

Kurokawa, who is Professor of Power Electronics in the Faculty of Technology at the TUAT, the Tokyo University of Agriculture and Technology, is Japanese chief delegate to TC82. As one of the key people at the conference, besides delivering opening and closing speeches, he was Chair of the 2006 Steering Committee, Chair of plenary sessions on various policy issues and also responsible for several of the posters displayed in the Photovoltaics, Biomass and Advanced power systems sections of the exhibition.

Renewable Energy 2006 coincided with Japan's first comprehensive international exhibition of renewable energy, covering 10 categories that included policy issues, photovoltaics, solar thermal applications, low-energy buildings, wind energy, biomass, hydrogen and fuel cells, ocean-energy, geothermal and advanced power systems.

The importance of renewable energy

In his introduction to the conference, Kurokawa stated, "The importance of the renewable energy technology field has been growing very significantly since the beginning of the 21st century and will continue throughout this century. The Organizing Committee of Renewable Energy 2006, was set up as a collaborative effort between academia, industry and the Japanese government. There is growing worldwide expectation that renewable energy technologies will prove to be a solution for increasingly apparent energy and global environmental problems. According to certain long-term world energy projections, renewable energy could be able to satisfy half of the world's energy needs by 2050. This would put renewable energy on the same level of importance as conventional energy."

Renewable Energy 2006

Some of the themes of the conference:

- Large and small scale photovoltaic systems and solar thermal projects being studied around the world as providers of additional energy;
- Japanese geothermal energy utilisation;
- A workshop on advanced renewable energy research in Russia;
- The implication of renewable energy on the sustainability of regions – 100 years ahead;
- The prospects of renewable energy in various areas in the world, particularly in light of high oil prices;
- Wind energy, with speakers from the UK, Greece, Norway and Japan;
- The energy recovery that is made possible by treating urban sewage sludge, marine biomass, wood, sugars, chicken manure slurry and other bio-energy conversion sources such as rice, charcoal, wind and waves.

Renewable energy to supply 60% of world's energy 2100

Kurokawa continued stating that "More aggressive forecasts predict that renewable energy might supply two-thirds of the world's energy by 2100. We, the specialists involved in the field of renewable energy technologies today, should accept this challenge and respond to such ambitious targets this century in an aim to provide new direction and quality to our lives. Knowing that renewable energy is the only green and peaceful resource present anywhere on earth, should inspire us to further its development and dissemination. The Organizing Committee sincerely believes that "Renewable Energy 2006" will provide an excellent opportunity for those in attendance to make an invaluable contribution to our planet by forming proposals to establish an ideal 'New Energy System' for the 21st century."

~ memo ~

~ memo ~

~ memo ~